KIT SCIENTIFIC REPORTS 7621

Nuclear Fusion Programme

Annual Report of the Association Karlsruhe Institute of Technology (KIT)/EURATOM

January 2011 - December 2011

KIT Scientific Publishing

I. Pleli (ed.)

Nuclear Fusion Programme

Annual Report of the Association Karlsruhe Institute of Technology (KIT)/EURATOM
January 2011 – December 2011

Karlsruhe Institute of Technology
KIT SCIENTIFIC REPORTS 7621

Cover page photograph

Breeder Unit Mock-up for European Blanket Module for ITER – Manufacturing process of Cooling plate with cooling channels (right side) and manifold (left side)

Fabrication Mock Up for demonstration of preliminary Welding Procedure Specification (pWPS) in accordance with ITER relevant codes and standards.
This is performed by Electron Beam welding technique, considering aspects of low distortion assembly, Post Welding Heat Treatment (PWHT) and Non Destructive(NDE) and Destructive Examination (DE) qualification processes.
Additionally, the following technologies are involved to ensure a high quality manufacturing result: Spark Erosion, 3-dimensional computerized numerical control (CNC) machining featuring smooth milling finishing, Electron beam drilling and later on 1-step Cooling Plate U-form bending.

Nuclear Fusion Programme

Annual Report of the Association
Karlsruhe Institute of Technology/EURATOM
January 2011 – December 2011

I. Pleli
(ed.)

KIT Scientific Publishing

Report-Nr. KIT-SR 7621

Impressum

Karlsruher Institut für Technologie (KIT)
KIT Scientific Publishing
Straße am Forum 2
D-76131 Karlsruhe
www.ksp.kit.edu

KIT – Universität des Landes Baden-Württemberg und
nationales Forschungszentrum in der Helmholtz-Gemeinschaft

KIT Scientific Publishing 2012
Print on Demand

ISSN 1869-9669

Overview

Preface

With Europe and the world increasingly conscious about the need to move towards sustainable energy production, fusion is receiving even more attention as an inherently sustainable and safe potential source of energy, and is called to accelerate its development path towards energy production. Urgency has now become particularly important in Germany, where the political consensus is to abandon nuclear energy within 10 – 12 years, and to shift completely towards sustainable energy by 2050. This path is mirrored by the recommendations of an independent expert panel charged by the European Commission in 2011 with the monitoring of the European fusion programme. The message by the panel, echoed by the Commission, is clear and has been well understood: The EURATOM programme should attain more urgency, and become even more ambitious.

The KIT Fusion Programme is well prepared, and certainly willing, to move along these lines. We are advancing many of the technologies that will be required to make a fusion power plant work efficiently and reliably, taking full benefit of fusion´s potential of being “clean” and inherently safe. This includes reduced activation materials, superconducting magnets and components, microwave plasma heating systems, vacuum and tritium systems of the fusion fuel cycle, high-duty components required inside the plasma vessel like the breeding blanket and the divertor, high-temperature He cooling systems, fusion neutronics, remote handling, plant system dynamics, plasma wall interaction mitigation, as well as specific safety studies. A number of these approaches will be crucial already to make the next step to fusion energy, i.e. ITER, a success.

All in all, taking into account the different sources of funding, about 250 experts from 8 KIT institutes (Institute for Advanced Materials / Applied Material Physics – IAM-AWP, -/ Material and Bio Mechanics – IAM-WBM, -/ Material Process Technology – IAM-WPT, Institute for Material Handling & Logistics – IFL, Institute for Pulsed Power and Microwave Technology – IHM, Institute for Neutron Physics & Reactor Technology – INR, Institute for Data Processing and Electronics – IPE, Institute for Technical Physics – ITEP) are contributing to the KIT Fusion Programme, organised in cross-border task forces and teams according to the competences required.

Concerning our participation in ITER construction, we reached a level of 16 active F4E grants, 6 of which were newly started in 2011. In most of these activities, we are relying on excellent cooperation with our partners from the other European fusion laboratories. Moreover, we could start one service contract directly with IO, referring to high voltage instrumentation feedthroughs, and two framework service contracts with F4E about the testing and characterisation of cryomaterials. Within the “Broader Approach”, we continued our dedicated work, inter alia, on the superconducting current leads for JT60SA, and on several contributions to IFMIF EVEDA.

Innovation and spin-offs are becoming more and more important to demonstrate that fusion research is bringing benefits already now, and we´ll not have to wait for tangible results until the second half of the century. In this sense, the KIT Fusion Programme was pleased to actively participate in the F4E workshop on “Managing Intellectual Property, Dispute Prevention and Technology Transfer in Fusion” that was held at the end of November at Barcelona. KIT presented 3 of its recently developed technologies, i.e., an advanced beam tunnel design,

developed for the W7-X gyrotrons, for application in any kind of medium and high power microwave tube, a “ductile” layered tungsten material, and a unique method for quench detection in high-current superconducting magnets. These examples are illustrating that fusion technology is a very versatile area with many applications in different fields.

Klaus Hesch
July 2012

Plasma Wall Interaction

In the tokamak reactors ITER and DEMO, transient events such as disruptions and edge localized modes (ELMs) can result in melt motion, vaporization and brittle destruction (BD) of the tungsten (W) and beryllium (Be) plasma facing components (PFCs). In order to simulate tolerable transients and disruption mitigation by massive gas injection (MGI), computer codes are being developed at KIT. The wall damages by the plasma and runaway electrons (RE) as well as the impact of eroded atoms on the plasma are also modeled.

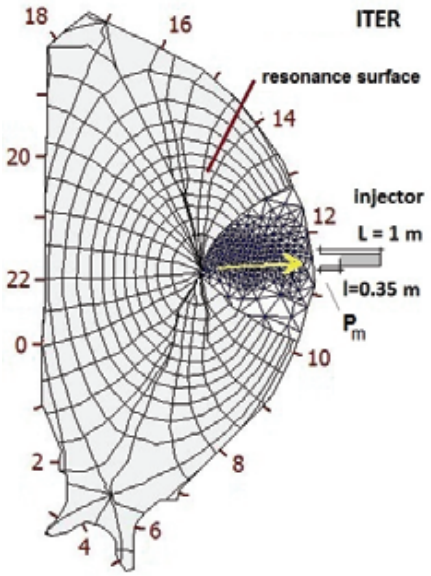

The triangular and magnetic flux meshes in the poloidal projection. The gas injector locates at the mid-plane.

The magneto-hydrodynamics and radiation tokamak code TOKES calculates, in a toroidally symmetric approach, MGI atoms and plasma contamination by diverse impurities in the vessel, and the plasma and radiation fluxes onto the wall. The fluid dynamics code MEMOS simulates the melt motions on W and Be surfaces and heat transport in material bulk. The thermo-mechanics code PEGASUS is used to simulate the BD of W. The RE energy deposition is modeled with the Monte-Carlo code ENDEP. Main models for melt motion, BD and MGI have been validated with experiments on plasma guns, electron beams and the tokamaks JET, TEXTOR and DIII-D.

A significant issue of ITER design is the occurrence of disruptions, which can limit the lifetime of PFCs. For **disruption mitigation**, MGI is a promising tool. Modeling with TOKES has been focused upon the plasma thermal quenching (TQ) caused by argon MGI. The code was successfully validated against two JET experiments: one with Joule heating and plasma energy content W = 0.8 MJ, and another one with neutral beam heating and W = 3.2 MJ. During TQ the injected gas is ionized and Ar ions of a temperature of ~100 eV expand making one toroidal turn during ~0.5 ms, which soon provides toroidal symmetry. Then a cooling wave terminates the plasma in ~3 ms. The TOKES radiation cooling model includes anomalous plasma thermal transport across ergodized magnetic surfaces.

Disruption mitigations by MGI can result in the generation of **runaway electrons (RE)**, which can damage the wall. Numerical simulations for the consequences of RE impact on the PFCs were carried out for JET, ITER and DEMO conditions. The energy distribution of RE was assumed to be exponential as $\exp(-E/E_0)$ or Gaussian as $\exp(-(E/E_0)^2)$ functions of the RE energy E. The characteristic energy E_0 depends on the device. The energy depositions calculated by ENDEP were used in MEMOS to examine melting (starting heating from a wall temperature of 800 K for ITER and DEMO, and from room temperature for JET). A reasonable agreement between ENDEP and MEMOS numerical simulations and JET experiments was achieved. Then predictive modeling on melt damage to the ITER vessel wall was performed. The simulations were performed for the RE deposition energy in the range of 30-100 MJm^{-2} over 0.05-0.3 s. Calculations of the RE impact on a hypothetical ITER mono-block blanket made of W with imbedded water cooling copper pipes resulted in the following conclusions. Main heat absorption in W occurs in the subsurface layer ~10 μm, 20% of impacting RE energy is converted into X-ray radiation, a fraction ~25% is reflected by back-scattered electrons, and due to strong bulk absorption only 0.5% of X-ray energy is released in the pipe. For a RE energy deposition of 30 MJ/m^2 and exposure time 0.1 s the W armor surface does not melt. In the case of DEMO, the RE impacts would probably result in W surface melting and evaporation, which is due to a large thickness of the W layer on the EUROFER substrate, required for providing a large PFC lifetime.

The validation of MEMOS by modeling experiments from the tokamak TEXTOR has been continued. MEMOS simulations were performed for long-time plasma heat loads with heat fluxes up to 30 MW/m^2 and duration τ ~ 5 s. The simulations have demonstrated a reasonable agreement with TEXTOR results. New calculations with MEMOS have been also carried out for ITER, focusing mainly on the magnitudes of melt splashing of Be and W under pulsed heat loads. Particular concern in the upper baffle region is about the misaligned leading edges between neighboring divertor cassettes. The melt damage is estimated for assumed misalignments of 3 mm, heat loads Q = 50 – 200 MJ/m^2 and τ ~ 0.5–3 ms. The main damage occurs there due to strong melt motion and a radiative vapor layer. A melt pool up to 0.4 mm and a wear layer about 0.1 mm are obtained after one pulse. These results initiated elaborations of ITER baffle design.

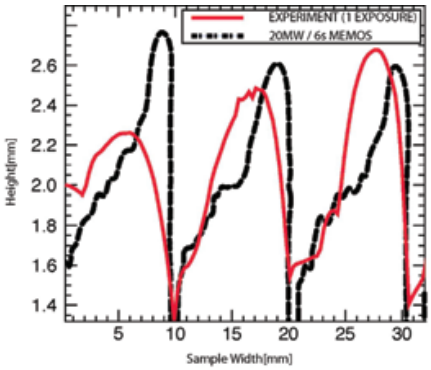

MEMOS profiles versus TEXTOR data. Comparison of the final erosion profile of W target; Q=20 MW/m^2, τ=6 s.

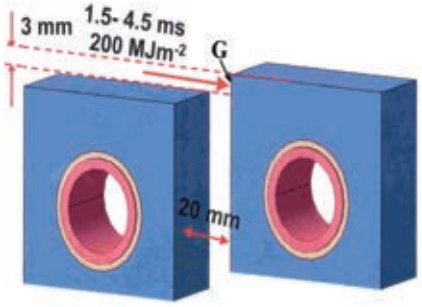

Sketch of a misaligned edge between monoblocks on the sides of two divertor cassettes.

Interpretation of dedicated experimental observations at the plasma gun QSPA-Kh-50 (Kharkov, Ukraine) has been performed aiming at further improvements of PEGASUS BD models for the W dust generation caused by ELM-like loads above the melting threshold. Analysis shows that the surface cracking after the resolidification can produce W dust with characteristic sizes of particles from 1 to 10 μm. The particles can leave the surface with the velocities up to 10 m/s. Then they cross the scrape-off layer (SOL) and evaporate in the confined plasma. For ITER, the resulting influx into the core is estimated about ~5×10^{18} W ions after one ELM of 0.75 MJ/m^2 power density and 0.25 ms duration. The corresponding radiation cooling produced by the W ions is roughly estimated to be about 150-300 MW, which can be intolerable.

Numerical investigations for DEMO using ENDEP and MEMOS were undertaken. The FW blanket module made from W-clad EUROFER steel mono-block with imbedded water or helium cooling tube was implemented in MEMOS. The blanket was numerically tested under the steady-state and transient heat loads of plasma and RE fluxes scaled from ITER. For VDE impact with Q ≥ 50 MJ/m^2 and τ ≤ 0.1 s the W thickness h required to prevent EUROFER from creeping is h ≥ 1.4 cm, however, then melting can occur. For h = 0.3 cm the sustainable steady-state loads are up to ~14 MW/m^2. The RE heat generation in W occurs in the subsurface layer of ~1 cm, thus the cooling pipes are not affected.

One of the most critical issues of DEMO is an excessive power loading to the plasma facing component, particularly to the divertor plates. Divertor concepts based on movable targets and some passive cooling, e.g., by radiation losses, could be an option to tackle the problem. Therefore, a preliminary assessment for replacing the conventional actively cooled divertor plates by a set of passively cooled moving targets was carried out. It is concluded that there are many potential difficulties with a moving divertor plate concept, which need to be addressed in a detailed engineering design and eventual testing. It is not yet clear whether a moving plate system would be more or less feasible than other similar ideas for a divertor, e.g., moving belts, pebble divertor or liquid walls.

Physics: Heating and Current Drive - ECRH

Electron Cyclotron Heating & Current Drive (ECRH & CD) will play a major role in forthcoming long pulse or continuous fusion devices like ITER, W7-X and DEMO. Due to its excellent coupling to the plasma and well localized power deposition in the plasma, microwaves in the range of 100 – 200 GHz are already applied in existing fusion machines to heat and stabilize the plasma and to drive a toroidal current, which would be of particular importance for a continuous tokamak. Since many years, KIT has been developing high power gyrotrons as microwave sources, diamond window units, and launchers to inject the power into the fusion plasma.

Together with several European institutions and with a commercial partner, KIT developed the gyrotrons for the W7-X heating system. Continuous progress is being reported on the tests of the series gyrotrons and the assembling of the complete ECRH system at IPP Greifswald.

The development of a 2 MW, CW, 170 GHz coaxial cavity gyrotron for ITER has been pursued within the EU Gyrotron Consortium, acting as a single scientific partner for F4E. The goal of this development is the supply of sources for 170 GHz ECH & CD to ITER, providing 8 MW CW power.

In another European consortium, the ITER ECRH Upper Launcher is being developed together with ultra-low loss diamond torus windows. The main purpose of these launchers is plasma stabilization, an additional equatorial launcher will provide central plasma heating.

For DEMO as the next step on the fusion step ladder towards power generation, new concepts of ECRH heating like frequency tuneable systems are under development, including ECRH RF sources, launcher components and broadband windows.

Microwave Heating for Wendelstein 7-X

The ECRH system for W7-X (10 MW, 140 GHz, CW) will be provided under the responsibility of KIT together with national and European partners. Many components of the transmission system, HV-systems and in-vessel-systems have been installed at IPP Greifswald, and have been already used for testing new concepts and components for ECRH. Progress has been made w.r.t. performance improvements of the series gyrotrons. In 2011, two series gyrotrons (SN4R, SN6) have been tested and successfully accepted, both showing the specified output power of 1 MW at CW operation. Several improvements have been included in the series gyrotrons, such as a corrugated beam tunnel, reduced RF loading of inner components, modified cooling of the output window and an enhanced beam sweeping system at the collector, resulting in a stable series production. Further work has been spent to include diagnostics and power measurement. All four ECRH plug-in launchers have successfully passed the tests and are ready to be installed in W7-X.

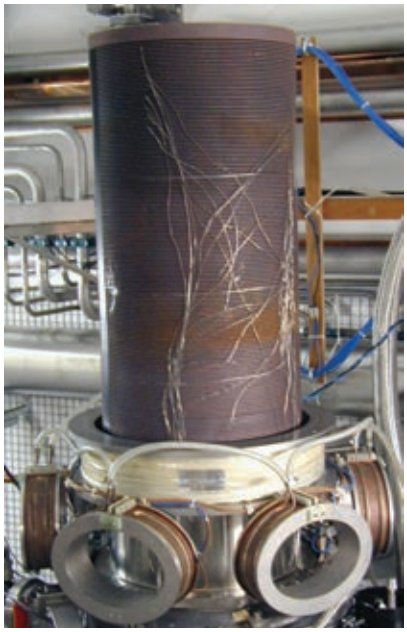

W7-X gyrotron collector and transversal field sweeping system.

Development of the European 170 GHz Gyrotron for ITER

The modified and refurbished first industrial prototype of the coaxial cavity gyrotron was delivered end of September 2011 to CRPP. Several experiments were performed until December 2011, yielding 2 MW output power and 45% efficiency in short pulse operation. Although the results were promising, the tests with the industrial proto-

type were terminated due to a fatal error in the cooling system. Based on that, F4E is considering to switch to an 1 MW backup solution.

At KIT, the short-pulse pre-prototype tube was operated with a new launcher, reducing the stray radiation from 7% to 5.5%. Activities have been started in order to design, manufacture and test a cooled normal-conducting (NC) coil for CW operation of the KIT Oxford instruments magnet, as required for 2 MW operation.

Other Developments on Gyrotrons

Besides the major scientific topics described above, several accompanying activities were ongoing. A new spectral measurement system was developed, allowing the calculation of instantaneous spectra and the identification of undesired mixing signals. A measurement example is shown in the figure below. This high dynamic and wide band measurement technique is essential for investigations on parasitic oscillations.

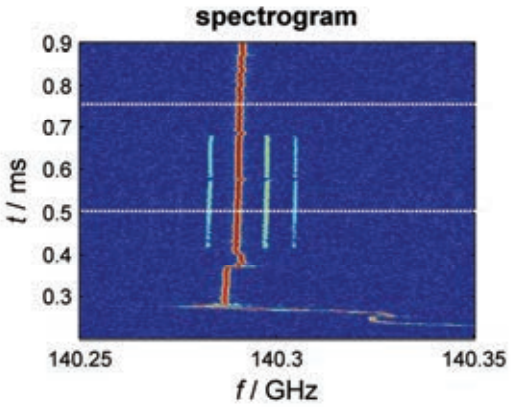

Measurement example of spectrum versus time at a W7-X gyrotron. It can be seen in the waterfall plot that, after a startup process, a modulation appears and vanishes again.

Since multi-frequency gyrotrons together with step-tuneability of the tubes is becoming more important for future devices, KIT is developing broadband technologies (e.g. Brewster angle diamond window) for these systems.

KIT is also involved in the development and definition of ECRH systems for next generation fusion devices (DEMO). It will require gyrotrons with improved performance, e.g. higher efficiency and reliabilty. Taking those requirements into account, in a first step the new design of an emitter concept for an electron gun of a gyrotron has been continued, aiming at innovative investigations on gun performance as well as at the qualification of improved emitter materials.

Design of the ITER ECRH Upper Launcher

After the successful Preliminary Design Review at ITER IO in end of 2009, it took two years until a follow up contract between Fusion for Energy and the developing Associations could be signed and started. The ECHULCA consortium (KIT, IPP/D, CNR/I, CRPP/CH, FOM/NL with KIT as the leading party) could reactivate the design of the ITER ECRH upper launcher with its main purpose of focused current drive for plasma stabilization. The goal of the ongoing design iteration is to improve the overall design and to finalize the components outside the vacuum vessel, waveguides, shutter valves and the millimeter wave diamond windows.

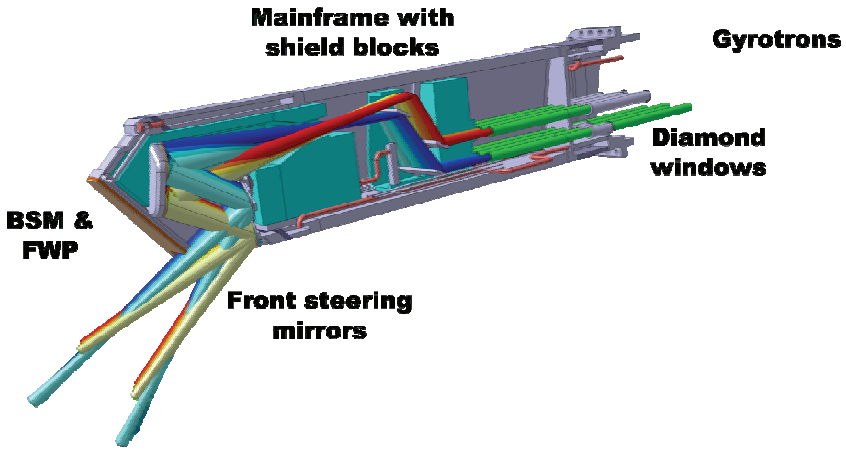

Preliminary design of the ITER ECRH Upper Launcher.

In a separate contract, the diamond window design could be improved, in cooperation with the colleagues at JAEA in Nara, Japan, where an installed diamond window prototype unit could luckily withstand the Tohoku earthquake in March 2011. The high power, long pulse tests at JAEA helped to mitigate non ideal millimeter wave mode content reducing the coupling of spurious higher order mode into small gaps of the assembly.

In parallel, the basis for the potential next ECRH generation window is being developed: a frequency tuneable system could make obsolete the state of the art fixed frequency angular steering system for electron cyclotron resonance matching. The critical key component for this step is a working diamond broadband window design. Three approaches are in development: tuneable double disk units (ASDEX UG), surface modified disks (anti-reflex surface texturing by laser) and a sophisticated window unit with the diamond disk asymmetrically brazed in the Brewster angle suppressing nearly all critical reflections. First prototypes have been designed and manufactured, tests have been started.

Accompanying the design activities for the ITER ECRH Upper Launchers, possible manufacturing routes have been checked with large scale prototypes tested in the Launcher Handling and Testing Facility Karlsruhe. A facility extension has been initiated allowing vacuum bake out experiments monitoring outgassing rates of prototype surfaces obtained from different manufacturing routes as welding, brazing or powder based hot isostatic pressing (HIP).

Magnets and Affiliated Components

The long-standing experience of KIT in the development of fusion magnets including associated components was exploited in 2011 to support design and construction of major fusion plants. Outstanding are the procurement of high temperature superconducting current leads for Wendelstein 7-X, the corresponding development for JT-60 SA, the materials testing of magnets structural parts for ITER at cryogenic temperatures, and the development of high temperature superconducting coils for future fusion power stations.

TORSION facility.

To characterize ITER components under axial as well as torsion load, a dedicated cryogenic test facility was commissioned. The performance characteristics of the TORSION facility allow for axial loads of +/- 100 kN and momentum of +/- 1000 Nm at temperatures down to 4.2 K. Within the development of high voltage axial breaks for ITER working at cryogenic temperature, this facility helped to perform mechanical quasi-static and fatigue tests at room temperature and 77 K. It was shown that the breaks met all specified mechanical requirements.

The procurement of **high temperature superconducting (HTS) current leads for Wendelstein 7-X** has started. After successful testing of two prototypes in 2010, series production is under way. Till the end of 2011, 4 of altogether 14 current leads were fabricated and tested in a special cryostat connected to the TOSKA facility.

Series production of HTS current leads for W7-X at KIT.

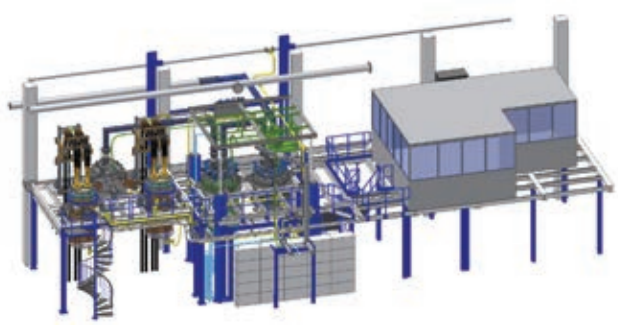

CuLTKa – Current Lead Test Facility Karlsruhe.

For the TF and CS magnets of **JT-60SA**, 6 leads for a maximum current of 26 kA and 20 leads with a maximum current of 20 kA are required. To come to a fast and economic testing sequence, the Current Lead Test Facility Karlsruhe (CuLTKa) is under construction. The present planning expects the assembly of CuLTKa being finished until end of 2012.

For fusion reactors beyond ITER, the use of **high temperature superconducting (HTS) magnets** would result in many economic advantages, e.g. tremendous saving of cooling power and abandonment of the thermal shield. A comparative study has been conducted based on REBCO (RE=Rare Earth-Ba-Cu-O) coated conductors that have high potential for use in fusion magnets due to their applicability at high fields and temperatures > 50 K. Four different cable designs propagated worldwide were compared including also the KIT concept using Roebel-Rutherford cables. Criteria comprised mechanical stability, AC losses, scalability in current performance and prospects for industrial manufacturing. The KIT solution, where Roebel cables are used as strands for Rutherford cables, turned out to be most advantageous.

Breeding Blanket

The development of breeding blankets, their integration in the core of a fusion reactor and their testing are central elements of KIT´s long term programme towards a fusion power reactor.

In particular KIT is developing Helium cooled concepts for these systems, namely the Helium Cooled Pebble Bed (HCPB) blanket. Several activities are also in support of the Helium Cooled Lithium Lead (HCLL) blanket concept developed by CEA. In addition, tasks have been performed for the improvement (in fabrication, characterization and modeling) of functional materials like Li-orthosilicate, Beryllium and Beryllium alloys.

R&D for helium-cooled blanket concepts has been done in 2011. Three Helium Cooled blanket concepts have been analyzed in this EFDA task: Helium Cooled Pebble Bed (HCPB); Helium Cooled Lithium Lead (HCLL) and Dual Coolant Lithium Lead (DCLL). The advantage of Helium Cooling is in the fact that Helium presents the better compatibility with all the materials used in the fusion reactor. The first two concepts (that are supported in the EU breeding blanket programme as candidates for the DEMO blanket and selected for the Test Blanket Programme in ITER) have been considered in more details. Open issues will be addressed in the future.

One important aspect for the application of the Helium Cooled Lithium Lead (HCLL) blanket concept is the understanding of the fundamental properties of magneto hydrodynamic **(MHD)** flows like pressure drop in generic geometric elements of liquid-metal circuits. For this, a closed liquid-metal circuit has been designed and manufactured. As working fluid, the liquid metal alloy GaInSn has been chosen, since this fluid is liquid at room temperature, non-toxic and nonflammable, which allows easy handling.

The EUROBREED training network is integrating almost the all the important aspects of the breeder blanket programme, including development of breeder materials, characterization and modelling of properties, testing of these materials in out-of-pile experiments, their integration in ITER, and also some aspects for the integration in the future DEMO reactor. In 2011, the activities related to the EUROBREED network were carried on in their full extent

for the third year; the conclusion of the network is foreseen for September 2012. Progress meetings were held in Madrid (May) and Karlsruhe (October) with presentation of the work by all the trainees, presentation and visit of the host laboratories and Meeting of the Coordination Board.

Heat removal from the first wall of the Helium-Cooled-Pebble Bed Test Blanket Module (HCPB TBM) was studied within an EFDA task. The purpose of the investigation was to experimentally prove the numerically found decrease of heat transfer coefficient due to the asymmetry of heat loads at the first wall of the HCPB TBM. This task was successfully accomplished. The investigation of heat transfer in the first wall has confirmed the 3D CFD models by experimental data. Based on detailed analysis of experimental and 3D CFD data in the framework of this task, an improved design of cooling channels in the first wall was proposed. An experimental facility named GRICAMAN has been designed for the investigation of the flow distribution in the coolant system of HCPB TBM, and construction has started. First results will be obtained in 2012.

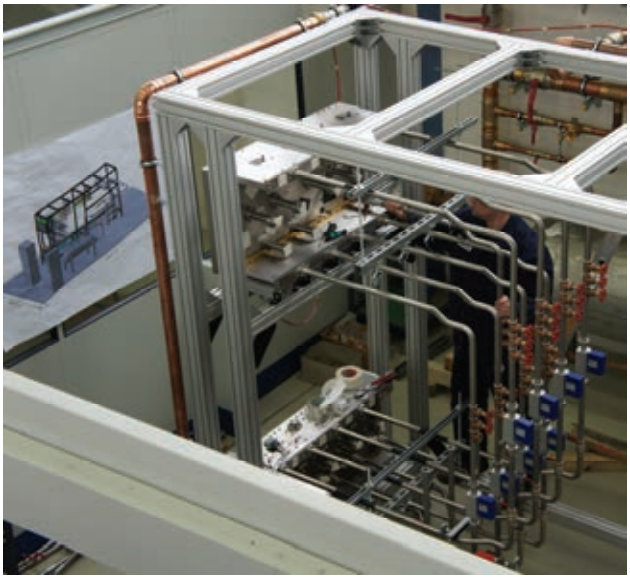

Final assembling of equivalent grid/cap channels.

The laboratories working on the European TBM programme have organized themselves in the **European Test Blanket Module Consortium of Associates** (TBM-CA, with the participation of KIT, CEA, ENEA, CIEMAT, RMKI and NRI), with KIT providing the project leader and hosting the central support team. A major activity for the design of the EU Test Blanket Systems in ITER was performed in the framework of an F4E Grant, where KIT has the responsibility to define the strategy to ensure a reliable and accurate tritium measurement at the outlet of the TBM in view of benchmarking the neutronics calculation. As a necessary step for this, a first conceptual design of the tritium accountancy system for the ITER TBM has been completed.

Procurement and Quality Control of Lithium Orthosilicate Pebbles. In collaboration with Schott AG, Mainz, KIT is developing and investigating slightly hyperstoichiometric lithium orthosilicate pebbles to be used in the HCPB blanket. In 2011, 4.7 kg of Li_4SiO_4 (OSi) pebbles were delivered and characterized in three batches (OSi 10/2). The batches showed clear differences between the material specifications, the SiO_2 excess and crush loads. Further investigations to clarify the reasons for this are in progress. As part of the Broader Approach DEMO activities**,** the **KALOS facility** (KArlsruhe Lithium OrthoSilicate) was assembled to investigate a modified fabrication process for the lithium orthosilicate pebbles. The new experimental setup was used to study blended breeder ceramics consisting of lithium orthosilicate, lithium metatitanate and also lithium metasilicate. It has been proven that the process can be operated successfully with the new setup and compositions. Additionally, these modifications also lead to higher process control resulting in a narrow size distribution.

Synthesis of Tritium Breeder Ceramics from Metallic Lithium. In the presently known powder or melt based fabrication processes for ceramic breeder pebbles, either lithium hydroxide hydrate or lithium carbonate is used as a starting material. For the fabrication of ^{6}Li enriched pebbles, which are needed for the last two phases of ITER, the variety of ^{6}Li enriched compounds is limited as most of the established enrichment techniques for lithium provide only metallic ^{6}Li. Metallic lithium though, cannot be directly used as a raw material in these processes. Therefore KIT investigated different chemical reaction routes to transform

Experimental setup – test facility (drawing), single nozzle beam and the new oven.

metallic lithium into nonmetallic compounds that are suitable as starting materials in the subsequent fabrication processes for breeder pebbles.

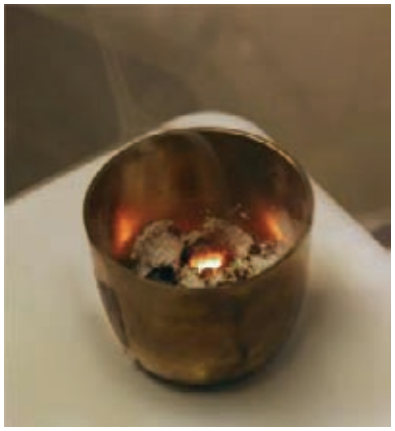

Reaction of liquid lithium and silica in a nickel crucible.

For the future use of breeder blanket material in the form of pebbles it is important to **model the Thermo-mechanics of Pebble Beds**. In reality, the pebbles produced by the manufacturer are polydisperse with a certain size distribution. The results of the stress-strain response show that the polydisperse pebble assemblies show a better behaviour as compared to mono sized assemblies. This suggests that the overall crush resistance for the polydisperse assembly is better; but the residual strain after unloading is higher, resulting in a large gap formation. Hence, the pebble size distribution should be chosen so as to make a compromise between the crush resistance and the gap formation.

Beryllium is considered as candidate material for the first wall of future fusion reactor and as neutron multiplier material for the fusion blanket, where its resistance against radiation is very important. Mobility of point defects produced under irradiation and their mutual interactions influence the formation of radiation induced microstructures and define the macroscopic response of irradiated material (e.g., swelling or irradiation growth) which in beryllium is significantly affected by gas production. A Combination of **ab initio and MD methods** proved to be a useful approach for the study of point defect clusters. In particular, several types of self interstitial atom (SIA) clusters were observed in MD and ab initio: (i) triangular configurations in basal plane (stacking fault), (ii) planar C-C clusters, which may present possible seeds for interstitial loop formation and (iii) non planar clusters. Further investigations are required to clarify their relations to a- and c-type interstitial loops experimentally observed in beryllium under irradiation. Macroscopic effects as, e.g., swelling of beryllium are greatly influenced by the amount of accumulated transmutation helium. Atomic scale simulations of beryllium behavior under irradiation are necessary for understanding of basic mechanisms and reliable prediction of microstructural changes. A very important conclusion of this work is that helium is essential for the stabilization of vacancy clusters, which are otherwise unstable. The direct consequence of this fact for the practice is that voids cannot grow in beryllium under electron irradiation, while helium bubbles can be formed under neutron irradiation due to helium produced by nuclear transmutations. Thus, it can be to concluded that the presence of transmutation helium is the necessary condition for the evolving of porous microstructures in beryllium.

Divertor

The development of divertors, their integration in the core of a fusion reactor and their testing are central elements of KIT´s long term programme towards a fusion power reactor. In particular, KIT is developing Helium cooled concepts for these systems, using W/W-alloy systems.

In 2011 a review of water-cooled Divertor Concepts in the EFDA 3PT frame was done, which serves as a starting point for appropriate design improvement. Also in the EFDA frame, a review of the status and perspective of development of the He-cooled divertor was done and the progress reported.

Successful deep draw attempts from 1 mm thick tungsten sheet for mass production of divertor thimble (Ø15 x 1).

Progress at KIT included investigating and developing W deep drawing for Tungsten divertor thimbles and High Heat Flux Tests on 1-Finger (more than 1000 cycles with 12 MW/m^2 were achieved) and 9-Finger modules.

Structural Materials - Steels

Reduced Activation Ferritic/Martensitic (RAFM) steels are reference structural materials for in-vessel components of a Fusion Power Plant because of their better irradiation resistance and improved radiological properties, as compared to commercial martensitic steels. EUROFER is the European development foreseen as material for structural parts of ITER-TBM and DEMO blanket and divertor. One of the most crucial items for the application of EUROFER is its performance under intense neutron irradiation. This question – which can be ultimately only answered by IFMIF – was tackled in 2011 activities of KIT.

A comprehensive assessment of the effects of neutron irradiation on blanket and divertor materials was done putting the emphasis on the review of the tensile, Charpy impact, fracture toughness and low cycle fatigue properties of EUROFER 97 steel irradiated up to a displacement damage dose of 80 dpa. The assessment also comprised irradiation experiments where He was artificially brought into the material matrix by doping the material with boron that builds up He under neutron bombardment as transmutation product. This technique tries to compensate for one of the shortcomings of fission reactor irradiations where, compared to irradiation under real fusion neutrons, the formation of He is inadequately small. An estimation of the helium induced extra embrittlement, expressed as the increase of the DBTT (Ductile-to-Brittle-Transition-Temperature), was done (cf. figure). These findings provide an important contribution to the estimation of service lifetime of in-vessel components in future fusion machines.

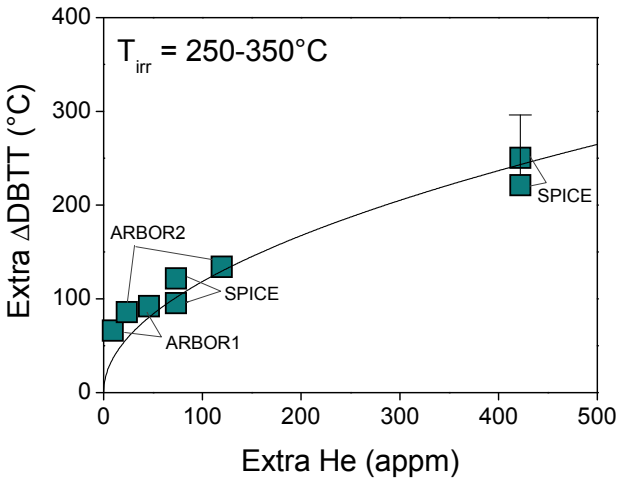

Helium induced extra embrittlement vs. extra helium amount for irradiated boron doped steels.

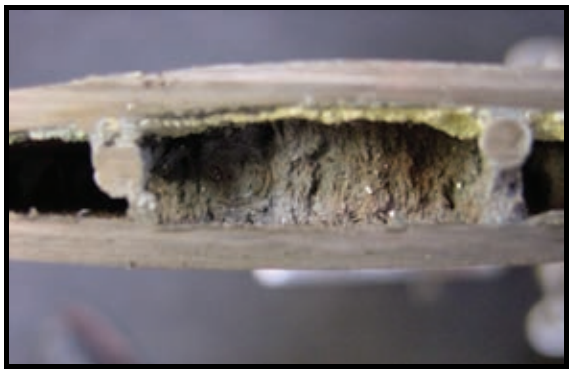

Plugging of the electro-magnetic pump by precipitates.

The HCLL concept for DEMO blankets and ITER TBM uses liquid metal Pb-15.7Li as breeding material. The aim of the PICOLO loop is to study the corrosion attack of flowing Pb-15.7Li on structural materials. For a closed testing loop it is difficult to describe the fate of the dissolved corrosion products in terms of transport, deposition, forming of precipitates etc. Refurbishment of several parts of the PICOLO loop gave the unique opportunity to carry out post mortem analyses of the magnetic traps and other drained components. The testing showed that oversaturation of Fe in Pb-15.7Li leads to precipitates at cooler sections of the system, and the installed magnetic trap for purification did not collect all existing particles leading eventually to the plugging of the EM pumping channel. These findings indicate the risks caused by corrosion products concerning safe and reliable operation of Pb-15.7Li systems.

The instrumented indentation technique, which is an enhancement of the conventional hardness measurement, allows the determination of multiple mechanical properties. In combination with the analysis by Artificial Neural Networks, the method reveals viscoplastic material properties like tensile and cyclic behaviour. Requiring only small testing volumes and offering the possibility to re-use already tested specimens, the indentation technique is specifically suited for the remote-handled use of irradiated specimens in a hot cell environment. Two indentation systems have been devised, developed, and recently installed at the KIT Fusion Materials Laboratory: The first one with operation parameters of up to 200 N and up to 600 °C and the second one, a high temperature indenter, with 2 N load and up to 1000 °C service temperature.

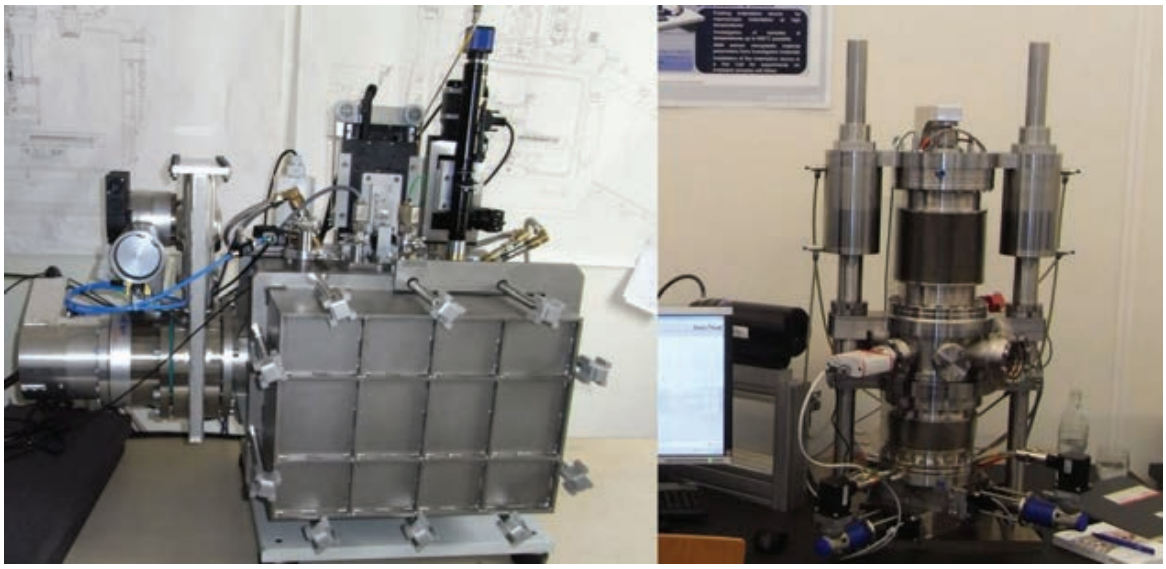

Hot Cell Indentation devices: 3 N / 1000 °C (left) and 200 N / 650 °C (right).

Structural Materials – Refractory Alloys

The development of a divertor for DEMO or a power plant is very challenging since heat loads of up to 10-15 MW/m² have to be removed in standard operation. KIT is pursuing a concept based on helium cooling and a modular arrangement of cooling fingers, which use refractory materials as a protective tile at the plasma facing side, and refractory materials as

structural material forming the cap of the cooling fingers. Tungsten and tungsten alloys are presently considered for both applications mainly because of their high temperature strength, good thermal conductivity, and low sputter rates. For armour materials, high crack resistance under extreme thermal operation condition is required, while for structural materials, sufficient ductility within the operation temperature range is mandatory. Both material types also have to be stable with respect to high neutron irradiation and transmutation rates.

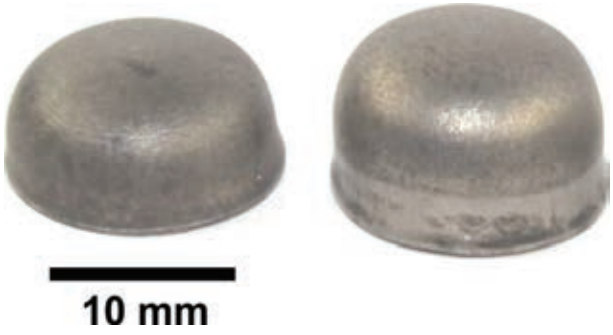

Deep drawing of tungsten thimbles performed in high vacuum at 600°C.

The reference concept for the helium cooled divertor implies the manufacturing of cooling fingers consisting of steel tubes connected to tungsten thimbles. To shape this cap, a tungsten plate with a thickness of 1 mm and a diameter of 26 mm was deep drawn in a universal testing device under a high vacuum and at high temperature into a thimble with a height of 10 mm and an outer diameter of 15 mm. The **deep drawing technique** combines two important benefits: (i) it fits the needs of a mass production technique which is necessary taking into account the large number of several hundred thousand cooling units required, and (ii) due to the weak grain boundaries of tungsten the grains should follow the contour of the thimble which is also realized by deep drawing a plate, in other words, 'grain boundary alignment'.

The use of tungsten as structural material in the reference concept is limited to the high temperature parts which must be connected to the lower temperature parts built from the reduced activation ferritic/martensitic steel ODS-EUROFER. Realizing such kind of joining by **diffusion bonding** is restricted by many problems related to the large differences in melting temperatures and coefficients of thermal expansion and the forming of brittle intermetallic layers. A low activation vanadium sheet was introduced as an interlayer to mitigate thermally induced residual stresses at the interface caused by different values of the thermal expansion. Comprehensive test series were carried out to find optimal diffusion bonding parameters, which on one hand can guarantee a sound bonding with high strength, ductility and toughness to survive the thermo-mechanical divertor loading, and on the other hand can mitigate the problem of induced residual stresses and the formation of carbon rich phases causing embrittlement. Optimal hipping parameters were found to be 700 °C for process durations of 1 h.

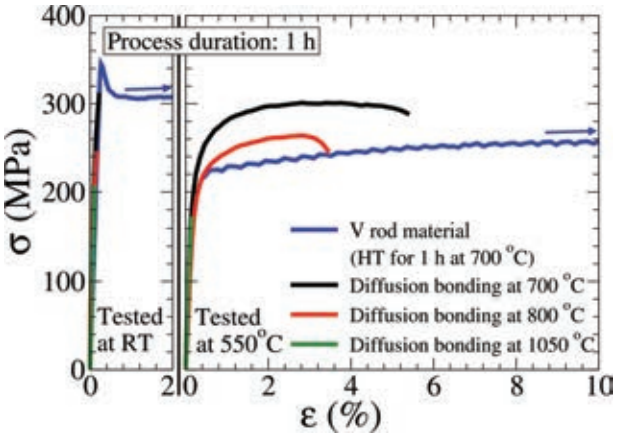

Improvement in strength and ductility of the joint by reducing the bonding temperature down to 700 °C and for process duration of 1 h, σ – ε curves for specimens tensile tested at RT and 550 °C.

Main drawback for the use of tungsten as structural material is its inherent brittleness at the favoured divertor operation temperature window. Based on the experience that bcc metals such as tungsten can become more ductile by prior cold working, several layers of thin tungsten foils with a thickness of 0.1 mm were assembled by brazing them together. In this way a **tungsten laminate** emerged. Charpy impact toughness tests demonstrated, that a tungsten laminate can dissipate energy at lower temperatures compared to tungsten plate material and that the idea of expanding the ductile properties of a tungsten foil to a bulk material by assembling and joining several layers of tungsten foil was successfully realized. A tungsten laminate pipe made by rolling-up a tungsten foil, followed by a subsequent brazing process

was manufactured. This component can dissipate high amounts of energy in a Charpy test and shows complete ductile fracture already at 200 °C. The development of a tungsten material that is ductile at lower temperatures can open a path to the design of gas cooled divertors consisting of larger parts with simpler geometry.

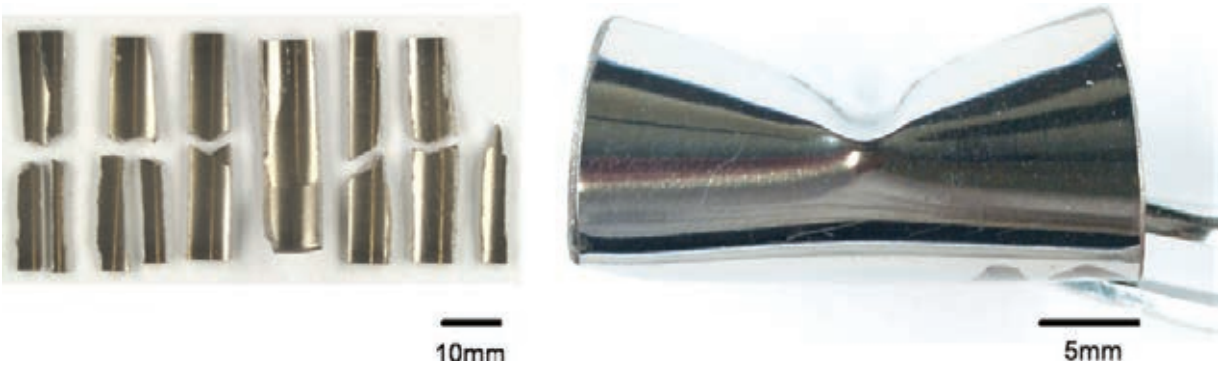

Charpy impact toughness tests at 300 °C with tungsten pipes made from rod material (left) and tungsten foil (right).

Nuclear Data

Theoretical and experimental activities have been conducted in the frame of F4E grants and contracts with ITER, EDFA-PPPT and EFDA-JET to provide nuclear data developments, including measuring techniques, and nuclear analyses for ITER and DEMO. The KIT contribution to the theoretical activities for nuclear data is on the evaluation of general purpose nuclear cross section data, the qualification of new and updated data evaluations and the development of advanced computational schemes for sensitivity calculations.

The experimental activities aim at providing the experimental data base required for the validation analyses and the development of experimental techniques needed for the nuclear TBM (Test Blanket Module) test programme in ITER. The focus of the KIT contribution is on measurements of nuclear responses in TBM mock-up experiments and on advanced measurement techniques both for ITER-TBM and for future experiments at JET.

Besides the regular support to KIT fusion projects, the fusion neutronics group at KIT has dedicated contributions to ITER and DEMO design by specific nuclear analyses comprising neutron/gamma transport simulations as well as shut-down dose rate calculations using the Rigorous-2-Step method (R2S).

The analyses of neutronics experiments on a mockup-up of the Helium-cooled Lithium-Lead (HCLL) TBM revealed a deviation from the nominal **Lithium concentration in PbLi**. To resolve this issue, several different measurements have been conducted to assess the real Li^6 concentration at various locations within the assembly. This includes time-of-arrival slow neutron spectra, transmission measurements with a moderated AmBe source (for relative differences), atomic absorption spectroscopy and ICP mass spectrometry. The results indicated a depletion in Li^6 (about 3.5 at%) at a Li content of 0.62 wt% in LiPb

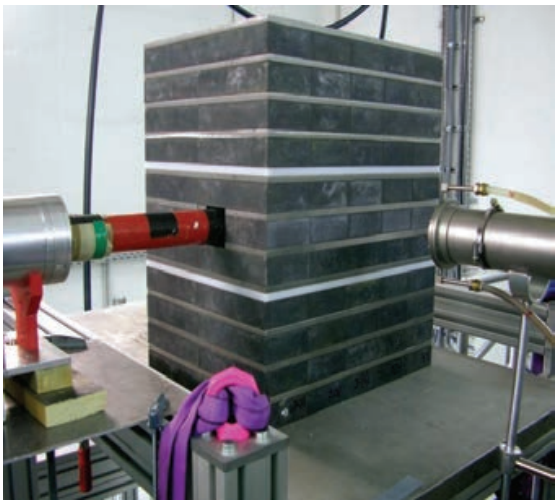

The HCLL-TBM neutronics mock-up.

Based on these and other confirmative measurements the **post-analyses of the experi-**

ments have been revised, and KIT contributed by sensitivity and uncertainty calculations for the tritium production rates using the MCSEN code.

For the development of a passive spectral neutron flux density measurement method in the ITER-TBM based on **material activation and a pneumatic transport system** for short irradiation and measurement cycles an activity on the selection of appropriate activation reactions and materials has been performed. Candidates have been selected and their responses to a HPGe gamma-ray detector have been simulated by combined EASY-2007 and MCNP calculations.

A task has been devoted to preliminary investigations of the suitability of a combination of **lithium glass scintillators, optical fibers and photodiodes** as candidates for TBM diagnostics. To this end, a pulse-height spectrum has been measured from a Cf-252 spontaneous fission source which showed a slightly lower energy resolution compared to using a photo multiplier tube instead of the photodiode.

For future experiments on JET for validation of shutdown dose rate predictions, an assessment of the suitability of neutron and gamma detectors has been conducted. KIT in collaboration with Technical University Dresden investigated a **Cadmium-Zinc-Telluride detector** with a special electrode arrangement. The small-size detector can be operated at room temperature and is suitable for measurement positions close to JET structures.

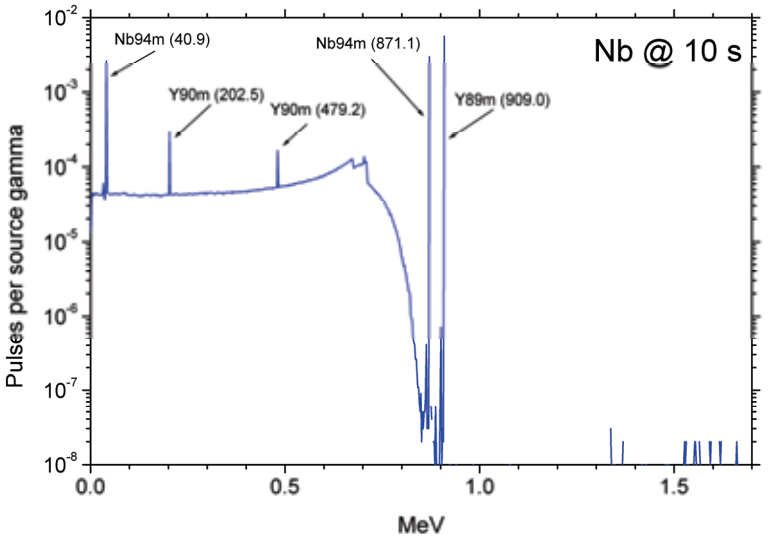

Calculated pulse height spectrum in a HPGe gamma-ray detector from Nb following a 30 s irradiation (10 s cooling time).

The **R2S approach**, developed originally at KIT, has been extended to mesh-based calculations (R2Smesh) recently. This scheme has been validated extensively and is utilized in a number of applications. For the previous dose rate measurement campaign at JET in 2009/2010, KIT provided R2Smesh calculations for the comparison to the experimental values and to complimentary Direct-1-Step calculations. To define a radiation map for DEMO both during and after plasma operation, KIT contributed with a first assessment focusing on remote handling issues to be extended in 2012.

The R2S scheme is part of the **neutronics computational services** provided to ITER Diagnostics Team in order to improve the shielding performance of the Diagnostic Generic Equatorial Port Plug (EPP) in ITER. Based on local models of the EPP, parametric analyses have been performed to find suitable design options, particularly to avoid neutron streaming through various gaps. A promising solution has been integrated in the general ITER neutronics model Blite for global assessments and further improvements.

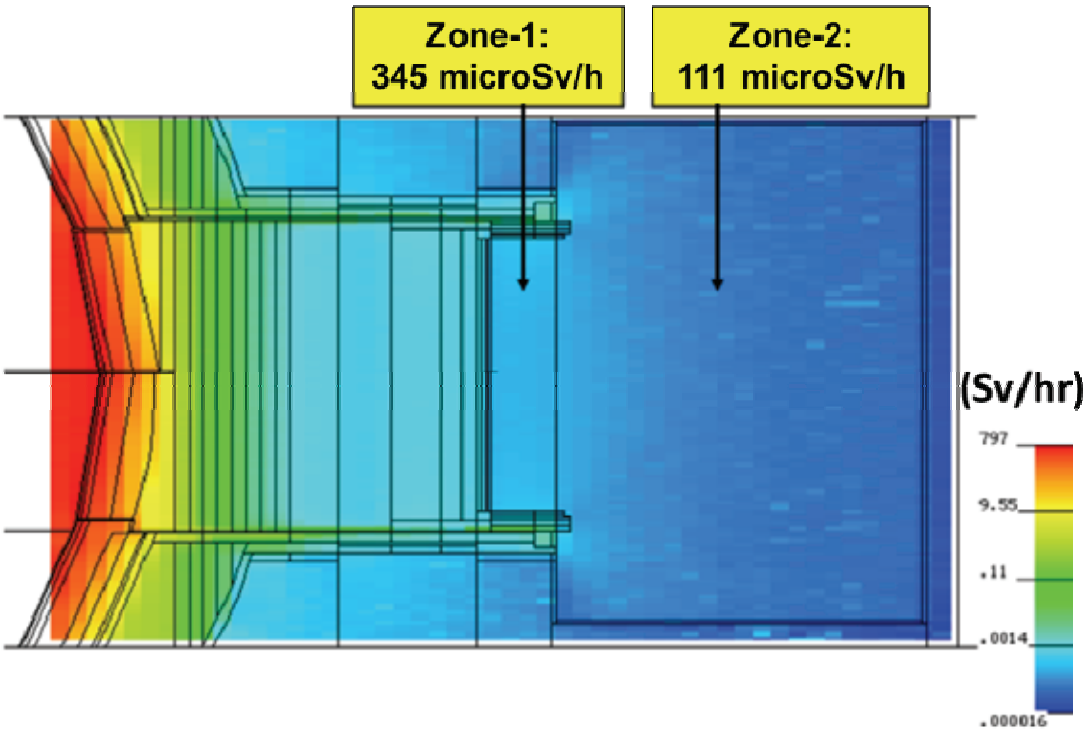

Shutdown dose rate (μSv/h) map for the local EPP model with optimal single labyrinth and vacuum boundary conditions.

International Fusion Materials Irradiation Facility (IFMIF)

Broader-Approach Activity: IFMIF Test Cell and High Flux Test Module

In the Engineering Validation and Engineering Design Activities (EVEDA) for the International Fusion Material Irradiation Facility IFMIF, which is an element of the Broader Approach activities launched jointly by several European countries and Japan, the German contribution includes engineering tasks for the IFMIF Test Cell and the IFMIF High Flux Test Module. According to the planning for EVEDA, these tasks will be performed in the timeframe up to 12/2013.

The IFMIF facility is dedicated to fusion-relevant irradiation of structural and functional material specimens, with the objective to create an experimentally validated material properties database suitable for design and licensing of future fusion power plants. The facility is composed of several subsystems, namely the 40MeV 250mA deuteron accelerator facility (AF), the lithium target facility (LF) and the test facilities (TF). The Target- and Test Cell (TTC) is part of the test facilities, containing the lithium target neutron source and the test modules. It has the primary function to shield the environment against the intense radiation generated by the target, and to safely contain all hazardous materials. Inside the TTC, the target and test modules are arranged, as shown in the Figure.

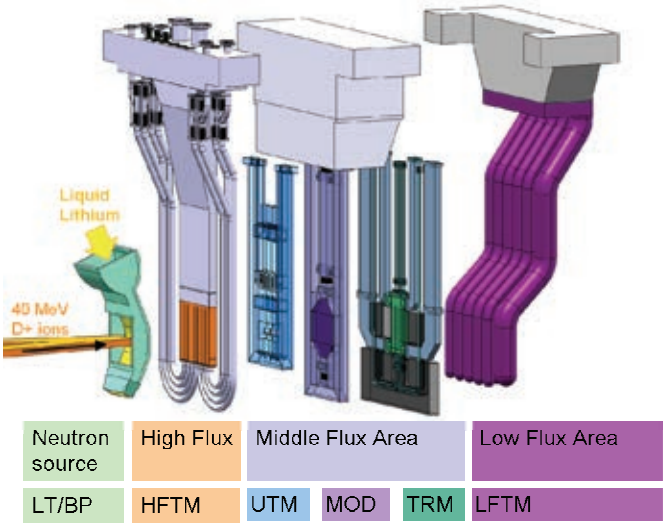

Overview on the irradiation experiments inside the IFMIF Target- and Testcell (TTC).

Engineering Design and Validation for the HFTM
The High Flux Test Module (HFTM) is the irradiation device for miniaturized samples of structural materials. The HFTM is positioned immediately behind the neutron source inside the TTC. The HFTM contains up to 24 irradiation rigs/capsules with approximately 80 SSTT samples each. It is possible to adjust individual temperatures for the specimens in each rig, in the range of 250 – 550°C. The design of the HFTM-Assembly has been improved regarding the assembly/disassembly process, which has to be performed partially under hot cell conditions by remote handling tools. It was sought to remove cost-driving and time consuming processes from the assembly, in order to improve the overall process in the IFMIF irradiation operation. A major step was the simplification of the finalizing weld-seams to close the HFTM-Assembly after insertion of the capsules.

Engineering Design of the Target- and Test Cell (TTC)
The design of the TTC has been significantly modified from the previous MTC concept. A driving motivation was the necessity to avoid polymer-based electrical connectors within the irradiation cavity.

Further Modifications are:

- The cross-section has been changed to a rectangular shape to adapt better to the test modules
- Instead of a vessel (bearing both mechanical and vacuum-pressure loads), the supporting walls are now made directly from the concrete of the radiation shield, with a steel liner inside to provide an inert and gas tight surface.
- The gas-sealing function has been moved above the top shielding plug, enabling the use of polymer-based sealing materials instead of difficult-to-handle metal gaskets.
- The electrical interfaces to the test modules are no longer performed by electrical connectors. Instead, the cables from the modules are fed-through gas tight plugs on the top of the modules.

The Preliminary Design Review for the new test cell design has been performed in 09/2011.

Neutronics Analysis for the IFMIF Test Facility and High Energy Beam Transport Section
The objective of this work was to support the engineering design of the IFMIF Test Facility (TF) with the Test Cell (TC) within the IFMIF-EVEDA/BA framework. The TC is the central part of IFMIF where two deuteron beams react with the liquid lithium target and the Test Modules (TMs) are placed for irradiation. Neutronic analyses are performed to provide various nuclear responses which are required for the engineering design of the facility (material damage, gas productions, heating, etc.) and for safety related assessments (activation of various components, air and gas, biological doses to work personnel and the public).

All previous nuclear analyses were conducted with a standard TC model that has been manually devised according to the CDR design. However, the TC presently designed has a very different geometry with significant impact on neutronic aspects. Therefore, a new TC model was converted into the geometry representation by utilizing the McCad conversion software developed at KIT.

The nuclear heating rate, displacement damage and gas production rates in the TC vessel wall were calculated with the new geometry model. Pronounced peaks were obtained around the beam ducts entrance region due to back-streaming neutrons. The helium production was shown to be too high if re-welding is considered. A wall thickness of more than 350 cm is needed to satisfy the dose rate limit during operation of less than 10 μSv/h in rooms adjacent to the TC. The dose rate on the top access cell floor is estimated to be around 20 μSv/h and well less than 100 μSv/h. Thus, substantial improvement has been achieved in the shielding capability for the access cell in the present TC design.

Fuel Cycle – Vacuum Pumping

Since two decades, KIT has been developing vacuum pumping systems for fusion reactors.

The concept of cryogenic pumping based on cryosorption at activated charcoal has been successfully demonstrated at KIT, and is now the common technology used for all primary vacuum pumping systems at ITER. As these cryopumps are part of the European procurement package for ITER, KIT has been charged with the elaboration of the complete build-to-print package of the torus and cryostat cryopumps and the neutral beam (NB) cryopumps. These pump designs are unique and will have to be validated by a 1:1 scale prototype. After manufacturing in the European industry, the prototype of the torus and cryostat cryopump (the so-called pre-production cryopump) will be tested in the TIMO-2 facility at KIT, whereas the NB prototype pump will be manufactured and tested in the neutral beam test facility MITICA which is under construction at Consorzio RFX, Padova, Italy.

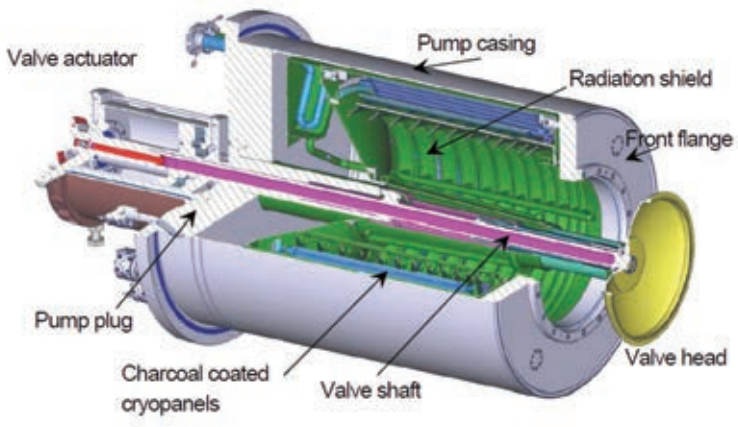

The build-to-print design of the ITER pre-production cryopump has been finalised.

As outstanding engineering highlight in 2011, the detailed design of the pre-production torus cryopump of ITER, could be finalised. The main challenge of this activity was to design this prototypical pump in such a way that it can be optionally used at ITER as a spare pump. This requires elaborating a design in compliance with requirements which were emerging at ITER for a long time, so that a strongly iterative working style had to be adapted. Besides the central 3D CATIA product, the final package contained a number of 230 2D manufacturing drawings and about 1400 weld descriptions. Along the design evolution process, off-normal event cases have been studied and a full thermal, mechanical and seismic load analysis was made to be able to demonstrate full compliance with EN 13445, the reference code for this component. The design was approved from F4E and ITER and will be given to the manufacturer who will be identified until mid 2012 in a call-for-tender procedure.

The detailed design development of the NB/MITICA prototype cryopump made excellent progress in 2011. The design could be further elaborated to the level of great detail already in many areas. The focus of the work in 2011 was given to an impressive catalogue of FEM analyses and a re-design of the cryopanels of the 4.5 K circuit. To ensure that the temperatures along the cryopanel fins stay acceptably low also in areas that are exposed to the very high electron heat loads originating from the ion source, the fins will now be copper plated, which ensures improved thermal conductivity.

In a parallel activity, KIT was supporting the Consorzio RFX team with specific know-how on the cryoplant concept design, based on the many years of experimental cryopump characterisation and TIMO operation. Until the end of 2011, a first draft of a Technical Specification for the cryoplant to operate the HNB cryopump could be elaborated.

The scientific highlight in 2011 was the successful organisation of an international workshop in the area of vacuum gas dynamics, held in May at Leinsweiler, with 60 participants from 19 countries from all over the world. This indicates the leading role of the KIT fusion programme in this field. For the first time, representatives of academia, engineering science and industry were brought together in an environment which allowed for perfect interaction and exchange. Many new contacts have been made which will definitely be helpful to initiate new collabora-

tions in the next future. The importance to simulate transient flow phenomena was clearly highlighted, as a result of which first activities have been launched in this direction. Another important topic discussed was the modelling of neutral gas flow patterns in the divertor in a physically consistent way that means combining the EIRENE/SOLPS approach for the plasma side with a sound Direct Simulation Monte Carlo approach for the neutral gas side. This work will be integrated in the upcoming EFDA ITER Physics Programme.

2011 was also characterised by the start of the new EFDA Power Plant Physics and Technology activity. A study of potential improvements and simplifications of the ITER inner fuel cycle in view of different power plant concepts with different requirements was conducted. As main outcome, the concept of Direct Internal Recycling (DIR) was developed, which introduces a short-cut for the torus exhaust gas around the tritium plant in order to reduce the tritium inventories, to improve the balance of plant, and to allow for shortest processing times. Within the new EFDA framework, a detailed assessment of potential vacuum system solutions for a fusion power plant was launched. It was clearly found that the ITER solutions are very specific and a simple extrapolation to the larger scale of a fusion power plant is not considered to be attractive. The main result of this study was a clear definition of the characteristics a vacuum system for a power plant must have, namely being continuous, non-cryogenic, and providing a separation between hydrogenic species and helium close to the divertor. KIT has developed a concept design of a candidate pumping system that fulfils these requirements and first proof-of-principle tests are planned for 2012.

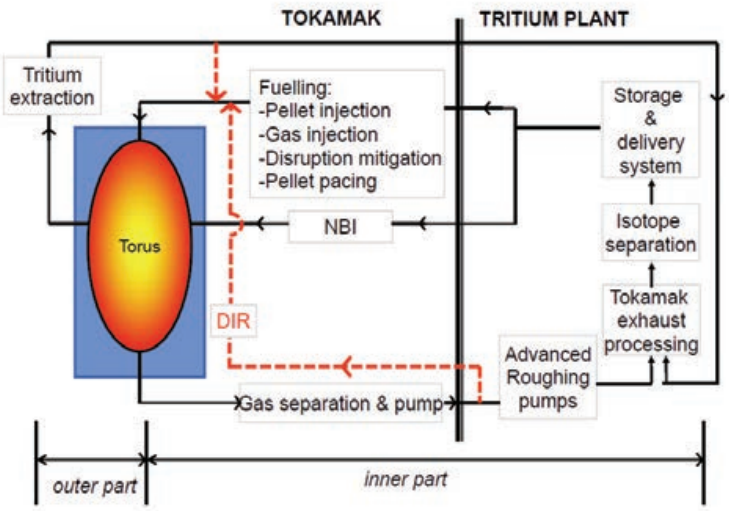

The concept of direct internal recycling (DIR) has been developed in order to simplify the fuel cycle for a fusion power plant significantly.

Fuel Cycle – Tritium Plant

The Water Detritiation System (WDS) and the Isotopic Separation System (ISS) of the ITER tritium plant will be European contributions. Both systems have been set up at technical scale in the Tritium Laboratory (TLK) of KIT in order to characterize the performances of various components for WDS and ISS processes in different working conditions and configurations as needed for ITER design.

The TRENTA facility has been upgraded and fully commissioned to the stage TRENTA-4, allowing **combined operation of the Water Detritiation System with the Cryogenic Distillation** representative of the ITER WDS and ISS protium separation column. Since the ITER WDS will be the final barrier against tritium discharges into the environment, tritiated streams from the ISS will be routed to the LPCE (Liquid Phase Catalytic Exchange) column of the WDS. The aim is to investigate interdependencies between the two systems taking into account different scenarios with composition fluctuations in the stream returned from the ISS.

Part of TRENTA facility.

An important result in 2011 was the determination of the **influence of deuterium** on the tritium separation performance of the LPCE column, essential component of the WDS. Up to 50% of D were in the tritiated feeding water. The outcome serves for benchmarking the modelling code as well as supporting the design of the ITER LPCE column.

The **TRIMO software** developed over the last decade for the dynamic simulation of the ITER fuel cycle was upgraded to the TRIMO++ version. This new version written in C++ takes the advantages of the programming language such as reliability and high flexibility offering the user the freedom to set up any configuration by linking of fuel cycle components in a modular way.

The water detritiation facility of TLK was used to demonstrate that it is possible to concentrate the volume of large amounts of **JET tritiated water**. During the last years of operation, JET has generated and temporarily stored on site tritiated water with an average rate of approximately 10 tonnes per year. JET is investigating alternative ways to the reference solution of shipping the tritiated water back to Canada. One drum of JET tritiated water containing about 180.5 l with an average tritium concentration of 0.41 GBq/kg was received by TLK for volume reduction and thus, tritium enrichment. The tritiated water had been purified before at SCK•CEN by passing the water through a series of ion filters. After processing the JET water in the TRENTA-3 facility at the TLK, the final reduced volume was only 6.25 kg with an average tritium concentration of 11.85 GBq/kg, which gives a volume reduction factor of about 29.

Fusion Programme Management Staff

Head of the Research Unit	Dr. K. Hesch	ext. 25460 e-mail: klaus.hesch@kit.edu
Secretariat:	Mrs. A. Knoll	ext. 25461 e-mail: anja.knoll@kit.edu
	Mrs. M.-E. Tuzia	ext. 22435 e-mail: maria-elena.tuzia@kit.edu
Program Budget, Administration, Reports, EU-Affairs	BW. M. Henn	ext. 25547 e-mail: michael.henn@kit.edu
	Mrs. I. Pleli	ext. 28292 e-mail: ingrid.pleli@kit.edu
Blanket and Divertor Development, HELOKA, IFMIF, Public Relations	Dr. D. Radloff	ext. 28750 e-mail: dirk.radloff@kit.edu
Fuel Cycle, Structural Materials, Superconducting Magnets, CAD-Office	DI. S. Gross	ext. 25468 e-mail: sigurd.gross@kit.edu
Plasma Heating Technology, Safety Studies, Neutronics, Physics	Dr. K. Hesch	ext. 25460 e-mail: klaus.hesch@kit.edu
Quality Management, Resource Loaded Planning, Document Management	Dr. J. Gafert	ext. 22923 e-mail: juergen.gafert@kit.edu
	Dr. I. Ignatiadis	ext. 85465 e-mail: Ioannis.ignatiadis@kit.edu
	Dr. M. Ionescu-Bujor	ext. 28325 e-mail: mihaela.ionescu-bujor@kit.edu
	Mrs. DI. B. Keim	ext. 24194 e-mail: birgit.keim@kit.edu
	Mrs. DI. Ch. Schweier	ext. 28325 e-mail: christine.schweier@kit.edu

Address: **Karlsruhe Institute of Technology**
Nuclear Fusion Programme Management

Post Office Box 3640, D - 76021 Karlsruhe / Germany

Telephone No: **0721-608-Extensions .....**

Telefax No: **0721-608-25467**

world wide web: **http://www.fusion.kit.edu/**

Contents

Page

Page

System Codes for DEMO

Structural Materials – Steels

Structural Materials – Refractory Alloys

Nuclear Data

Page

Plasma Wall Interaction

Modelling of Cracked and Molten Divertor and First Wall Material under High Transient Loads-benchmark against Experiments for ITER Transient Power Load Simulation (WP11-PWI-04-03-01 and WP11-PWI-04-03-02)

Introduction

In fusion tokamak-reactor (ITER, DEMO) the transient and off-normal plasma events (ELM, RE, VDE and disruption) may produce strong erosion (vaporization, melting and cracking) of the PFC materials (beryllium, tungsten, CFC etc.).

For modelling of armour materials erosion, particularly a melt motion damage including heat transport into bulk materials, the incompressible fluid dynamics code MEMOS has been used. The validation of MEMOS by modelling experiments from plasma gun QSPA-T and from the tokamak TEXTOR has been continued. Also new calculations with MEMOS has been carried out, focusing mainly on the magnitudes and the thresholds of melt splashing of Be and W under pulsed heat loads.

Brittle destruction (cracking) of tungsten armour under action of ELMs is considered as a serious problem for ITER divertor. The cracking can produce W dust with characteristic sizes of particles ranged between 1 and 10 μm. The particles can leave the surface with the velocities up to 10 m/s, then they cross the scrape-off layer (SOL) and evaporate in the confined plasma. For W surface cracking due to loads below the melting threshold the thermo-mechanics code PEGASUS was earlier applied. The code PEGASUS describes such processes in W and CFC as crack formation, thermal conduction and dust production. In 2011 interpretation of experimental observation at the plasma gun QSPA-Kh-50 aiming further validation and improvements of PEGASUS models has been performed.

Validation of MEMOS code and simulations of PFC melt layer erosion in ITER and DEMO

The tungsten melt layer deformation caused by **J**x**B** force at TEXTOR has been modeled with the code MEMOS [1]. In the case of RE impact and long-time VDE a melt layer can exist up to several seconds. TEXTOR Experiments show that the **J**x**B** force generated by the thermo-emission electrons accelerates the melt layer and leads to a large scale melt motion damage (up to 1 mm per event). MEMOS simulations were performed for long-time plasma heat loads with heat fluxes in the range 15 – 30 MW/m^2 on the timescale of 5-6 s in a strong magnetic field. The model of space-charge limited thermo-emission current based on the modified Child-Langmuir expressions was implemented. The heat loads Q = 18, 20, 22 and 30 MW/m2, τ =5 and 6s having rectangular space profile and time shape were applied. The brush size is taken D=1 cm with the distance between brushes of 0.05 cm and radius of the brush edge rounding *Re*=0.2 cm, thickness of the tungsten target is taken of 3 mm. It is also assumed that the back side of the tungsten target is passive-cooled by radiation. Results of simulations carried out for the heat loads in the range 18–30 MW/m^2 over 5-6 s have demonstrated a reasonable agreement with TEXTOR data (Fig.1 and Fig. 2).

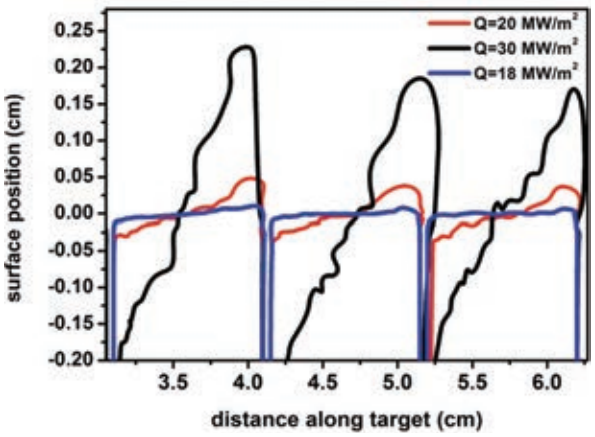

Fig. 1: MEMOS final erosion profile of W target for different heat loads Q=18 MW/m^2, τ=6 s; 20 MW/m^2, 6 s; 30 MW/m^2, 6 s.

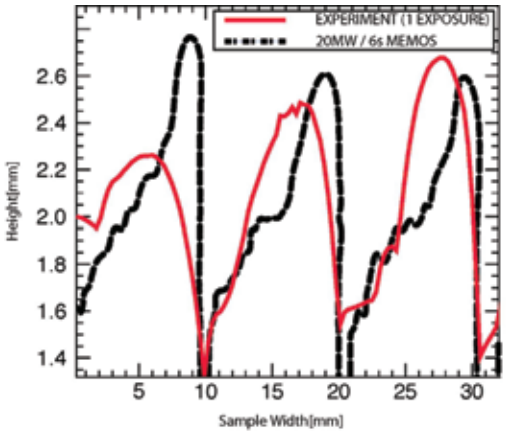

Fig. 2: MEMOS profiles vs. TEXTOR data. Comparison of the final erosion profile of W target; Q=20 MW/m^2, τ=6 s

Application of PEGASUS code for interpretation of QSPA-Kh50 experiments

The dust production rate due to ELM-like heat load is investigated in the quasi-stationary plasma accelerator QSPA Kh-50 [2]. It is shown that W surface under ITER ELM-like heat loads of 0.75 MJ/m^2 melts and under 0.45 MJ/m^2 does not melt. Analysis shows that the surface cracking under action of thermo-stress results in solid dust ejection. W influx into the ITER is estimated about ~5×10^{18} W atoms per one ELM of 0.75 MJ/m^2 power density and 0.25 ms time duration. Corresponding radiation cooling power of produced W impurities is roughly estimated to be about 150-300 MW.

The mass loss at 0.75 MJ/m^2 (above melt threshold) is ~5 μg/cm^2/pulse after 200 pulses (Fig. 3). Irradiation of the second tungsten target has been performed with 260 repetitive shots below the melting threshold. At 0.45 MJ/m^2 (below melt threshold) the mass loss is ~1.6 μg/cm^2/pulse. Since the erosion rate for the dust particles does not depend on the plasma density, for ITER it should be approximately the same as in the QSPA-Kh50 facility.

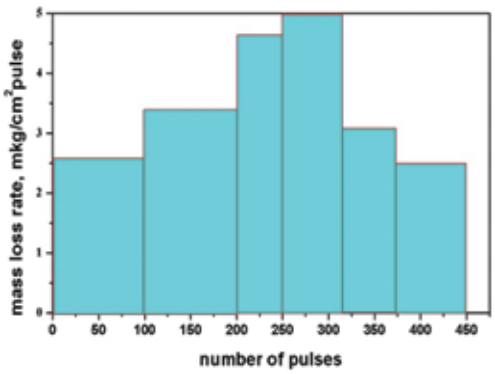

Fig. 3: Target mass loss rate vs. the number of pulses in the QSPA-Kh50 facility for the shots with surface heat load of 0.75 MJ/m^2.

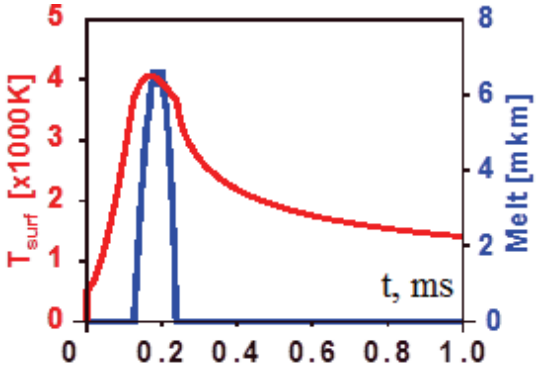

Fig. 4: Calculated time dependences for the surface temperature and the melt layer depth for the QSPA-Kh50 shot with energy density of 0.75 MJ/m^2. The melt layer totally re-solidifies at 0.23 ms.

The measured W particles are produced from cracking of solid tungsten surface, because all they start from the surface after 0.2 ms from the plasma arrival at the target. Results of PEGASUS simulation show that the particles are starting probably after re-solidification of melt layer, which occurs at 0.23 ms from the start of heating (Fig. 4).

Effect of off-normal events on reactor first wall

The energy deposition and erosion of W/EUROFER blanket module for the FW of DEMO reactor due off-normal events (VDE, ELMs) is calculated [3]. The simulations were performed for the RE deposition energy in the range of 30-100 MJm^{-2} over 0.05-0.3 s. In the case of a "hot" VDE, all stored plasma energy is deposited to the FW area over 0.3 - 1sec. It is shown that the minimum W thickness needed to prevent failure of the W/ EUROFER bond (assumed to be the EUROFER creep point) is so large that armour surface melts.

A possible option for DEMO's FW design is a sandwich type block structure, which consists of a water coolant tube embedded in the EUROFER heat sink, to which the W armour is attached. EUROFER has a creep temperature point assumed to be ~750°C.

The calculations were performed by the codes ENDEP and MEMOS. Most of RE energy is deposited within ~0.1 mm of armour layer. In the case of VDE, almost all plasma energy is converted into heat melting and W surface evaporation . In the case of RE, the percentage of absorbed energy in W armour reaches ~60%, while the percentage of energy emitted as photons is ~11-15%. The rest of RE energy is reflected off by back-scattered electrons (~16-34%) The EUROFER creep point limits the minimum W thickness (indicated in Fig. 5 by vertical arrows for 30 MJ/m^2/0.1s and 50 MJ/m^2/0.05s cases). For instance, for the RE case with moderate energy deposition density and exposure time (50 MJ/m^2 and 0.05s, respectively), the W armour thickness must be ≥ 1.4cm in order to reduce the EUROFER temperature below the creep point. However, at that thickness the W armour will melt. Only in the case of 30 MJ/m^2/0.1s for thickness ≤ 0.8cm the W surface doesn't melt and it is possible to avoid the creep thermal stresses. The total molten and evaporated thickness is ~2 mm for W, this, depending on the VDE and RE frequencies, would seriously restrict the armour lifetime.

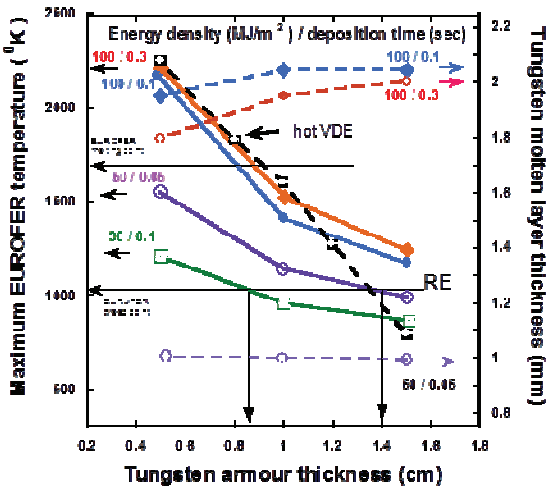

Fig. 5: The maximum of EUROFER temperature and maximum W melt layer as a function of W armour thickness.

The energy deposition into the W armour is a surface phenomenon. For RE deposition at energy densities ≥ 50 MJ/m^2 and deposition times ≤ 0.1s, the minimum armour thickness required to prevent EUROFER from creep or thermal stresses is ≥1.4cm. Almost always melting occurs. The loss of creep strength at relatively low temperature represents the main drawback of EUROFER as a structural material.

PFC lifetime in fusion reactor under steady state operation

The feasibility of the FW sandwich type blanket made of W/EUROFER (see Fig.6) is analyzed in fusion reactor steady-state operation under normal conditions [4]. The energy deposition into W armours of various thicknesses and the level of erosion caused by the RE and VDE impact were performed with the codes ENDEP and MEMOS.

During normal operation the erosion of the FW could mainly occur due to collisions with hot neutral atoms and actions of transients. Fig. 7 shows that when incoming heat flux Q reaches ~14 MW/m^2 the interlayer temperature exceeds the critical creep point T_{crit} ~ 50ºC for EUROFER and the structural material can experience strong thermal distractions. Such values of Q one can expect in DEMO for transient events like ELMs or convective radial plasma losses, associated with unstable convective cells in the SOL region during steady-state op-

eration. Under steady-state operation for heat flux value~13.5 MW/m^2 the surface armour temperature increases with the armour thickness (but stays below the melting point) and heat flux into water coolant remains below CHF value. For heat flux ≥ 10 MW/m^2 W temperature approaches a limit of~900-1050 K beyond which the degradation of the structural properties and crack formation can be expected. To keep the W surface temperature below 1 keV, the armour thickness must be ≤ 3-4 mm. It is estimated that the layer of that thickness could be sacrificed within three years of continuous operation owing to sputtering erosion.

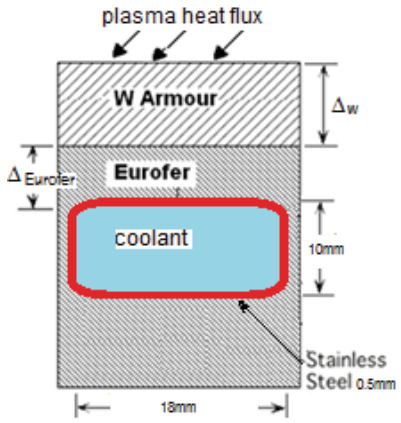

Fig. 6: Sketch of blanket module used for the computation of the plasma impact.

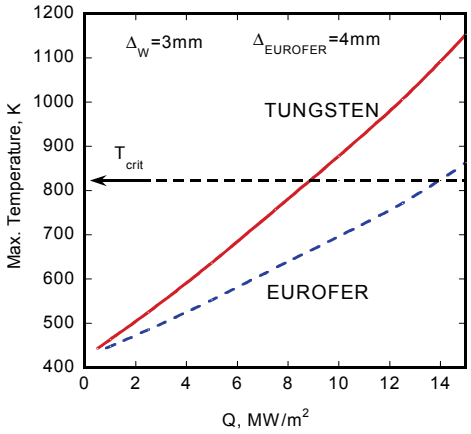

Fig. 7: W surface temperature & max. EUROFER temperature vs. heat power flux Q under steady-state operation.

Simulation of transient heat flux damage on leading edges in the ITER all-tungsten divertor

The consequences for W material damage as a result of plasma heat loads on the vertical faces of the misaligned leading edges between the divertor cassettes due to the downwards vertical displacement events expected on ITER is investigated by using the MEMOS code [5]. Melting can occur more readily under transient heat loads mainly on the leading edges on which plasma fluxes can impinge at nearly normal incidence. Particular areas of concern are the edges present on either side of gaps between neighbouring divertor cassettes, in the upper baffle region of the outer vertical target plates. Simulations of W melting are performed. Estimated heat loads on W mono-blocks in the worst expected ITER VDEs can exceed several hundred MJ/m^2 flowing parallel to the magnetic field for durations of a few ms. Melt layer damage is estimated for single plasma loads in the range Q = 50 – 200 MJ/m^2, with pulse durations between 0.5 – 3 ms and edge misalignments (Fig. 8, the lateral surface G) up to several mm in order to cover the worst possible mechanical misalignment in the current divertor design. The principal finding is that the most significant contributors to damage on misaligned edges are the radiative vapour shielding coupled with a strong melt motion.

Calculations show that the incoming plasma flux heats the surface up to high temperature such that significant evaporation occurs (see Fig. 9). The evaporated material expands towards the incoming plasma and essentially screens the target surface from the plasma stream (so that the direct heating by the plasma is reduced by a large factor). The evaporated material is heated by the plasma up to rather high temperatures so that the plasma shielding layer becomes the source of intense radiation (at the level of several GW/m^2). This intense radiation lasts for a slightly longer time than the plasma loads. Typical plasma pressures in the plasma shield region are comparable with the pressure of the incident plasma stream and will be on the order of several bars for the intense VDE loads at near normal incidence considered here. The radiation from the plasma shielding heats the target surface and surrounding components and can cause significant damage even in shadowed regions.

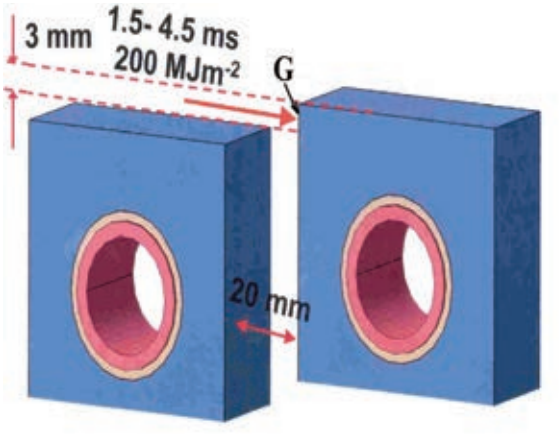

Fig. 8: Sketch of misaligned edge between monoblocks on sides of two neighbouring divertor cassettes.

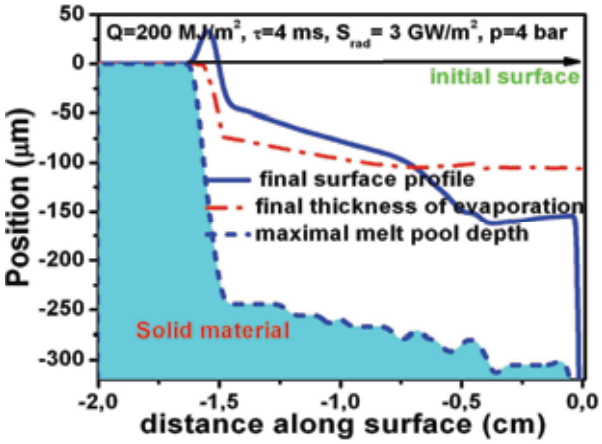

Fig. 9: Surface profiles, max. melt pool depth and evaporation profile along the lateral surface G; Q = 200 MJ/m^2, τ = 4 ms.

Staff:

B.N. Bazylev
Yu. L. Igitkhanov
I.S. Landman
S.E. Pestchanyi

Literature:

[1] B. Bazylev et. al., Workshop PFMC-13 Rosenheim, May 2011, to be published (in Physica Scripta)

[2] S. Pestchanyi et. al., Workshop PFMC-13 Rosenheim, May 2011, to be published

[3] Yu. Igitkhanov et al., Workshop PFMC-13 Rosenheim, May 2011, to be published

[4] Yu. Igitkhanov et al., 19th PSI Conference, San Diego, May 2010, to be published

[5] B Bazylev et al., Conf. ICFRM-15, Charleston, Oct 2011, presented for publication

[6] Yu. Igitkhanov et al., Conf. ISFNT-10, Portland, Sep 2011, to be published

[7] Yu. Igitkhanov et al., Conf. ICFRM-15, Charleston Oct 2011, presented for publication

Acknowledgement

This work, supported by the European Communities under the EFDA contract of Association between EURATOM and Karlsruhe Institute of Technology (KIT), was carried out within the framework of the European Fusion Development Agreement. The views and opinions expressed herein do not necessarily reflect those of the European Commission.

Development of the PWI Basis in Support of Integrated High-Z Scenarios for ITER. Demonstration of Liquid Plasma-facing Components Behaviour under ELM-like Load (WP11-PWI-04-04-01)

Introduction

The behaviour of Li layer on various porous substrates is now under investigations at different tokamaks (FTU, NSTX). Experiments demonstrated that the 'lithization' of vessel surface leads e.g. to strong reduction of heavy impurities in the plasma and longer wall lifetime for high power heat loads. A heating system increases the Li temperature above the melting point (450 C) resulting in a thin (from several microns to several tens microns) lithium film formation on the chamber wall. The impact of the hot confined plasma transients can contaminate plasma by Li ions owing to physical sputtering, melting and evaporation. The behaviour of Li coated PFC materials still remains an important issue.

In 2011 the melt motion code MEMOS was upgraded to take into account capillary porous system and Li layer recovery under transients (ELM) impact. New numerical simulations were performed under the following conditions: the melt motion and the evaporation of Li film on impermeable tungsten substrate, the Li coating of 5-50 μm thickness on W bulk material and W capillary porous system. The reference heat load Q = 0.1 MJ/m^2 during the reference pulse load time τ = 0.5 ms was assumed, magnetic field B = 5 T, tangential pressure varied in the range 2×10^{-4} to.2×10^{-3} bar, electric current component normal to the target surface varied in the range 5 – 50 A/cm^2, initial surface temperature T_0 = 30 C (assuming that Li can melt during the transient). The thickness of evaporation layer has been investigated for the reference pulse duration and heat load ranged between 0.1 and 0.4 MJ/m^2. The applied force and the energy flux correspond to the rectangular pulse shape. The time shape of the pulse were simulated as

$$Q(t) \propto \left(1+\left(\frac{\tau}{t}\right)^2\right)\left(\frac{\tau}{t}\right)^2 \exp\left(-\left(\frac{\tau}{t}\right)^2\right) \qquad (1)$$

recoiling the "real ELM" shape.

The results show that significant evaporation starts at heat loads ≥ 0.2 MJ/m^2 (Fig. 1). For the reference heat load the vaporization is negligible, and the melt motion only causes the melt layer damage. In calculations the effects of tangential plasma pressure and the **J**x**B** force on liquid Li motion were investigated as well as the dependence of the surface damage on the pulse shape.

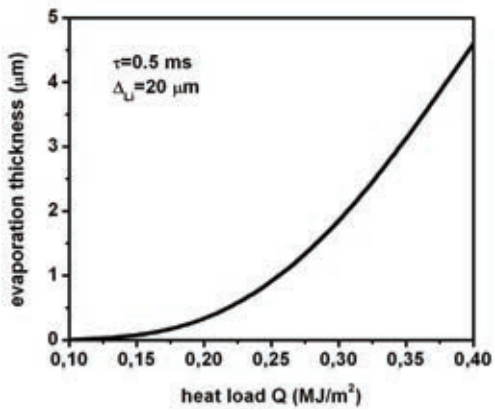

Fig. 1: Depth of evaporation vs. heat loads. Thickness of Li layer Δ=20μm, No motion. Pulse shape given by Eq. (1).

The effect of different ELMs pulse shape on the formation of crater is shown in Fig. 2 and Fig. 3, where craters are caused by the tangential pressure for different thickness of Li layer and after 3 ms from pulse trail. The rectangular pulse shape demonstrates somewhat higher surface damage in comparison with the "real ELM" pulse shape. In scenarios with Δ_{Li} = 5 μm, the removed melted materials from the crater bottom is recovered by the capillary forces from the W porous matrix and the thickness of liquid Li at the crater bottom remains about 0.4 μm (see Fig. 3).

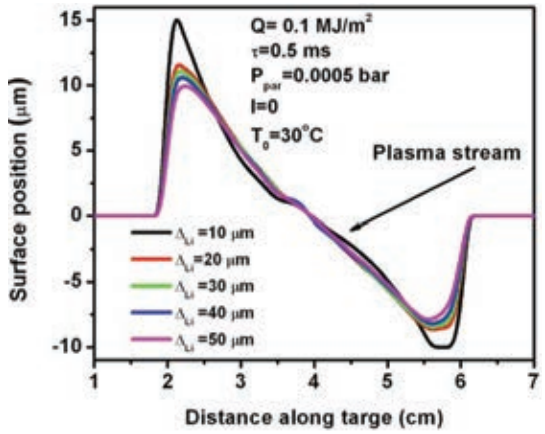

Fig. 2: Crater shape caused by the tangential pressure for different thickness of Li layer after 3 ms from pulse trail. Rectangular pulse shape.

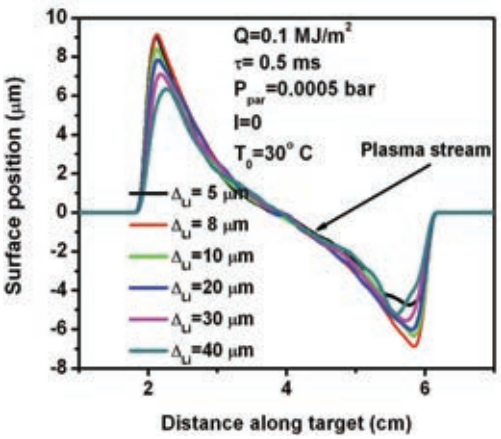

Fig. 3: Crater shape caused by the tangential pressure for different thickness of Li layer after 3 ms from pulse trail. Pulse shape given by Eq. (1). Capillary porous system is taken into account.

Conclusions

A model of porous substrate has been implemented into the MEMOS code and its effect on the melt motion damage was analysed. The effect of porous substrate on the melt motion damage was investigated for low heat loads accounting for the Li vapour shielding influence on melt layer thickness. It is concluded that for transients like weak ELMs the compensation of Li losses by the substrate source will not be so effective against evaporation or molten layer removal. The remaining liquid Li layer is estimated to be below 0.4 μm, which could easily evaporate under high heat loads.

Staff:

B.N. Bazylev

Acknowledgement

This work, supported by the European Communities under the EFDA contract of Association between EURATOM and Karlsruhe Institute of Technology (KIT), was carried out within the framework of the European Fusion Development Agreement. The views and opinions expressed herein do not necessarily reflect those of the European Commission.

Optimization of Disruption Mitigation Techniques – Analysis and Modelling (WP11-PWI-06-02-02 and WP11-PWI-06-02-03)

Numerical Modelling of Heat Deposition by Runaway Electrons and MGI Validation Simulations against JET

Introduction

A significant issue of ITER operation is the occurrence of disruptions, which can limit the lifetime of plasma facing components (PFCs). During the thermal quench of disruption relativistic runaway electrons (RE) can appear. In big tokamaks probably RE by avalanches will be generated. Disruption mitigation by massive gas injection (MGI) can also result in generation of RE. Runaway electrons can damage the first wall. Therefore, theoretical analyses and numerical simulations for RE stopping power in plasma and consequences of RE impact on the PFCs has been carried out in 2011, for ITER and DEMO conditions. To estimate the RE damage dedicated numerical simulations have been performed with the energy deposition Monte-Carlo code ENDEP for CFC, Be and W targets, for theoretically predicted RE beam parameters. The energy distribution of RE was assumed to be exponential as $\exp(-E/E_0)$ or Gaussian function $\exp(-(E/E_0)^2)$ with RE energy E. The characteristic energy E_0 depends on the device.

Another activity has concerned modelling of massive gas injection (MGI) of noble gas argon with the integrated tokamak code TOKES. In the simulations, the injected gas gets ionized in the core and then the contamination results in fast loss of plasma energy by radiation emission. TOKES MGI model is successfully compared with two argon experiments on tokamak JET.

Comparison of CFC and tungsten mono-block blanket concept for fusion reactor

Estimations of the RE impact on the ITER mono-block FW blanket made of CFC or W with imbedded Cu pipes with water cooling result in the following conclusions [1]. Heat generation in W occurs at the subsurface layer ~10μm, and in CFC ~1000 μm. W surface does not melt and CFC does not experience a brittle destruction.

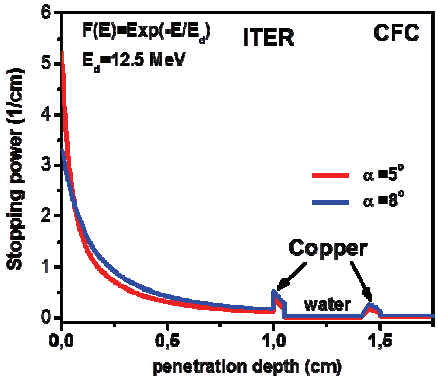

Fig.1: Heat release in CFC and in Cu pipe as a function of radial distance from FW surface for RE energy of 30MJ/m^2 over 0.1s.

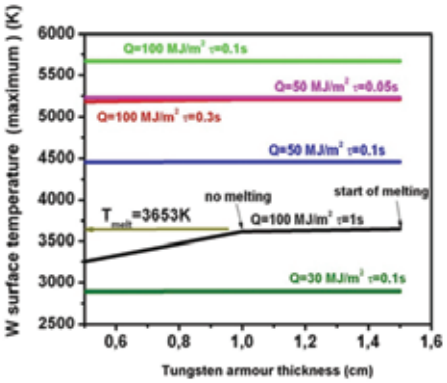

Fig. 2: Maximum W surface temperature as a function of distance from the surface to the Cu pipe.

Calculations show that in the case of W 20% of RE energy is converted into X-ray radiation, but due to strong absorption inside bulk W only 0.5% of X-ray energy is released in the Cu pipe. For the CFC case, a small but significant heat generation can occur in the Cu water pipe (see Fig. 1). The maximum W surface temperature as a function of distance from the surface to the Cu pipe is shown in Fig. 2: for mono-energetic RE beams and incident angle ~1º. For a RE energy deposition of 30MJ/m2, which is the value expected in ITER, and 0.1s

exposure time, the W armor surface does not melt. However, for the DEMO case RE electrons will evaporate and melt the W surface.

The evolution of the CFC and W surface temperature during and after RE impact has shown in the Fig. 3. It is seen, that the melting point for W is reached at ~0.4ms for RE pulse duration of 10ms and energy of 30 MJ/m^2. The evolution of temperature at the Cu pipe for the CFC and W case in ITER for runaways of a power 30MW/m^2 lasting 0.1 and 0.01sec is shown in Fig. 4.

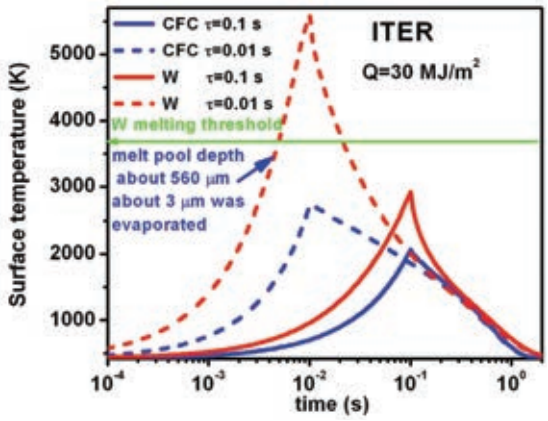

Fig. 3: The evolution of the surface temperature for CFC and W during and after RE exposure times at 0.1-0.01s and RE energy of 30MJ/m^2.

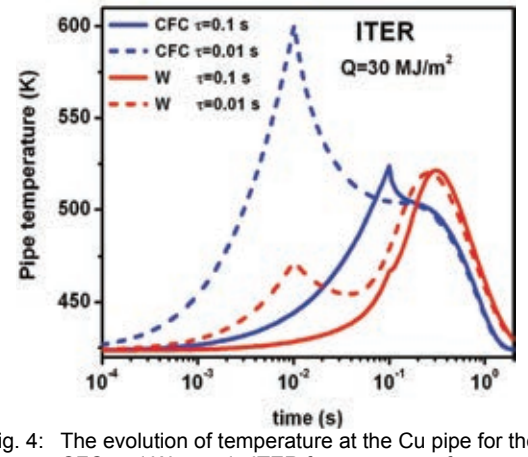

Fig. 4: The evolution of temperature at the Cu pipe for the CFC and W case in ITER for runaways of a power 30MW/m^2 lasting 0.1 and 0.01sec (dashed lines).

For DEMO (PPCS model C) the RE energy deposition and erosion of W/EUROFER blanket module for the first wall is estimated. The simulations were performed for the RE deposition energy in the range of 30 – 100 MJ/m^2 over 0.05 - 0.3 s. Mono-energetic RE beams (50 and 80 MeV) and RE beams with a Gaussian energy distribution centred at the energy $E_0 \approx$ 18,5 MeV is assumed. The energy deposition time of RE is in a range of 0.05 – 1 s. It is shown that the minimum W thickness needed to prevent failure of the W/ EUROFER bond (assumed to be the EUROFER creep point) is so large that armour surface melts.

Estimations of the runaway elastic scattering cross-section in multi-component fusion plasma with massive gas injection [2] have shown, that the increase of effective charge number with RE energy reduces the growth rate of the primary and secondary (avalanche) electron production. This effect can explain the absence of RE in some experiments with MGI.

Calculations have been done for energy deposition and erosion of W/EUROFER blanket module for DEMO first wall due to the runaway electrons and vertical displacements events (VDE) [3]: For RE with energy density ≥ 50MJ/m^2 and deposition times ≤ 0.1s the armor thickness required to prevent EUROFER from creep or thermal stresses is ≥1.4cm. However, in this case, the heat transfer to the coolant is insufficient and the W surface melts. VDE causes surface energy deposition into the W armour, which results in a vaporization, which cannot reduce the heat transfer. Therefore, both RE and VDE transients will pose a major lifetime problem in DEMO design.

Calculations of the required thickness of W armor for preventing W melting and evaporation, and EUROFER creeping under steady-state DEMO conditions keeping tolerable impurity concentration have been presented in [4]: For 13.5 MW/m^2 and 4 mm W/EUROFER sandwich structure the minimum thickness of the tungsten armor of 3mm will keep the maximum EUROFER temperature below the critical limit for EUROFER steel.

Modelling of runaway electrons impact for ITER and DEMO

For DEMO (PPCS model C) the RE energy deposition and erosion of W/EUROFER blanket module for the first wall has been estimated. The simulations were performed for the RE deposition energy in the range of 30-100 MJ/m^2 over 0.05-0.3s. Mono-energetic RE beams (50 and 80 MeV) and RE beams with a Gaussian energy distribution centred at the energy E_0 ≈ 18,5MeV have been assumed. The energy deposition time of RE has been considered in a range of 0.05-1s. The results show that the minimum W thickness needed to prevent failure of the W/ EUROFER bond (assumed to be the EUROFER creep point) is so large that the armour surface melts.

For RE with energy densities ≥ 50MJ/m^2 and deposition times ≤ 0.1s the armor thickness required to prevent EUROFER from creep or thermal stresses is ≥1.4cm. However, the heat transfer to the coolant is insufficient and W surface melts. VDE causes surface energy deposition into the W armor, which results in a vaporization, which cannot reduce the heat transfer. Therefore, both RE and VDE transients will pose a major lifetime problem in DEMO design.

Simulation of massive gas injection (MGI) with tokamak code TOKES

Tokamak experiments demonstrated effective ionizations of injected atoms G (G = Ne, Ar, He) during MGI, the following MHD activity, which causes the thermal quench (TQ) within a few ms when the ionization front reached the magnetic surface of safety factor q = 2, and a radiation flush. On the short time scale, the ionization of G-atoms localized near the jet entry can have as result a strong variation of the plasma parameters on poloidal coordinate y. For example, the electron temperature T_e decreases drastically near the jet. This can significantly decrease the ionization rate resulting in deep jet penetration.

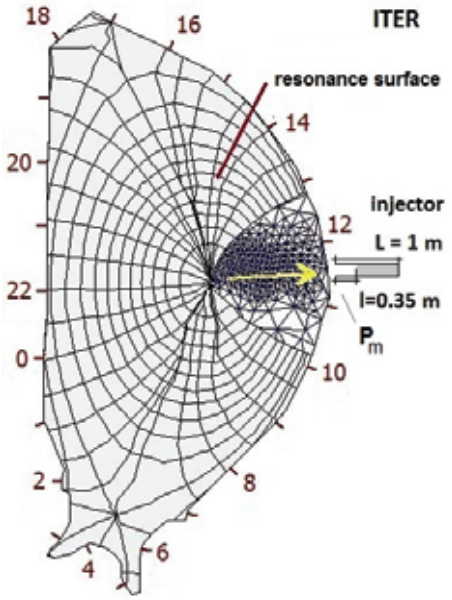

Fig. 5: TOKES triangular and magnetic flux meshes. Position of gas injector.

In 2011, the modelling with the tokamak code TOKES has been focused upon further development of the code aiming MGI simulations (Fig. 5). The plasma transport is calculated in the confined region with closed magnetic surfaces, as well as in the SOL and in the private region, where the unclosed surfaces cross the wall. Preliminary predictive simulations for ITER have been performed, with the conclusion that after the radiation flush the maximum wall temperature can exceed the beryllium melting point.

TOKES has been successfully validated against two JET experiments on argon MGI [5]. Experimental results on MGI of noble gas into the various JET discharges have been analysed and two of them has been chosen for simulation. These are JPN76314 with ohmic heating only, plasma energy content W=0.8 MJ and H-mode discharge JPN77806 with W=3.2 MJ. The injected gas is ionized and plasma of the temperature T_{Ar} = 100-50 eV expands with velocity of $V_{||} = 2.5C_s \sim 5\times10^6$ cm/s and makes one toroidal turn during ~0.5 ms, which soon provides toroidal symmetry.

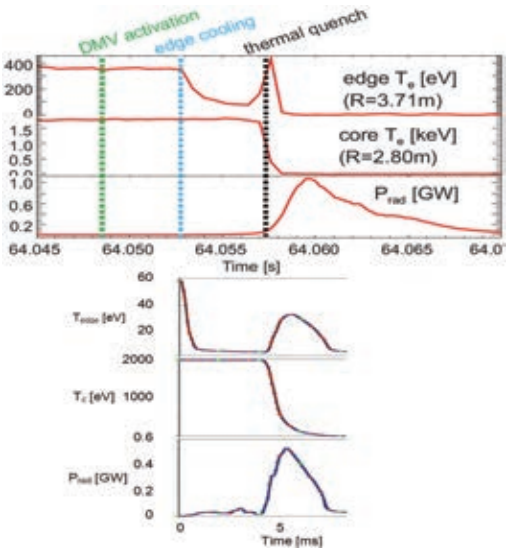

Fig. 6: Comparison of time dependences for edge and core temperature and radiation power P_{rad} measured in JET pulse JPN76314 (upper panel) with the corresponding simulation (lower panel).

Fig. 6 demonstrates the comparison of simulated and experimental centre temperature $T_{e0}(t)$. The good fitting indicates that the simulation reproduces main processes of thermal quench. TOKES radiation model was coupled with plasma thermal transport across deteriorated magnetic surfaces. The first consequence of the core instabilities appears to be the small deteriorations of toroidal symmetry and thus slight overlapping of nested magnetic surfaces, which drastically increases electron cross-transport by thermal conductivity along entangled magnetic field lines (3D thermal transport). After the start of cooling plasma periphery the instabilities can develop at many rational values of q in the core, but they remain moderate until $t > t_{q2}$. The coupling parameter which drives the thermal conductivity is the ratio of plasma energy to radiation loss energy.

Conclusions

Numerical simulations of W armour damage under the runaway electron heat loads are carried out using the codes ENDEP and MEMOS. For the energy density deposition of RE ≥ 50MJ/m^2 and deposition times ≤ 0.1s into the W armour, the minimum armour thickness required to prevent EUROFER from creep or thermal stresses is ≥1.4cm. Almost always melting occurs. Thus, the loss of creep strength at relatively low temperature represents the main drawback of EUROFER as a structural material. Therefore, RE will pose a major lifetime issue in DEMO depending on disruption frequency.

For MGI modelling for ITER, TOKES radiation model was coupled with plasma thermal transport across deteriorated magnetic surfaces. For MGI, the obtained results provide useful benchmarks, but more work is needed for further development of the code TOKES in order to reach reliable integrated modelling including plasma and surface aspects as the injector gas dynamics in the vessel. The TOKES scenario for the thermal quench of MGI at JET has been developed based on available JET experimental database. For two different JET discharges a reasonable agreement has been reached.

Staff:

B.N. Bazylev
Yu.L. Igitkhanov
I.S. Landman
S.E. Pestchanyi

Literature:

[1] Yu. Igitkhanov, B. Bazylev, On tokamak DEMO first wall concepts Paper ID15-445 Conf. ICFRM-15, Charleston Oct 2011, presented for publication

[2] Yu. Igitkhanov, On the generation of Runaway Electrons during Massive Gas Injection, 13th International Workshop on Plasma Edge Theory in Fusion Devices, PET-13, September, 2011, presented for publication

[3] Yu. Igitkhanov, B. Bazylev, Effect of Off-Normal Events on Reactor First Wall, Workshop PFMC-13 Rosenheim, May 2011, to be published (in Physica Scripta)

[4] Y. Igitkhanov, B. Bazylev, Plasma facing material lifetime in DEMO reactor, Conf ISFNT-10, Portland, Sep 2011, to be published

[5] S. Pestchanyi I. Landman, Verification of TOKES simulations against the MGI experiments in JET, Conf ISFNT-10, Portland, Sep 2011, presented for publication

[6] B. Bazylev, Yu. Igitkhanov, I. Landman, S. Pestchanyi, A. Loarte, J. Nucl. Mat. V417, 1-3 (2011) 655-658

[7] B. Bazylev G. Arnoux, W. Fundamenski, Yu. Igitkhanov, M. Lehnen, and JET EFDA Contributors. J. Nucl. Mat v. 415, 1 (2011) S841-S844.

[8] Yu Igitkhanov, B Bazylev and I Landman, Calculation of runaway electrons stopping power in ITER. J. Nucl. Mat. 415 (2011) S845-S848

[9] Yu. Igitkhanov, B. Bazylev, The PFC erosion in DEMO due to Runaway electrons, Fusion Science and Technology, Vol. 60, Num 1, July 2011, Pages 349-353 (TOFE)

[10] Yu. Igitkhanov, B. Bazylev, Electric Field and Hot Spots Formation on Divertor Plates J. Modern Phys., 2011, 2, 131-135

[11] I.S. Landman, S.E. Pestchanyi, Yu. Igitkhanov, R. Pitts Fus. Eng. Des. V86, 9-11 (2011) 1616–1619

Acknowledgement

This work, supported by the European Communities under the EFDA contract of Association between EURATOM and Karlsruhe Institute of Technology (KIT), was carried out within the framework of the European Fusion Development Agreement. The views and opinions expressed herein do not necessarily reflect those of the European Commission.

Preliminary Concept Studies of Alternative Concepts for Heat Removal in Future Fusion Reactors based on Moving or Liquid Targets, or Hybrid Systems of it (WP11-PEX-01-ACT3-01)

Introduction

The most critical issue of a fusion reactor is an excessive power loading to the plasma facing component, particularly to the divertor plates. For the electric power production P_{net} = 1 GW, operation availability A = 0.5 and the heat-electricity transformation efficiency η = 0.3 the power exhausted in the vessel follows as $P_{exh} = f_n P_{net}/(A\eta) \approx 1.3$ GW with f_n = 0.2. As a reference case we consider a DEMO with centre plasma major radius R_0 = 8m. The heat flux is estimated as $Q_{exh} = P_{exh}/2(2\pi R)w_s \approx 260 MW/m^2$, assuming the width of the power fall-off as w_s = 5 cm and neglecting the radiation losses. This heat flux exceeds the technically acceptable limit for any material. The power loading mitigation scenarios using intensive radiation by externally launched impurities has not been proved yet against its consistency with burning plasma operation and will not be considered here. Tilting the divertor plate in poloidal plane is another option. However, in order to reduce power load to acceptable level of 5 MW/m^2, the plates must be tilted to very small angle in respect to plasma stream: 5/260 = 0.019 rad $\approx$ 1 grad. This seems unrealistic; the poloidal size of inclined target becomes rather large: 2.5m. Furthermore, a critical issue of such a divertor is the compatibility with the cooling system. In general, the actively cooled tokamak divertor concept has many drawbacks. mong those drawbacks are the erosion of the divertor plates and the material redeposition, the requirement of the frequent removal of the plates, the requirement of high temperature of the PFCs > 600°C for efficient electric power generation. PFC surfaces must be thin enough to conduct the heat to the coolant and to avoid erosion, yet thick enough to protect interlayer and structural material from destruction. Divertor concepts based on movable targets and passive cooling could be an option. This work consists of a preliminary assessment of some concepts based on replacing the conventional actively cooled divertor plates by a set of passively cooled moving targets.

Designs with steadily rotating target

In Fig.1 an array of rotating discs of small thickness is considered as divertor targets, which experience the power flux of incident plasma. Thin plasma stream locally hits (strike zones) the discs and due to rotation, the absorbed heat is rather homogeneously distributed over the disc volume. Each disc is hollow, being connected to its rotation axis via conical binding, so that there are no places on the disc and the binding, which are heated permanently. In practice the binding and the disc experience a homogeneous distribution of radiation power over irradiated surface. In the designs the cooling occurs in a special chamber surrounding the hot target plates. The chambers could contain water or helium as a coolant. The fast replacement of the coolant substance in the chamber provides an effective removal of the heat and the radiation. Rest of power leaks through the gaps of the cooling system, reaches the remote surfaces of the vacuum vessel of tokamak and exhausts there. The radiation losses can be estimated by Stefan-Bolzmann formula, which in the case of tungsten for the surface temperature T_s = 3000 K gives $q_{rad} \approx 1.4$ MW/m^2. Then, for the value of the exhausted power per toroidal length $P_{exh}/2(2\pi R)$ = 13 MW/m, the required radius of disk is about $R_d \approx 3$ m, which is too large to be appropriate. In Fig. 2 some variant is introduced hinting that the discs can also be inclined and how to use momentum of the plasma stream shifting it for keeping disc rotation without an additional engine.

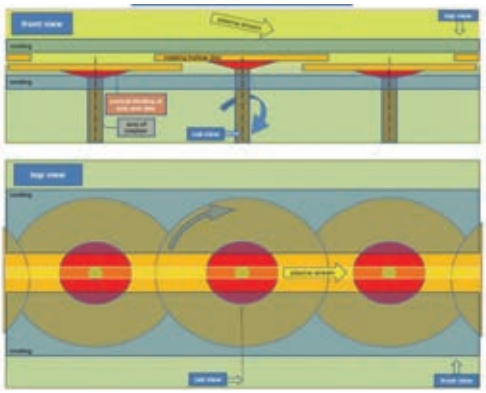

Fig. 1: Divertor pales made from W as rotating discs: front and top view.

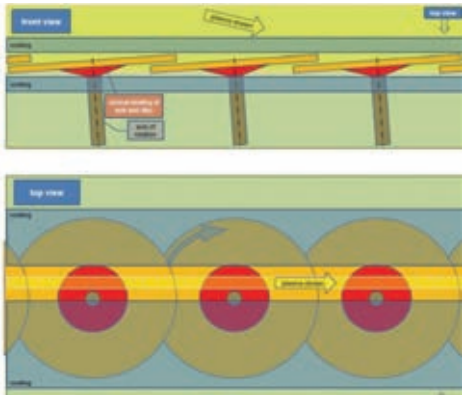

Fig. 2: Alternative design of oblique discs shifted aside of plasma stream.

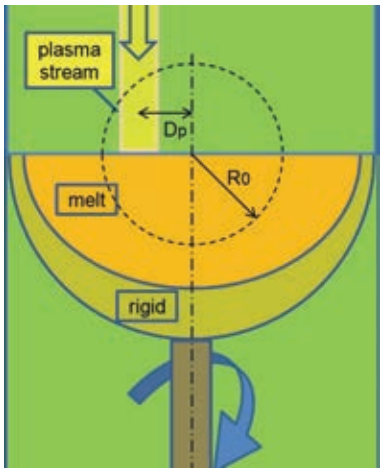

Fig. 3: Rotating spheroid with partially melted W.

The radius of plasma facing surface can be reduced in another design based on a spinning segment of spheroid, which resembles a half-egg spinning about its vertical axis (Fig. 3). Estimations show a technically acceptable size of the spherical target. However, high vapour pressure of W surface p_{sat}~0.36 bar for expected temperatures T_s ~ 5500 K will strongly contaminate plasma. Large p_{sat} is an serious obstacle for applying radiation cooling of the target. However, the target can be isolated from the confined plasma by using the cooling chamber with rather narrow slot for plasma incoming to the target. Only unimpeded W vapour flow near the plasma has chance to get into the gap. It can be shown that impurities near the target can be effectively entrained by the plasma stream and brought back to the target. Some part of W atoms can penetrate into the SOL and bulk. Detailed 3D calculations are required to assess the impurity behaviour in the main plasma. The main drawback of the model is the accidental contact of the plasma stream with the slot edge with consequent thermal erosion and strong contamination.

Concept of toroidally moving divertor segments

The alternative divertor concept considered here is based on rapidly moving toroidally divertor plates on rails (Fig. 4). These divertor plates would absorb the plasma heat flux with their thermal inertia, after which they would be removed from the vessel for processing. When outside the tokamak, these plates could be cooled, cleaned etc., and then returned to the vessel in an automated loop. This scheme could provide near optimal divertor surfaces at all times, and avoid the need to stop machine operation for repair of damaged or eroded plates.

In this model the plates are toroidally segmented and form a ring around the bottom of a tokamak, with the two divertor strike zones. The plates could be inserted and removed. These plates could be inserted vertically down into position to cover the divertor strike points, which would face these surfaces as shown at the right, and then could be removed from below. This plate exchange could be done at each toroidal segment, or the plates could be rotated in the toroidal direction within the vessel. The plates would be inserted and removed between the TF coils and carried on a conveyer belt to a plate processing area.

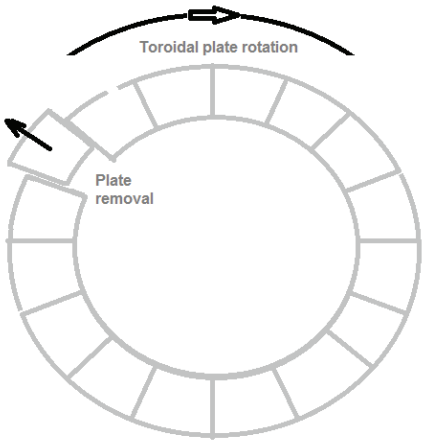

Fig. 4: The horizontal plates are replaced with a radial motion and rotated in an offset toroidally to sweep the heat flux over the plate radius.

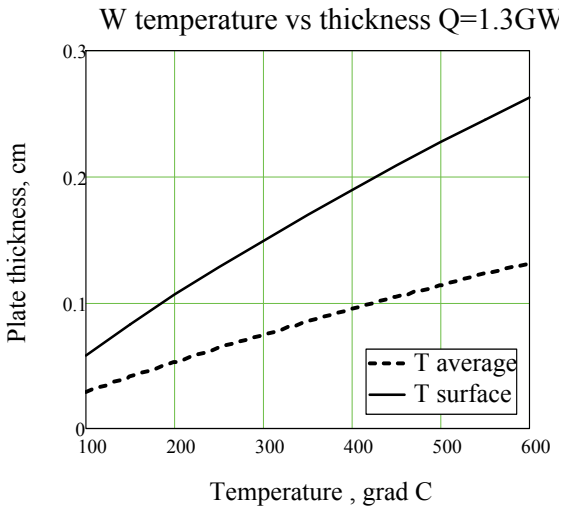

Fig. 5: The tungsten plate thickness as a function of the surface and average bulk temperature for P_{exh} = 1.3 GW.

The required plate speed can be determined by the thermal diffusion times and the width w of the heated region at the divertor strike points. If the divertor plates are not actively cooled, their thickness and thermal diffusion time within the tokamak will be determined by the maximum allowable surface temperature and the incident plasma heat flux. We assume that a thermal heat load of *Q* (Watts) is absorbed by the plates over an area determined by the toroidal circumference *2πR* (cm) and the width of the plasma-heated region of the divertor plates *w* (cm*). V=2π R w d*. The plate thickness *d* (cm) over which the heat penetrates during an exposure time τ (sec) can be estimated from the thermal diffusivity D of the plate material (cm^2/sec) as*: D = d*^{2} /3τ. We take this distance "*d*" to be the optimal thickness for the plates. The thermal diffusivity is *D* = (κ/cρ) where κ is the thermal conductivity, c the heat capacity, and ρ the plate density. The average temperature rise T_{ave} of the plates over the thickness *d* after an exposure time τ is $T_{ave} \sim Q\tau/[c2\pi Rw]$. The optimal plate thickness is linearly proportional to the assumed max average temperature and inversely proportional to the local power density on the plate (Fig. 6).

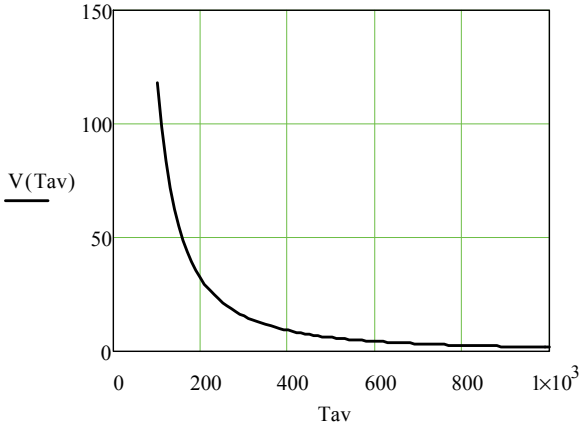

Fig. 6: The toroidal speed of plate vs the average plate temperature T_{av}.

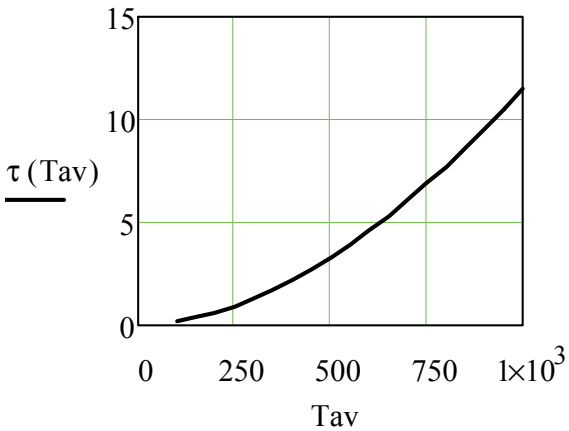

Fig. 7: The time over which plate remains exposed by Q for given temperature T_{av}.

The required plate speed can be determined by the thermal diffusion and the width of the heated region at the divertor strike points, $V_{plate} \sim w/\tau$ so that a new region of each plate is exposed whenever the plate was near its local temperature limit. Fig. 6 and Fig. 7 show the plate velocity as a function of an average temperature and the thermal diffusion time vs plate

thickness. For example, for a tungsten plate, w = 15cm, T_{ave} = 600ºC, the vertical sweep rate would be $V_r \sim w/\tau \sim$4.4 cm/sec, so if the plate length is~300 cm the residence time of the plate in the divertor region would be ~ 68 sec. Plasma thickness is taken as 15 cm and diffusion time 4.6 sec.

There are many potential difficulties with such a moving divertor plate concept, which would need to be addressed in a detailed engineering design and eventual testing. It is not yet clear whether a moving plate system would be more or less feasible than other similar idea for a divertor, e.g. moving belts, pebble divertor or liquid walls.

Staff:

Yu.L. Igitkhanov
I.S. Landman

Acknowledgement

This work, supported by the European Communities under the EFDA contract of Association between EURATOM and Karlsruhe Institute of Technology (KIT), was carried out within the framework of the European Fusion Development Agreement. The views and opinions expressed herein do not necessarily reflect those of the European Commission.

Review of Problems for Steady-state DEMO Variants (WP11-DAS-PLS-P02-01)

Introduction

The difference between a steady state DEMO design and a pulsed one is expected to be so significant, that they will in fact be two different machines. Projecting the existing long-pulse experiments in tokamak (TORE SUPRA) and stellarator (LHD) to DEMO one can conclude that on the plasma physics side, efficient external current drive will need high temperature and low density, which might be in conflict with high density operation and exhaust at high P/R. This would need a compromise. Also, the need for alignment of pressure and current profiles may need sophisticated control, maybe in conflict with the limited diagnostics capabilities allowed on DEMO. On the technology side, pulsed operation will introduce additional mechanical and thermal cyclic loads which will impact on the structural materials. The need for efficient external current drive calls for a high electrical efficiency of the H&CD systems [1].

Here we are reviewing some problems related to the DEMO steady-state operation, namely:

1) the plasma impact on the FW during a long range steady-state operation and
2) the plasma–wall interaction associated with sputtering erosion during a long pulse exposition of heat and particle flux into the FW material and consequent bulk plasma contamination [2].

The plasma impact on the FW during a long range steady-state operation

Here we consider steady state DEMO operation under normal conditions, when the sandwich type blanket first wall module is considered (see Fig.1). Heating of a W-clad EUROFER PFC by radiation and neutral flux as well as by transients like ELM is discussed. We have analysed the cases, when heat fluxes into coolant (water) remains under critical heat flux (CHF) value. We assume the heat transfer into rectangular tube of 10mm x 18mm cross-section with a water temperature of 150°C. The rest parameters and limitations are similar to ITER blanket cooling system [3].

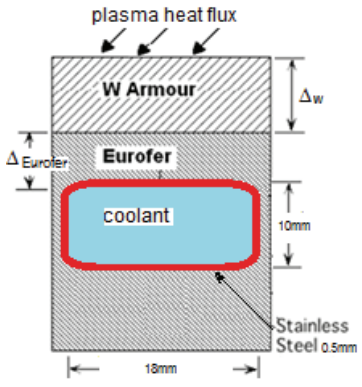

Fig. 1: Sandwich type blanket first wall module used for the Monte Carlo MEMOS computation of the plasma impact.

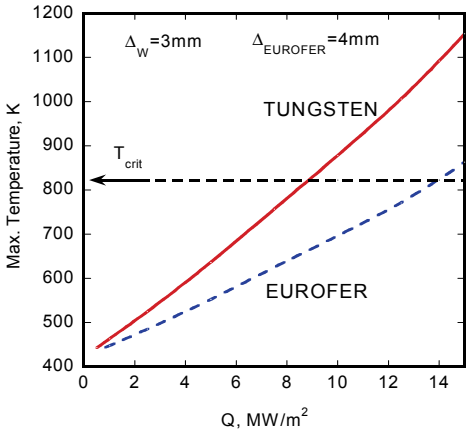

Fig. 2: W surface temperature and maximum EUROFER temperature vs net incoming heat flux Q under steady-state operation.

During normal operation the erosion of the FW and baffle surface could mainly occur due to collisions with hot neutral atoms. Undergoing charge–exchange collisions with the hot ions at the separatrix or in pedestal region, energetic neutrals will deliver the plasma energy to the armour surface, thus producing a strong sputtering. Fig. 2 shows the armour surface temperature and the maximum EUROFER temperature (interlayer temperature) for different incoming heat flux values Q. When Q reaches~14 MW/m^2 the interlayer temperature exceeds the critical value T_{crit}.~ 550ºC and EUROFER can experience intolerable thermal distraction [4].

Such values of Q can be expected in DEMO due to transient events like ELMs or convective radial plasma losses, associated with unstable convective cells in the SOL region during steady-state operation. Calculations show that for expected incoming fluxes the W surface temperature remains below the melting point and evaporation is negligible. Calculations have been performed for armour thickness Δw=3mm and for EUROFER thickness ΔEUROFER = 4mm. Fig. 3 shows the maximum W temperature under design heat load (13.5 MW/m^2 for the limiter, and 0.5 MW/m^2 for the FW) as a function of the W armour thickness. It is shown that under steady-state operation for heat flux value~13.5MW/m^2 the surface armour temperature increases with increasing the armour thickness, whereas the W/EUROFER interlayer temperature remains almost unchanged. For low power load of~0.5MW/m^2 a weak dependence of the armour surface temperature and the interlayer temperature on armour thickness is shown. Under expected steady-state operation heat loads and the thickness of W armour, surface temperature remains well below the vaporization and melting points and, as calculations also show, coolant heat flux remains below CHF, thus avoiding severe degradation of the heat removal capability.

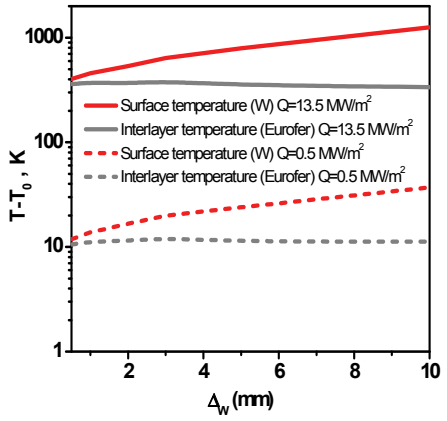

Fig. 3: Maximum armour surface temperature and maximum EUROFER temperature vs armour thickness ΔW for two cases of incoming heat fluxes Q=13.5MW/m^2 and 0.5MW/m^2; SS water cooled rectangular channel; $\Delta_{EuROFER}$= 4mm, Δ_{SS} =0.4mm, Tcoolant=150 ºC. The temperature is calculated from the initial value $T_0 = T_{coolant}$.

For incoming heat flux ≥10MW/m^2 W temperature approaches a soft limit of~900-1050K based on the degradation of the structural properties and on possible crack growth through the W, the EUROFER could eventually be affected . To keep the W surface temperature below 1keV, the armour thickness should be taken ≤ 3-4 mm. As it will be shown further, this thickness could be sacrificed during three years of continuous operation by taking into account only the sputtering erosion.

Variation of the surface armour temperature and interlayer temperature with EUROFER thickness is shown in Fig. 4, for given DW =3mm and Q=13.5MW/m^2. Under these conditions and ΔEUROFER ≤ 4.5mm, there will be no thermal degradation of the structural material properties. Fig. 5 shows heat loads and corresponding thickness of EUROFER when operation causes no thermal degradations (region below the curve). Arrow indicates the thickness value for the same case as in Fig. 4.

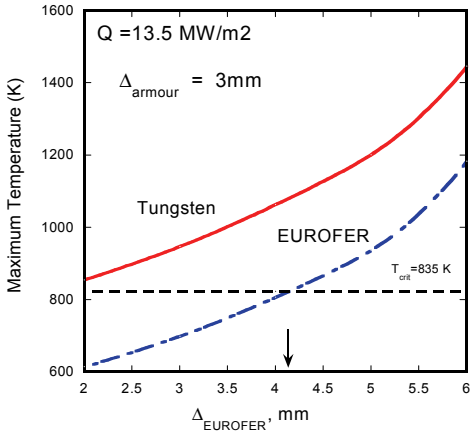

Fig. 4: Maximum temperature of W and EUROFER vs EUROFER thickness. For $\Delta_{EUROFER}$ < 4.3 mm max. EUROFER temperature remains below the critical value.

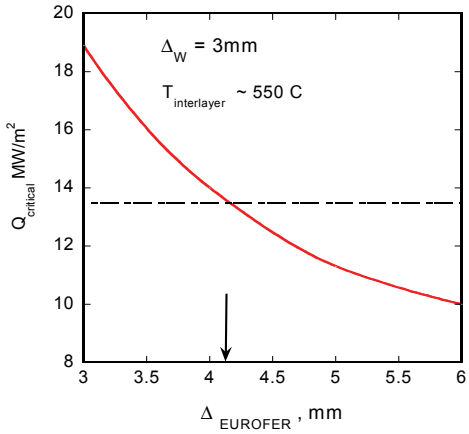

Fig. 5: Critical incident heat flux Q_{crit} vs EUROFER thickness when interlayer EUROFER temperature exceeds the critical value~550 ºC that poses a thermal stress problem; W armour thickness Δ_w=3mm.

Calculations show that the volumetric heating associated with the neutrons is not particularly demanding for the first walls blanket design, whereas the surface heating is important in term of allowable temperatures and stresses.

Sputtering erosion in a long-range operation

The important erosion process for the FW and baffles under steady-state DEMO operation is expected to be physical sputtering, since the W surface temperature remains below the melting point and ignition of arcing is insufficient for life-time limitation under normal operation [5]. The thickness, d, of plasma facing elements (e.g., the FW blanket armour, limiter, etc.) sputtered during Δt operation time by incident particle fluxes Γ_j of different species j, can be expressed as [6]

$$d(t) = \Delta t \cdot \frac{A_t \cdot m_p}{\rho_t} \cdot \sum_j \left\langle Y_j \Gamma_j \right\rangle \qquad (1)$$

where A_t is the target atomic mass (in amu), ρ_t is the target material density, Yj(E,θ) is the sputtering yield of particle j with energy E and angle of incidence θ, and Γ_j is the flux of particles j. The brackets in (1) represent an average over the angular and energy distribution of the incident particles. Thus, the precise determination of the erosion rate needs the correct form of the energy distribution function of the incident particles and the sputtering yield $Y_j(E,\theta)$. Here we present the results of erosion rate calculations taking into account deviation from the Maxwellian distribution function at the divertor plates due to the sheath acceleration and the angular dependence of the sputtering yield.

Following [6] the averaged sputtering yield, defined as the yield averaged over the distribution of energy and angle of incidence of the projectiles, is given by

$$\overline{Y_j}\left(\frac{atom}{ion}\right) = S_0 \int_0^1 \int_{\varepsilon^*}^{\infty} \exp\left(-\frac{\varepsilon}{\beta}\left(1-t^2\right)\right) \times \exp\left[-\left(\sqrt{\frac{\varepsilon}{\beta}t^2 - \delta} - M_0\right)^2\right] \cdot tS(\varepsilon,t) \cdot \varepsilon d\varepsilon \qquad (2)$$

where $S_0 = \frac{2E_{Th}^2}{T_i^2 F(M_0)}$, $t \equiv \cos\theta$, $\varepsilon = E/E_{Th}$ $\varepsilon^* = \max(1,\delta)$; $\beta = T_i/E_{Th}$, $\delta = Z_j e\varphi_0 / T_i$

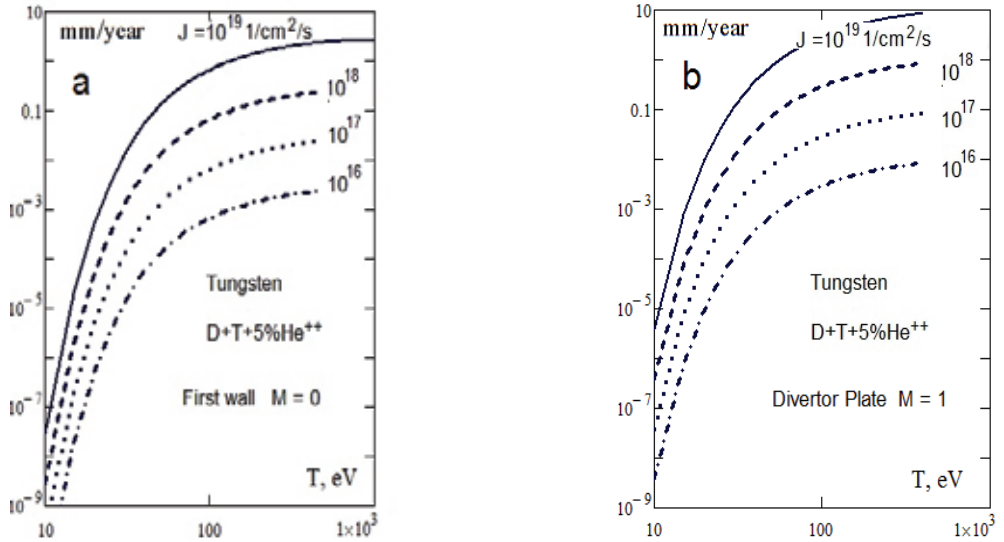

Fig. 6: The thickness of (a) W armour of First Wall and (b) divertor plate sputtered during one year of continuous operation by various particle fluxes of D/T/5%He of incident ions J($cm^{-1}sec^{-1}$).

Here M_0 is a Mach number of incoming particle flux (which must be taken to one at the divertor plate according to Bohm condition and to zero at the FW), S(ε, t) represents the sputtering yield for a certain energy and angle of incidence of the particles. This dependence can be described by the revised Bohdansky formula [7] for the energy dependence and the Yamamura formula [8] for the angular dependence. Using these formulas, the erosion rate of the W armour sputtered during one year of continuous operation by various particle fluxes of D+T+5%He++ incident ions is shown in Fig.6a for the FW and in Fig. 6b for divertor plates. The stronger erosion of the divertor plates compared with the FW erosion is due to the acceleration of incoming ions in the sheath potential and the deviation of energy distribution function from Maxwellian. It is seen that at temperatures ≤ 100eV sputtering of W material is negligible. However, for neutrals, undergoing the charge-exchange collisions in the pedestal region, strong erosion can be expected for particle fluxes several orders of magnitude exceeding the DEMO expected values: 10^{14}-10^{15}/cm^2/s. The most intensive W ions release due to charge-exchange collisions is expected from baffles. However, due to rather low level of W sputtering rates even for higher pedestal temperatures and expected particle fluxes of hydrogen isotopes and 5% of helium, the impurity concentrations will remain below the fatal values for W impurities~0.005% under steady-state operation and normal conditions. However, the sputtering with external impurity ions could pose a problem and must be simulate numerically by a transport code.

Conclusions

Our calculations show that under steady state operation and ITER like coolant conditions the interlayer temperature is weakly dependent on the W armour thickness in the wide range of incoming heat fluxes.

The maximum W armour thickness is limited by the maximum allowable temperature of EUROFER under maximum steady-state design loads. The armour surface temperature increases with the armour thickness increase and for the reference case of ~3mm remains well below the tungsten melting point.

Both temperatures of the W surface and the EUROFER interlayer are increasing with an increase of incoming heat flux. For reference conditions (Δw~3mm, $\Delta_{EUROFER}$~4mm), the maximum heat flux which does not causes intolerable thermal stresses in structural material is about ~13.5MW/m^2. Calculations show that for DEMO envisaged conditions [9] (particle fluxes and boundary temperatures) the total sputtering erosion of the W armour by the charge-exchange neutrals could reach~1mm during one year of steady-state operation.

In the case of off-normal events, the calculations show that in the ‘hot’ VDE case the energy deposition into the W armour is very shallow (~nm) and causes surface melting and evaporation. The absorption of slow VDE power requires thicker W armour to maintain the maximum heat flux and temperature in the material structure to acceptable level. It is shown that the presence of a vaporized layer and a macroscopic molten layer is unavoidable for expected exposition times and power loads. The RE deposit their energy deeper into armour and for energies ≥ 50MJ/m^2 and deposition times ≤ 0.1s, the minimum armour thickness required to prevent EUROFER from thermal distraction is ≥1.4cm.However, this size of layers doesn’t prevent the W surface from melting. At higher RE energy deposition rates (≥100MJ/m^2 in 0.1s), the required armour thickness to prevent creeping destruction is even larger so that the bulk of the armour layer will melt and evaporate.

Although W/EUROFER bound is compatible with high neutron fluencies, the loss of creep strength at relatively low temperature represents the main drawback of EUROFER as a structural material. Our estimations of erosion of the FW by charge-exchange neutrals and the divertor plates by incoming ions show the importance of angular dependence of sputtering yield and, particularly, the sheath potential effect.

Staff:

B. Bazylev
Yu. L. Igitkhanov

Literature:

[1] H. Zohm: On the minimum size of DEMO, Fusion Science and Technology 58

[2] Yu. Igitkhanov et al., PFMC-13 Rosenheim

[3] ITER DDD, WBS 1.6, Blanket System, G 16 DDD 2 98-06-2 W 0.5, June 1998;

[4] R. Lindau, A. Möslang, Fusion Engineering and Design 75-79, (2005) 989

[5] Yu. Igitkhanov, B. Bazylev, Journal of Modern Physics, 2011, 2, 131-135; R. Raffray, G. Federici, Journal of Nuclear Materials 244 (1997) 85-100

[6] V. Abramov, Yu. Igitkhanov, V. Pistunovich and V. Pozharov, J. Nucl. Mater. 162-164 (1989) 462.

[7] W. Eckstein, C. Garcia-Rosales, J. Roth and W. Ottenberger, Max-Planck-Institut für Plasmaphysik Report, IPP 9/82 (1993).

[8] Y. Yamamura, Y. Itikawa and N. Itoh, Nagoya University Report, 1PPJ-AM-26 (1983)

[9] D Word and W Han., DEMO. Results of Systems Studies for DEMO, TW6-TRP-002, DEMO/UKAEA/ PROCESS, 5 July 2007

Acknowledgement

This work, supported by the European Communities under the EFDA contract of Association between EURATOM and Karlsruhe Institute of Technology (KIT), was carried out within the framework of the European Fusion Development Agreement. The views and opinions expressed herein do not necessarily reflect those of the European Commission.

Simulation of ITER First Wall Energy Loading during Mitigated Disruptions and Runaway Electrons (F4E-GRT-315 (PMS-PE))

Introduction

Disruptions in ITER are the most serious threat to plasma-facing component (PFC) integrity. Stored energies during burning plasma operation will be much higher than anything which can be achieved in today's devices and ITER will face the prospect of very serious plasma induced damage to first wall and divertor armour.

The objective of this task is to provide estimates of expected energy loading and consequences for armour material. In particular, the calculations should address two specific issues: the energy loading and any resulting material damage on the FW due to photonic radiation loads at the thermal quench (TQ) resulting from disruptions mitigated by massive gas injection (MGI); and damage resulting from runaway electron (RE) impact during the current quench (CQ).

Current state of work

The first activities have been started in October. So far the implementation of ITER vessel surface shape into the integrated tokamak code TOKES was done. The triangular grid needed for description of injected neutrals of noble gases is generated (Fig. 1). Two-dimensional data on magnetic flux configuration is decoded and it seems it can be used in TOKES. The location of gas injector and injector parameters such as sort of gas are also delivered and going to be implemented.

Concerning the first wall damage calculations using the ENDEP and MEMOS codes, some additional data (the geometry of the first wall panel(s) (2D), the incident angle of RE impact, the slow/fast RE loss specifications) should be provided by IO in order to perform the first calculations.

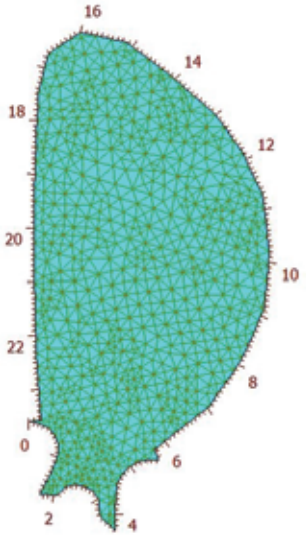

Fig. 1: ITER shape and triangular grid.

Staff:

B. Bazylev
I. Landman
S. Pestchanyi

Acknowledgement

This work was supported by Fusion for Energy under the grant contract No. F4E-GRT-315 (PMS-PE). The views and opinions expressed herein reflect only the author's views. Fusion for Energy is not liable for any use that may be made of the information contained therein.

Physics: Heating and Current Drive – ECRH

Microwave Heating for Wendelstein 7-X (CoA)

Introduction

In the recent years electron cyclotron resonance systems have been established as a standard method for localised heating (ECRH) and current drive (ECCD) in fusion relevant plasmas. Thus, ECRH will be the basic day-one heating system for the stellarator W7-X, which is currently under construction at IPP Greifswald. In the first stage W7-X will be equipped with a 10 MW ECRH system operating at 140 GHz in continuous wave (CW). The complete ECRH system will be provided by KIT, which in 1998 established, together with EU partners, the 'Projekt Mikrowellenheizung für W7-X' (PMW). The responsibility covers the design, development, construction, installation and integrated tests of all components required for stationary plasma heating on site at IPP Greifswald. PMW also coordinates the contributions from Institut für Plasmaforschung (IPF) of the University of Stuttgart (IPF), which is responsible for the microwave transmission system and part of the HV-system, and from the team at IPP Greifswald, which is responsible for the in-vessel components and for the in-house auxiliary systems. PMW benefits also from the collaboration with Centre de Recherche de Physique des Plasmas (CRPP) Lausanne, Commissariat à l´Energie Atomique (CEA) in Cadarache and Thales Electron Devices (TED) in Vélizy.

A contract between CRPP Lausanne, FZK Karlsruhe and TED, Vélizy, had been settled to develop and build the continuously operating series gyrotrons. The first step of this collaboration was the development of a prototype gyrotron for W7-X with an output power of 1 MW for CW operation at 140 GHz. This step has been finished successfully.

Seven series gyrotrons have been ordered at the industrial company TED. First operation and long pulse conditioning of these gyrotrons are being performed at the teststand at KIT, where pulses up to 180 s at full power are possible (factory acceptance test, FAT), 30 minutes shots at full power are possible at IPP (site acceptance test, SAT). Including the preprototype tube, the prototype tube and the 140 GHz CPI-tube, ten gyrotrons will be available for W7-X. To operate these gyrotrons, in addition to the Oxford Instruments and Accel magnets, eight superconducting magnetic systems have been manufactured at Cryomagnetics Inc., Oak Ridge, USA.

The completion of the project made further progress in 2010. Most of the components of the transmission system, HV-systems and in-vessel-components have been ordered, manufactured, delivered and are ready for operation at IPP Greifswald. A part of the existing ECRH system has been already used to test new concepts and components for ECRH. Some delay arose in the project during the last 1-2 years due to unexpected difficulties in the production of the series gyrotrons.

Series Gyrotrons

The first TED series gyrotron SN1 has been tested successfully at FZK and IPP in 2005 (920 kW/1800 s). It fulfilled all the specifications; during the acceptance test no specific limitations were observed. In order to keep the warranty this gyrotron has been sealed, one prototype gyrotron is routinely used for experiments.

The next series gyrotrons showed a more or less different behavior with respect to parasitic oscillations excited in the beam tunnel region. These oscillations resulted in an excessive heating of the beam tunnel components, in particular of the absorbing ceramic rings. The gyrotrons re-opened after operation showed significant damages due to overheating at the ceramic rings and the brazing of the rings. A possible solution was proposed and successfully tested by KIT. As the main difference to the usual beam tunnel this design features corrugations in the copper rings which handicap the excitation of parasitic modes. The first W7-X gyrotron equipped with an improved beam tunnel was delivered and tested at KIT in 2010.

During the tests at KIT no parasitic oscillations originating from the beam tunnel region were observed. In early 2011 this tube was delivered to IPP for final Site Acceptance Tests (SAT). This gyrotron produced 1.02 MW directed RF power at the output window (0.95 MW in the absorber load) with an efficiency of 42%. The pulse length was limited to 353 s due to arcing in the absorber load.

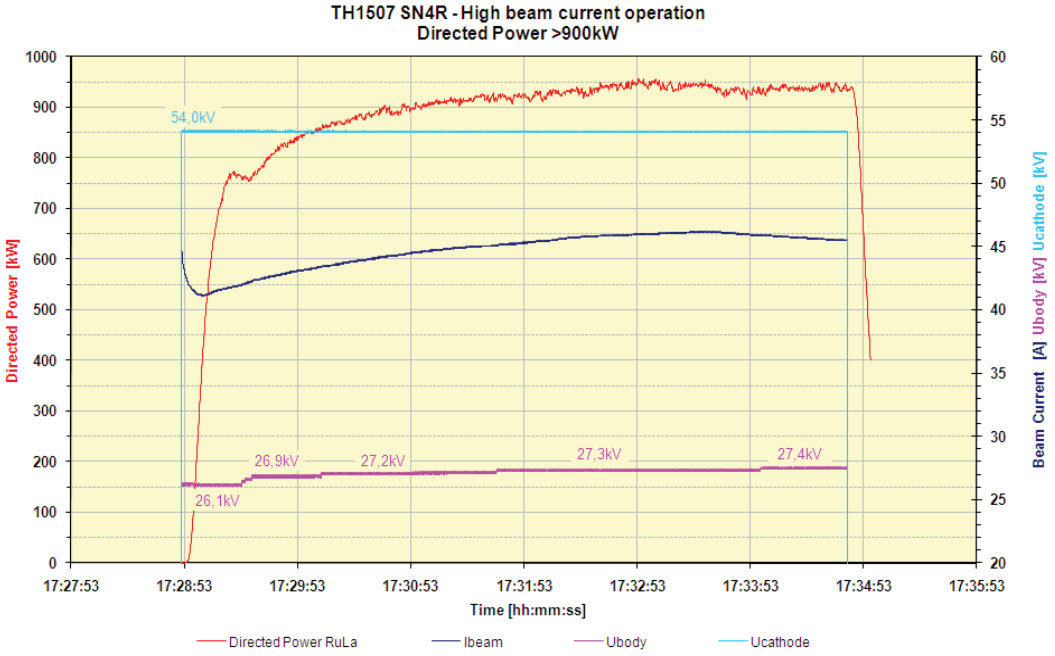

Fig. 1: Output power, beam current and operating voltages of series gyrotron SN4R, measured at IPP Greifswald in the absorber load.

At IPP an advanced beam sweeping system at the collector was used. This system is a combination of the usual vertical field sweeping (VFSS) and a transversal field sweeping (TFSS), which results in a strong decrease of the peak temperature at the collector and a more homogeneous distribution of the thermal loading (see Fig. 2).

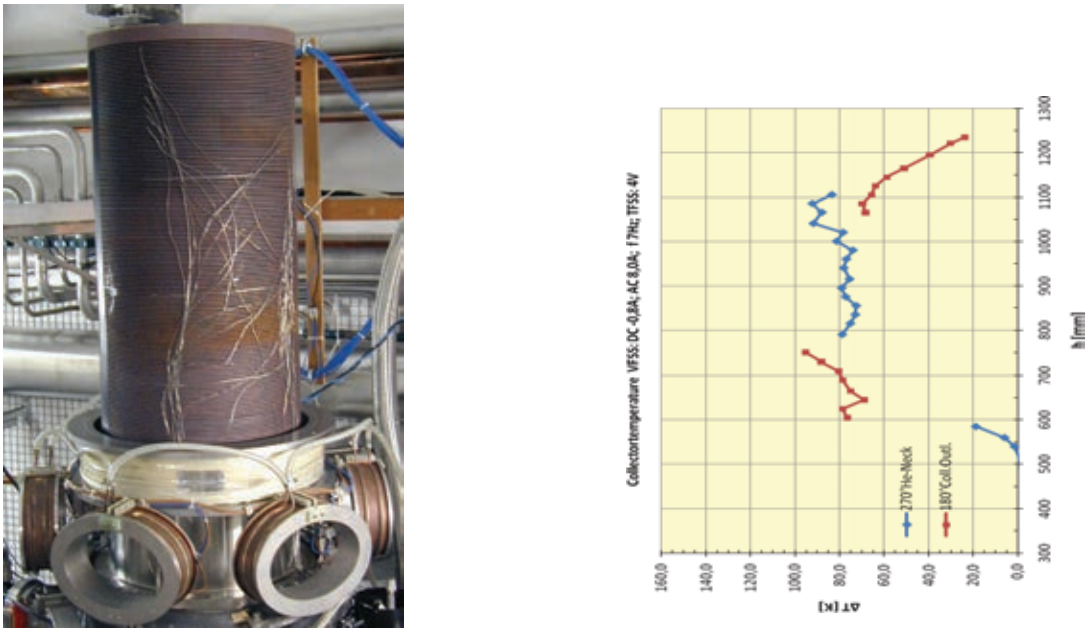

Fig. 2: Gyrotron collector and transversal field sweeping system (left), temperature distribution of the loaded collector along the axis of SN4R (right).

Due to this sweeping system it was possible to operate SN4R at a higher beam current with increased output power.

The next series gyrotron SN6 has been taken into operation at KIT in short pulse. First tests show an output power of 1.024 MW at 50 A. The Gaussian beam content of the RF output beam has been measured with an IR system, the analysis of the profiles gave a TEM_{00} content of 97%. Further conditioning and long pulse tests are being performed.

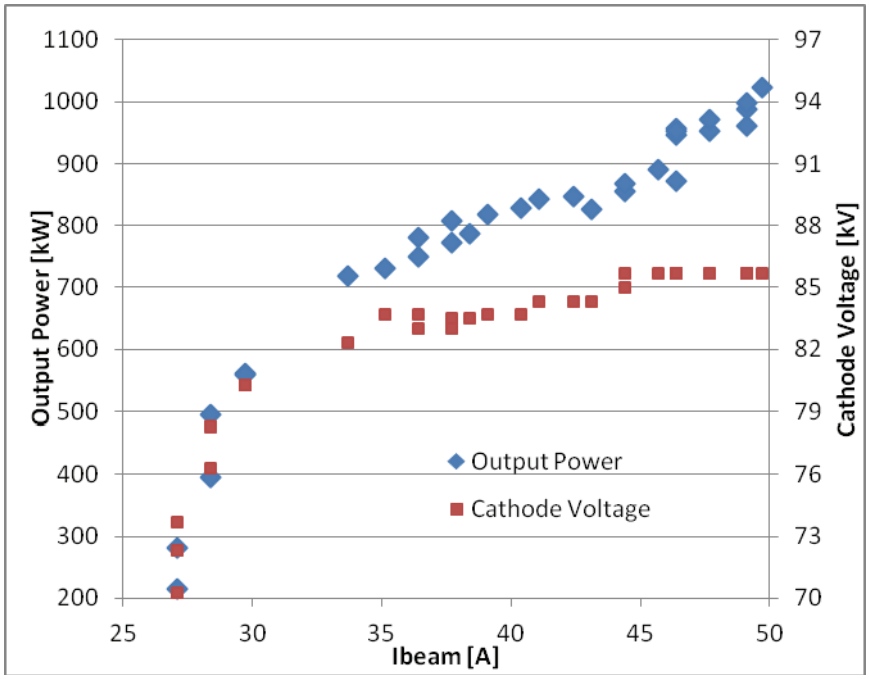

Fig. 3: Output power and cathode voltage versus beam current for series gyrotron SN6, measured during first short pulse tests at KIT.

Transmission Line

The transmission line consists of single-beam waveguide (SBWG) and multi-beam waveguide (MBWG) elements. For each gyrotron, a beam conditioning assembly of five single-beam mirrors is used. Two of these mirrors match the gyrotron output to a Gaussian beam with the correct beam parameters, two others are used to set the appropriate polarization needed for optimum absorption of the radiation in the plasma. A fifth mirror directs the beam to a plane mirror array, the beam combining optics, which is situated at the input plane of a multi-beam wave guide. This MBWG is designed to transmit up to seven beams (five 140 GHz beams, one 70 GHz beam, and one channel connected to the N-port launchers via a switch) from the gyrotron area (entrance plane) to the stellarator hall (exit plane). To transmit the power of all gyrotrons, two symmetrically arranged MBWGs are used. At the output planes of the MBWGs, two mirror arrays (beam distribution optic, BDO) separate the beams again and distribute them via two other mirrors and CVD-diamond vacuum barrier windows to individually movable antennas (launchers) in the torus.

The manufacturing and installation of the components of the basic transmission system have been completed. Cooling tube manifolds to supply the mirrors and stray radiation absorbers mounted in the towers in front of the stellarator are being prepared for installation early next year.

In 2011, gyrotron SN4R was installed in Greifswald, and beam characterization and the subsequent design and manufacturing of the surfaces of the two matching mirrors for this tube

has been performed. SN6 is presently under test at KIT Karlsruhe, where the beam parameters are being measured.

Further remaining work includes diagnostics and power measurement of the gyrotron beams. The receivers attributed to the directional couplers on the mirrors M14 and related alignment control are in fabrication. The water-cooled version of the "long load" was put into operation and tested successfully. This load (Fig. 4) consists of a 23 m long stainless steel tube with a water jacket, which is tapered down towards the end. The inner diameter is reduced from 56 mm at the beam input down to 38 mm at the load end in three steps in order to match the power absorption of the waveguide to the power loss along the guide. A non-linear horn (diameter 80 – 56 mm) at the input avoids spill-over of the Gaussian input beam at the waveguide entrance. The calculated absorption of the waveguide is 80 %. The remaining power is dumped in a standard calorimetric load, which is designed for 1 MW power in repetitive short-pulse operation. This load can be operated in CW mode at lower power. The present tests have demonstrated a CW capability of at least 140 kW. High-power test of the long load in combination with the calorimeter and the Maquette gyrotron showed that the absorption of the stainless-steel waveguide is somewhat dependent on the power level as well as on the input polarization within a range of 74 to 82 %. This is explained by the increase of damping with increasing wall temperature in the waveguide, as well as by finite precision in the alignment of the whole system. The power level used for the test was up to 820 kW, short-pulse, and 650 kW at 60 s, limited by the output power of the Maquette tube. Further tests are planned in the frame of acceptance of the next series gyrotron.

Fig. 4: Input section of the long load, showing matching horn, and the absorbing waveguide with cooling connection.

In the past years, the ECRH system at IPP -Greifswald was used as a test bed for novel components, e.g. for test of high-power diplexers. These devices are developed for use as a combiner for the power of two gyrotrons as well as a fast directional switch (FADIS) between two outputs, and therefore are of potential interest for ITER.

Based on the experience gained from the tests, very compact diplexers have been designed and built. The diplexer MC IIIb is compatible with the corrugated waveguides system used at ASDEX Upgrade, and is intended to be used there for in-line ECE experiments. For this purpose, a new resonator mirror drive was built by TNO in Delft, and the diagnostics for the drive control was upgraded and simplified. Commissioning at ASDEX Upgrade is planned for next year. An evacuated version (MQ IV) compatible with the ITER system is being designed at present (see Fig. 5). Provided that funding for the manufacturing is available, high-power tests on the ITER test system at JAEA, Naka are foreseen.

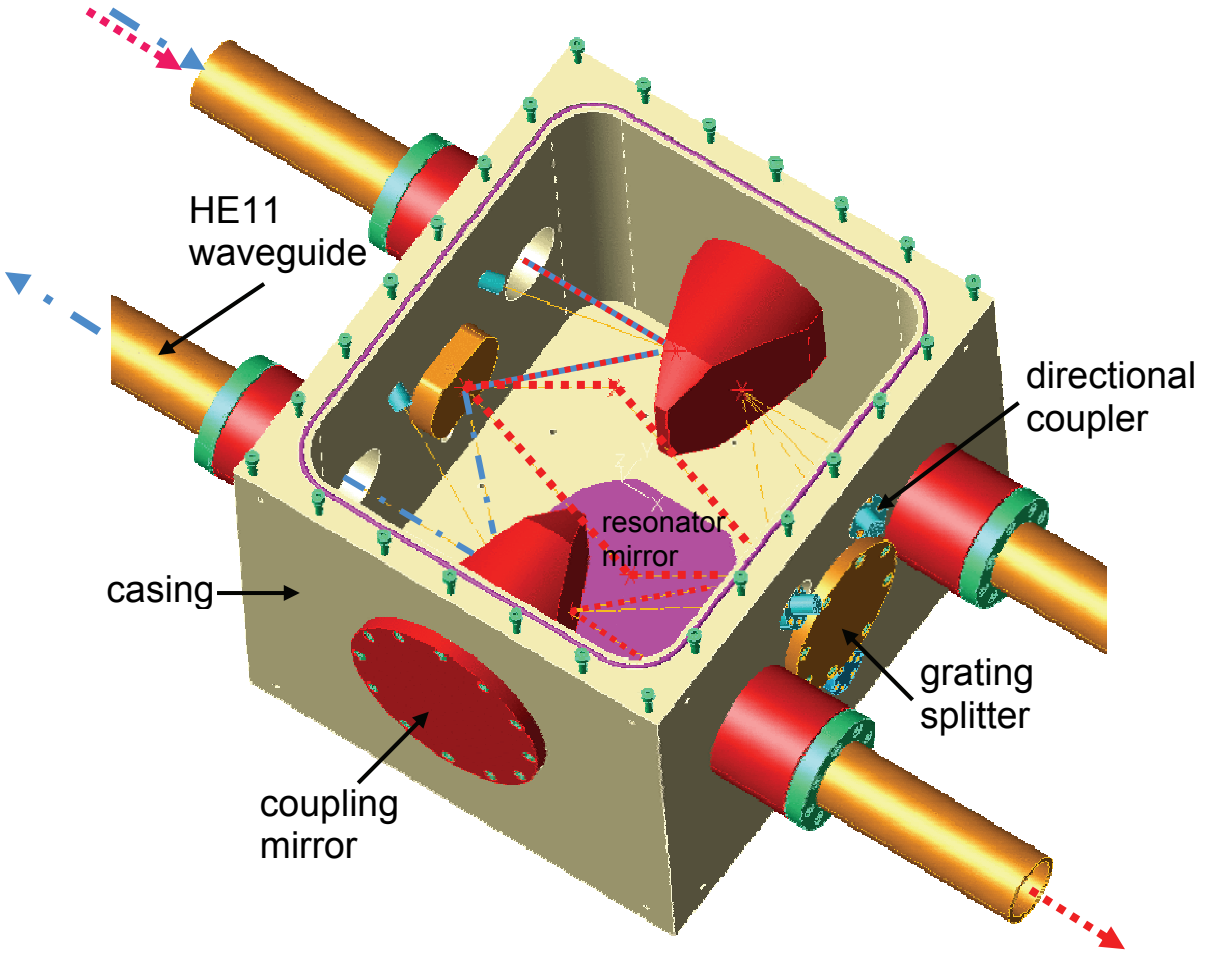

Fig. 5: Design of the diplexer MQ IV compatible with the ECRH system on ITER (waveguide diameter 63.5 mm, distance of adjacent guides 300 mm). The top plate with the mirror drive and the absorber tubes is removed to reveal the resonator geometry and the beam path shown in red dotted (resonant channel) and blue dash-dotted lines (non-resonant channel).

In-vessel components

The four refurbished ECRH-plug-in launchers have successfully passed the official vacuum leak test for W7-X in-vessel components. They also demonstrated the robustness and reliability of their motor drive mechanism in mechanical cycling tests of the front steering mirrors in the MISTRAL-chamber in vacuum.

For two of the N-ports of W7-X, "remote-steering" (RS) launchers are foreseen. This is due to the fact that front steering launchers as used in the A and E ports will not fit into these narrow ports. The remote-steering properties are based on multi-mode interference in a square waveguide leading to imaging effects: For a proper length of the waveguide, a microwave beam at the input of the waveguide (with a defined direction set by a mirror system outside of the plasma vacuum) will exit the waveguide (near the plasma) in the same direction. For W7-X, the vacuum window, a vacuum valve as well as a mitre bend must be incorporated into the 4.6 m long waveguide, as shown in the conceptual design Fig. 6.

In 2011, the N-port engineering design activity was frozen. The project is waiting for the final approval of a BMBF application on support for developing and constructing two remote-steering launchers. This application (collaboration of IPP with IPF and two industrial partners) was filed in 2011, with the expectation to start early 2012.

Basic research on the optimization of remote-steering antennas was continued at IPF Stuttgart.

In the frame of a diploma thesis, investigations on the influence of a mitre bend and gap in the waveguide were performed on a slightly scaled antenna mock-up made from square corrugated waveguide. The results show that both elements can be included in the launcher without remarkably reducing the performance in the reachable steering range of $-12° < \varphi < 12°$.

In parallel, the IPF-FD3D full-wave code has been adapted to the problem of finding the waveguide dispersion relation for arbitrarily deformed waveguide cross sections. A waveguide cross-section with outward bulges resulting in an increased angular steering range has been identified. The PROFUSION code was extended to calculate the remote-steering qualities of the deformed waveguide.

A first mock-up for investigations of deformed waveguide cross-sections was built, and measurements are underway.

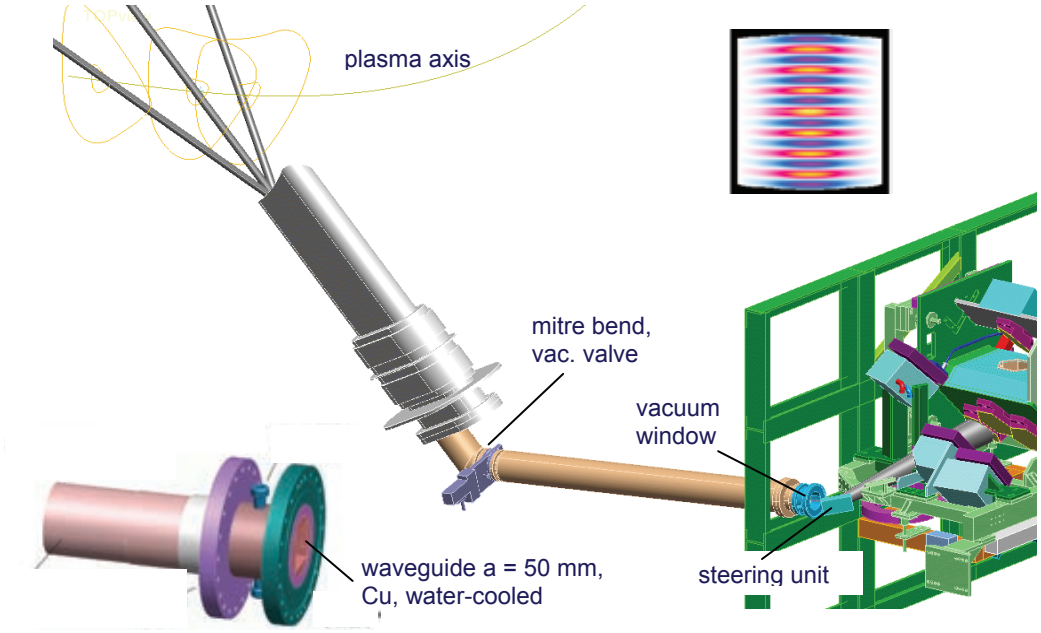

Fig. 6: Conceptual design of the remote steering launcher, which is designed for the narrow N-ports of W7-X. The insert left, bottom shows the design of the corrugated (nearly) square waveguide with vacuum flange and cooling connection. The insert top, right shows the transverse field structure of an m= 15 mode in the slightly bulged waveguide cross-section.

The final design of electron cyclotron absorption (ECA) diagnostics, which measures the transmitted ECRH power, the beam position and polarization, was completed. A prototype waveguide bundle was successfully test-assembled in the W7-X vacuum chamber. A minor rerouting of the waveguides in the plasma vessel had become necessary, due to collisions with other in-vessel components. The design is officially approved as collision free now and the production drawings were completed. The counter part of the plasma vessel waveguide bundles are the four B-port inserts with vacuum interfaces for the waveguides. Vacuum leak tests of the first B-port insert showed, that some of the mica vacuum interface windows were damaged by a superelevated compacting pressure. Therefore, the waveguide vacuum interfaces have been slightly modified. They were reassembled into the B-port plug-in and are presently leak-tested.

The microwave material test chamber, which measures the material properties at 140 GHz with low-power stray radiation, was upgraded within a Bachelor thesis in co-operation with the Humboldt University Berlin. A detailed investigation of the radiation field inside the sphere

helped to improve the measurement accuracy significantly. This small chamber is also used to calibrate the stray radiation detectors for the MISTRAL chamber and for W7-X.

The stray radiation in W7-X will also be monitored by so called “sniffer” probes, which are highly over-moded spherical resonators. It is planned to install at least one probe in every W7-X module. The probes have been characterized in collaboration with the Eindhoven University of Technology (TU/e). The detailed design for their integration into W7-X plasma vessel is ongoing.

Staff:

IHM / KIT
K. Baumann
K. Boschert
G. Dammertz
G. Gantenbein
H. Hunger
S. Illy
J. Jelonnek
S. Kern
R. Lang
W. Leonhardt
M. Losert
D. Mellein
S. Miksch
A. Papenfuß
B. Piosczyk
A. Samartsev
M. Schmid
W. Spiess
D. Strauss
J. Szczesny
M. Thumm
J. Weggen

IPF (University of Stuttgart)
H. Höhnle
W. Kasparek
H. Kumric
C. Lechte
R. Munk
F. Müller
B. Plaum
P. Salzmann
K.H. Schlüter
U. Stroth
A. Zeitler

M. Bohner
H. Dadgostar,
X. Glad
J. C. Ruiz

IPP (Greifswald/Garching)
B. Berndt
H. Braune
V. Erckmann (PMW)
F. Hollmann
L. Jonitz
H. Laqua
G. Michel
F. Noke
F. Purps
T. Schulz
P. Uhren
M. Weißgerber

Humboldt Universität Berlin
R. Brose
G. Fußmann

Eindhoven University of Technolgy
J.W. Oosterbeek
S. Paquay

Literature:

[1] Borie, E.; Gantenbein, G.; Illy, S.; Kern, S.; Leonhardt, W.; Smartsev, A.; Schlaich, A.; Schmid, M.; Thumm, M., Development of 140 GHz, 1 MW, CW gyrotrons for fusion applications. Status and recent results,. 10th School of Fusion Physics and Technology, Volos, GR, May 9-13, 2011

[2] Braune, H.; Erckmann, V.; Laqua, H.P.; Michel, G.; Noke, F.; Purps, F.; Schulz, T.; Wagner, D. ; W7-X ECRH Teams at IPP, IPF and KIT, Gyrotron high power long pulse operation. Challenges and solutions., 23rd Joint Russian-German Meeting on ECRH and Gyrotrons, Karlsruhe/Stuttgart/Garching, May 23-28, 2011, Viewgraphs on CD-ROM

[3] Erckmann, V.; Kasparek, W.; Petelin, M.I.; Bruschi, A.; Bin, W.; Braune, H.; van den Braber, R.; Doelman, N.; Gantenbein, G.; Laqua, H.P.; Lechte, C.; Lubiako, L.; Marushchenko, N.B.; Michel, G.; Plaum, B.; Thumm, M.; W7-X ECRH-Teams at IPP Greifswald, IPF Stuttgart, and KIT, ECRH with advanced CW systems,. 8th Internat.Workshop 'Strong Microwaves and Terahertz Waves : Sources and Applications', Nizhny Novgorod, Russia, July 9-16, 2011, Proc. S.15-16, Nizhny Novgorod : Russian Academy of Sciences, 2011

[4] Erckmann, V.; Kasparek, W.; Plaum, B.; Lechte, C.; Petelin, M.I.; Bruschi, A.; D'Arcangelo, O.; Bin, W.; Braune, H.; van den Braber, R.; Doelman, N.; Gantenbein, G.; Laqua, H.P.; Lubiako, L.; Marushchenko, N.B.; Michel, G.; Thumm, M. ; W7-X ECRH-Teams at IPP Greifswald, IPF Stuttgart, and KIT, Large scale CW ECRH systems: meeting a challenge,. Joint Meeting of the 19th Topical Conf.on Radio Frequency Power in Plasmas and the US Japan RF Physics Workshop, Newport, R.I., June 1-3, 2011

[5] Erckmann, V. ; PMW- and W7-X Teams at KIT and IPP W7-X and ECRH. Status and prospects. 23rd Joint Russian-German Meeting on ECRH and Gyrotrons, Karlsruhe/Stuttgart/Garching, May 23-28, 2011, Viewgraphs on CD-ROM

[6] Floristán, M. ; Müller, P. ; Gebhardt, A. ; Killinger, A. ; Gadow, R. ; Cardella, A. ; Li, C. ; Stadler, R.; Zangl, G.; Hirsch, M. ; Laqua, H. P.; Kasparek, W., Development and testing of 140GHz absorber coatings for the water baffle of W7-X cryopumps. Fusion Eng. Des. 86 (2011) 1847-1850

[7] Gantenbein, G.; Erckmann, V.; Illy, S.; Kern, S.; Kasparek, W.; Lechte, C.; Leonhardt, W.; Lievin, C.; Samartsev, A.; Schlaich, A.; Schmid, M.; Thumm, M., 140 GHz, 1 MW CW gyrotron development for fusion applications. Progress and recent results. Journal of Infrared, Millimeter, and Terahertz Waves, 32(2011) S.320-328, DOI:10.1007/s10762-010-9749-2

[8] Gantenbein, G.; Braune, H.; Dammertz, G.; Erckmann, V.; Illy, S.; Kern, S.; Kasparek, W.; Lechte, C.; Leonhardt, W.; Lievin, C.; Michel, G.; Noke, F.; Purps, F.; Samartsev, A.; Schlaich, A.; Schmid, M.; Thumm, M., New results of the 140 GHz / 1 MW series gyrotrons for W-7X., 23rd Joint Russian-German Meeting on ECRH and Gyrotrons, Karlsruhe/Stuttgart/Garching, May 23-28, 2011, Viewgraphs on CD-ROM, US-EU-JPN RF Heating Technology Workshop, Austin, Tex., October 10-12, 2011

[9] Gantenbein, G.; Dammertz, G.; Kern, S.; Latsas, G.; Piosczyk, B.; Rzesnicki, T.; Samartsev, A.; Schlaich, A.; Thumm, M.; Tigelis, I., Progress in stable operation of high power gyrotrons,. Prater, R. [Hrsg.] Electron Cyclotron Emission and Electron Cyclotron Resonance Heating (EC-16) : Proc.of the 16th Joint Workshop, Sanya, China, April 12-15, 2010, Singapore [a.o.] : World Scientific, 2011 S.347-352, Incl.CD-ROM, ISBN 978-981-4340-26-7

[10] Gantenbein, G.; Braune, H.; Dammertz, G.; Erckmann, V.; Illy, S.; Kern, I.S.; Kasparek, W.; Lechte, C.; Leonhardt, W.; Lievin, C.; Michel, G.; Noke, F.; Purps, F.; Samartsev, A.; Schlaich, A.; Schmid, M.; Thumm, M., Status of 1 MW, 140 GHz series gyrotrons for W7-X, 36th Internat.Conf.on Infrared, Millimeter and Terahertz Waves (IRMMW-THz 2011), Houston, Tex., October 2-7, 2011

[11] Illy, S.; Gantenbein, G.; Schmid, M.; Weggen, J., Design, construction and first tests of a stainless steel load for high power mm-wave radiation, 23rd Joint Russian-German Meeting on ECRH and Gyrotrons, Karlsruhe/Stuttgart/Garching, May 23-28, 2011, Viewgraphs on CD-ROM

[12] Kasparek, W.; Erckmann, V.; Hollmann, F.; Michel, G.; Noke, F.; Purps, F.; Plaum, B.; Brand, P.; Lechte, C.; Filipovic, E.; Saliba, M.; Doelmann, N.; van den Braber, R.; Bongers, W.; Krijger, B.; Petelin, M.; Shchegolkov, D.; Koposova, E.; Lubyako, L.; Bruschi, A.; Bin, W.; D'Arcangelo, O.; Stober, J.; Wagner, D. ; Groups at IPF Stuttgart, IAP N.Novgorod, IPP Garching and Greifswald, IFP Milano, KIT Karlsruhe, TNO Delft and FOM Rijnhuizen, Status of development of compact diplexers for ECRH applications,. 23rd Joint Russian-German Meeting on ECRH and Gyrotrons, Karlsruhe/Stuttgart/Garching, May 23-28, 2011, Viewgraphs on CD-ROM

[13] W. Kasparek, W. ; van den Braber, R. ; Doelman, N. ; Fritz, E. ; Erckmann, V. ; Hollmann, F. ; Michel, G. ; Noke, F. ; Purps, F. ; Bongers, W. ; Krijger, B. ; Petelin, M. ; Lubyako, L. ; Bruschi, A. ; et al. High-Power Performance of a Resonant Diplexer for advanced ECRH. Fusion Sci. Technol. 59 (2011) 729 - 741

[14] Schlaich, A.; Choudhury, A.R.; Gantenbein, G.; Illy, S.; Kern, S.; Lievin, C.; Samartsev, A.; Thumm, M. Examination of parasitic after-cavity oscillations in the W7-X series gyrotron SN4R. US-EU-JPN RF Heating Technology Workshop, Austin, Tex., October 10-12, 2011

[15] Schlaich, A.; Illy, S.; Kern, S.; Samartsev, A.; Thumm, M., Recent examinations of the W7-X-SN4R gyrotron RF output spectrum, 23rd Joint Russian-German Meeting on ECRH and Gyrotrons, Karlsruhe/Stuttgart/Garching, May 23-28, 2011, Viewgraphs on CD-ROM

[16] Thumm, M.; Gantenbein, G.; Illy, S.; Kern, S.; Leonhardt, W.; Samartsev, A.; Schlaich, A.; Schmidt, M.; Erckmann, V.; Kasparek, W.; Lechte, C.; Lievin, C., 140 GHz, 1 MW, CW gyrotron development for the ECRH system of the stellarator Wendelstein 7-X., 2011 IEEE Internat.Vacuum Electronics Conf. (IVEC 2011) : Proc.of a meeting held in Bangalore, IND, February 21-24, 2011, Piscataway, N.J. : IEEE, 2011 S.105-106, ISBN 978-1-4244-8662-5

[17] Thumm, M.; Braune, H.; Dammertz, G.; Gantenbein, G.; Erckmann, V.; Illy, S.; Kern, S.; Kasparek, W.; Lechte, C.; Leonhardt, W.; Lievin, C.; Michel, G.; Noke, F.; Purps, F.; Samartsev, A.; Schlaich, A.; Schmid, M.; Schulz, T., Recent progress on the 1 MW, 140 GHz, CW series gyrotrons for W7-X., 8th Internat.Workshop 'Strong Microwaves and Terahertz Waves : Sources and Applications', Nizhny Novgorod, Russia, July 9-16, 2011, Proc. S.45-46, Nizhny Novgorod : Russian Academy of Sciences, 2011

[18] Vaccaro, A.; Aiello, G.; Meier, A.; Scherer, T.; Schreck, S.; Spaeh, P.; Strauss, D.; Gantenbein, G., Silicon oil DC200(R)5CST as an alternative coolant for CVD diamond windows,. Prater, R. [Hrsg.] Electron Cyclotron Emission and Electron Cyclotron Resonance Heating (EC-16), Proc.of the 16th Joint Workshop, Sanya, China, April 12-15, 2010, Singapore [a.o.] : World Scientific, 2011 S.401-409 Incl.CD-ROM, ISBN 978-981-4340-26-7

Analysis of Design Issues, Interfaces and Preparation of the Procurement Arrangement for the ITER Gyrotron (F4E-2009-GRT-034-01)

Design and Development of the European Gyrotron (F4E-2009-GRT-049-01)

Introduction

The development of a 2 MW, CW, 170 GHz coaxial cavity gyrotron for ITER is pursued within the European Gyrotron Consortium (EGYC, consisting of CRPP, Switzerland; KIT, Germany; HELLAS, Greece; CNR; Italy), which acts as one scientific partner for F4E, and in cooperation with ISSP, Latvia. The goal of this development is the supply of sources for 170 GHz ECH & CD at ITER providing 8 MW CW power, to cover the EU contingent on ECH & CD sources in ITER. In contrast to other contributors to ECH & CD on ITER, the EU plans to provide sources with 2 MW RF power per unit (ITER minimum specification: 1 MW) in order to reduce cost and space requirements, to be able to double the system power if requested and to establish the - essentially more powerful - coaxial technology.

While the industrial gyrotron prototype, built by Thales Electron Devices (TED, France), is tested at CRPP, KIT provides support to the development through component design, scientific investigations and collaboration, as well as low and high power tests. The latter are done with KIT's modular pre-prototype gyrotron (see figure 1). In particular, KIT is solely responsible for the design of cavity, uptaper and mode converter system, and, with the position change or Dr. Ioannis Pagonakis from CRPP to KIT, also for the electron gun and other aspects of the electron optical system up to the collector. KIT also supports the experimental phases at CRPP in the frame of mobility missions.

In parallel to the coaxial 2 MW gyrotron activities, a 1 MW conventional cavity design was prepared in 2010 as a fallback solution. Since the coaxial ITER gyrotron project is strongly delayed due to an unexpected repair cycle of the prototype, the strategic decision about keeping the 2 MW design or switching to a conventional 1 MW design is under strong discussion and will be taken early in 2012.

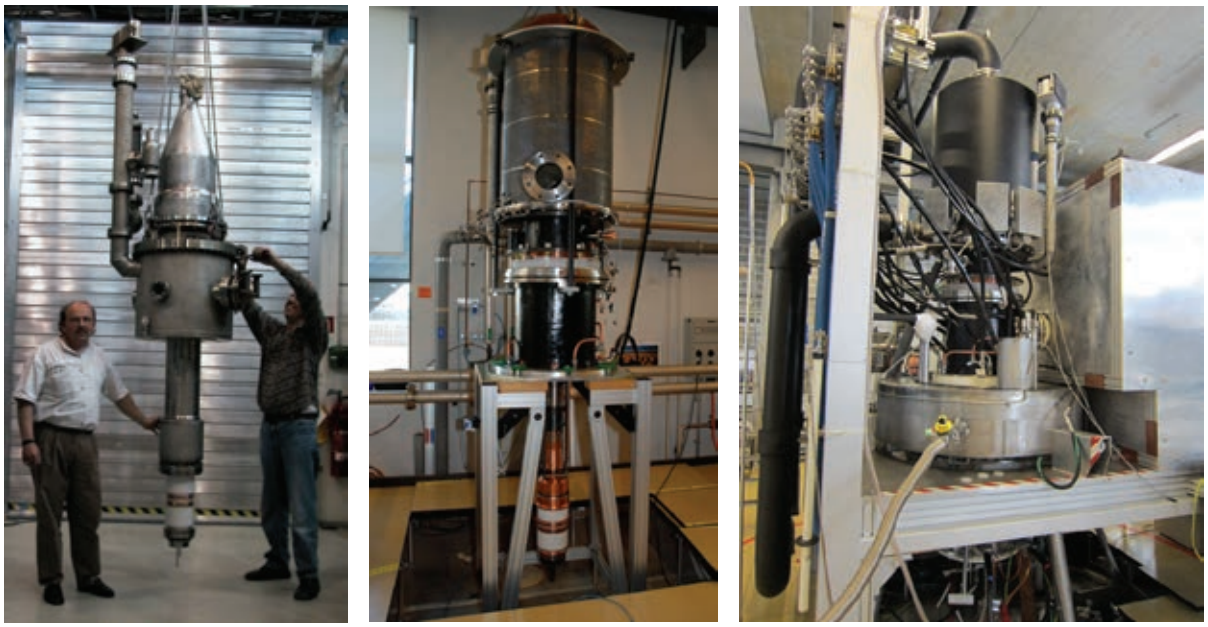

Fig. 1: Coaxial 2.2 MW 170 GHz short pulse pre-prototype gyrotron at KIT (left); the refurbished industrial long pulse prototype at delivery end September 2011 (mid); and the same prototype, installed at the CRPP test stand inside the ASG magnet (right).

Status of work at the beginning of 2011

The refurbishment of the industrial prototype for the ITER gyrotron was started in 2009 and aimed at delivery to CRPP Lausanne in summer 2010. Due to various delays, the delivery date had to be shifted first to end March 2011 – finally, the delivery took place end September 2011. The first problem was a leaky brazing at the ceramic collector insulator during the final bake-out of the tube.

To fill this gap of experiments, the KIT pre-prototype was equipped with the old 165 GHz-gun, after the 170 GHz-gun also failed due to a crack in a gun insulator. In former short-pulse experiments with the new KIT dimpled-wall launcher, an internal stray radiation of 7% was measured. The next hot experiments with a different launcher-antenna designed by IAP Nizhny Novgorod were set up to determine the change of stray radiation level due to the launcher exchange.

Since it was obvious that, on the one hand, the KIT electron guns reached the end of their life time, on the other hand, an increase of pulse length was highly desirable for more scientific insight and for a better support to the long pulse experiment with the industrial prototype at CRPP, the so-called modular project was started. In 2009 the pre-prototype produced a world-record power of 2.2 MW at 170 GHz with good efficiency, which was a major step forward and now requires validation at longer pulses. The modular project should transform the short pulse pre-prototype into a modular medium-pulse and, if possible, into a pre-tested long-pulse tube.

Regarding theory and simulation, first steps for a further improvement of the quasi-optical system through phase correcting mirrors or smoothing of the launcher structure have been made, initiated within the dissertation of Dr. Matthias Beringer on a 4 MW coaxial gyrotron, which was finalized end 2010. A different dissertation on simulation code improvement was started, aiming at a better interaction description through realistic magnetic field modelling. The simulation work on GRT-034 regarding the influence of stray-magnetic fields in the ITER environment was also started, in strong collaboration with CRPP.

After the successful redesign of the beam tunnels of the coaxial gyrotron and the conventional tubes at KIT, the investigations on parasitic oscillations were extended to investigations on dynamic ACI and the possible influence of tolerances and misalignments on parasitic oscillations.

Achievements in 2011

High power tests with the industrial prototype at CRPP

After a large number of unexpected delays caused by smaller damages and process problems, the modified and refurbished first industrial prototype was finally delivered end September 2011 to CRPP. The experiments have been performed until 9th of December and have been strongly supported by all EGYC associations, including continuous presence of KIT experts at the experiment.

First of all, the experiment had to prove that the site acceptance test criteria were fulfilled, such that the tube could be accepted by the customer F4E. After this, F4E would take over the ownership from the manufacturer TED, and the actual RF experiments could be started. After a first four days of rapidly improving RF operation, with a performance close to the specification, the tube broke on 9th of December, The first observation was quite disappointing, since the gyrotron arrived with a leak that developed during transport. The leak could be sealed by a special resin, as shown in figure 2, but the tube fell back to an unbaked condition, which made long pulse operation questionable. Despite this problem, the vacuum could be regained and quickly improved; during all subsequent experiments the vacuum behaviour

was clearly better than that of an unbaked tube, which raised hopes on long pulse operation, but this was finally disabled by the terminating accident.

Fig. 2: C. Lievin (TED) fixing the vacuum leak.

The achievements of the site acceptance test and the short phase of RF experiments are in overview:

- The SAT acceptance tests were successfully completed at the end of November:
  - The gun design changes have been validated. The tube stood the high voltage without any problem without and with magnetic field - in strong contrast to the first design - and permitted the operation at nominal parameters.
  - Good alignment of the inner rod has been done (0.06mm accuracy), and the overall tube position in the magnet has also been verified.
  - The conditioning time needed to reach high power operation was surprisingly short, especially if the leak is taken into account.

- RF tests started on December 5th:
  - The tube showed excellent potentialities: Within four days, it was possible to reach nominal parameters (90 kV, 75 A) and extract 2 MW of output power with an efficiency of 45% on the right mode. Pulse lengths were limited to ca. 1 ms pulses. It should be noted that no particular optimization other than the magnetic field value was done, in particular the depression voltage was arbitrarily set to 30.5kV – at the nominal 35 kV, the efficiency would have exceeded 48%. Further optimization appeared easily possible. See figures 3 and 4.
  - No low frequency oscillations were observed. The new beam tunnel concept was again (after the pre-prototype measurement) validated at short pulse on this tube.
  - The microwave beam symmetry was measured with thermal paper and found to be very good, and in agreement with experiments and simulations made at KIT (see figure 5).
  - One strange observation is that the mode’s starting currents were unexpectedly high.

- An internal ceramic RF absorber failed on December 9th during an accidental (but not uncommon) operation under wrong mode rotation, putting an early end to the experimental phase. It is under discussion if the mode jump is indicating a reduced stability region.

The short reminder of the year was dedicated to post-evaluation of the event and the measurements, as well as on discussions of the implications. This will be continued in 2012, the possible consequences and conclusions are not established at the end of 2011.

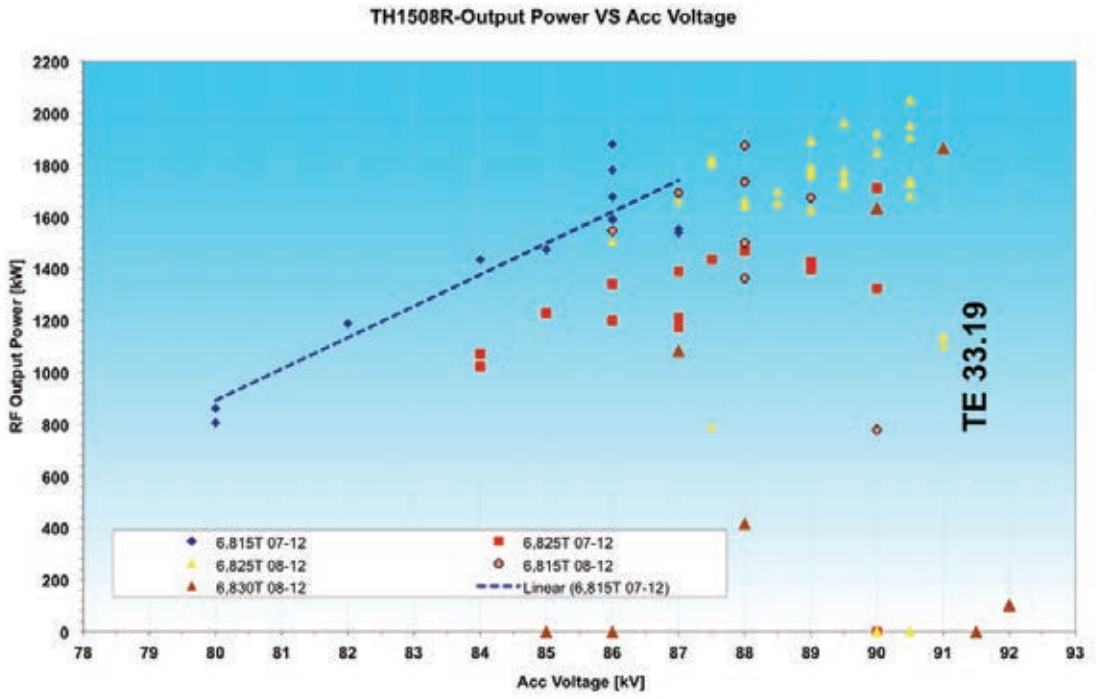

Fig. 3: Measured RF output power of the industrial prototype for different magnetic field settings.

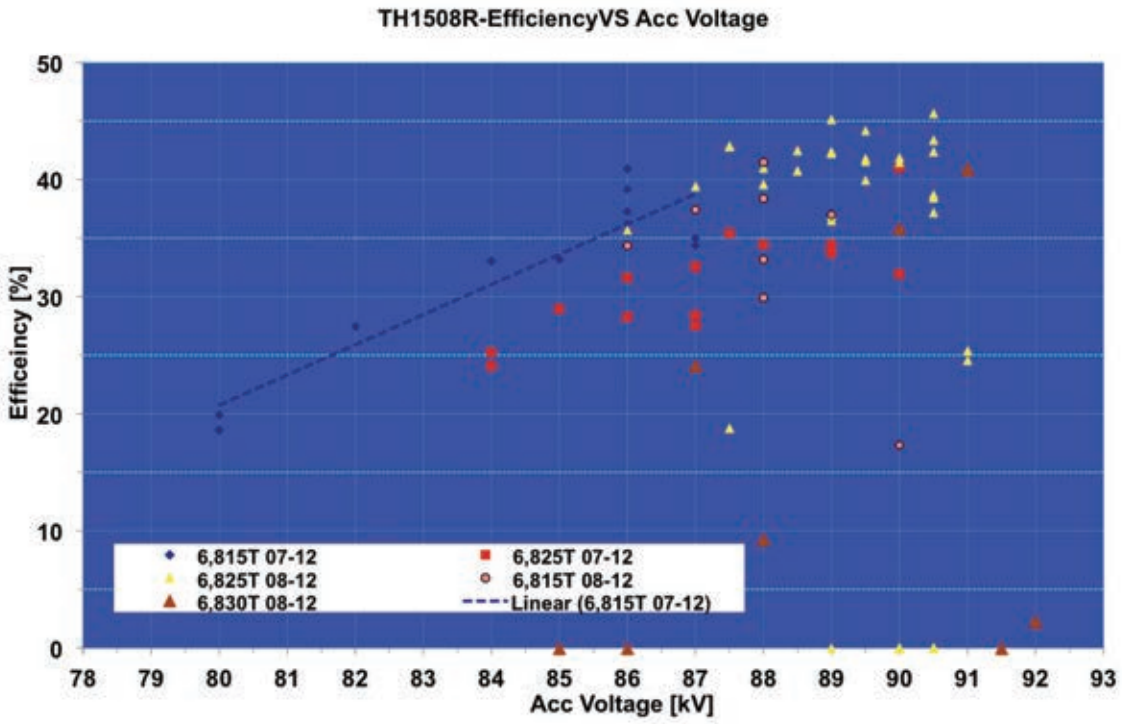

Fig. 4: Measured total efficiency of the industrial prototype for different magnetic field settings. Note that due to the short experimental time the efficiency was not optimized.

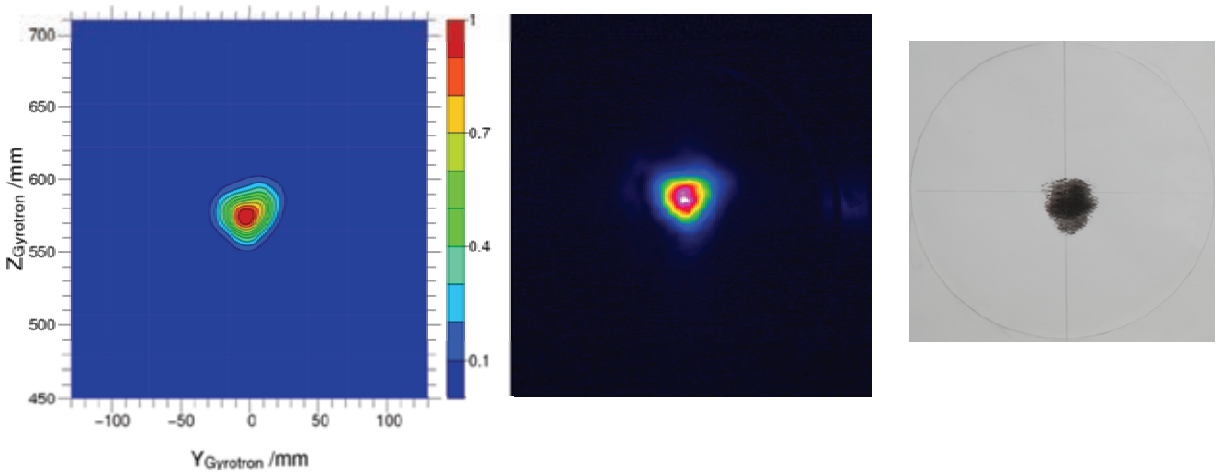

Fig. 5: The RF output beam pattern of $TE_{34,19}$ in simulation (left, linear scale), thermal camera measurement at the KIT-pre-prototype (mid) and in thermal paper measurement at the refurbished prototype (right) shows very good agreement and beam alignment at the RF window.

High power tests at KIT and redesigns of the pre-prototype

Since no high power experiments could be done in 2010, the plans for these experiments were shifted to 2011. After several problems were solved, it was possible to operate the pre-prototype again in short pulses with the 165 GHz gun. This gun is unfortunately not suitable for application of the additional normal conducting coil, which would be necessary for 2 MW operation, so only some 1 MW working points from former tests could be reproduced. The major result of these investigations was that the stray radiation could be reduced from 7% to 5.5% by employing the IAP launcher. This result motivates the further work on smoothed KIT rippled-wall launchers. During this experiment, it became obvious that the the gyrotron could not not be operated furthermore using the old gun, so the experiments were stopped after that result.

In order to regain the capability for hot experiments, the modular project was taken further. First, the aim was to use the refurbished KIT 170 GHz-gun in June to do a fast validation experiment relevant for the redesigned electron gun of the industrial prototype. This experiment appeared to be of strategic relevance, since the decision on keeping or dropping the 2 MW concept was, and is still, under investigation through the TAP expert group on gyrotrons for F4E – this group was set up to elaborate a recommendation for TAP on the 2 MW program. After both the gun delivery and the decision point were delayed until end of the year, no further high power tests were done at KIT in 2011. The next tests are scheduled in February 2012. The preparation activities for these tests were running throughout the year, starting with design, manufacturing and test of a cooled normal-conducting (NC) coil for CW operation of the KIT Oxford instruments magnet, as required for 2 MW operation. The tests done in 2009 used a pulsed uncooled NC coil. Mid of the year, after the gun delivery was delayed, the decision was taken to modify the pre-prototype already in the first step by equipping it with a small shaft that fits the cooled NC coil (see figure 6). These mechanical modifications, together with other mechanical adaptions and improvements, lasted until end of 2011 and will be finalized for the first tests.

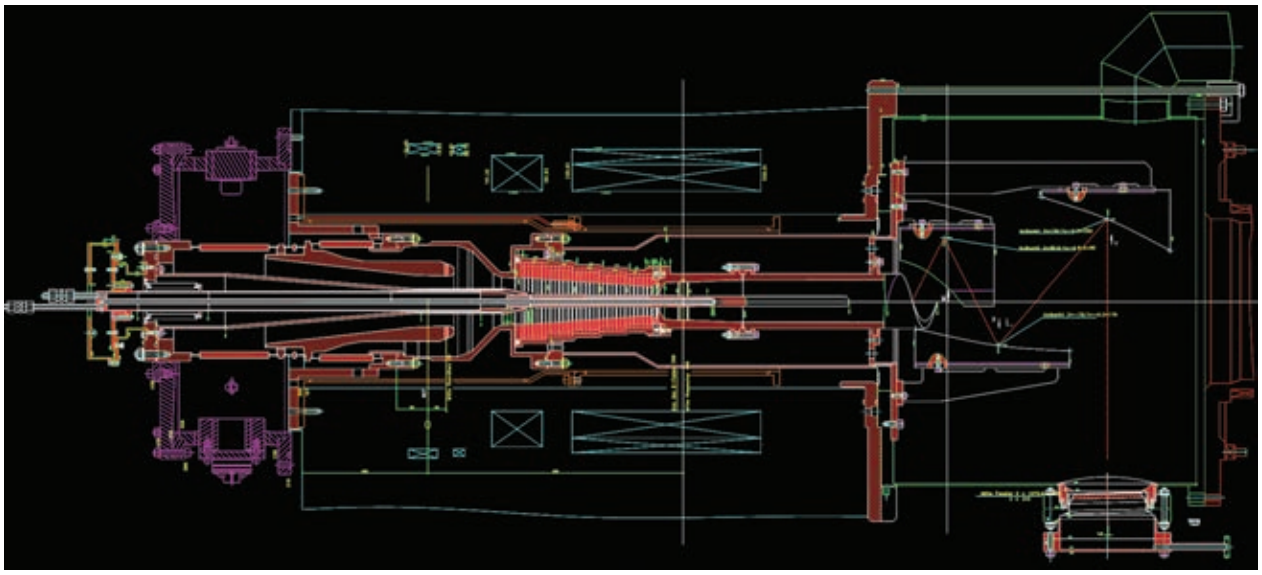

Fig. 6: Sketch of the KIT pre-prototype gyrotron with small gyrotron body inside the magnet (rotated; up is right side). The brown shape is the cooled NC coil inside the magnet (blue), and the red thick material at the upper magnet end is a new isolating spacer that shifts the gyrotron in the right position and also allows depressed collector operation with high voltage standoff.

Quasi-optical systems for ITER gyrotrons

The pre-prototype experiments mentioned above have shown clearly that the level of stray radiation created by the rippled-wall launcher and its quasi-optical system needs to be reduced. In addition, it was desired to increase the fundamental Gaussian mode content of the RF output beam further above 96%. Two approaches were pursued, first to equip the existing “first version” launcher with phase correcting mirrors (figure 7) to increase the Gaussian Content, and second to refine the launcher design by smoothing its surface to achieve both lower stray radiation and higher Gaussian content, even with smooth mirrors. Both approaches required some code work and investigations on the best filtering methods for smoothing without degrading performance. Finally, both approaches succeeded and resulted in design improvements: While the phase correcting mirrors approach could increase the Gaussian content even to 99%, as shown in simulation (in cold tests 97% has been measured), the smoothed launcher approach reached around 97% in simulation with an significant reduction of stray radiation. The hardware for both designs is now available, cold measurements of the smoothed launcher are scheduled at the beginning of 2012, and both system variants will be tested in high power tests during 2012, too.

In addition, some redesign work for the 1 MW ITER backup design was started, since a check of the manufacturer TED showed that the first design would not fit the foreseen housing.

Finally, the dissertation of Jens Flamm on efficient simulations of tapered launchers was nearly finished by the end of the year, resulting in a new analysis code that can directly consider the small taper angles of real world launchers – until now, this could only be done in slow analysis codes like SURF3D.

Last not least, it should be mentioned that the KIT quasi-optical millimetre-wave VNWA had to be upgraded from outdated software and operating systems to make these measurements possible. In addition, the RF backward-wave tube sources had to be replaced by solid state devices, which in return called for new mixers to maintain system sensitivity. All these redesign and upgrade works were being done and are continued by trying to bring the backward wave tubes into operation again, for even increased system dynamic.

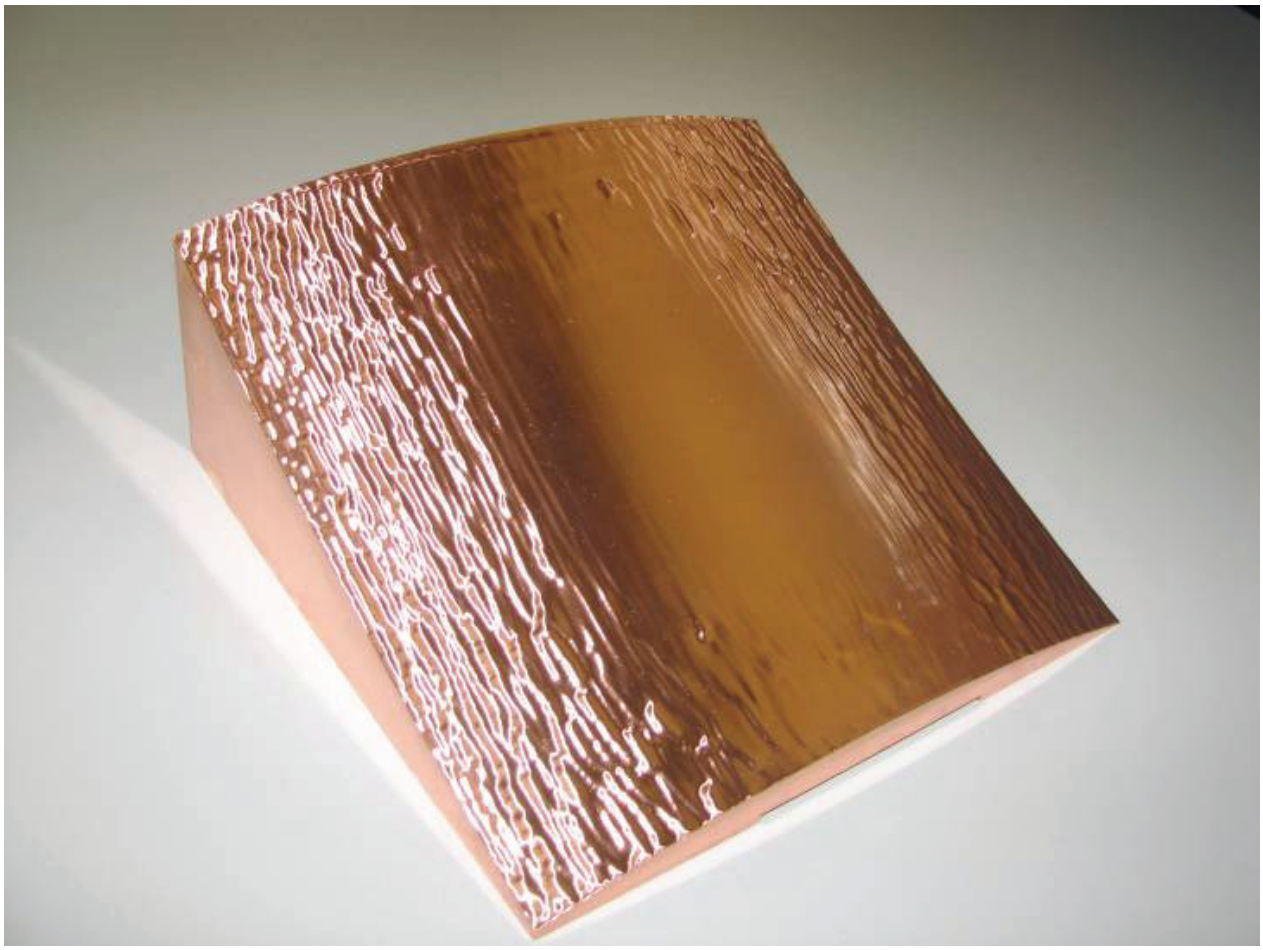

Fig. 7: Phase correcting mirror for improved Gaussian RF beam content.

Investigation of the ITER stray magnetic field on gyrotron operation

In the context of the F4E GRT-034 Task No. 1, the effect of the ITER stray magnetic field (SMF) on the operation of the European gyrotron has been studied. The SMF include the magnetic field generated by neighbouring gyrotrons, the ITER tokamak and also fields generated by the ferromagnetic structural materials used in the ECRH building. The 3D self-consistent electrostatic code ARIADNE has been used for the evaluation of the stray magnetic field effect on the electron beam in the cavity and the collector region. It is shown that the beam parameters at the cavity of the gyrotron are not significantly affected by the SMF. On the other hand, the magnetic field lines in the collector region are significantly deformed in the presence of the SMF. A part of the electron beam is guided to the non-appropriately cooled part of the collector surface, while the electron beam power is distributed in a significantly smaller area of the collector walls. In order to address the problem, the use of an advanced transverse sweeping system is proposed, which would allow to compensate the stray magnetic field and to improve the collector operation. A manuscript dedicated to this study with title "Study of the ITER SMF Effect on the EU 170 GHz 2 MW Coaxial Cavity Gyrotron" has been submitted to the journal IEEE Transaction of Plasmas Science.

Investigation of the modulation capability of the ITER gyrotron

In the framework of the F4E GRT-034 Task No. 2, the power modulation capabilities of the 2MW, 170 GHz gyrotron for ITER have been addressed. One of the critical parts of the tube is the collector, which will experience an increased load in the case of modulated operation of the gyrotron (where the averaged efficiency will be decreased).

One of the main results obtained from the transient thermomechanical analysis with ANSYS show that the less efficient modulation with the body power supply will raise the peak temperature and therefore the thermomechanical stress inside the collector wall beyond critical values and therefore should be avoided. As a consequence, the more efficient modulation with the main power supply should be preferred. Nevertheless, even in this case the peak temperature and stress will be slightly increased compared to the nominal operation point. Therefore, more investigations are needed to optimize the collector surface shape or to increase the sweeping frequency.

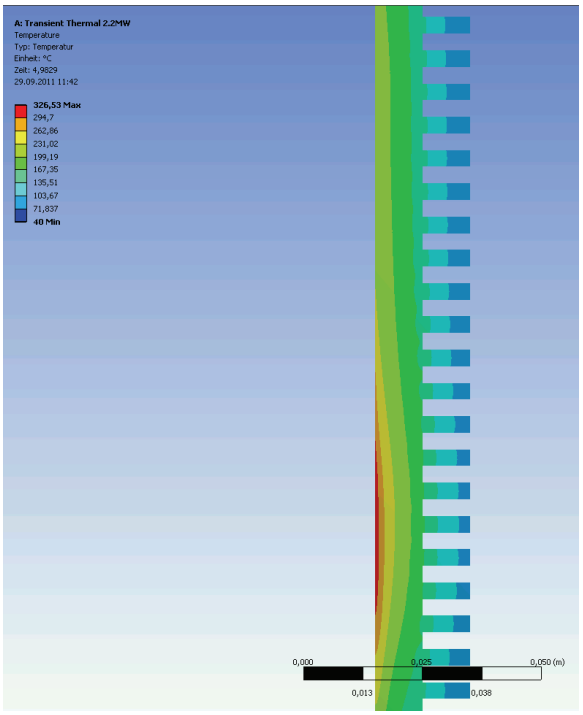

Snapshot of the temperature distribution in the collector wall during nominal operation (obtained with ANSYS)

Theoretical and experimental investigations on parasitic oscillations and related effects: Simulation code improvement, ACI investigations and measurement system development

Triggered by the investigations on beam tunnel oscillations started in 2009, there is a growing interest on parasitic oscillations and their implications. While the beam tunnel oscillation problem appears solved, the search for parasitic frequencies in experiment resulted in a number of observations of high interest for further research. This coincided with observations of dynamic after cavity interaction (ACI) processes in simulation that led to similar RF spectra and had a clear influence on performance. For this reason, the activities on code improvement, particular ACI investigations as well as improving spectral millimetre wave measurement systems and applying them at gyrotron experiments were and are continuing.

Code improvement is done in the frame of a dissertation, aiming at incorporating enhanced numerical models for non-uniform magnetic fields in interaction simulations. The older code versions were assuming a constant magnetic field only or a simplified model, which is suitable inside the resonator, but increasingly loses dependability outside, in locations where the parasitic oscillations are generated. First versions of the new code are being tested; one simulation example featured a surprisingly good coincidence between simulated and parasitic frequencies.

In a broader view, investigations on the influence of numerically induced reflections on ACI and their reduction are ongoing, in strong collaboration with colleagues from HELLAS and CRPP. First results show a strong influence of numerical reflections on ACI, but it is also found that when these influences are removed, strong dynamic ACI can still appear. All these code improvement activities are continued, aiming at creating a simulation tool that can reliably predict the appearance of parasitic oscillations and support their suppression by design.

On the experimental side, the next spectral measurement system is being developed as a part of another dissertation work. With the system developed in 2009, it became possible to display millimetre wave spectra in large bandwidth with high dynamic resolution, as long as the oscillations remained stationary enough over a millisecond range. The new system is utilizing fast digital oscilloscopes, receiving a downmixed time domain signal with bandwidths

exceeding 2 GHz. This permits the calculation of instantaneous spectra, and with a special dual-receiver technique, undesired mixing signals can be safely excluded while actually increasing the usable bandwidth. The system is under development, with the particular problem of having to acquire large amounts of data very quickly and over long time ranges. A measured example is shown in figure 8. This high dynamic and wide band measurement technique is essential for investigations on parasitic oscillations, especially when the aim is to check by measurement that no such oscillation appears. Here it can be said that in the coaxial pre-prototype, after being equipped with the corrugated beam tunnel, it could be shown through such measurement systems that no parasitic RF oscillations were generated. While this result appears of little interest seen from the measurement technique side, it is very hard to obtain and at the same time it is an important performance feature of the gyrotron. Other gyrotrons, which are also under investigation, are still creating parasitic oscillation spectra, thus justifying the further development of the measurement systems.

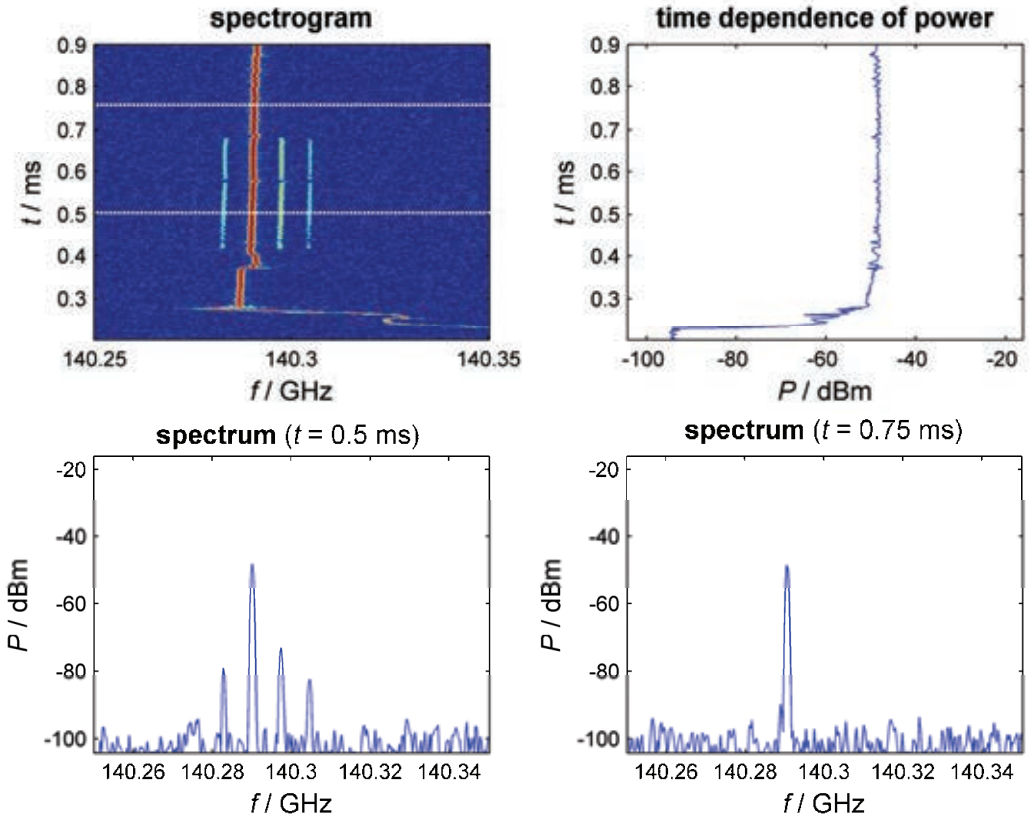

Fig. 8: Measurement example of spectrum versus time at the SN6 W7-X gyrotron. It can be seen in the waterfall plot (top left) that, after a startup process, a modulation appears and vanishes again. The example is just shown in small band; the actual measurement bandwidth expands over two separate ranges of 2 GHz each.

Conclusions and prospects

The unfortunate conditions for the coaxial gyrotrons during 2011 can only partly be balanced be the impressive list of successes during the four days RF experiment phase of the industrial prototype. A significant part of 2012 will be dedicated to the post-evaluation of the measurements and of the damage event. However, it should not be overlooked that even the short measurement campaign represents a quantum leap for the industrial prototype: For the first time, a coaxial industrial prototype was operated reaching the high design power of 2MW at high efficiency of 45% and at good beam quality, without any parasitic oscillations.

Since the damage comes under high time pressure and also otherwise difficult times for fusion technologies, a re-evaluation of project plans should be considered. It is currently open

if the 1 MW backup design project will be re-activated. In any case, KIT will prepare for such an event.

Another parallel opportunity to go on with coaxial gyrotron developments is the modular project, which actually was set up to be a substitute in exactly such a damage case as experienced. This project will in any case start through the next pre-prototype tests scheduled in February right after the refurbished gun was delivered. This experimental phase concentrates on component tests in short pulse, and the most important component to be redesigned and validated is the RF absorber scheme at the mirror box. In addition, this experiment will be operated with depressed collector, opening another chance to quickly determine efficiency limits in short pulse. Other components to be tested during the year are the new quasi-optical systems and several different beam tunnels.

The test stand will need further modifications in view of upcoming longer pulse tests. These activities will go on through the whole year. The same is true for the efforts on code improvement and measurement systems mentioned above.

Industrial Partner

TED Thales Electron Devices, Velizé, France ;
TED is the manufacturer of our gyrotrons and their components, formally associated to the F4E grants through procurement contracts with F4E.

Staff:

K. Baumann
E. Borie
G. Dammertz
D. D'Andrea
J. Flamm
G. Gantenbein
H. Hunger
S. Illy
J. Jelonnek
J. Jin
S. Kern
R. Lang
W. Leonhardt
M. Losert
D. Mellein
K. Nussbaum
I. Pagonakis
B. Piosczyk
T. Rzesnicki
A. Samartsev
A. Schlaich
M. Schmid
R. Schneider
W. Spieß
J. Szczesny
M. Thumm
J. Weggen

Literature:

[1] Albajar, F.; Bonicelli, T.; Alberti, S.; Avramides, K.A.; Cirant, S.; Gantenbein, G.; Goodman, T.P.; Illy, S.; Ioannidis, Z.; Hogge, J.P.; Jin, J.; Kern, S.; Latsas, G.; Pagonakis, I.G.; Piosczyk, B.; Rzesnicki, T.; Thumm, M.; Tigelis, I.; Tran, M.Q.; Vomvoridis, J.; Benin, P.; Lievin, C.; Darbos, C.; Gassmann, T.; Henderson, M. The European 2 MW gyrotron for ITER. Prater, R. [Hrsg.] Electron Cyclotron Emission and Electron Cyclotron Resonance Heating (EC-16) : Proc.of the 16th Joint Workshop, Sanya, China, April 12-15, 2010 Singapore [u.a.] : World Scientific, 2011 S.331-338 ISBN 978-981-4340-26-7

[2] Beringer, M.H. Design studies towards a 4 MW 170 GHz coaxial-cavity gyrotron. Dissertation, Karlsruher Institut für Technologie 2010 Karlsruhe : KIT Scientific Publ., 2011 (Karlsruher Forschungsberichte aus dem Institut für Hochleistungsimpuls- und Mikrowellentechnik ; Bd.1) ISBN 978-3-86644-663-2

[3] Flamm, J.; Jin, J.; Thumm, M. Comparison of different models of wave propagation in launchers of quasi-optical mode converters. 23rd Joint Russian-German Meeting on ECRH and Gyrotrons, Karlsruhe/Stuttgart/Garching, May 23-28, 2011

[4] Flamm, J.; Jin, J.; Thumm, M. Cylindrical wave decomposition in launchers of gyrotron quasi-optical mode converters. 2011 IEEE Internat.Vacuum Electronics Conf. (IVEC 2011), Bangalore, IND, February 21-24, 2011

[5] Flamm, J.; Jin, J.; Thumm, M. Cylindrical wave decomposition in launchers of gyrotron quasi-optical mode converters. 2011 IEEE Internat.Vacuum Electronics Conf. (IVEC 2011) : Proc.of a meeting held in Bangalore, IND, February 21-24, 2011 Piscataway, N.J. : IEEE, 2011 S.111-112 ISBN 978-1-4244-8662-5

[6] Flamm, J.H.; Jin, J.; Thumm, M.K. Wave propagation in advanced gyrotron output couplers. Journal of Infrared, Millimeter, and Terahertz Waves, 32(2011) S.887-896 DOI:10.1007/s10762-011-9800-y

[7] Jin, J.; Gantenbein, G.; Kern, S.; Rzesnicki, T.; Thumm, M. A matching optics unit (MOU) for coaxial-cavity ITER gyrotron. 23rd Joint Russian-German Meeting on ECRH and Gyrotrons, Karlsruhe/Stuttgart/Garching, May 23-28, 2011

[8] Jin, J.; Gantenbein, G.; Kern, S.; Rzesnicki, T.; Thumm, M. Design matching optics unit (MOU) for coaxial ITER gyrotron. 2011 IEEE Internat.Vacuum Electronics Conf. (IVEC 2011), Bangalore, IND, February 21-24, 2011

[9] Jin, J.; Gantenbein, G.; Kern, S.; Rzesnicki, T.; Thumm, M. Design matching optics unit (MOU) for coaxial ITER gyrotron. 2011 IEEE Internat.Vacuum Electronics Conf. (IVEC 2011) : Proc.of a meeting held in Bangalore, IND, February 21-24, 2011 Piscataway, N.J. : IEEE, 2011 S.271-272 ISBN 978-1-4244-8662-5

[10] Jin, J.; Rzesnicki, T.; Kern, S.; Thumm, M. High-efficiency quasi-optical mode converter for the coaxial cavity gyrotron. Fusion Science and Technology, 59(2011) S.742-748

[11] Kern, S.; Roy Choudhury, A.; D'Andrea, D.; Schlaich, A.; Avramides, K.; Alberti, S. Recent advances in gyrotron interaction simulations. 23rd Joint Russian-German Meeting on ECRH and Gyrotrons, Karlsruhe/Stuttgart/Garching, May 23-28, 2011

[12] Kern, S.; Avramides, K.A.; Roy Choudhury, A.; Dumbrajs, O.; Gantenbein, G.; Illy, S.; Samartsev, A.; Schlaich, A.; Thumm, M. Simulation and experimental investigation on dynamic after cavity interaction (ACI). 36th Internat.Conf.on Infrared, Millimeter and Terahertz Waves (IRMMW-THz 2011), Houston, Tex., October 2-7, 2011

[13] Li, F.; ALberti, S.; Hogge, J.P.; Pagonakis, I.G. Calculation of stray magnetic field effects on the operation of the ITER electron cyclotron system. 38th IEEE Internat.Conf.on Plasma Science (ICOPS) and 24th Symp.on Fusion Engineering (SOFE), Chicago, Ill., June 26-30, 2011

[14] Li, F.; ALberti, S.; Hogge, J.P.; Pagonakis, I.G. Calculation of stray magnetic field effects on the operation of the ITER electron cyclotron system. 38th IEEE Internat.Conf.on Plasma Science (ICOPS) and 24th Symp.on Fusion Engineering (SOFE), Chicago, Ill., June 26-30, 2011 Piscataway, N.J. : IEEE, 2011 Paper SP2-27 ISBN 978-1-4577-0669-1 Proc. also publ. online e-ISBN 978-1-4577-0667-7 DOI:10.1109/SOFE.2011.6052289

[15] Pagonakis, I.Gr.; Illy, S.; Piosczyk, B.; Kern, S.; Hogge, J.P.; Alberti, S. A new criterion for gyrotron gun design. 23rd Joint Russian-German Meeting on ECRH and Gyrotrons, Karlsruhe/Stuttgart/Garching, May 23-28, 2011

[16] Pagonakis, I.Gr.; Illy, S.; Piosczyk, B.; Li, F.; Alberti, S.; Darbos, C.; Henderson, M. The effect of the ITER stray magnetic field on the operation of the EU 2 MW coaxial cavity gyrotron. 23rd Joint Russian-German Meeting on ECRH and Gyrotrons, Karlsruhe/Stuttgart/Garching, May 23-28, 2011

[17] Pagonakis, I.Gr.; Li, F.; Alberti, S.; Illy, S.; Piosczyk, B.; Hogge, J.P.; Kern, S.; Ferran, A.; Henderson, M.; Darbos, C. The effect of the ITER stray magnetic field on the operation of the EU 2 MW coaxial cavity gyrotron. 8th Internat.Workshop 'Strong Microwaves and Terahertz Waves : Sources and Applications', Nizhny Novgorod, Russia, July 9-16, 2011

[18] Roy Choudhury, A.; Kern, S.; D'Andrea, D.; Schlaich, A.; Thumm, M. Influence of tapered magnetic field on gyrotron interaction calculation. 23rd Joint Russian-German Meeting on ECRH and Gyrotrons, Karlsruhe/Stuttgart/Garching, May 23-28, 2011

[19] Rzesnicki, T.; Piosczyk, B.; Illy, S.; Jin, J.; Kern, S.; Pagonakis, I.; Samartsev, A.; Schlaich, A.; Thumm, M. 2 MW, 170 GHz coaxial-cavity gyrotron for ITER. Results obtained with a short pulse pre-prototype at KIT. 8th Internat.Workshop 'Strong Microwaves and Terahertz Waves : Sources and Applications', Nizhny Novgorod, Russia, July 9-16, 2011

[20] Rzesnicki, T.; Piosczyk, B.; Illy, S.; Jin, J.; Kern, S.; Pagonakis, I.; Samartsev, A.; Schlaich, A.; Thumm, M. 2 MW, 170 GHz coaxial-cavity gyrotron for ITER. Results obtained with a short pulse pre-prototype at KIT. 8th Internat.Workshop 'Strong Microwaves and Terahertz Waves : Sources and Applications', Nizhny Novgorod, Russia, July 9-16, 2011 Proc. S.121-122 Nizhny Novgorod : Russian Academy of Sciences, 2011

[21] Rzesnicki, T.; Piosczyk, B.; Gantenbein, G.; Illy, S.; Jin, J.; Kern, S.; Losert, M.; Pagonakis, I.; Samartsev, A.; Schlaich, A.; Thumm, M. 2 MW, 170 GHz coaxial-cavity gyrotron for ITER. Experimental results obtained with a short-pulse pre-prototype tube. US-EU-JPN RF Heating Technology Workshop, Austin, Tex., October 10-12, 2011

[22] Rzesnicki, T.; Piosczyk, B.; Gantenbein, G.; Illy, S.; Jin, J.; Kern, S.; Pagonakis, I.; Samartsev, A.; Schlaich, A.; Thumm, M. Recent experimental investigations on the 2 MW, 170 GHz coaxial cavity pre- prototype gyrotron for ITER. 23rd Joint Russian-German Meeting on ECRH and Gyrotrons, Karlsruhe/Stuttgart/Garching, May 23-28, 2011

[23] Samartsev, A.; Gantenbein, G.; Illy, S.; Kern, S.; Latsas, G.; Thumm, M.; Tigelis, I. Numerical simulation of parasitic gyro-BWO interaction in a gyrotron beam tunnel. 36th Internat.Conf.on Infrared, Millimeter and Terahertz Waves (IRMMW-THz 2011), Houston, Tex., October 2-7, 2011

[24] Schlaich, A.; Choudhury, A.R.; Gantenbein, G.; Illy, S.; Kern, S.; Lievin, C.; Samartsev, A.; Thumm, M. Examination of parasitic after-cavity oscillations in the W7-X series gyrotron SN4R. US-EU-JPN RF Heating Technology Workshop, Austin, Tex., October 10-12, 2011

[25] Schlaich, A.; Illy, S.; Kern, S.; Samartsev, A.; Thumm, M. Recent examinations of the W7-X-SN4R gyrotron RF output spectrum. 23rd Joint Russian-German Meeting on ECRH and Gyrotrons, Karlsruhe/Stuttgart/Garching, May 23-28, 2011

[26] Thumm, M. Computer engineering in radio physics at KIT. Design in high power microwave technology. Symp.on Computer Engineering in Physics and Geophysics, Novosibirsk, Russia, September 22-24, 2011

[27] Thumm, M. Progress on gyrotrons for ITER and future thermonuclear fusion reactors. IEEE Transactions on Plasma Science, 39(2011) S.971-979 DOI:10.1109/TPS.2010.2095042

[28] Thumm, M. Progress on gyrotrons for ITER, W7-X and future magnetic confinement fusion reactors. Vortr.: Novosibirsk State Technical University, 6.Dezember 2011

[29] Thumm, M.K.A.; Arzhannikov, A.V.; Astrelin, V.T.; Burdakov, A.V.; Ginzburg, N.S. ; Kalinin, P.V.; Kuznetsov, S.A.; Makarov, M.A.; Mekler, K.I.; Peskov, N.Yu.; Polosatkin, S.V.; Popov, S.A.; Postupaev, V.V.; Rovenskikh, A.F.; Sergeev, A.S.; Sinitsky, S.L.; Sklyarov, V.F.; Stepanov, V.D.; Vyacheslavov, L.N.; Zaslavsky, V.Yu. Generation of high power THz waves in relativistic electron beam. 3rd Shenzhen Internat.Conf.on Advanced Science and Technology - Terahertz Science and Technology (the 3rd SICAST), Shenzhen, China, November 21-26, 2011 Book of Abstracts S.26

[30] Thumm, M.K.A. Recent developments on high-power gyrotrons. Introduction to this special issue. Journal of Infrared, Millimeter and Terahertz Waves, 32(2011) S.241-252 DOI:10.1007/s10762-010-9754-5

Acknowledgement

This work was supported by Fusion for Energy under the grant contracts No. F4E-2009-GRT-034-01 and No. F4E-2009-GRT-049-01 with collaboration by EPFL, Switzerland; HELLAS, Greece; and CNR, Italy. The views and opinions expressed herein reflect only the author's views. Fusion for Energy is not liable for any use that may be made of the information contained therein.

Technological Requirements of an Electron Cyclotron Current Drive System for DEMO (WP11-DAS-HCD-EC-01)

ECRH systems have demonstrated successful heating, current drive and plasma stabilisation in several fusion experiments. With growing RF power, pulse length, efficiency and reliability of gyrotrons, ECRH has become one of the first choices for heating and plasma stabilisation in existing and planned fusion devices.

Today, 2 MW CW RF windows (small band) and transmission lines, and 1 MW CW sources (single or dual frequency) with 50 % efficiency are considered state of the art up to 170 GHz. 2 MW gyrotrons are under investigation, even 4 MW sources appear feasible, and investigations on broadband concepts have been launched.

With its small RF wave length and easy plasma access, ECRH offers the advantage of small antenna structures and torus openings together with a well controlled localized heating, which is particularly useful for plasma stabilisation and shaping current drive profiles.

In this task the specific R&D needs and a development roadmap for an ECH&CD system for DEMO are analysed. The technology requirements and specifications for a nuclear environment are assessed for the power sources, transmission lines, RF windows, antenna, diagnostics, interfaces and remote handling issues. The activity includes a RAMI analysis (reliability, availability, maintainability, inspectability).

Based on the assumptions of a DEMO 1 (ITER like) and DEMO 2 (CW machine with a large amount of non-inductive current drive) tokamaks the technological developments in the various fields (gyrotron, window, launcher, remote handling, critical issues) are being addressed. The main differences between ITER and DEMO with respect to the ECH&CD system are mentioned and necessary developments towards DEMO are analysed.

Staff:

G. Gantenbein
S. Kern
D. Strauss

Acknowledgement

This work, supported by the European Communities under the contract of Association between EURATOM and Karlsruhe Institute of Technology, was carried out within the framework of the European Fusion Development Agreement. The views and opinions expressed herein do not necessarily reflect those of the European Commission.

Advanced Gyrotron Development
Studies on Electron Beam Diagnostic Systems (CoA)

Introduction

One of the big unknowns in experimental gyrotron diagnostic is still the electron energy distribution at the absorption in the collector. Even though the distribution can be simulated with many tools today, a measurement in full operation is impossible yet. On one hand, the energy distribution is one of electron beam features that determines the possible energy recovery, on the other hand, the measurements performed after interaction would give valuable insight into the interaction mechanisms, as well as a good tool for code validation.

One possibility for creating a diagnostic tool for energy distribution is to measure the X-ray spectra that are emitted as bremsstrahlung at the collector. One of the problems is the reconstruction of the electron's energy distribution through de-convolution. Other problems are uncertainties and possible error sources through shielding. With such a diagnostic in hand, an important tool would be available for further optimisation of gyrotron efficiencies and simulation codes.

Status of work at the beginning of 2011 and achievements in 2011

The X-ray electron beam diagnostic is currently developed within a collaboration among KIT and the St. Petersburg State Polytechnical University (SPbSPU), Russia. In 2010, an extensive theoretical study on the calculation of electron energy distributions from bremsstrahlung was accomplished. The result was that a very good reconstruction of energy distributions is possible if the radiation is measured through materials and walls which don't absorb strongly, like the ceramic isolators on the gyrotron or additional windows, for example at the collector.

In 2011, an X-ray spectrometer "AmpTek X-123CdTe" was purchased and sent to St. Petersburg for first experimental tests. Unfortunately, the transfer caused customs problems in Russia, which delayed the whole project by several months and made it impossible to continue the measurements on a KIT gyrotron at the end of the year. Nevertheless, experimental measurements could be done with an "Introvolt 120" X-ray source. Several spectra were investigated (see figure 1). It was found that the calculation of electron energies from measured data required a code modification in order to take into account the distortions and the characteristic lines and to pre-process the measured data accordingly. It was subsequently possible to reconstruct test spectra by running the source sequentially at different voltages. Using such measurements, the influence of the pre-processing parameters was studied in detail (figure 2). After these tests finished successfully, a shielding box for the spectrometer was designed to reduce the influence of both external electromagnetic influences as well as the strong static magnetic field at the gyrotron.

Conclusions and prospects

The experimental tests foreseen at KIT could not be performed due to the lack of a suitable gyrotron experiment. Through the experimental preparation with the "Introvolt 120" X-ray source and the corresponding code modifications, the necessary experience was gathered to continue with measurements on a gyrotron at KIT. For this purpose, the step-tunable gyrotron will be equipped with a dedicated collector that features a top window for measurements. The shielding box for the spectrometer was already built.

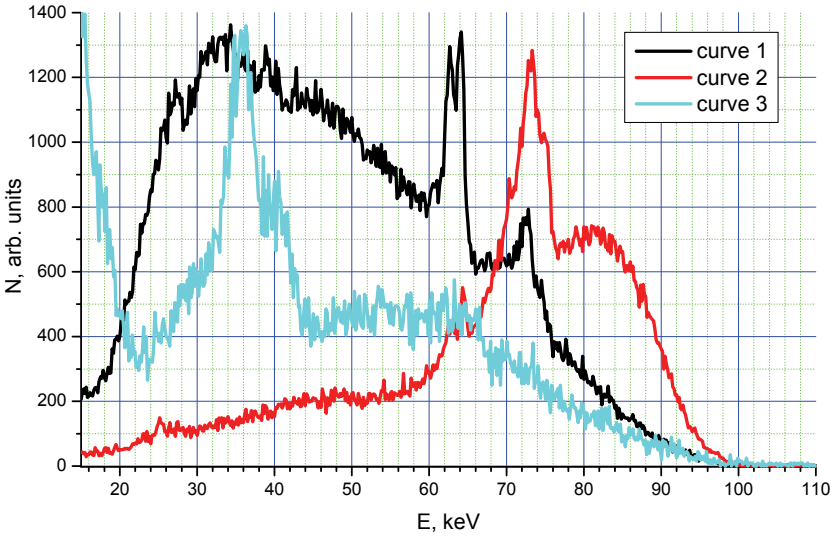

Fig. 1: Photon spectra of different types measured with X-ray tube with tungsten target at U = 100 kV – for different conditions of X-ray generation and propagation to spectrometer sensor.

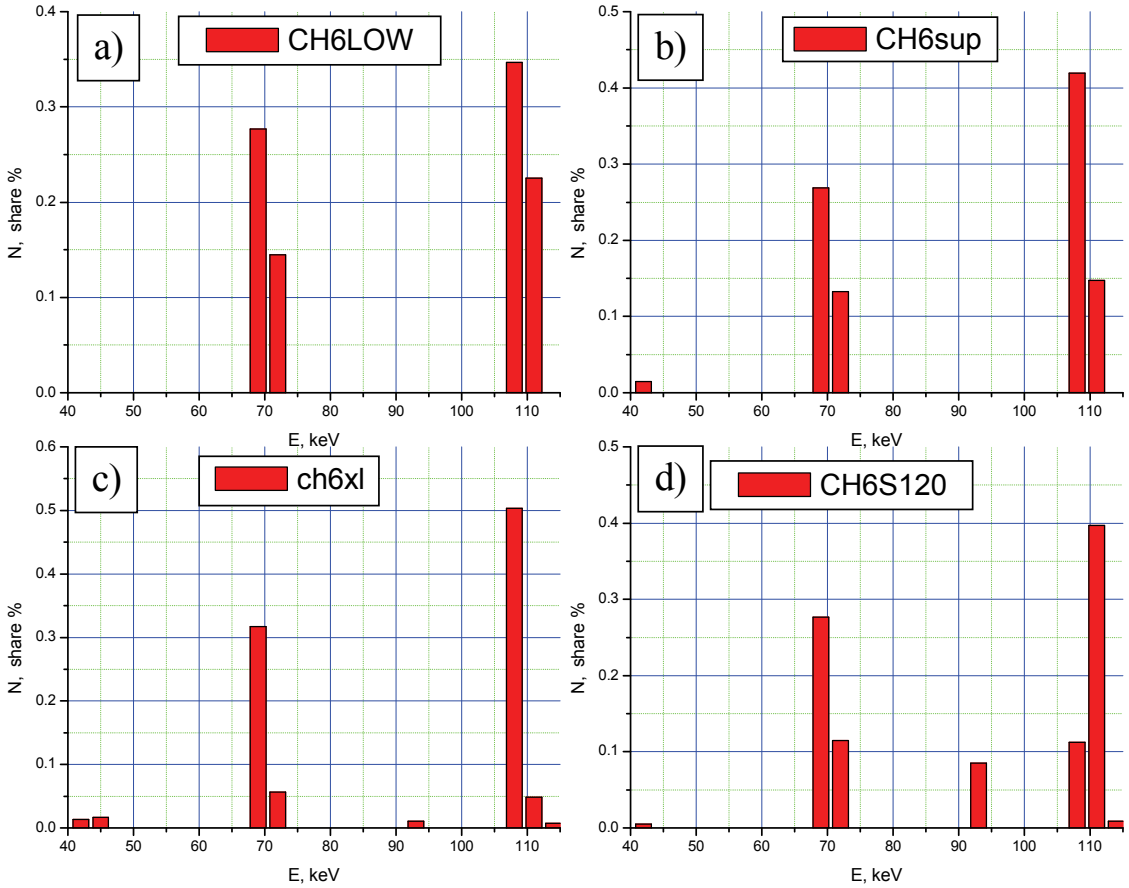

Fig. 2: Electron energy distributions reconstructed from X-ray spectrum for X-ray operation regime “100 s at 110 kV + 75 s at 70 kV” with usual basis (energy points are eU= 33, 36,…, 120 keV, step 3 keV) and different weight functions on energy discretization intervals and steps:
(a) the usual weight function $W = E^2$;
(b) the same weight function divided by 3 in an interval near characteristic radiation lines;
(c) the same weight function divided by 10 in an interval near characteristic radiation lines;
(d) weight function is equal to basic function for the highest energy $W = A_{120}(E)$.

Design of a low power gyrotron for the test of a new emitter concept

The design phase of a 28 GHz, 15 kW gyrotron for the test of a new segmented emitter is nearly finished. The new emitter type is based on small individual emitter rods, heated in the rear part of the segment. The goal of this project is to combine several segments to a ring-shaped structure to replace the conventional emitter ring. This concept allows the influence of the emission current of each emitter segment and therefore enables the control of the azimuthal homogeneity of the emission, which is not possible in the case of conventional ring-shaped emitters.

This work is done in collaboration with Calabazas Creek Research (USA), which will design and build the cathode part of the tube in two variants, one equipped with the new segmented emitter (see Fig.3 left part) and one with a conventional ring-shaped emitter, for comparison measurements.

All other parts of the gyrotron are under development at IHM and reached now the final design phase (see Fig.3 right part), including the electron beam optics, cooling, material selection and UHV technology. First brazing tests with relevant materials have been performed at the IHM mechanical workshop.

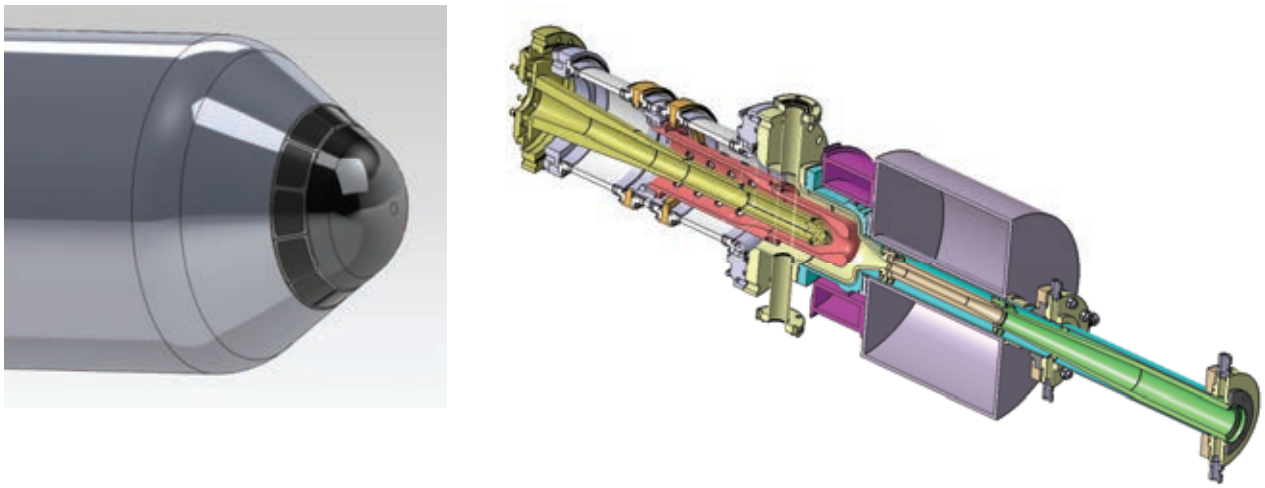

Fig. 3: Drawings of the cathode section with segmented emitter (left) and of the complete test gyrotron (right).

Design and test of a high power stainless steel microwave load

Conventional high power microwave loads usually use a ceramics coating to absorb the RF power. Unfortunately, this concept has the drawback that local hot-spots may appear on the load surface that will cause ablation of the coating. To avoid this problem, we designed a load manufactured solely from stainless steel and increased the overall absorbing area of the device with additional U-shaped stainless steel pipes. Since experiments in 2010 without active cooling of the load showed promising results, we equipped the inner pipe structure with water cooling (leaving the outer structure still without active cooling). The results obtained with this set-up allowed RF pulses of 550 kW for 30 s and 780 kW for 20 s, respectively, indicating a significant performance increase compared to the measurements of 2010.

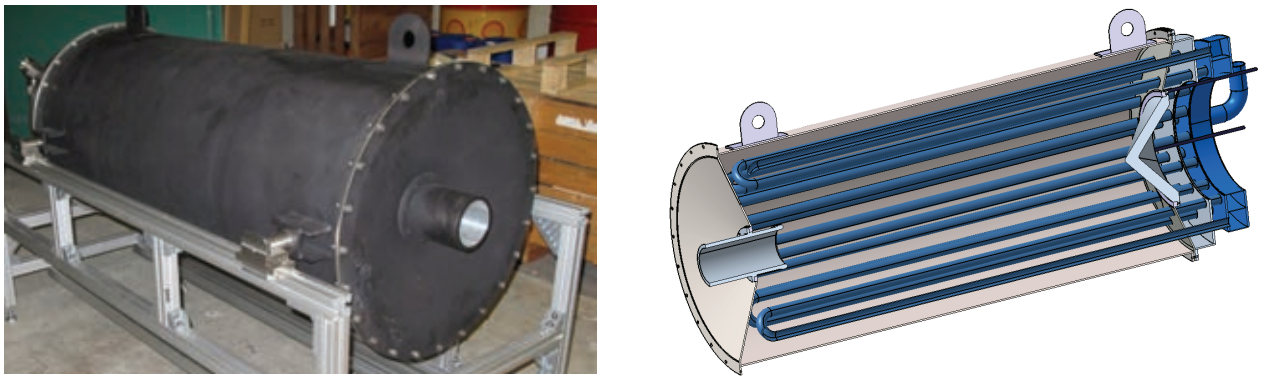

Fig. 4: The stainless steel microwave load prepared for the second measurement in 2011.

Staff:

G. Dammertz
G. Gantenbein
S. Illy
S. Kern
R. Lang
A. Malygin
B. Piosczyk
W. Spiess
J. Szczesny
M. Thumm
J. Weggen

Advanced Gyrotron Development
Step-Tunable Gyrotron (CoA)

Introduction

In recent years electron cyclotron resonance heating and current drive (ECRH and ECCD) has been established as a successful instrument in magnetically confined fusion plasmas. Gyrotrons are the unique devices which meet the extraordinary requirements of those applications: output power in the MW range, 100 – 200 GHz output frequency, and pulse length of several seconds up to continuous wave (CW). Due to its excellent coupling to the plasma and the very good localization of the absorbed RF power, ECRH is applied in present day machines and is also foreseen in large forthcoming fusion project: it will be the main heating system for the stellarator W7-X which is currently under construction and it will play a major role in the ITER tokamak. In particular, advanced tokamaks are operated in a plasma regime, where MHD instabilities which may limit the performance are present. To a large extent the stability in a tokamak is influenced by the distribution of the internal plasma currents, which can be manipulated by the injection of RF waves. The location of the absorption of RF waves with the angular frequency ω is dependent on the resonance condition $\omega - k_z v_z = \omega_c$ (k_z: z-component of the wave number, v_z: electron velocity along z-axis). Thus, by changing the wave frequency ω the absorption can be moved to any radial position where the local cyclotron frequency of the electrons ω_c holds for the expression above.

Industrial gyrotrons in the relevant frequency range with an output power of about 1 MW are usually designed for a fixed frequency. However, frequency tunable gyrotrons are not a standard product, since these broadband tubes require additional optimization of major components of the gyrotron like the electron beam forming optics, cavity, quasi-optical mode converter and output window.

For experiments on plasma stabilization at ASDEX Upgrade (IPP Garching) with advanced ECRH and ECCD, multi-frequency tunable (105 – 143 GHz) 1-MW long-pulse gyrotrons are highly needed.

Experiments with modified profile of resonator

According to our program established in 2010 it was decided to modify the profile of the up-taper in the resonator in order to suppress the effect of After Cavity Interaction (ACI) of the spent electron beam with a traveling EM wave. The ACI effect was observed in numerical simulations and was believed to be the possible reason for low mode purity of the RF beam at the output window, and reduced efficiency of the gyrotron.

The machining of the new resonator was performed at the IHM workshop in order to reduce the costs. The profile of the produced resonator was measured and it was found within the range of acceptable tolerances.

Experiments with a new resonator started in August and continued until October 2011. During that period various comparative measurements have been performed allowing conclusions on the influence of the up-taper geometry on the performance of the gyrotron, based on the assumption that parasitic frequencies are excited in the up-taper. Experimental measurements showed that at usual operation condition a specific parasitic oscillation was still present with each excited cavity mode (at different frequencies). A detailed study of the dependency of the frequency of parasitic oscillations on cathode voltage and magnetic field was performed.

The power measurements were made for several cavity modes at different frequencies for comparison with the original resonator and, in addition, at higher frequency range four modes with radial number 9 were studied.

With the short pulse experiment It was found that for a number of modes, which have the matching caustic radius, it was possible to obtain nearly one megawatt power at nominal beam current and a efficiency of about 26 %. Though according to the calculations of the electron beam properties the pitch factor (ratio of perpendicular to parallel electron velocity) is larger than a nominal one. Operation of the gyrotron at higher power was followed by the appearance of both high frequency parasitics and low frequency electron beam instability in the range of few tens megahertz.

In Table 1 the list of measured modes is reproduced with achieved power and beam properties used during operation.

Table 1: Frequency, power and efficiency of measured modes at nominal parameters of operation.

Mode	Frequency, [GHz]	U_{cath}, [kV]	I_{beam}, [A]	Power, [kW]	Efficiency, %
$TE_{19,7}$	119,5	93,0	41,1	880	23,0
$TE_{20,7}$	124,1	91,7	41,0	890	23,6
$TE_{22,7}$	130,9	90,0	40,0	900	25,0
$TE_{22,8}$	140,0	91,7	41,0	960	25,5
$TE_{23,8}$	143,3	90,3	39,1	980	27,5
$TE_{24,9}$	155,9	91,7	41,1	980	26,0
$TE_{25,9}$	159,2	91,0	40,4	1000	27,2
$TE_{26,9}$	162,5	89,7	40,4	990	27,3
$TE_{27,9}$	165,9	90,0	40,4	950	26,1

In the table the efficiency of short pulse operation is calculated without taking into account the effect of voltage depression. In a long pulse operation one could expect higher efficiency to be obtained.

In order to characterize the possible limitations of the output power one could measure its dependence on the beam current. Such dependency was measured for two modes: $TE_{22,8}$ and $TE_{23,8}$, which is shown in Fig. 1.

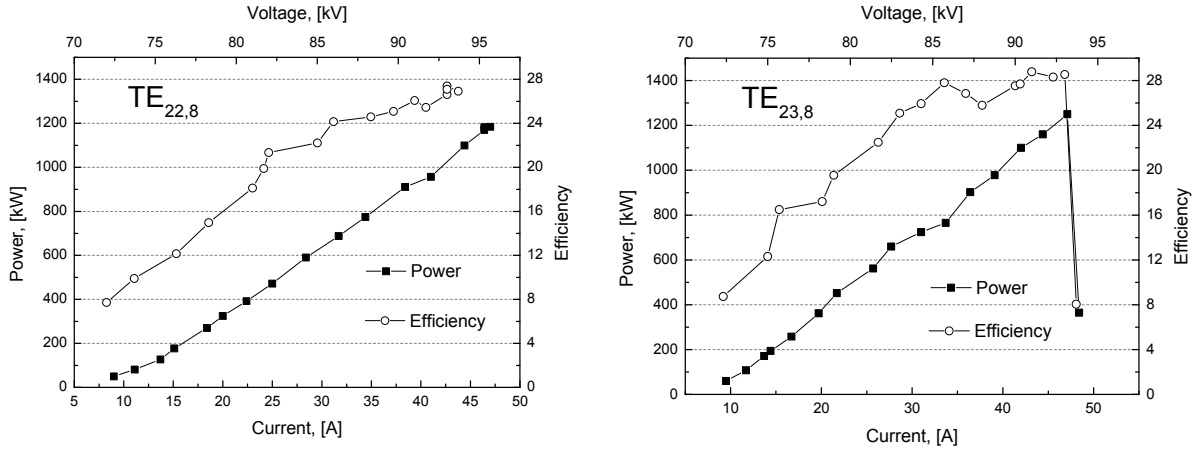

Fig. 1: Output power in dependence of the beam current for the modes $TE_{22,8}$ and $TE_{23,8}$.

A further increase of the beam current was limited by the heating power supply of the cathode. In both cases the power depends linearly on the current. The interesting point is that in both plots the efficiency does not reach saturation and is still growing with the current. From this result we may conclude that, in order to improve the performance, the resonator itself may be optimized.

ESRAY calculations of the electron beam parameters such as pitch factor and radius for operation in the $TE_{23,8}$ mode show that the pitch factor exceeds the nominal one (≅1.3) significantly. Operation of the gyrotron at reduced pitch factor close to the nominal one shows an output power reduction of approx. 200 kW. The inconsistency between the theoretical calculations and experimental performance is still the subject of study.

The frequency dependency of parasitic modes on the cathode voltage and magnetic field was studied. The results of the measurements are plotted in Fig. 2 (a) and (b). Parasitic oscillation demonstrates gradual dependence both on the beam voltage/energy and magnetic field amplitude. The change of the working mode in the cavity from $TE_{22,8}$ to $TE_{23,8}$ nearly does not affect the frequency of the parasitics. From this we may conclude that parasitic and gyrotron oscillations are not strongly coupled and the parasitics may occur at different sections of the resonator or even in the downtaper of the beam tunnel section. In addition, in contrast to the gyro mode the parasitics show a stronger dependence on the magnetic field and the cathode voltage change which is characteristic for BWO type interaction.

At the moment the origin of this oscillation is still the subject of investigation.

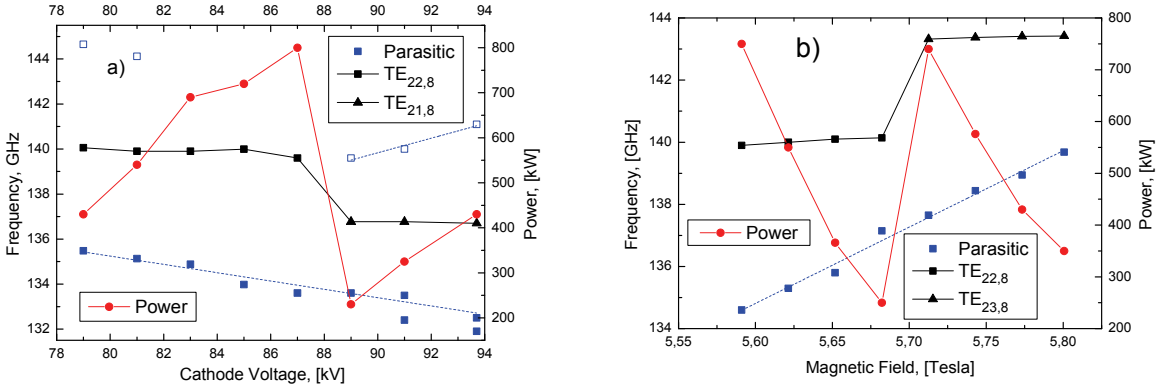

Fig. 2: Frequency of resonator and parasitic modes in dependence of the voltage (a) and magnetic field (b).

A special study was performed to investigate the influence of beam disposition on the RF field profile pattern measured by IR-camera. The Gaussian content detected for the main mode $TE_{22,8}$ is at the value 79% instead of 93% expected from calculations of the Quasi Optical System (QOS). Such a low value of Gaussian content was stably reproduced at different positions of the electron beam in the cavity and various regimes of operation by the same mode of oscillation. In principle, in the case of multimode oscillation the power of each mode must be sensitive on the operation. Therefore, the beam pattern must strongly vary, which was not the case. A new type of QOS having higher efficiency is developed (see below).

New quasi-optical mode converter

A new type of quasi-optical mode converter for the step-tunable gyrotron was developed with the use of an improved code for the launcher and mirrors synthesis. The improvements of the code reduce the stray radiation from the launcher and, therefore, thermal loading on inner construction parts of gyrotron. Generally the Gaussian content is higher for the main operating modes.

The Fundamental Gaussian Mode Content (FGMC) of the field calculated at the last section of the launcher is presented in Table 2.

The launcher will be used together with a quasi-elliptical mirror and two new toroidal mirrors.

Table 2: Calculated Fundamental Gaussian Mode Content at the last Brillouin zone of the launcher for 9 modes.

Mode	Frequency [GHz]	FGMC [%]
$TE_{17,6}$	104.9	97.8
$TE_{18,6}$	108.2	96.8
$TE_{19.6}$	111.5	94.7
$TE_{19.7}$	120.8	97.8
$TE_{20.7}$	124.1	98.9
$TE_{21.7}$	127.4	98.2
$TE_{21.8}$	136.7	93.2
$TE_{22.8}$	140.0	95.6
$TE_{23.8}$	143.3	97.4

CVD-diamond Brewster window

The efficient operation for a large number of operating modes at different frequencies is only possible by using a broadband synthetic diamond Brewster window fabricated by chemical vapor deposition (CVD). Due to the large Brewster angle of 67.2° deg, the diameter of the disk has also to be rather large in order to have sufficient aperture for the RF beam. One disk with a thickness of 1.7 mm and a diameter of 140 mm was developed by Element Six and already delivered. This disk can be used for the elliptic shape of a Brewster window with an effective aperture of 50 mm.

Because of the ellipticity, the stresses during the brazing procedure are different from circular disks. These stresses were calculated to be increased by a factor of 1.3. After successful preliminary brazing tests at TED with a quartz disk and a small diamond disk the brazing of the 140 mm diamond disk was finished at TED. This disk will be introduced into housing, experiments with the gyrotron are foreseen.

Staff:

G. Dammertz
J. Flamm (KIT, CS)
G. Gantenbein
S. Illy
S. Kern
W. Leonhardt
M. Losert
J. Jelonnek
J. Jin
D. Mellein
A. Papenfuss
B. Piosczyk
A. Samartsev
T. Scherer (IAW-AWP)
A. Schlaich (KIT, CS)
M. Schmid
R. Schneider
W. Spieß
D. Strauss (IAW-AWP)
J. Szczesny
M. Thumm

Literature:

[1] Samartsev, A.; Gantenbein, G.; Dammertz, G.; Illy, S.; Kern, S.; Schlaich, A.; Thumm, M., Current status of multi-frequency gyrotron development, 23rd Joint Russian-German Meeting on ECRH and Gyrotrons, Karlsruhe/Stuttgart/Garching, May 23-28, 2011, Folien auf CD-ROM

[2] Samartsev, A.; Gantenbein, G.; Dammertz, G.; Illy, S.; Kern, S.; Leonhardt, W.; Schlaich, A.; Schmid, M.; Thumm, M., Development of frequency step tunable 1 MW gyrotron at 131 to 146.5 GHz, 2011 IEEE Internat.Vacuum Electronics Conf. (IVEC 2011), Bangalore, IND, February 21-24, 2011

[3] Samartsev, A.; Gantenbein, G.; Dammertz, G.; Illy, S.; Kern, S.; Leonhardt, W.; Schlaich, A.; Schmid, M.; Thumm, M., Development of frequency step tunable 1 MW gyrotron at 131 to 146.5 GHz, 2011 IEEE Internat.Vacuum Electronics Conf. (IVEC 2011) : Proc.of a meeting held in Bangalore, IND, February 21-24, 2011, Piscataway, N.J. : IEEE, 2011 S.269-270, ISBN 978-1-4244-8662-5

[4] Samartsev, A.; Gantenbein, G.; Illy, S.; Kern, S.; Latsas, G.; Thumm, M.; Tigelis, I., Numerical simulation of parasitic gyro-BWO interaction in a gyrotron beam tunnel, 36th Internat.Conf.on Infrared, Millimeter and Terahertz Waves (IRMMW-THz 2011), Houston, Tex., October 2-7, 2011

Fusion Researcher Fellowship (WP11-FRF-KIT/D'Andrea)

Implementation of a 3D Particle-in-cell Code for the Simulation of Gyrotron Components

The main purpose of this project is the numerical simulation of the launcher and cavity resonator and mode converter of gyrotrons using a state-of-the-art, high-order, MPI-parallelized kinetic code, which is highly flexible, and equipped with a multitude of physical models for a wide range of applications in space and laboratory plasma physics, namely HALO-PIC.

The first gyrotron component, which was successfully simulated with the high order HALO-PIC code at IHM, is the complete 140 GHz $TE_{22,6}$ mode with a simple Vlasov launcher. The numerical experiment is initialized by an analytical (time dependent) electromagnetic wave at the entrance of the wave guide. The whole computational domain was discretized with ~2.6 x 10^6 tetrahedrons with a characteristic discretization length of ~10^{-3} (about 0.5λ: λ wavelength) and the fields were approximated by a fourth order method. Furthermore, this simulation required 512 processors of the LAKI cluster at the HLRS (Höchstleistungsrechenzentrum Stuttgart) for about 10 CPU hr. Perfect conducting boundary conditions are prescribed on the metallic parts, while open boundaries are assigned at the border of external space. The picture shown below is recorded at t=2.1ns and clearly shows that, as expected, the wave travels the cylindrical part and then propagates in the free space with an almost plane shape. In the external area interferential phenomena are taking place and it is also possible to recognize that some waves are possibly travelling inside the cylinder. A cylindrical section was cut at the cylinder radius R_0 and then "unwrapped" to be able to inspect the resolution around the reflection area (see figure right). This area is extremely important since it is from here that the electromagnetic wave exits the launcher and then hits the mirrors system. The code simulates the emitted wave accurately and the results show how other waves that reach this area can deviate the outcoming wave.

In the next step the cavity of a $TE_{3,1}$ second harmonic gyrotron will be modeled and simulated.

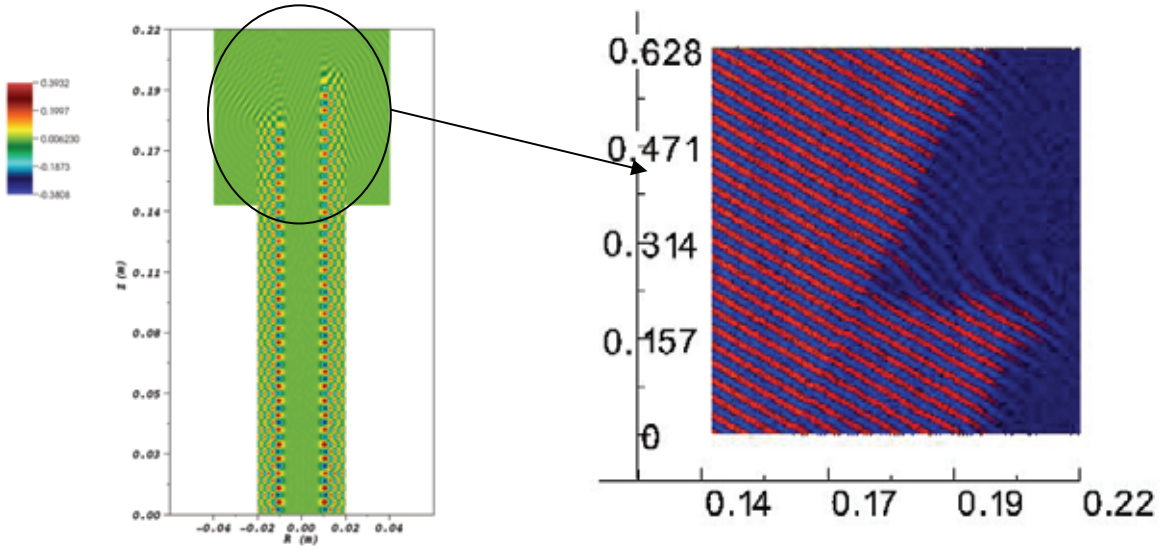

X-Z cross section showing the field amplitude (B_z) of the $TE_{22,6}$ launcher and Z-θ representation of the $TE_{22,6}$ launcher cut region (right).

Staff:

D. D'Andrea
S. Illy

Acknowledgement

This work, supported by the European Communities under the contract of Association between EURATOM and Karlsruhe Institute of Technology, was carried out within the framework of the European Fusion Development Agreement. The views and opinions expressed herein do not necessarily reflect those of the European Commission.

Design, Analysis and Documentation to Produce the ITER EC H&CD Upper Launcher Final Design - Part 1 (F4E-GRT-161-01)

Introduction

This grant is a contract between F4E and the recently formed European EC Upper Launcher Consortium of EURATOM Associates ECHUL-CA, in which the best qualified European laboratories in the area of ECH antenna, namely KIT Karlsruhe (D, project leadership), IPP Garching (D, together with IPF at University Stuttgart), CRPP (CH), CNR (I) and ITER-NL (specifically: FOM, NL) have joint forces to develop a high quality ITER ECH antenna system. The development starts with the preliminary design (figure 1) as developed in former contracts between the EFDA and the Associates involved.

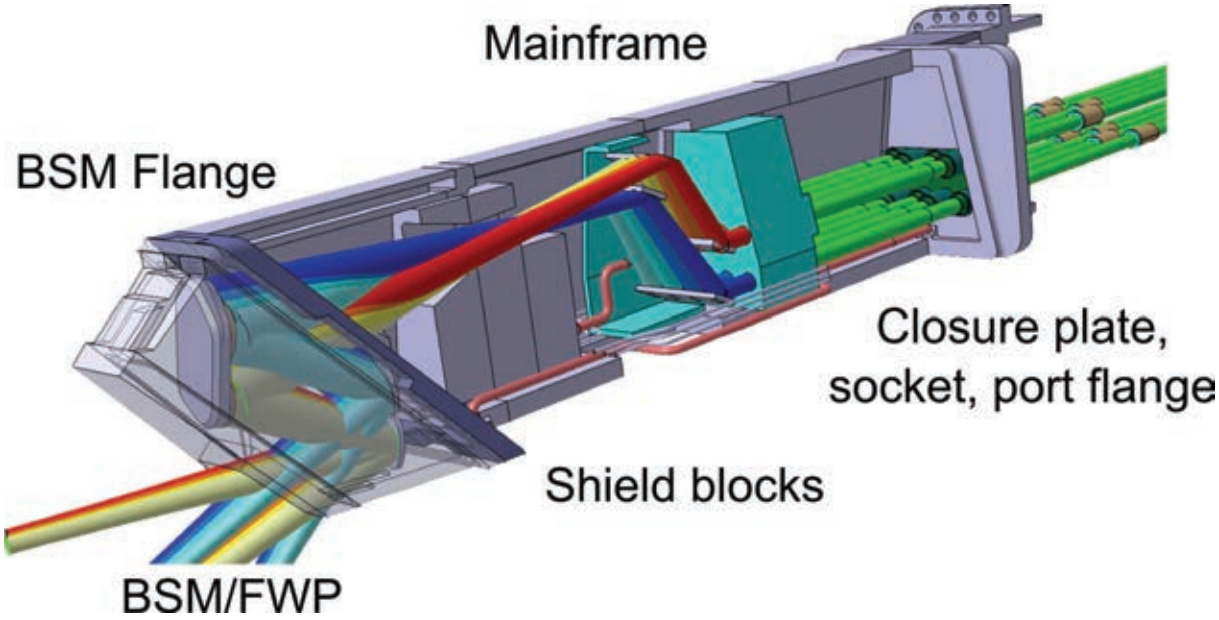

Fig. 1: Preliminary design of the ITER ECH Upper Port Plugs.

In this project with a duration of 24 months the following design activities for the four ITER ECH upper launchers will be defined: Firstly, the final design of components related to the first confinement system, which are essentially the closure plate, the external waveguides and the sophisticated high power diamond windows. Secondly, one design iteration step of the in-vessel launcher components is foreseen, including the quasi-optical system with the different mirror sets, and the structural system including actively cooled components close to the plasma such as the first wall panel.

Status of work

In 2011, a detailed proposal has been successfully elaborated, and the contract between F4E and ECHUL-CA could be signed in October. After the kick-off meeting at the end of November, first activities have been started, and the first intermediate reports are in progress.

Staff:

U. Fischer
T. Scherer
D. Strauß

Acknowledgement

This work was supported by Fusion for Energy under the grant contract No. F4E-GRT-161-01 with collaboration by CRPP Switzerland, FOM Netherlands, CNR Italy and IPP Germany. The views and opinions expressed herein reflect only the author's views. Fusion for Energy is not liable for any use that may be made of the information contained therein.

Manufacturing of ITER ECH Upper Port Plug Structural System Prototypes (BMBF Reference No. 03FUS0010)

Introduction

The ITER ECRH (Electron Cyclotron Resonance Heating) system features four upper launchers to inject up to 20 MW of mm-wave power into the plasma. They will be installed into upper ports in order to counteract plasma instabilities.

An upper launcher basically consists of the launcher port plug and the mm-wave system. The port plug is the casing of the launcher. It accommodates the launcher mm-wave system, which is composed of individual waveguides and a set of mirrors to inject the microwaves precisely to the targeted plasma instabilities. In combination with dedicated shielding elements, the port plug provides protective and accurate installation of the mm-wave components. Figure 1 shows the launcher, mounted in one of the upper ports of the ITER Tokamak.

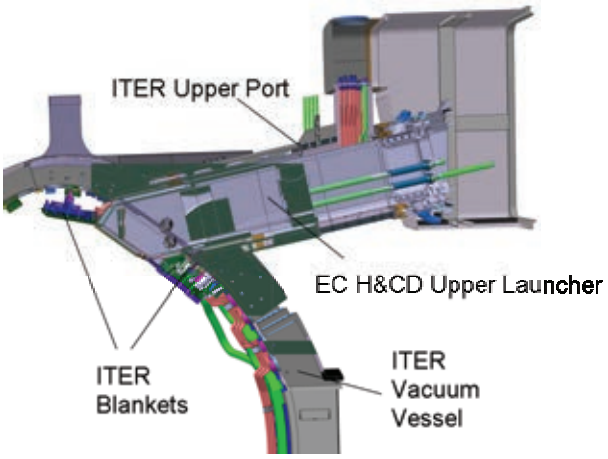

Fig. 1: Outline of the ECRH Upper launcher.

Preliminary design of an EC H&CD port plug

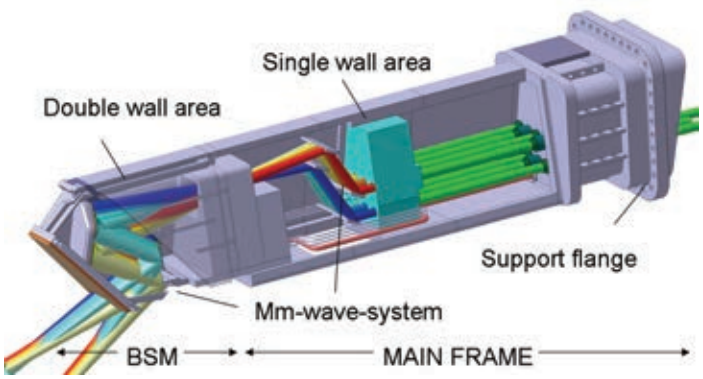

Fig. 2: The EC H&CD upper launcher.

The outer structure of the launcher consists of two main components, the plasma-facing Blanket Shield Module (BSM) and the launcher main frame, and is designed as a cantilevered beam, bolted at the port extension of the vacuum vessel [1]. The launcher has to withstand very high moments during plasma disruptions [2], causing strong bending of the launcher [3]. In the front area of the launcher, very high nuclear heat loads will occur. These heat loads decrease with radial distance from the plasma. For the specific part of the launcher structure directly behind the BSM, a double-wall frame has been designed, consisting of two shells of stainless steel with ribs in between, forming meandering cooling channels. Figure 2 gives an outline of the present launcher design.

Motivation for double wall prototyping

The mechanical design of the ECRH port plug structure introduces high-level requirements for potential manufacturing procedures. The very high mechanical loads during plasma disruptions require a rigid structure to comply with the maximum allowable limits of deflection of the plug. The welding of such strong joints usually causes shrinkage and distortion of the welded structure, while the installation of precisely performing mm-wave-components requires high dimensional accuracy. Therefore prototyping is mandatory to gain experience on the behavior of the component during manufacturing. To benefit optimally from the results of prototype manufacturing, a full-size mock-up of the double wall segment was envisaged to

provide maximum experience on the influence of the welding parameters, shrinking effects and dimensional accuracy. The double-wall prototype is also foreseen to be tested at the Launcher Handling Test Facility (LHT) at KIT, where structural components can be tested under ITER operating conditions [5] to verify simulations on heat removal and flow characteristics of coolant.

Design of the double wall prototype

The design of the prototype was basically derived from the preliminary design of the double wall area of the launcher. It consists of two shells, forming the trapezoidal contour of the mock-up, and two cover plates at the front and the rear side of the prototype. The gap between the shells is used as cooling passage. To verify the heat removal performance of the prototype, standard flanges at the entrance and the exit of the cooling path provide connections for proper installation at LHT [6]. Figure 3 illustrates the design and the coolant flow scheme.

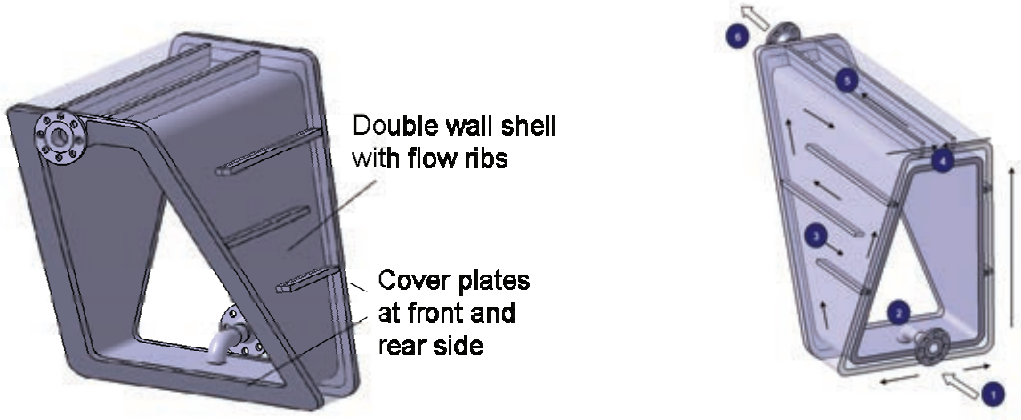

Fig. 3: Double wall section prototype with coolant flow scheme.

The coolant enters the prototype in the bottom area and is branched off into two symmetrical channels to provide homogenous cooling for both of the side walls. The cooling water is recombined again in the top area to leave the prototype at its front side. Ribs between the sidewalls and in the top area are forming meandering channels. To avoid dead-flow zones in the corners, leakage gaps between the ribs and the cover plates are foreseen.

The typical dimension of the prototype is 1200 x 1100 x 800 mm³. The wall thickness is 30 mm, while the distance between the shells (and thus the width of the cooling channels) is 20 mm. The mock-up was considered to be made from ITER-grade stainless steel. However, the availability of this material is very restricted, thus the use of stainless steel 316L, which has rather identical chemical and mechanical properties, is envisaged.

Manufacturing concepts

After the successful manufacturing of the single wall prototype [7] by MAN Diesel & Turbo in Deggendorf/Germany, it was decided to continue this collaboration. Based on the KIT design, MAN D&T developed three different manufacturing strategies for the double wall mock-up:

- *Design with ribs*

The inner shell is welded out of two bent shells. Ribs will be welded onto the inner shell. They are designed to provide the mechanical stiffness and rigidity of the assembly. The outer shell consists of four parts, of which the lateral segments feature dedicated cut-outs for proper connection with the ribs. The double wall structure is closed by plates on the front and the back side.

- *Design with studs*

The inner and the outer shell consist of two bent shells each. Welded bolts between the shells provide mechanical integrity of the structural system. Dedicated baffles between the shells form the coolant flow duct without rigidly coupling the casing elements. The double wall structure is closed by plates on the front and the back side.

- *Design by deep-drilling*

The basic profile of the trapezoidal structure will be made by welded sheets. Cooling channels are machined into these sheets by deep-drilling. The cooling channels will be connected by machined manifolds on both face sides. As for the other design concepts, cover plates close the body.

A first evaluation of the three different manufacturing variants was performed. It turned out, that the design variant with ribs requires a big amount of weld metal deposit, which would cause unacceptable deformation of the casing; therefore this variant was abandoned. To compare the two remaining manufacturing routes, it was decided to fabricate two pre-prototypes on a small size level, representing a section of the prototype side wall. The typical dimensions of the pre-prototypes are 1000 x 500 x 80 mm³, including the sharp bend profile of the prototype, thus the challenging geometry of the original cooling channels will be simulated as well.

Analysis and manufacturing of pre-prototypes

Pre-prototype with stud design

For proper removal of heat loads, it is necessary to have an optimum arrangement of the studs and the ribs to get a uniform velocity profile of the cooling water flow. Therefore the flow characteristics were analyzed by numerical simulation. The basic model features three meandering flow channels with a cross-section of 20 x 125 mm each. The ribs are just linear joints between the studs. In the flow reversal areas, there are leakage gaps with 5 mm width. The coolant mass flow is 2.25 kg/s. Figure 4 shows the simulation of the coolant flow.

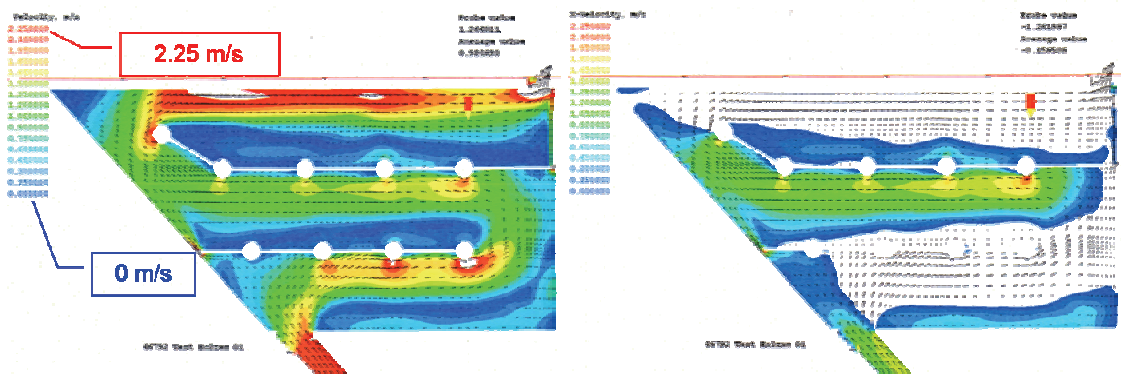

Fig. 4: Flow regime of the basic model (stud design).

The figure on the left hand side shows the coolant velocity related to flow direction. It illustrates the substantially inhomogeneous distribution of the water flow. The right hand picture shows the x-vector. The blue areas in the lower and the upper channel and the non-colored area in the mid channel show even effects of return flow. The first leakage gap between the first and the second channel works very well, while the second one between the second and the third channel is almost without effect due to very low flow velocity. The pressure loss within the basic model was calculated to 0.015 MPa. The flow characteristics of the basic model will lead to very inhomogeneous cooling with potential hot spots in the structure. To optimize the cooling performance, additional baffles were installed in order to homogenize

the flow. This was done in an iterative process to find the optimum arrangement of the baffles.

The installation of the baffles led to a considerable uniformity of the velocity profile, except in the sharp edged bends at the entrance and between channel two and three, where strong gradients occur. However, this effect is even advantageous, because these gradients activate turbulences and thus improve the heat transfer. For comparison purposes, the ribs close to the plugs were only installed in channel one and two. The left hand picture in figure 5 shows the total velocity of the optimized flow regime. As above, the right hand picture shows the x-vector and indicates the disappearance of the return flow. An additional positive effect of the baffles is the decrease of the pressure loss, which is about a third less than for the basic model and adds up to approximately 0.01 MPa.

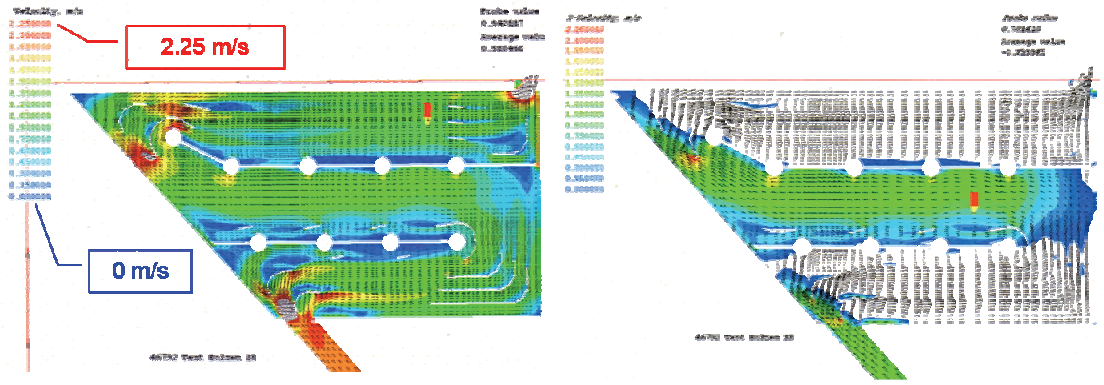

Fig. 5: Flow regime of the refined model (stud design).

The plug design was manufactured of 30 mm stainless steel plates. The basic shapes of the plates were formed by jet-cutting. The plugs were machined from rolled steel. Appropriate weld preparation was performed and a specific sequence of the welding was applied to minimize shrinking and warping of the component. Finally, the manifolds on both face sides were closed by welded cover plates.

Pre-prototype with deep-drilling design

The deep-drilled pre-prototype was manufactured out of 80 mm stainless steel plates. The basic shapes of the plates were formed by jet-cutting. For the given dimensions, the deep-drilling could be performed in one working step; thus a stageless shape of the bores was achieved. The manifolds on both face sides were closed by welded cover plates.

The deep-drilled pre-prototype features three meandering coolant channels, each formed by four parallel deep-drilled bores of 30 mm diameter. The distance between the longitudinal axes of the bores is around 36 mm. Combining four bores to one cooling channel results in a cross section of about 2800 mm², which is slightly larger than for the plug design. Also the leakage gaps were designed.

The fluid dynamics simulations were performed. The basic model features three meandering flow channels, each consisting of a bundle of four cylindrical sub-channels. The coolant mass flow is 2.25 kg/s. Figure 6 shows the results of the fluid dynamics simulations.

It can be shown that substantial discrepancies in terms of flow velocity and pressure occur inside the different cylindrical sub-channels. The right hand sided illustration in figure 6, where the x-vector of the coolant flow is given, shows an extremely critical situation in the first cooling channel, where a return flow can be observed in the lowermost sub-channel. Thus a certain ratio of the coolant forms a loop, which reduces the cooling capability significantly. This effect can also be observed in the second channel (obviously in opposite direc-

tion). In the third cooling channel no return flow occurs, however there are strong differences of coolant velocity from 0.3 m/s up to 1.3 m/s.

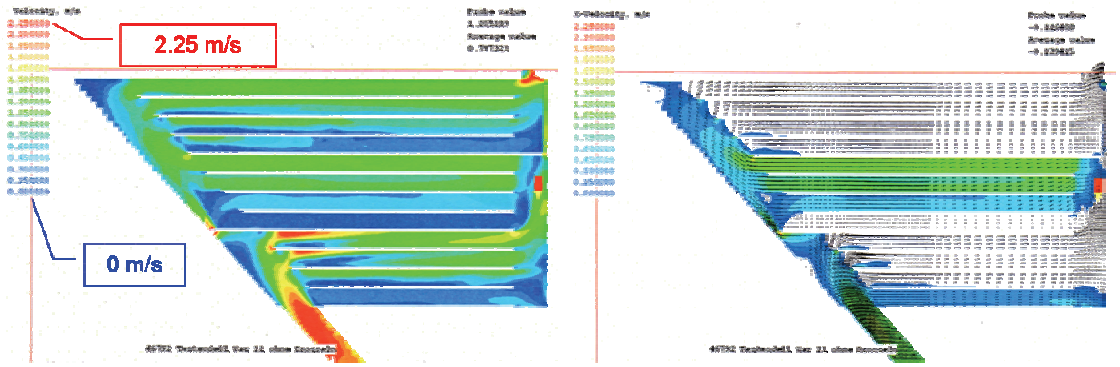

Fig. 6: Flow regime of the basic model (deep-drilled).

To optimize the flow characteristics of the deep-drilled pre-prototype, throttles were inserted into the particular sub-channels. After performing several iteration steps, an optimum combination of throttles of different sizes was found to provide a flow regime of reasonably homogenous properties. The pressure loss of this model was calculated to be less than 0.007 MPa. Figure 7 shows the flow velocities along the cooling channels and the almost uniform flow directions inside the sub-channels.

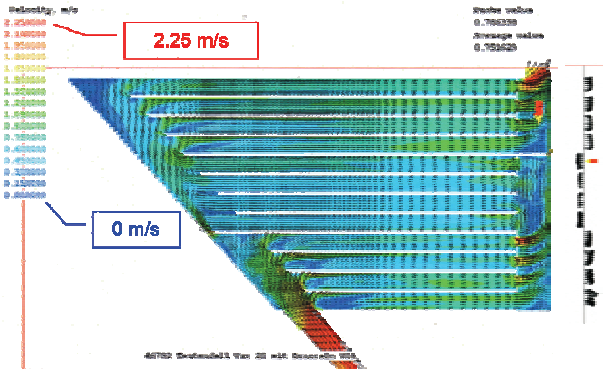

Fig. 7: Flow regime of the refined model (deep-drilled).

Comparison of the pre-prototypes

Based on the fluid dynamics simulations and the manufacturing of the pre-prototypes, an evaluation of the manufacturing routes was made. The fluid dynamic simulations showed insufficient flow regimes for both of the basic design approaches. However, by placing baffles (for the stud design) and throttles (for the deep-drilled design), the coolant flow can be optimized to guarantee proper removal of nuclear heating. Having done this, both pre-prototypes show good flow characteristics and shall be deemed as equal, however the pressure loss is around 30% smaller for the deep-drilled one.

The difference on manufacturing effort is substantial. Total manufacturing time is about twice for the stud design, compared to the deep-drilling design. Due to the significantly lower number of welded joints, the geometrical accuracy of the deep-drilled layout is superior to the stud design. To match the required tolerances, additional machining of the surfaces would be necessary for the stud design. However, additional machining, in particular polishing, is necessary anyway to fulfill the surface quality requirements of structural In-vessel components under vacuum conditions [8]. The machining of the circular cooling channels matches the tolerances within 1 mm. The material consumption is slightly higher for the deep-drilled variant.

Conclusion and next steps

To verify the preliminary design of the ITER EC H&CD upper launcher and to identify optimum manufacturing procedures for rigid port plug structures, prototyping of dedicated segments of the launcher structure is mandatory. For the double wall segment of the launcher

main frame, a manufacturing study is under progress. To identify the preferable design and the optimum manufacturing route, two pre-prototypes were sketched and manufactured. Fluid dynamic simulations have been performed in order to evaluate and optimize the cooling performance of the different designs. Both prototypes were delivered in July 2011 by the manufacturer MAN Diesel & Turbo Deggendorf to KIT, where they were recently tested. Based on these test results the decision about the manufacturing route for the full size prototype will be made [9].

Staff:

G. Aiello
A. Meier
T. Scherer
S. Schreck
A. Serikov
P. Späh
D. Strauss
A. Vaccaro

Industry cooperation with:
MAN Diesel & Turbo, D-94452 Deggendorf, Germany

Literature:

[1] P. Spaeh et al., The ITER EC H&CD upper launcher: Structural design, Proceedings of the 26th SOFT conference, Porto, Portugal, 2010

[2] A. Vaccaro et al., The ITER EC H&CD upper launcher: Transient mechanical analysis, Proceedings of the 26th SOFT conference, Porto, Portugal, 2010

[3] D. Strauss, Deflections and Vibrations of the ITER ECRH Upper Launcher, EC-16 meeting, 12-15 Apr. 2010, Sanya, China

[4] A. Serikov et al., Nuclear-Safety-Related and Shielding Analyses of the ITER Quasi-Optical ECH Launcher, IEEE Transactions on Plasma Science, V. 38, Issue 3, 224 (2010)

[5] S. Schreck et al., Prototype manufacturing and testing of components of the ECH upper launcher for ITER, 23rd IAEA Fusion Energy Conference, Daejeon, Korea, October 11-16, 2010

[6] T. Scherer et al., Prototyping and testing of ITER ECH upper launcher components, 21st Joint Russian German workshop on ECRH and gyrotrons, Greifswald, Germany, May 11-16, 2009

[7] P. Spaeh et al., Manufacturing studies of structural components for the ITER EC Upper launcher", ISFNT-9, 2009, Dalian, China, Fusion Engineering and Design 85 (2010) 1406–1409

[8] G. Aiello et al., Outgassing measurements for the ITER EC H&CD upper launcher, 23st Joint Russian German workshop on ECRH and gyrotrons, Karlsruhe, Germany, May 23-28, 2011

[9] P. Spaeh et al., Manufacturing studies of double wall components for the ITER EC H&CD Upper Launcher, Proceedings of the ISFNT-10, 2011, Portland, US.

Acknowledgement

This work was financially supported by the Ministry of Research and Education (BMBF) under the grant No. 03FUS0010. The views and opinions expressed herein do not reflect necessarily those of the BMBF or the European Commission.

Goal Oriented Training Network on Remote Handling (WP10-GOT-GOTRH)

Overview

The aim of the EFDA Goal Oriented Training Network on Remote Handling (RH) "GOT RH" is to train engineers for activities in support of the ITER project and the long-term fusion programme within the European Associations, Fusion for Energy, the ITER Organization, and industry. The GOT-RH is a practical level project for increasing the coherence of RH training within a collaborative context, involving 5 EURATOM Associations: TEKES - Finland; coordination, CEA - France, CIEMAT - Spain, FOM - Netherland,and KIT - Germany. The project, which will last for 3 - 4 years (depending on the time neded for the recruitment of the trainees), was started on October 1st 2010.

Planned activities and status

The work of GOT RH is organised in three work packages. WP1 covers case studies with mentoring support on the ITER RH system requirements with concept and design development including virtual reality (VR) prototyping. WP2 is dedicated to the ITER RH control system requirements, architectures and designs including VR prototyping. WP 3 includes high level training courses and workshops.

The KIT trainee will be involved in the topic *"Maintenance of components of the ECH Upper Port Plug",* which is part of WP1. The aim is to identify the major requirements and to elaborate RH procedures for providing a high availability of the ECH Upper Port Plug system.

The trainee will work on two basic aspects of remote handling: first on the optimization of the Upper Port Plug design (components and structure) with respect to remote handling procedures, and second, on the use of standardized tools where possible, and the development of specialized tools where necessary. Additionally, he will get familiarized with F4E's quality management. The training includes stays at the partner laboratories and attending the project meetings, the participation to relevant conferences (e.g. SOFT, SOFE) and the presentation of the work progress at the RH workshops of the GOT-program.

The KIT trainee has started his work on the 1st of September 2011.

The first event of the common training for the GOT-RH Trainees (WP3) was the 5th Karlsruhe International School on Fusion Technologies, Karlsruhe, September 19-30, 2011, which was attended by the GOT-RH trainees from TEKES, CIEMAT and FOM as well.

In this early stage until the end of 2011, the training was concentrated on the introduction to design and analysis tools (e.g. CATIA V5 and ANSYS), to ITER design (UPP and HC) and to DEMO/FPP conceptual design, on the acquisition of basic knowledge on the ECH-UL system and on Remote Handling issues (including review of ITER documentation).

Staff:

G. Grossetti (trainee)
S. Schreck

Acknowledgement

This work, supported by the European Communities under the contract of Association between EURATOM and Karlsruhe Institute of Technology, was carried out within the framework of the European Fusion Development Agreement. The views and opinions expressed herein do not necessarily reflect those of the European Commission.

Candidate Remote Maintenance Schemes and Solutions (WP11-DAS-RH-00-01, -01-01, -04-01 and -06-01)

Introduction

This Task Agreement describes the review and assessment work to be conducted as part of the EFDA Power Plant Physics & Technology Work Programme 2011, to evaluate the remote maintenance schemes for future Fusion Power Plants (FPPs). Although the main emphasis is on the maintenance of in-vessel components, future work will encompass ex-vessel activities linked to the maintenance of in-vessel components, in particular transport between the vessel and the hot cell, and suitable ex-vessel maintenance activities. The proposed review activities on RAMI and on standardisation should therefore not be limited to in-vessel maintenance operations. The review is being co-ordinated jointly by a representative of the Associations and a representative of industry.

Part of these activities will also contribute to the execution of the DEMO Design Activities (DDA) in the IFERC Project under the Broader Approach (BA) Agreement, whose implementation is under the responsibility of Fusion for Energy. Following the F4E Governing Board Decision approving a proposal from F4E to seek the collaboration of EFDA for the implementation of the DDA, the EFDA Steering Committee agreed to conduct these activities within the PPPT programme.

WP11-DAS-RH-00-01: Task Coordination

The different activities to be carried out within this task need overall coordination. In particular, it has to be noted that in some cases, several associations are participating in the execution of each subtask, and therefore special care has to be devoted to ensure efficient communication between the various groups in order to maximise synergies and avoid duplications.

WP11-DAS-RH-01-01: Review of the ITER/PPCS divertor maintenance scheme

An updated review of the applicability of the ITER divertor maintenance scheme shall be carried out including an analysis of the availability, feasibility and reliability of the system.

Activities to be planned for the period of 2012-2013 shall be defined according to the analysis above.

WP11-DAS-RH-04-01: Connection of in-vessel components

Connecting technologies are critical to all remote maintenance approaches.

The operation of a fusion reactor will create unprecedented levels of neutron damage and transmutations in the steel of the cooling pipes and the structures, affecting the quality and reliability of the welds contained. Furthermore, the high background radioactivity will have a impact on the posibility to conduct volumetric weld inspection by conventional means.

Therefore, the following studies are foreseen to define further studies in 2012-2013:

- Literature study to evaluate the impact of transmutation on weldability. Consultation with industry is advisable to examine alternative weld technologies, their relative heat input to the joints and the consequential impact on re-weldability. Alternative joining techniques such as metal seals or others shall be examined to make an initial assessment of their applicability for the anticipated temperature, pressures and radiation levels in a DEMO environment, and to different cooling media (water, Helium and liquid metals).

- Literature search and review to evaluate which technologies could be applied to conduct weld inspection within the DEMO environment.

WP11-DAS-RH-06-01: Preliminary Definition of the DEMO Port Plugs

This sub-task is an attempt to preliminarily define the DEMO port plugs. Significant differences are expected between the pulsed and the steady-state options, so that these two approaches have to be considered separately.

The activity includes the preliminary definition of the port plugs opening number and size in the pulsed and steady state DEMO cases. Input from other groups working on assessment of H&CD systems and from the task coordinator is expected.

The blanket MMS segmentation, that was analysed in the PPCS study, was rather optimistic with respect the toroidal space assumed, that is needed to accommodate the toroidal field coils: the approach was based on certain assumptions with respect the main reactor configuration. The assumptions made for the segmentation of the MMS have to be revisited, considering the differences expected between pulsed and steady state devices. In particular, the expected impact of the change in the Port Plug dimensions and number has to be taken into account, checking to which extent the flexible conceptual design proposed for the MMS segmentation can be adapted. From the results of this sub-task, further work to be carried out in 2012-2013 shall be identified.

Status of work

First activities were started after the kick-off meeting in October 2011; the final report is to be delivered in March 2011. A follow up contract by EFDA is in preparation.

Staff:

M. Mittwollen
P. Norajitra
D. Strauß

Acknowledgement

This work, supported by the European Communities under the contract of Association between EURATOM and Karlsruhe Institute of Technology, was carried out within the framework of the European Fusion Development Agreement. The views and opinions expressed herein do not necessarily reflect those of the European Commission.

Review of the Vertical Maintenance System Concept (WP11-DAS-RH-02-01)

Introduction

In a Fusion Reactor the plasma facing components (mainly Blankets and divertors) are subjected to intense neutron, thermal, EM and particle loading. All these loads constitute a limitation in the lifetime of these components. This leads to the necessity of a scheduled replacement of them during the lifetime of the reactor. The replacement operation of the blankets has analogy to the re-fuelling of a nuclear reactor; the plant has to be shut-down for a relatively long time, the Vacuum Vessel (VV) should be open and high irradiated parts of the reactor core need to be assembled / disassembled in Remote Handling (RH) procedures. Analogous case is the divertor; due to intense particle loading the expected lifetime of solid target plates is limited to few full power years (FPY); this means that the divertor components will require several replacements during the reactor life. The duration of these replacement operations will constitute the major contribution to the reduction of availability of the reactor and it is considered one of the major issues that have to be solved in the fusion plant design in direction of an economical viable energy source.

Very few concepts of reactor maintenance have been proposed and studied in detail. One of this is the Vertical Maintenance System (VMS) that has been adopted in almost all EU studies as reference concept for DEMO and for a Fusion Power Plant (FPP). This concept was adopted in the NET project, in ITER CDA and later in the DEMONET version that was the basis for the European Breeding Blanket Development up to 2000. Only during the PPCS studies an ITER-like system (“large modules”) has been used as basis for the comparison of the different reactor models. In successive studies the VMS was again considered as reference concept; like in the short DEMO studies of 2006-2008. In this study a model of reactor was elaborated by EFDA (EFDA design 2007) on the basis of PROCESS system code optimizations. The final DEMO conceptual results on in-vessel integration issues have been developed by different organisations (KIT, CEA and EFET) following the same requirements and the same parameters to obtain consistent outcoming. KIT elaborated a conceptual design of DEMO that is illustrated in Figure 1.

The VMS is based on large vertical ports located at the top of the VV in the space between two adjacent TF-coils; this allows to extracting the blanket that is segmented in vertical elements. Usually each blanket sector (16 sectors in a 16-TF-coils-machine) is divided in 5 vertical segments (3 outboard and 2 inboard segments) that are small enough to be extracted from the port. In-vessel movements of the segments are supported by RH-machines operating inside the vacuum vessel. The vertical ports are used also to route the pipes coming from the segments allowing a direct access to the pipe connection for cutting and re-welding operations.

In general the divertor concept is excluded from this type of maintenance. Single null reactor configurations with a divertor in the lower part of the VV require a separate maintenance system that in general is based on cassette like in ITER. However, the rail of the cassette system can be integrated in the VMS giving the support for in-vessel machines necessary to move the segments inside the VV.

The classical VMS implementation requires the opening of all the 16 vertical ports and the use of all these ports for the segment extraction. In this case large casks are adopted to transport the blanket segments to the Hot Cell Facility (HCF) avoiding contamination of the reactor buildings.

Discussion

The VMS concepts is one of the most studied concepts of DEMO/FPP maintenance; it gives a conceptual solution to several key issues in the fusion reactor maintenance:

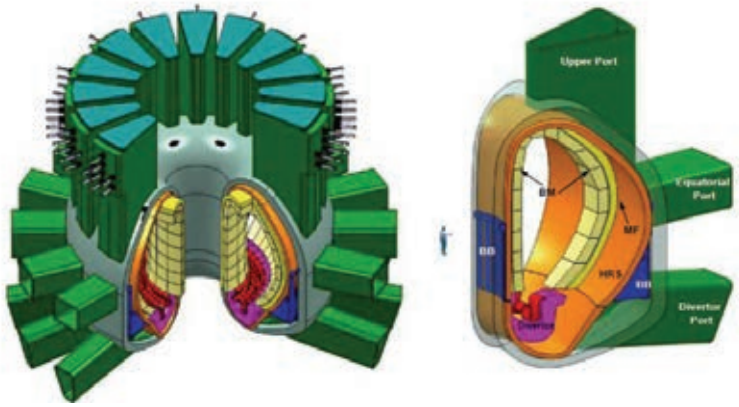

Fig: 1: KIT DEMO lay-out (E. Magnani et al.: Design conflicts arising between different tasks for in-vessel integration DEMO conceptual studies, EFDA TW6-TRP-007-D2-D3, Final Report (2008).

- Necessity to reduce drastically the replacement time for components of the power core like blanket and divertor systems whose lifetime is much lower than the foreseen plant lifetime (condition that become more mandatory increasing the performance of the plant in direction to an economically viable FPP). For this reason it is required to reduce the number of replaceable units, reducing handling operations in VV of hydraulic, mechanics and electric connections. The standard VMS concept (applied to a 16-sector-reactor) requires 80 segments each with own independent hydraulic connections (e.g. for cooling and tritium extraction purposes).
- Necessity to have good accessibility of the connections of the replaceable units and protect them vs. neutron heating and damages. This requirement calls for moving these connections in outer part of the in-vessel region (beyond shielding structures). In particular reweldable connections should be protected by He transmutation reactions and RH attachment by neutron heating and damages. In the VVS the hydraulic connections of the segments are moved in the vertical access port in a zone of relatively simple accessibility and lower radiation field.
- Possibility to use a crane for the movemnt of the large segments that is enabled by a vertical access to the power core.
- Possibility to design all the parts of the removable units at the same lifetime class avoiding operation of refurbishment in hot cell for reusing less irradiated sub-components. In any case blanket and divertors (for which a large difference in the lifetime is foreseen) are almost independently handled (vertical port only for the blanket and lower ports for the divertors). Also the thickness of the blanket segments can be tailored in order to optimise the volume of the materials that need to be frequently replaced.
- The mentioned studies have also highlighted the drawbacks and issues related to this concept. The following list is not exhaustive:
- Necessity to handle very large and heavy components through relatively small access ducts with high precision. In particular the movement required by these components in the vessel is complex. Only the mid outboard segments could be moved in a straight vertical movement; for the others it is necessary to move the sector in toroidal-radial direction to reach their final position in the reactor. Additional movements will be also necessary to cope with the selected attachment system. The kinematic has to be studied in more detail and the assistance inside of the VV of RH machine seems essential.

- The removable units have to be mechanical attached to the VV to withstand several large loads (e.g. EM loads). The design of this attachment system is complicated by the thermal mismatch among the inner power core at high temperature (it is required to have sufficient efficiency of the power generation system especially in FPP conditions) and the outer power core that can be fixed to the VV at lower temperature level (usually 100-150°C). In DEMO-2007 two concepts have been studied: High Temperature and Low Temperature Shield. An assessment of the two concepts has been done in the past and in the frame of this work. The conclusion of the authors indicates an advantage of the first, for the following reasons:
  - relatively simple basic idea of attachment with shear keys and bolts (at the bottom) between parts that can be kept at the same temperature level.
  - simpler RH machinery, it can be avoided to have a separate, special robot in the upper region;
  - no necessity of additional connections among group of elements;
  - no separate cooling is required for the attachment elements, they can be integrated into the general cooling system of the MMS;
  - more precise installation, no link between installation errors
  - attachment more adaptable for “special cases” (e.g. considering insertion of Port Plug based systems)
  - bending bar behind the shield, can be a lifetime component
- The maintenance scheme doesn’t allow a selective replacement of segments (e.g. in case of unscheduled maintenance due to component failure). Also in the “standard” system in which all the vertical ports are used for maintenance, other segments in the ports have to be removed before to accessing the “faulted” one.
- The opening of all the ports for replacement poses issues that are often underestimated. The opening of a single port is a major undertaking due to several operations that have to be done (e.g. opening of confinement barrier, removing piece of shield and pipes, cutting of closure plates, installing a double port system) and their implication to the safety regulations in force. It could be requested to reduce the number of maintenance ports (e.g. to only 2). This possibility has been examined and its feasibility is linked to the addition of further restrictions like a more demanding geometry of the segments and more complicated kinematics in the VV to reach the maintenance port.
- The external logistic is also very demanding in order to manage the transfer of the large segment between reactor and Hot Cell Facility (HCF). Two different concepts have been analysed in the context of the 2-port-maintenance concept: namely the corridor and the cask concepts. No study is known for the “all-ports” concept. The conclusions are at the moment only at a very preliminary stage, but several issues are already envisaged.
- The impact on the HCF requirements (in term of space, time and equipment) has not been studied in detail. Each proposed variants of each steep of the maintenance concept can have very different outcome. In general the requiremnt in term of space seems to be very demanding (but this is also for other maintenance concepts). If no refurbishment of the MMS is required as scheduled operation, some requiremnt can be relaxed. However, precise requirement for wasting (or recycling) of materials after irradiation are still incomplete to start a detailed study.
- Impact of radiation field on the RH operations and machinery. The compatibility of the DEMO/FPP environment to these operations has to be investigated. It is certainly orders of magnitude more sever in comparison to ITER; in DEMO will be strongly dependent on the preformance of the selected machine.
- Impact of different auxiliary systems like the H&CD and Control Diagnostic to the VMS. These systems are assumed to be allocated in dedicate VV ports and their maintenance

should be based on a Port Plug maintenance approach. Conflicts with the segmentation of the power core and with the pipe routing have been already identified.

Conclusions

Looking at the different studies done in the last 30 years on maintenance systems for DEMO/FPP like the VMS or the Large Sector Maintenance Systems, it is difficolt at this moment to proceed to a selection of a “reference” DEMO maintenance concept as all the needs to be further developed and transferred to a future high performance FPP; in fact to many issues are unsolved as far as we move from the ITER machine in direction on more high-performance (e.g. in term of neutron fluences or thermal level) configurations. Furthermore, reliability consideration should be integrated in more consistently into the design. The solution for the blanket/divertor maintenance is and will remain in the next years a critical issue for the development of the fusion reactor and will necessitate the investment of large effort and resources.

As far as the VMS is concerned, it is one of the few promising concepts that can solve the major requirements of the FPP. It is suggested that intense work is dedicated on this in order to clarify all the remaining unsolved issues. A list of then can be deduced by the discussion in this task; the main points can be highlighted (many of these are interconnected) in order to arrive to a conceptual design:

- Clarification of the requirents for the maintenance system according to the selected DEMO/FPP configuration. Different requirements can lead to the selection of different solutions whilst under certain reactor working condition cannot be adopted by other configurations.
- Revision of the RH kinematics of the segments and of the attachment sequences in the HTS and LTS options. Definition of feasibility criteria.
- Study of mechanical attachment systems. This include bending bar, shear-keys, bolts, etc.
- Study of hydraulic connection systems for different kinds of pipes.
- Concepts of in-vessel and ex-vessel machine and equipments to accomplish the VMS. Study of compatibility with proposed fusion reactor environments.
- Revision of the feasibility of a power core segmentation in order to minimise the number of segments.
- Revision of the design of the MMS in order to optimise the dimensions and weight.
- Study of external logistic taking into account different number of maintenance port options (e.g. 2 ports in comparison to all-ports, but only 2-3 under parallel maintenance). This is connected also to the feasibility of a cask concept for transfering the MMS to the HTF. Feasibility of a corridor concept possible for the “all-maintenance-ports” VMS.
- Study of HCF requirements for different variants of VVS replacement concepts (e.g. number of maintenance ports, segmentation).
- Impact on the VMS of the integration of auxiliary systems like the H&CD and Control Diagnostic.
- Impact of the maintenance to the design of the blanket and divertor components and vice versa.

Staff:

L.V. Boccaccini
F. Cismondi
D. Nagy (HAS)

Acknowledgement

This work, supported by the European Communities under the contract of Association between EURATOM and Karlsruhe Institute of Technology, was carried out within the framework of the European Fusion Development Agreement. The views and opinions expressed herein do not necessarily reflect those of the European Commission.

Alternative Plant Architectures: Review of the Large Port Maintenance System Concept (WP11-DAS-RH-03-01)

Introduction

Among the very few concepts of reactor maintenance that have been proposed and studied in more detail, the Large Port Maintenance System (LPMS) has been adopted and investigated in the majority of US and Japanese Power Plant Studies, namely the Japanese DREAM, CREST and SlimCS and the US ARIES-RS and ARIES-AT. The implementation of the LPMS has been is based on principles that are summarized and discussed in the following:

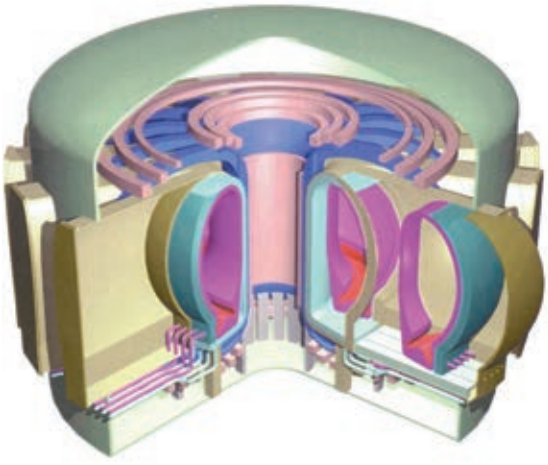

Fig. 1: Schematic view of the large port configuration.

Large Equatorial Ports: Extending the radial outboard dimensions of the VV, it is possible to realize ports between two adjacent TF-coils able to allow the extraction of a complete power core sector in a direct radial movement. The principle is illustrated in Figure 1.

Toroidal Segmentation. The tendency is to reduce the number of sectors (and so of TF coils). 12 sectors were considered in DREAM and in the most recent SlimCS, 14 in CREST, while 16 are assumed in both US ARIES studies. This reduction is advantageous under the point of view to reduce the number of required maintenance actions.

Magnetic System. To allow the extraction of each sector through all the corresponding horizontal ports it is necessary to have a design of the TF coils enlarged in the outboard radial direction. The related supporting structure can be located only in the upper and lower part of the TF in order to not interfere with the large ports leaving the outer legs without supporting. Also the PF coils should be adapted to the necessity of high horizontal port. The PF coil location has to be moved in the upper or in the lower region in order to not interfere with the extraction movement of the sectors.

Vacuum Vessel Design. The horizontal ports should be dimensioned to allow the replacement with a straight radial movement of the whole sector. Several important engineering issues have to be addressed in the design of the VV, like the helium-tight-closure of large opening, the supporting of large VV port extensions in reduced place and pipe routing compatible with RH operations.

Removable Sector design: The removable part (a power core sector) should be realised in a integrate design; this design is in form of a robust poloidal ring. This choice allows to speed-up the replacement time and to design a structure able to withstand large loads (e.g. electromagnetic loads, weight, etc).

Sector support inside the VV: The sectors necessitate a support inside the VV to withstand the turnover torques during central disruption and vertical loads during Vertical Displacement Events (VDE). Some of the designs suggest a radial rail support, DREAM proposed flanges to the other sectors. A good description of requirements and design details is tbd.

Piping lay-out and connections. The different reactor concepts revised in this study have different concepts for the lay-out and the disconnection of the pipe that feed the power core. However, in all the considered concepts the pipes of a given sector are routed inside the re-

lated portion of the VV to the outside. In ARIES-RS, -AT and in CREST the pipes are routed through the VV Closure Plate into a maintenance area realized in the maintenance port duct. This area is closed by a closure plate at the maintenance door. From here, the pipes are routed from the maintenance area into the duct walls so that they can leave the maintenance duct area and keep free the maintenance door. This means that the replacement operation have the following sequence: a) opening of the maintenance closure plate, b) cutting of the sector pipes, c) opening of the VV closure plate and withdraw of the whole sector. In SlimCS only one closure port is considered; the pipes are routed directly through the closure plate and are handled outside the cryostat boundary. DREAM considered pipes routing from the inboard; this concept has been abandoned in following designs as it is difficult to find sufficient space for maintenance operation (and also for piping) in the inboard side.

Sector transport mechanism. To move the sector in radial direction along the port duct, rail system can be used.

Transfer Casks. The most common option proposed to transport the sectors from the reactor to the HCF (and vice versa) is to use large cask. This cask is able to dock to the maintenance port of the reactor and to the HCF door allowing the transfer without spreading tritium and dust. The cask has large dimensions in order to contain an entire sector and the necessary equipment to handle the sector, the closure plates and to connect/disconnect the piping.

Maintenance logistic. All the studies consider in the baseline a HCF maintenance approach. This means that old sectors are immediately replaced with new ones during the maintenance period. This requires a spare sector in the HCF for each port that is maintained in a maintenance period. Alternatives like corridor maintenance have been considered but at the end not included in the baseline.

Plant Availability. All the studies offer estimation of the sector replacement time as well as of the total plant availability. A comparison is difficult according to the different plant design and assumptions used in the assessment. An important parameter to evaluate the availability of the plant is the fraction of power core that is replaced during a maintenance period. Replacement of the entire core reduces the maintenance time in comparison to a fractioned approach. However, in the calculation of the final plant availability other factors have been considered, too. A replacement strategy based on 1/2 of the power core is proposed as the optimised solution according to ARIES-AT studies, while Japanese studies like CREST and SlimCS are based on a full replacement at the operational lifetime of the sector. Also the sector operational lifetime is assumed differently in the studies from 2FPY in SlimCS to 4FPY in ARIES-AT. For the plant for which availability estimation is given the values are between 85 and 93%. EU assessments of these availability values tend to corrected this value down to 77-81%.

Hot Cell Requirements. The impact on the HCF requirements (in term of space, time and equipment) is very strong dependent on the different variants used in the maintenance systems. Each proposed variants of each steep of the maintenance concept can have different outcomes to these requirements. In general the requirement in term of space seems to be very demanding (but this is also for other maintenance concepts). The choice of different fraction of power core that is replaced during a maintenance period has an impact of spares that have to be stored in HCF. 1/1 fraction maintenance is the most demanding in term of spare and space in HCF. Also the design of the replaced sector and the classification of lifetime classes of its components (blanket, divertor, shield, etc) have a large impact on the HCF operations, equipments and space. In any case the refurbishment operation of the sector is judged a long time operation that is usually is done during operation time. This is the reason of the necessity of spares.

Discussion

The Large Port Maintenance System (LPMS) gives a conceptual solution to major key issues in the fusion reactor maintenance:

- Necessity to reduce drastically the replacement time for components of the power core. For this reason it is required to reduce the number of removable units, reducing handling operations in VV of hydraulic, mechanics and electric connections. The standard LPMS concept (applied to a 16-sector-reactor) requires only 16 removable units (sectors).
- Necessity to have good accessibility of the connections of the removable parts and protect them vs. neutron heating and damages. In this concept the main mechanical and hydraulics connection for the sectors are realised in the outer outboard structure of the Blanket well beyond the main shielding structures. Open issue is the necessity to have support structure inside the vacuum vessel for the sectors.
- Avoid the use of RH machines inside the VV. This can be a strong advantage considering the very high dose in the torus that could make it impossible to use these machines.
- Also if the sectors are very large removable units, the replacement movement is only a straight radial extraction/insertion. Furthermore, the units can be supported by the floor with the use of rail concepts that can allow a reliable and precise movement of the structures.

The mentioned studies have also highlighted the drawbacks and issues related to this concept. The following list is not exhaustive:

- The concept requires a particular configuration of the magnet system that leads to larger components. This is of course a complication for the design and adjunctive costs for a system (i.e. the magnet system) that contributes as major item to the cost of the plant (maybe a cost increase of 10%). An engineering challenge is the support of the turnover forces on the outer TF legs due to lack of supporting structure. Also the lay-out of the PF coils should be adapted to the necessity of high horizontal port leading to a more demanding design (i.e. higher currents).
- The design of the VV presents additional engineerig issues: 1) large closure plates that need to be handled and closed helium-tight remotely; 2) integration of large ports on the toroidal structure; 3) realisation of flanges (in particular for doors at the VV radius) in very restricted space.
- The design of transport casks and related handling equipment for very large removable units represent also an engineering challenge. The whole system has to operate completely under RH to accomplish all the operations of handling of large closure plates, cutting/rewelding of pipes, withdraw of sectors, etc.
- The removable units include components of different lifetime classes. To optimise the waste it is necessary to perform several operations of refurbishment in HCF to reuse less irradiated sub-components. This means RH disassembly of used sectors (dividing waste to reusable components) and assembly of new sectors using also already irradiated parts. A modular design of the removable units can help to accomplish this task simplifying the operations.
- Each removable unit has to be mechanical attached to the VV to withstand several large loads (e.g. EM loads) during reactor operation. The studied systems suggested different possibility, like radial rail or flanges. Solutions necessitate to be studied in more detail.
- Inside of a sector an attachment system should be provided between parts at different level of temperature. The design of this attachment system is complicated by the thermal mismatch among the inner power core at high temperature (>300°C, in fact it is required to have sufficient efficiency of the power generation system especially in FPP conditions)

and the outer power core that have to be fixed to the VV at lower temperature level (usually 100-150°C).

- The opening of very large ports is a major undertaking due to several operations that have to be done (e.g. opening of confinement barrier, removing piece of shield and pipes, cutting of closure plates, installing a double port system) and their implication to the safety regulations in force.
- The external logistic is also very demanding in order to manage the transfer of the large sectorst between reactor and Hot Cell Facility.
- The impact on the HCF requirements (in term of space, time and equipment) has not been studied in detail. In general the requirement in term of space seems to be very demanding (but this is also for other maintenance concepts).
- Impact of different auxiliary systems like the H&CD and Control Diagnostic to the LPMS. These systems necessitate penetrations to the in-vessel region from the extern. Conflicts with the sector segmentation of the power core and with the large port ducts have to be carefully considered.

Conclusions

The LPMC is one of the few proposed concepts that offer a solution for the major requirements of the FPP. However, extensive work is necessary to clarify the unsolved engineering issues. A list of them can be deduced by the discussion in this section; the main points can be highlighted (many of these are interconnected) in order to arrive to a conceptual design:

- Clarification of the requirements for the maintenance system according to the selected DEMO/FPP. Different requirements can lead to the selection of different solutions and possible solutions under certain reactor working conditions cannot be adopted for other configurations.
- Study of mechanical attachment systems for the connection of the sectors to the VV. This includes the flange connection and e.g. radial attachment rails.
- Study of hydraulic connection systems for different kind of pipe.
- Concepts of ex-vessel machine and equipments to accomplish the sector replacement. Study of compatibility with proposed fusion reactor environments.
- Study of external logistic taking into account different number of maintenance port that can be operated in parallel. Optimisation of cask number
- Study of HCF requirements for different variants of LPMS replacement concepts.
- Impact on the LPMS of the integration of auxiliary systems like the H&CD and Control Diagnostic.
- Impact of the maintenance to the design of the blanket and divertor components and vice versa.

Staff:

L.V. Boccaccini
F. Cismondi

Acknowledgement

This work, supported by the European Communities under the contract of Association between EURATOM and Karlsruhe Institute of Technology, was carried out within the framework of the European Fusion Development Agreement. The views and opinions expressed herein do not necessarily reflect those of the European Commission.

Goal Oriented Training Programme “ITER Port Plug Engineering” (WP08-GOT-ITER-PPE (FU07-CT-2008-00047))

A revised design approach of the attachment system for the ITER EU-HCPB-TBM based on a central cylindrical connection element

The Test Blanket Module (TBM) is one important component that will be tested in ITER. It has the task to breed tritium, contribute to the shielding and to remove heat from the plasma. Two TBMs are located inside an equatorial port plug in vertical arrangement. The TBMs are connected to the port plug shield by the attachment system.

The TBM is a plasma-facing and therefore a highly cooled component. This leads to a strong thermal gradient in radial direction of the TBM during plasma operation (up to ~250°C). The attachment system has to compensate the differential expansion between the back plate of the TBM and the port plug shield (~120°C). Another operating state with a high temperature difference between the TBM and the shield is tritium outgassing (TBM at 500°C homogeneous temperature, shield 120 °C).

On the other side, high mechanical loads act on the TBM. The mechanical loads that are considered the most demanding for the attachment system are caused by electro-magnetic effects during different operating states and plasma scenarios (e.g. disruptions or VDE) as well as by the dead weight. These loads have to be transferred to the shield by the attachment system.

Different concepts have been developed to address these two contradicting requirements over the past years. The latest development of a concept based on a cylindrical central connection element for the EU-HCPB-TBM is investigated as well as the results of the analyses of a fast Vertical Displacement Event (VDE) type II and the operating state tritium outgassing are evaluated.

The steady-state and transient thermal-structural analyses were performed with the simulation software ANSYS. The connection to the shield was not modeled in detail. In order to reduce the number of elements a shell model of the TBM box has been used for the transient analyses. Due to the uncertainties in the determination of the damping factor, a conservative assumption has been made by specifying only a small numerical damping factor of 0.05 in order to damp the higher frequency modes.

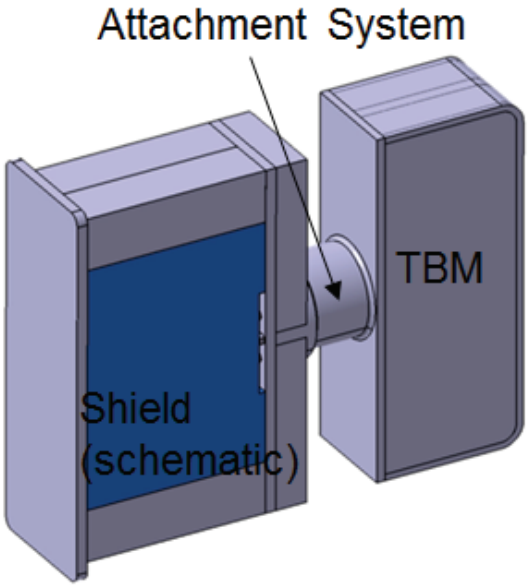

Fig. 1: Cylindrical attachment system between TBM box and a portion of the shield.

The attachment system that connects the TBM box and the shield can be seen in figure 1. The connecting cylinder is welded to the TBM box. In order to avoid welding of dissimilar materials the connection to the shield is established by a splined shaft and additional screws to prevent an axial movement.

The recent design approach is the first one that fulfills the requirements given by the relevant design codes. In a next step, the connection to the shield and the TBM box has to be further developed with focus on feasibility of the manufacturing and the mounting sequence. In addition, the design of the piping between shield and TBM has to be considered in detail.

Staff:

H. Neuberger
C. Zeile

Literature:

[1] A revised design approach of the attachment system for the ITER EU-HCPB-TBM based on a central cylindrical connection element, presented at the 10th ISFNT 2011, to be published in Fusion Engineering and Design, Proceedings of the ISFNT 10.

Acknowledgement

This work, supported by the European Communities under the contract of Association between EURATOM and Karlsruhe Institute of Technology, was carried out within the framework of the European Fusion Development Agreement. The views and opinions expressed herein do not necessarily reflect those of the European Commission.

Goal Oriented Training Programme "ITER Port Plug Engineering" (WP08-GOT-ITER-PPE (FU07-CT-2008-00047))

In the framework of the fusion training programme PPE (Port Plug Engineering) the trainee Gaetano Aiello fills the third work package under the supervision of PD Dr. Theo Scherer. The subject of the package is devoted to materials, manufacturing and assembly of upper port plug structures, with particular reference to the Electron Cyclotron Heating and Current Drive Upper Launcher (ECH&CD UL) in ITER. The trainee finished his training activity in August 2011.

Design of double wall components

Figure 1 shows a cutaway of the upper launcher. The front part of the main frame is exposed to substantial nuclear heat loads up to 0.8 W/cm^3. To meet the high cooling requirements, it is designated as a double wall steel structure with a specific cooling path for the water.

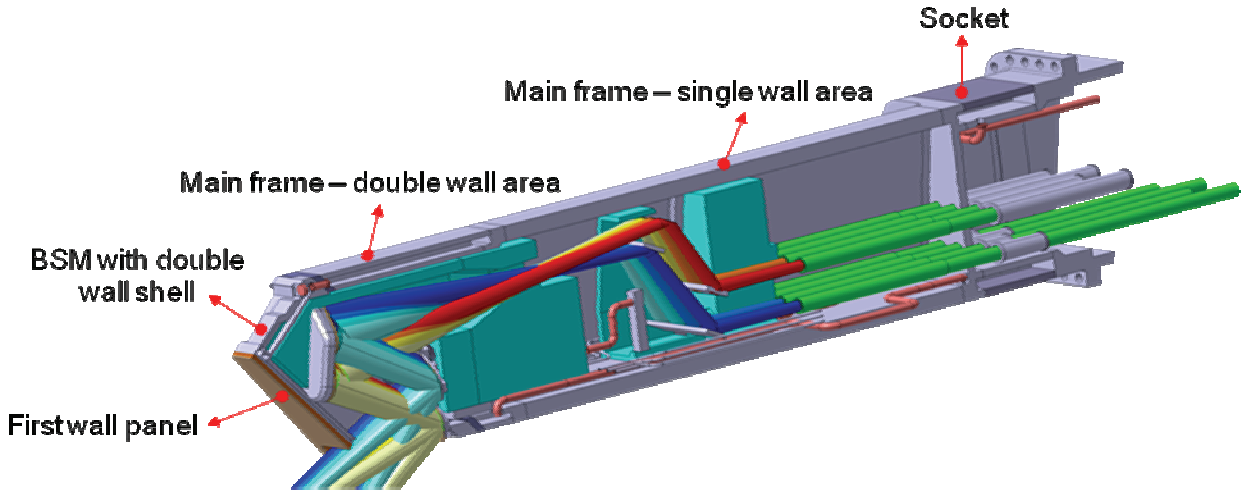

Fig. 1: Cutaway of the upper launcher.

Several manufacturing options are taken into account in order to find the best one in terms of mechanical and fluid dynamic performance, reliability, feasibility and costs. Prototyping and testing are therefore necessary. The industrial partner MAN in Deggendorf is in charge of building two prototypes of this double wall steel structure according to two different manufacturing techniques:

1. SS 316L prototype obtained from a single main body where the cooling path is carried out by deep hole drilling,
2. SS 316L prototype obtained from two parallel plates kept together by welded bolts and where the cooling path is carried out by welding ribs and baffles to the plates.

In the frame of the training programme, the trainee spent three weeks in the company working at the design of the second prototype by using CATIA V5 (figure 2). With the help of MAN experts, he performed the design taking into account the real manufacturing process and the DIN norms. The prototype was manufactured and thermo-hydraulic tests will be carried out in our Launcher Handling Test facility.

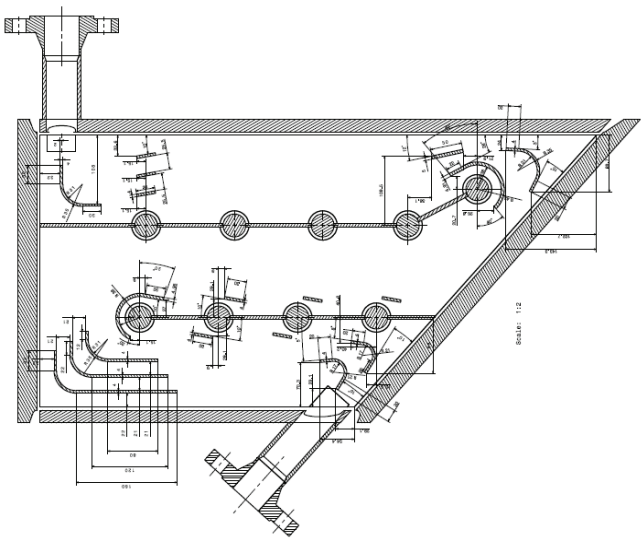

Fig. 2: Section view of the double wall prototype with bolts.

Analysis of a CVD diamond window unit

CVD diamond window units are used for microwave transmission in the ECH&CD systems. The transmission of high power microwave beams through these barrier windows might induce thermo-mechanical stresses in the diamond which, in some cases, can lead to crack formation. The units are usually made up by artificially grown CVD-diamond disks brazed to window housings and analyses are carried out to check the performance of such units during operating conditions.

A double disk CVD diamond window unit was tested at the ASDEX Upgrade tokamak in Garching with a transmitted power of 580 kW at 140 GHz. CFD and thermo-mechanical analyses were performed using respectively ANSYS CFX and ANSYS WORKBENCH to evaluate the thermal deformation and stress fields in the diamond disk.

The analyses regard the disk on the gyrotron side for conservative reasons. Figure 3 shows a section view of half window unit. The diamond disk is 106 mm of diameter and 1.806 mm of thickness with an aperture for the mm-wave beam of 80 mm. Two copper cuffs of 1 mm thickness are brazed to the disk: the inner and the outer cuffs, which are connected to a steel flange respectively through a copper ring and a copper spacer. The spacer helps to more relax the stress distribution in the window unit. The power absorbed by the disk is partially removed by direct contact between the diamond and the water and partially diffuses in the inner and outer cuffs. The water enters the unit from the right side through a pipe inside the flange and first cools the outer cuff and the diamond as a middle cuff is welded to the copper ring. Then, the water cools the inner cuff and leaves the unit from the left side through a pipe inside the flange. The pipes are concentric.

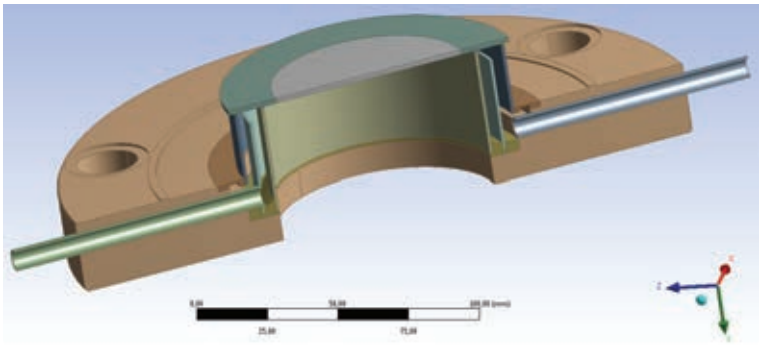

Fig. 3: Section view of half window unit.

The results of the performed analyses show that the temperature gradient in the diamond disk, due to the absorbed power, causes a stress field (first principal stress) with a maximum value of 186 MPa against a fracture limit of diamond of 500 MPa [1]. This maximum stress is located at the brazing region between the disk and the inner copper cuff (figure 4). The maximum thermal deformation is instead located at the border of the disk and it is very small (31.8 µm only).

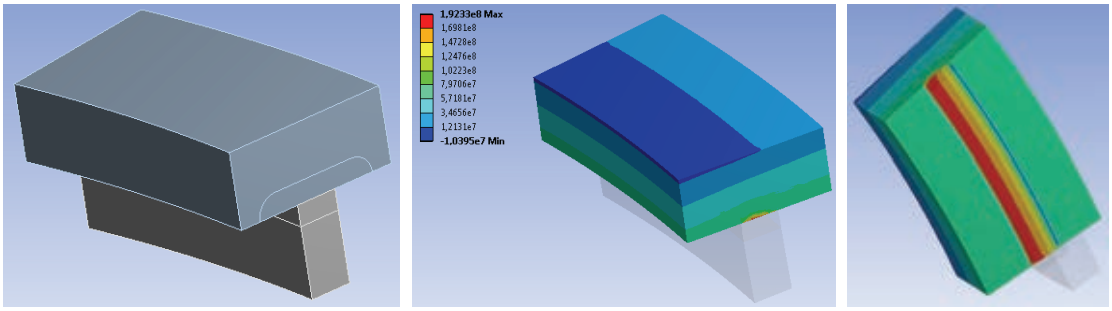

Fig. 4: A submodel was performed in the region of the coarse model where the highest first principal stress is located. It includes a portion of the diamond disk and the inner copper cuff. The first principal stress distribution is shown with values in Pa.

Staff:

G. Aiello
A. Meier
T. Scherer
S. Schreck
P. Spaeh
D. Strauss
A. Vaccaro

Literature:

[1] Thumm M., State-of-the-art of High Power Gyro-Devices and Free Electron Masers, KIT Scientific Reports 7575, Update 2010.

Acknowledgement

This work, supported by the European Communities under the contract of Association between EURATOM and Karlsruhe Institute of Technology, was carried out within the framework of the European Fusion Development Agreement. The views and opinions expressed herein do not necessarily reflect those of the European Commission.

Magnets and Affiliated Components

Conductor Jacket Mechanical Testing Reference Laboratory (ITER/IO/10/4300000292)

Background and Objectives

The stainless steel jacket for the ITER TF, CS, and PF magnet conductors will be procured by six Domestic Agencies from 2010 – 2013. Recent status reports from the DAs indicate that there is significant variation in the test methods employed to characterize the critical mechanical properties of the jacket (yield strength, ultimate tensile strength, and elongation), and further there is significant variation in the final mechanical properties of the material. Given the limited margin in the specification (particularly for yield strength and elongation) and the wide range of test results, it is required to establish a mechanical test reference laboratory to support the standardization of test procedures used to characterize the jacket material, and to deconvolute variation due to real jacket performance from that due to test procedure variation. Further, the ITER requirement for testing of full-size weld specimens at cryogenic (< 7 K) temperatures requires some significant development, particularly for the round-in-round jacket of the TF conductor.

At present KIT is capable of providing both testing of sub-size samples according to ITER standardized procedure, and also testing full-size jacket tubes at helium cryogenic temperatures.

Scope of Work

Under this Framework agreement, a steering committee consisting of one Responsible Officer (RO) from both ITER and KIT shall define Tasks to be completed under the agreement. The scope of the tasks shall include:

- Perform mechanical tests on full-size jacket specimens for ITER conductors.
- Perform sample preparation (stretching, heat treatment, and sample sectioning) of jacket tubes from ITER magnet conductors
- Perform mechanical tensile tests on sub-size specimens
- Perform fatigue (SN) testing on sub-size specimens
- Perform fracture toughness and fatigue crack growth rate testing
- Perform post-testing analysis such as fracture surface analysis by SEM microscopy
- Perform additional characterization as agreed by both parties, such as chemical or micro-structural assessment of the jacket material.

All tests have to be performed at helium cryogenic temperatures (T < 7 K).

Mechanical Investigation of Jacket Material

Several samples of TF, CC and CB jacket material and candidate material was provided by ITER within 2011. Specimens were machined by EDM and tested at 4.2 K. The TF material coming from different DA suppliers (Europe, R. of Korea, China) was investigated and main point was to reach the specification given by ITER, especially the total elongation after heat treatment should be >20%. The suppliers managed to be qualified for TF conductor production. However, controlling the parameters that influence an embrittlement due to cold work and the heat treatment is difficult. To understand the different results from TF material tested, SEM picture are made to investigate the failure surface in detail.

Beside the TF jacket, material of the Correction Coil (CC) and Corrector Busbar (CB) was provided by ITER (origin ASIPP China). Small size specimen for tensile testing at 4.2 K were

machined and tested. In Figure 1 the material and tested small-size specimen can be seen. Table 1 summarizes the results.

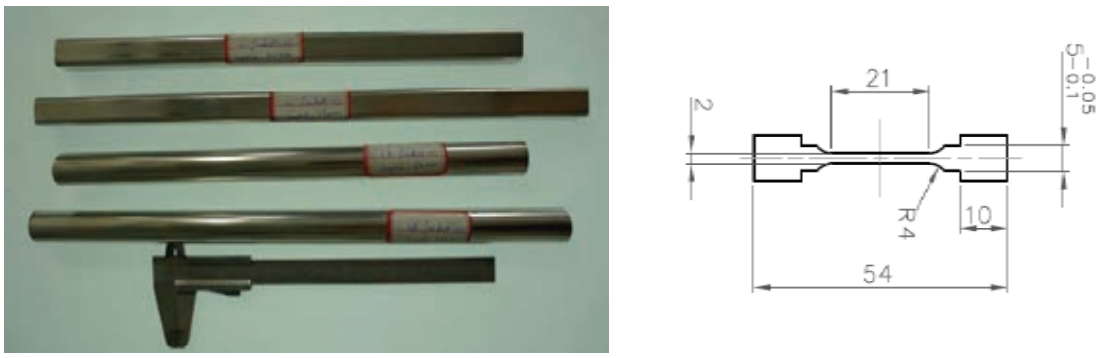

Fig. 1: Jacket material and machined small size specimen for test.

Table 1

File-name	Temperature	Young's Modulus	Yield Strength	Ultimate Tensile Strength	Uniform Elongation	Total Elongation
-	K	GPa	MPa	MPa	%	%
P1(CB)	4.2	211.8	659	1331	38.9	42.3
P2(CB)	4.2	213.0	698	1285	37.1	37.2
P3(CC)	4.2	212.4	697	1641	43.7	44.3
P4(CC)	4.2	184.5	732	1649	39.4	42.5

Cooperation:

Joint work within conductor production. Mechanical analysis of stainless steel 316LN/316L material.

ICAS, Italy
POSCO, R. of Korea
ASIPP, China

Radial plate production material qualification.

Schmiedewerke Gröditz, Germany
METSO, Finland
CNIM, France

Staff:

B. Purr
V. Tschan
K.-P. Weiss
S. Westenfelder

Acknowledgement

This work was supported by ITER Organization under the service contract No. ITER/IO/10/4300000292. The views and opinions expressed herein reflect only the author's views. The ITER Organization is not liable for any use that may be made of the information contained therein.

Mechanical and Physical Characterisation of Materials at Cryogenic Temperatures (F4E-OPE-084 (ES-MF))

Background and Objectives

The performance of materials is crucial for the operation of fusion reactors, so their quality needs to be assured with high certitude. Material characterisations and microscopic inspections are needed in order to support the construction and development of components and materials for ITER and other fusion-related facilities under the responsibility of F4E. The Framework Contract concerns testing of materials at cryogenic temperatures, which are present in particular in the ITER machine's magnet system operating at 4 K.

Scope of Work

The aim of the Framework Contract is to support the European manufacturing of magnet components for ITER and other fusion facilities, such as the JT-60 SA, during their lifecycle from the R&D phase to the series production. In particular the following material characterisation activities are included:

Mechanical testing (at 4 K – 77 K typical):

- Tensile tests to determine material's tensile strength, yield strength, elongation, reduction of area, pull strength of joints, etc
- Shear tests
- Interlaminar shear strength of electrical insulation materials
- Fatigue tests to determine material's fatigue strength, develop Wöhler-curves, fatigue crack growth rates (FCGR, da/dN)
  - Number of cycles range for Wöhler-curves up to 10^6
  - Required R ratio is R = 0.1
- Fracture toughness (Critical stress intensity factor K1C)
- Charpy-V impact test (standard size or mini-Charpy-V)

Physical properties measurements (at 4 K – 77 K typical):

- Electrical conductivity
- Thermal conductivity
- Magnetic properties (magnetic permeability, susceptibility)
- Thermal contraction from RT to 4 K

Specimen sizes and types shall follow relevant EN, ISO, ASTM or equivalent standards. Typical materials concerned are:

- Structural metals: stainless steels, steels, copper alloys, aluminium alloys, titanium base alloys, nickel base alloys
- Glass/resin composites and other electrical insulation materials
- Weld-, braze etc. joints and other kind of combinations of the above-mentioned materials

ITER TF Jacket Analysis

To qualify a new heat treatment process and to follow the change in mechanical properties through the different process steps of the TF jacket, the jacket material was tested at the following stages during the manufacturing process:

- As received

- Cold worked (compacted + 2.5% stretching)
- Heat treated according to heat treatment 1 specification (old)
- Heat treated according to heat treatment 2 specification (new)

Table 1

Heat treatment 1	Heat treatment 2
Heating-up: 5 °C/h till 595 °C 160 hours at 595 °C 5 °C/h till 620 °C 320 hours at 620 °C Cooling down: 5 °C/h till 500 °C	Heating up: 5-500 °C /h 200 hours at 650 °C Ramp down: 50 °C /h until 500 °C
last cool down stage below 500 °C can be proposed by KIT (oven thermic inertia)	

ITER TF-coil Case Closure Weld Qualification

Tensile and fracture toughness tests were performed for the pre-qualification of the ITER TF-coil case closure welds. The material of the case is 316LN and the type of weld was narrow-gap hybrid laser and GMAW. The results vary due to voids within the weld. Table 2 gives the results of the fracture toughness in the center of the weld. Further improvement of the weld process is necessary and has to be verified by non-destructive testing of the weld and by new 4K mechanical characterization campaign.

Table 2

Filename	Temperature	Fracture Toughness
-	K	MPa m^0.5
Weld – 35/11 – 25.22.2 LMN		
1CT1	4.2	128
1CT2	4.2	208
1CT3	4.2	136

Cooperation:

Joint work within conductor production. Mechanical analysis of stainless steel 316LN/316L material.
ICAS, Italy
POSCO, R. of Korea
ASIPP, China

Radial plate production material qualification.
Schmiedewerke Gröditz, Germany
METSO, Finland
CNIM, France

Staff:

B. Purr
V. Tschan
K.-P. Weiss
S. Westenfelder

Acknowledgement

This work was supported by Fusion for Energy under the service contract No. F4E-OPE-084 (ES-MF) The views and opinions expressed herein reflect only the author's views. Fusion for Energy is not liable for any use that may be made of the information contained therein.

Current Leads for Wendelstein 7-X and JT-60SA (CoA; BMBF Ref. No. 03FUS0013)

Current Leads for Wendelstein 7-X

The stellarator W7-X presently under construction at the Greifswald branch of the Max-Planck-Institute for Plasma Physics consists of 50 non-planar and 20 planar coils with a maximum conductor current of 17.6 kA. KIT will deliver the current leads for the magnet system. In total 14 current leads are required (maximum design current I_{max} = 18.2 kA, nominal current I_{nom} = 14 kA).

Prototype current lead test

After the successful test of the prototype currents, IPP has approved the fabrication of the series current leads.

Series current lead manufacturing (Status of Nov 2, 2011)

Due to the tight schedule it was decided to manufacture and assemble the series current leads for W7-X in KIT. Except the heat exchangers which are being fabricated in time, all other components have been prefabricated. Four series current leads have been fabricated and successfully tested. Series current leads 5 and 6 are assembled and prepared for the test. The assembly of series current leads 7 and 8 is underway. The assembly of series current leads 9 and 10 has started.

Current Leads for JT-60SA

In the frame of the Broader Approach Agreement between Japan and the EU and concomitantly to the ITER project, a satellite tokamak project called JT-60SA has been agreed. The magnet system of JT-60SA consists of 18 toroidal field coils (25.7 kA), 4 central solenoid modules (20 kA) and 7 poloidal field coils (20 kA). Following the commitment of the German Government to the EU, FZK shall design, construct and test the current leads. In total 6 leads for a maximum current of 26 kA and 20 leads with a maximum current of 20 kA, mounted in vertical, upright position are required.

Status

The status is as follows:

- All HTS stacks for the TF and CS/EF current leads have been manufactured and delivered by Bruker HTS.
- The design of the HTS current lead for TF and CS/EF coils of JT-60SA has been finalized and all interfaces frozen and approved by the project team. In particular an agreement was achieved between F4E and KIT that EU rules, codes and standards will be used in the fabrication of the current leads.
- The detailed design including fabrication drawings of the heat exchangers have been finalized and sent to TÜV for approval. This is required before launching contracts to industry for delivery of materials and fabrication of components. Some requests for quotation have been sent to potential suppliers.
- The test facility CuLTKa is under construction and will be commissioned end of 2012 to be ready for the test of the current leads for JT-60SA.

Staff:

W7-X CL:	JT-60SA:
W.H. Fietz	W.H. Fietz
R. Heller	R. Heller
M.S. Darweschsad	B. Ganninger
G. Dittrich	M. Gehrlein
S. Eckerle	R. Heger
S. Fink	M. Hollik
U. Fuhrmann	C. Lange
M. Gehrlein	U. Saller
F. Gröner	A. Opitz
R. Heger	
M. Heiduk	
S. Heuser	
M. Hollik	
C. Lange	
R. Lietzow	
I. Meyer	
R. Müller	
R. Rotondo	
E. Specht	
V. Zwecker	
A. Kienzler	
C. Molnar	
T. Vogel	
P. Wagner-Nagy	

Literature:

[1] R. Heller, W. H. Fietz, S. Fink, M. Heiduk, A. Kienzler, C. Lange, R. Lietzow, T. Möhring, P. Rohr, T. Rummel, T. Mönnich, K. Buscher, “Test results of the high temperature superconductor prototype current leads for Wendelstein 7-X”, IEEE Trans. on Appl. Supercond. 21(3) (2011), 1062-1065

[2] W. H. Fietz, S. Fink, M. Heiduk, R. Heller, C. Lange, R. Lietzow, T. Möhring, P. Rohr, M. Süßer, T. Rummel, “Test arrangement for the W7-X HTS-current lead prototype testing”, IEEE Trans. on Appl. Supercond. 21(3) (2011), 1058-1061

[3] R. Heller, W.H. Fietz, A. Kienzler, R. Lietzow, “High Temperature Superconductor Current Leads for Fusion Machines”, Fusion Engineering and Design 86 (2011) 1422–1426

[4] E. Rizzo, R. Heller, L. Savoldi Richard, R. Zanino, “Heat exchanger CFD analysis for the W7-X high temperature superconductor current lead prototype”, Fusion Engineering and Design 86 (2011) 1571-1574

[5] S. Drotziger, W.H. Fietz, M. Heiduk, R. Heller, C. Lange, R. Lietzow, T. Möhring, “Investigation of HTS current leads under pulsed operation for JT-60SA”, submitted for publication in IEEE Trans. on Appl. Supercond.

[6] E. Rizzo, R. Heller, L. Savoldi Richard, R. Zanino, “CFD analysis and performance assessment for a 68 kA HTS current lead heat exchanger”, submitted for publication in IEEE Trans. on Appl. Supercond.

[7] E. Rizzo, R. Heller, L. Savoldi Richard, R. Zanino, “Parametric analysis of pressure drop and heat transfer in the meander-flow heat exchanger of HTS current leads for fusion applications”, submitted for publication in Cryogenics

Acknowledgement

This work was financially supported by the Ministry of Research and Education (BMBF) under the grant No. 03FUS0013 and is done in the Project JT-60SA under the Broader Approach Agreement between Europe and Japan. The views and opinions expressed herein do not reflect necessarily those of the BMBF or the European Commission.

Quench Detection System for Fusion Magnets (HGF)

Redesign of KIT´s new basic quench detector electronics completed

To meet challenging requirements regarding measurement accuracy and potential separation for future applications of the KIT-Quench detection system the existing detector electronics had to be redesigned in 2010. After successful test and validation of the first prototypes a new small system consisting of 16 (max. 24) detectors was manufactured with the beginning of 2011.

The new Quench detectors UNIQD Type 3420 perform the expected enhancement of measurement and detection accuracy combined with lower drift over the temperature range.

Some properties of the new Quench detector UNIQD Type 3420:

- Capable of up to 30 KV potential separation to ground (ITER spec.)
- Reliable Quench detection at lowest thresholds of 5-10 mV
- Full parameterization during operation possible
- Low drift design allows simplified or lapse of climatisation

Fig. 1: Revised KIT-Quench detector UNIQD TYPE 3420.

The new detector layout serves as a basic platform for fusion and non-fusion applications (e.g. accelerator coils). By variation of assembly, different specifications can be fulfilled (e.g. potential separation from 10 to 30 KV). This allows simplified handling of the detector and an additional reduction of costs.

Software *QVision Release 3.0*

The software *QVision* is the “All-In-One” tool for parameterization, diagnostics and operational supervision of the KIT-Quench-detection system unit (= cabinet with an amount of max.

128 detectors UNIQD). The software is now available in English language (multilingual version).

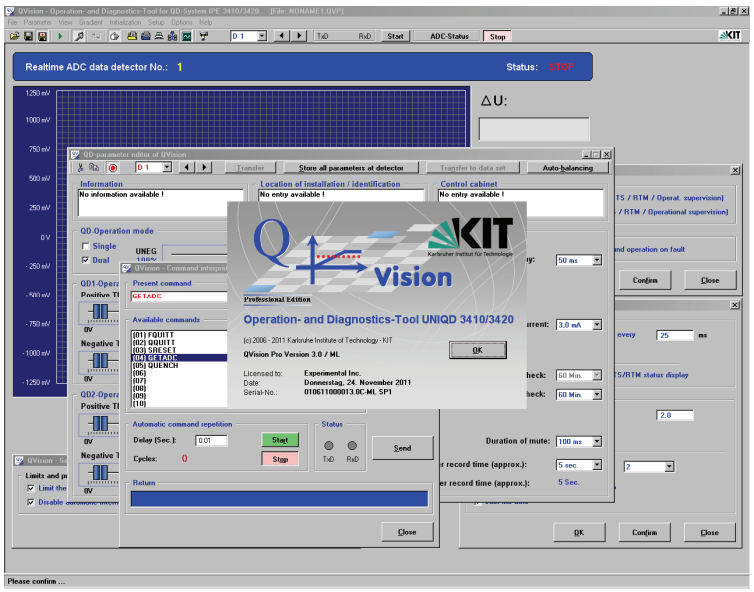

Fig. 2: All-In-One software tool *QVision* with integrated operational supervision mode and remote-interface (interface to control center).

Additional features of the new release QVision 3.0 (extraction):

- Extended remote interface for common control / linking of up to 512 system units (= more than 65000 detectors)
- Scalable permissions to system operators
- Full log operational supervision mode with complete event recording / event monitoring
- Auto-balancing menu for fast and accurate sequential balancing of two coils (or coil with co-wound wire)
- Interface to data base systems (option) and online help menus

The software now includes new safety options (e.g. password protection etc.) and comes with extended interfaces for online data access during operational supervision (status of cabinet, status of detectors, differential voltage (ADC-data), temperature etc.). Adapted to Windows ® 7 the software is now able to work in a user dependent mode.

Staff:

A. Ebersoldt
K. Petry
D. Tcherniakhovski

Conception, Design and Analysis of the Feeder - Power Distribution System Interface Conceptual Design and Analysis (ITER/CT/09/4100001296)

Objectives

One of the most critical components of the HTS current leads for ITER is the room temperature terminal (RT-termination) which serves as the interface between the current lead heat exchanger and the room temperature bus bar.

Several possibilities have been discussed within ITER IO as well as within the HTSWG:

- Air-cooling of the RT-termination (i.e. no water in dry box),
- Water-cooling of the RT-termination (water cooled flexible interface bus bars and possibly water cooled HTSCL termination), and
- Hybrid option (water cooled HTSCL termination, air-cooled flexible interface bus bars).

All options need to be studied and the pros and cons to be analysed. So ITER IO and KIT agreed to perform a design study in the frame of a service contract ITER/CT/09/4100001296.

Study

The study composes of three parts:

Subtask 1.1: Design Options
An air-cooled, a water-cooled and a hybrid option for the design of the PS-feeder interface were developed. The most promising solution is the active water cooling of the room temperature bus bars. It will be used to perform Sub-task 1.2.

Subtask 1.2: Detailed Analysis of the Three Design Options
As a result of sub-task 1 only the water-cooled option was analyzed in detail with respect to the thermal performance. This analysis was performed for four cases: the nominal operating case, the off-duty (zero-current) case, the over-heating case (faulty contact) and the freezing scenario (~150 K at HTSCL termination). As no detailed design of the CS and PF current leads are available, the study was concentrated on the TF current leads. The present design of the RT-termination of the 68 kA HTS current lead taking into account the actual dimensions of the water cooled power cables should work for 68 kA steady state operation, standby and it can also handle the fault condition in standby. But the following requirements are mandatory:

- It has to be considered that the water cooling of the cables has to keep into operation during standby.
- If this can not be guaranteed the heater power installed in the RT-termination has to be increased from 1 kW to at least 3 kW.

It should be noted that the He outlet temperature is not influenced by the heater power imposed on the RT-termination. If the He outlet pipes have to be free of ice all the time, i.e., independent of the operating conditions, a dry box is required.

Therefore the following design is proposed:

- Use dry box to prevent icing
- Use heaters large enough to compensate the temperature gradient in all operating conditions
- Use water cooling of flexible cables to reduce heater power in operation because water is much more effective that the heater cartridges.

Subtask 1.3: Final Recommendation for the PS-feeder Interface Design
Based on the findings in subtask 1.2 the optimal solution for the interface was proposed.

- As a result of the study presented in the report for subtasks 1.2 and 1.2 the use of a water cooled PS-feeder interface is strongly recommended. Integrated water cooling of the RT-termination seems not to be necessary if the termination itself is properly designed. Of course the design has to take care about the movement of the current lead during cool down and during current operation as well.
- Air cooling seems to be very ineffective and requires a lot of additional infrastructure like huge air blowers and air/water heat exchangers. There seems to be no space within and in the neighbourhood of the dry-box as well. Therefore a hybrid solution has not been investigated in detail because there is no single advantage compared to the water cooled option.

Status

It has been agreed with ITER RO to close this task after successful finalization of work end of 2011.

Staff:

W.H. Fietz
R. Heller
C. Lange

Acknowledgement

This work was supported by ITER Organization under the service contract No. ITER/CT/09/4100001296. The views and opinions expressed herein reflect only the author's views. The ITER Organization is not liable for any use that may be made of the information contained therein.

HTS Materials for High Current HTS Magnet Cables (WP11-DAS-HTS-02-01)

For use in fusion magnets, the second generation of high temperature superconductors, the coated conductors have to be considered due to the current carrying performance and radiation aspects. The commercial availability of HTS 2G material is actually very limited. At the moment a critical current of >1000 A/cm width at 77 K in self-field conditions in a 16 m long sample is reported as record for REBCO tapes (1530 A/cm for short samples). Over the last years the performance of coated conductors has continuously improved, mainly due to the application of controlled, oriented, artificial pinning sites. Tapes are mainly produced in USA, Korea, Germany, and in Japan. Commercially available tapes can be ordered from SuperPower, AMSC, and with some restrictions from Fujikura. Other companies are expected to come to the market the next years. Commercial materials peak with currents up to about 300 Amperes per cm-width of the conductor.

Cable concepts from 2G HTS tapes

REBCO coated conductors are restricted to tape geometries with no in-plane-bending. This requires new concepts for cabling. Different designs for high current cables for magnets were proposed in the last years. At the moment there are four major coated conductor cable concepts which are able to carry large currents in fusion relevant magnetic background fields with reasonable AC losses.

Coaxial cable (NIST-USA): This cable design is similar to power cables where the industrial assembling procedure was already solved. The number of applied HTS tapes is limited to the machinery which feeds the tape from reels to the central cable former.

Twisted Stack (MIT): The cable design requires the application of stacks of conductors. A single stack cannot be provided in long lengths from a reel, it needs to be assembled during fabrication of the cable from a number of reels for each tape. Changing the grooved central former to higher number of HTS stacks allows increasing the cable current carrying capability.

Roebel (KIT): The Roebel cable can be prepared in quite different configurations. Restricted to single stacked strand configuration, the scalability in current is given but also limited by changing the transposition length. Machinery for automatic cabling was demonstrated by IRL-NZ for this case with big success. For further increased currents, multi-stacking of strands is one option with similar arguments and limitations as in the case of the Twisted-Stack concept.

Rutherford cable (KIT): The Rutherford cable is designed using Roebel cables as strands. The advantages of this concept are the low AC loss features and a large variety of cable features and dimensions. Important cable features as cooling channel and reinforcements can easily be applied in the concept. The scalability of the cable is good.

Using the different cable concepts at an operation temperature of 50 K, the expected operation current density at magnetic fields of 12, 15 and 20 T is shown in table 1.

Table 1: A rough estimation of the maximum current for specific magnetic fields of different cable concepts at 50 K.

Cable concept	#Tapes	12 T	15 T	20 T
Coaxial1	24	0.54 kA	0.37 kA	0.2 kA
Coaxial2 (2-phase)	80	1.8 kA	1.25 kA	0.66 kA
Twisted Stack	120	2.7 kA	1.9 kA	1 kA
Rutherford	1000	11.2 kA	7.8 kA	4.1 kA

Table 2: Scalability with focus on industrial production.

	Coaxial	Twisted-stacked	Roebel	Roebel-Rutherford
AC losses	+	+	++	+++
mechanical stability	++	++	+	++
Bending	+	?	++	+
Scalability in current performance	++	+	+	++
Prospects for manufacturing in long lengths	+++	+	++	++

In table 2 a rough evaluation of the different cable concepts with respect to selected key performance aspects and the scalability to an industrial production is given. From the view on the AC loss performance the Rutherford and the Roebel cable have a clear advantage due to their sophisticated structure with intensive transposition of the conductors. The mechanical properties depend strongly on the source of stresses, tensile or bending. In this context the more simple concepts as the stacked and coaxial cable design have distinct advantages. Scalability is considered with respect to the required current carrying level on one hand, to meet the magnet design values, and on the other hand regarding manufacturing details as assembling procedures and long length fabrication of the cable components. Here a clear advantage of the helical concept is seen since it is very flexible in the number of applied strands and requires only a simple standard winding process. For the Roebel concept an automatic assembling was proved with limited flexibility and for the Rutherford cable an assembling procedure for given strands is not very complicated and also suitable for an automatic device. The stacked system has the general disadvantage that stacks cannot be stored on reels in long lengths which limits the number of tapes in one strand.

Staff:

W. Fietz
W. Goldacker

Acknowledgement

This work, supported by the European Communities under the contract of Association between EURATOM and Karlsruhe Institute of Technology, was carried out within the framework of the European Fusion Development Agreement. The views and opinions expressed herein do not necessarily reflect those of the European Commission.

Development of HTS Conductors (CoA)

The work that has been done on HTS solutions for fusion applications in 2011 concentrated on several main topics:

- Improvement of AC loss measurement techniques as upgrade of magnetic measurements and transport measurement
- Applying modelling to understand the behaviour of HTS cables
- Further optimisation of the Roebel cable technique, preparation of medium lengths and revision of the automatic punching machine for small cables
- Further work on a Rutherford cabling concept for HTS conductors with I > 10 kA, B > 10 T and T > 50 K.

Improvement of AC loss equipment

Magnetic measurements
In an environment of liquid nitrogen (LN_2) a so called “Calibration free technique”, has the advantage of directly measuring the absolute values of the AC losses, without the need of calibration. This magnetic method allows measuring also the contribution of strand or filament coupling. Therefore, an equipment for cable samples is requested with an upgrade of the dimensions. The advantage of this system is that it is able to reliably measure AC losses in standard superconductors (such as BSCCO and REBCO coated conductors), structured REBCO coated conductors, samples with ferromagnetic substrate as well as cables made of these conductors, which allows a direct comparison.

We designed and partially constructed the special type of coils required for this method, shown in figure 1. First experiments were performed at low fields and proved the system’s sensitivity and reliability. The Roebel cable has a transposition of the current path, which is important to reduce the AC losses. Modifications of the cable for lower losses are:

(1) Reduction of the width of the meander shaped strands.

(2) Decrease of the cable aspect ratio.

(3) Introduction of striations in the individual strands to reduce the effective width of the superconducting layer.

These modified cables are the candidates for the ongoing work.

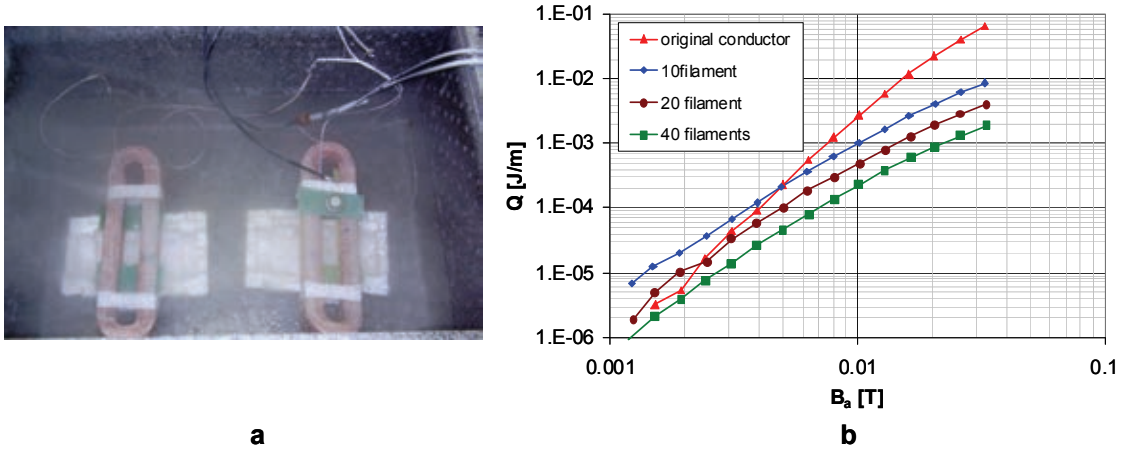

Fig. 1: a: The “Calibration free system” in the cryostat.
b: Measured AC loss in structured *RE*BCO coated conductors.

Transport AC loss measurements

The standard technique for transport AC loss measurement usually uses a single return conductor. The sample is connected to a transformer by means of a copper braid conductor. The second end of the sample is connected to another copper braid conductor, this conductor returns to the transformer at a certain distance from the sample. This configuration is schematically shown in figure 2 together with the apparatus.

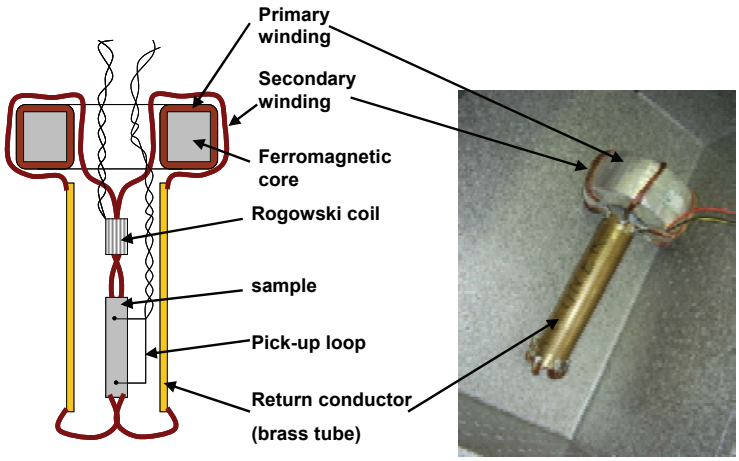

Fig. 2: Schematic view and photo of system for transport loss measurements with coaxial arrangement.

The measured losses on BSCCO and CC agree very well with the analytical prediction of the corresponding model and critical current and proved the successful functionality of the device.

Modelling of HTS Roebel cables

Roebel cables are very complex structures with a very inhomogeneous self field. All strands go through each position along the cable, passing all values of the self field. This gives changing critical currents along the strand and the need of current redistribution when the cable is operated close the transport critical current of the cable. In figure 3 investigations of a single Roebel cable are shown, illustrating the situation. The upcoming investigations will extend to a stack of Roebel cables where the self field situation is much different and the current distribution consequently too.

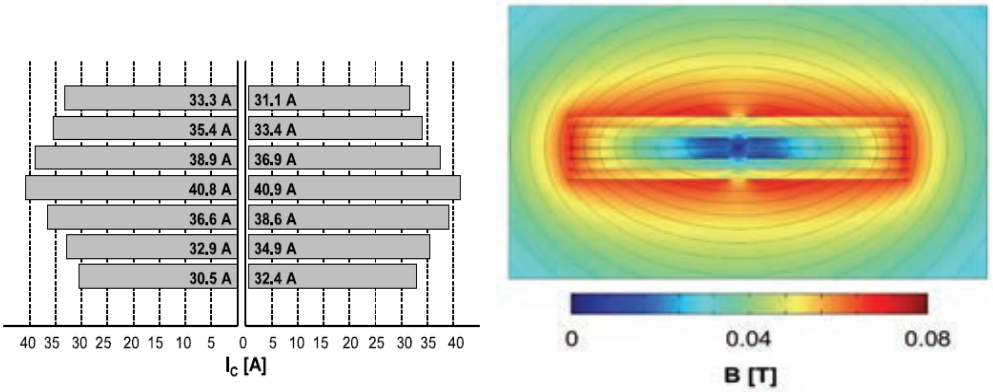

Fig. 3: Modelling the self field pattern across the cross section of a Roebel cable and the calculated critical current values in the coated conductor strands (left side).

Optimisation of Roebel cables

Assembling a Roebel cable is a quite complicated step. An automatic robotic machine was developed and patented by the Industrial Research Laboratory in NZ. The disadvantage of the device is the size of about 8 m length, the costs of several 100 k€ and the very limited flexibility to change the cable design. From these reasons an automatic assembling machinery was not considered for our actual research. F&E questions actually focus on lengths of a few meters. Therefore, the technique of hand-made cables was optimized which can be applied for lengths of 5 m and more. A cable with 4.5 m length was demonstrated as shown in Fig. 4. Very important for this sample was the test of the punching accuracy along a length of 50 meter conductor. For non sufficient constancy of the transposition length, the preparation of a cable will fail. The accuracy of the punching machine was excellent, no change of the transposition was found. This qualifies the tool for industrial lengths!

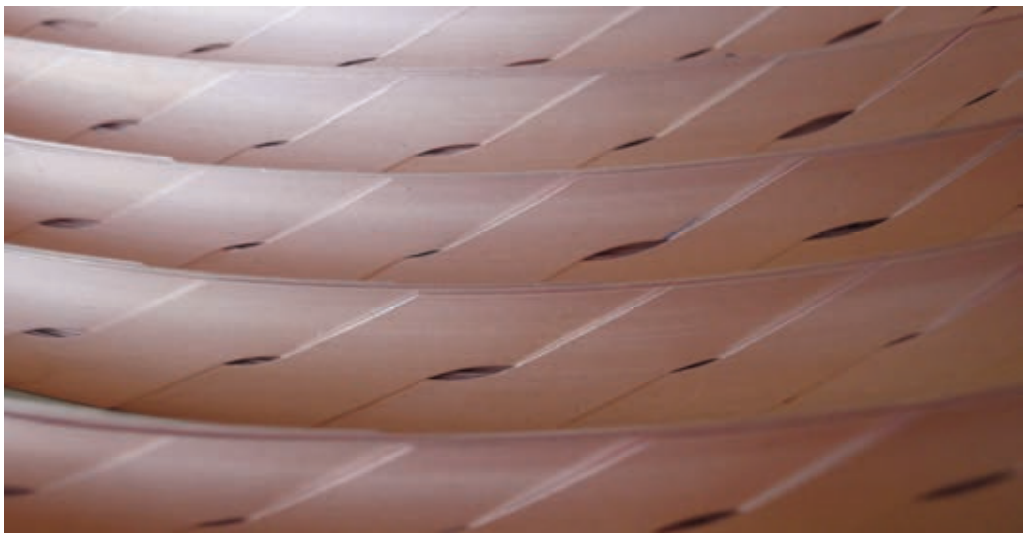

Fig. 4: Long length of a Roebel cable with 4.5 m, 10 strands and 12 mm width.

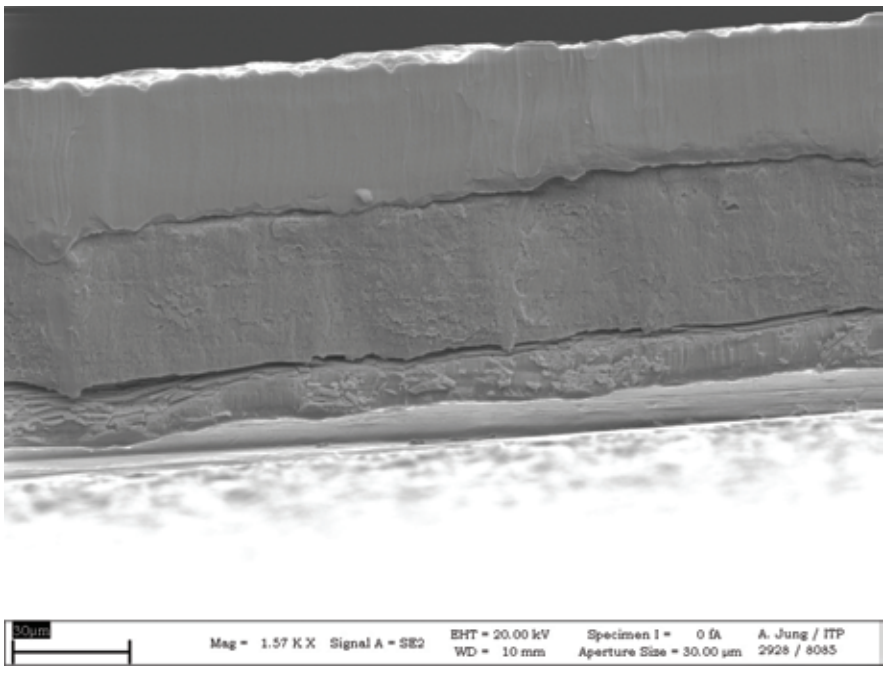

Fig. 5: Delamination effects of the coated conductor composite as consequence of a non-optimized punching tool. The layers are from top: Cu, substrate Hastelloy, buffer(thin)+YBCO, **the delamination gap (light gray),** and Ag+Cu.

The automatic punching device of KIT was working not accurate enough to punch small tape widths (Fig. 5).

Coated Conductor Rutherford Cable (CCRC) with HTS Roebel strands

ITEP presented this idea 2010 and started with the development of a subsize CCRC demonstrator (Fig. 6) with Roebel cables as strands to approach the current regime of 20 kA at 50 K and 12 T background field. In CCRCs all strands are fully transposed and experience similar fields and forces in a magnet winding. By assembling stacks of tapes instead of single tapes, a current carrying capability of 1320 A for a 4 mm wide Roebel cable with 50 punched strands was achieved in 2009 giving some idea of the potential of the strands. One of the most critical steps making a cable is the bending of the strands around the corner of the central former of the cable. A special continuous edge bending strain rig (CEBSR) was developed to study the bending of the fundamental tapes and the Roebel strands (see figure 7). A further optimization of the rig with a lot of test measurements was performed and a reliable operation of this unique facility was now achieved. In figure 8 the complete data set of the bending behaviour of the coated conductors being exposed to a variety of bending situations is shown.

Fig. 6: CAD drawing of the sub-size CCRC demonstrator cable.

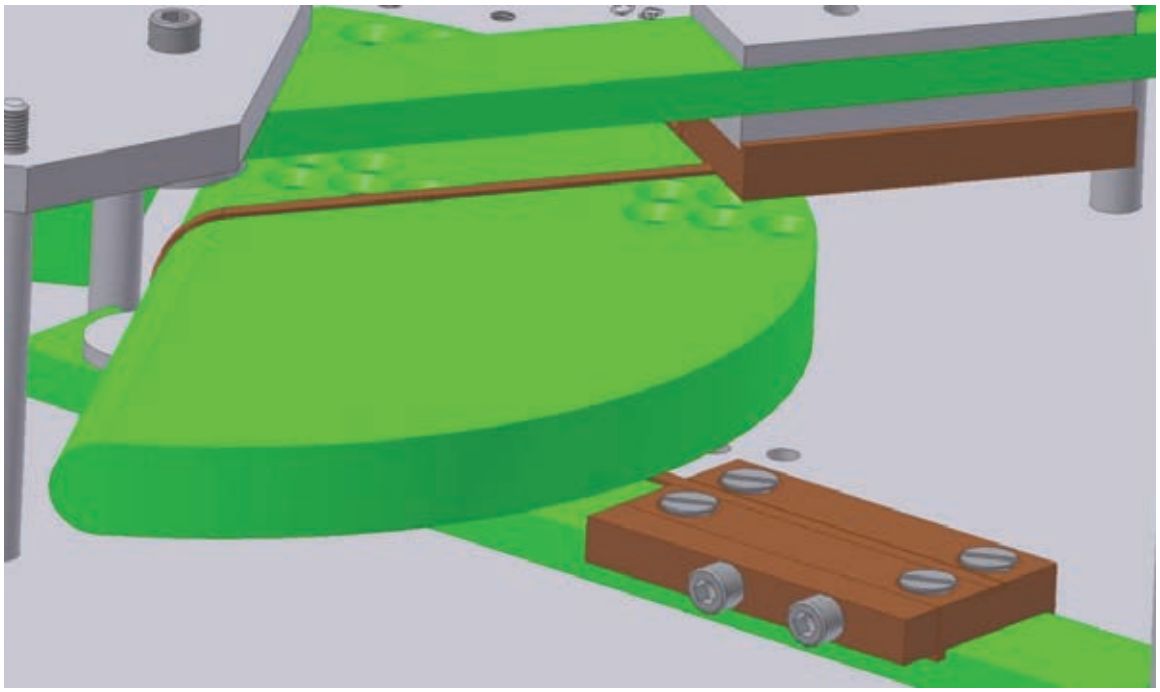

Fig. 7: Continuous edge-bending device to simulate strain effects on the currents of tapes and cables in step-over region of CCRCs.

The plateau like behaviour of the degradation for narrow bending radius looks very likely to be a contribution of shear effects which were observed earlier in torsion bending experiments. To confirm this interpretation more investigations are necessary.

Another very important outcome is the different behaviour of the conductor for a SC layer outside (convex side) or inside (concave side) oriented. For very sharp edges the inside orientation is much better and withstands smaller bending radii. This is an extremely important result for the CCRC since applying Roebel strands one has the option of both orientations. These results propose to orient the SC layers of the strands towards the central former. Verification on the model cable needs to done as one of the next steps.

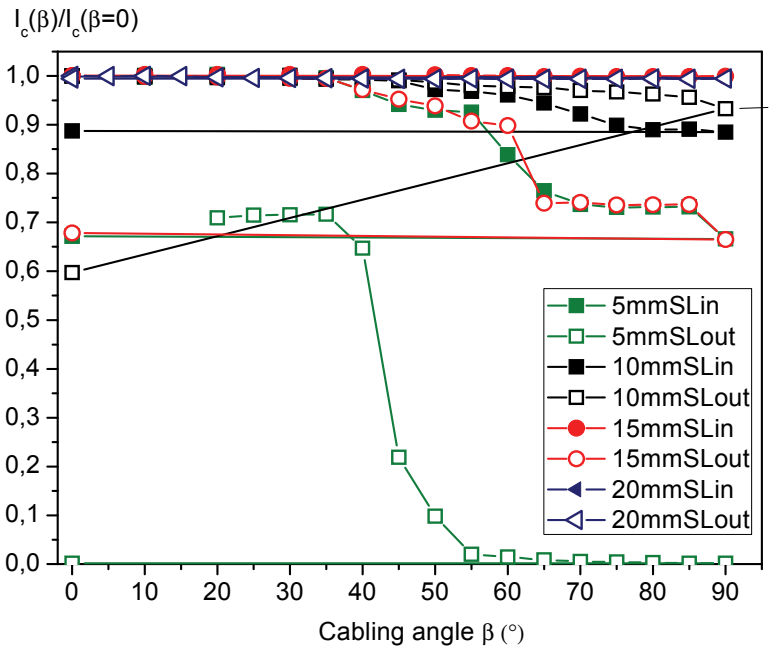

Fig. 8: CEBSR measurements for SuperPower coated conductors and different edge radius [unpublished]. The numbers indicate the radius of the bending edge and SLin and SLout means the orientation of the superconducting layer inside or outside the bending shape.

Future Work

The investigations of Roebel strand properties on the EBSR will be performed as the next important step. After qualifying the strands for the cable, the CCRC demonstrator cable will be equipped stepwise with 1 and 3 strands at minimum and investigated with respect to current feed in situation, transport current and current redistribution at the critical current. The reliability of the conductors in this stress loaded arrangement on cooling cycles is also a critical feature of the cable.

Staff:

A. Kario
H. Fillinger
W. Goldacker
F. Grilli
A. Kling
R. Nast
B. Ringsdorf
B. Runtsch
A. Jung
S. Schlachter
M. Vojenciak

Literature:

[1] Vojenciak, M.; Grilli, F.; Terzieva, S.; Krueger, P.; Nast, R.; Holubek, T.; Schlachter, S.I.; Kling, A.; Goldacker, W.: Experimental techniques for magnetization AC loss investigation. Superconductivity Centennial Conf., European Conf.on Applied Superconductivity, Den Haag, NL, September 18-23, 2011

[2] Terzieva, S.; Vojenciak, M.; Grilli, F.; Nast, R.; Souc, J.; Goldacker, W.; Jung, A.; Kudymov, A.; Kling, A.: Investigation of the effect of striated strands on the AC losses of 2G Roebel cables. Superconductor Science and Technology, 24(2011) S.045001/1-5

[3] Schlachter, S.I.; Goldacker, W.; Grilli, F.; Heller, R.; Kudymow, A.: Coated conductor Rutherford cables (CCRC) for high-current applications: concept and properties. IEEE Transactions on Applied Superconductivity, 21(2011) S.3021-3024

[4] Grilli, F.; Pardo, E.; Vojenciak, M.: Self-field effects, Jc(B) dependence and ac losses in ROEBEL-assembled YBCO coated conductor cables. Superconductivity Centennial Conf., European Conf.on Applied Superconductivity, Den Haag, NL, September 18-23, 2011

[5] Goldacker, W.; Schlachter, S.I.: Low loss high current 2G-cables for power applications. Superconductivity Centennial Conf., European Conf.on Applied Superconductivity, Den Haag, NL, September 18-23, 2011

Cryogenic Infrastructure (CoA)

Introduction

The cryogenic infrastructure of the ITEP supplies different experiments within the ITEP and other institutes of the Karlsruhe Institute of Technology (KIT), which are working for the Fusion Programme with refrigeration power or liquid helium. Such experiments in the ITEP are tests of superconductive components in the TOSKA facility, experiments for the ITER-cryopump in TIMO, and mechanical material tests in different cryostats equipped with traction engines.

Fig. 1: 2 kW-refrigerator with valve box and calorimeter.

For these experiments the cryogenic infrastructure comprises among other things:

- A 2 kW-refrigerator at 4.4 K with a liquefaction rate of 21 g/s (equivalent to 600 litres/h).
- A 300 W-refrigerator at 1.8 K with a liquefaction rate of 5 g/s (equivalent to 145 litres/h).
- A high pressure helium purifier working at 200 bars with a continuous purification mass flow of 14 g/s and a discontinuous purification mass flow of 28 g/s. The residual impurity content is lower than 1 ppm.
- Three recovery compressors with a pressure increase from one to 200 bars and a maximum mass flow of 26 g/s or 527 standard cubic meters respectively.
- A helium storage system consisting of:
  - stationary liquid helium vessels with a capacity of 15,000 litres or 1,875 kg respectively
  - storage tanks for impure helium with a capacity of 1,075 kg
  - storage tanks for pure helium with a capacity of 1,275 kg

  The whole storage system has consequently a capacity of 4,225 kg or 23,985 standard cubic meters respectively, see Fig. 3.

Fig. 2: 8-ary vacuum pump station of the 300 W@1.8 K-refrigerator.

Fig. 3: Helium storage system.

- A liquid nitrogen storage vessel with a capacity of 32,650 litres for the supply of all experiments and a filling station to distribute liquid nitrogen in transport vessels.

The cryogenic infrastructure is controlled by a state-of-the-art control system based on PCS7 and WinCC. The operation of the components can be done in two control rooms or via clients installed directly at the experiments.

A team of five operators, three engineers and one academic staff member is responsible for maintenance, repair, upgrading and extension of the cryogenic infrastructure for new or changed experiments.

Additional tasks are the supervision of peripheral installations such as

- Energy distribution system
- Re-cooling water unit
- Compressed-air distribution system.

Also, maintenance, repair, upgrading and extension of the

- Vacuum systems
- Different safety devices like oxygen monitors

are tasks of this group.

Beyond these regularly routine works this report is focused on selected extension projects, as well as giving an overview of the cryogenic supply activities for fusion projects.

Selected maintenance and extension works

2 kW (4.4 K) refrigerator

The following selected maintenance and extension works at the 2 kW-refrigerator were done in 2011:

- Reconstruction of the control systems AS1, AS2 and AS3 from Siemens Teleperm system AS 235 to AS 488
- Implementation of new vacuum measurement devices
- Implementation of new program blocks for valves and motors with individual alarm signals
- Programming for automatically cool down and warm up of the current lead tests in TOSKA
- Filter changes at two oil-sealed screw compressors for helium

Fig. 4: Filter changes at two oil-sealed screw compressors for helium.

300 W (1.8K) refrigerator

The following selected maintenance and extension works at the 300 W-refrigerator were done in 2011:

- Exchange of the control unit PCAS 121
- Reconstruction of the relubrication unit for the turbines

He-recovery and purification system

The following selected maintenance and extension works at the He-recovery and purification system were done in 2011:

- Reconstruction of the power supply system for the process control; now the network components of the profibus participants will be centrally supplied to avoid a bus breakdown during a disconnection of one participant.
- Exchange of oscillating dampers for a He-recovery compressor.
- Reconstruction and change of the safety valves for a He-recovery compressor.
- TÜV-checkups.
- Calibration and maintenance works for the He-scale.
- Repairing work at compressors.

Fig. 5: TÜV-checkups

Miscellaneous

- Supervision of the assembly of the control cabinets for CuLTKa

Cryogenic supply for the Fusion Programme

The different experiments for the Fusion programme in ITEP are supplied with circa 31,054 litres liquid. In addition the refrigerators ran nearly 1030 hours in 2011 for the supply of refrigeration power.

For comparison, the average consumption for such experiments in the period between 2001 and 2010 is about 23,054 litres liquid helium and 1,809 hours of refrigeration power. So in 2011 we had a higher liquefaction rate and a lower refrigeration power than the mean values of the years before.

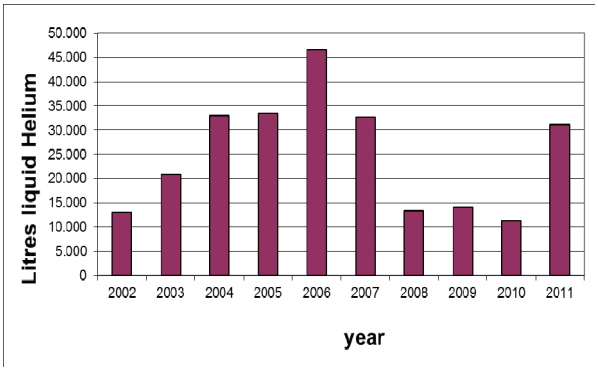

Fig. 6: Liquid helium supply between 2002 und 2012.

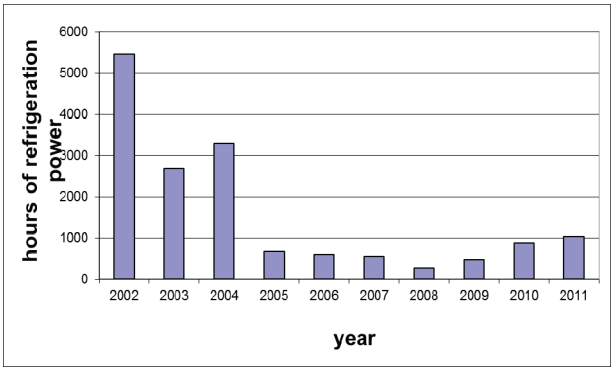

Fig. 7: Hours of refrigeration power between 2002 und 2011.

Staff:

A. Baumgärtner
S. Bobien
M. Duelli
U. Fuhrmann
H. Neumann
B. König
K. Metzger
D. Wetzel
H. Zimmermann

Fusion Researcher Fellowship (WP11-FRF-KIT/Vojenciak)

Objectives

High-temperature superconductors (HTS) are potentially very interesting for future fusion applications. These materials underwent substantial development in the direction of high critical currents and long production lengths. However, cabling techniques and techniques of AC loss reduction still require a lot of research and development.

The goal of this project for the year 2011 is building, testing and routinely using a comprehensive experimental facility to fully characterize HTS conductors, both in DC and AC. The main objects of investigation are Roebel cables and MgB_2 cables.

Description of the facility

For full characterization of a HTS conductor from the AC loss point of view one needs to measure the transport AC losses and the magnetization AC losses. MgB_2 cables will be characterized at temperature of 4.2 K, while Roebel cables made of *RE*BCO superconductor will be characterized at temperature of 77 K. Summary of required measurement is:

- Magnetization AC loss at 77 K
- Transport AC loss at 77 K
- Magnetization AC loss at 4.2 K
- Transport AC loss at 4.2 K

A universal device for all mentioned requirements would be very complex. Therefore it was decided to build a system with some parts to be used in all the experiment types and some parts peculiar to each experiment type. The experimental facility consists of a cryogenic part (including both power and signal detecting parts), measuring devices, and a computer for control. The cryogenic part is the only variable part.

Apparatus for magnetization AC loss measurements in LN_2 environment

In an environment of liquid nitrogen (LN_2) we use so called “Calibration free technique” [1], which has the advantage of directly measuring the absolute values of the AC losses, without the need of calibration. The system consists of two sets of coils, one containing the sample to be measured, the other one empty used as reference. The advantage of this system is that it is able to reliable measure AC losses in standard superconductors (such as BiSCCO and *RE*BCO coated conductors), structured *RE*BCO coated conductors, samples with ferromagnetic substrate as well as cables made of these conductors.

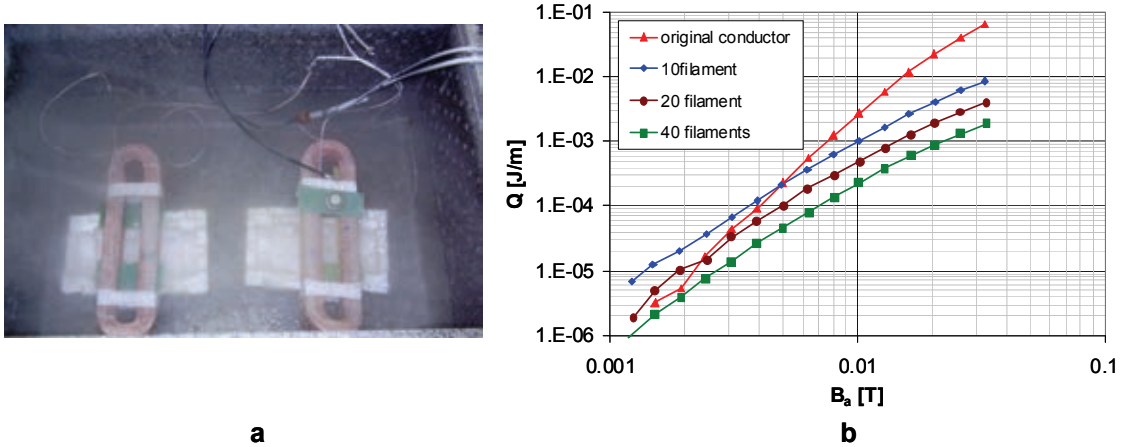

Fig. 1: a – The “Calibration free system” in the cryostat. b – Measured AC loss in structured *RE*BCO coated conductors.

Typical measurement results of structured samples of *RE*BCO coated conductors are shown in figure 1b. The measurements prove the theoretical prediction that magnetization AC losses at high fields decrease by increasing the number of filaments.

Apparatus for transport AC loss measurements in LN_2 environment

The standard technique for transport AC loss measurement usually uses a single return conductor. The sample is connected to a transformer by means of a copper braid conductor. The second end of the sample is connected to another copper braid conductor, this conductor returns to the transformer at a certain distance from the sample. This configuration is schematically shown in figure 2.

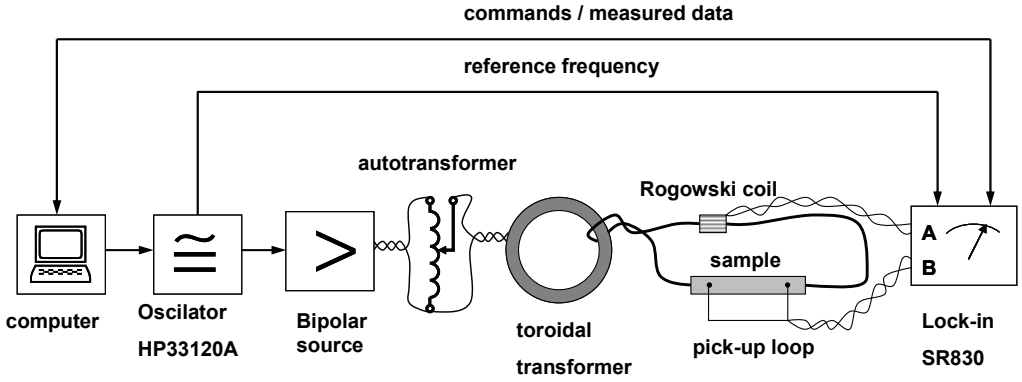

Fig. 2: Schematic view of the apparatus for transport AC loss measurement.

A photo of the cryogenic part inside the cryostat is shown in figure 3a. The advantage of this configuration is that it is easily adaptable to different shapes and sizes of the sample. There is also enough free space around a sample; therefore it is possible to utilize various kinds of contacts (e.g. pressure contacts, as it is shown in figure 3b). A disadvantage of this configuration is the relatively high leakage magnetic flux, which causes high induced voltage in the power circuit. For this reason the power of the bipolar source must be relatively high, especially for high currents and high frequencies.

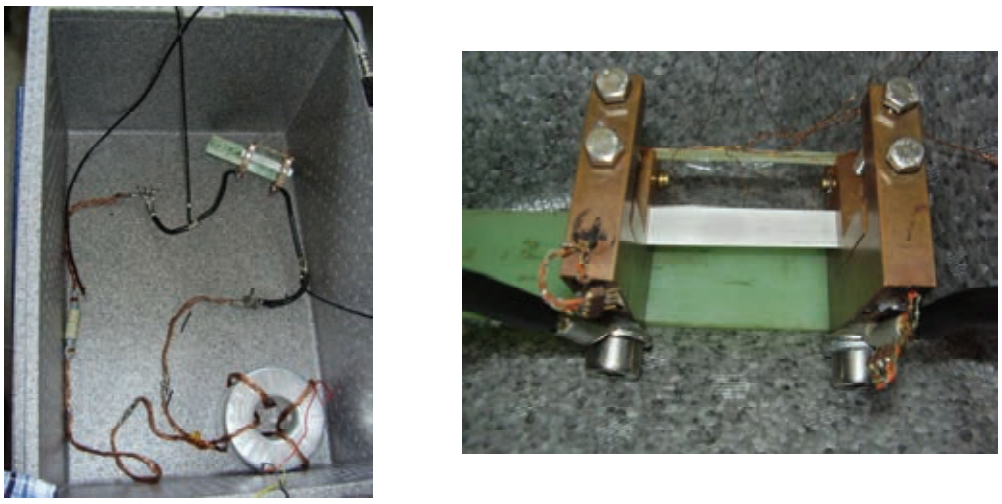

a **b**

Fig. 3: The cryogenic part of the system with single return conductor. a – overall view of the high current part of the circuit. b – detail of the sample holder with pressure contacts.

We measured three commercial samples of superconducting tape. One sample of BiSCCO tape (so called 1st generation of HTS) and two samples of YBCO tape (so called 2nd genera-

tion of HTS) with width of 4 mm and 12 mm, respectively. The experimental results are compared with the analytical predictions of Norris's formulas in figure 4. The measured losses agree very well with the analytical prediction of the corresponding model and critical current.

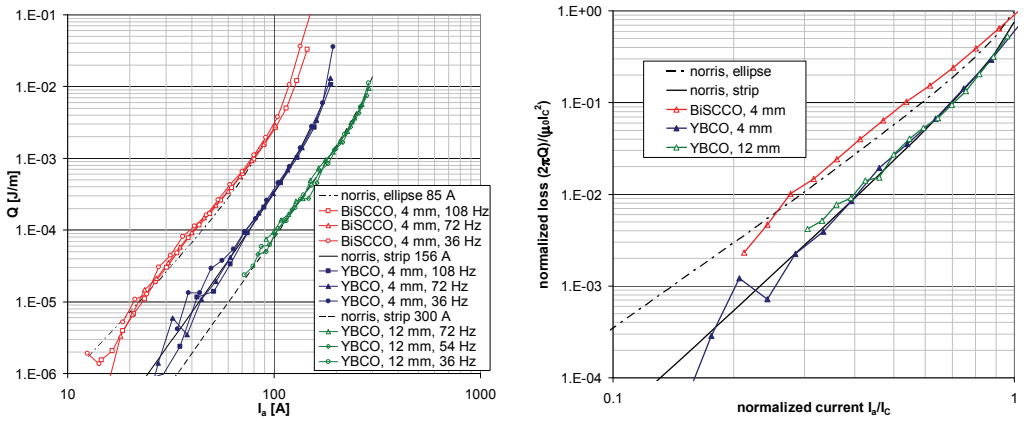

a b

Fig. 4: Measured loss per one cycle of AC transport current. a – dependence of loss per unit length on amplitude of transport current. b – dependence of normalized loss on normalized transport current.

Apparatus for magnetization AC loss measurements in LHe environment

For measurement of magnetization AC loss in liquid helium (LHe) environment we use a thermal method. This method is sensitive and the thermal response from the sample is reasonably fast because of the low specific heat at temperatures around 4.2 K. An AC loss in the sample causes increase of the temperature on the sample's surface. The sample is thermally insulated from the helium bath in order to have a sufficiently high temperature increase. For this purpose we use a fiber-glass tube with low pressure (~100 Pa) helium gas inside as a thermal insulation. With this configuration we are able to measure AC losses with precision around 1 μW.

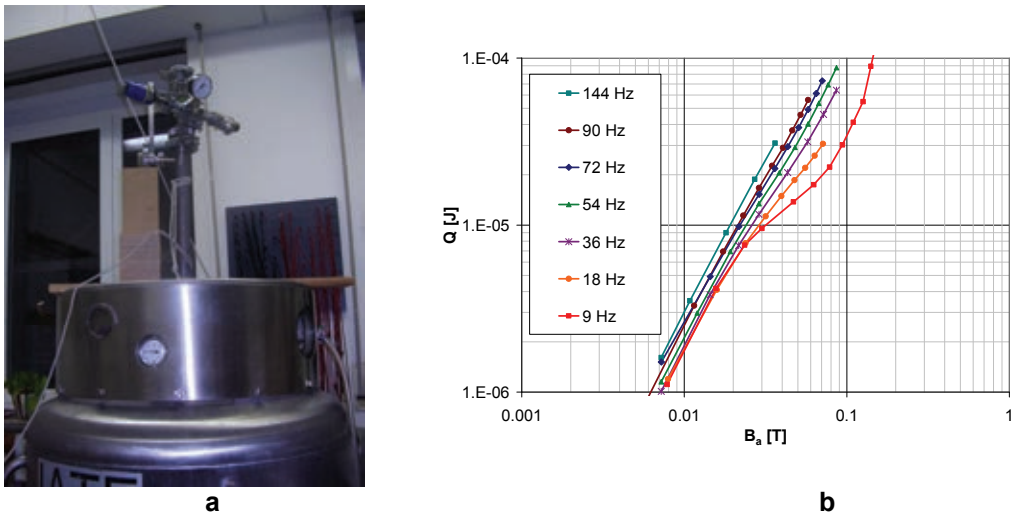

a b

Fig. 5: a – apparatus for magnetization AC loss measurement in LHe environment. b - Measured AC loss in structured *RE*BCO coated conductors.

We used this apparatus for measuring the AC losses in a sample of MgB_2 cable. This cable was made out of multifilamentary MgB_2 wire with monel sheath. This is a very complicated structure from AC loss point of view. There is combination of hysteretic losses in the ferromagnetic material – monel, hysteretic losses in the superconductor and coupling losses be-

tween filaments and individual wires in a cable. Experimental results are shown in figure 5b. From our measurements we can conclude that losses in ferromagnetic material are important only in low fields (up to 70 mT) and low frequencies (up to 36 Hz). At high fields and high frequencies the coupling loss is the most important loss mechanism.

Apparatus for transport AC loss measurements in LHe environment

We have made preliminary tests of the system for transport AC loss measurement in LHe environment. This system is built and has been successfully tested in LN_2 environment. In contrast to the system for LN_2 environment, this system uses a configuration with coaxial return conductor. This configuration is schematically shown in figure 6.

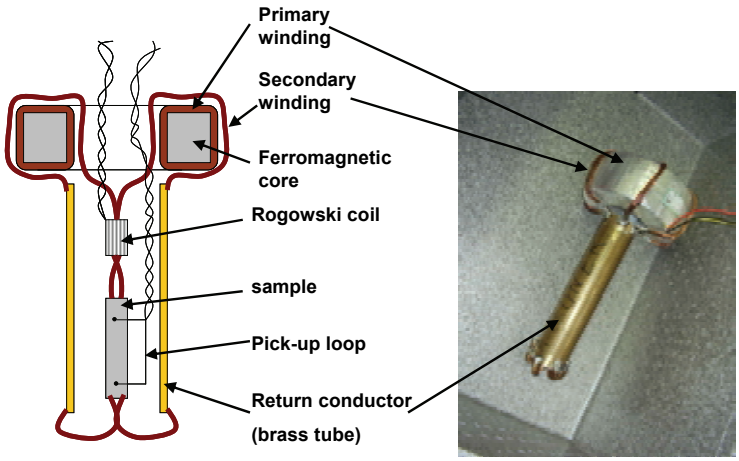

Fig. 6: Schematic view and photo of system for transport loss measurements with coaxial arrangement.

The coaxial configuration uses a conducting tube as a return conductor in contrast to the configuration with single return conductor. The sample together with a Rogowski coil is placed inside the tube. Several copper braid conductors are used for connections between the sample and the tube. This configuration has the advantage of low leakage magnetic flux and thus low induced voltage in the power circuit.

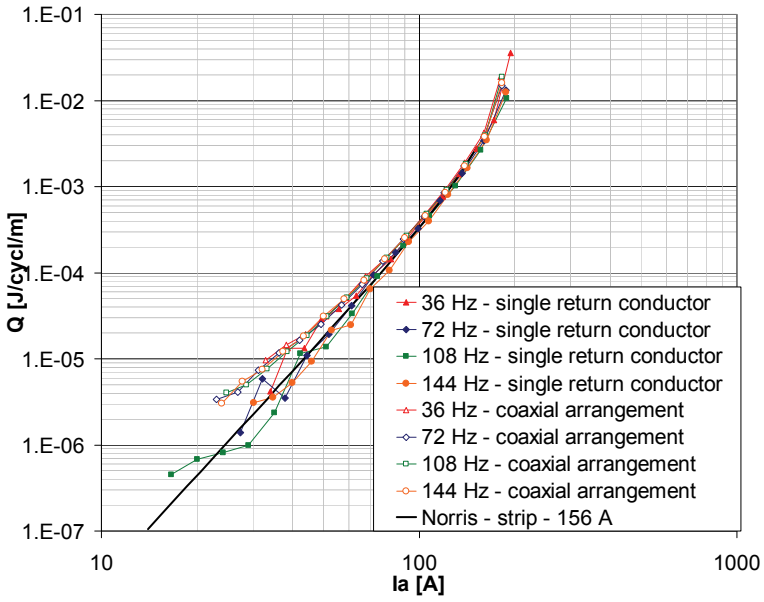

Fig. 7: Comparison of transport AC loss of the same sample measured in a system with single return conductor and in a system with coaxial arrangement. Results agree very well at medium and high currents.

We compared the results of measurement on the sample with single return conductor and system in coaxial configuration. For this measurement we have used a 4 mm wide YBCO tape with a critical current of 156 A.

We expect that this configuration is suitable for measurements in a liquid helium bath. There is only a very low AC magnetic flux in the system's ambience and therefore a metal cryostat could be used. This apparatus will be tested in a liquid helium bath in the year 2012.

Staff:

M. Vojenciak

Literature:

[1] Šouc, J., Gömöry, F., and Vojenčiak, M.: Calibration free method for measurement of the AC magnetization loss, Supercond. Sci Technol. 18 (2005) 592-595.

Acknowledgement

This work, supported by the European Communities under the contract of Association between EURATOM and Karlsruhe Institute of Technology, was carried out within the framework of the European Fusion Development Agreement. The views and opinions expressed herein do not necessarily reflect those of the European Commission.

Goal Oriented Training Programme " Cyrogenic Training Programme for Fusion" (WP10-GOT-GIRO (FU07-CT-2010-00065))

Objectives

In the frame of a structured training program, it is intended to train early-stage engineers during 3 years. This program will take place within a collaborative group to provide the technical know-how and the skills which are necessary for the engineering of components for ITER or fusion program and for the management of ITER relevant projects. The aim of the training is to reinforce the knowledge of the trainees thanks to their involvement in an engineering team constituted of experts in various domains.

Status

The contract was signed end of June 2010. A first coordination meeting was held in Porto end of Sept. 2010 with attendees of the 3 involved associations KIT, CEA and JET. At a task meeting in Sept. 2011 it was clarified that all trainees except one trainee at CEA were identified. KIT found the second trainee (M. Schrank) for the field "Design of measurement and control system for large cryogenic systems".

Staff:

W.H. Fietz
B. Kuffner
R. Lietzow
M. Schrank
M. Süßer

Acknowledgement

This work, supported by the European Communities under the contract of Association between EURATOM and Karlsruhe Institute of Technology, was carried out within the framework of the European Fusion Development Agreement. The views and opinions expressed herein do not necessarily reflect those of the European Commission.

Breeding Blanket

R&D for Helium-cooled Blanket Concepts (WP11-DAS-IVCC-06-01)

Introduction

Three Helium Cooled blanket concepts have been analysed in this task:

1. The Helium Cooled Pebble Bed (HCPB);
2. The Helium Cooled Lithium Lead (HCLL); and
3. The Dual Coolant Lithium Lead (DCLL).

The advantage of Helium Cooling is in the fact that Helium presents the better compatibility with all the materials used in the fusion reactor. Furthermore, it can be adapted to a wide range of temperature windows to cope with almost all the materials; in addition it can be employed at very high temperatures increasing the efficiency of the power generation cycle. However, this last feature will be strongly limited by the necessity to high pumping power to circulate the coolant in the blanket which is counterproductive.

The first two concepts (that are supported in the EU breeding Blanket as candidates for the DEMO blanket and selected for the Test Blanket Programme in ITER) have been considered in more details. The DCLL is mentioned as an attractive concept, but using a more advanced technologic extrapolation in comparison of the first ones.

The following table summarizes the characteristic of the near term concepts:

	HCPB	**HCLL**
Breeder:	Li_4SiO_4 in form of a pebble bed, monodispers (0.3-0.6mm diameter) at 40% ^{6}Li enrichment	PbLi in eutectic composition (15.8 t% at Li) at 90% ^{6}Li enrichment
Neutron Multiplier:	Be or Be alloy in form of a mono size pebble bed (1mm diameter).	PbLi accomplish also this function.
Helium coolant:		
– pressure	8 MPa	8 MPa
– Inlet temperature	300°C	300°C
– Outlet temperature	500°C	500°C
– Purification requirements (O, N, C, etc)	tbd	tbd
– Max T contents	Tbd (<1Pa)	Tbd (<1Pa)
Tritium Extraction:	He Purge flow through the breeder and beryllium beds at <0.4 MPa). 0.1% H is added to facilitate the T extraction.	The PbLi is recirculating outside the blanket at a slow velocity (the pressure is geodetic, ~1MPa)
FW protection layer:	2 mm W (average)	2 mm W (average)
Li burn-up control:	No system proposed	Possible on-line with chemistry control of the PbLi flow in the external loop.

	HCPB	HCLL
Purge/PbLi Loop:	Helium at 0.1-0.4 MPa, with velocity of few cm/s.	about 0.068 m^3/s considering 10 inventory recirculation per day
Surface Heating:	Max 0.5 MW/m^2 on all the blanket FW.	Max 0.5 MW/m^2 on all the blanket FW.
Neutron Wall Load:		
– PPCS	1.8 (2.3) MW/m^2 av(peak)	1.84 (~2.5) MW/m^2 av(peak)
– DEMO-2007		1.56 (~2.0) MW/m^2 av(peak)
Tritium Breeding Ratio:		
PPCS (2000)	1.07 @ 20% 6Li 1.12 @ 30% 6Li for b_{IB}=39cm and b_{OB}=49cm	
PPCS (2004)	1.10 @ 30% 6Li 1.12 @ 20% 6Li 1.14 @ 40% 6Li for b_{IB}=36 cm and b_{OB}=46 cm	1.14 @ 90% 6Li for b_{IB}=53 cm and b_{OB}=78 cm
DEMO-2007		1.10 @ 90% ^{6}Li for b=56cm 1.10 @ 60% ^{6}Li for b=60cm
IB: inboard, OB: outboard		
Energy multiplication:		
– PPCS	1.33	1.18
Pressure drops in Blanket Loop:	0.22 - 0.41 MPa	0.29 - 0.45 MPa
Pumping Power in Blanket Loop:	154-288 MW @ 3966 MW_{th}	218-333 MW @ 4219 MW_{th}
Gross thermodynamic cycle efficiency	0.41 - 0.42	0.44

Conclusions

The following table summarizes the open R&D issues for the development of these concepts

	R&D Objectives
Common Topics	
Helium cooling technology for fusion reactors	Improvements in the design to compensate lower performance in terms of heat transfer and power pumping. Development of cooling loops and components (e.g. high temperature axial compressors) for DEMO conditions.
Steel development and Fabrication technologies	Complete the RAFM (EUROFER) development with the target requirements to operate in a range of about 300-550°C, low neutron damage up to 70 dpa (with possibility to extend it to about 150 in a FPP) and low activation properties. Qualification of manufacturing processes like diffusion bounding (e.g. HIP processes) and joint technologies (e.g. laser, EB, TIG) for fusion components.
Neutronic performances	Improve of the predicting capability for the determination of the Tritium Breeding Ratio (TBR) in the design phase. Particulary important for the solid breeder. Improvement of the design in order to optimise the TBR.
Tritium extraction and recovery	Complete the lay-out of the tritium purge flow loop/PbLi loop T-extraction in DEMO/FPP. Impact on T-self-sufficiently. Development of T recovery equipments.
Tritium control: coolant purification & permeation barriers.	Development of Coolant Purification systems for DEMO/FPP. Safety studies on T control in DEMO/FPP; definition of safety requirement for T control (e.g. permeation barriers).
Tritium inventory	Safety studies on T inventory limits in DEMO/FPP (definition of safety requirement for T inventory). Impact on the T-self-sufficiently.
Diagnostics	Integration of plasma control diagnostic in the blanket system. Interlock and safety signals from Blanket System.
Reactor Integration	Integration of blankets in the selected maintenance systems.

HCPB topics	
Ceramic Breeder Development	Complete the in-pile characterisation.
Beryllium (as Neutron Multiplier) Development	Complete the in-pile characterisation. Development of Be alloy (if requested).
Thermo-mechanics of the Pebble Bed (temperature control in pebble beds).	Complete measurements of bulk/surface thermal conductivity in pebble beds and related modelling. Include irradiation effects.
Be/steam, Be/air reaction (safety analyses)	Study on new materials (Be-alloys) to reduce the reaction rate with air/steam. Safety study of for the use of Beryllium as multiplier in DEMO/FPP and definition of related safety requirements.
Tritium retention in Be	Characterisation of T release in irradiated Be (e.g. in HIDOBE) and improve the modelling.

HCLL topics	
Development of eutectic PbLi	Improve operation procedures for chemistry control.
Magneto-Hydrodynamic (MHD) Design.	Improve modelling capability and design.
PbLi/steam reaction (safety analyses)	Safety study of for the use of PbLi as breeder in DEMO/FPP and definition of related safety requirements.
PbLi-steel Corrosion	Complete investigation and modelling (e.g. effect of Magnetic field). Definition of operational requirements.
PbLi Purification	Development to cope with activation products (e.g. Po production).

Staff:

L.V. Boccaccini
F. Cismondi
I. Maione
S. Kecskes

Acknowledgement

This work, supported by the European Communities under the contract of Association between EURATOM and Karlsruhe Institute of Technology, was carried out within the framework of the European Fusion Development Agreement. The views and opinions expressed herein do not necessarily reflect those of the European Commission.

Magneto-hydrodynamic Flows for Fusion Blankets (CoA)

Experiments

A closed liquid-metal circuit has been designed and manufactured with the main purpose of having a flexible device to study fundamental properties of magnetohydrodynamic (MHD) flows like pressure drop in generic geometric elements of liquid-metal circuits. The loop has further the possibility to serve for testing of measuring techniques for applications in ITER test blankets. As working fluid the liquid metal alloy GaInSn has been chosen, since this fluid is liquid at room temperature, non-toxic and nonflammable, which allows easy handling. The final optimized design of the experimental loop, as shown in Fig. 1, has been obtained as a result of theoretical considerations and by the support of numerical calculations. It consists of a double loop arrangement that allows feeding the test section in a symmetric way and obtaining the most uniform entrance conditions. The central channel, which represents the test section where measurements are taken, is connected by bends to two ducts. Each of these lateral channels has an electromagnetic pump, formed by two large Cu-electrodes connected to a current source, and an electromagnetic flow meter. All other elements are fabricated from electrically insulating material and components can be exchanged easily.

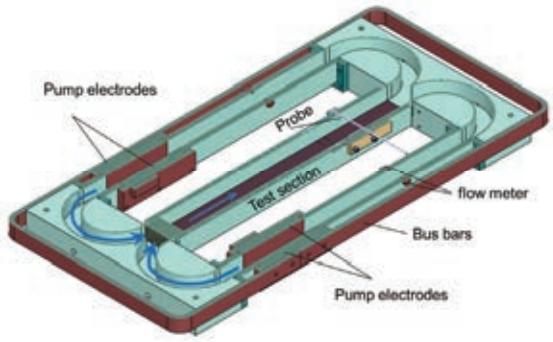

Fig. 1: Experimental loop formed by two pump channels fitted with copper electrodes and a central duct for measurements and sensor tests.

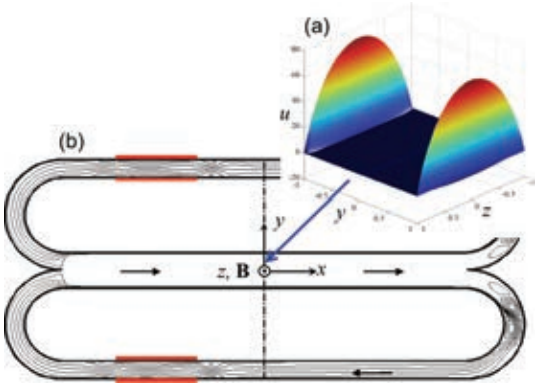

Fig. 2: (a) 3D view of velocity distribution at x = 0. (b) Isolines of electric potential in the double loop on the symmetry plane for a magnetic field of about 0.8 T.

The layout of the circuit by simple design equations has been confirmed by detailed 3D numerical simulations of the entire double-loop. Calculations have been carried out by using the open source software OpenFoam in which MHD equations have been implemented [1]. As electric boundary conditions we assume insulating walls everywhere, except at the pump electrodes, where by an applied potential difference a current is imposed that drives the flow, and in the test-section at walls perpendicular to the magnetic field. The latter ones called Hartmann walls are chosen perfectly conducting, since under these conditions the flow is characterized by a high pressure drop, the fluid in the core of the duct is almost stagnant and practically all flux is carried by thin jets along the insulating lateral walls. This is shown in Fig. 2(a) where the calculated velocity distribution is displayed in the middle of the test section for an applied magnetic field of about 0.8T. In Fig. 2(b) contours of electric potential are shown as indication for velocity streamlines in the horizontal symmetry plane of the duct for a stable laminar MHD flow. Near the edges of the pump electrodes 3D disturbances are present, which decay after a short distance so that at the entrance of the test section the flow is laminar. When the liquid-metal approaches the test section it is rapidly distributed into the side layers, along walls parallel to the magnetic field, in which it flows at high speed. This type of flow tends to develop instabilities near the side walls and their occurrence and flow pattern will be the subject of a detailed experimental program.

During the experimental campaign it is foreseen to measure the electric potential distribution on the channel walls and the local potential gradients in a duct cross section using a movable

probe whose position can be precisely adjusted by using a driving mechanism as shown in Fig. 3. On both side walls of the duct a row of non-equally spaced potential sensors is present to record time-dependent signals along the channel axis. Numerical results displayed in Fig. 4 give already indications that the flow in the test section tends to develop interesting time-dependent instabilities that will be investigated experimentally using the present device. Detailed knowledge about near-wall unstable flow and turbulent MHD flows is important for accurate predictions of heat and mass transfer (e.g. transport of tritium and corrosion products) for applications for instance in the European helium-cooled lead lithium (HCLL) test blanket module for ITER.

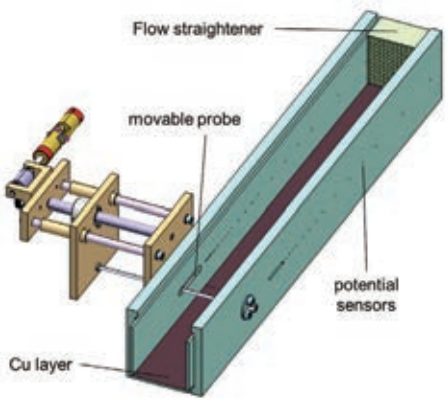

Fig. 3: Test section (middle channel) and mechanism to move a traversable electric potential probe.

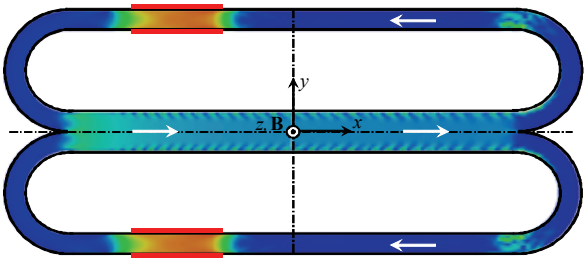

Fig. 4: Contours of the magnitude of calculated electromagnetic force for an unstable MHD flow in the test section on the horizontal symmetry plane.

Additional details on design equations and simulations used to define the characteristics of the experimental liquid metal loop have been published in references [2] [3] [4].

Further experimental results about MHD effects in a scaled mock-up of an HCLL blanket module have been published and presented in references [5] [6].

Numerical studies of MHD flows with strong magnetic fields (EFDA HPC-FF – HCP-MHD)

In the framework of the study of a HCLL blanket concept for ITER, numerical tools are developed to complement experimental activities. Simulations support for instance selection and validation of physical models for 3D coupled phenomena, like magneto-convection.

A finite volume solver has been developed for simulating MHD flows for intense applied magnetic fields, i.e. when the characteristic flow parameter called *Hartmann number* Ha is large. The code is able to predict MHD flows in geometries with walls of arbitrary electric and thermal conductivity. The equations have been implemented in the open source CFD code OpenFOAM. An important characteristic of the developed MHD solver is the use of an interpolation procedure of current fluxes from cell-faces to cell-centers, which preserves the conservative properties of the current density field. The code has been fully validated against available analytical and asymptotic solutions [1] [10].

In the currently proposed HCLL blanket design the liquid metal serves mainly to breed tritium and the heat flux is removed by helium flowing at high pressure in channels grooved in the walls. The use of a separate coolant has the advantage that the liquid metal can flow in the blanket with smaller velocities compared to those required in self-cooled blanket concepts. As a result the buoyant-convective flow caused by non-uniform thermal conditions and gravity may be comparable or even exceed the forced flow foreseen for tritium removal. Therefore, knowledge of buoyancy-driven MHD flows becomes fundamental to understand how the liquid metal circulates in the blanket.

Equations describing buoyant-MHD flows have been implemented in the developed solver in OpenFOAM. Heat and current conductance in solid domains and the coupling with buoyant MHD convection in fluids have been modeled and thoroughly validated. The code has been applied to get an overview of convective flow patterns in long vertical channels under various thermal and electric boundary conditions. The influence of wall conductivity, of the orientation of the imposed heat flux and of the duct aspect ratio on buoyancy driven MHD flows has been numerically investigated [7] [8]. Before studying complex fusion-related geometries, the fundamental physics of MHD-buoyant flows has to be fully understood in order to give the correct physical interpretation of coupled 3D phenomena.

Let us consider the stationary MHD flow in a vertical channel that is sufficiently long to ensure fully developed flow conditions in a large axial part. In the following discussion the electric conductivity of the wall is characterized by the *conductance parameter* c that gives the ratio of wall to fluid electrical conductance. A uniform magnetic field $\mathbf{B}$ is imposed in z-direction (see Fig. 5(a)). Walls parallel to $\mathbf{B}$ are called *side walls* and those perpendicular to it are the *Hartmann walls*. In a first example a temperature difference is applied between isothermal side walls ($\nabla \mathrm{T} \perp \mathbf{B}$) so that, in case of no internal heat generation, a linear temperature distribution $\mathrm{T} = y$ is present. The duct walls are perfectly electrically conducting ($c = \infty$). As shown in Fig. 5(b) the velocity distribution is characterized by two counter-flowing jets that develop in the side layers along walls parallel to the magnetic field. The fluid moves upwards near the heated wall and downwards at the colder wall. In Fig. 5(c) the axial velocity is plotted in half of the duct ($y \geq 0$) at z = 0 for various conductance parameters c. It can be observed that when reducing c, i.e. when the electrical conductivity of the wall becomes smaller, a larger flow rate is carried by the jet near the side wall at y = 1 and the flow in the core increases so that finally the jet disappears as $c \rightarrow 0$. In an electrically insulating duct (c = 0), the axial velocity varies linearly in the core and it starts reducing when approaching the side walls due to the additional contribution of viscous forces (see Fig. 6(a)).

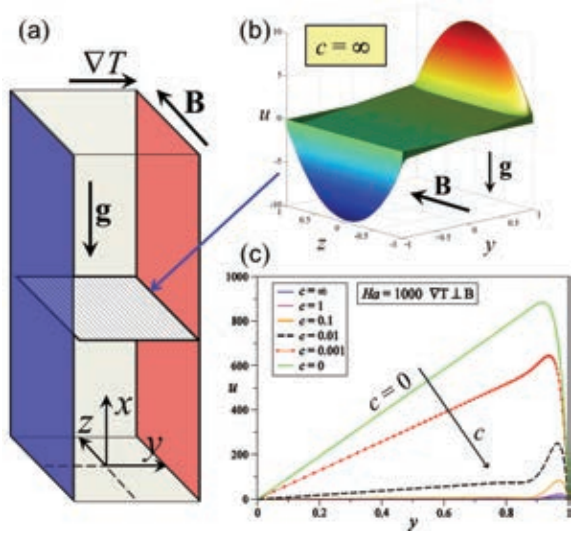

Fig. 5: Buoyancy-driven MHD flow in a long duct, with $\nabla \mathrm{T} \perp \mathbf{B}$, for Ha = 1000. (a) Geometry and reference system, (b) axial velocity distribution in case of c = ∞, (c) axial velocity profile at z = 0 for various conductance parameters c.

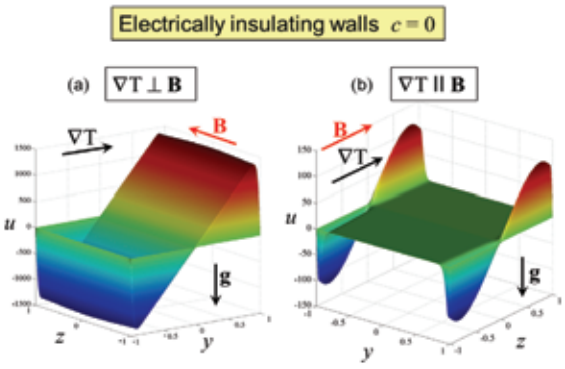

Fig. 6: Axial velocity distribution for buoyancy-driven MHD flow in electrically insulating ducts (c = 0), for Ha = 1000, with (a) $\nabla \mathrm{T} \perp \mathbf{B}$ and (b) $\nabla \mathrm{T} \parallel \mathbf{B}$.

In the case in which a linear temperature distribution is applied between Hartmann walls, i.e. when $\nabla \mathrm{T} \parallel \mathbf{B}$, the liquid metal in an electrically insulating channel distributes as shown in Fig. 6(b). The velocity in the side layers is an odd function of z and the fluid flows upwards in the half of the duct near the hot wall (z > 0) and downwards by the cold wall (z < 0). The dif-

ferent flow structure in the two cases studied (Fig. 6) is related to the changed organization of electric currents and potential in the channel.

Results show that the electrical conductivity of duct walls determines the profile and the magnitude of the velocity in the channel and therefore it affects the performance of a device in terms of mass and heat transfer. Hence, numerical studies of buoyancy-driven MHD flows for fusion blanket applications should be carried out by using geometries with the most realistic values of wall electrical conductivity. It has been shown that by applying the same thermal boundary conditions (e.g. $\nabla T \perp \mathbf{B}$), while reducing the electrical conductivity of the walls, the maximum velocity in the side layers increases by almost two orders of magnitude and a much stronger core flow is present. The results described show the appearance of high-velocity jets in the boundary layers along the duct side walls. Such flows should exist when inertia forces are negligible compared to the electromagnetic ones. In the performed study it is assumed that the flow remains laminar. However, future stability analyses are required to determine the range of flow parameters for which the discussed solution is valid.

Additional work on modeling of MHD flows and examples of application of the developed code have been published and presented by the MHD group at IKET in references [9] [10].

Acknowledgement

This work, supported by the European Communities under the contract of Association between EURATOM and Karlsruhe Institute of Technology, was carried out within the framework of the European Fusion Development Agreement. The views and opinions expressed herein do not necessarily reflect those of the European Commission.

Staff:

L. Bühler
H.-J. Brinkmann
S. Ehrhard
C.Mistrangelo

Literature:

[1] C. Mistrangelo and L. Bühler. Development of a numerical tool to simulate magnetohydrodynamic interactions of liquid metals with strong applied magnetic fields. Fusion Science and Technology, 60(2):798-803, 2011.

[2] L.Bühler, C. Mistrangelo, and C. Köhly. Design of a flexible liquid metal loop for investigation of MHD flows related to fusion blanket applications. In Proceedings of the 24th Symposium on Fusion Engineering, SOFE 2011. Porto, Portugal, June 2011.

[3] L. Bühler, C. Mistrangelo, and C. Köhly. Layout of an experimental liquid metal circuit based on MHD considerations. IEEE Transactions on Plasma Science, under review, 2011.

[4] L. Bühler, C. Köhly, and C. Mistrangelo. MHD experiments using GaInSn for basic research and sensor qualification in strong magnetic fields. In Satellite Meeting on Liquid metal application on Fusion Science, Porto, September 30. 2010.

[5] L. Bühler and C. Mistrangelo. Liquid metal flow in the European concept for a fusion test blanket under the influence of spatially varying magnetic fields. In Proceedings of the 8th Pamir International Conference on Fundamental and Applied MHD, Borgo, Corsica September 5-9, pages 405-409. 2011.

[6] L. Bühler, C. Mistrangelo, and S. Horanyi. Experimental detection of MHD flow reversals in sub-channels of a liquid metal test blanket for ITER. 4th International Symposium on bifurcations and instabilities in fluid dynamics, Barcelona, Spain, July 18-21, 2011.

[7] C. Mistrangelo and L. Bühler. Numerical analysis of buoyant-convective liquid metal flow in channels exposed to strong magnetic fields. In Proceedings of the 24th Symposium on Fusion Engineering, SOFE 2011. Porto, Portugal, June 2011.

[8] C. Mistrangelo and L. Bühler. Numerical study of fundamental magneto-convection phenomena in electrically conducting ducts. IEEE Transactions on Plasma Science, accepted.

[9] C. Mistrangelo and L. Bühler. Instabilities in electrically driven MHD flows. In Proceedings of the 8th Pamir International Conference on Fundamental and Applied MHD, Borgo, Corsica September 5-9, pages 175-179. 2011.

[10] C. Mistrangelo. Simulation of MHD flows in OpenFOAM: Capabilities and new features. In Workshop on Numerical Simulation of MHD Flows, 18-20 October 2010, Karlsruhe, Germany.

Goal Oriented Training “Power Supply Engineering” (EFDA-WP08-GOT-PSE (FU07-CT-2009-00084))

The Power Supply Engineering plays an important role in the design, operation and exploitation of the fusion experimental devices and relevant test facilities. The role of the power supply engineers in this sense is a key role, as the power supplies are active devices which can be designed, optimized and upgraded to satisfy the requirement. These are the power supply engineers needed for ITER and to form them in this sense is the main objective of this training program.

The training activities are divided into two main areas:

- General engineering training and experience including personal development.
- Training and experience in specific technical areas to conclude with involvement in and/or management of one or more significant technical projects.

The general training consists mainly of a collaborative training program in coorporation with the participating associations, based on comprehensive set courses and shadowing activities on the operation of the facilities present in each laboratory. In 2011 the trainee attended to two-week-courses at all the participating institutions (ENEA, Frascati; Consorzio RFX, Padova; IRFM, Cadarache; CCFE, Culham and KIT). As a highlight it shall be mentioned only one of the huge amount of topics covered in the courses, which was an analysis of the ITER Steady State Power Supply Network which was done in ENEA, Frascati in October.

The specific training consists of practical work experience at the Helium Loop Karlsruhe – High Pressure (HELOKA-HP) experimental facility. The object of HELOKA-HP is to test the HCPB-blanket concept and to gain experience in operating such kind of helium facilities. In this sense it also acts as a prototype for the ITER TBM helium cooling system.

In 2011 most of the work was dedicated to the commissioning of the second stage of the Data Acquisition and Control System of the HELOKA-HP facility and several devices of the helium loop. For example, in June 2011 the 750 kW helium heater and its power supply have been successfully commissioned. Together with the installation of the instrumentation and helium supply system, the loop is now operational. Some work is still continuing on the automated control of the plant. After this has been completed the integration of the test section and the preparation for the experimental campaign can be started. This will be the third stage of DACS and the main work for 2012.

The first experiments are planned to start with tests of a reduced size first wall mock-up. The first wall is the plasma facing surface of the blanket which has to withstand a thermal radiation of up to 500 kW/m². One of the experimental requirements is to reproduce this heat flux. For the current set-up this means that about 150 kW have to be deposited onto the surface of the first wall by a suitable heating device. Amongst others the possibility to use an induction heater was therefore investigated (see Fig. 1). In order to come to a decision about the final heating device a report has been issued. When the final method is chosen the procurement of the power supplies for the heater and the integration into the test section of HELOKA will be the main tasks for 2012.

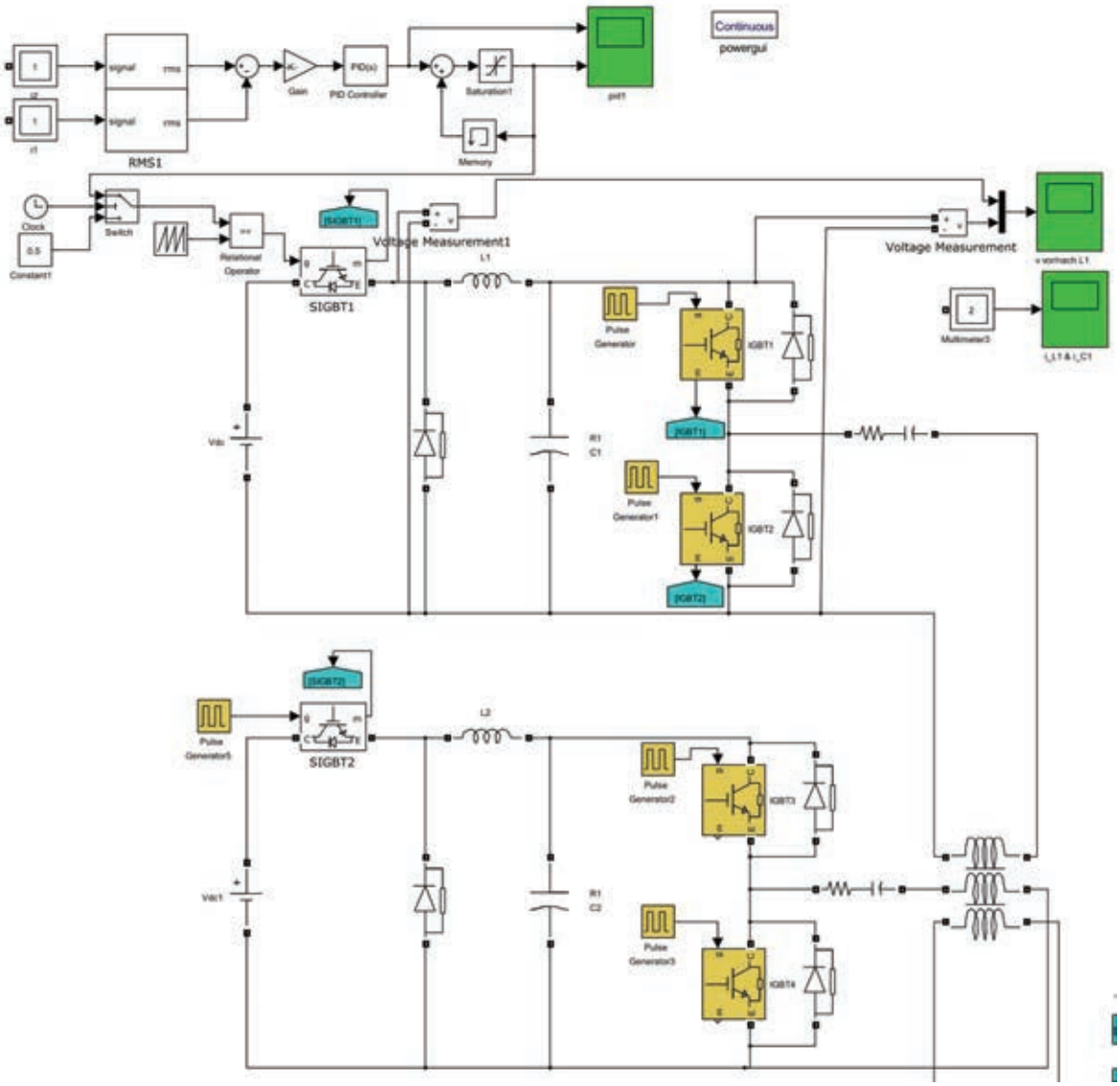

Fig. 1: Part of the model of a three-phase, current controlled high frequency current generator for an induction heater in Matlab/Simulink SimPowerSystems.

Cooperation with Industry

Andreas Hofer Hochdrucktechnik GmbH, Germany, contractor:
- supply and commissioning of a helium compressor

Klöpper-Therm GmbH & Co. KG, Germany, contractor:
- supply and commissioning of a helium heater

Siemens AG Karlsruhe, Germany, contractor:
- supply of several power and control cubicles
- installation of instrumentation
- implementation of hard- and software into control system

ATE, Czech Republic, contractor: - supply of several power supply cubicles

ATEKO/VUES, Czech Republic, contractor: - supply of frequency converters

Staff:

A. Kunze
M. Schmid

Acknowledgement

This work, supported by the European Communities under the contract of Association between EURATOM and Karlsruhe Institute of Technology, was carried out within the framework of the European Fusion Development Agreement. The views and opinions expressed herein do not necessarily reflect those of the European Commission.

Goal Oriented Training Programme “Breeding Blanket Developments for Fusion Reactors” (WP08-GOT-EUROBREED (FU07-CT-2008-00047))

The EUROBREED network is integrating almost the all the important aspects of the breeder blanket programme including development of breeder materials, characterisation and modelling of properties (e.g. thermo-mechanics and tritium release), test of these materials in out-of-pile and in-pile experiments, integration of them in ITER, and also some aspects for the integration in the future DEMO reactor. Thus, the broad range of competences required in the European breeder development in the future is addressed, and the proposed project will provide a significant and necessary improvement in the expert basis required.

EUROBREED, jointly conducted by KIT, AEUL, CEA, CIEMAT, ENEA, NRG, HAS-University of Budapest, and CCFE, consists of eight work packages (WP). Two of them are hosted at KIT (WP1 and WP2): WP1 is entitled “Design, procurement and test of solid breeder units” and WP2 “Pebble bed development and testing for the EU solid breeder blanket”. Furthermore KÍT is in charge of the Coordination of this network.

In 2011 the activities related to EUROBREED network continued regularly for the third year; the conclusion of the network is foreseen in September 2012. Progress meetings were held in Madrid (May) and Karlsruhe (October) with presentation of the work by all the trainees, presentation and visit of the host laboratories and Meeting of the Coordination Board.

The only issue was the anticipated conclusion of WP-4; in fact the trainee left her position in Cadarache for a new job. The network is now reduced to only 7 work packages.

In **work package No. 1**, the technical programme of the trainee consists of three parts: (1) the design and analyses of a TBM Breeder Unit (BU), (2) fabrication, procurement and assembly of a BU mock-up and (3) testing of the BU mock-up. The three years long training period started on the 24th of August 2009.

With the completion of the 2nd year the trainee completed the final design of the BU: during the 3rd year he will concentrate on the mock-up procurement and on the design of a consistent experimental plan. Carrying out these activities he will contribute to the design of the Helium loop layout and procurement of the loop components.

The actual possibility to test a BU mock-up for the trainee is shifted because the design and construction time of the related Helium facility in KIT is delayed due to technical and design-change reasons. In order to allow the trainee to complete the BU mock-up testing campaign, the trainee program will be integrated in a PhD program of the trainee. The overall activities performed within the training will be completed by the experimental activities, including validation of the mock-up performances and benchmark of the design codes used in the design process, to be performed in the PhD specific extension period.

After completion of the training program, 2 additional years are considered to complete the PhD plan: in this period the trainee will finalize the mock-up and helium facility procurement phase and will follow up the experimental campaign and evaluate the results of the experiments. The main goal will be to evaluate the BU expected thermo mechanical performances and to validate the set of computational tools used for the BU design assessment.

For the last year of the training program the revised technical programme consists in:

- Adaptation of the TBM BU design to the BU mock-up design, including relevant parameters (material, manufacturing processes, Post Welding Heat treatments).
- Procurement of the structural components of the BU mock-up (follow-up the manufacturing process directly in the manufacturing company during critical manufacturing steps).

- Preparation of an experiment plan including selection of parameters, selection and installation of dedicated diagnostic systems and experimental devices.

For the specific aspects listed above the trainee will be involved in the design and commissioning of the KATHELO Helium loop layout.

This technical program requires interfaces/collaboration with different experts in KIT itself but also in other European Associations. A close collaboration will be required with manufacturing and material experts from KIT and CEA and then from the industry.

Staff:

L.V. Boccaccini
F. Hernandez (trainee)
F. Cismondi

Literature:

[1] F. Hernández, F. Cismondi, B. Kiss, Thermo-mechanical analyses and assessment with respect the design codes and standards of the HCPB Breeder Unit, Presented as poster at the ISFNT-10 (Portland 2011), doi:10.1016/j.fusengdes.2012.02.088.

[2] F. Cismondi, B. Kiss, F. Hernandez, E. NDiaye, G. Legradi, J. Reimann, M. Ilic, The fundamental role of fluid dynamic analyses in the design of the solid EU Test Blanket Module, Presented as poster at the ISFNT-10 (Portland 2011), doi:10.1016/j.fusengdes.2012.02.089

Acknowledgement

This work, supported by the European Communities under the contract of Association between EURATOM and Karlsruhe Institute of Technology, was carried out within the framework of the European Fusion Development Agreement. The views and opinions expressed herein do not necessarily reflect those of the European Commission.

Manufacturing and Testing of a FW Channel Mock-up for Experimental Investigation of Heat Transfer with He at 80 bars and Reference Cooling Conditions. Comparison with Numerical Modelling (TW5-TTBB-001 D 10)

Purpose and methods applied for investigation of heat transfer in the first wall

The Task TW5-TTBB-001 D10 deals with investigations of heat removal from the first wall of Helium-Cooled-Pebble Bed Test Blanket Module (HCPB TBM). The purpose of investigations was to experimentally prove the numerically found decrease of heat transfer coefficient due to the asymmetry of heat loads at the first wall of HCPB TBM.

The investigations have been done experimentally by manufacturing and testing of a mock-up for a cooling channel in the first wall as well as computationally by developing of corresponding 3D CFD models. The mock-up named HETRA (HEat TRAnsfer) involves one U-sweep of the cooling channel in the first wall of HCPB TBM Version 1.1. The heated HETRA section involves two channel bends and a long straight section which simulates the plasma adjacent part of the first wall. This section is heated only on the surface representing plasma facing side. The heat flux at the plasma facing side of the first wall is simulated by a set of discrete ceramic heaters.

The heated section is made of TBM relevant Eurofer steel. TBM relevant parameters of Helium coolant (pressure of 80 bar and temperature of 300 ^{0}C) are provided by connection of HETRA test section to the HEBLO loop. The connection is made by the side channels.

The heated section has been made replaceable what provided examination of cooling channels with different surface roughness. In conducted experimental campaign two heated sections have been considered: (i) a channel with hydraulically smooth walls (surface roughness less than 2μm) and (ii) an artificially roughened channel with maximal roughness height in order of ~20μm.

The main goal of investigations was to determine a detailed temperature distribution in the Eurofer wall of the cooling channel. For that purpose, six sets of temperature measurements have been performed along the heated HETRA section. The measurements have been done applying thermocouples with a diameter of 0.5 mm. The pattern of thermocouples has been arranged in such a way that temperature data along two lines in channel cross-section can be obtained. In the front (heated) channel wall with strong temperature gradients three thermocouples have been placed for each measuring line. In the back (not heated) wall only two thermocouples along a measuring line have been applied. Therefore, within each of six sets the Eurofer temperature could be measured at 10 positions.

In all of the six experimental runs the Helium mass flow rate has been set to 80 g/s (due to strong resistance of HETRA test section, higher mass flow rates could not be realized in the HEBLO loop). Measurements with both, smooth channel and rough channel, have been performed for Helium inlet temperature of 300 ^{0}C (as TBM relevant temperature) and temperature of 50 ^{0}C (by which heat loses from the test section were negligible low). Finally, measuring series with hydraulically rough channel and Helium inlet temperature of 300 ^{0}C are conducted for three levels of heater power: 2x2600 W, 2x2100 W and 2x1600 W which respectively correspond to surface heat flux of ~270 kW/m^2, ~216 kW/m^2 and ~166 kW/m^2.

Numerical investigations of fluid flow and heat transfer in HETRA test section have been performed by use of 3D CFD code STAR-CD. The computational domain has been arranged to mimics the test section in detail – from the involved materials up to the geometry of electrical heaters. Boundary conditions on the channel walls have been imposed using high Reynolds number approach. The power of heaters has been modelled by defining the volumetric source terms in the conductor part of the heaters. Outer boundary of test section has been considered as adiabatic, while heat loses have been accounted for by decreasing the power

of heaters according to the measured data. 3D CFD simulations have been conducted for each of the aforementioned measuring series.

Results of experimental and numerical investigation of heat transfer in the first wall

The experimental results could be retrieved by corresponding 3D CFD computational scenarios with satisfactory accuracy (see Figure 1).

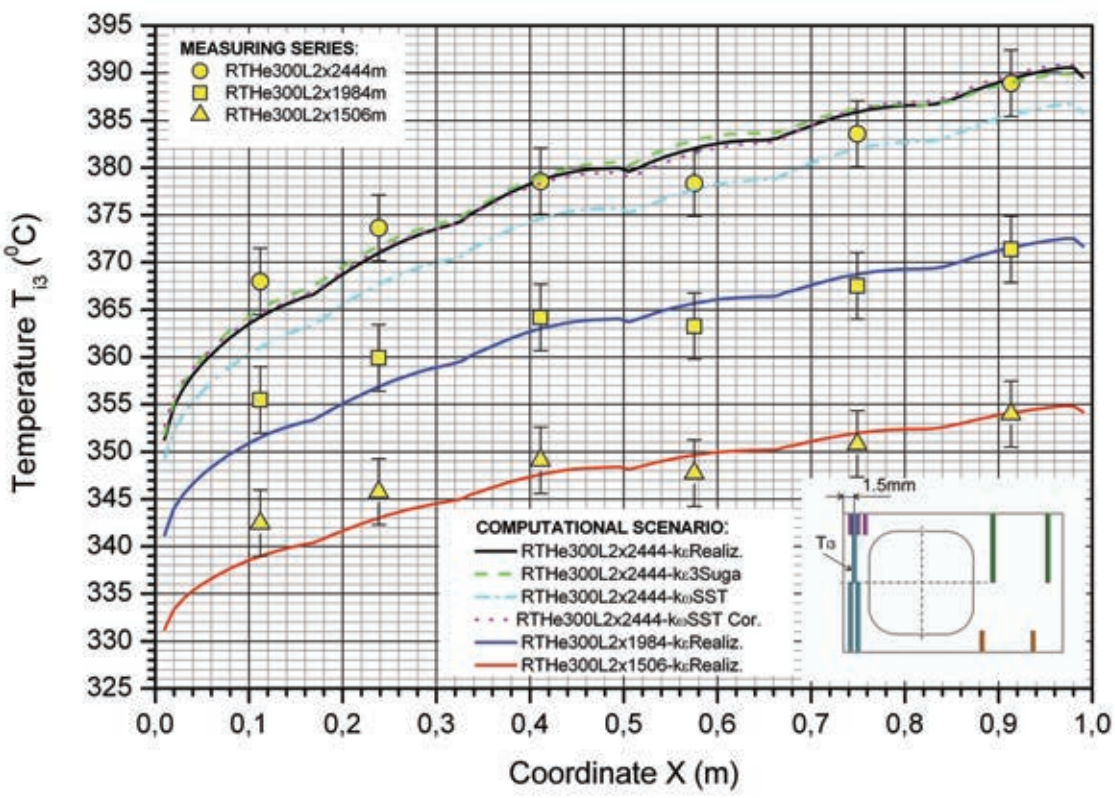

Fig. 1: Measured and 3D CFD computed temperature distribution along the heated section of HETRA test channel (for Legend notation see Nomenclature).

On the other side, so-called 1D CFD approaches, where heat transfer is evaluated on the basis of Helium bulk temperature and mean heat transfer coefficient obtained by use of common engineering correlations, could not be verified against experimental data for Eurofer temperature (see Figure 2): in the front heated channel wall the measured temperatures were strongly underestimated (~15-17 ^{0}C), while in the back non-heated wall an overestimation of measured temperatures of ~5 ^{0}C has been discovered. This finding is of particular importance because it means that the use of the aforementioned 1D CFD approaches in conditions of the first wall would inevitably lead to dangerous underestimation of maximal Eurofer temperature as well as underestimation of temperature gradients across the first wall and therefore underestimation of thermal stresses.

An analysis of methods for improved treatment of heat removal from the first wall by codes for structural analysis (like ANSYS code) has shown that the use of mean heat transfer coefficient and fluid bulk temperature as representative parameters should be abandoned. Instead, 3D CFD data for local heat transfer coefficient defined in relation to Helium temperature in wall adjacent fluid layer should be adopted. To apply this method, data on both variables should be extracted from 3D CFD results along the channel perimeter at several longitudinal positions, transferred to ANSYS model and then properly interpolated over the channel surface. Evaluations performed in this way for conditions of HETRA test section showed acceptable agreement with measured data.

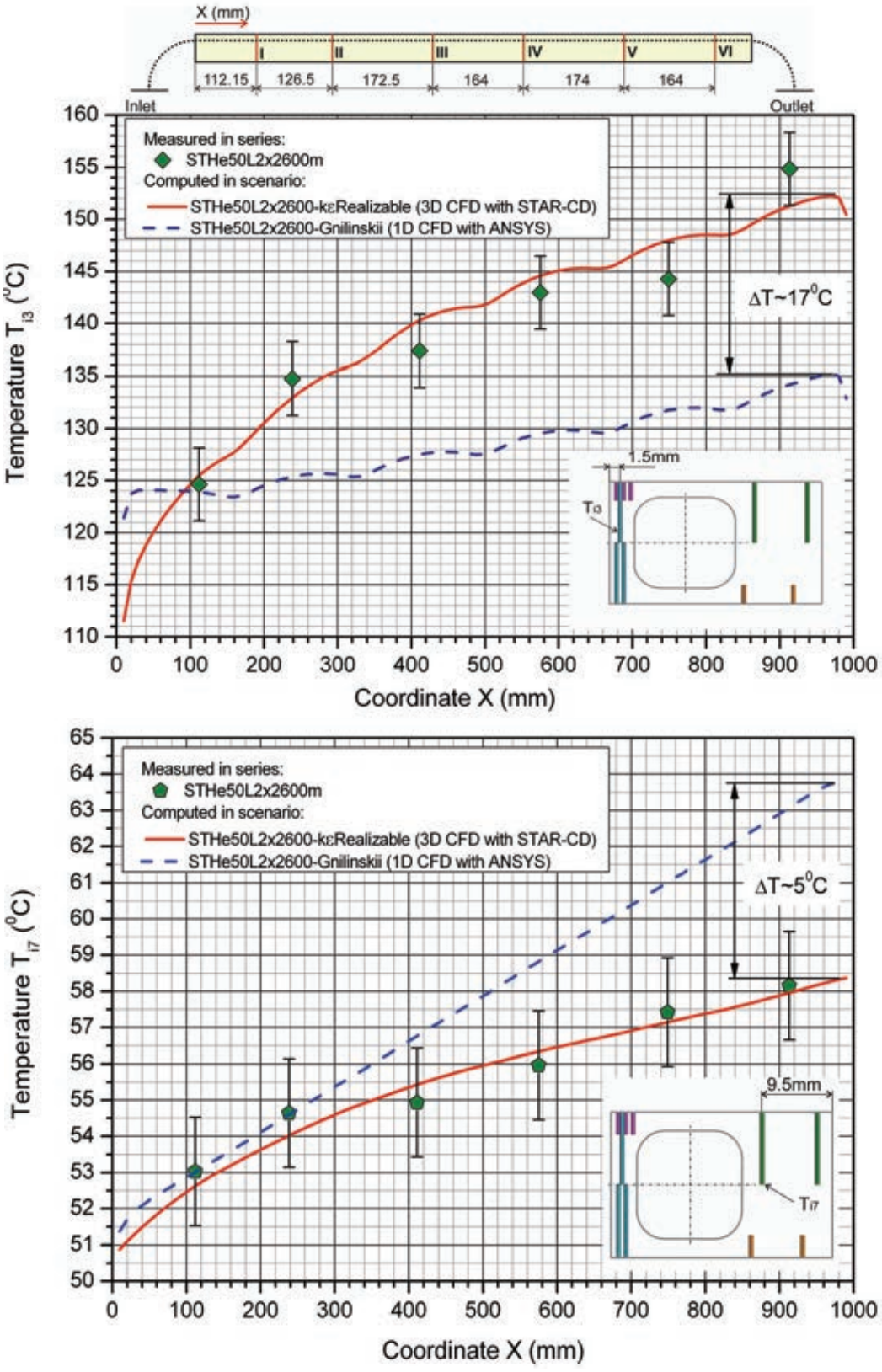

Fig. 2: Temperature distribution computed by 1D CFD approach (ANSYS model with heat transfer coefficient α=4821 W/m^{2}K according to Gnilinskii correlation for Nusselt number) in comparison with 3D CFD results and measured data (for Legend notation see Nomenclature).

The comparison of results for hydraulically smooth and hydraulically rough test channel has shown that the influence of surface roughness on improvement of heat transfer is quite modest (see Figure 3) – for TBM relevant Helium inlet temperature of 300^{0}C a decrease of Euro-

fer temperature of ~6-7^{0}C has been found in the front heated channel wall. Such a situation is not surprising when one takes into account that the channel is only slightly rough – evaluated dimensionless roughness height r^+~13.5 is close to the lower edge of transitional rough regime.

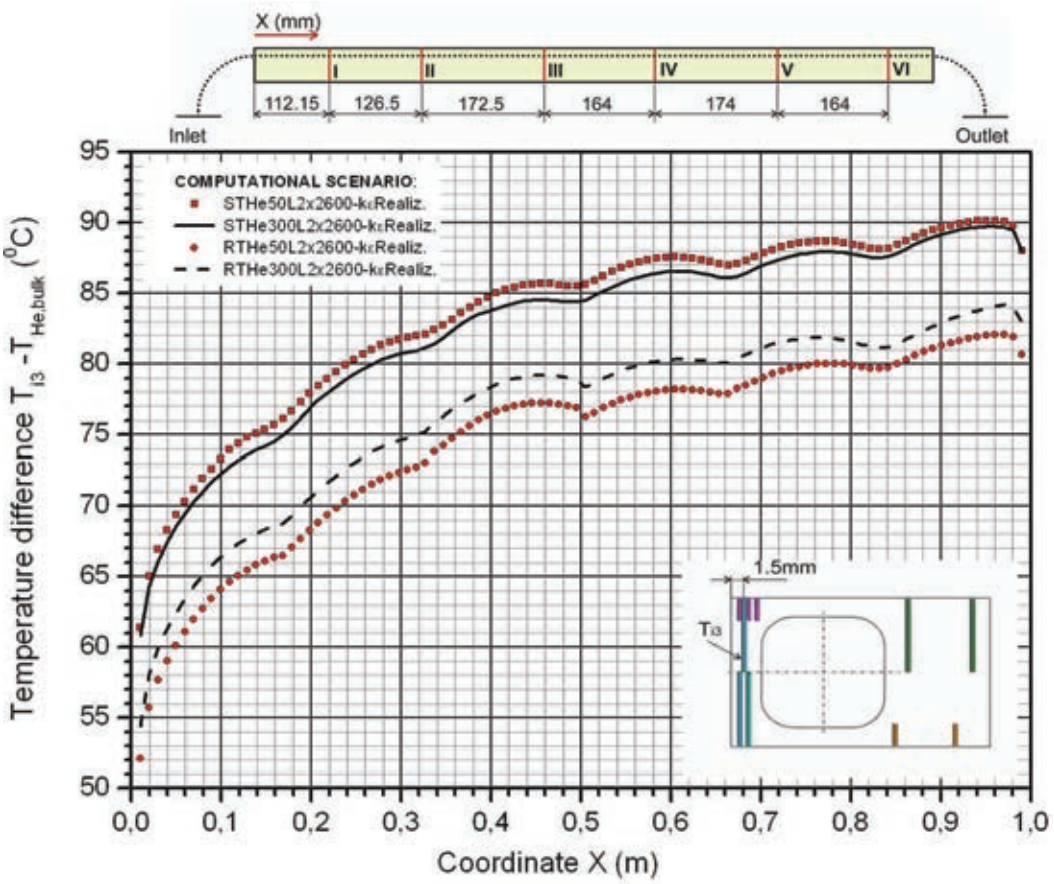

Fig. 3: Eurofer temperature in heated wall computed for hydraulically smooth / rough channel and inlet coolant temperature of 50^{0}C / 300^{0}C. Results are presented relative to Helium bulk temperature (for Legend notation see Nomenclature).

Finally, an analysis of temperature field in channel cross-section (see Figure 4) has revealed that the back non-heated channel wall is practically inactive in heat transfer. The heat coming from the front heated side of the channel is transferred to Helium coolant before it reaches the back part. A further analysis has shown a steep temperature distribution of Helium coolant in cross direction. This means that the Helium close to the front hot wall takes most of the heat, while Helium close to the back cold wall does not contribute significantly to the heat removal from the first wall.

This finding has been used to propose an alternative design of the cooling channel in the first wall of HCPB TBM Version 2.1 which can be summarized in the following way: (i) current square like channel cross section of 15x15 mm with 4 mm pellet radius has been replaced by a rectangular like channel cross section of 15x8 mm with rounded shorter sides, (ii) 12 parallel cooling channels each consisting of two in series connected U-passes foreseen in the current design were replaced by 24 parallel channels with only one U-pass and (iii) mass flow rate per channel of 1.33/12=0.1108 kg/s in the current design has been replaced by mass flow rate per channel 1.33/24=0.0554 kg/s.

3D CFD analyses have shown that with the aforementioned alternative design of the cooling channel the first wall can satisfactorily be cooled; even when the channel walls are hydraulically smooth (maximal Eurofer temperature of 531 ^{0}C has been found). On the other side, channel walls in the current design would probably have to be roughened since maximal Eu-

rofer temperature computed for smooth channel surface (547.3 ^{0}C) is too close to the maximal allowed value of 550^{0}C. Finally, the real advantage of the alternative to the current design of cooling channel in the first wall lies in its significantly better hydraulic performance – pumping power for the alternative design of the cooling channel is ~30-35% of those necessary in the case of the current channel design.

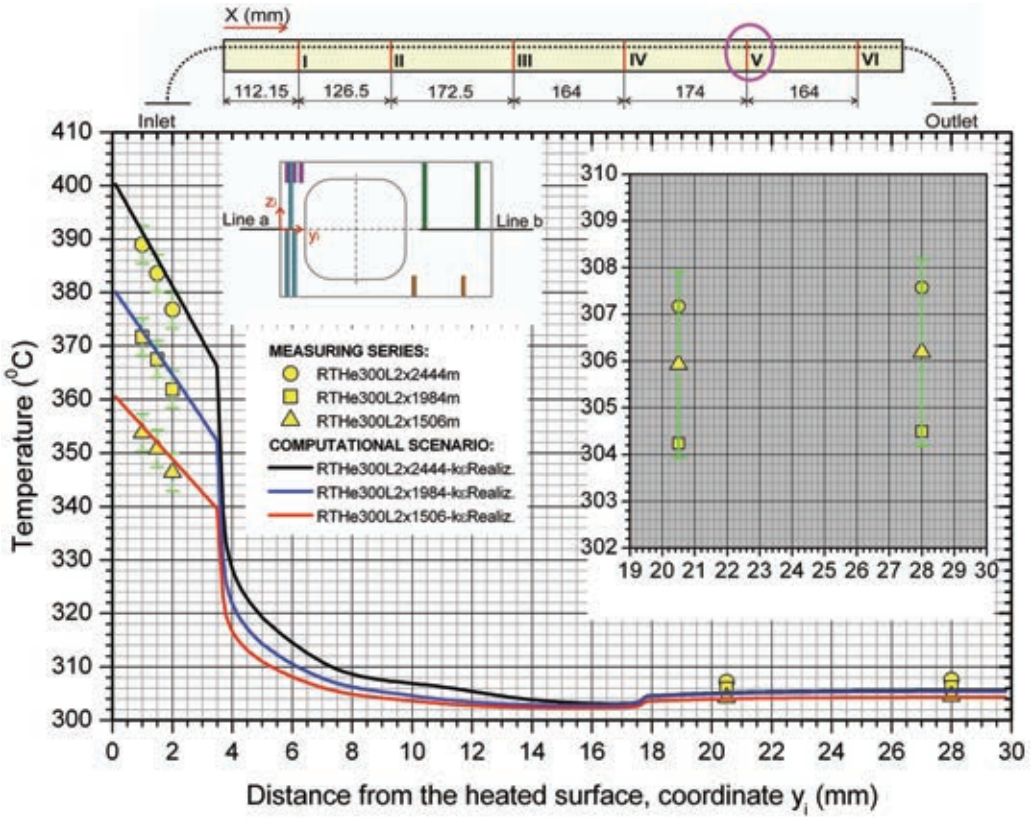

Fig. 4: Temperature distribution in cross-section of HETRA test channel (measuring plane V) (for Legend notation see Nomenclature).

Conclusions and outlook

The activities within this Task have been completed in 2011 and a Final Report has been issued. The investigations of heat transfer in the first wall have shown that: (i) by use of experimental data it was possible to verify 3D CFD models and (ii) 1D CFD approaches in which heat transfer in the first wall is evaluated on the basis of common engineering correlations for heat transfer coefficient failed in comparison with experimental data.

Finally, based on detailed analysis of experimental and 3D CFD obtained in the framework of this Task an improved design of cooling channels in the first wall could be proposed. The authors recommend further investigations to find out an optimal solution for cross-section of the cooling channel.

Nomenclature

Notation of measuring series/computational scenarios in Figure 1-4:
S/R-hydraulically smooth/rough channel;
THe50 / The300 - Helium inlet temperature 50^{0}C/300^{0}C;
L2x2600 - heating power (in W) transferred to Helium coolant over surface $19.3 \cdot 10^{-3} m^2$ (heat losses are negligible);
L2x2444, L2x1984 and L2x1506 - heating power transferred to Helium coolant over surface $19.3 \cdot 10^{-3} m^2$ (heat losses of ~6% are accounted for).
Names of computational scenarios include applied turbulence model.

Staff:

M. Ilic
S. Kecskes
B. Kiss
G. Messemer
V. Szabo
K. Zinn

Acknowledgement

This work supported by the European Communities under the contract of Association between EUROATOM and Karlsruhe Institute of Technology, was carried out within the framework of the European Fusion Development Agreement. The views and opinions expressed herein do not necessarily reflect those of European Commission.

Manufacturing and Testing of Mock-ups for Investigation of Coolant Flow in the Manifold System of HCPB TBM (GRICAMAN Experiments) (TW5-TTBB-003 D 1)

For the investigation of flow distribution in the coolant system of HCPB TBM an experimental facility named GRICAMAN has been designed and is under construction (see Figure 1). The flow domain to be investigated in GRICAMAN experiments is defined to be the upper poloidal half of HCPB TBM Version 2.1 bounded at the outlets of the first wall channels, at the outlets of by-pass pipes and at the inlets of breeding units, i.e. involving one half of manifold 2, cooling channels in four horizontal and eight vertical stiffening grids, 8 cooling channels within two cap halves, half of manifold 3 and inlets of 8 breeding units. Significant simplifications of the experimental facility are achieved (i) assuming that the flow is adiabatic, (ii) replacing helium with air pressurised at 3 bar and ambient temperature and (iii) representing complicated stiffening grid- and cap channels by simple pipes with the equivalent flow resistances (named equivalent grid/cap channels). The facility is designed keeping real geometry of manifold 2 and manifold 3 and replacing complicated grid and cap cooling channels with simple pipes having the same flow resistance as the real channels. This report presents activities done in 2011 on the further development of GRICAMAN facility.

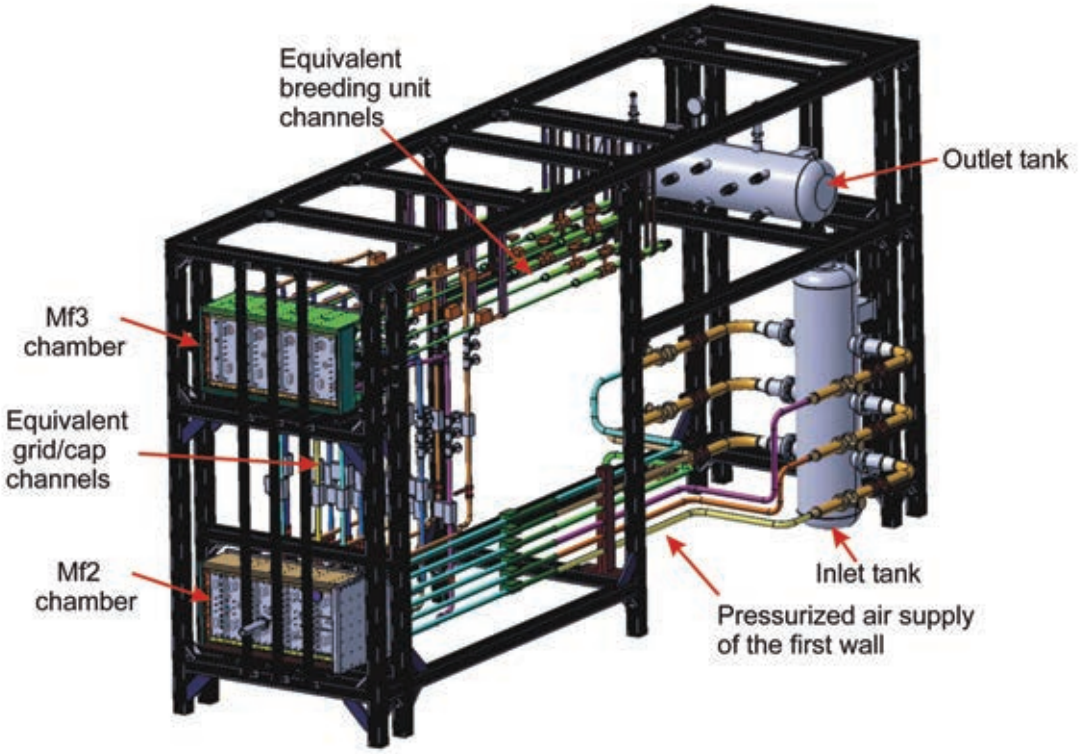

Fig. 1: CAD design of Gricaman facility and Gricaman frame.

All lines for supply/exhaust of the working fluid (air pressurized at 3 bar and at ambient temperature) have been built and tested. All auxiliary components of GRICAMAN facility (like inlet distributor, outlet collector, etc.) have been mounted and tested. A probe assembling of two manifold chambers has been done. All equivalent grid/cap channels have been assembled and hydraulically adjusted.

An especially demanding task was to assemble and adjust the equivalent grid/cap channels. Therefore, as these channels are tightly packed in limited space between two manifold chambers, their final assembling had to be done in situ (see Figure 2). For that purpose manifold chambers had to be mounted and properly fixed at the GRICAMAN frame. How-

ever, in this phase no final assembling of manifold chambers could be done, i.e. no sealing rings has been applied. This is due to high temperatures which occur when equivalent channels were welded to corresponding flanges (screwed at manifold parts). The assembling of these channels has been done by the company Kraftanlagen Heidelberg GmbH.

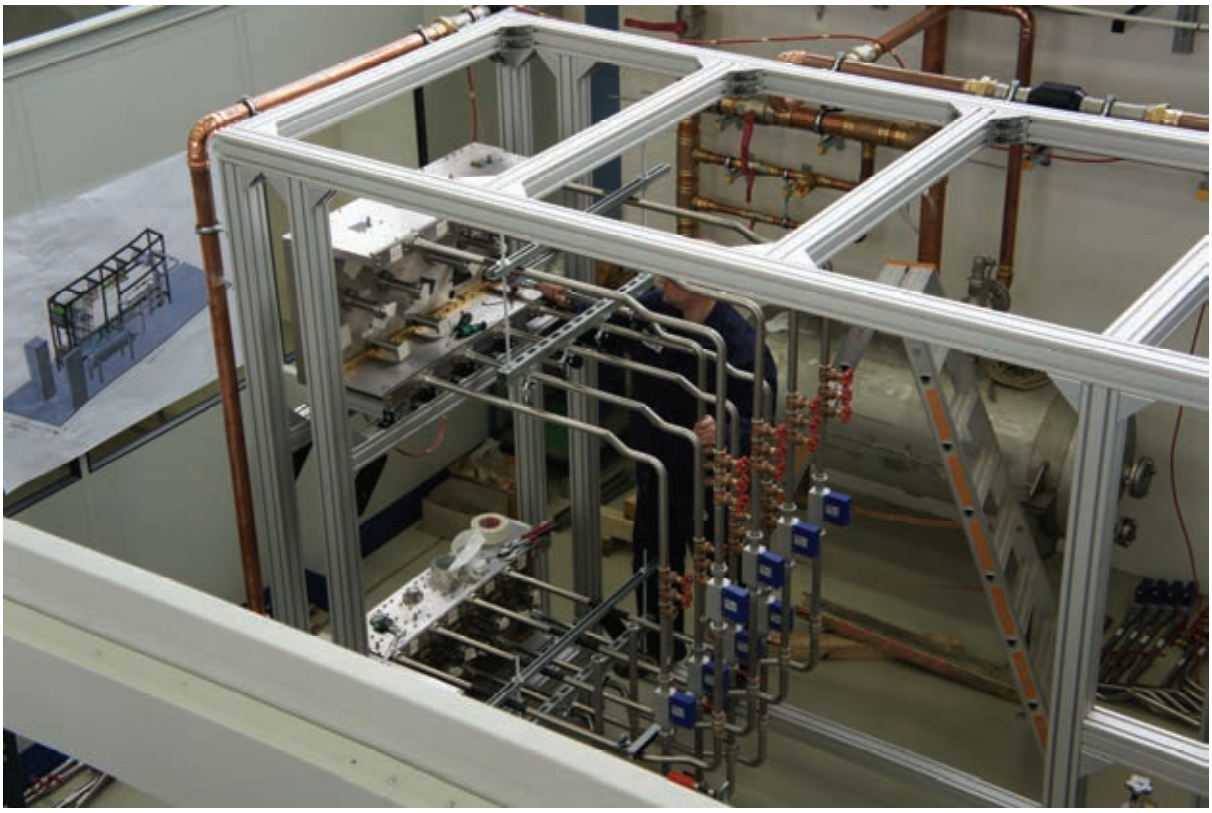

Fig. 2: Final assembling of equivalent grid/cap channels.

In the next step each of 20 grid/cap channels had to be hydraulically adjusted. For that purpose at each channel three slide valves have been foreseen by the design, so that the resistance of the channel could be increased / decreased by turning the valve stem on/off. For a proper practicing of this procedure, it was of extreme importance to know the exact position of each valve stem. As no appropriate device could be found at the market, we designed and manufactured the sub-assembly presented in Figure 3. Replacing the standard valve wheel with this sub-assembly provided tracking the position of the valve stem up to 1/12 of its pitch (corresponds to turning the wheel on/off of 30^0). In this way hydraulic resistance of equivalent grid/cap channels could be related to the position of the valve stem. The applied practice is illustrated in Figure 4 with an example of an equivalent vertical grid channel. Therefore, for a given mass flow rate of air (here nominal mass flow rate) the pressure loss between the channel inlet and outlet has been measured for different positions of the valve stem. Next, from the pressure curve obtained in such a way the position of valve stem could be found which corresponds to the pressure loss de-

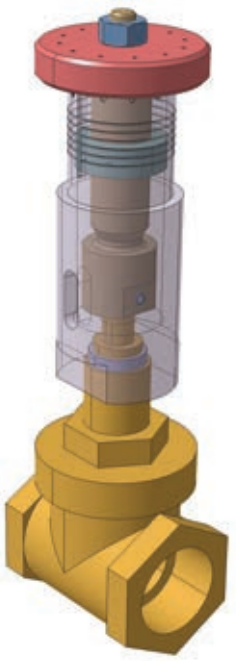

Fig. 3: CAD design of sub-assembly for control of position of valve stem. The sub-assembly has been applied for an adjustment of hydraulic resistance of equivalent grid/cap channels.

termined for the real grid channel. Note that position of the valve stem in Figure 4 is presented by the number of full turns starting from the fully opened position (presented with regular number) and the number of additional 30^0 steps (presented as superscript).

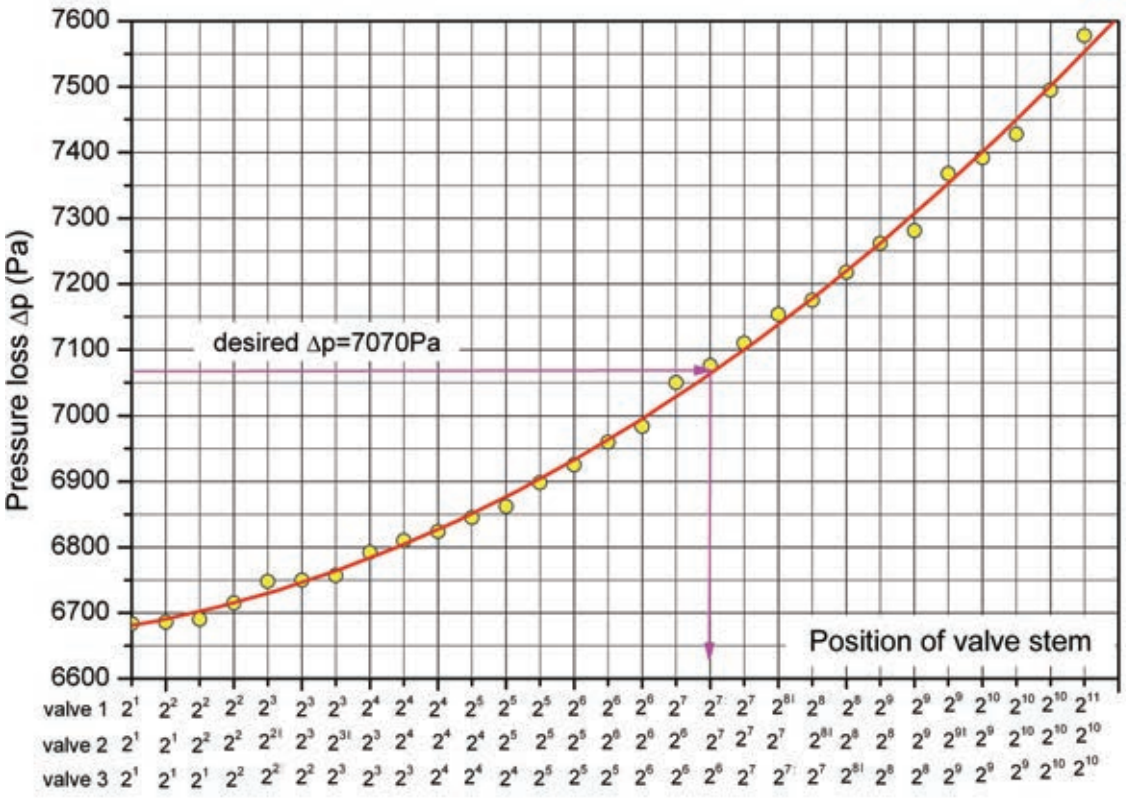

Fig. 4: An example of experimental adjustment of hydraulic characteristic of equivalent channels in Gricaman facility (equivalent vertical grid channel is presented). For notation of valve stem position see the text.

The status of GRICAMAN activities is as follows. Currently, the final mechanical assembling of manifold chambers (with sealing rings) is under preparation. The installation of instrumentation will be done till end of January 2012. In February 2012 tests will be started. Simultaneously the 3D CFD model of GRICAMAN flow domain is under development. It is planned that all GRICAMAN activities will be completed at the beginning of June 2012, when the Final Report for this Task will be issued.

Staff:

O. Albrecht
O. Bitz
M. Ilic

Acknowledgement

This work supported by the European Communities under the contract of Association between EUROATOM and Karlsruhe Institute of Technology, was carried out within the framework of the European Fusion Development Agreement. The views and opinions expressed herein do not necessarily reflect those of European Commission.

Conceptual Design of the Tritium Accountancy Systems for the European Test Blanket Systems (F4E-GRT-254 (PNS-TBM) – Action 2)

Scope and objectives

One of the major ITER missions is to test breeder blanket concepts so as to increase the confidence level that the next reactor (i.e. DEMO) can demonstrate the required tritium self-sufficiency. Europe will operate two different Test Blanket Modules (TBM) in ITER: the Helium Cooled Pebbles Bed (HCPB) and the Helium Cooled Lithium Lead (HCLL) concepts.

The objectives of this grant managed by the European Consortium of Associates for the TBM (TBM-CA) are the following:

- Action 1 by CIEMAT: develop a numerical tool for tritium migration in the breeder blanket to perform a sensitivity study for different scenarii (pulse length and frequency, different structure materials, different TBM sizes);
- Action 2 by KIT-TLK: define the strategy to ensure a reliable and accurate tritium measurement at the outlet of the TBM in view of benchmarking the neutronics calculation.

Previous results

During the previous period, the review and consolidation of the processes to be used in the Tritium Extraction system (TES) and Coolant Purification System (CPS) of the EU TBM has been completed [1-3]. In particular, different traps have been selected to remove from the Helium purge and coolant streams the tritiated species:

- Adsorption Column (AC) containing zeolite material to remove tritiated water vapour (noted Q2O) [4];
- Getter Beds (GB) containing zirconium alloy to remove tritiated hydrogen (noted Q2).

Such traps are working in adsorption / desorption cycles, so that two traps are needed to achieve quasi continuous process. The regenerated Q2 can directly be sent to the tritium plant while the regenerated Q2O need additional process. A PERMCAT reactor [5-7] placed downstream of the AC has been finally retained to recover the tritium from Q2O in the Q2 form [8, 9].

Achievement in 2011 for the design of the tritium accountancy system for the ITER TBM

The first activities were focused on the clarification and validation of the input data for the expected tritium production (input from CIEMAT) and the tritium system configuration / operation (input from ENEA). From this, the expected regenerated streams from all the components containing tritium have been characterised in terms of total flow rates and tritium levels (Figure 1).

Afterwards, different strategies have been studied to define the best proposal for the tritium accountancy system (TAS). The expected performances of different analytical techniques to measure tritium (as well as the overall chemical composition) have been used to evaluate meticulously two different cases, i.e. the static (gas collection) or dynamic (on-line real-time) approach. A multi-criteria decision analysis considering accuracy, space, operation, and price has been performed for all the 8 streams of Figure 1. Finally the tritium accountancy system (TAS) has been selected [10] as shown in Figure 2. It consists mainly in dynamic accountancy measuring the mass flow rate and the tritium activity using ionisation chambers [11]. This approach has been mainly retained since it allows minimising the space needed, and improves both the reliability and the DEMO relevancy.

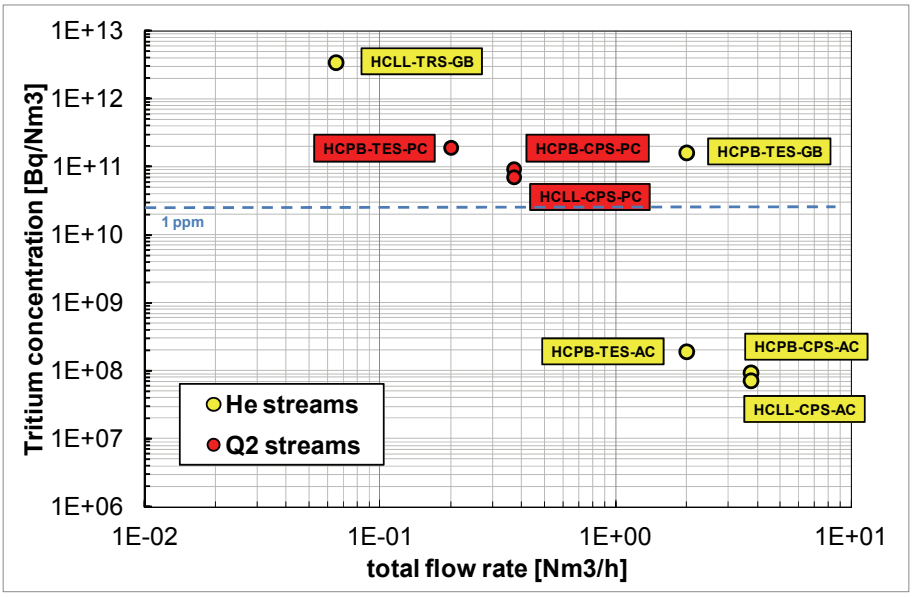

Fig. 1: Tritiated streams expected from the regeneration of the different components.

Solely for the HCLL-TRS, a static accountancy using 2 parallel collecting vessels (for pVT) working in sequence connected to a gas chromatograph has been retained. This has been motivated due to the rather small flow rate and the expected large variation of the chemical composition that makes it difficult to ensure a good accuracy using the dynamic approach. For all streams routed to TP containing significant tritium amounts, tritium accountancy as good as 5% should be achievable.

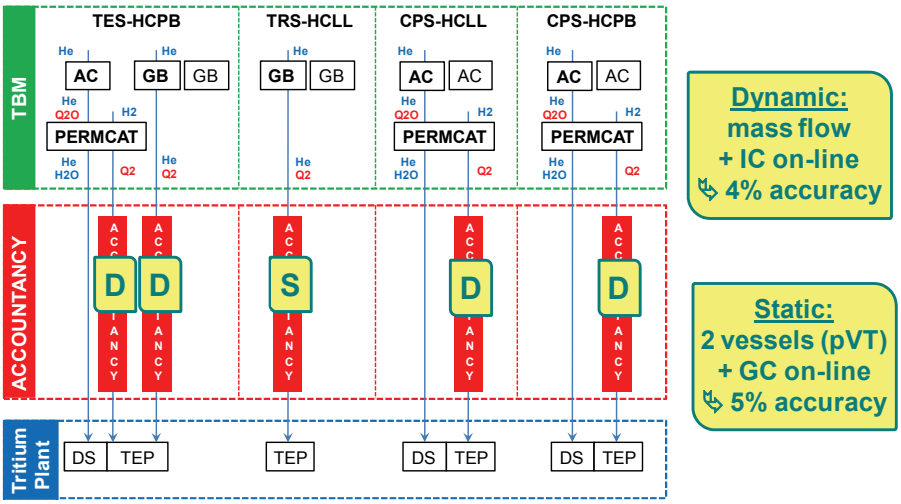

Fig. 2: Architecture of tritium processes in EU TBM, indication of best TAS and interface with the tritium plant.

Based on this proposal that has been acknowledged by F4E, the work has been pursued to provide the detailed pipe and flow diagram, the preliminary operation manual, and finally the 3D CATIA model as shown in Figure 3. Thanks to the mainly retained dynamic approach as well as the static approach using 2 vessels in parallel, the space allocation has been reduced to the minimum. All the instrumentation and components required can be accommodated in a glove box of about 6 m^3.

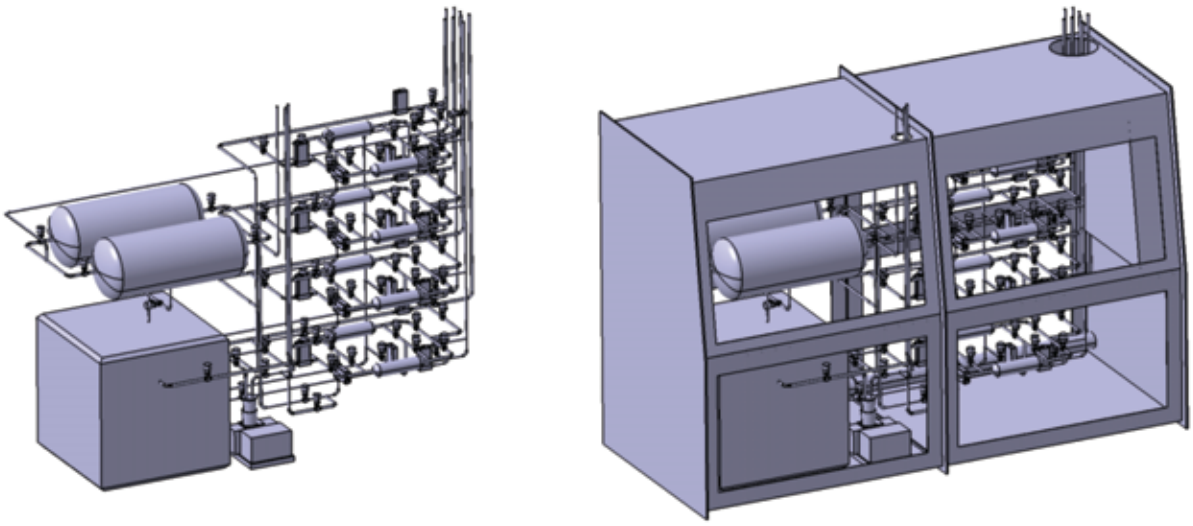

Fig. 3: 3D CATIA view of TAS (left) hosted in a TLK standard glove box.

Conclusion and perspectives

The first conceptual design of the tritium accountancy system for the ITER TBM has been completed. This is an important milestone for the overall TBM programme since it will ensure a relevant and valuable experimental programme in ITER in view of neutronics validation and tritium self-sufficiency in DEMO. The next activities should focus on the experimental demonstration of such accountancy principle. The announced performances should be verified within the large range of flow rate and tritium levels.

Staff:

C.G. Alecu
D. Demange
M. Schwarz
R. Wagner

Literature:

[1] A. Ciampichetti, A. Aiello, G. Coccoluto, I. Ricapito, K. Liger, D. Demange, C. Moreno " The coolant purification system of the European test blanket modules: Preliminary design" *Fusion Engineering and Design* **85** (2010) 2033.

[2] K. Liger, A. Ciampichetti, D. Demange "HCLL and HCPB coolant purification system: preliminary measurement and instrumentation plan" *Fusion Science and Technology* **60** (2011) 1431.

[3] A. Ciampichetti, F.S. Nitti, A. Aiello, I. Ricapito, K. Liger, D. Demange, L. Sedano, C. Moreno, M. Succi "Conceptual design of tritium extraction system for the European HCPB test blanket module" *presented at ISFNT-10, Portland, USA, 11.16 September 2011, submitted to Fusion Engineering and Design*

[4] D. Demange, N. Bekris, U. Besserer, T.L. Le, F. Kramer, A. Parracho, R. Wagner "Overview of processes using zeolite at the Tritium Laboratory Karlsruhe" Proceeding of 5th international FEZA conference, 3rd – 7th July, 2011, Valencia, Spain; ISBN: 978-84-8363-722-7.

[5] S. Welte, D. Demange, R. Wagner "Characterisation of a multi-tube PERMCAT reactor in view of a technical facility for highly tritiated water processing at the Tritium Laboratory Karlsruhe" *Fusion Engineering and Design* **86** (2011) 2237.

[6] S. Welte, D. Demange, R. Wagner, N. Gramlich " Development of a technical scale PERMCAT reactor for processing of highly tritiated water" *presented at ISFNT-10, Portland, USA, 11.16 September 2011, submitted to Fusion Engineering and Design*

[7] K. Munakata, D. Demange "Development of numerical simulation code of membrane reactor for detritiation" *Fusion Engineering and Design* **86** (2011) 2334.

[8] D. Demange, E. Fanghänel, B. Kloppe, T.L. Le, F. Scheel, K.H. Simon, R. Wagner, S. Welte "CAPER modifications and first experimental results on highly tritiated water processing with PERMCAT at the Tritium Laboratory Karlsruhe" *Fusion Science and Technology* **60** (2011) 1317.

[9] A.I.R.T. Parracho, D. Demange, S. Knipe, L.T. Le, K.H. Simon, S. Welte " Process of highly tritiated water desorbed from molecular sieve bed using PERMCAT" *presented at ISFNT-10, Portland, USA, 11.16 September 2011, submitted to Fusion Engineering and Design*

[10] D. Demange, C.G. Alecu, N. Bekris, O. Borisevich, B. Bornschein, S. Fischer, N. Gramlich, Z. Köllö, T.L Le, R. Michling, F. Priester, M. Röllig, M. Schlösser, S. Stämmler, M. Sturm, R. Wagner, S. Welte " Overview of R&D at TLK for process and analytical issues on tritium management in breeder blankets of ITER and DEMO" *presented at ISFNT-10, Portland, USA, 11.16 September 2011, submitted to Fusion Engineering and Design*

[11] R. Wagner, U. Besserer, D. Demange, H. Dittrich, T. L. Le, K. H. Simon, K. Guenther "Improvement and characterization of small cross-piece ionization chambers at the Tritium Laboratory Karlsruhe" *Fusion Science and Technology* **60** (2011) 968.

Acknowledgement

This work was supported by Fusion for Energy under the grant contract No. F4E-GRT-254 (PNS-TBM) with collaboration by CIEMAT, Spain and ENEA Italy. The views and opinions expressed herein reflect only the author’s views. Fusion for Energy is not liable for any use that may be made of the information contained therein.

Design and Development of the European Test Blanket Modules (TBM) – Non-destructive Testing (NDT) (BMBF Reference No. 03FUS0011)

Objective

The objective of this task are to investigate the welded joints of TBM mockups, flat cooling plate and L-shaped first wall mockup, before and after heat treatment by using non-destructive ultrasonic immersion testing for the quality assurance and defect quantification.

Task current status

For quality assurance of the HIP joints and material characterization in the TBM mockup cooling plates, the plates were non-destructively tested by ultrasonic immersion technique. For the tests, the institute's own diving equipment system KC 200 from GE Inspection Technologies was used. The ultrasonic testing has been performed intermitting straight- and angle beam examinations using a 20 MHz sensor and by amplification of 80 dB (Fig. 1).

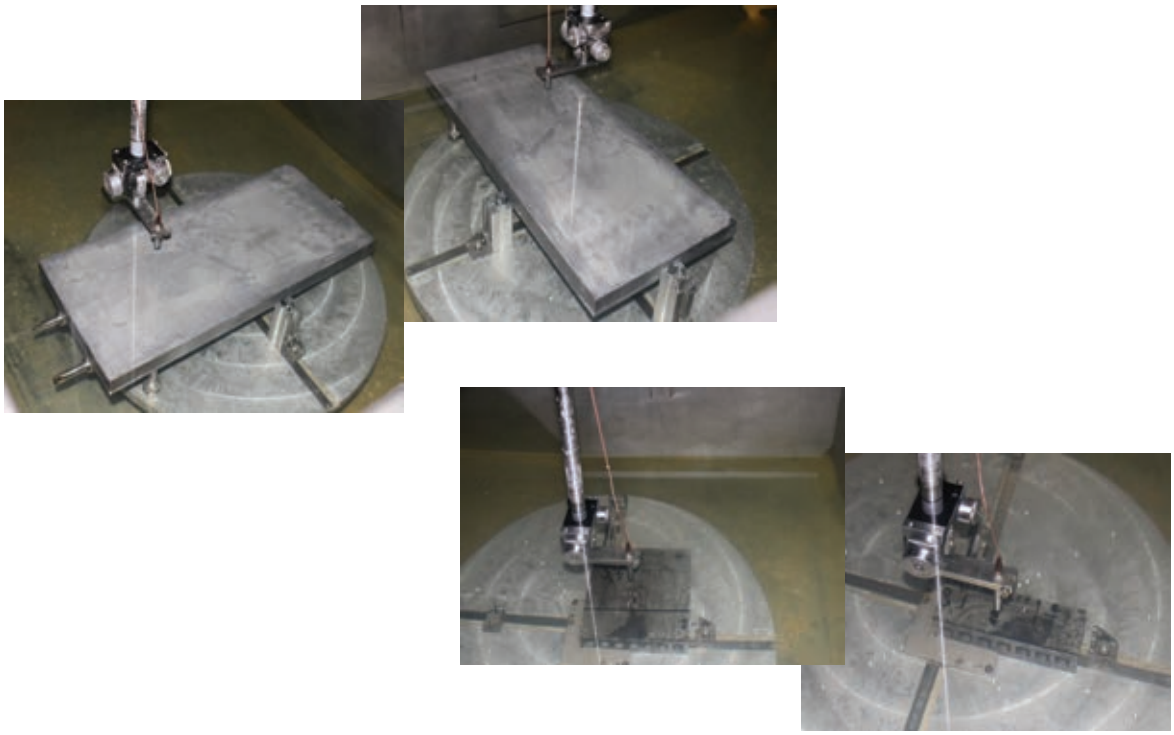

Fig. 1: Various TBM mockup cooling plates during scanning in ultrasonic bath.

During the ultrasonic immersion testing different inaccuracies were identified. In the TBM mockup cooling plates gaps directly at the HIP connections with lengths up to 1.2 mm, channel curvature, as well as pores or non-metallic inclusions (from 50 µm till 150-200 µm) were detected (Fig. 2, 3).

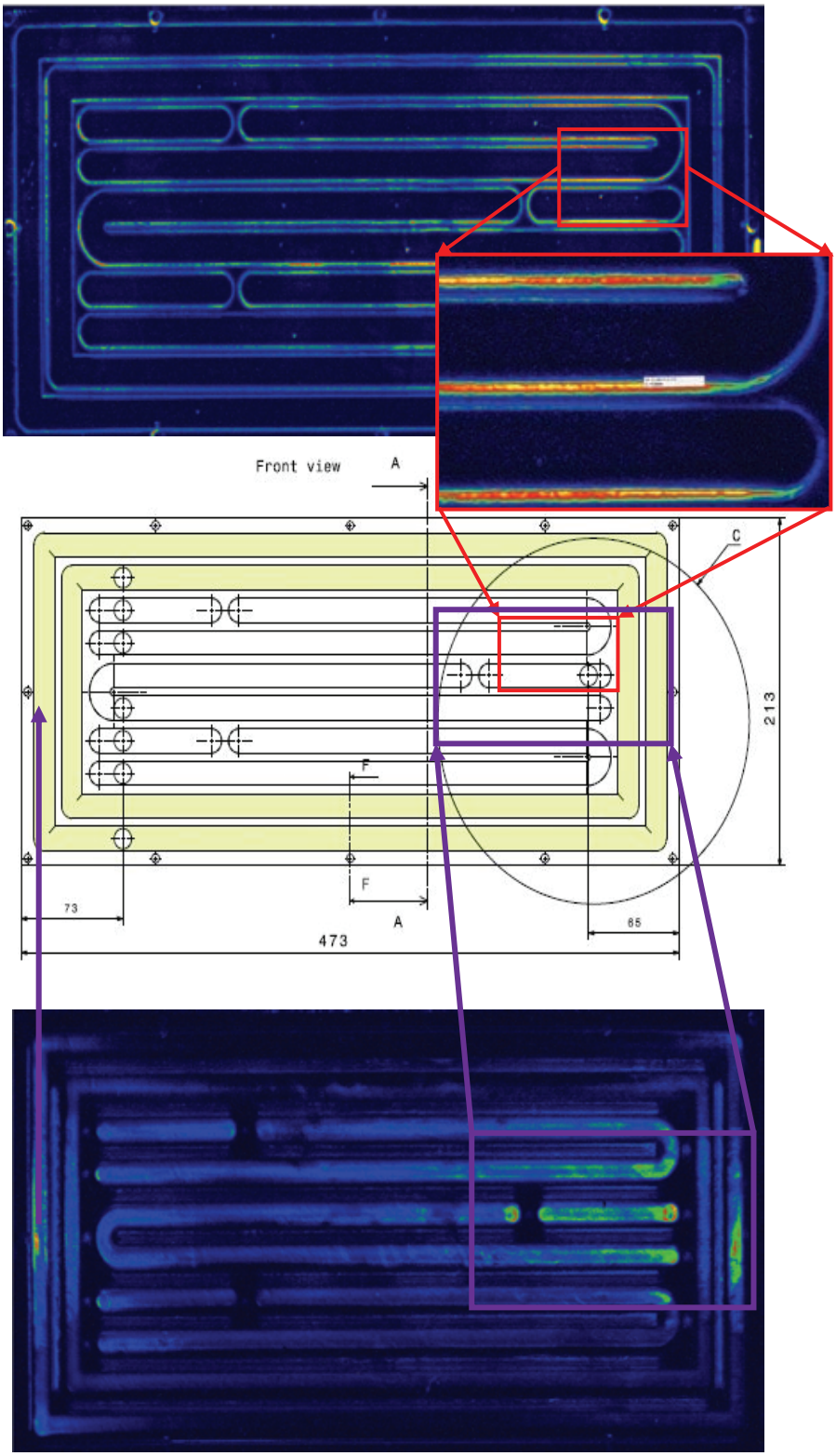

Fig. 2: Sketch of the TBM mockup plate with C-scan ultrasonic images.

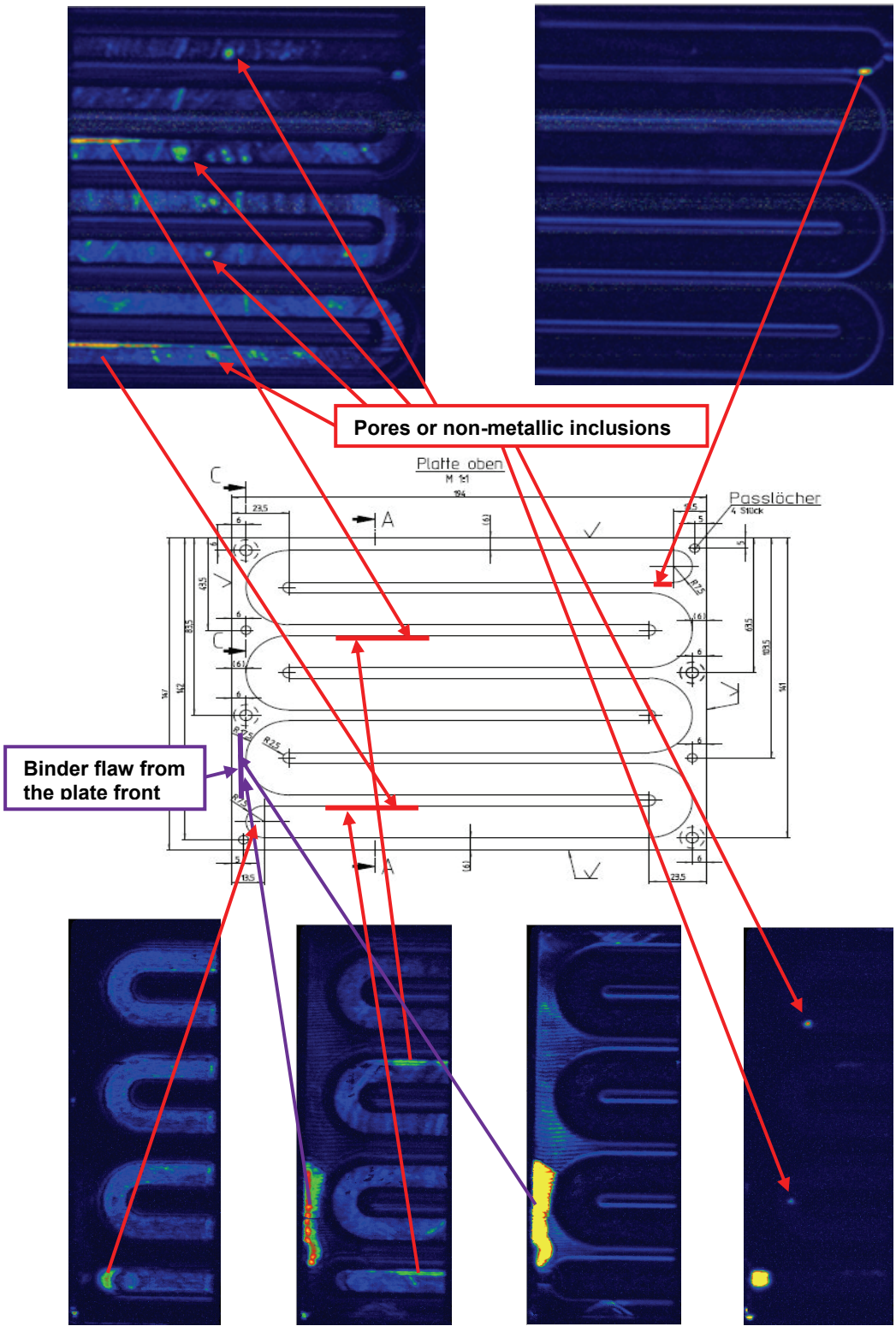

Fig. 3: Sketch of the TBM mockup plate with C-scan ultrasonic images.

Using the same NDT setup the L-shaped first wall mockup plate has been investigated before and after heat treatment (Fig. 4).

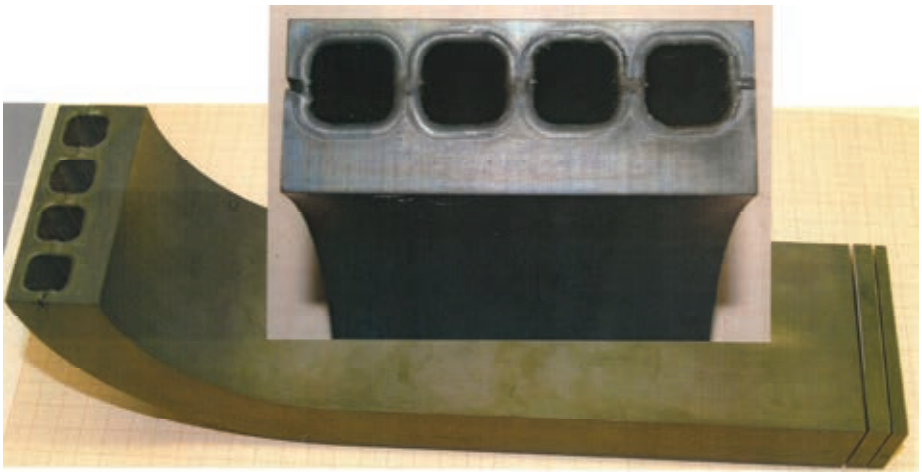

Fig. 4: View of the L-shaped plate first wall mockup.

In the ultrasonic examination irregularities (in the width of about 50-100 µm and along the entire plate), pores or non-metallic inclusions (from 50 µm till 150-200 µm) could be found (Fig. 5, 6).

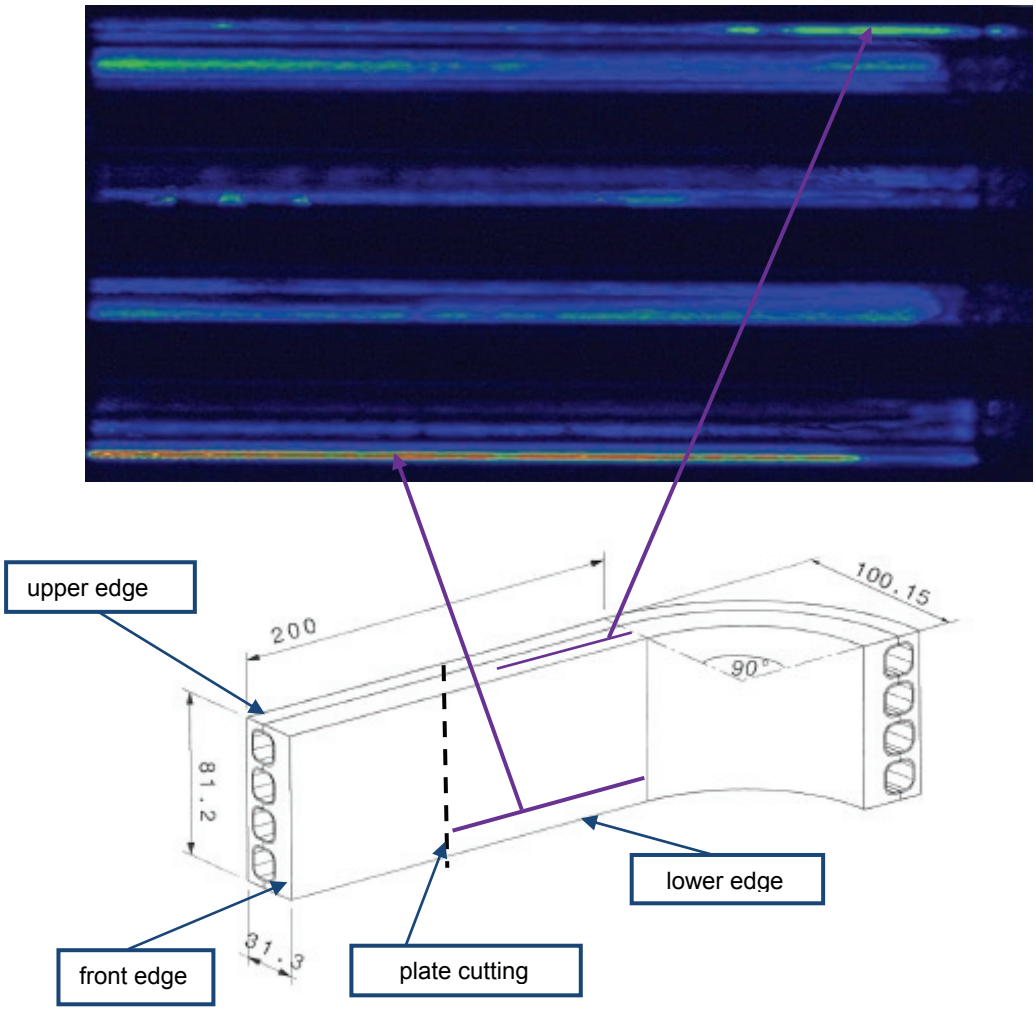

Fig. 5: View of the L-shaped first wall mockup with C-scan ultrasonic image.

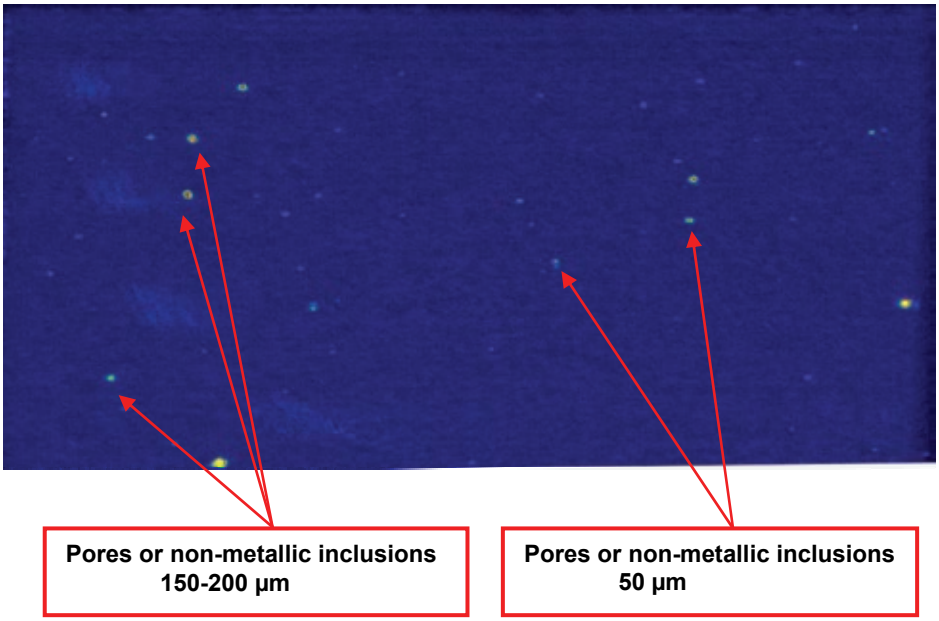

Fig. 6: C-scan ultrasonic image of the L-shaped first wall mockup plate.

Currently a first wall mockup fabricated by a new manufacturing technique for the realisation of curved inner cooling channels is investigated. The main focus lies on the relatively complicated geometry of the many diffusion bonded interfaces both on the stiffening plates, as well as on the bending place and their inspectability using the immersion ultrasonic technique established to date.

Staff:

J. Aktaa
S. Knaak
T. Martin

Acknowledgement

This work was financially supported by the Ministry of Research and Education (BMBF) under the grant No. 03FUS0011. The views and opinions expressed herein do not reflect necessarily those of the BMBF or the European Commission.

.

Procurement and Quality Control of Lithium Orthosilicate Pebbles – OSi 10/2 (HGF)

In collaboration with Schott AG, Mainz, the Karlsruhe Institute of Technology is developing and investigating slightly hyperstoichiometric lithium orthosilicate pebbles to be used in the HCPB blanket. The pebbles with a surplus of 2.5 wt% SiO_2 are produced by melting a mixture of $LiOH \cdot H_2O$ and SiO_2 powders and then spraying the liquid material in air. The characteristics of the final product are influenced by the batch wise melt-spraying process, which is rather difficult to control in the small facility. Consequently, the reproducibility from one production run to the other is not very high, and it is therefore necessary to control the quality of each batch of pebbles received from the industrial producer, in order to provide a well-defined standard material in all experimental activities with pebbles or pebbles beds.

In autumn 2010, 4.7 kg of Li_4SiO_4 (OSi) pebbles were delivered and characterized in three batches (OSi 10/2). The pebbles with diameters ranging from 250 to 630 µm were characterised in the initial state according to the standard test program for quality control. Characterisation included optical and scanning electron microscopy, size distribution, density, porosity, specific surface area, crush loads and chemical and phase analysis using X-ray powder diffraction.

The three batches that were tested showed clear differences between the material specifications, the SiO_2 excess and crush loads (see Table 1). To investigate the differences in the mechanical stability for each batch, crush load measurements were performed on 40 pebbles with a diameter of 500 µm. Mean values of about 4 N were determined with standard deviations of 1.5 N. These average crush loads appear significantly lower than previous batches such as OSi 10/1 (5.8 - 6.8 N) or OSi 08 (5.8 – 7.1 N).

Table 1: Physical properties of lithium orthosilicate pebbles OSi 10/2

Batch	**OSi 10/2-1**	**OSi 10/2-2**	**OSi 10/2-3**
Principal Constituents / wt% (Schott)			
Li_2O	48.53	48.51	48.58
SiO_2	50.85	51.01	50.77
excess SiO_2	*2.06*	*2.24*	*1.93*
Size Distribution			
d_{50} / µm	310	320	325
He-Pycnometry			
closed porosity (calc.) / %	0.5 ± 0.0	0.3 ± 0.0	0.5 ± 0.0
Hg-Porosimetry			
density / g cm^{-3}	2.26 ± 0.0	2.25 ± 0.01	2.26 ± 0.02
density / % TD*	94.3 ± 0.2	93.4 ± 0.2	94.2 ± 0.7
open porosity / %	4.8 ± 0.5	5.8 ± 0.2	4.6 ± 0.2
Pebble Bed Density			
tap density / g cm^{-3}	1.44 ± 0.03	1.44 ± 0.01	1.44 ± 0.01
Crush Load Tests			
mean crush load / N (IMF II)	4.1 ± 1.5	4.1 ± 1.5	4.0 ± 1.2

* A theoretical density of 2.4 g cm^{-3} was assumed for the OSi material.

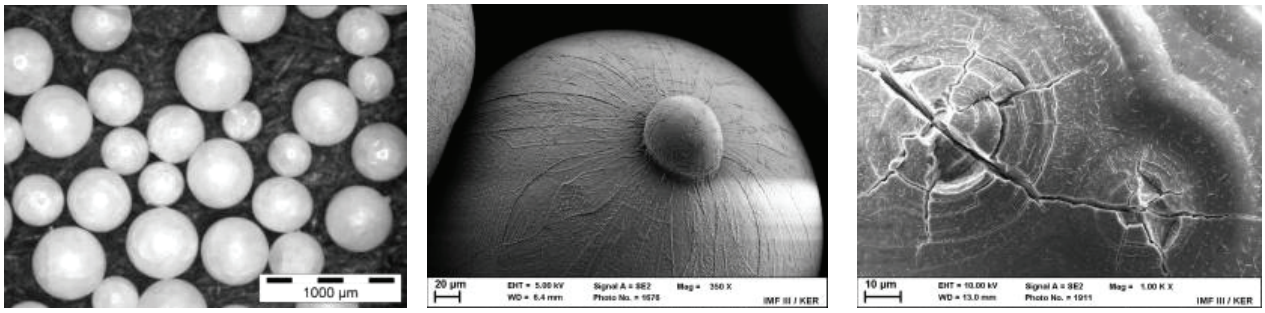

Fig. 1: Pebble morphology, pebble adhering to larger pebble & surface defects.

Optical microscopy examinations showed that all the OSi 10/2 pebbles exhibited a pearly white surface (Fig. 1). However, all of the batches contained pebbles with severe defects. A lot of the larger pebbles had smaller pebbles adhering to their surface, while nearly all had indentations or cracks on the surface, which is also shown using a scanning electron microscope in Fig. 1. However, the amount of large pores and cavities seems lower than usual. An examination of the pebble morphology, the microstructure at surfaces and at etched cross-sections for two of the batches OSi 10/2-1 and OSi 10/2-2 is given in Fig. 2.

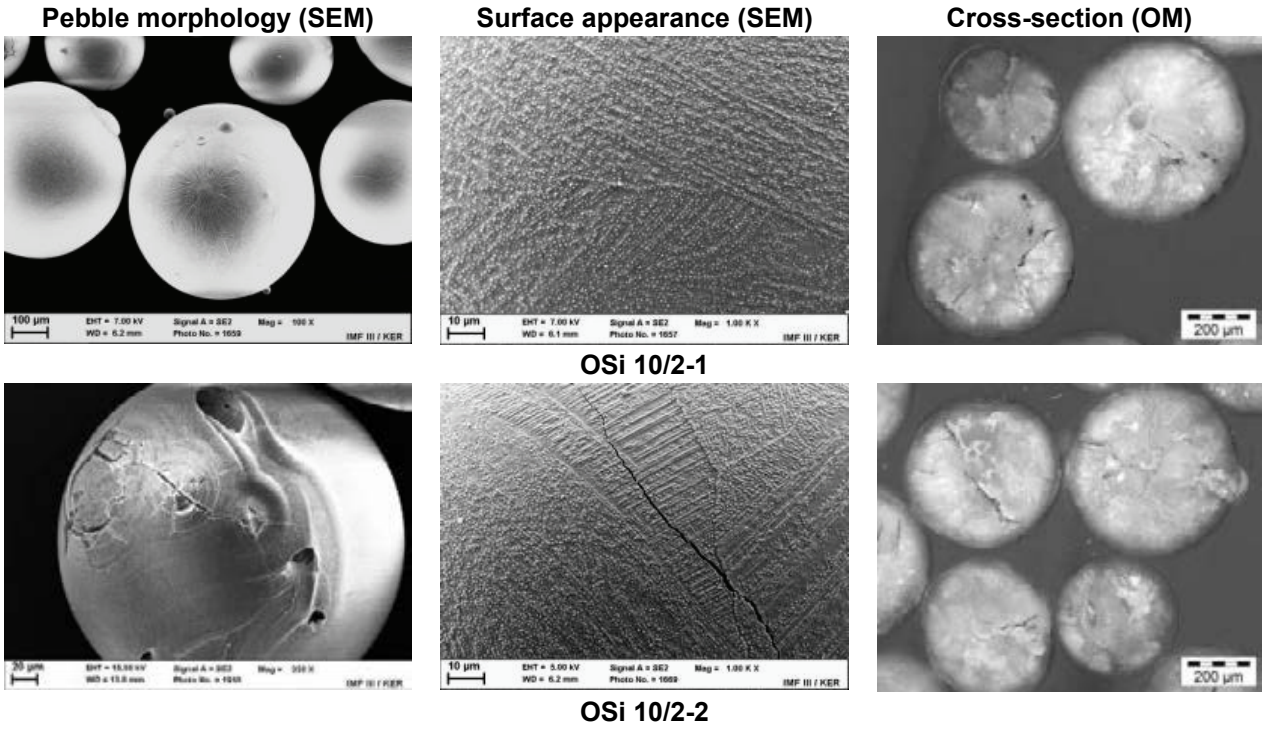

Fig. 2: Morphology and microstructure of lithium orthosilicate pebbles in the initial state.

The delivered pebbles were screened to a diameter range of 250-630 µm, resulting in fractions with a mean pebble diameter (d_{50}) between 310 and 325 µm for all three pebble batches of OSi 10/2 (Figure 3). The maximum of the distribution in each case is asymmetrically shifted to smaller diameters, which is similar to results obtained for previous batches.

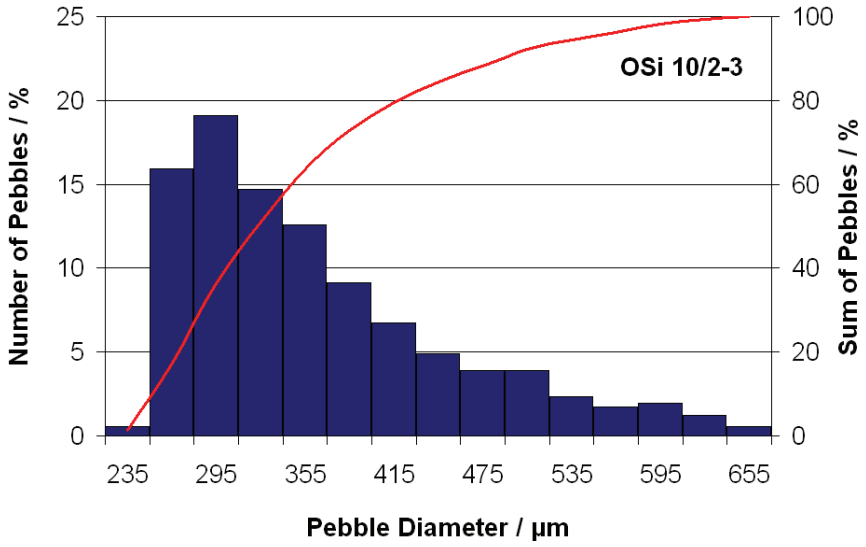

Fig. 3: Example of pebble size distribution for OSi 10/2-3.

Porosity and density of the orthosilicate pebbles were measured by He-pycnometry and Hg-porosimetry (Table 1). The inner density was measured by He-pycnometry, where the open porosity is neglected and only the closed porosity can be calculated. Closed porosities of 0.5 % were calculated for batch OSi 10/2-1 and OSi 10/2-3, and a somewhat lower value of 0.3 % for batch OSi10/2-2. By Hg-porosimetry relatively low densities in the range of 93.4 – 94.3 %TD were calculated based on a theoretical density of 2.4 gcm^{-3}. Open porosities of 4.6 – 5.8 % were also determined for the three pebble batches.

Small samples of the lithium orthosilicate pebbles were annealed at 950°C for 1 week under air to obtain the thermodynamically stable phases, lithium ortho- and metasilicate and a homogeneous microstructure in all pebbles. The results obtained for the conditioned pebble batches are summarised in Table 2. By thermal annealing, the crush load of each batch decreased slightly to a crush load of about 3 ± 1 N.

Table 2: Physical properties of conditioned lithium orthosilicate pebbles OSi 10/2-c.

Batch	**OSi 10/2-1-c**	**OSi 10/2-2-c**	**OSi 10/2-3-c**
Pebble Bed Density			
tap density / g cm^{-3}	1.45 ± 0.01	1.41 ± 0.00	1.44 ± 0.01
Crush Load Tests			
mean crush load / N	3.4 ± 1.0	2.9 ± 1.0	3.1 ± 0.9

* A theoretical density (TD) of 2.4 g/cm³ was assumed for the OSi material.

Investigations by SEM were performed for all batches in order to show the surface and inner structure represented by cross sections (Fig. 4). The appearance of the conditioned pebbles after annealing is very similar to that of the initial state. Most of the pebble surfaces display grains of lithium orthosilicate that have formed as a result of the decomposition of the high temperature phase $Li_6Si_2O_7$ into the stable phases Li_4SiO_4 and Li_2SiO_3 during the heat treatment. However, the inferior pebble morphology is still visible and Figure 4 shows that many of the cracks and defects are still present after the annealing process.

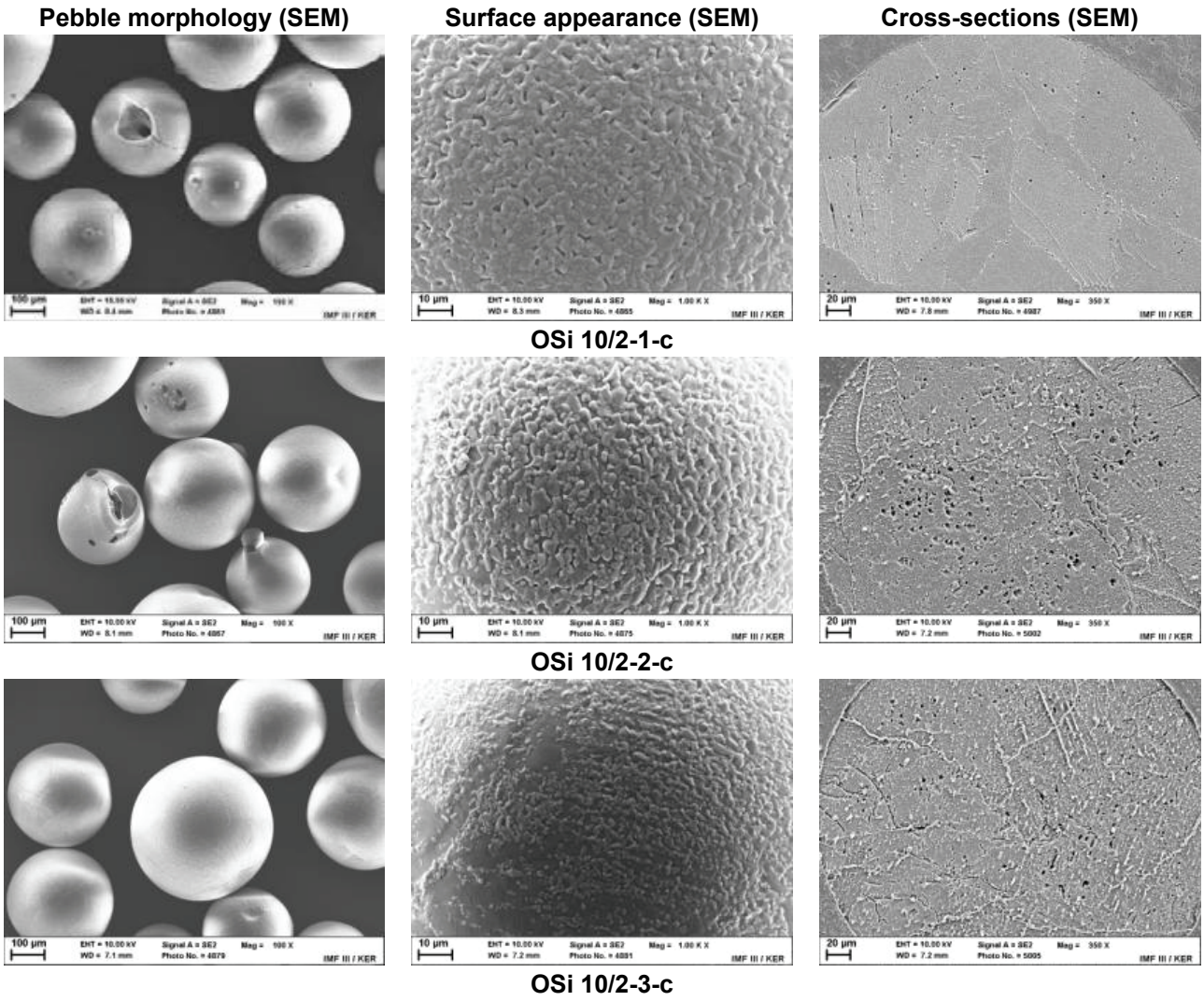

Fig. 4: Morphology and microstructure of lithium orthosilicate pebbles after conditioning.

Cooperation with Industry

The company Schott AG, Mainz, Germany, is the deliverer of the established lithium orthosilicate pebbles. The material development is carried out in close cooperation with KIT (former Research Center Karlsruhe).

Staff:

B. Dörzapf
U. Kaufmann
R. Knitter
M. Kolb
O. Leys
U. Maciejewski
C. Odemer

Literature:

[1] Abou-Sena, A., Löbbecke, B., von der Weth, A., Knitter, R., Effect of Post Welding Heat Treatment of the HCPB TBM on the Eurofer and Lithium Orthosilicate Pebbles, Fusion Eng. Design 86 (2011) 2254-2257.

[2] Zmitko, M., Poitevin, Y., Boccaccini, L., Salavy, J-F., Knitter, R., Moeslang, A., Magielsen, A.J., Hegeman, J.B.J., Lässer, R., Development and qualification of functional materials for the EU Test Blanket Modules: Strategy and R&D activities, J. Nucl. Materials 417 (2011) 678-683.

[3] Munakata, K., Mochizuki, K., Wajima, T., Wada, K., Hara, K., Shinozaki T., Takeishi, T., Knitter, R., Bekris, N., Fuji, T., Yamana, H., Okuno, K., Tritium release from ceramic breeder materials deposited with noble metals, J. Nucl. Materials 417 (2011) 731-734.

[4] Knitter, R., Chaudhuri, P., Feng, Y.J., Hoshino, T., Yu, I.-K., Recent developments of solid breeder fabrication, ICFRM-15, 16.-22. Oct. 2011, Charleston, USA, to be published in J. Nucl. Mater.

Production of Advanced Breeder Pebbles by a Modified Process (BMBF Reference No. 03FUS0012)

As part of the BA DEMO activities, the KALOS facility (KArlsruhe Lithium OrthoSilicate) was assembled to investigate a modified fabrication process for lithium orthosilicate pebbles. In 2010, several batches were fabricated to study the influence of process parameters such as pressure, cooling conditions and drop height on the pebble properties [1-3]. As a new acquisition in 2011, an oven with separate heating zones for crucible and nozzle was integrated into the facility. It will also enable the employment of larger batch sizes in future experiments. To avoid corrosion of the crucible, the upper region is kept at a slightly lower temperature than the lower region. The higher temperature in the lower part simultaneously compensates for extra heat losses around the nozzle (Fig. 1). The new experimental setup was used to study blended breeder ceramics consisting of lithium orthosilicate, lithium metatitanate and also lithium metasilicate. Therefore the composition of the melt was modified by additions of TiO_2.

Fig. 1: Experimental setup – test facility (drawing), single nozzle beam and the new oven.

It has been proven that the process can be operated successfully with the new setup and compositions. Additionally, these modifications also lead to higher process control resulting in a narrow size distribution as shown in Fig. 2.

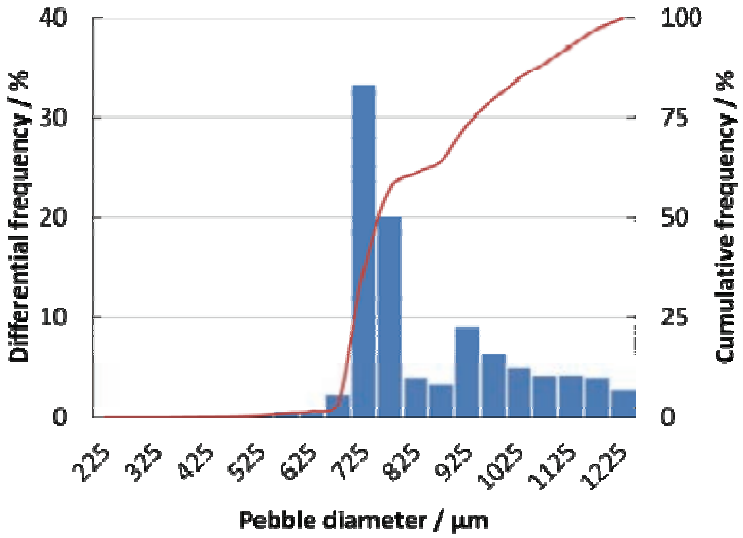

Fig. 2: Example of pebble size distribution for the modified process.

Due to the nature of the process, we currently aim to fabricate pebbles with a diameter of 700-750 µm. Although this value is significantly larger than the average diameter of pebbles produced by SCHOTT (ca. 320 µm), it still allows meaningful comparison of pebbles in the 500 µm range.

The blending of lithium orthosilicate and lithium metatitanate was done in order to optimize the pebble properties. Various experimental batches have been performed with additions of titanium dioxide and silicon dioxide to the melt to encourage the formation of secondary phases of up to 20 mol% of lithium metatitanate (Li_2TiO_3) and up to 15 mol% of lithium metasilicate (Li_2SiO_3) respectively [4,5]. Below are mappings of titanium and silicon compared to the standard scanning electron image (Fig. 3). It can be seen that the titanium is present at the grain boundaries of the dendritic lithium orthosilicate microstructure.

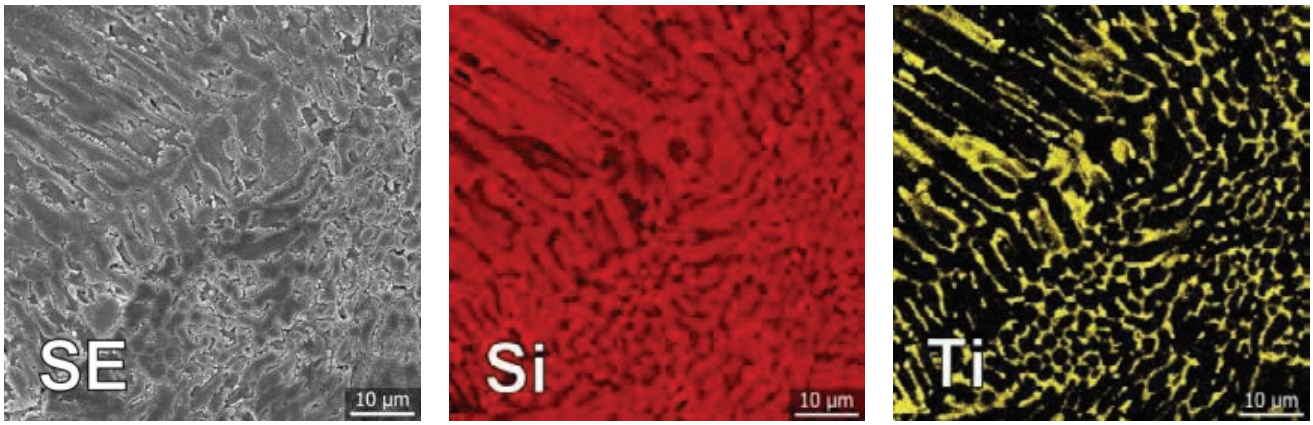

Fig. 3: Scanning electron mappings of silicon and titanium in pebble microstructure.

The main advantage of the addition of titanium dioxide is the apparent increase in crush load. An initial addition of 5 mol% drops the average crush load slightly. However, further increases in lithium metatitanate show a clearly increasing trend (Fig. 4).

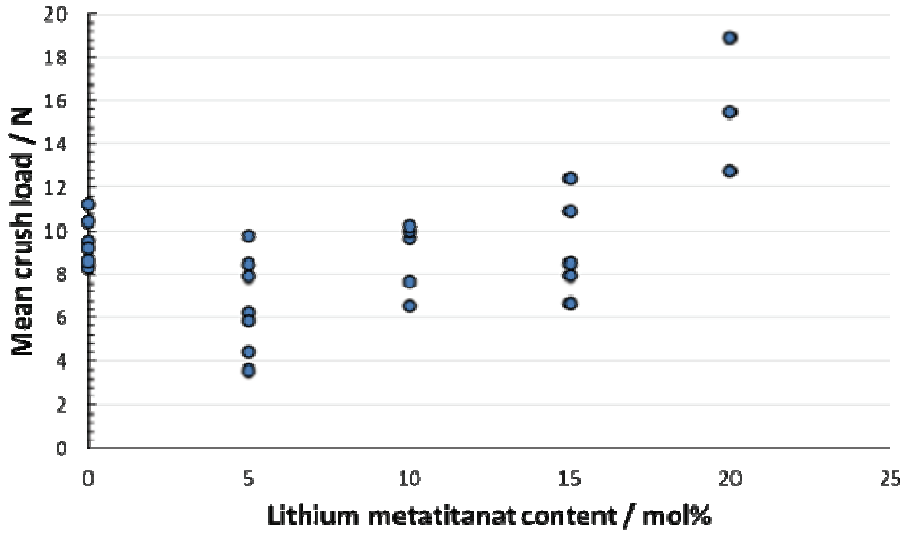

Fig. 4: Crush load results for pebbles with a diameter of 1000µm.

It was also found that the addition of titanium dioxide has the additional bonus of lowering the possible operating temperature of the crucible, which is favoured with respect to corrosion issues, as the melting point of the mixtures was reduced. This has also been verified by differential scanning calorimetry.

However, the phase equilibria for these compositions are not explored yet. It is thought that higher molar fractions of lithium metatitanate will, at some unknown value, start to increase the overall melting point of the mixture due to the high melting point of pure lithium metatitanate. It was also noted that an increase in lithium metatitanate also caused an increase in closed porosity of the pebbles (Fig. 5). The reason for the increase in the closed porosity is yet not clear, but it is assumed that it is caused by a lower density of the melt and thereby a higher increase of the density during crystallisation.

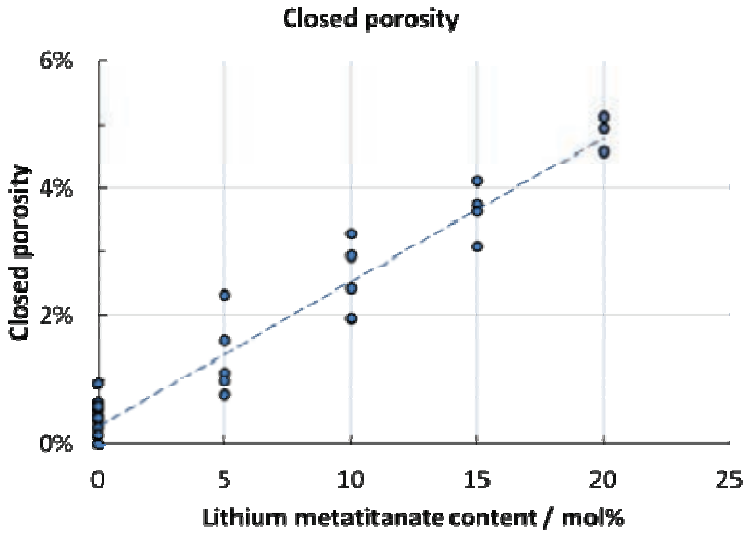

Fig. 5: Closed porosity as a function of lithium metatitanate content.

The effects of annealing the pebbles have also been studied. X-ray diffraction showed that a metastable disordered cubic modification of Li_2TiO_3 is formed during fabrication. This phase can easily be transformed to monoclinic lithium metatitanate by a short heat treatment. Different batches were conditioned at 950°C for a time period of 1 week and 3 weeks to examine the evolution of the microstructure at higher temperatures. In Figure 6 below, it can be seen that the metatitanate grain structure remains relatively stable over the annealing periods, and even during 3 weeks no significant grain growth occurs.

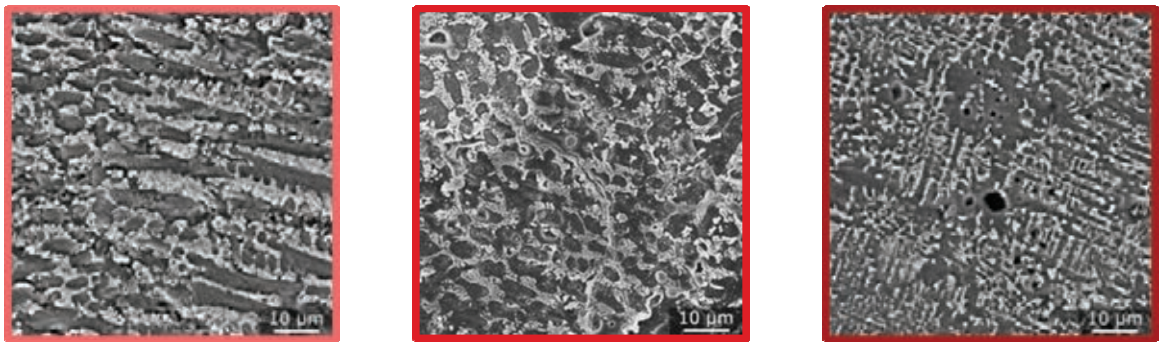

Fig. 6: Microstructure as received, after 1 week and after 3 weeks respectively.

The optimum content of titanium for metatitanate strengthened lithium orthosilicate pebbles will be evaluated in the near future. Furthermore, a modification of the cooling section is under progress to enable a more controlled cooling and crystallization of the pebbles with the aim to minimize the generation of cracks.

Cooperation with Industry

The company Goraieb Versuchstechnik, Karlsruhe, Germany, is involved in the BMBF project to develop an alternative production route for advanced lithium orthosilicate pebbles. The company is responsible for the technical setup and the operation of the facility. The optimization of the facility and the material development is carried out in cooperation with KIT.

Staff:

B. Dörzapf
U. Kaufmann
R. Knitter
M. Kolb
O. Leys
U. Maciejewski
C. Odemer

Literature:

[1] Kolb, M.; Knitter, R.; Kaufmann, U.; Mundt, D.: Enhanced fabrication process for lithium orthosilicate pebbles as breeding material. Fusion Eng. Design 86 (2011) 2148-2151.

[2] Kolb, M., Knitter, R., Enhanced Melt-Spraying Process for Tritium Breeder Pebbles, CBBI-16, 8-10 Sept. 2011, Portland, OR, USA.

[3] Kolb, M., Knitter, R., Advancements in the melt-based fabrication of tritium breeder pebbles, BA Workshop Meeting on Tritium and Blanket Technologies, Portland, OR, USA, 14.09.2011.

[4] Knitter, R., Kolb, M., Kaufmann, U., Goraieb, A.A., Fabrication of modified lithium orthosilicate pebbles by addition of titania, ICFRM-15, 16.-22. Oct. 2011, Charleston, USA, to be published in J. Nucl. Mater.

[5] Odemer, C., Maciejewski, U., Kolb, M., Knitter, R., Gefügeuntersuchungen an schmelzprozessierten Lithiumorthosilikatkugeln, 45. Metallographietagung, 14.-16. Sept. 2011, Karlsruhe.

[6] Abou-Sena, A., Löbbecke, B., von der Weth, A., Knitter, R., Effect of Post Welding Heat Treatment of the HCPB TBM on the Eurofer and Lithium Orthosilicate Pebbles, Fusion Eng. Design 86 (2011) 2254-2257.

[7] Zmitko, M., Poitevin, Y., Boccaccini, L., Salavy, J-F., Knitter, R., Moeslang, A., Magielsen, A.J., Hegeman, J.B.J., Lässer, R., Development and qualification of functional materials for the EU Test Blanket Modules: Strategy and R&D activities, J. Nucl. Materials 417 (2011) 678-683.

[8] Munakata, K., Mochizuki, K., Wajima, T., Wada, K., Hara, K., Shinozaki T., Takeishi, T., Knitter, R., Bekris, N., Fuji, T., Yamana, H., Okuno, K., Tritium release from ceramic breeder materials deposited with noble metals, J. Nucl. Materials 417 (2011) 731-734.

[9] Knitter, R., Chaudhuri, P., Feng, Y.J., Hoshino, T., Yu, I.-K., Recent developments of solid breeder fabrication, ICFRM-15, 16.-22. Oct. 2011, Charleston, USA, to be published in J. Nucl. Mater.

Acknowledgement

This work was financially supported by the Ministry of Research and Education (BMBF) under the grant No. 03FUS0012. The views and opinions expressed herein do not reflect necessarily those of the BMBF or the European Commission.

Synthesis of Tritium Breeder Ceramics from Metallic Lithium (HGF)

In the presently known powder or melt based fabrication processes for ceramic breeder pebbles, either lithium hydroxide hydrate or lithium carbonate is used as a starting material. For the fabrication of ^{6}Li enriched pebbles, which are needed for the last two phases of ITER, the variety of ^{6}Li enriched compounds is limited as most of the established enrichment techniques for lithium provide only metallic ^{6}Li. Metallic lithium though, cannot be directly used as a raw material in these processes. Therefore we investigated different chemical reaction routes to transform metallic lithium into nonmetallic compounds that are suitable as starting materials in the subsequent fabrication processes for breeder pebbles [1, 2].

In principal two different routes exist to transform the pure metal into the candidate breeder ceramics lithium orthosilicate and lithium metatitanate. The first route involves a reaction with the respective oxide, silica ($Li + SiO_2$) or titania ($Li + TiO_2$), while the second route uses the reaction of the elements. Since titanium and lithium are virtually insoluble and intermetallic phases do not exist as in the system lithium-silicon, the second route is only applicable for lithium orthosilicate ($Li + Si$). The melting of lithium and the subsequent reaction with silica, titania or silicon was carried out in argon atmosphere to prevent unwanted reactions with air. Figure 1 shows the reaction of liquid lithium and silica in a nickel crucible at about 450 °C. It can easily be observed that this reaction is strongly exothermic.

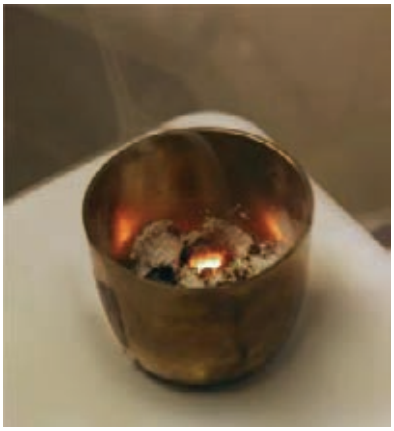

Fig. 1: Reaction of liquid lithium and silica in a nickel crucible.

Due to the absence of oxygen during the reaction with liquid lithium, it is not possible to obtain the desired breeder compositions of lithium orthosilicate or lithium metatitanate directly after synthesis. Instead, several intermediate or precursor phases were observed by x-ray diffraction, using an airtight sample holder (Fig. 2). To convert the formed precursor phases to the desired compounds, a second heating step in air is necessary. Heating the products to 900 °C proved to be sufficient (Fig. 2). The products can be used directly in melt-spraying processes or, presumably after a milling step, in the established shaping and sintering processes.

The reaction enthalpy of liquid lithium and silica, titania or silicon was studied by differential scanning calorimetry (DSC) (Fig. 3). The reaction of lithium and silica showed the highest reaction enthalpy (2614 J/g), followed by the reaction of lithium and titania (2247 J/g) and the reaction of lithium and silicon (1907 J/g). Because of the smaller reaction enthalpy, the synthesis route using silicon instead of silica is regarded to be the most convenient way. Another advantage of this route is that silicon is available in extraordinarily high purity compared to silica, so that activating impurities dissolved in the final breeder ceramic can be avoided.

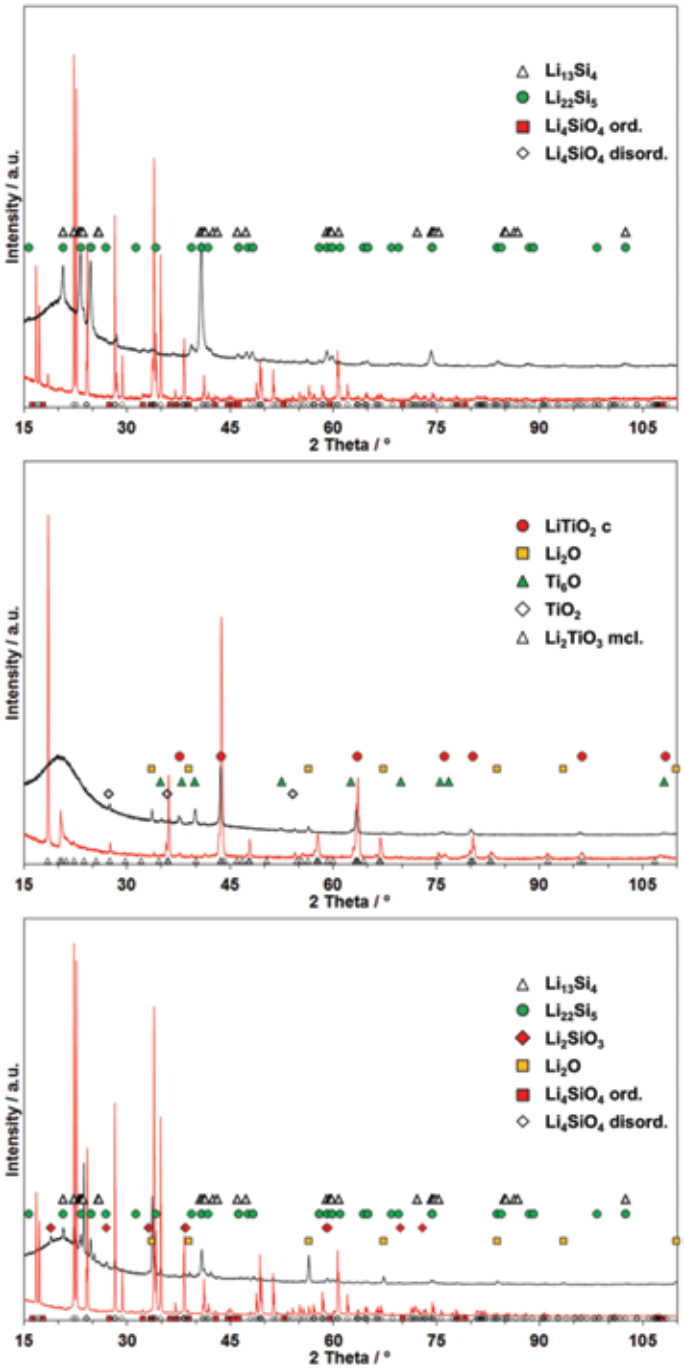

Fig. 2: X-ray diffraction histograms taken from samples of the investigated reaction routes *Li* + SiO_2 (top), *Li* + TiO_2 (middle) or *Li* + *Si* (bottom). The histograms detailed with a black line were taken right after the synthesis in argon atmosphere. In red the histograms are detailed after the final heating step. The most prominent reflexes are indicated with respect to the identified phases.

Staff:

B. Dörzapf
U. Kaufmann
R. Knitter
M. Kolb
O. Leys
U. Maciejewski
C. Odemer

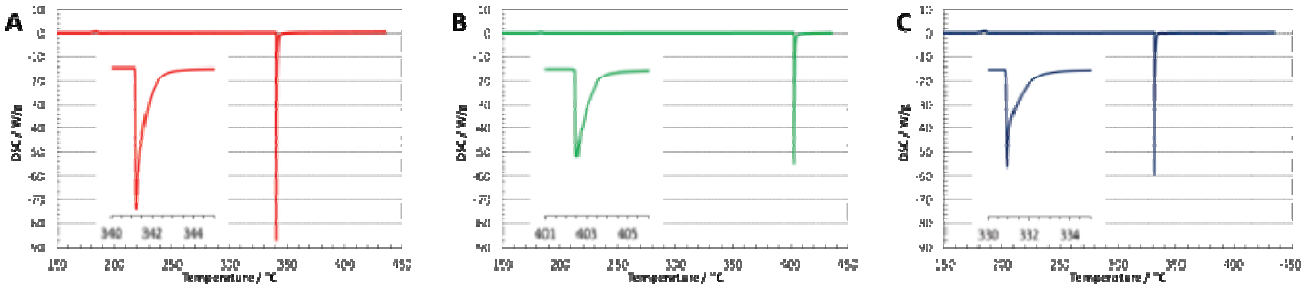

Fig. 3: Investigations of the reaction of lithium with silica (A), titania (B) or silicon (C) with DSC.

Literature:

[1] Kolb, M., Odemer, C., Knitter, R., Synthesis of tritium breeder ceramics from metallic lithium, ISFNT-10, 11.-16. Sept. 2011, Portland, Oregon, USA.

[2] Knitter, R., Kolb, M., Odemer, C., Synthesis of Tritium Breeder Ceramics from Metallic Lithium, J. Nucl. Mater. 420 (2012), 268-272.

[3] Abou-Sena, A., Löbbecke, B., von der Weth, A., Knitter, R., Effect of Post Welding Heat Treatment of the HCPB TBM on the Eurofer and Lithium Orthosilicate Pebbles, Fusion Eng. Design 86 (2011) 2254-2257.

[4] Zmitko, M., Poitevin, Y., Boccaccini, L., Salavy, J-F., Knitter, R., Moeslang, A., Magielsen, A.J., Hegeman, J.B.J., Lässer, R., Development and qualification of functional materials for the EU Test Blanket Modules: Strategy and R&D activities, J. Nucl. Materials 417 (2011) 678-683.

[5] Munakata, K., Mochizuki, K., Wajima, T., Wada, K., Hara, K., Shinozaki T., Takeishi, T., Knitter, R., Bekris, N., Fuji, T., Yamana, H., Okuno, K., Tritium release from ceramic breeder materials deposited with noble metals, J. Nucl. Materials 417 (2011) 731-734.

[6] Knitter, R., Chaudhuri, P., Feng, Y.J., Hoshino, T., Yu, I.-K., Recent developments of solid breeder fabrication, ICFRM-15, 16.-22. Oct. 2011, Charleston, USA, to be published in J. Nucl. Mater.

Modelling of Thermo-mechanics of Pebble Beds (CoA)

Objective

The thermo-mechanical response of polydisperse pebble assemblies is investigated. First, the effect of pebble size distribution and volume fraction on a binary pebble assembly is carried out and then the analysis is extended to the case of polydisperse pebble assemblies. A set of master curves are obtained showing a relation between the microscopic and macroscopic properties of the system.

Binary Pebble Assemblies

Binary pebble assemblies are characterized by two parameters: radius ratio (r*) and relative volume fraction (V*) defined as: $r^* = r_{min}/r_{max}$; $V^* = V_{max}/(V_{min}+V_{max})$, where r_{min} is the radius of the small pebble and r_{max} is the radius of the large pebble in the assembly. V_{max} and V_{min} are the total volume of large and small pebbles in the assembly, respectively.

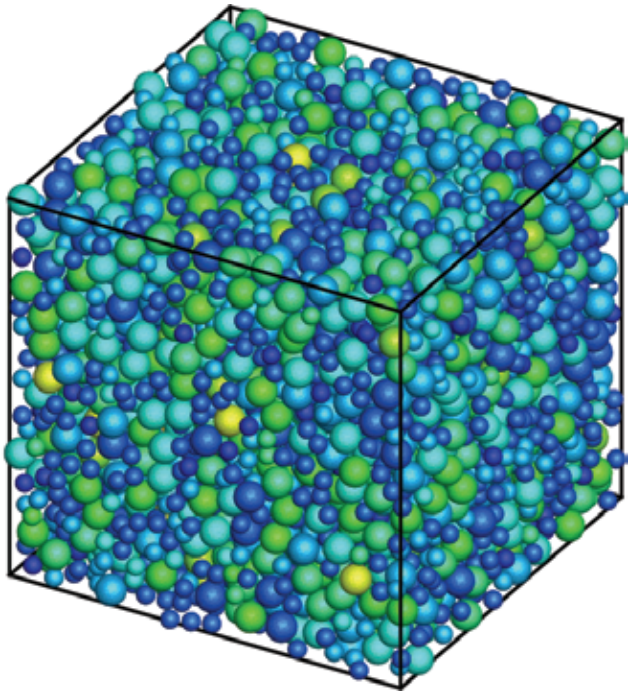

Fig. 1: A binary pebble assembly with r* = 0.6 and V* = 0.7. The colors indicate the stored potential energy at 1.5% strain.

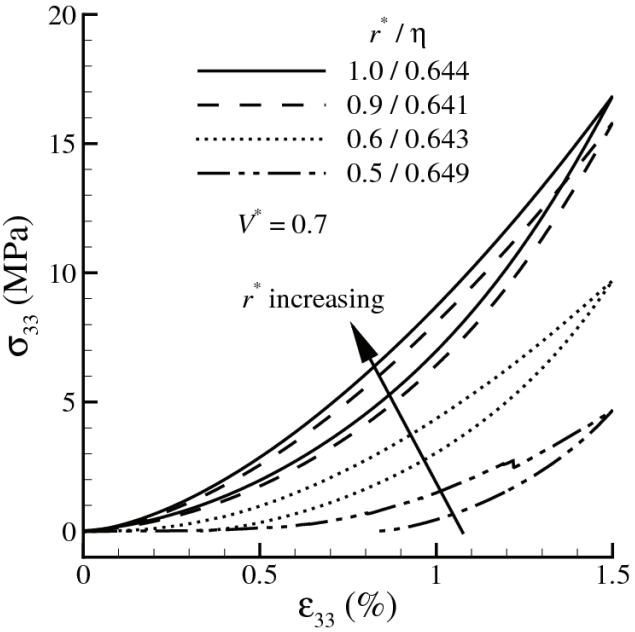

Fig. 2: Stress-strain response of a binary assembly showing the effect of radius ratio r* for a given relative volume fraction V*=0.7.

The binary pebble assembly is subjected to uni-axial compression of 1.5% strain with periodic boundary conditions mimicking the uni-axial compression tests done at KIT. The thermo-mechanical response of the pebble assembly is studied using the discrete element method (DEM) [1]. Figure 1 shows the configuration of a binary pebble assembly with $r^* = 0.6$ and $V^*=0.7$. The colour indicates the potential energy stored in each pebble. Figure 2 shows the average stress-strain response of the pebble assembly for different radius ratios. It should be noted that each radius ratio (r*) is associated with a different packing factor (η) as it is difficult to generate assemblies with different r* values and the same packing factor. Hence, while analyzing, the effect of packing factor should also be taken into consideration.

Figure 2 shows that with increasing r* value the response becomes more stiff for a given value of V* and η. This suggests that the mono size assemblies are generally stiff compared to binary assemblies. When there is a size distribution in the assembly, the small pebbles can accommodate the strain by moving between the large pebbles exhibiting a net compliant

response as compared to the mono size assemblies. A similar behavior is also observed in the experiments [2] referred to as ball-bearing effect. However, in the above results the effect of packing factor is also included which is overshadowed by the effect of size distribution in the assembly (compare dashed and dotted lines).

Polydisperse Assemblies

In reality, the pebbles produced by the manufacturer are polydisperse with a size distribution as shown in Figure 3. Hence, we have investigated the stress-strain response of the assemblies with a realistic pebble size distribution as shown in Figure 3. The polydisperse assembly is generated by modifying the Random Close Packing algorithm used in [1]. Figure 4 shows the stress-strain response of a mono size, binary and polydisperse assembly demonstrating clear size distribution dependence. The mono size assembly shows the stiffest response despite having the lowest packing factor. Also, it should be noted that the net compliance of the system affects the residual strain after unloading to a stress-free state. The assembly with most compliant response results in a large residual strain after unloading (conform Figure 2 and Figure 4). The residual strain after unloading signifies the gap formation in the pebble beds in the loading/unloading cycles.

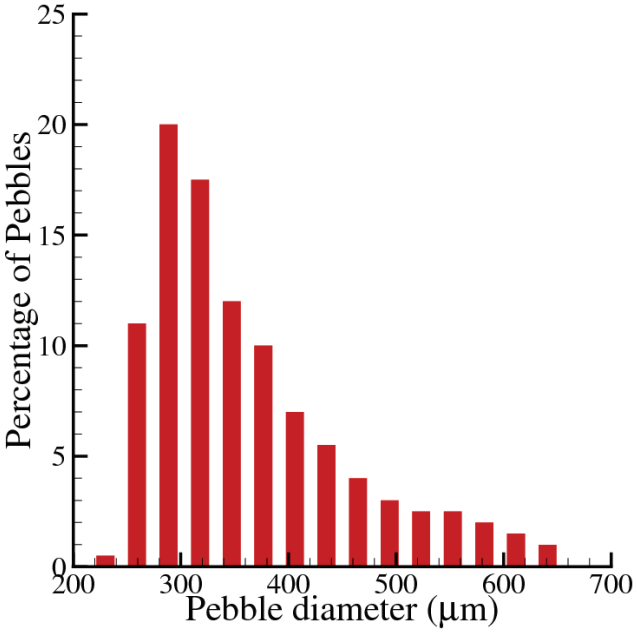

Fig. 3: Typical pebble size distribution in a lot obtained from Schott AG measured at KIT.

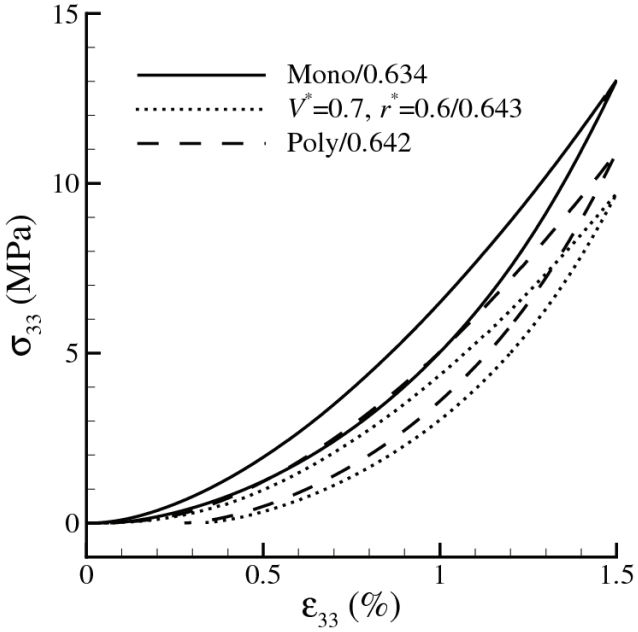

Fig. 4: Stress-strain response of pebble assemblies showing the effect of pebble size distribution from mono size to polydisperse.

Discussion

The above results show the macroscopic response of the pebble assemblies with different size distributions and packing factors. However, the strength of DEM lies in its ability to establish a correlation between response of the system at microscopic and macroscopic scales. The average contact force between individual pebbles and the average coordination number in the assembly are the two important microscopic response parameters which help us understand the thermo-mechanical response with more insight in terms of effective thermal conductivity and crush resistance. Hence, such correlations between average contact force and hydrostatic pressure, average coordination number and hydrostatic pressure have been obtained in [1]. A similar correlation for the polydisperse assemblies is shown here. Figure 5 shows the normalized average normal force for all the simulations (mono size, binary and polydisperse with different packing factors and size distributions) as a function of hy-

drostatic pressure. In the normalized average force, the average scaled radius <r> is given by

$$< r >= \sqrt[3]{\sum_{p=1}^{P} \frac{N_p}{N} r_p^3},$$

with pebbles of *p* different sizes. Figure 6 shows the scaled average coordination number as a function of hydrostatic pressure. Both the figures show a striking universal behaviour demonstrating the independence on the pebble size distribution, packing factor and relative volume fractions. Hence, these master curves can be used to predict the mechanical strength of the pebble assemblies with different configurations.

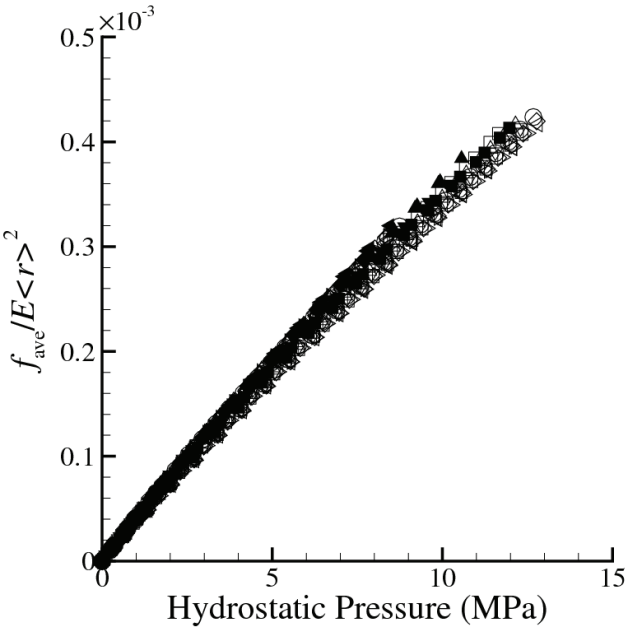

Fig. 5: Normalized average contact force vs hydrostatic pressure for mono, binary and polydisperse assemblies.

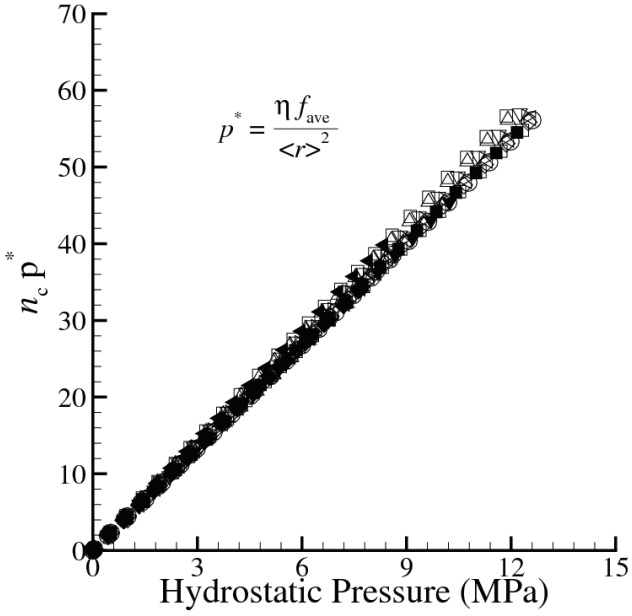

Fig. 6: Normalized average coordination number vs hydrostatic pressure for mono, binary and polydisperse assemblies.

Conclusions and Outlook

The results of the stress-strain response show that the polydisperse pebble assemblies show a compliant behaviour compared to mono size assemblies. This suggests that the overall crush resistance for the polydisperse assembly is better; but the residual strain after unloading is more resulting in a large gap formation. Hence, the pebble size distribution should be chosen so as to make a compromise between the crush resistance and the gap formation.

In future, the DEM model should be improved to predict the over all thermal conductivity. A parallel development of phenomenological models for the new Breeder Unit being developed at INR is to be carried out in the coming year 2012.

Staff:

R. K. Annabattula
M. Kamlah

Literature:

[1] Gan, Y. & Kamlah, M. Discrete element modelling of pebble beds: With application to uniaxial compression tests of ceramic breeder pebble beds. *Journal of the Mechanics and Physics of Solids* **58**, 129-144(2010).

[2] J. Reimann, E. Arbogast, M. Behnke, S. Mueller and K. Thomauske, Thermo-mechanical behaviour of ceramic breeder and beryllium pebble beds, Fusion Engineering and Design, **49-50**, 643-649 (2000).

Interatomic Bonding and Phase Stability (WP11-MAT-REMEV-01-01)

Multiscale Study of Small Self-Interstitial Clusters in Beryllium

Introduction

Beryllium is considered as candidate material for the first wall of future fusion reactor and as neutron multiplier material for fusion blanket, where its resistance against radiation is very important. Mobility of point defects produced under irradiation and their mutual interactions influence formation of radiation induced microstructure and define macroscopic response of irradiated material (e.g., swelling or irradiation growth) which in beryllium is significantly affected by gas production.

The properties of vacancies and their gas-filled clusters have been already investigated in our previous paper [1]. Therefore this work is focused on the study of the stability of self-interstitial atoms (SIAs) and their clusters in hcp beryllium as well as on investigation of SIA diffusion pathways. Some non-trivial interstitial configurations and their diffusion paths were obtained in molecular dynamic runs using recently developed interaction potential for beryllium [2]. *A priori* known and newly obtained configurations were relaxed using first-principles density functional theory (DFT) code VASP [3], while migration barriers were estimated by means of the nudged elastic band method implemented in VTST package (see e.g. [4]).

Results and Discussion

Single interstitials

Previously we have investigated eight high-symmetry interstitial configurations in beryllium [1].

According to their formation energies (see Fig. 1) these configurations can be roughly divided in two groups: those lying mainly (i) in basal (Ef is below 4.5 eV) and (ii) out of basal plane with higher formation energies. The defect energetics and atomic positions were obtained by conjugate gradient relaxation using VASP with ultrasoft and PAW pseudopotentials. Six configurations from eight are apparently stable: i.e. the interstitial atom after relaxation had the same neighbors as before. Other configurations are unstable: basal crowdion (BC) undergo spontaneous transition to basal octahedral (BO) position, while basal tetrahedral (BT) relaxes to tetrahedral one (T).

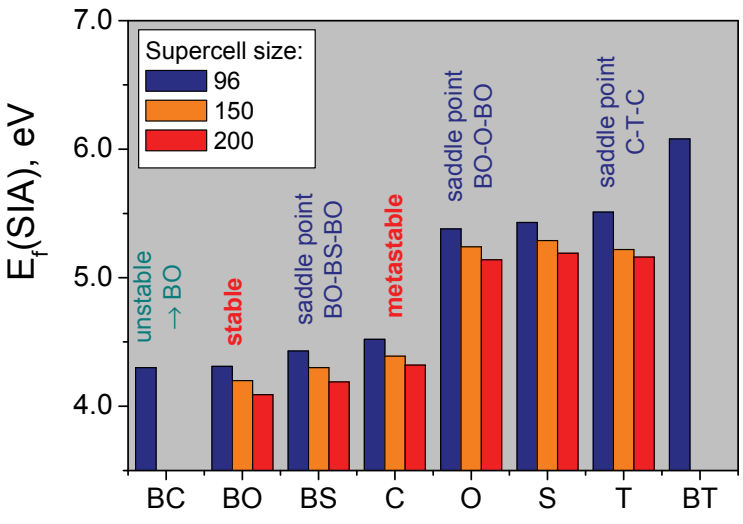

Fig. 1: Formation energies of various SIA configurations in beryllium [1].

Using the same approach we have investigated single SIA diffusion pathways, which are summarized in Fig. 2. The easiest diffusion path is in-basal plane rotation (BO-BS-BO) requiring only 0.12 eV. SIA movement perpendicular to basal plane is much less favorable and needs 1.1 eV (BO-O-BO). Another path which combines in- and out-of-basal plane components (BO-C-BO) has intermediate diffusion barrier of 0.27 eV. It is seen in Fig. 2c that BO

position is the lowest energy ground state, while non-basal crowdion (C) is only a shallow local minimum, which requires only 0.06 eV for decay to BO. Fig. 2a and b also show that BS and O positions are saddle points of respective diffusion jumps and were therefore apparently stable during relaxation.

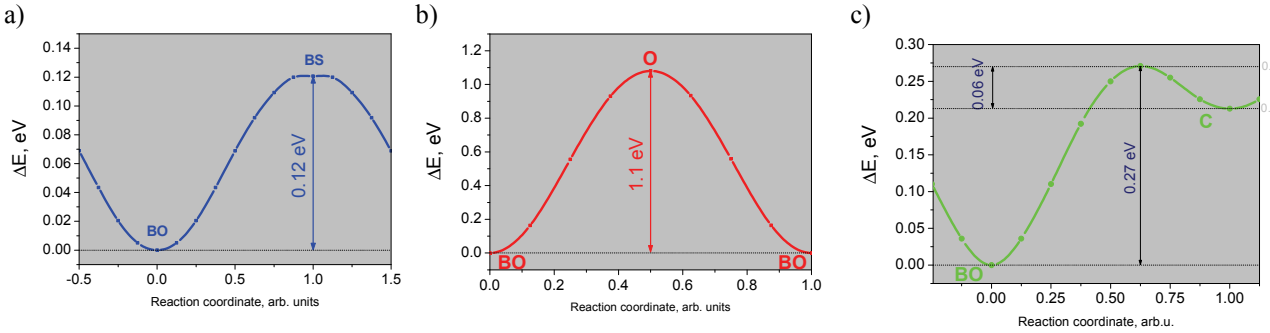

Fig. 2: Diffusion paths of self-interstitials: in-basal-plane path BO-BS-BO (a), path along c axes BO-O-BO and the path inclined with respect to basal plane BO-C-BO.

Di-interstitials

Di-interstitials can be formed in particular from two BO interstitials. During this process they push the regular lattice atom located between them (the central atom in Fig.3a) into another neighbouring BO position forming planar triangular cluster of three BOs around one empty lattice site.

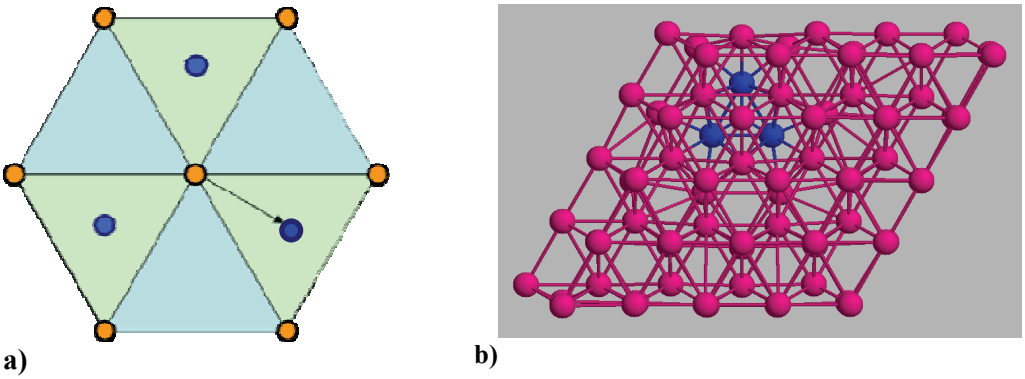

a) **b)**

Fig. 3: Formation of SIA cluster containing 3 interstitial atoms and one vacant lattice site (a) formation mechanism by reaction BO+BO→(BO_3Vac_1) ≡ (3,1); (b) relaxed configuration in 100 atom supercell.

We checked that two BO interstitials placed at the second nearest neighbor separation spontaneously form triangular cluster during relaxation indicating the lack of diffusion barrier for this transition.

In addition various forms of non-planar clusters were observed in molecular dynamics runs, which will be not described here due to the lack of space.

Mechanism of formation and nature of planar triangular interstitial clusters

Addition of another BO to the BO_3Vac_1 cluster will result in displacement of two additional lattice atoms into BO positions (see Fig.4a): (BO_3Vac_1)+BO→(BO_6Vac_3) (see Fig. 4). This process can be continued: (3,1) → (6,3) → (10,6) → (15,10) → … →((n+1)(n+2)/2, n(n+1)/2), where the first number in parenthesis is a number of interstitials and the second is a number of vacancies in the cluster with sequential index n.

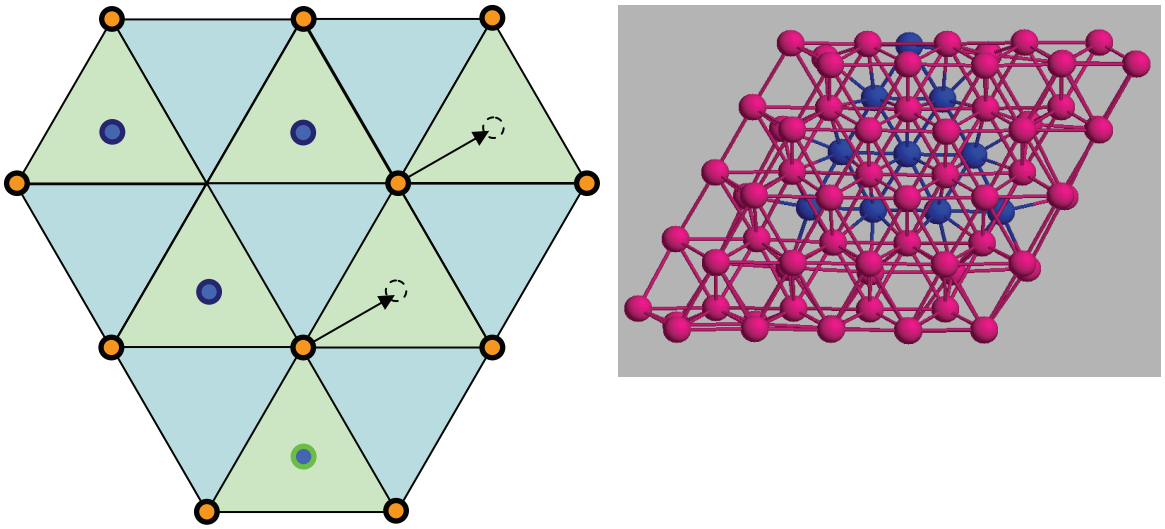

Fig. 4: Formation of SIA cluster containing 6 interstitial atoms and 3 vacant lattice sites: (a) formation mechanism by reaction (3,1)+BO→(6,3); (b) relaxed configuration in 100 atom supercell.

This reaction uncovers a new mechanism of basal self-interstitial cluster formation and self-similar growth in hcp materials with stable BO interstitial configuration by clustering of two BO or by attachment of BO to planar triangular SIA cluster. As was mentioned above this clustering does not require overcoming additional energy barrier.

These planar clusters might be confused with interstitial loops, however they do not add an additional crystalline plane as real interstitial loops should do, but present another stacking sequence of planes locally. They can be considered as local stacking faults with the stacking sequence of layers along c axis: ABABCBABA, where ABC sequence is that native for fcc lattice, while hexagonal close packing consists of AB layers.

Such clusters were also observed in molecular dynamics simulations of atomic displacement cascades in zirconium together with irregular and prismatic SIA clusters [5]. The later are formed from several basal SIA clusters stacked on each other and were recognized as I2 intrinsic stacking faults with two fcc stacking sequences on the top and bottom of the prism.

One could suppose that planar clusters of that kind can grow infinitely forming a complete stacking fault layer. However, our molecular dynamics calculations indicated that large planar clusters are unstable against formation of non-planar configurations inserted in planar cluster. For example, one of the cluster atoms can be replaced with a split dumbbell along c-axis.

As have been shown previously di- and tri-vacancy clusters are not stable in beryllium [1], therefore we decided to check whether triangular clusters similar to those described above but formed by agglomeration of vacancies (analog to stacking fault tetrahedral (SFT) observed in fcc metals) are stable. However, our preliminary DFT calculations have shown that formation of SFT in beryllium is energetically unfavorable.

Conclusions

Combination of ab initio and MD methods proved to be a useful approach for the study of point defect clusters. In particular, several types of SIA clusters were observed in MD and ab initio: (i) triangular configurations in basal plane (stacking fault), (ii) planar C-C clusters, which may present possible seeds for interstitial loop formation and (iii) non planar clusters.

Further investigations are required to clarify their relations to a- and c-type interstitial loops experimentally observed in beryllium under irradiation.

Staff:

A. Möslang
P. Vladimirov

List of External Contributors:

V. Borodin (RNC Kurchatov Institute)

Literature:

[1] M. Ganchenkova, P. Vladimirov, V. Borodin, J. Nucl. Mater. **386-388** (2009) 79-81

[2] C. Björkas, N. Juslin, H. Timko, K. Vörtler, K. Nordlund, K. Henriksson and P. Erhart, J. Phys.: Cond. Matter **21** (2009) 445002

[3] G.Kresse, J.Hafner, Phys. Rev. B (1993) **47**, 558; ibid. (1994) **49**, 14251; G.Kresse, J.Furthmüller, Comput. Mat. Sci. (1996) **6**, 15; G.Kresse and J.Furthmüller, Phys. Rev. B (1996) **54**, 11169

[4] D. Sheppard, R. Terrell, and G. Henkelman, J. Chem. Phys. **128**, 134106 (2008)

[5] R. Voskoboinikov, Yu. Osetsky, D. Bacon, Nucl. Instr. Meth. Phys. Res. B **242** (2006) 530–533

Acknowledgement

This work, supported by the European Communities under the contract of Association between EURATOM and Karlsruhe Institute of Technology, was carried out within the framework of the European Fusion Development Agreement. The views and opinions expressed herein do not necessarily reflect those of the European Commission.

Helium Behaviour in Beryllium (HCP-FF – HeliBery)

Introduction

Beryllium is an effective neutron multiplier material widely exploited in nuclear applications. It will be used in the helium cooled beryllium pebble bed of fusion reactor blankets for increasing the efficiency of tritium production. Such macroscopic effects as, e.g., swelling of beryllium are greatly influenced by the amount of accumulated transmutation helium. Atomic scale simulations of beryllium behavior under irradiation are necessary for understanding of basic mechanisms and reliable prediction of microstructural changes.

In this study we investigate the behavior of interstitial and substitutional helium, its diffusion pathways and interaction with point defects present in irradiated beryllium by means of static and molecular dynamics *ab initio* simulations.

Computational details

In this work static and “state of the art” dynamic first principles density functional theory (DFT) based calculations are used for the identification of possible defect configurations and their diffusion pathways.

Ab initio calculations are performed with plane-wave VASP computer code [1]. Full geometry optimization is carried out using Generalized Gradient Approximation (GGA) with Perdew-Wang non-local exchange-correlation functional [2] and the scalar relativistic PAW [3]. The calculations involve typically 13x13x13 Monkhorst-Pack k-point mesh [4] and 450 eV for cut-off energy. Migration barriers were estimated by means of the drag method. Rhombohedral supercells with sizes of 64 and 96 lattice sites are applied.

Molecular dynamics simulations are performed by VASP code on the so-called exact adiabatic Born-Oppenheimer surface [5]. In metals fast moving electrons can adapt their motion to the much slower motion of nuclei. It means that total electronic energy minimization (ground state search) is performed at each step of molecular dynamics. Simulations are performed in the NVT ensemble where the system temperature is controlled by means of the Nose-Hoover thermostat.

Results and Discussion

Single helium interstitials

Eight possible high symmetry configurations for interstitial helium atoms have been tested: octahedral (O), basal octahedral (BO), tetrahedral (T), basal tetrahedral (BT), non-basal crowdion (C_N), basal crowdion (BC), split along c-axis (S) and basal split mixed dumbbell (BS_m). Most of these configurations were found to be stable for self-interstitial atoms, therefore we checked if they are suitable for helium interstitial atom too. After relaxation a half of configurations appears to be stable, namely: C_N, BO, BT, BS_m (only two of them were reported by us previously [6]). Formation energies of various interstitial helium configurations are shown in Figure 1. These calculations were performed using supercells containing 64, 96 and 128 atoms to assess the effect of the supercell size. As can be seen from the figure for stable configurations the difference does not exceed 0.02 eV. Thus one can conclude that even a supercell with 64 atoms is sufficient for reliable description of interstitial helium behavior in beryllium.

It should be noted that the ground state configuration for interstitial helium in beryllium is a mixed dumbbell located in basal plane (BS_m). This configuration was observed most of the time in the first principle molecular dynamics runs supporting the results of static simulations.

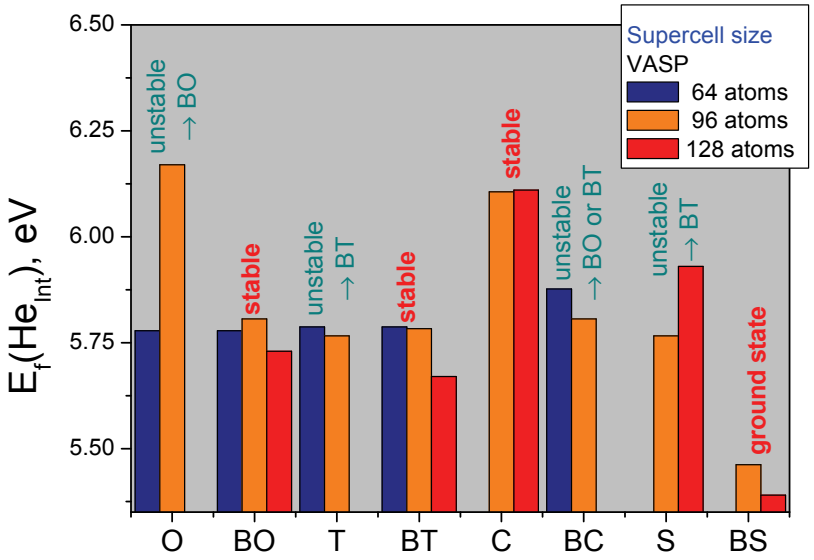

Fig. 1: Formation energies of interstitial helium at various positions.

In accordance with this the FPMD runs have revealed that at temperatures of 800-1000 K helium atom avoids the neighborhood of BO being effectively caged in the triangle around BT position. It can form mixed dumbbell with any of the three atoms at the triangle corners, but jumps between triangles occurs by flip: the mixed dumbbell turns over going out of basal plane while helium atom jumps in the other triangle. Diffusion jumps observed during the simulation runs occurred only within the basal plane, i.e. at low temperatures interstitial helium diffuses two-dimensionally.

At 1200 K the energy of helium atoms is sufficient to jump over BO containing triangle, so on-site rotations of the mixed dumbbell are possible. Therefore at high temperatures helium can change triangles without flip. On the other hand helium jumps between two adjacent basal planes through a tetrahedral-like configuration were observed. As a result a mixed interstitial diffuses three dimensionally at higher temperatures.

Interstitial helium pairs

As in many metals helium interstitials in beryllium are attracting each other. FPMD calculations have shown that there are two types of helium interstitial pairs: in-basal plane pair and out-of-basal plane pair (see Figure 2). The in-basal plane configuration diffuses by in-basal

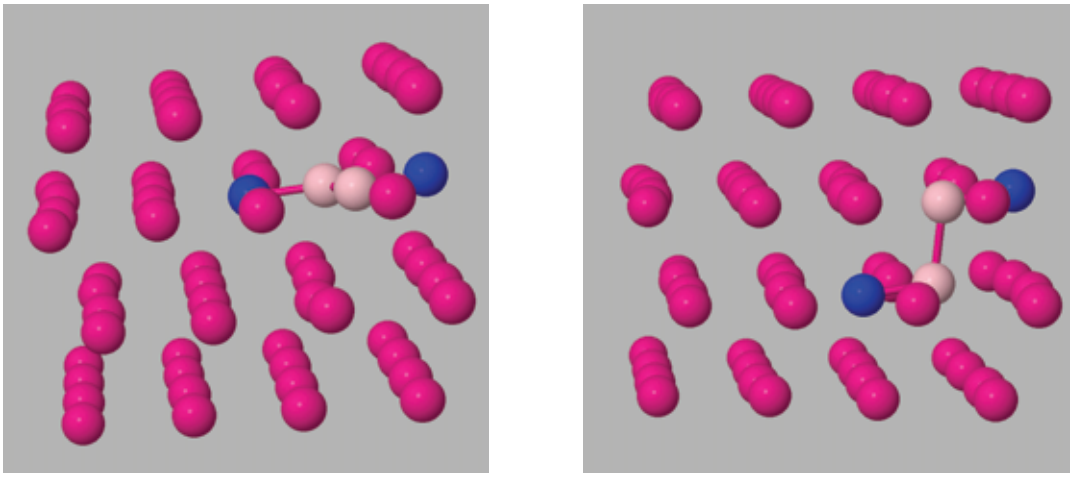

Fig. 2: Pairs of interstitial helium. (a) In-basal-plane pair, (b) out-of-basal plane pair. Helium atoms are colored rose, while beryllium atoms constituting mixed dumbbells are colored blue.

plane rotations and is also essentially caged within triangle. However, even at 800 K out-of-basal plane rotation with formation of out-of-basal plane pair is possible. In spite of the fact that the second configuration has significantly higher binding energy (1.35 eV cf. 0.83 eV for the first one) a reverse transformation was also observed in FPMD run at 800 K.

Helium vacancy clusters

As it was shown previously [6-7] di-vacancy clusters are unstable in beryllium. The same behavior was recently predicted by DFT calculations for tungsten [8] and aluminum [9-10]. In this work we calculated binding energies of helium atom with di-vacancy clusters in various orientations. It appears that helium atoms effectively stabilize di-vacancy clusters in one basal plane and in adjacent planes, but cannot stabilize di-vacancy along c axes, where vacancies are separated by additional basal plane between them. The binding energy of He_1Vc_2 cluster with respect to decay into two separate vacancies and helium interstitial is about 3.0-3.7 eV depending on di-vacancy orientation. Certainly the binding energies with respect to the decay into substitutional helium and vacancy are significantly lower: 0.3-0.4 eV.

In FPMD simulation at 1000 K two diffusion jumps of He_1Vc_2 cluster were observed. It appears that diffusion of the in-basal-plane cluster occurs by classical ring mechanism in basal plane. Initial and final configurations of the jump were relaxed using static *ab initio* and migration barrier was estimated by means of the drag method. Jumping atom was fixed along the direction of the jump while it was allowed to relax in two other directions. To avoid shifting of the lattice as a whole one or in some cases two atoms far from the jumping atom were fixed in all three directions.

The observed in-basal plane jump sequence occurs through the intermediate dissociated configuration (see Fig. 3):

$$(He_1Vc_2)_{aa} \rightarrow He_{sub} + Vc.$$

It can be seen from Fig. 3 that another two in-basal plane jumps are possible. One jump (aa3) also results in the dissociation of He_1Vc_2 cluster while the other (aa2) does not require dissociation. Surprisingly the jump without dissociation (aa2) has higher migration barrier of 1.6 eV than those with dissociation: 0.9 eV for aa3 and 0.7 eV for aa1. It was the lowest energy migration path, which was observed in the described above ring diffusion mechanism.

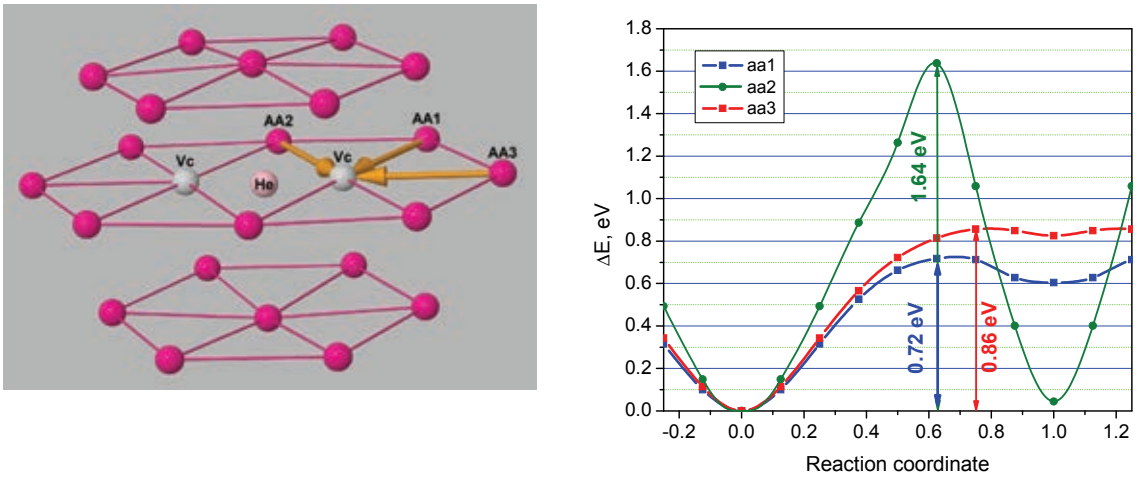

Fig: 3: (a) Three possible in-basal-plane jumps of beryllium atoms labeled as aa1, aa2 and aa3 into He1Vc2 complex situated in the same basal plane. In the cases aa1 and aa3 dissociation of basal (He1Vc2)aa complex occurs: (He1Vc2)aa → HeS + Vc, while in the case of aa2 jump (He1Vc2)aa complex changes its orientation.
(b) Energy profiles corresponding to these migration pathways.

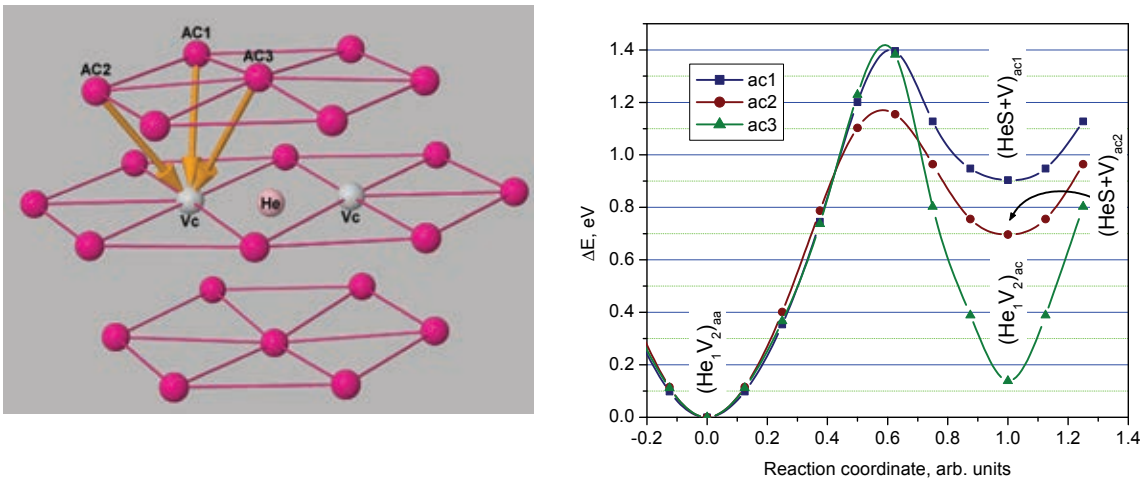

Fig. 4: (a) Three possible jumps of beryllium atoms labeled as ac1, ac2 and ac3 from one basal plane into He_1Vc_2 complex situated in the adjacent basal plane. In the cases ac1 and ac2 dissociation of basal $(He_1Vc_2)_{aa}$ complex occurs, while in the case ac3 a new $(He_1Vc_2)_{ac}$ non-basal complex is formed.
(b) Energy profiles corresponding to these migration pathways.

To complete the study we have calculated the diffusion barriers for three possible beryllium atom jumps from the adjacent basal plane. Two jumps are those when beryllium atoms labeled as ac1 and ac2 are jumping into one of the vacancies (see arrows in Fig. 4a). Helium atom is pushed into another vacancy. In these cases helium-vacancy cluster is dissociating as far as the new vacancy is not a nearest neighbor of the old one. In case of the third jump (ac3) the newly formed vacancy is a nearest neighbor of the helium atom again. Therefore helium takes intermediate position between the vacancies, but now the vacancies are in different basal planes and helium is between these planes too. The results of these calculations are presented in Fig. 4b.

This analysis suggests that $HeVc_2$ cluster is migrating preferentially in basal plane with approximately the same rate as vacancy (0.7 eV), while it needs to overcome the two times higher barrier (1.4 eV) to move between basal planes. On the other hand the barrier for dissociation (ac2) is slightly lower (1.2 eV).

Conclusions

Combination of static and dynamic ab initio methods proved to be a useful approach for the study of point defect migration pathways.

It was shown by static relaxations that mixed He-SIA dumbbell is a ground state for helium at interstitial position in beryllium. Interstitial helium is a fast diffuser: mixed dumbbell diffuses at low temperatures two dimensionally (within one basal plane), but at higher temperatures can jump between adjacent basal planes as well (undergo three dimensional diffusion). Mixed dumbbells are bound to each other building planar and non-planar configuration. These configurations are mobile and diffuse by rotation within basal plane or by jumps between adjacent basal planes.

Substitutional helium diffuses only as a vacancy cluster. It was shown by molecular dynamics calculations that He1Vc2 cluster migrates by classical ring diffusion mechanism. Calculation of diffusion barriers has shown that this cluster diffuses only two dimensionally in the basal plane as far as the barrier for the jump between two adjacent basal planes is higher than the barrier for the cluster dissociation.

Very important conclusion of this work is that helium is essential for stabilization of vacancy clusters, which are otherwise unstable. The direct consequence of this fact for the practice is that voids cannot grow in beryllium under electron irradiation, while helium bubbles can be

formed under neutron irradiation due to helium produced by nuclear transmutations. Thus it is possible to conclude that the presence of transmutation helium is the necessary condition for the development of porous microstructure in beryllium.

Staff:

A. Möslang
P. Vladimirov

List of External Contributors:

V. Borodin (RNC Kurchatov Institute)

Literature:

[1] G. Kresse, J. Hafner, Abinitio Molecular-Dynamics for Liquid-Metals, Phys Rev B, 47 (1993) 558-561.

[2] [J.P. Perdew, Y. Wang, E. Engel, Liquid-Drop Model for Crystalline Metals - Vacancy-Formation, Cohesive, and Face-Dependent Surface Energies, Phys Rev Lett, 66 (1991) 508-511.

[3] G. Kresse, D. Joubert, From ultrasoft pseudopotentials to the projector augmented-wave method, Phys Rev B, 59 (1999) 1758.

[4] H.J. Monkhorst, J.D. Pack, Special points for Brillouin-zone integrations, Phys Rev B, 13 (1976) 5188.

[5] G. Kresse, W. Bergermayer, R. Podloucky, E. Lundgren, R. Koller, M. Schmid, P. Varga, Complex surface reconstructions solved by ab initio molecular dynamics, Applied Physics A: Materials Science & Processing, 76 (2003) 701-710.

[6] [M.G. Ganchenkova, P.V. Vladimirov, V.A. Borodin, Vacancies, interstitials and gas atoms in beryllium, J Nucl Mater, 386 (2009) 79-81.

[7] [M.G. Ganchenkova, V.A. Borodin, Ab initio study of small vacancy complexes in beryllium, Phys Rev B, 75 (2007) -.

[8] [C.S. Becquart, C. Domain, Ab initio calculations about intrinsic point defects and He in W, Nucl Instrum Meth B, 255 (2007) 23-26.

[9] [K. Carling, G. Wahnstrom, T.R. Mattsson, A.E. Mattsson, N. Sandberg, G. Grimvall, Vacancies in metals: From first-principles calculations to experimental data, Phys Rev Lett, 85 (2000) 3862-3865.

[10] L. Yang, X.T. Zu, F. Gao, Ab initio study of formation, migration and binding properties of helium-vacancy clusters in aluminum, Physica B-Condensed Matter, 403 (2008) 2719-2724.

Acknowledgement

This work, supported by the European Communities under the contract of Association between EURATOM and Karlsruhe Institute of Technology, was carried out within the framework of the European Fusion Development Agreement. The views and opinions expressed herein do not necessarily reflect those of the European Commission.

Screening of an Alternative Production Route/Capacity for Be Pebbles (F4E-2009-GRT-030 (PNS-TBM) - Action 2)

Introduction

The general objective of the Action 2 of this Grant is the screening of alternative Be pebbles production routes and to qualify the pebbles produced by these routes with respect to their applicability for fusion reactor blankets.

- The characterization of three batches of Be pebbles with different sizes of grains produced by Bochvar Institute, Russia was performed. Mechanical milling of beryllium hot-pressed blocks or ingots was used for the production of the batches.
- Together with MATERION (Brush Wellman Inc., USA) the development of new production route of Be-pebbles were investigated. First successful trials were performed in 2011 and reported at the Int. Workshop on Beryllium Technology for Fusion Applications (BeWS-9.5), 25-26 October 2011, Perrysburg & Elmore, Ohio, USA. A small batch of the new pebbles for characterization will be purchased in the next year.

Preliminary results on the characterization of Be pebbles produced by Bochvar Institute

Investigations of microstructure

Investigations of microstructure of three batches of Be pebbles produced by Bochvar Institute with various sizes of grains (10-30 μm, 30-60 μm and >100 μm) have shown differences in surface morphology, internal porosity and crack propagation behavior.

4. Be pebbles with the smallest grains (10-30 μm) have compact matrix practically free of pores and cracks. Some few surface defects and cracks attached to them were observed.
5. Be pebbles with the grain sizes in the range of 30-60 μm have loosely bound grain structure, which resulted in the fallout of individual grains of the matrix during grinding and polishing.
6. Be pebbles with the grain sizes exceeding 100 μm contain a great number of small pores and inclusions presumably referring to the history of material fabrication. Compared to Be pebbles with the grain sizes ranging 30-60 μm, the change of behavior of the crack propagation from intergranular to transgranular takes place.

Common properties of all three batches of Be pebbles include:

- No obvious preferred grain orientation (texture) in material matrix was observed.
- The presence of surface oxidation was observed by EDX analysis of the Be pebbles surfaces.
- Contamination with iron and aluminum was found on the surfaces of Be pebbles from all batches. Presumably, these impurities originate from the process of material fabrication.

Analysis of chemical composition

Similar quantitative results for Cu, Ni, Fe and Mn contents were obtained for all three batches. Presumably, these elements are homogeneously distributed in the sample volume. On the other hand, some deviation between Cr and Ti contents in material matrix and on the surfaces of Be pebbles was found, which might be related to surface contamination during fabrication.

Analysis of tritium release characteristics of Be pebbles

Three major release peaks were observed. Positions of the peaks depend on the temperature ramping rate due to a presence of a certain delay needed for tritium diffusion. At heating rate of 15°C/min all peaks are shifted to higher temperatures by about 100-150°C. This fact suggests that hydrogen diffusion in the bulk of grains is taking place. This also confirms that hydrogen is not trapped exclusively on the surface of pebbles, but penetrates inside the grains during thermal loading.

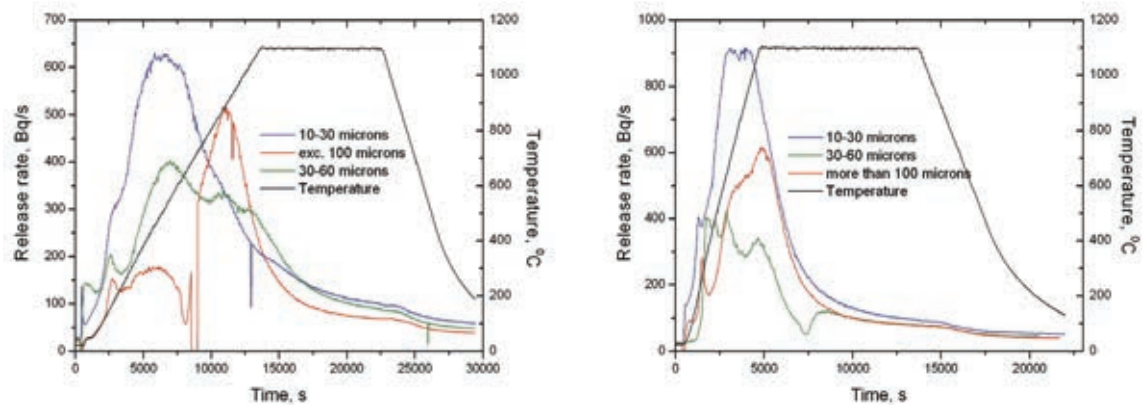

a) b)

Fig.1: Tritium release rate from Be pebbles with different sizes of grains at heating rate (a) 5°C/min and (b) 15°C/min.

At slow heating rate (5°C/min) the heights of the first and second peaks are increasing with decreasing of the grain size, while the height of the third peak is decreasing. In particular, the third peak for the batch with the grain size of 10-30 μm is observed as a small shoulder, while for the batch with the largest grain size (>100μm) it dominates tritium release. For the faster temperature ramping this clear tendency versus grain size is not observed.

Investigations of packaging densities of Be pebbles

The largest packing factors (γ ≈ 63%) were obtained when testing pebbles with grain sizes more than 100 μm. This packing factor is comparable with that of 1 mm NGK pebbles investigated previously. These pebbles are characterized by smooth surfaces, irregular pebble shapes (rather brick-type than spherical), wide size distribution (fractions of mm to several mm). At flat walls, mostly, the largest pebble surface is in contact with the wall, which is probably favorable for heat transfer.

The batches with grains more than 100 μm, 10-30 μm and NGK pebbles behave in a very similar way showing relatively close values of the packing factors for different container heights.

Compared to the batches with grains more than 100 μm and 10-30 μm pebbles, the batch having 30-60 μm grains differ significantly in the surface roughness, although pebble shape and size distribution are not very different. The large surface roughness reduces the packing factor remarkably.

Preliminary conclusions on a potential suitability of investigated Be pebbles for TBM purpose

Since different characteristics of Be pebbles were examined in the frame of this work, it makes sense to prepare a table which represents corresponding material properties by marking as "best", "medium", "worst" or questionable - "?" which means that these points are still under discussion from the point of view of TBM application (see Table 1). The judgment on

chemical composition is based on information on contamination with iron which is a highly-activated element under neutron irradiation.

Table 1: Comparison of different properties of Be pebbles from the point of view of TBM application.

Characteristic of material/Material batch	Be pebbles with the grain sizes of 10-30 µm	Be pebbles with the grain sizes of 30-60 µm	Be pebbles with the grain sizes exceeding 100 µm
Packing density	best	worst	best
Chemical composition	best	medium	worst
Tritium release measurement	best	medium	worst
Material density	medium	best	worst
Pebble size	?	?	?

These preliminary considerations show the advantages of Be pebbles with the grain sizes ranging from 10 to 30 µm. Good performance was also shown by the pebbles with the grain sizes of 30-60 µm, although their packing density was slightly lower than packing densities of other types of pebbles. Coarse-grained Be pebbles along with the pebbles with 10-30 µm grains have a good performance only by investigations of packing density. Other characteristics (tritium release measurements, chemical composition and pebble density) are not in favor of the large-grained Be pebbles. The influence of the sizes of pebbles on the stable and reliable work of TBM is still under discussion.

Presently it is difficult to make final conclusion on a potential suitability of the investigated Be pebbles for TBM application since the costs and market availability of these pebbles are still not verified.

Staff:

A. Abou-Sena
V. Chakin
P. Kurinskiy
A. Möslang
R. Rolli
H.-C. Schneider
P. Vladimirov

List of External Contributors:

E. Alves (ITN)
J. Reimann (KBHF)

Acknowledgement

This work was supported by Fusion for Energy under the grant contract No. F4E-2009-GRT-030(PNS-TBM) - Action 2 - with collaboration by ITN Portugal. The views and opinions expressed herein reflect only the author's views. Fusion for Energy is not liable for any use that may be made of the information contained therein.

Breeder and Neutron Multiplier Materials: Development of Beryllium and Beryllium Alloy Pebble Beds with Improved Tritium Release Characteristics (BMBF Reference No. 03FUS0012)

Introduction

The most relevant properties of Be-Ti alloys besides their ability as neutron multiplier are their thermo-physical, chemical and tritium release properties. In particular, $Be_{12}Ti$ is considered to be one of the promising materials for neutron multipliers in future fusion power plants. Laboratory-scale tests aimed to produce $Be_{12}Ti$ samples and the study of their relevant properties were performed.

One should note that beryllium and its compounds are high toxic materials (especially, fine particles in air) so that special glove-boxes under controlled argon atmosphere were used for R&D works.

Preparation of equipment

In this year a glove-box system which consists of three sections was designed and built in a special beryllium laboratory (KBHF) located at KIT. The new enlarged glove-box, which is shown in Fig. 1, allows making several investigation/production steps in one closed system. These steps include:

- Preparation of fine powders by wet ball milling in a new NETZSCH milling device which has a capability to mill up to 2 kg of Be powders per cycle.
- Investigations by means of KEYENCE optical digital microscope. This microscope also allows evaluation of both – polished surfaces and fine milled powders.
- Vertically built sintering oven (temperature range up to 1400 ^{0}C). This oven can be used for sintering of Be-Ti rods or pebbles. The possibility to apply inert gas pressure (up to 1 MPa) inside this oven is also foreseen.

Fig. 1: New glove-box system consisting of three sections (the third section is in the background).

Fabrication and characterization

The operation of new milling machine was successfully tested using coarse Ti powders. Fine-milled particles having the sizes of a few microns were obtained after a several hours of milling in a fluid oxygen-free tetradecane ($C_{14}H_{30}$).

Curve showing the influence of time of milling and two different rotor speeds (800 rpm and 1500 rpm) on the average particle sizes of milled titanium powder is shown in Fig. 2. Eleven powder probes were sampled during the process of milling for further investigations by REM.

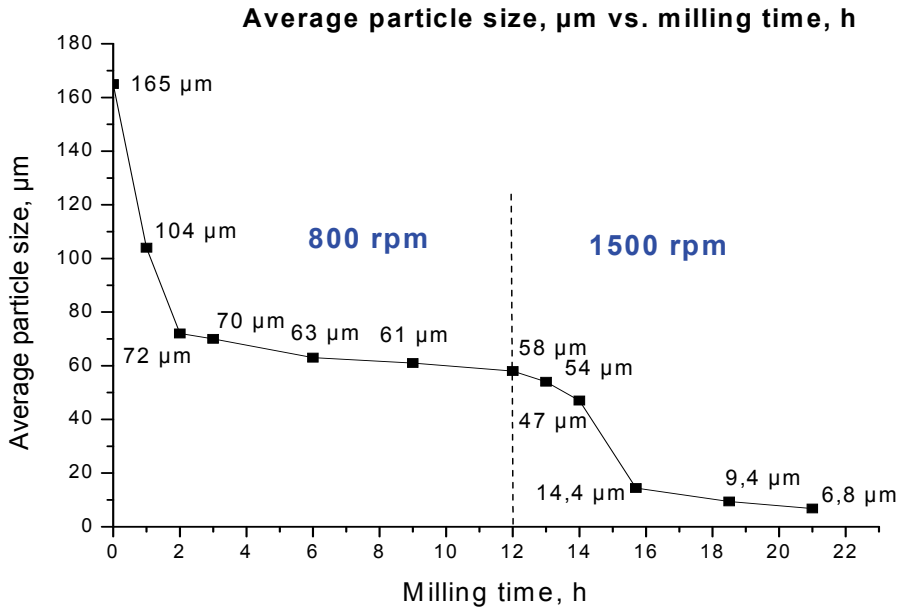

Fig. 2: Dependence of the particle sizes of milled Ti powder on milling time and rotor speed.

The view of milled Ti particles placed on the plastic sample holder is shown in Fig. 3. KEYENCE microscope integrated into a newly developed glove-box system was used to obtain this image.

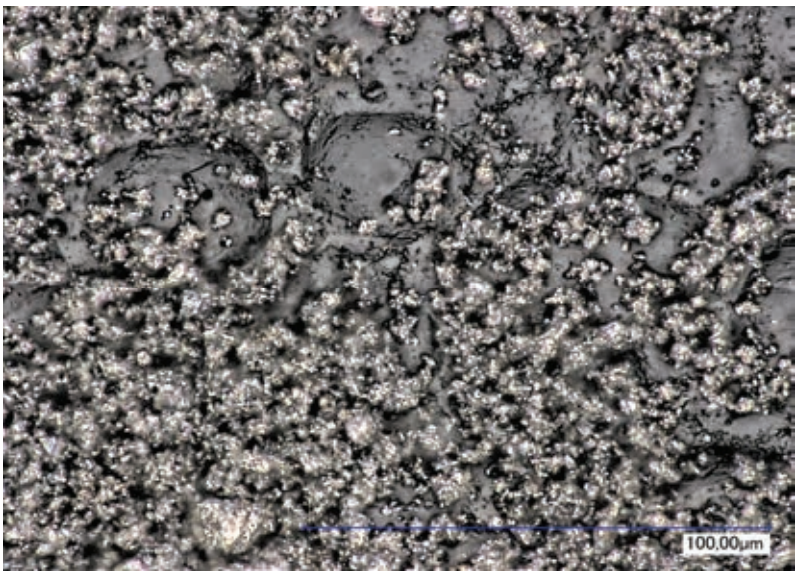

Fig. 3: View of fine titanium particles milled in tetradecane C14H30.

It is expected that kilograms of beryllium fine powders will be obtained within the next months. Fine-grained milled powders are needed for further works aiming to produce beryllides by means of sintering, HIP, etc.

In year 2011 a comparative study of tritium release properties after preliminary saturation with "hydrogen-tritium" gas mixture was performed [1]. Tritium release behaviour of different types of beryllides were compared to pure beryllium. It was shown that beryllides have a lower ability to retain tritium if compared to pure beryllium. Fig. 4 shows two curves corresponding to different types of $Be_{12}Ti$ samples and one curve relating to S-65H beryllium grade.

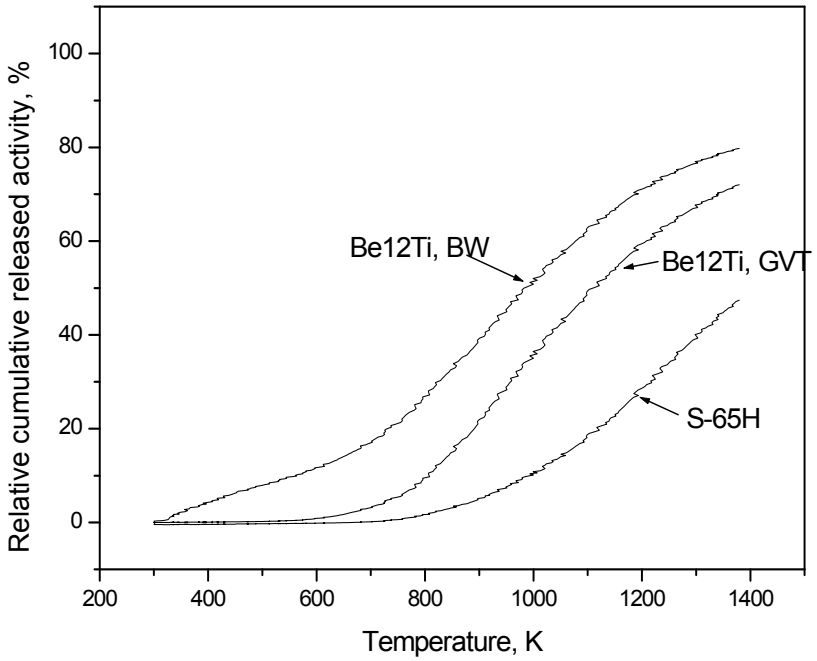

Fig. 4: Activity of released tritium depending on a sample temperature for three kinds of beryllium-based materials.

Since the gas release properties of beryllium-based materials are in a strong dependency on the thickness of oxide layer, the evaluation of the thickness and structure of the surface oxide layer is necessary.

The phase composition of the near-to-surface layers of $Be_{12}Ti$ and $Be_{12}V$ specimens was investigated at the SCD beamline at ANKA synchrotron facility after air-annealing at 800 ^{0}C. A high surface sensitivity of measurements was achieved at grazing incidence conditions by varying the incidence angle. Since beryllium has low values of X-Ray absorption, the near-surface regions having depths from 2 up to 20 μm were investigated. Totally, the structure of six surface layers has been investigated. The main objective was the evaluation of composition of the reactant products which can influence the parameters of retention and release of radiogenic gases [2]. Fig. 5 shows layer-by-layer investigation of crystal structure of near-surface layers of oxidized $Be_{12}Ti$ sample.

Also, the results on study of mechanical properties and oxidation resistance of $Be_{12}Ti$ and $Be_{12}V$ samples delivered by Company Materion, USA, were published this year [3].

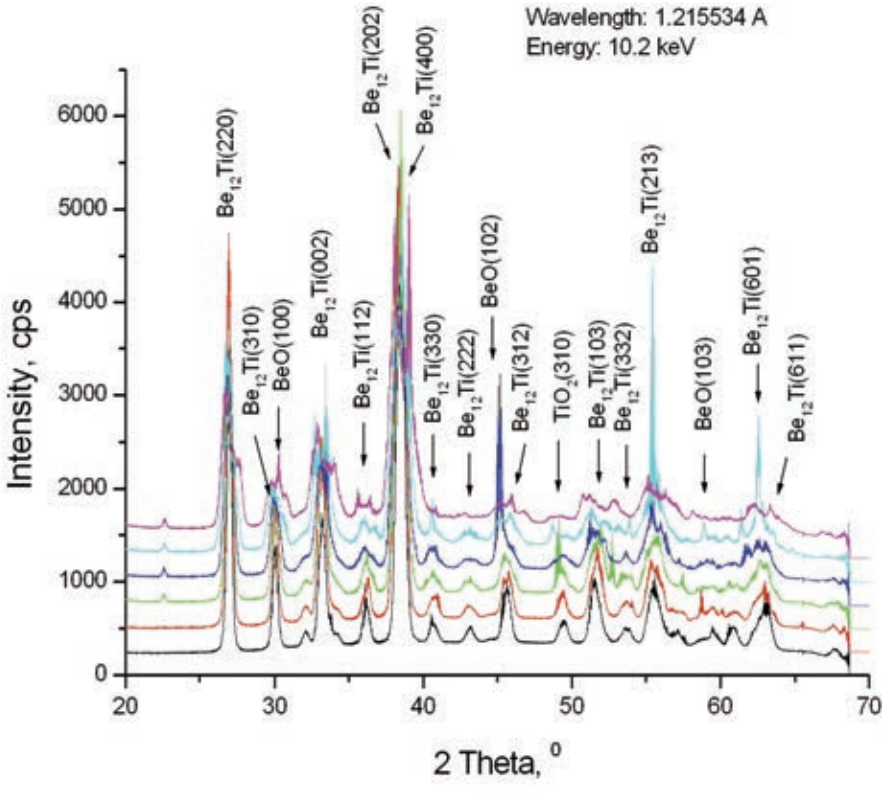

Fig. 5: X-Ray diffraction patterns obtained by means of synchrotron radiation from the surface of $Be_{12}Ti$ sample.

Conclusions and future plans

Principally, the possibility of production of Be-Ti rods which contain, mainly, $Be_{12}Ti$ phase was shown in previous years. The possibility to fabricate $Be_{12}Ti$ pebbles is under investigation now.

Production of a few kilograms of Be-Ti powder mixture with the use of a new NETZSCH milling machine is foreseen in the future. Fine Be-Ti powder with the particle size of 2-5 µm is needed for further works aimed to manufacture compact beryllide samples by:

- Sintering tests
- Hot pressing (HIP or hot extrusion)

Cooperation with industrial partners:

Several $Be_{12}Ti$ and $Be_{12}V$ specimens for investigations of their fusion-relevant properties were supplied by company Materion Corp., USA (http://materion.com/). Materion Corp. is a world's wide leader in the manufacturing of beryllium-based materials for nuclear applications.

Staff:

V. Chakin
P. Kurinskiy
A. Möslang

Literature:

[1] V. Chakin, M. Klimenkov, R. Rolli, P. Kurinskiy, A. Moeslang, C. Dorn, Microstructural and tritium release examination of titanium beryllides, Journal of nuclear materials, 417 (2011) 769-774.

[2] P. Kurinskiy, A. Moeslang, V. Chakin, T. Slobodskyy, A.A. Minkevich, T. Baumbach, Ch. Dorn, A.A. Goraieb, X-Ray study of surface layers of air-annealed $Be_{12}Ti$ and $Be_{12}V$ samples using synchrotron radiation, Fusion Engineering and Design, In Press.

[3] P. Kurinskiy, V. Chakin, A. Moeslang, R. Rolli, E. Alves, L.C. Alves, N. Franco, Ch. Dorn, A.A. Goraieb, Comparative study of fusion relevant properties of $Be_{12}V$ and $Be_{12}Ti$, Fusion Engineering and Design, Vol. 86, Oct. 2011, pp. 2454-2457.

Acknowledgement

This work was financially supported by the Ministry of Research and Education (BMBF) under the grant No. 03FUS0012. The views and opinions expressed herein do not reflect necessarily those of the BMBF or the European Commission.

Post Irradiation Examination of Be Materials irradiated in HIDOBE-01 Campaign (F4E-2009-GRT-30 (PNS-TBM) - Action 3)

KIT continued post-irradiation examinations of unconstrained beryllium pebbles and titanium beryllide pellet fragments irradiated within HIDOBE-01 experiment at HFR, Petten. The irradiation campaign HIDOBE-01 started in June 2005 and was finished in October 2007 after completion of 25 reactor cycles, or 649 days at full reactor power (>40 MW). The irradiation parameters of the investigated beryllium samples are as follows. The maximum neutron fluence in the central plane of the core was 8.92×10^{25} m^{-2} (E>1 MeV), corresponding to a damage dose of 18.1 dpa, and accumulations of 2950 appm helium and 285 appm tritium. The minimum irradiation parameters were as a neutron fluence of 5.69×10^{25} m^{-2} (E>1 MeV) which corresponds to a damage dose of 11.3 dpa, and accumulations of 1890 appm helium and 176 appm tritium. The average irradiation temperatures were as 630, 740, 873, and 948 K.

Tritium release and creep tests, and also microstructure investigations by optical metallography (OM), scanning (SEM) and transmission electron microscopy (TEM) were performed in 2011 according to the “HIDOBE-01: Detailed PIE plan” [1].

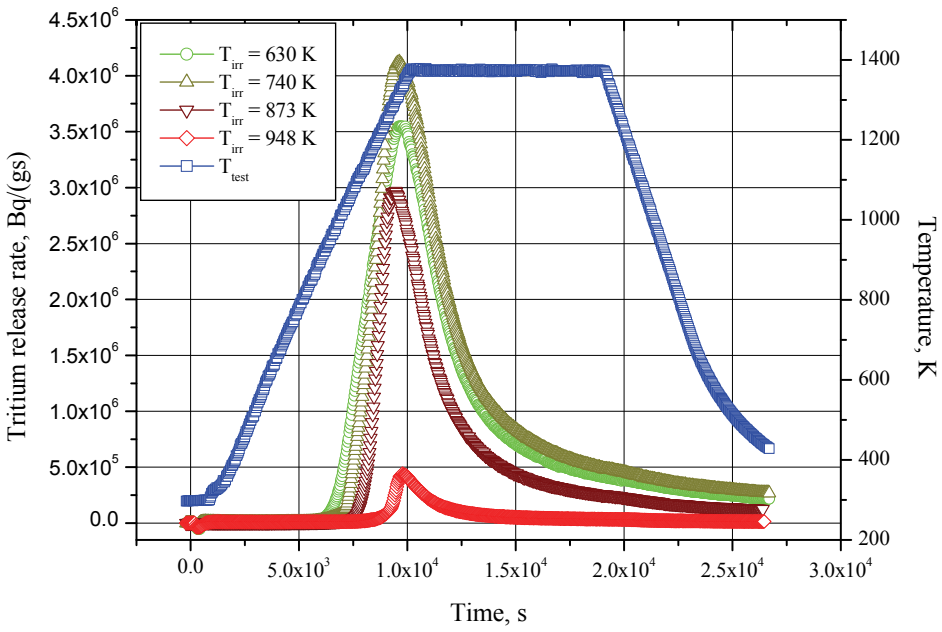

Fig. 1: Tritium release rate versus time exposure for irradiated beryllium pebbles.

Fig. 1 shows tritium release rates from beryllium pebbles with 1 mm diameter fabricated by Rotating Electrode Method (REM) as a function of time for four irradiation temperatures. All tritium release spectra are similar to each other. The tritium release starts to increase significantly after t = 3000-5000 s from the test beginning at temperatures which depend on irradiation temperatures. In particular, a higher irradiation temperature causes a more significant shift of the increase of the release rate. After t = 8000-10000 s all curves reach maximums and then monotonically decrease but slower with time when the testing temperature is kept constant at 1373 K. Thus, for each irradiation temperature only one peak is shown at temperatures of 1200-1400 K. The long-term neutron irradiation (649 days) at a definite irradiation temperature T_{irr} forms in beryllium a microstructure which is very stable for testing temperatures $T_{test} \leq T_{irr}$. This means that tritium can be released from traps only at temperatures higher than the irradiation temperature. A sharp decrease of the released activity occurs above the irradiation temperature of 873 K. At the maximum irradiation temperature (948 K)

the residual measured tritium is 6-8 times lower than at other irradiation temperatures. This means that tritium was mainly released from the pebbles during irradiation. A direct conclusion from these analyses is that at irradiation temperatures higher than 873 K a quite significant part of the produced tritium is able to escape already during neutron irradiation and that above this temperature the tritium remaining in the pebbles decreases further substantially with temperature. This strong decrease of the residual tritium in the irradiated beryllium pebbles with increasing irradiation temperature is of outstanding importance for a sound evaluation of the integral tritium inventory in highly neutron irradiated HCPB pebble beds.

The planned creep tests were performed on individual pebbles of 1 mm (2003) from all four irradiation temperatures. The loading values were changed from 10 up to 100 N, the duration of the tests was 80 h, the testing temperatures were equal to the irradiation temperatures. It was shown that creep rates had high values which directly depend on loading values and testing temperatures.

The microstructures of pebbles irradiated at 630 K and 740 K are quite similar to the non-irradiated state of the beryllium pebbles. Being produced via melting the pebbles have a coarse grain microstructure where the grain sizes can sometimes reach 400 µm. No clearly visible oxidation layers are present on the surface of the pebbles irradiated at 630 K and 740 K. However, some small objects of white color on the pebble surface are noticeable. The objects can be presumably identified as isolated islands of beryllium oxide BeO or a mixture of beryllium metal and BeO. Also no visible pores and gas bubbles have been observed on these cross sections. Contrary to lower irradiation temperatures, numerous pores (or bubbles) have been found in the microstructure after irradiation at 873 K. They have large sizes (up to 50 µm) and are distributed both over the bulk of the grains, and on the grain boundaries. Oxide films with a thickness of up to 8 µm are visible on the cross section of the pebble. It is quite dense and mainly skintight to the pebble surface. The film consists of two layers, a dark, compact, dense layer and a light one which is fragmentary located on the external surface of the dark layer. Probably, the light layer is the beryllium metal which diffuses during the oxidation process from the beryllium matrix through the beryllium oxide layer to the surface. At the highest irradiation temperature of 948 K, the number of pores is much larger (see Fig. 2 a). The thickness of the surface oxide layer remains below 8 µm but its morphology is changed (see Fig. 2 b). The surface layer consists of only one dark layer which is only loosely attached. Moreover, between the oxide layer and the beryllium surface large pores or gaps are visible.

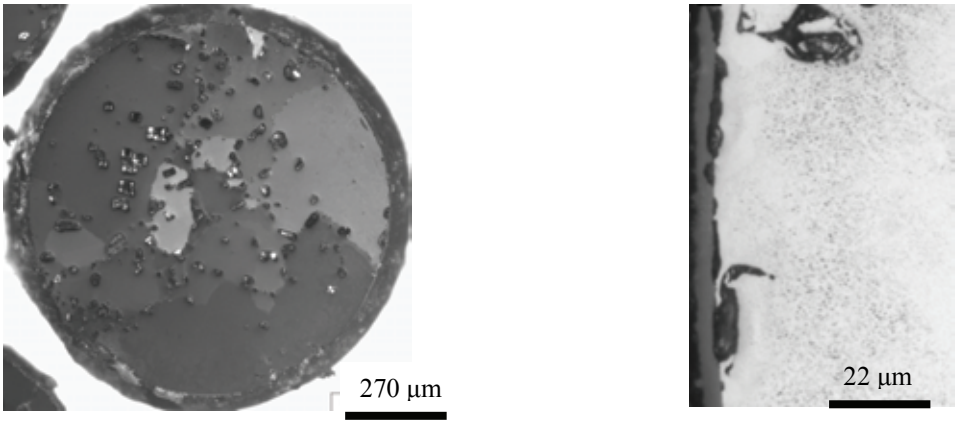

a b

Fig. 2: Cross-sections of beryllium pebbles irradiated at T_{irr} = 948 K.

In order to investigate the evolution of the beryllium pebble microstructure, transmission electron microscopy (TEM) was used (see Fig. 3). A high density of gas bubbles, presumably filled with helium, was detected in both investigated irradiated samples. After irradiation at 630 K (Fig. 3 a) helium bubbles with typical diameters of 8 nm are homogenously distributed

in the microstructure forming sometimes chains of bubbles. In the top left corner of Fig. 3 (a) some bubbles show an elongated narrow shape of about 4 nm thickness – presumably due to the changed orientation to the imaging plane. After irradiation at 948 K (see Fig. 3 b) the helium bubbles are much larger, ranging from 10 to 130 nm. These large bubbles mostly show a hexagonal faceted shape, however in contrary to the minimum irradiation temperature of 630 K only the small part of the bubbles can be identified as disk like shape.

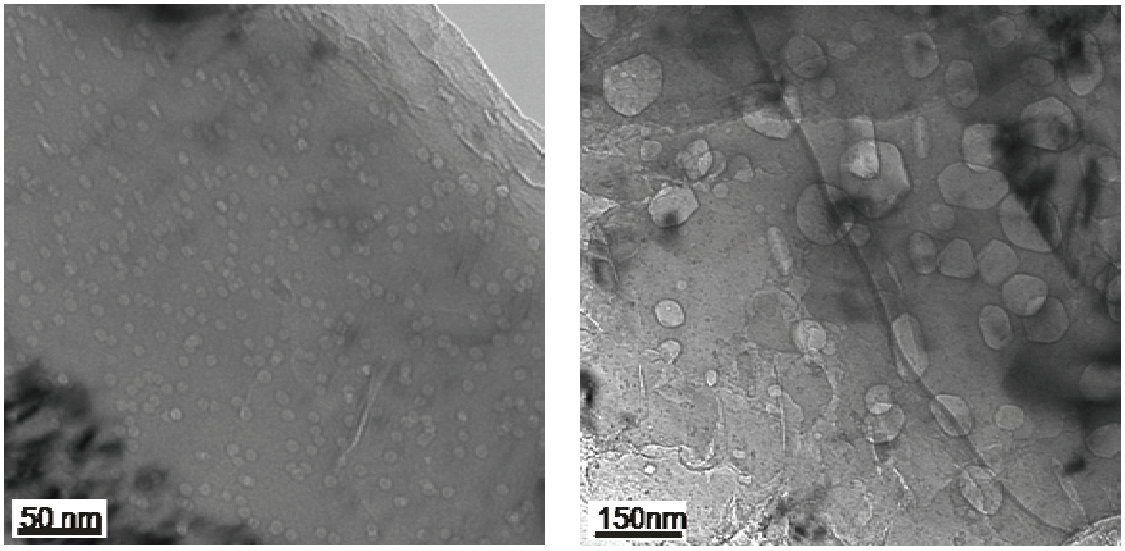

a b

Fig. 3: TEM images of irradiated beryllium pebbles: a)T_{irr} = 630 K; b) T_{irr} = 948 K.

During 2011 the new quadrupole mass-spectrometer from the company MKS production has been installed at FML (IAM-WBM) in the glove box. Fig. 4 shows a view of the mass-spectrometer before installation into the box. Now the mass-spectrometer is fully in function. First tests were successful performed with beryllium pebbles loaded by hydrogen-tritium gas mixture at a high temperature. This device will allow to measure not only released activity under heating but also will give an information about which atomic masses were escaped from irradiated beryllium meaning hydrogen and helium isotopes. Following thermo-desorption tests on F4E-2009-GRT-030 (PNS-TBM) - Action 3 will be performed using available proportional counter as well as the new mass-spectrometer.

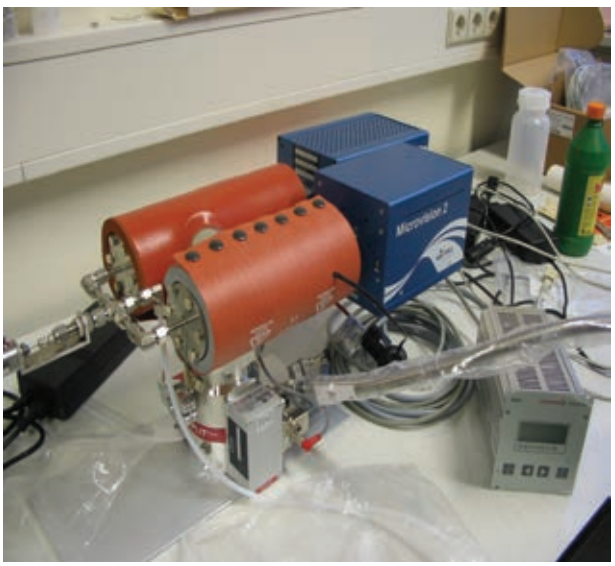

Fig. 4: A view of the new quadrupole mass-spectrometer.

Staff:

P. Barié
V. Chakin
J. Ehrmann
A. Erbe
M. Gilpert
M. Holzer
H. Jackisch
M. Klimenkov
P. Kurinskiy
S. Lautensack
G. Mangei
A. Moeslang
H. Ries
M. Rietschel
G. Rösch
R. Rolli
I. Sacksteder
R. Schmidt
H.-C. Schneider

Literature:

[1] S. van Til, HIDOBE-01: Detailed PIE plan, Under the contract of Fusion for Energy F4E-2009-GRT-030 (PNS TBM) - Action 3, NRG, the Netherlands, 14 October 2010.

[2] V. Chakin, R. Rolli, A. Moeslang, M. Klimenkov, M. Kolb, P. Vladimirov, P. Kurinskiy, H.-C. Schneider, S. van Til, A.J. Magielsen, M. Zmitko, Tritium release and retention properties of highly neutron irradiated beryllium pebbles from HIDOBE-01 experiment, Proceedings of the ICFRM-15, Charleston, USA, October 2012, to be published in Journal of Nuclear Materials, 2012.

Acknowledgement

This work was supported by Fusion for Energy under the grant contract No. F4E-2009-GRT-030(PNS-TBM) - Action 3 - with collaboration by NRG Petten, The Netherlands; ITN Sacavém, Portugal and ISSPI, Riga, Lativa. The views and opinions expressed herein reflect only the author's views. Fusion for Energy is not liable for any use that may be made of the information contained therein.

Divertor

Review of Water-cooled Divertor Concepts (WP11-PEX-01-ACT2-02 and WP11-DAS-IVCC-08-01)

The objective of this task is to review the existing water-cooled divertor (WCD) conceptual designs and to identify the potential weak points, which serve as a starting point for appropriate design improvement. The only existing example of an actual WCD was the ITER divertor that has been well developed. All WCD designs are therefore addressed to the ITER divertor concept and/or based on it, such as the PPCS-A divertor concept, studied in the framework of the EU Power Plant Conceptual Study. Within the frame of the current EU PPP&T DEMO-1 study, the useability of a WCD is to be investigated.

The first step of work has begun with a comprehensive literature review [4], which provides information on the applied heat load, cooling conditions, geometrical and material specification for the monoblock and cooling tubes. Because of their diversity, the studies performed in the different associations in the EU, RF, US and JP can be categorized from operational point of view into two main lines: Low/Medium temperature- and high temperature operation:

a) Low temperature operation: Most of the studies performed in the EU, RF and US were based on medium pressured water in the order of 3–4 MPa, cooling water pipe diameter of ~10 mm and flow velocities of ~10 m/s. The coolant temperature of these studies has been in the order of 100 °C.

b) High Temperature operation: The operational domains of these concepts are significantly higher with regard to the temperature (order of 300°C) and pressure level (up to 15 MPa).

In particular, JAEA (Japan Atomic Energy Agency) has been developing high performance cooling tubes with pressurized water flow for many years. The cooling tube posses a flow promoter in form of helical triangular fin (a quasi screwed tube) on its inner surface to enhance the heat transfer. The high heat flux experiments were focused mainly on critical heat flux testings. The screwed tube design were developed primarily for the JT60-SC tokamak, but JAEA also performed critical heat flux experiments under relevant cooling condtitions for DEMO divertor.

As one of the leading research institutes in Europe, ENEA mainly focused its activity in the past 5-6 years on developing and utilizing the Hot Radial Pressing (HRP) bonding technique to join the CFC or W monoblock with CuCrZr cooling tube. The HRP manufacturing process was validated on different scaled mock ups in several european high heat flux test facilities (EFREMOV, AREVA/CEA, FZJ). Successful results were obtained by the thermal fatigue tests carried out in accordance with the requirements for ITER.

Material aspects: From the literature it could be inferred that CuCrZr material was used as a structural material for ITER divertor under moderate boundary conditions (i.e. low neutron dose, low temperature). The use of high thermal conductivity of CuCrZr heat sink may allow for a high performance of the divertor, on the one hand. On the other hand, its embrittlement at high neutron flux, as well as a reduction of its fracture toughness at a neutron damage dose of above 0.3 dpa, especially at elevated coolant temperatures, was reported in [5] and [6], respectively. Therefore, the applicability of such a material is questionable, when operating in a fusion power plant or DEMO environment under high neutron flux and maybe at elevated coolant temperatures. This can be viewed as a handicap for the use of such a water-cooled concept for DEMO, unless a substitute material can be found which simultaneously satisfies all the thermal-hydraulic and thermo-mechanics design requirements.

A thermal analysis for water cooling with heat sink material made of austenitic steel [7] shows that a surface heat load of up to 5 MW/m^2 can be dissipated. The use of RAFM steel

is not possible due to the low coolant temperature lying below its DBTT limit of 350 ° C under irradiation.

Staff:

L.V. Boccaccini
S. Kecskes
P. Norajitra
H. Neuberger
J. Reiser
M. Rieth

Literature:

[1] M. Ferrari, L. Giancarli, K. Kleefeldt, C. Nardi, M. Rödig, J. Reimann, et al., Evaluation of divertor conceptual designs for a fusion power plant, Fusion Engineering and Design 56–57 (2001) 255–259.

[2] V. Barabash, A. Peacock, S. Fabritsiev, G. Kalinin, S. Zinkle, A. Rowcliffe, et al., Materials challenges for ITER—current status and future activities, Journal of Nuclear Materials 367–370 (2007) 21–32.

Acknowledgement

This work, supported by the European Communities under the contract of Association between EURATOM and Karlsruhe Institute of Technology, was carried out within the framework of the European Fusion Development Agreement. The views and opinions expressed herein do not necessarily reflect those of the European Commission.

Helium-cooled Divertor (WP11-DAS-IVCC-09-01)

The objective of this task is to review the status and perspective of development of the He-cooled divertor. The development of the helium-cooled divertor has been started under the EU PPCS in 2000 [1] with the goal of reaching 10 MW/m^2. This divertor type with helium cooling was applied in most of the PPCS reactor models (i.e. A-B, B and C). After the helium-cooled divertor has been selected as reference for the EU DEMO application, its development has been vigorously pursued at KIT since 2003. Today's reference concept [2] is based on a modular design of small tungsten-based cooling fingers. Each of them consists of a tile as thermal shield which is brazed to a thimble as heat sink part; both are made of tungsten material. The fingers themselves are then connected with the steel body by means of brazing. The fingers are cooled with helium impinging jets at 10 MPa and 600°C. The helium temperature was adapted to the tungsten material property, in particular the DBTT (assumed about 600°C). In 2004, a combined HHF test facility helium loop with EB in Efremov, St. Petersburg, Russia was built for proof of design principle. This facility allows mock-up testing under the specified DEMO conditions (without neutron). Already in the first test series, the cooling performance of the finger concept with helium has been confirmed under the defined heat load of 10 MW/m^2 and several load cycles. Since then, the design terms of robustness (i.e. thermal stress reduction) and the production quality of tungsten parts were gradually improved to enhance the lifetime of the cooling finger against thermo-cyclic loads as large as possible (goal is reaching 1000 cycles). In the last tests of 2010 [3], the first breakthrough was achieved when such a cooling finger of the currently best design already survived > 1000 cycles without damage. Currently R&D is focused on tungsten joining technology (i.e. high-temperature brazing) [4], non-destructive testing, and – due to the large quantity of finger units required (> 250,000) – on the mass production of divertor components (i.e. W deep drawing [4] and tungsten injection molding [5]). Future planning is the construction and testing of bigger components (i.e. target plates and divertor cassette) in HELOKA. The use of the divertor in DEMO was envisaged for about 2040.

Staff:

P. Norajitra
L.V. Boccaccini

Literature:

[1] P. Norajitra et al., Conceptual design of the dual-coolant blanket within the framework of the EU power plant conceptual study (TW2-TRP-PPCS12), Final Report, Forschungszentrum Karlsruhe, Wissenschaftliche Berichte, FZKA 6780, 2003.

[2] P. Norajitra, et al., He-cooled divertor development for DEMO, Fusion Eng. Des. 82 (2007) 2740–2744.

[3] P. Norajitra et al., Progress of He-cooled Divertor Development for DEMO, SOFT-26, 27.09.-01.10.2010, Porto, Portugal. To be published in FED.

[4] P. Norajitra, S. Antusch, W. Basuki, L. Spatafora, V. Toth, Newly developed innovative manufacturing technologies for He-cooled DEMO divertor, proceedings of the 2011 IEEE/NPSS 24th SOFE, June 26-30, 2011, Chicago, Illinois, USA, IEEE Catalog #: CFP11SPF-CDR, ISBN: 978-1-4673-0103-9.

[5] S. Antusch, P. Norajitra, V. Piotter, H.-J. Ritzhaupt-Kleissl, Powder Injection Molding for mass production of He-cooled divertor parts, J. Nucl. Mater. 417 (2011) 533–535.

Acknowledgement

This work, supported by the European Communities under the contract of Association between EURATOM and Karlsruhe Institute of Technology, was carried out within the framework of the European Fusion Development Agreement. The views and opinions expressed herein do not necessarily reflect those of the European Commission.

Investigating and Developing W Deep Drawing (HGF)

In a continuation of deep drawing experiments, a newly developed tool was used. This time 1 mm thick, round tungsten slices of 20 mm and 24 mm diameter, respectively, were deep drawn successfully. Figure 1 shows the deep-drawn product in the form of a divertor thimble (outer diameter 15 mm) with a height of 8 and 11 mm, respectively (bottom right in the figure). The parameters used are: 700 °C operating temperature and 20 kN maximum compression force equivalent to about 160 MPa projected normal contact pressure on the stamp.

Fig. 1: Successful deep draw attempts from 1 mm thick tungsten sheet for mass production of divertor thimble (Ø15 x 1).

Staff:

W. Basuki
P. Norajitra
L. Spatafora
V. Toth

HHF Tests on 1-Finger and 9-Finger Modules (HGF)

Three 1-finger modules with new brazing materials [1] were successfully HHF tested. The mock-ups survived 944, 223, and 171 cycles at 10 MW/m^2, respectively. The failure occurred was due to the He-leakage through cracks in the thimble wall. As the cause of this, a high surface pressure of the pimples of the quasi-bayonet connection was suspected. Therefore, the joint design must be improved further in the next step. The following table shows the overall result of the number of cycles of the mock-ups tested till now, as a measure of robustness, regardless of type and driving style.

Table 1: Results of all HHF tests (Best Case)

Heat flux [MW/m²]	Max. achieved number of cycles before failure
10	940
12	1110
13	69
14	38

As part of the HHF test programs for divertor components, two 9-finger modules are under manufacturing. Figure 1 shows the components of a 9-finger module just before final assembly. The fabrication sequence for this is described in [2] in detail.

Fig. 1: 9-finger module manufacturing. Left: individual parts, right: assembly view.

Staff:

S. Antusch
S. Berberich
P. Norajitra
L. Spatafora

Literature:

[1] Nuclear Fusion Programme, Annual Report of the Association Karlsruhe Institute of Technology/EURATOM, January 2010 - December 2010, KIT Scientific Publishing, KIT Scientific Reports 7592, 2011, ISSN 1869-9669.

[2] P. Norajitra, L. Spatafora, Technological study on manufacturing of multi-finger module of He-cooled DEMO divertor, ICFRM-15, Charleston, South Carolina, USA, 16-22 October 2011. To be published in Fusion Science & Technology.

System Codes for DEMO

Review of Technology / Engineering Assumptions / Models used in the Code. (WP11-SYS-01-ACT2-01 + WP11-SYS-01-ACT2-02) Identification of Improvement Needs and Plans for Implementation (WP11-SYS-01-ACT7-01)

Introduction

The Technology Guidelines are intended to assist the design of a fusion power plant. This design will start from the running of the System Code that at the moment is the main target of this report.

Aim of this task is to prepare a preliminary document establishing a Table of Contents and collect for each identified items information available. From the beginning of the task, the aim was not to prepare a final document; to this goal larger resources would be necessary and in any case this document is a “living one” subjected to modifications as soon as decisions in the requirements of the new DEMO are taken by the EU Project Leadership.

The parameters included in this document are mostly collected from some reactor study done in the past. In particular the Power Plant Conceptual Study (PPCS) have been taken into account for the definition of five reactor models with a relative wide spectrum of materials (structural, breeder, coolant, etc.) and configurations. In addition the studies conducted on DEMO-2007 have been considered as start point for the configuration of the new DEMO.

System codes

A systems code is a computer program that includes simple algebraic formulae of all parts of a reactor system, from the basic plasma physics to the generation and transmission of electricity. Using such a systems code allows one to roughly evaluate reactor design parameters, e.g., physics and engineering requirements and cost of electricity, consistently with physics and engineering constraints based on analysis design philosophy. In a series of reactor design processes, a systems code is used to make a basis of a reactor design that is initial determination of reactor operation points (or windows).

Several system codes (e.g., PROCESS, HELIOS, ARIES, KAREI) have been developed since the eighties with different objectives and appropriate architecture and level of development, to explore possible operating condition ranges of a fusion power reactor and/or (more often) find an optimized configuration around a given operating point. Most of the above mentioned codes are based on a plasma physics’ zero dimensional model incorporating technological constraints, e. g. max heat flux on the divertor or max current density in the coils. “Technological modules” are integrated or coupled with this core in the most advanced tools, whilst relevant parameters are used as input data in other codes. For instance, a calculation of system code starts from a first guess of radial building and the output can be provided as input to 3D neutronic calculations. Output of 3D-neutronic is an optimized radial build-up. This can be used again in the system code to refine the configuration. It is an iterative process that should started at a convergence point.

PROCESS has been developed in CCFE and was widely used in the past EU Reactor Studies, ARIES Code has been developed in the US in the framework of ARIES activities, KAERI Code in Korea and SYCOMORE, a new code is under development in CEA.

Discussion

The guideline document is divided in sections dedicated to systems of the fusion power plant (e.g. magnets, blankets, etc.) and overall process estimations (e.g. Plant Power Balance, Availability, Cost of Electricity, etc.). For each of these systems/processes requirements, technological constrains, etc. have been collected.

Magnet system: In this section several points are addressed; first the lay-out of the coils on the basis of the PROCESS Code. “Mechanical Design Criteria” and “Superconducting cable design criteria are collected in the other sections”. Finally, “fluence and nuclear heating limits” are reported, which are important in the determination of the radial build-up of the reactor in view of magnet protection.

Vacuum Vessel and Maintenance Concepts: The lay-out of the reactor (e.g. radial build-up, blanket coverage, etc.) is strongly impacted by the maintenance system adopted as basis of the reactor concept (e.g. dimensions of the magnets and of the supporting in-vessel region). In this report all the considerations are based on the system analyzed during the DEMO-2007 studies, namely the Vertical Maintenance System (VMS) with a design of the replaced blanket segments based on the Multi Module Segment (MMS) concept.

Blanket System: In this section the values used for the thickness of the different blanket zones are discussed in relation to Tritium Breeding Ration (TBR) performances and neutron shielding capability. A section is dedicated to lifetime consideration related to this component.

Divertor System: The plasma facing components (PFCs) have to be designed to withstand high power loads, allow for efficient Helium exhaust, control particle recycling and limit the impurity release. The key physics parameters with which the plasma boundary properties can be controlled are:

- the radiation level from impurities at the plasma edge which influences the power flow to the divertor plate;
- the plasma edge density which influences the radiation level (impurities and charge exchange) and the plasma temperature (sputtering);
- transient phenomena (ELMs, disruptions) which cause peak heat loads and
- the type of impurity species which enter the edge plasma either via erosion of wall materials or via impurity seeding.

They have to be chosen such that the technical boundary conditions are satisfied, e.g.:

- the maximum heat load density on divertor plates
- the maximum average heat flux on the wall
- thermal fatigue properties and thermal stress
- materials surface properties (sputter yields, chemical reactivity, melting, sticking probability etc.)

The PFCs should survive a number of off-normal events. Erosion processes will finally limit the life time of PFCs, once the thermal load issue is solved and off-normal events are more or less inhibited.

Heating systems: The steady state operation of a tokamak reactor relies upon the fact that the electrical current necessary for plasma confinement can be driven non-inductively. It then consists of two parts, (i) a self-generated current stemming from the density and temperature gradients (the neoclassical bootstrap effect), and (ii) an externally driven current which comes from the application of high power heating through the interaction of neutral beams or radio frequency waves with the various particle species. Since the amount of recirculated power must be minimized in an attractive reactor design, it is essential that the bootstrap current fraction and the current drive efficiency of the external heating systems are both as large as possible. The present assessment is of course highly subject to the level of progress one can reasonably anticipate during the operation of ITER and the required R&D will be outlined.

Fuelling and Tritium System: The development of tritium cycle for DEMO fusion reactors is at its first stages and significant effort on conceptual design activities, modeling and experimental appear as compulsory. The main activities related to the tritium system study should start with a review of existing available documentation related with: Key tritium analyses in the Tritium Cycle (TC) source term (breeding blanket concepts), actual reference configuration lay-outs for the total cycle and integrating systems and selection of relevant tritium processing key technologies for code development. In a DEMO reactor study a reliable tritium Process Flow Diagram (PFD) modeling tool for DEMO Tritium Cycle (TC) should be developed and implemented in a System Code. This tool is, at present, being conceived to provide dynamically global quantitative evaluation of tritium paths from source unit (breeding blanket structures) into the main Tritium Cycle systems. From the system analysis point of view, a detailed definition of all components composing the entire Tritium Cycle should be foreseen.

Plant Power Balance: A proposed schema for the Power Flow is illustrated in Figure 1. The Fusion Power is a source term which is constituted by two separated contributions: the neutron power and the alpha power. The neutron power is associated to the neutron kinetic energy and includes 80% of the FP, while the alpha power includes 20 %. In a magnetized plasma, alpha particles will interact with the magnetic field and the particles of the plasma

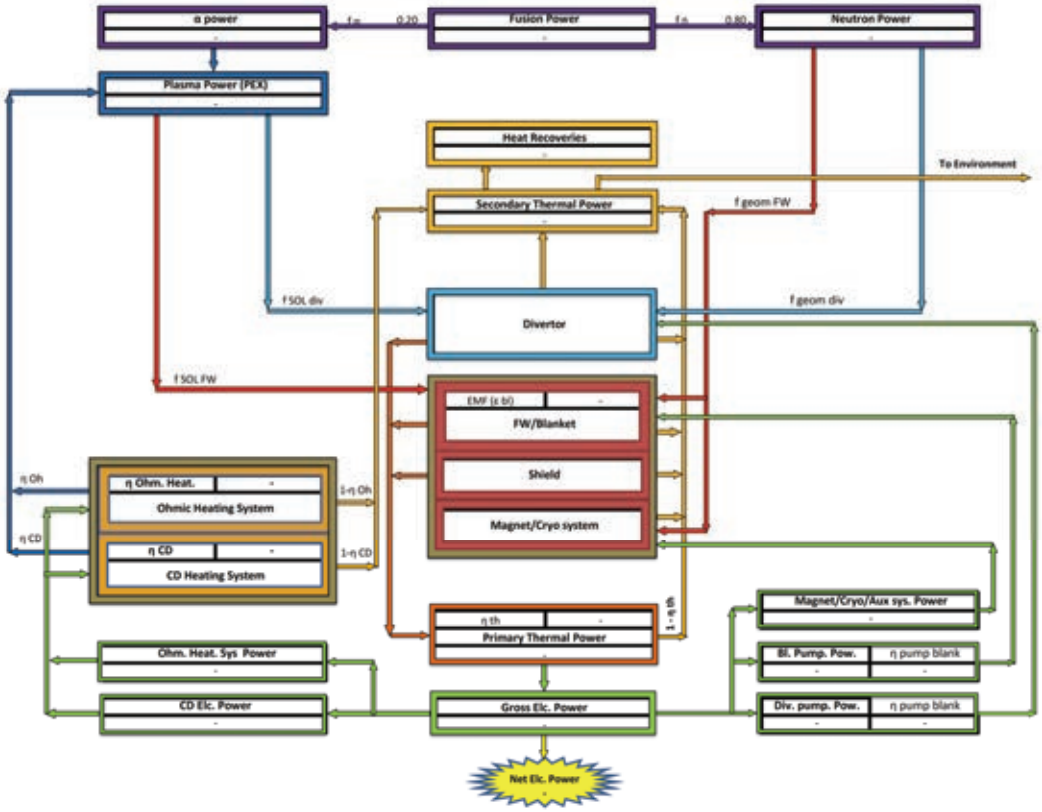

Fig. 1: Plant Power Balance Scheme.

core. The plasma core energy receives also the contribution of the Heating and Current Drive Systems. At steady state this energy crosses the Scrape-off layer (SOL) boundary in form of radiation from the plasma core and in form of particles from the SOL region. The sum of these power terms constitutes the Power Exhaust. Following different patterns, this energy will be deposited mostly in the Plasma face components of the Blanket and Divertor Systems. We distinguish among two main systems for the heat removal from the Vessel/in-vessel components, namely a Primary Thermal Power (PTP) and a Secondary thermal Power (STP). The PTP is usually heat collected by a coolant at high temperature that can be used for high efficiency electricity production. The STP (associated to coolants at low temperature

or in general to thermal power terms present in the plant and balancing the total power distribution) can be used only in a reduced fraction to increase the efficiency of the Power Generation Systems (e.g., in a Rankine cycle can be used for the pre-heating of the water coming from the condenser, as indicated in the term “Heat Recoveries”). Most of the energy transported by the STP is then discharged from the plant. The total electrical power produced by the power conversion system is called “Gross electrical power” (GEP). Part of this power is re-introduced inside the plant to feed all the auxiliary systems. The total amount of electrical power feeding the auxiliary system is given by: Heating and Current Drive system power, Divertor and Blanket pumping power, and Magnet/Cryogenic/Other Auxiliary electrical power.

Plant Lifetime and Availability and Costing model. This part could be addressed only partially in the task and necessitate to be improved in further work.

Conclusions

The work (also if limited) was able to provide some suggestions for the future development of PROCESS (or for a new code):

- It is suggested to use a modular form of a System Code in which different models with different grade of accuracy and complexity could be integrated allowing to perform different tasks, like exploring wide operating condition ranges of a fusion power reactor, or searching for an optimized configuration around a given operating point and/or providing configuration parameters that are used as input data in other codes (or code platforms) in which the conceptual design is further developed. This strategy is reflected by identifying two areas of work: 1) Inside the actual System Codes improving the interaction among plasma and technological aspects (design, design criteria, materials properties, system performances, etc.) of the fusion machine; 2) Creating the connection to more sophisticated Engineering tools (“Integrated Engineering System”) that that are necessary to perform the DEMO Design even in the Conceptual Phase. For this work it is necessary to “translate” many of the parameters optimized in the System Codes in input (e.g. loads) usable for the Conceptual Design. In the future this do not exclude the possibility to create more integrated systems that allow feedback mechanisms to re-assess reactor configurations caused by changes in the design (e.g., necessity of increased blanket thickness or magnets geometry).
- Among the technological parameters that have a major impact on System Code previsions the radial build-up is a very sensitive one. In the past experiences of PPCS and DEMO-2007 design the necessity of iterations between proper system codes (like PROCESS, in which this thickness is only an input value) and neutronics-thermal-hydraulic-structural tools (necessary to confirm the radial building vs. design criteria) created several issues in managing the reactor configurations. It would be interesting to develop more sophisticated models to treat this part up to including some simplified neutronic routines to check design parameters related to e.g. Tritium Breeding Ratio, Magnet neutron shielding and power balance among the different components constituting the fusion reactor.
- Power Flows: the model can be improved taking into account a more detailed power distribution and also pulsed operation regimes (i.e., start up or shut down of the machine). In particular a more improved neutron power distribution among the different systems should be foreseen (e.g. combination with a neutronic model). The scheme used by PROCESS can accommodate different plant configurations simply modifying few parameters. A more general model could be interesting allowing more details in the power flow. In any case loading conditions on the single component/system as a result of the power in the exhaust should be improved, thereby improving PEX modeling.
- Geometry: An interesting feature of PROCESS is to consider a 2D (axial-symmetric) geometry for the calculation of several parameters. This 2D section is a good basis for the connection to other tools that are necessary to proceed with the conceptual design. Also if

this part has not been analyzed in detail, some improvements seem possible to increase this capability.

- It is interesting to note that some issues as Tritium Breeding Ratio or Tritium Fuel Cycle are very poor (or not) addressed in System codes. The First issue can be considered in the Blanket Section, the second maybe could require modeling the Tritium Fuel Cycle. Further assessment is necessary.

Staff:

L.V. Boccaccini
F. Franza
I. Maione

Acknowledgement

This work, supported by the European Communities under the contract of Association between EURATOM and Karlsruhe Institute of Technology, was carried out within the framework of the European Fusion Development Agreement. The views and opinions expressed herein do not necessarily reflect those of the European Commission.

Structural Materials – Steels

Issues Related to Radiation on Blanket and Divertor Materials (WP11-DAS-MAT-M02-01)

Objectives

Several experiments are performed to study the influence of the neutron irradiation on the mechanical properties and microstructure of DEMO Blanket and Divertor relevant structural materials. The current proposal aims at assessment of the mechanical properties of neutron irradiated RAFM steels. The emphasis will be put on the assessment of tensile, Charpy impact, low cycle fatigue (LCF) and fracture toughness properties of EUROFER 97 and EUROFER ODS (9% Cr) steels irradiated up to a displacement damage dose of 80 dpa. The effects of the neutron irradiation temperature and dose will be investigated. The influence of neutron irradiation on divertor materials will be assessed depending on the availability of relevant data. For the assessment of the issues related to helium production and its influence on the mechanical properties of RAFM steels the experiments simulating helium production under neutron irradiation (e.g. by 10B doping) will be reviewed.

Task Current Status

The data to be assessed within the current task has been collected by retrieving existing databases and literature. The mechanical testing results on EUROFER 97 and EUROFER ODS (9%Cr) steels from various *low* (IRFUMA up to 2 dpa [SCK-CEN], SUMO, SIWAS up to 9 dpa [NRG]), *medium* (WTZ RUS 01/577, SPICE up to 15 dpa [KIT]) and *high* dose (ARBOR 1 up to 33 dpa [KIT], ALTAIR up to 42 dpa [CEA], ARBOR 2 up to 70 dpa [KIT] and 80 dpa [CEA]) European irradiation programmes have been reviewed. For straightforward comparison of the results from different irradiation programmes the details about investigated materials, specimen dimensions and extraction directions, irradiation conditions, testing parameters etc. have been collected.

Fig. 1 shows the dose evolution of hardening for EUROFER 97 and other different RAFM steels for Tirr =300-335 °C and Ttest = 300-350°C. The full symbols represent the KIT results, whereas the open symbols stem from literature (SCK-CEN, NRG, CEA). Neutron irradiation leads to substantial increase in the Yield Stress with the dose. The Yield Stress increase is rather steep at doses below 10 dpa. The hardening rate appears to be significantly decreased at the achieved damage doses for all investigated steels. At achieved damage doses the hardening indicates a clear tendency towards saturation for EUROFER 97 (Heat E83697). A comparison of high dose irradiation results obtained on EUROFER 97 (E83697), pre-irradiation heat treated EUROFER 97 HT (E83697) and EUROFER 97 (E83698) reveals however that high dose hardening behaviour can be observably modified by variation of different metallurgical variables (thermal treatment, heat, etc.). Hardening quantified for F82H-mod and 9Cr2WTaV (British Steel, Heat VS3104) steels

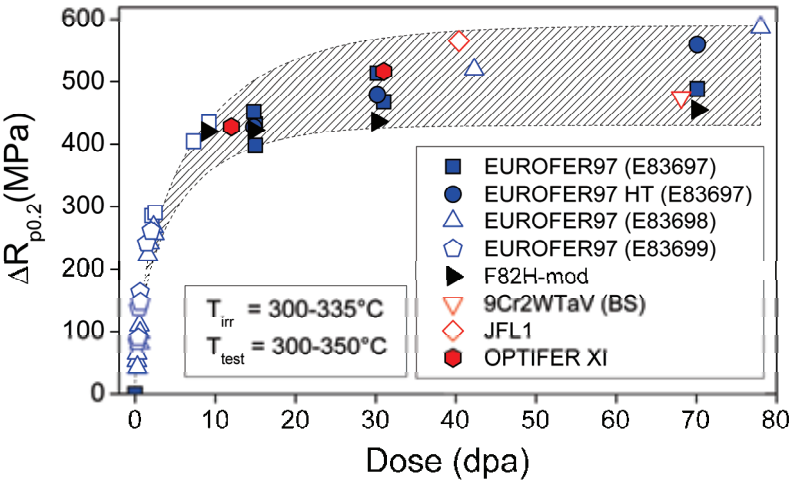

Fig. 1: Irradiation hardening vs. irradiation dose for EUROFER 97 and other RAFM steels for T_{irr} =300-335 °C and T_{test} =300-350 °C. The full symbols represent KIT results. The open symbols are from different European irradiation experiments carried out by SCK-CEN, NRG, CEA. The hatched area marks the scattering band for the high dose results and is guide for the eye.

at 70 dpa is comparable to that of EUROFER 97 (Heat E83697). Furthermore, similar to EUROFER 97 (Heat E83697) F82H-mod steel indicates saturation of hardening at the achieved damage doses. The hatched area marks the scattering band of the high dose hardening for different RAFM steels. It is important to note that to the reasons for observed data scattering belong not only the differences in the metallurgical variables, but also variations and uncertainties in the irradiation conditions. The limited number of available irradiated samples does not allow detailed statistical analysis of the results.

The evolution of the neutron irradiation induced embrittlement (measured in impact tests) with dose for EUROFER 97 and F82H steels at irradiation temperatures between 300 and 337 °C is shown in Fig. 2. For comparison the neutron irradiation induced embrittlement for OPTIFER and 9Cr2WVTa (BS) steels are also included. In case of EUROFER 97, differentiation is made between specimens machined from as-delivered products and specimens machined from the plates subjected to pre-irradiation HT. The results on F82H and F82H-mod are plotted together for different heat treatments and material compositions. The pre-irradiation HT of EUROFER 97 leads to considerable improvement of the irradiation resistance at doses up to 30 dpa. At the achieved damage doses, however, the embrittlement of EUROFER 97 HT becomes comparable to that of EUROFER 97. All investigated steels show steep increase in the ΔDBTT with dose below 10 dpa. With farther increasing the damage dose the embrittlement rate decreases and a clear tendency towards saturation is observed at the achieved damage doses. F82H-mod irradiated to 65 dpa at 337 °C behaves somewhat poor compared to the EUROFER steels with respect to embrittlement. The embrittlement of OPTIFER XI and OPTIFER XII steels after low temperature irradiation to 12 dpa (and 31 dpa in case of OPTIFER XI) confirms the embrittlement trend of EUROFER 97 steels.

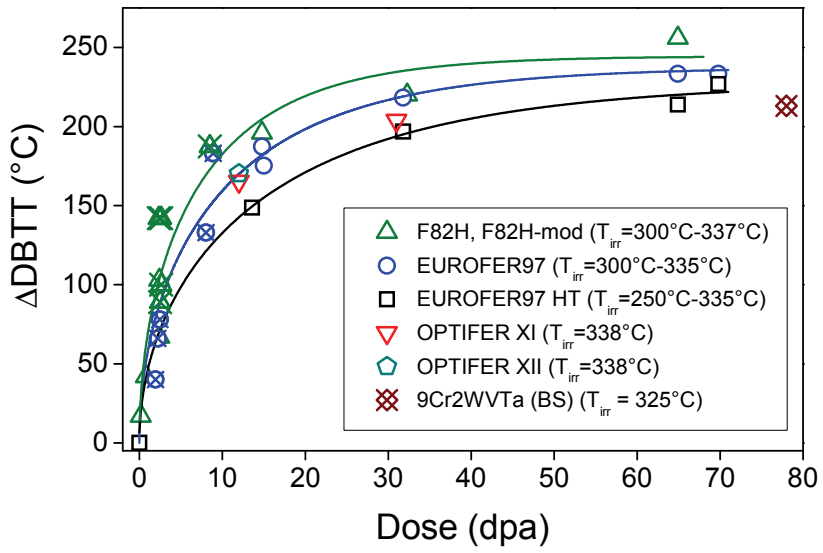

Fig. 2: Irradiation shifts of the DBTT vs. dose for EUROFER 97 and other RAFM steels. The open symbols represent KIT results and the crossed symbols represent NRG and CEA results. The solid lines are a model description of the data.

The post irradiation annealing experiments yielded very promising results. The post-irradiation annealing of e.g. 70 dpa@335°C irradiated EUROFER 97 HT at 550 °C for 3 h leads to a reduction of the DBTT from 135 to -43 °C resulting in a residual embrittlement (shift in DBTT) of just 48 °C compared to the unirradiated state. The residual embrittlement of F82H-mod irradiated to 65 dpa and annealed is about 106 °C. Post irradiation annealing of 70 dpa@332°C irradiated EUROFER 97 lead in addition to a nearly complete recovery of the tensile properties with respect to both the strength and ductility.

The effects of the neutron irradiation on the microstructure and mechanical properties of the RAFM steels depend strongly on the irradiation temperature. The irradiation induced hardening and embrittlement is substantially reduced at irradiation temperatures above $T_{irr} \geq 350$ °C. So the DBTTs of the several RAFM steels irradiated at or above 350 °C to 15 dpa in SPICE irradiation remain below -24 °C and, hence, well below the material application temperature. On the basis of this observation a temperature window between 350 and 550 °C is proposed for operation of the First Wall and breeding bBlanket components.

The neutron irradiation induced hardening may differently affect the low cycle fatigue behaviour of the irradiated RAFM steel specimens. The increase of the elastic part of the cyclic deformation and the related reduction of the inelastic strain amplitude due to irradiation induced hardening lead to the increase of the fatigue lifetime especially at low strain ranges. The radiation hardening induced increase of the stress level might, however, lead to enhanced damage evolution and hence to lifetime reduction especially at high strain ranges.

Despite large efforts of the scientific community the effects of the helium production on the performance of the RAFM steels is not sufficiently understood due to absence of the irradiation facility with a fusion reactor relevant neutron spectrum. Investigation of helium effects in neutron irradiated boron doped EUROFER 97 based steels lead to a progressive material embrittlement with increasing the produced helium content up to 432 appm.

Conclusion

The state-of-the-art structural materials are highly suited for the special fusion reactor design with the operating temperature range for the FW and BB being between 350 and 550 °C. The thermal recovery experiments yielded very promising results. After possible validation of this method through the study of the repeatability of these experiments, recovery heat-treatments can also be utilized for extension of the operating temperature range down to RT. Helium effects in RAFM steels are not sufficiently understood due to absence of the irradiation facility with a fusion reactor relevant neutron spectrum and have to be a subject of future investigations.

Staff:

E. Gaganidze

Literature:

[1] E. Gaganidze, C. Petersen, E. Materna-Morris, C. Dethloff, O. J. Weiß, J. Aktaa, A. Povstyanko, A. Fedoseev, O. Makarov, V. Prokhorov, *Mechanical properties and TEM examination of RAFM steels irradiated up to 70 dpa in BOR-60*, J. Nucl. Mater. 417 (2011) 93-98.

[2] E. Gaganidze, C. Petersen, J. Aktaa, A. Povstyanko, V. Prokhorov, E. Diegele and R. Lässer, *Low cycle fatigue properties of reduced activation ferritic/martensitic steels after high-dose neutron irradiation*, Nucl. Fusion 51 (2011) 083012.

Acknowledgement

This work, supported by the European Communities under the contract of Association between EURATOM and Karlsruhe Institute of Technology, was carried out within the framework of the European Fusion Development Agreement. The views and opinions expressed herein do not necessarily reflect those of the European Commission.

TEM Investigation of Neutron Irradiated EUROFER 97 and Boron Containing Alloy (WP11-MAT-REMEV-05-04)

Introduction

Material research for innovative fission and fusion nuclear systems has become a field of growing relevance worldwide. Reduced activation ferritic martensitic steels (RAFM) with 8-10%Cr-WTaV are leading candidates for the application in fusion reactors. The EUROFER 97 with 9% Cr has become the European reference RAFM steel for fabrication of blanket material for the future fusion reactor. It is expected that structural materials in a fusion reactor will be exposed to very high levels of irradiation induced displacement damage of more than 100 displacements per atom (dpa) and relatively high helium concentrations of up to 10 appm He/dpa, the latter due to inelastic transmutation reactions of energetic fusion neutrons.

Embrittlement induced by the formation of copper precipitates under irradiation is a problem for some Russian and American nuclear reactor pressure vessel steels (e.g., 15Kh2MFA and ASTM A302B) with increased copper content (~0.1wt%), which are mostly used in the reactors of 2^{nd}-generation, for example, PWR or VVER type. Especially sensitive to this kind of embrittlement are welds, which receive additional copper from welding wires. In modern reactors this problem is avoided by a careful control of the copper content of the base and weld material. On the other hand, the problem of the copper induced embrittlement is directly related to the extension of the end of life of the existing reactors. Post irradiation heat treatment of reactor pressure vessel anneals irradiation induced defects and changes the morphology of copper precipitates.

As fission neutrons produce typically about 30 times less helium per unit time compared to fusion neutrons, in the absence of fusion reactors helium effects have to be simulated, e.g. by an addition of ^{10}B that decays into ^{4}He during neutron irradiation thus increasing the helium production. The neutron irradiation of this alloy allows studying of both the effect of high concentration of helium bubbles and their interaction with Cu precipitates, thus giving a unique opportunity for understanding its severe impact on tensile and fracture toughness degradation.

Method

The boron alloyed specimens have been prepared from the EUROFER 97 with addition of 0.116% wt ^{10}B and 0.56%wt. Cu. After complete transmutation (approximately corresponding to a displacement damage dose of 1 dpa) this amount of boron produces about 5800 appm He. After fabrication, the ferritic-martensitic alloy has been heat treated at 1040 °C for 30 min and normalized at 750 °C for 90 min, to obtain the tempered martensite structure. In the present study the specimens have been neutron irradiated up to 16.3 dpa at 300 °C and 400 °C in the mixed spectrum reactor HFR, Petten and have been characterized together with unirradiated control specimens using analytical transmission electron microscopy (TEM).

Samples with a thickness of 0.2-0.3 mm have been thinned by electro-polishing in a TENUPOL device using H_2SO_4 + 80% CH_3OH as electrolyte. From that material, disks with diameter of 1 mm have been punched. TEM investigations have been performed using a FEI Tecnai 20 FEG microscope with an accelerating voltage of 200 kV, the scanning unit for performing scanning TEM (STEM) equipped with the high angle annular dark field (HAADF) detector and the energy dispersive x-ray (EDX) detector for elemental analysis.

Results

Unirradiated specimen

The analytical detection limit of the EDX method for copper is close to 0.5 wt.%. As a consequence, copper cannot be detected if it is homogeneously distributed in solid solution, but only if it segregates to precipitates. As far as numerous lattice defects as well as precipitates and inclusions of different kind hardly allow an imaging of Cu-rich precipitates in the bright field mode, the elemental EDX mapping of areas varying between 150×150 nm2 and 2×2 µm2 allows their unequivocal detection e.g. on grain or lath boundaries. It should be noted that at relatively high concentrations used in this work copper precipitates after heat treatment even without irradiation, while at lower concentrations cascade forming irradiation would be necessary for the precipitation.

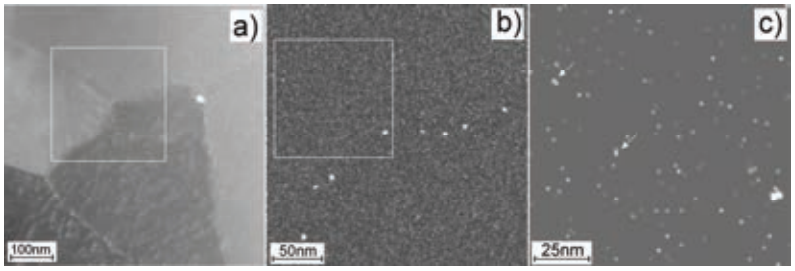

Fig. 1: TEM characterisation of unirradiated specimen. a) HAADF image of the investigated area, b) the Cu map of the area marked with a square, c) the enlarged image of the area marked in (b) with enhanced contrast.

Fig. 1a shows a HAADF image of an investigated area which contains a grain boundary. Copper clusters of 3-5 nm in diameter are clearly visible along the grain boundary. A further magnification of Fig. 1b shows a high number density of copper precipitates in the bulk with typical diameters of ~1 nm (Fig. 1c). This size is close to the resolution limit of TEM used in these investigations. The well detectable clusters of about 1.5nm size are marked with arrows.

Specimen irradiated at 300 °C

Fig. 2b shows the Cu map of an area marked in the HAADF image (Fig. 2a) with a typical grain boundary. It is clearly visible that Cu precipitates decorate the grain boundaries and are present inside grains as well. The size of the observed clusters varied from 1.5 to 7 nm. Even larger clusters with sizes up to 12 nm were found occasionally on grain or lath boundaries. In this study we were unable to confirm the decoration of dislocation loops or dislocation lines by Cu clusters.

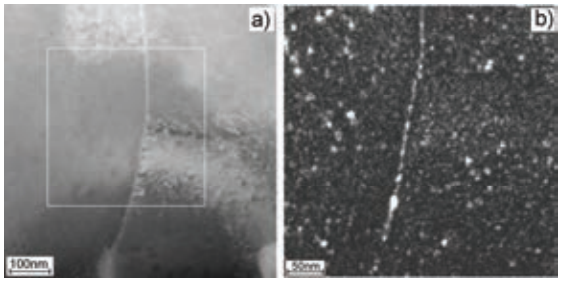

Fig. 2: TEM investigation of the specimen after neutron irradiation at 300 °C (16.3dpa). HAADF image of the investigated area is shown in the part (a) and Cu map of the area marked with the square in the part (b).

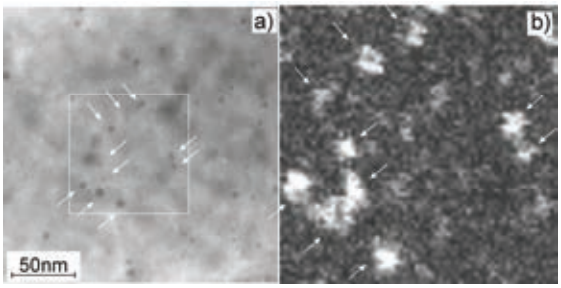

Fig. 3: TEM investigation of the specimen after neutron irradiation at 300 °C (16.3dpa). HAADF image of the investigated area is shown in the part (a) and Cu map of the area marked with the square is shown in the part (b).

Our studies have shown that the Cu clusters inside grains are always located on helium bubbles. Fig. 3 presents the HAADF image of a 100×100 nm^2 area with several He bubbles (marked by arrows), visible as the darker spots. The spatial distribution of Cu clusters, which are also marked by arrows, shows the same pattern as helium bubble distribution.

Specimen irradiated at 400 °C

The TEM investigations of the specimen irradiated at 450 °C demonstrate the influence of the irradiation temperature on the clustering process. The clusters are large so that they can be imaged even using large area scans. Fig. 4 shows the results of EDX mapping of a 3×3 μm^2 large area. The presence of Cu-clusters on grain and lath boundaries as well as inside grains is clearly visible. The presence of $M_{23}C_6$ carbides on the grain boundaries does not influence the distribution and size of Cu clusters. The comparison of the Cu and Cr maps does not show any indication for favorable precipitation on carbides.

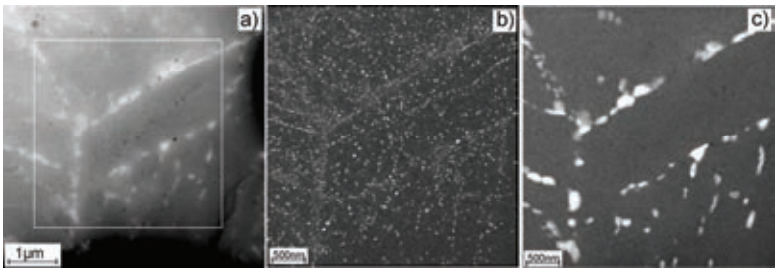

Fig. 4: TEM investigation of the specimen after neutron irradiation at 400 °C (16.3dpa). The HAADF image of the investigated area is shown in the part (a), Cu and Cr maps of the area marked with the square are shown in the pars (b) and (c).

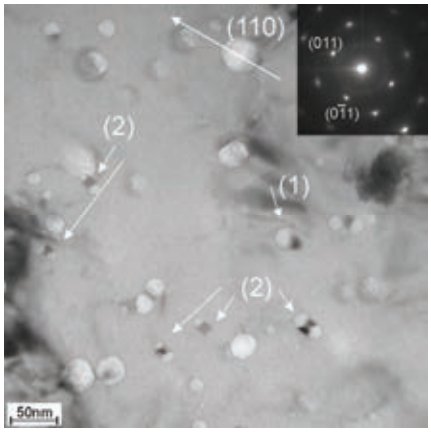

Fig. 5: Bright field TEM image shows the different type of Cu clusters which are marked with arrows.

The results of the elemental mapping of a 500×400 nm^2 area are presented in the Fig. 5. The Cu clusters are mainly located on the grain boundary. Several clusters inside grains are always located closely to the He bubbles. At the same time the He bubbles exist without closely located Cu cluster. This is clearly visible in the Fig. 5 by comparing of Cu and HAADF image, where the He bubbles are visible as the darker round spots. In the bottom part of the scanned area numerous clearly visible bubbles are without Cu cluster. The size of the Cu-clusters varied from 5 nm to 25 nm.

The analysis of TEM images shows the formation of two types of the Cu clusters. The clusters of the first type are the small ones located on the surface of He bubbles. One cluster of this type marked for example by the arrow number (1). The Cu clusters of the second type form together with He bubbles a “dumbbell”, where two helium bubbles are formed at opposite sides of a Cu cluster. Clusters of such type are marked by the arrow number (2) in the same figures. As it is seen from the image, the dumbbells are usually oriented along the [110] direction. The indexed diffraction pattern from this area is presented in cutout (Fig. 5).

Discussion

Copper precipitation was found to be a major reason for radiation induced embrittlement of reactor pressure vessel steels and, especially, of their welds. This finding has raised the interest for experimental investigations of this effect. Experimental studies have shown that copper precipitation takes place under neutron, but not under electron irradiation. This result stressed the importance of atomic displacement cascades for the nucleation and growth of copper-rich precipitates. Hardening increase observed after electron irradiation was attributed to the formation of copper-vacancy pairs, induced by isolated vacancies.

Theoretical studies have considered various mechanisms that explain the Cu cluster formation. Copper atoms being slightly oversized with respect to the matrix form substitutional solid solution in iron and ferritic steels. Substitutional impurities diffuse usually by vacancy mechanism. However, the particular details of diffusion mechanism depend on whether impurity is bound to vacancy. The muon spin rotation experiments performed by one of us have

revealed that copper atom dissolved in bcc iron matrix is slightly bound to vacancy with a binding energy of about 0.14 eV. It is interesting to note that ab initio calculation performed some decades later provided a very close value of 0.17 eV. Positron annihilation studies of irradiated copper doped iron have also confirmed that copper enriched zones formed under irradiation contain large number of vacancies. After understanding of the key role of copper precipitation for the embrittlement of reactor pressure vessel steels under irradiation a large number of computer simulations of this process were performed. The majority of the studies is dealing either with kinetic Monte Carlo simulation of copper precipitation process or with determination of diffusion coefficients of small copper-vacancy clusters.

The role of small gas-vacancy clusters was also understood in the studies related to formation and growth of helium bubbles under irradiation. It was known that helium induces formation of gas-filled voids due to their stabilization (increase of binding energy) by addition of helium atoms. The binding energy of a vacancy with helium (~0.5 eV) is higher than with copper and therefore helium-vacancy clusters are more stable. It seems that the formation of mobile small impurity-vacancy clusters plays an essential role not only for the nucleation stage but also for the precipitate or gas bubble growth as far as it is limited by impurity mass transport. Moreover mobility and stability of impurity-vacancy clusters can be important for the duration of the nucleation stage. It was known that copper does not decorate void surfaces. Our studies confirmed that copper atoms do not decorate the surface of gas bubbles as well, but often form precipitates attached to them.

Conclusions

Within the scope of this study, the EUROFER 97 alloyed with B and Cu was analyzed by TEM before and after neutron irradiation up to 16.3 dpa at 300 °C and 400 °C. The investigation of the unirradiated material shows that copper forms a higher density of very small clusters that are with a diameter of about 1 nm at the TEM resolution limit, and larger clusters at grain or lath boundaries with typical diameters of 2.3 nm. It is likely that a certain fraction of Cu is in solid solution before irradiation and therefore not visible in the TEM. The irradiation at 300 °C and 400 °C leads to the formation of more pronounced well detectable Cu clusters, which usually are located on the grain or lath boundaries and at the surface of He bubbles. The size of the clusters varied from 3 to 10 nm in the specimen after irradiation at 300 °C and increases to the 10-25 nm range after irradiation at 400 °C. The formation of He-Cu-He “dumbbells” is typical and can be explained by the trapping and accumulation of helium atoms. The production of helium from the neutron induced decay of 10B is completed already after about 7% of the irradiation time, while the irradiation induced production of Cu precipitates and its coarsening continues throughout the entire neutron irradiation.

Staff:

M. Klimenkov
E. Materna-Morris
A. Möslang
R. Rolli
H.-C. Schneider
P. Vladimirov

Literature:

[1] M. Klimenkov, P. Vladimirov, A. Möslang. E. Materna-Morris, H.-C. Schneider „ TEM study of irradiation induced copper precipitation in boron alloyed EUROFER97 steel” International Journal of Materials Research 102 (2011) 1089-1093

[2] M. Klimenkov, E. Materna-Morris, A. Möslang, H.C. Schneider Microstructural characterisation of boron alloyed EUROFER 97 after neutron irradiation. 15th Internat.Conf.on Fusion Reactor Materials, Charleston, S.C., October 16-22, 2011

[3] M. Klimenkov, E. Materna-Morris, P. Vladimiriov, A. Möslang, H.C. Schneider TEM study of irradiation induced copper precipitation in the presence of helium.15th Internat.Conf.on Fusion Reactor Materials, Charleston, S.C., October 16-22, 2011

Acknowledgement

This work, supported by the European Communities under the contract of Association between EURATOM and Karlsruhe Institute of Technology, was carried out within the framework of the European Fusion Development Agreement. The views and opinions expressed herein do not necessarily reflect those of the European Commission.

Quantitative Microstructural Investigations of Irradiated Specimens from WTZ and ARBOR 1 (WP11-MAT-REMEV-05-03)

Objectives

The current task aims at continuation of analyzing the neutron irradiation induced evolution of the microstructure in the RAFM steel EUROFER 97 and its boron doped variant addressing (a) irradiation dose dependence of *sizes* and *volume densities* of radiation defects (e.g. defect clusters, dislocation loops, voids, helium bubbles, precipitates); (b) neutron flux dependence of *sizes* and *volume densities* of radiation defects. A long term goal is the correlation of the neutron irradiation induced changes in the microstructure to the changes in the mechanical properties, as well as the development of a phenomenological model describing the evolution of radiation defects in RAFM steels. The specimens to be studied in this task stem from SPICE (15 dpa/300 °C, HFR, NRG, Petten), WTZ (15 dpa/330 °C, Bor-60, JSC "SSC RIAR", Dimitrovgrad), ARBOR 1 (32 dpa/ 330 °C, Bor-60, JSC "SSC RIAR", Dimitrovgrad) and ARBOR 2 (70 dpa/ 330 °C, Bor-60, JSC "SSC RIAR", Dimitrovgrad) irradiation programmes. The neutron fluxes (>0.1 MeV) for Bor-60 and HFR irradiations were 1.8×10^{19} $m^{-2}s^{-1}$ and 4.0×10^{18} $m^{-2}s^{-1}$, respectively.

Task Current Status

The microstructure of EUROFER 97 and boron doped specimens irradiated in the WTZ and ARBOR 1 irradiation programmes was analyzed quantitatively with the high resolution FEI Tecnai G² F20 X-TWIN TEM installed in the hot cells of the FML. Fracture appearance of selected specimens has been studied by SEM. TEM specimens were prepared from the undeformed parts of KLST specimens.

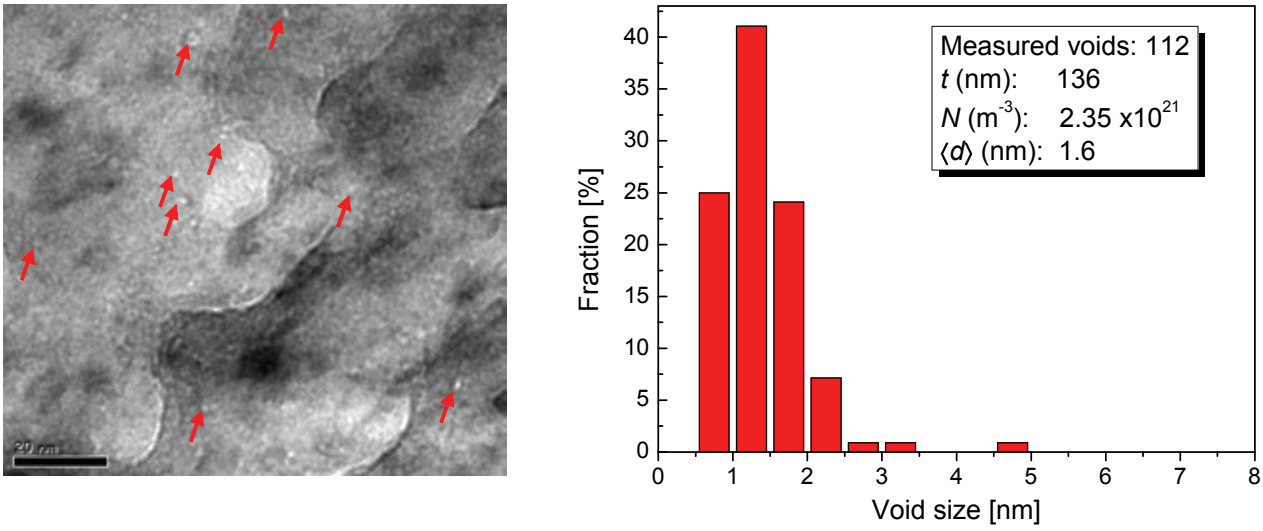

Fig. 1: a) Underfocused Bright-field (BF) image of EUROFER 97 irradiated to 32 dpa showing irradiation induced voids.
b) Density and size distribution of voids for the corresponding specimen.

After investigation of dose dependence of size distributions of defect clusters and dislocation loops the emphasis was put on the quantitative analysis of voids and helium bubbles. Determination of average size and densities of voids in 15 dpa irradiated EUROFER 97 yielded 2.6 nm and 3.6 x 10^{20} m^{-3}, respectively. By analyzing EUROFER 97 specimens irradiated to 32 dpa in the BF image mode small cavities became visible when going off-focus. A systematical through-focus series analysis showed that the contrast of these defects changes from a white dot with a black ring to a black dot with a white ring (Fresnel contrast) when going from underfocus to overfocus, which confirms the presence of voids or bubbles. Fig. 1a shows an underfocused BF micrograph with several voids. As depicted in Fig. 1b size distri-

bution and density of voids in the 32 dpa specimens were determined. The sample thickness *t* has been determined by applying CBED technique. The density of voids was 2.35 x 10^{21} m^{-3}, about one order of magnitude higher than observed in the 15 dpa sample, whereas the average size was 1.6 nm. The results of the quantitative investigations are summarized in Table .

Table 1: Quantitative microstructural data from TEM investigations of neutron-irradiated EUROFER 97 irradiated up to 32 dpa at 330-332 °C.

Irrad. programme	Dose (dpa)	$\langle d \rangle_{loops}$ (nm)	$N_{loops,max}$ (m^{-3})	$\Delta\sigma_{loops}$ (MPa)	$\langle d \rangle_{voids}$ (nm)	$\langle N \rangle_{voids}$ (m^{-3})	$\Delta\sigma_{voids}$ (MPa)
WTZ	15.0	3.4	1.58 x 10^{22}	252	2.6	3.6 x 10^{20}	56
ARBOR 1	31.8	4.8	2.22 x 10^{22}	355	1.6	2.3 x 10^{21}	110

To correlate the irradiation induced changes in the microstructure to the changes in the mechanical properties we applied the dispersed barrier hardening model (DBH), which uses simple geometrical considerations to calculate the hardening $\Delta\sigma_x$ caused by the interaction of moving dislocations with randomly distributed obstacles of type x.

$$\Delta\sigma_x = M_T \alpha_x \mu b \sqrt{\sum_{i=1}^{i_{max}} N_i d_i} \qquad (1)$$

Here M_T is a Taylor factor (3.06 for bcc metals), α_x is the obstacle strength of the defects *x*, μ is the shear modulus, *b* is the magnitude of the Burgers vector ($0.5a_0\sqrt{3}$ for bcc, where a_0 is the lattice parameter) and N_i and d_i are distributions of density and diameter of the defects. The material parameters μ and a_0 were taken for Fe-10Cr model alloy at a temperature of 300 °C, they are 75.3 GPa and 0.288 nm, respectively. According to recent Molecular Dynamics simulations results available in the literature the interaction strength for loops/clusters at a given temperature was chosen to be about 0.6. Voids were assumed to be rigid obstacles, so their barrier strength is 1. Since a fraction of defects/dislocation loops is always invisible in the micrographs it is reasonable to pick the maximum observed defect density N_{max} as input parameter for calculating the hardening. In contrast to the density the sizes of the defects do not depend on their orientation with respect to the electron beam, so using $\langle d \rangle$ is appropriate. These parameters together with resulting hardening values are summarized in Table 1. The dose-dependent hardening $\Delta R_{p0.2}$ (0.2% offset yield stress) of EUROFER 97 determined by tensile tests is given in Fig. 2. The line represents a phenomenological description of a hardening within the framework of Whapham and Makin model by assuming a single defect type only which predicts saturation of hardening at high damage doses. The hardening by loops/clusters calculated with Eq. (1) using the obtained quantitative data in Table 1 is displayed as filled diamonds. The crosses were calculated using $\langle d \rangle$ and $\langle N \rangle$, whereas the error bars represent the experimental scattering of $\Delta\sigma_{loops}$ when actual size distribution of defects/dislocation loops is used as input parameter. The yield strength increase due to loops alone is considerable lower than measured $\Delta R_{p0.2}$. In order to account the contribution of other microstructural defects e.g. voids an adequate hardening superposition law has to be used. A quadratic superposition law seems to be appropriate one in order to take into account contribution of voids and dislocation loops, as the corresponding obstacle strength are comparable, i.e.

$$\Delta\sigma_{tot} = \sqrt{\Delta\sigma_{loops}^2 + \Delta\sigma_{voids}^2} \qquad (2)$$

Since the density of voids in EUROFER 97 is one (32 dpa) respectively two (15 dpa) orders of magnitude lower than that of the loops, the calculated total hardening increases only very slightly from 252 to 258 MPa at 15 dpa and from 355 to 372 MPa at 32 dpa when the hardening contributions of voids are included in addition to loops/clusters using Eq. (2). So in our case the contribution of voids can be neglected. There are several possible reasons for the difference (factor ≤ 1.8) between estimated and tensile hardening. Firstly, a considerable number of loops or clusters are invisible due to their orientation with respect to the electron beam. Secondly, certain types of defects, like vacancy clusters or nano-sized precipitates cannot be detected by TEM. Thus studies with different complementary methods like TEM, PAS and SANS are needed to get full quantitative information on radiation damage.

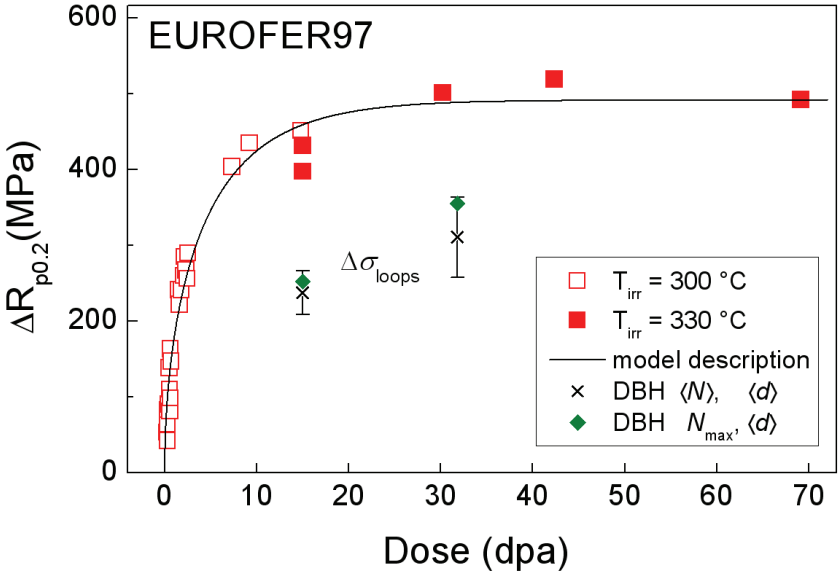

Fig. 2: Estimation of hardening by dislocation loops using the DBH model. Both the maximum defect density (N_{max}, filled diamonds) and the average one (<N>, crosses) were used as input parameters. In comparison the dose-dependent hardening $\Delta R_{p0.2}$ of EUROFER 97 determined by tensile tests is shown (squares). These data points comprise results from KIT and from literature. The solid line is a description of hardening according to Whapham and Makin model.

After irradiation of EUROFER 97 based model steel ADS3 doped with 0.0083 wt.% ^{10}B within ARBOR 1 programme to 22.4 dpa at 332 °C about 43 appm He was produced due to boron-to-helium transmutation. The fracture surface of KLST specimens revealed a transgranular cleavage with no sign of intergranular fracture. Similar to the EUROFER 97 base material radiation-induced defects like dislocation loops were visible in ADS3 under TEM. In addition, by recording BF through-focal series He bubbles became visible in ADS3, see Fig. 3. Their contrast changed from white dots surrounded by a black Fresnel fringes in the underfocused image in Fig. 3 (b) to dark dots with white fringes in the overfocused image in Fig. 3 (c). The presence of helium inside the cavities was proved by means of EELS analysis yielding a helium-to-vacancy ratio of approximately 0.33. The bubbles were of spherical shape and rather homogeneously distributed within the steel matrix with no sign of preferential nucleation at line dislocation or grain boundaries. An average bubble size was 1.4 nm and an average bubble density was 2.3×10^{22} m^{-3}.

A phenomenological model describing helium bubble growth kinetics under neutron irradiation has been developed within the HRJRG-13 project. The model is based on kinetic rate equations and is solved by a Fortran code. Simulations were performed for the EUROFER 97 based boron doped alloys ADS2 and ADS3, which differ in the alloyed ^{10}B amount and therefore produce different helium concentrations under irradiation. Characteristic irradiation conditions of SPICE and ABROR 1 experiments were taken into account by adapting the parameters like temperature, diffusivity and varying helium generation rates due to different boron transmutation cross sections in the considered irradiation programs.

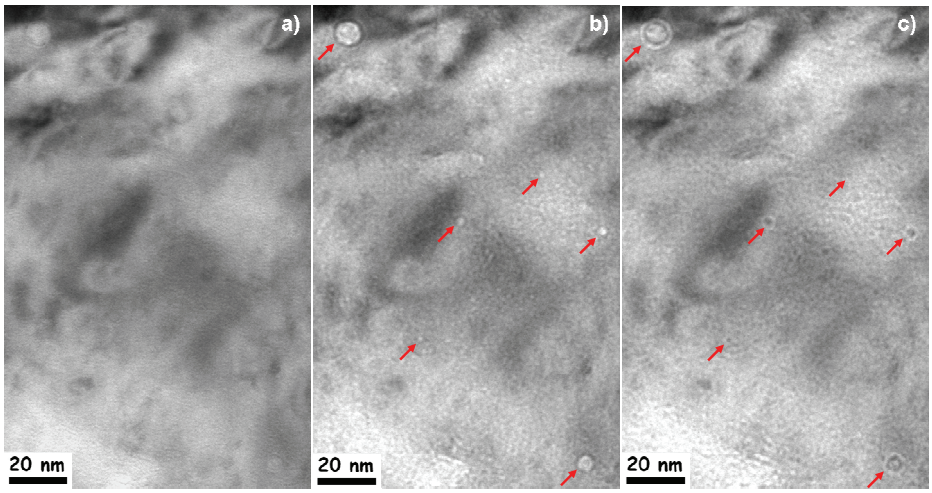

Fig. 3: TEM micrographs showing He bubbles in irradiated ADS3 from ARBOR 1 (a) in-focus (b) underfocus (-750 nm) (c) overfocus (+750 nm).

Calculated final bubble size distributions for ADS2 and ADS3 after SPICE and ARBOR 1 irradiations are used to assess helium induced hardening by applying the DBH model according to Eq. (1). The barrier strength of helium bubbles is assumed to be weak to intermediate, resulting in a variation of α_{He} between 0.2 and 0.4. Fig. 4 shows a comparison of hardening derived from simulations and experiments. A linear superposition of hardening contributions from helium and other radiation induced defects was used for estimation of helium hardening from tensile and instrumented Charpy impact experiments. Under these conditions simulation results agree well with experiment. It has to be noted that by applying a quadratic superposition law according to Eq. (2) to hardening contributions from helium and other radiation induced defects, the hardening derived from simulated bubble size distributions underestimates the influence of helium bubbles.

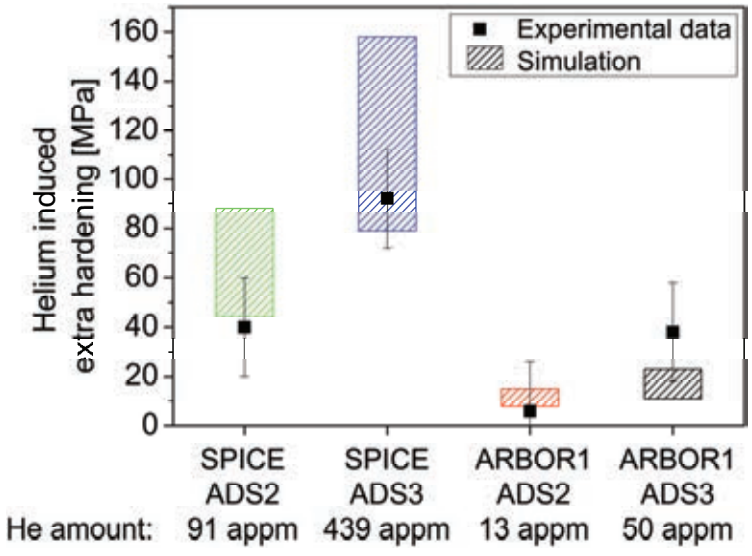

Fig. 4: Comparison of helium induced hardening on the basis of simulations with experimentally determined results. DBH model was applied on simulated bubble size distributions assuming helium bubbles as weak/intermediate obstacles. A good agreement of simulations with experiments is observed assuming a linear superposition of hardening contributions from helium and other radiation defects.

Conclusion and Outlook

The volume densities and size distributions of the dislocation loops and voids were quantified for EUROFER 97 samples after irradiation to 15 and 31.8 dpa at 330-332 °C. Based on the

obtained quantitative data the irradiation-induced hardening was estimated with the DBH model. The calculated hardening was significantly smaller than determined in the post-irradiation tensile tests, which shows that additional complementary methods like PAS and SANS are needed to get full quantitative information on radiation damage. Quantitative TEM investigations of neutron irradiated boron doped steel revealed a homogeneous distribution of helium bubbles with no sign of preferential nucleation at microstructural sinks.

Further TEM investigations of irradiated EUROFER 97 will be conducted at high damage doses with respect to quantification of sizes and volume densities of radiation induced defects (e.g. defect clusters, dislocation loops, voids/bubbles precipitates). The activities will particularly include analysis of Cr-rich alpha-prime precipitation in EUROFER 97 (WTZ, ARBOR 1 & 2) as well as investigation of helium bubble distribution in high dose irradiated boron containing steels (ARBOR 2). The results of quantitative microstructure analysis will be used for verification of models for evolution of the radiation defects in RAFM steels.

Staff:

C. Dethloff
E. Gaganidze
O. Weiß

Literature:

[1] E. Gaganidze et al., Mechanical properties and TEM examination of RAFM steels irradiated up *to 70 dpa in BOR-60*, J. Nucl. Mater. 417 (2011) 93-98.

[2] E. Gaganidze, C. Dethloff, O. J. Weiß, V. Svetukhin, M. Tikhonchev, J. Aktaa, Modeling and TEM Investigation of Helium Bubble Growth in RAFM Steels under Neutron Irradiation, presentation at the 25th ASTM Symposium on Effects of Radiation on Nuclear Materials, June 15th to 17th, 2011, Anaheim, USA.

[3] O. J. Weiß, E. Gaganidze, J. Aktaa, Quantitative Microstructural Characterisation of High-dose Irradiated EUROFER97, presentation at the 15th International Conference on Fusion Reactor Materials, 16th-20th October, 2011, Charleston, USA.

[4] C. Dethloff, E. Gaganidze, V. Svetukhin, J. Aktaa, Modeling of Helium Bubble Growth in 10B-doped RAFM Steels under Neutron Irradiation, presentation at the 15th International Conference on Fusion Reactor Materials, 16th-20th October, 2011, Charleston, USA.

Acknowledgement

This work, supported by the European Communities under the contract of Association between EURATOM and Karlsruhe Institute of Technology, was carried out within the framework of the European Fusion Development Agreement. The views and opinions expressed herein do not necessarily reflect those of the European Commission.

Operation of the Fusion Materials Laboratory (Underlying Technology) (CoA)

The Fusion Materials Laboratory provides the infrastructure for the performance of tasks defined in the EFDA and F4E work programmes related to the characterisation and testing of irradiated and non-irradiated materials. Methods such as optical and electron microscopy, tritium adsorption and desorption, He pycnometry and Hg porosimetry, crush load, micro hardness, creep, charpy impact, tensile, LCF and instrumented indentation tests as well as long-time annealing tests are applied. The work includes Post Irradiation Examinations (PIE) of Reduced Activation Ferritic Martensitic (RAFM) steels (reference material for DEMO and ITER-TBMs) and tungsten as well as investigations on materials relevant for the HCPB blanket (ceramic breeder materials, beryllium) and technical aspects (glasses).

PIE on selected samples from the HFR IIB and BOR 60 experiments were performed. For this purpose, in 2011 mostly LCF tests were carried out. Tested specimens' small cuts were prepared for LOM, SEM, and TEM and examined. Broken halves of charpy specimens were prepared for instrumented indentation and served for identifying material parameters and Vickers hardness. The aim of the investigations is to study the irradiation effects on the mechanical and structural properties of these materials and to investigate the possibilities of a post-irradiation heat-treatment in order to reduce irradiation defects.

The investigation of blanket materials was continued. Lithium orthosilicate pebbles were investigated by LOM and their porosity and deformation hardness were determined. Different batches of materials were characterised with respect to the influence of parameters of the fabrication process on the mechanical and structural properties. Tritium adsorption / desorption tests and creep tests were done on irradiated and unirradiated beryllium, beryllium vanadium, and beryllium titanium alloys and on BeO-doped beryllium, both on single pebbles and on pebble beds.

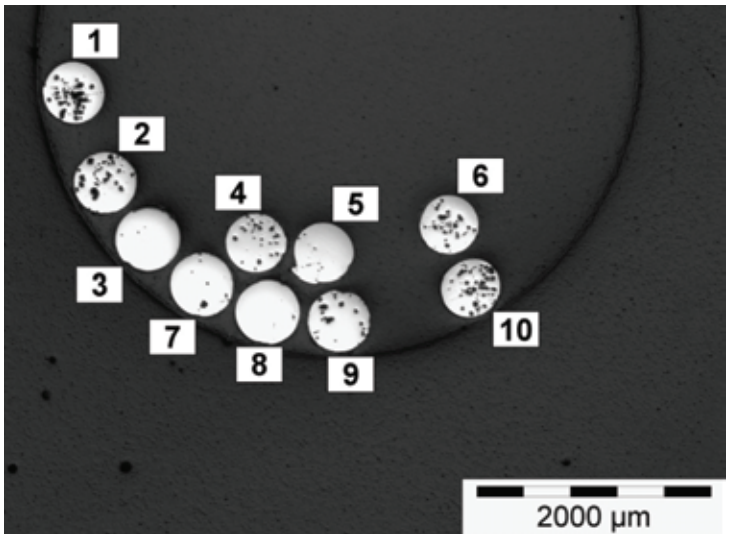

Fig. 1: New preparation technique of irradiated beryllium to produce cross-cuts by embedding and grinding of pebbles of 0.5 mm diameter.

Adsorption and desorption experiments were also done with unirradiated beryllium titanium pebbles. Furthermore different beryllium titanium alloys were characterized by LOM and SEM. Porosity measurements and creep tests were performed. Activated beryllium from the HIDOBE irradiation was investigated by LOM and SEM, by densiometry, and specimens were prepared for SANS experiments. To produce cross-cuts for LOM and SEM, a multi-step embedding and grinding process of very small and highly radiating beryllium was developed. For TEM investigations, another new preparation method for the extremely brittle irradiated beryllium was developed, producing thin fragments by crush-test and fixing them on meshes. Further on, release experiments on tritium-loaded glass windows were performed.

Detailed results and consecutive analysis of the measurements are reported in the respective chapters of this report.

For the PIE the following equipment was used:

- Charpy impact, LCF and tensile testing devices, indentation device for instrumented ball-indentation and Vickers hardness-test

- LOM, SEM, and TEM with analysis of chemical elements
- Desorption device with high temperature furnace for tritium and helium release measurements
- He-pycnometer and sphere crush and creep testing apparatus.

Operation of the new 200 kV high resolution TEM for investigation of radioactive material down to atomic scale was continued. Various results, identifying the damage mechanisms in highly irradiated steel, could be published. A new glove-box for safe electrochemical preparation and plasma-cleaning of TEM specimens was taken in operation. The SEM was equipped with a new, shielded EDX system to identify elements down to beryllium in highly radioactive specimens. The new mass spectrometer, able to identify the tritium release and retention of fusion-relevant materials, was installed in its new glove box and started operation with tritium gases.

The installation of the gamma spectrometer and it's shielding and safe transfer units could be finished, a calibration system could be procured in the reporting period.

Fig. 2: New mass spectrometer in glove box (left above) and tritium release unit and pipe installation (right).

Fig. 3: Gamma spectrometer with shielding device for specimen and detector (left), transport unit for transfer from Hot Cell (right).

For high temperature indentation, the manufacturing of both machines was finished in the reporting period. Both machines are designed for remote-handled use in the Hot Cell with highly active specimens; they furnish loads and maximum temperatures of 2 N and 1000 °C resp. 200 N and 600 °C. Assembly und first test runs of both machines at manufacturers are done; both machines were delivered end of 2011, optimization of parameters is going on.

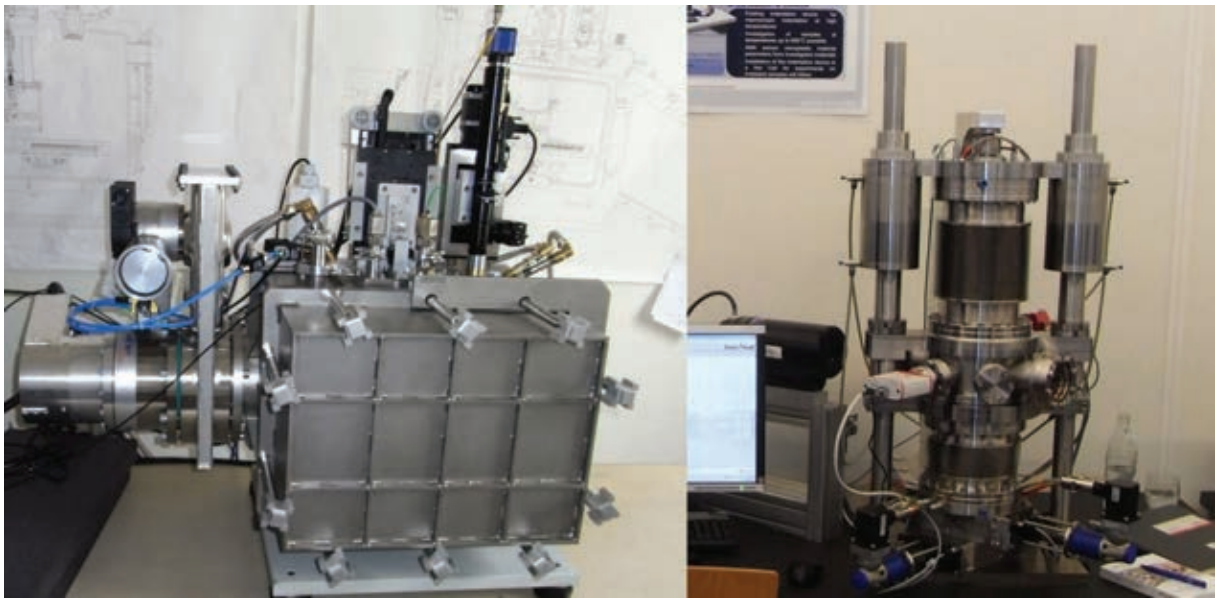

Fig. 4: Indentation devices for indentation up to 3 N / 1000 °C (left) and up to 200 N / 650 °C (right).

Future activities:

Continuation of measurements as referred to above:

- PIE of the HFR II B irradiation phase, 15 dpa
- PIE of the BOR 60 irradiation campaign, 15 – 30 dpa
- PIE of the OSIRIS FURIOSO high temperature irradiation, WL10-tungsten, 5 dpa
- PIE of the HIDOBE irradiations
- Calibration and regular operation of the new mass spectrometer
- Installation of new devices for instrumented indentation at elevated temperatures
- Characterization of new batches of ceramic breeder materials and beryllium
- Operation of the gamma-ray spectrometer to study the activation of RAFM steels.

Staff:

B. Albinski
P. Barié
J. Ehrmann
A. Erbe
M. Gilpert
M. Holzer
W. Ibbe
S. Lautensack
G. Mangei
U. Meyer
H. Ries
M. Rietschel
R. Rolli
I. Sacksteder
M. Scherwitz
R. Schmidt
H.-C. Schneider
H. Steinle
M. Weber

Literature:

[1] Chakin, V., Rolli, R., Schneider, H.-C., Moeslang, A., Kurinsky, P., Van Renterghem, W.: Pores and cracks in highly neutron irradiated beryllium. Journal of Nuclear Materials, 416(2011) 3-8

[2] Chakin, V., Klimenkov, M., Rolli, R., Kurinskiy, P., Moeslang, A., Dorn, C.: Microstructural and tritium release examination of titanium beryllides. Journal of Nuclear Materials, 417(2011) 769-774

[3] Chakin, V., Möslang, A., Kurinskiy, P., Rolli, R., Schneider, H.-C., Alves, E., Alves, L.C.: Tritium permeation, retention and release properties of beryllium pebbles. Fusion Engineering and Design, 86(2011) 2338-2342

[4] Gaganidze, E., Petersen, C., Materna-Morris, E., Dethloff, C., Weiß, O.J., Aktaa, J., Povstyanko, A., Fedoseev, A., Makarov, O., Prokhorov, V.: Mechanical properties and TEM examination of RAFM steels irradiated up to 70 dpa in BOR-60. Journal of Nuclear Materials, 417(2011) 93-98

[5] Gan, Y., Kamlah, M., Riesch-Oppermann, H., Rolli, R., Liu, P.: Crush probability analysis of ceramic breeder pebble beds under mechanical stresses. Journal of Nuclear Materials, 417(2011) 706-709

[6] Klimenkov, M., Vladimirov, P., Möslang, A., Materna-Morris, E., Schneider, H.-C.: TEM study of irradiation induced copper precipitation in boron alloyed EUROFER97 steel. International Journal of Materials Research, 102(2011) 1089-1093

[7] Klimenkov, M., Materna-Morris, E., Möslang, A.: Characterization of radiation induced defects in EUROFER 97 after neutron irradiation. Journal of Nuclear Materials, 417(2011) 124-126

[8] Kurinskiy, P., Chakin, V., Moeslang, A., Rolli, R., Alves, E., Alves, L.C., Franco, N., Dorn, Ch., Goraieb, A.A.: Comparative study of fusion relevant properties of Be12V and Be12Ti. Fusion Engineering and Design, 86(2011) 2454-2457

[9] Materna-Morris, E., Möslang, A., Rolli, R., Schneider, H.-C.: Effect of 16.3 dpa neutron irradiation on fatigue lifetime of the RAFM steel EUROFER97. Fusion Engineering and Design, 86(2011) 2607-2610

[10] Sacksteder, I., Schneider, H.-C., Materna-Morris, E.: Determining irradiation damage and recovery by instrumented indentation in RAFM steel. Journal of Nuclear Materials, 417(2011) 127-130

[11] Weiß, O.J., Gaganidze, E., Aktaa, J.: Quantitative TEM investigations on EUROFER 97 up to 32 dpa. Vincenzini, P. [Ed.] Selected Papers from the 5th Forum on New Materials, Part of CIMTEC 2010 - 12th Internat.Conf.on Modern Materials and Technologies, Montecatini Terme, Trans Tech Publ., (2011) 118-123

Production and Characterization of Laboratory-scale Batches of Nano-structured ODSFS (WP11-MAT-ODSFS-01-01)

Introduction

Up to date fusion power plant concepts are based on materials which can be operated at higher temperatures and up to higher neutron doses. Oxide dispersion strengthened (ODS) steels – produced by mechanical alloying – with chromium contents of 9 and 14 wt.% (or even more) are typical candidate materials due to their excellent high temperature strength and good corrosion resistance.

The production route for these ODS materials is complex and contains several preparation steps, such as mechanical alloying and hot isostatic pressing. Microstructural characterization of mechanically alloyed powder allows direct investigations of the influences of milling parameters on the microstructure and herewith on the mechanical properties of the prepared material. Another important factor is the distribution of Y_2O_3 phase inside or on the mechanically alloyed powder particles. In the past year the influence of the milling time on the evolution of the Y_2O_3 phase was examined. Complete dissolution of this phase during mechanical alloying is essential for a homogeneous distribution of oxide nanoparticles and grain size distribution in the compacted material. Undissolved Y_2O_3 leads to coarser, micrometer sized particles and very poor mechanical properties after compacting and thermo-mechanical treatment.

Powder characterization was followed by mechanical tests and microstrucutural characterization of as-hipped and as-rolled materials. These materials contained different oxide additions.

Materials, Study and Results

To validate the ODS production process, a small experimental series with the same powders but different milling times was done. Argon gas atomized steel powder was produced from a steel alloy with a composition of Fe13Cr1W0.3Ti. The exact composition of the material can be found in Table 1. The powder was mixed with Y_2O_3 with a fine particle size (d90<10 µm) and ball milled in a ZOZ SimoloyerCM01 with steel balls. The ratio of powder/steel balls was

Table 1: Materials, fabrication details and experiments performed/planned.

Material	Milling-time	Process	Experiments performed / planned
Fe13Cr1W0.3Ti + Y2O3	24h	MA	Powder characterization
Fe13Cr1W0.3Ti + Y2O3	48h	MA	Powder characterization
Fe13Cr1W0.3Ti + Y2O3	80h	MA	Powder characterization
Fe13Cr1W0.3Ti + Y2O3	80h	MA+HIP	Charpy, TEM characterization, EBSD
Fe13Cr1W0.3Ti + Y2O3	80h	MA+HIP+HR	Charpy, TEM characterization,
Fe13Cr1W0.3Ti + La2O3	80h	MA+HIP+HR	Charpy, TEM characterization,
Fe13Cr1W0.3Ti + Ce2O3	80h	MA+HIP+HR	Charpy, TEM characterization,
Fe13Cr1W0.3Ti + Zr2O	80h	MA+HIP+HR	Charpy, TEM characterization,
Fe13Cr1W0.3Ti + MgO	80h	MA+HIP+HR	Charpy, TEM characterization,

1:10, with a batch consisting of 200 g powder and 2000 g of steel balls. Milling was done at 1200 rpm. For all the different milling times, one batch was mechanically alloyed (MA). The powder was examined after 24, 48 and 80 hours milling time. Due to the massive amount of metallic surfaces, the mechanically alloyed (MA) powder is highly reactive with oxygen in the air. For this reason, the milling itself and all further treatment during the production process

took place under the excess of oxygen in argon atmosphere. The powder samples for further investigation were prepared and embedded into capsules with epoxy in an argon filled glove-box.

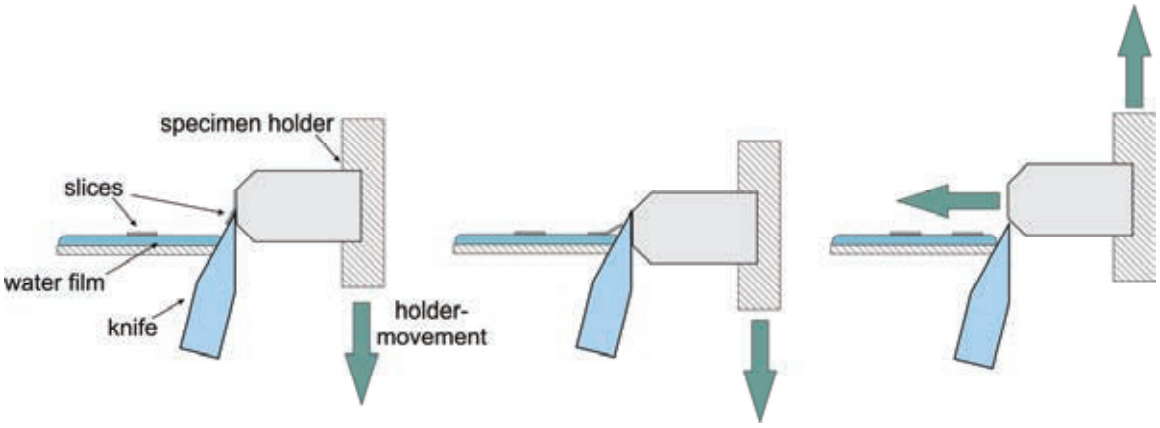

Fig. 1: TEM sample preparation via Microtom.

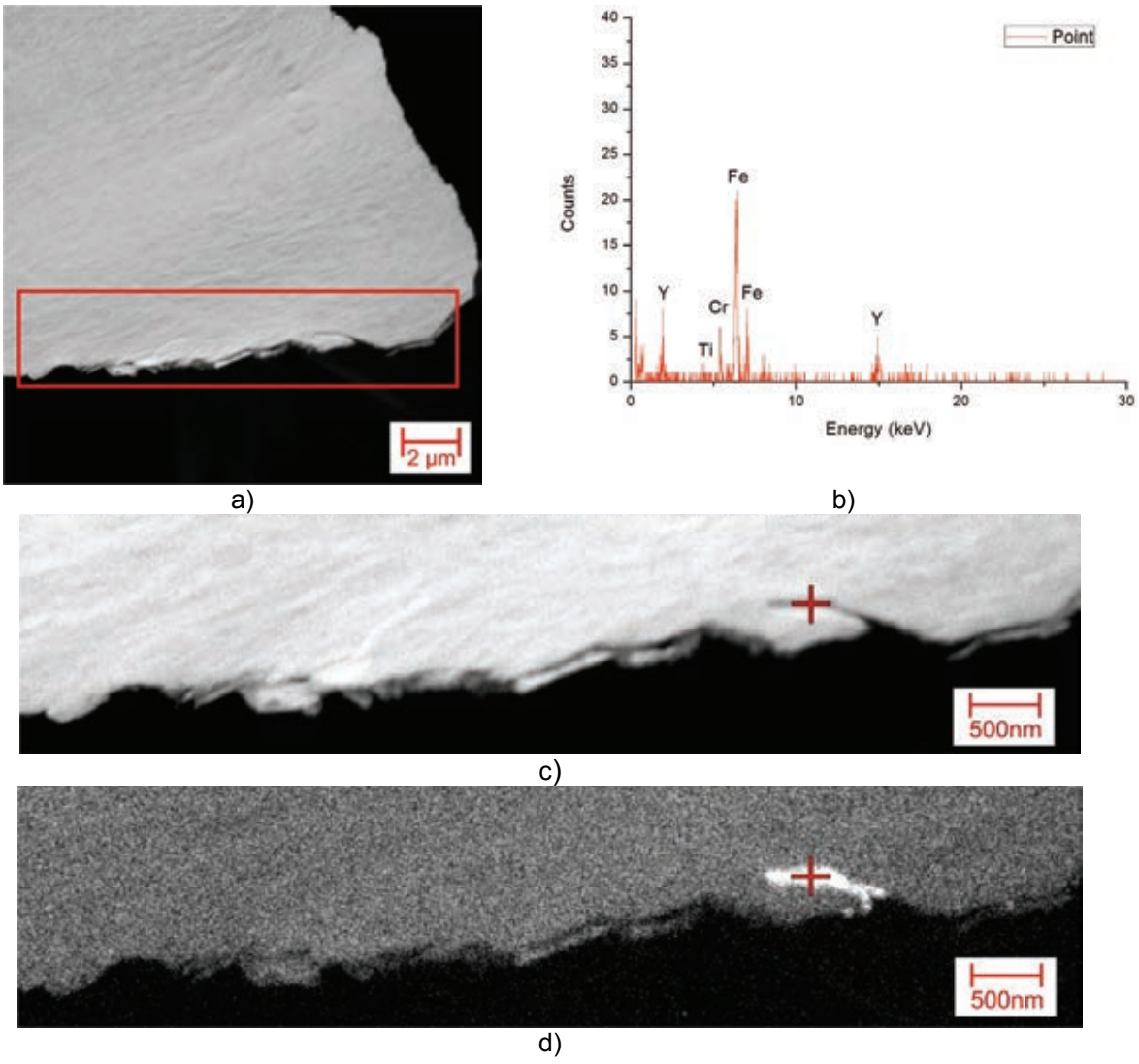

Fig. 2: a) HAADF image of powder particle. (b) EDX point analysis. (c) elemental mapping of iron (d) elemental mapping of yttrium.

Then, the capsules were trimmed, to have a small and defined tip of 100 by 100 microns and attached to the microtom holder (Fig. 1). The holder moves up and down and a diamond

blade cuts off very thin slices (approx. 80 to 100 nm thickness). These slices are collected on a water film and gathered onto a standard carbon-plated TEM copper net. The blade can cut through epoxy and even divide the steel particles to make them thin enough for TEM-examinations. Several slices (around 5 to 7) are collected and put onto one copper net. Each slice contains up to several cut powder particles, dependent how equally distributed the particles were in the TEM capsule. Usually around 1-2 particles could be found in the epoxy slices. For the analyses, a FEI TECNAI-20F (200kV) Transmission Electron Microscope equipped with HAADF detector for scanning TEM was used. The elemental analysis has been performed using energy dispersive X-ray spectroscopy. Examples of the results can be found in Fig. 2.

After validation of the production process, steel powders were mixed with different oxides and milled for 80 hours. Details of the materials produced can be found in table 1. HIPing of the alloys was performed at 1150 °C and 100 MPa at Bodycote, Munich. Then, the capsules were hot-rolled at 1100 °C at University of Clausthal and reduced from approx. 40 mm diameter to 6 mm thickness. All the tests and following analysis were performed in as-rolled condition.

Conclusions

TEM sample preparation for MA steel powders by microtomy, proved to be a fast method for the validation of the milling time. Small batches of a new material can be milled for different times and examined using TEM + EDX. Then, the mechanical alloying process can be checked and validated without going through the complete ODS production process, which is highly time consuming and expensive.

The experimental series showed that milling the given steel powder with Y_2O_3 for 24 hours is not enough to achieve full mechanical alloying. The mixture needs to be milled for at least 48 hours. Further milling beyond 48 hours leads to finer and more homogenous particle sizes, even beyond the as-received condition.

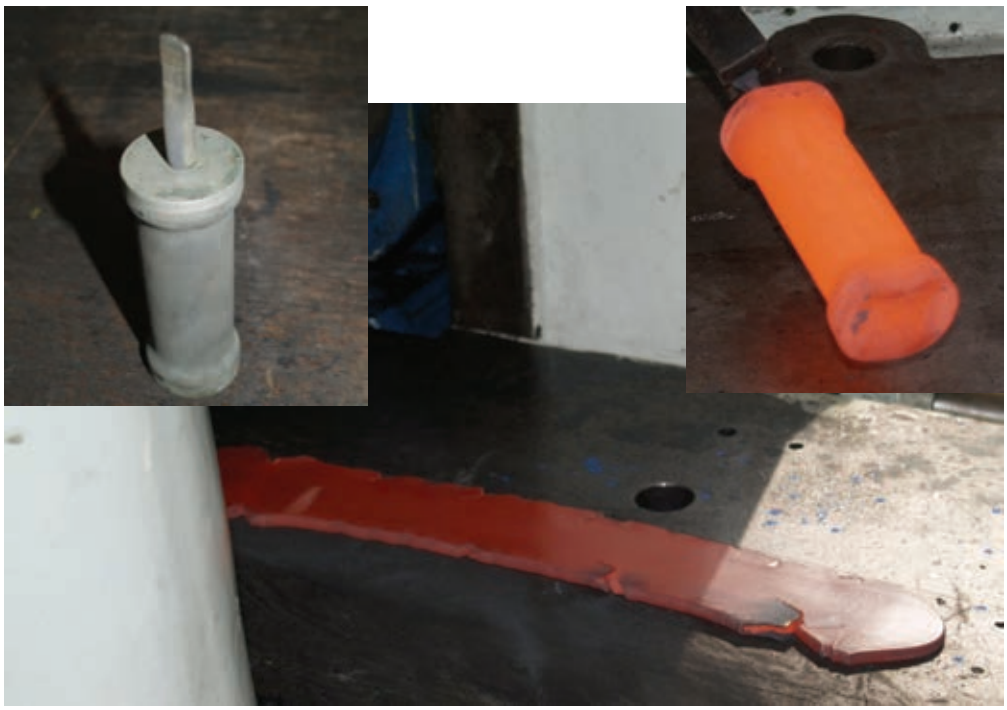

Fig. 3: Capsules after HIPPing, and during hot-rolling.

Alloys containing different oxides were successfully hipped and hot-rolled (Fig. 3). First mechanical and microstructural characterization (Fig. 4 + Fig. 5) showed major differences be-

tween the various oxides. These differences and correlations between microstructure and mechanical properties are a main subject of the future work.

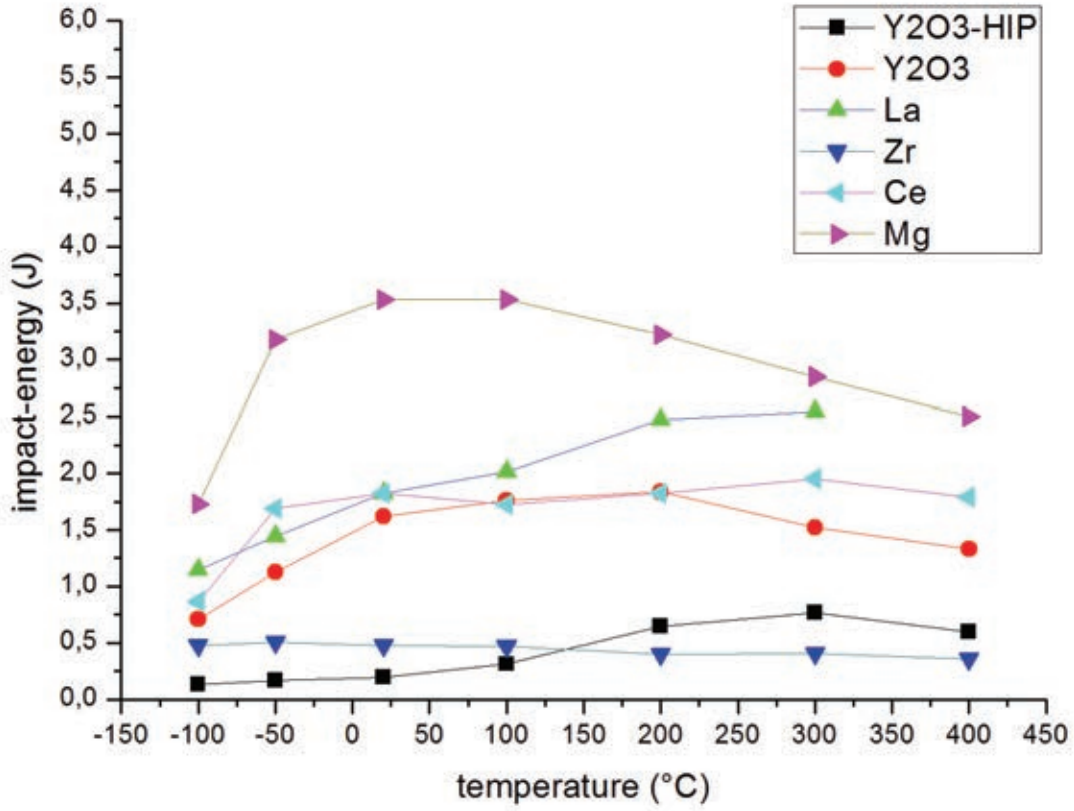

Fig. 4: Results of Charpy impact tests (as-rolled and as-hipped condition).

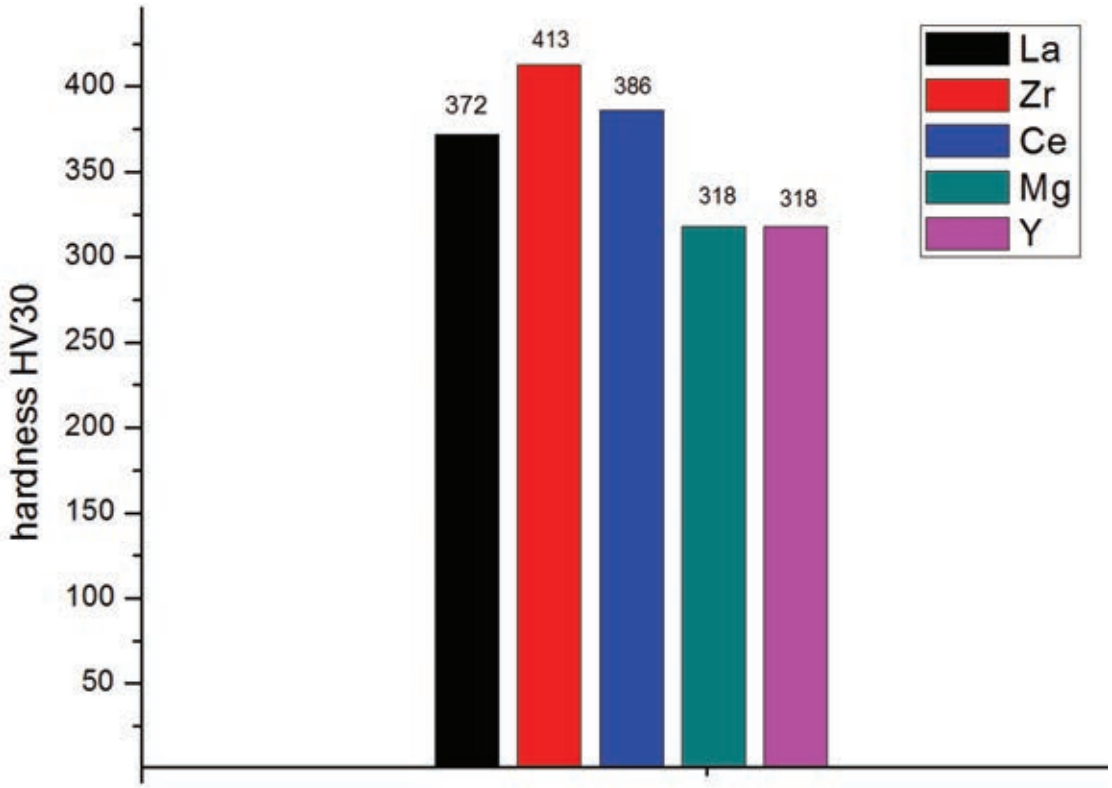

Fig. 5: Vickers hardness of the different alloys (as-rolled condition).

Staff:

S. Baumgärtner
L. Commin
B. Dafferner
S. Heger
J. Hoffmann
U. Jäntsch
M. Klimenkov
R. Lindau
A. Möslang
J. Reiser
M. Rieth
R. Ziegler
H. Zimmermann

Literature:

[1] J. Hoffmann, M. Klimenkov, R. Lindau, M. Rieth, TEM study of mechanically alloyed ODS steel powder, Journal of Nuclear Materials (2011), DOI: 10.1016/j.nucmat.2011.09.034

[2] J. Hoffmann, M. Klimenkov, R. Lindau, M. Rieth, Validation of the mechanical alloying process of ODS steel, Proceedings of the Jahrestagung Kerntechnik 2011, May 17-19, Berlin, Germany.

[3] J. Hoffmann, Rainer Lindau, Michael Rieth, Mechanical and microstructural characterization of different oxides for oxide-dispersion-strengthened (ODS) steels, Gordon Research Conference – Physical Metallurgy 2011, August 3., Boston, USA

[4] J. Hoffmann, Characterization and optimization of a nanoscale ferritic oxide-dispersion-strengthened (ODS) alloy, Fusion PhD Seminar 2011, June 27-28, Bad Herrenalb, Germany

Acknowledgement

This work, supported by the European Communities under the contract of Association between EURATOM and Karlsruhe Institute of Technology, was carried out within the framework of the European Fusion Development Agreement. The views and opinions expressed herein do not necessarily reflect those of the European Commission.

Production and Characterization of Industrial Batches of Nano-structured ODSFS (WP11-MAT-ODSFS-02-01)

Introduction

The developmental work on nano-structured ODS steels in Europe is carried out in laboratories at universities and research centres at laboratory scale, i.e. small batches of a few grams to about 200 grams. The presently identified applications in future nuclear fusion reactors require instead amounts of material that are orders of magnitude larger and need therefore an industrial-scale fabrication. Among others, the transferability of the results gained in lab-scale to industrial scale production has also to be proven. A cooperation of a research centre with a single industrial partner as it was the case in the ODS-EUROFER development performed by KIT (formerly FZK) with PLANSEE is no longer possible due to the decision of PLANSEE to give up the ODS production.

This very fruitful cooperation lead in several developmental steps to a reduced activation ferritic martensitic 9Cr ODS-steel with acceptable mechanical properties that allow to increase the operational temperature compared to the non-ODS EUROFER 97 steel by about 100 °C to 650-700 °C making the material suitable for application in the blanket and divertor of a DEMO-type reactor.

Due to the α-γ phase transformation in these steels, the application temperature of this ODS-steel is limited to temperatures of about 800 °C. To avoid this drawback the development of ODS ferritic steels (ODSFS) which do not show such a phase transformation is pursued.

To establish a production route in industrial scale it was decided to divide the fabrication process into single steps and to find industrial partners for each production step. In preceding studies each step was analysed in laboratory scale in view of scalability to industrial scale.

This task is strongly interwoven with other tasks in which the influences of composition and production parameters on the properties of ODSFS are investigated.

Materials, results and discussion

In continuation of the work performed until the last reporting period, where the influence of Ti content in 14 Cr ferritic ODS alloys was studied, the effect of thermo-mechanical treatment i.e. the influence of mechanical deformation and heat treatments was investigated. Several batches of 200 g to 1 kg of 14 Cr ODS steels were produced in the usual process from pre-alloyed 13.5Cr-1.1W-0.3Ti powder by adding 0.3wt.% Y_2O_3. The fabrication process consisted of mechanical alloying under hydrogen gas, encapsulation, degassing and hot-isostatic-pressing for consolidation of the powders. While the small batches were used to investigate the microstructure and mechanical properties in the hipped state, the larger batches were foreseen to be rolled to 6 mm thick plates. Additionally, batches without any Yttria were produced and treated in the same manner for comparison.

It is worthwhile mentioning that the whole powder handling during the powder-metallurgical production route was performed under protective gas atmosphere to keep the oxygen content as low as possible. Fig. 1 shows cylindrical (200 g) and prismatic (1000 g) types of capsules after hot isostatic pressing (HIP). The prismatic type of HIP capsules should be used for subsequent rolling. Therefore these capsules were machined to slabs prior to the rolling. The rolling was performed in cooperation with the Technical University of Clausthal. A cross rolling technique which includes turning of the slabs between different rolling passes was applied. This procedure should lead to homogenous in-plane mechanical properties. Fig. 2 gives an impression of the hot rolling of the slabs in a 12 inch Duo Mill (left side).

From the 6 mm thick rolled plates, blanks for the fabrication of small scale specimens for tensile, LCF and impact testing were cut by spark erosion. The geometry of these specimens has been developed for irradiation in IFMIF and is meanwhile well established and has been used in several irradiation experiments in HFR (SPICE) and Bor 60 reactor (ARBOR). Fig. 2 shows also on the right hand side, how the blanks were taken in order to test the mechanical properties with respect to the direction of the last rolling pass (indicated by arrows).

Fig. 1: Different types of HIP capsules after HIP (left) and after milling (right).

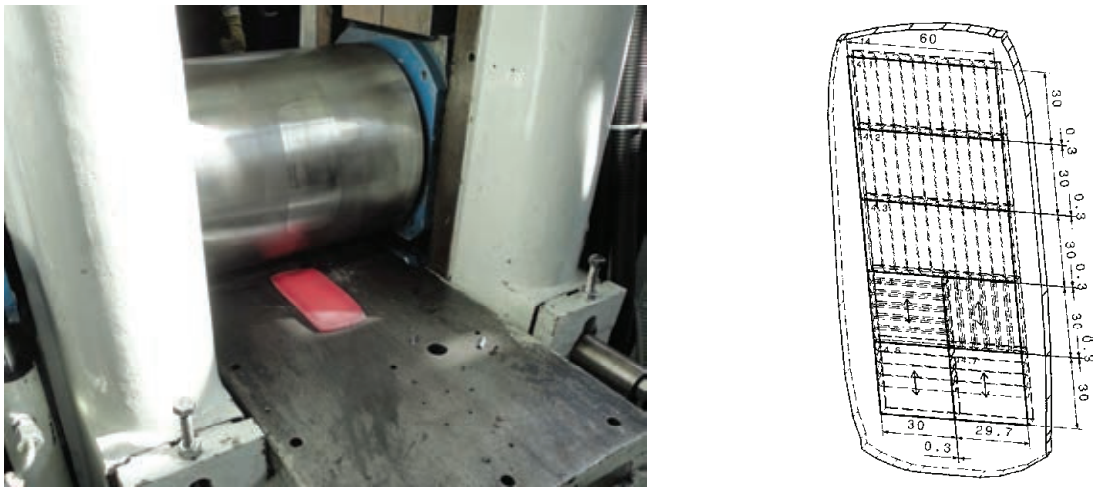

Fig. 2: Rolling of the 1 kg slabs in a 1,800 kN 12 inch Duo Mill (left) and partitioning of rolled plate for specimen fabrication (right).

For the different Ti-contents, the correlation between microstructure and mechanical properties was analyzed by means of scanning electron microscope (SEM) and transmission electron microscope (TEM) equipped with energy- dispersive X-ray spectrometer (EDX) and electron energy loss spectrometer (EELS). A bimodal grain size distribution was observed in all as-hipped Ti-containing ODS alloys as it was seen earlier [1,2]. These alloys consisted of coarse grains typical ranging from 1 µm to 8 µm and fine grains well below 1 µm in diameter. The addition of Ti resulted in the formation of spherical Ti oxides rather than Cr oxides owing to the stronger affinity of Ti. The influence of Ti on particle size refinement was striking and the optimum effect was obtained when adding 0.3% Ti. Vickers hardness measurements (HV30) increased consistently with increasing in Ti content. The ODS alloys with 0.3% Ti exhibit the highest strength due to the optimum refinement of mean ODS particle size. Detailed results of the microstructural investigations and of the mechanical characterisation are given in [3].

The effect of rolling compared to hot isostatic pressing on the mechanical properties is shown in Fig. 3 to 5. Fig 3. shows the temperature dependence of the ultimate tensile strength of 13.5Cr-1.1W-0.3Ti with or without 0.3wt% Yttria addition. The ultimate tensile

strength for the experimental 13.5%Cr ODS alloy (olive green symbols) in the hipped (circles) and rolled condition (squares) over the range from RT to 700 °C is shown in Fig. 3 in comparison with data for the 13.5%Cr unmilled base alloy without any Yttria (navy blue symbols). The ultimate tensile strength of the ODS alloy is remarkably enhanced compared to the base material and exceeds the values for EUROFER-ODS (blue dotted lines) and is, independent of the sampling direction, slightly higher than of the only hipped material.

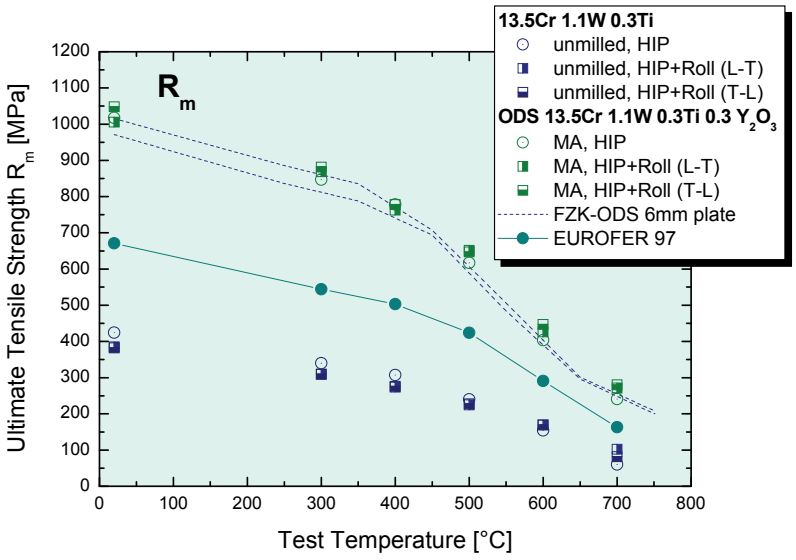

Fig. 3: Temperature dependence of ultimate tensile strength for a 13.5Cr-1.1W-0.3Ti-0.3Y_2O_3 ODS alloy in the hipped and rolled state compared to 9%Cr EUROFER -ODS steel and the basic steels.

The non-ODS material shows an opposite effect. While the tensile strength until 500 °C is slightly lower for the rolled material, it is higher above this temperature. Also no dependence from the sample direction was observed. The base material without Yttria shows by far the lowest tensile strength of all shown materials.

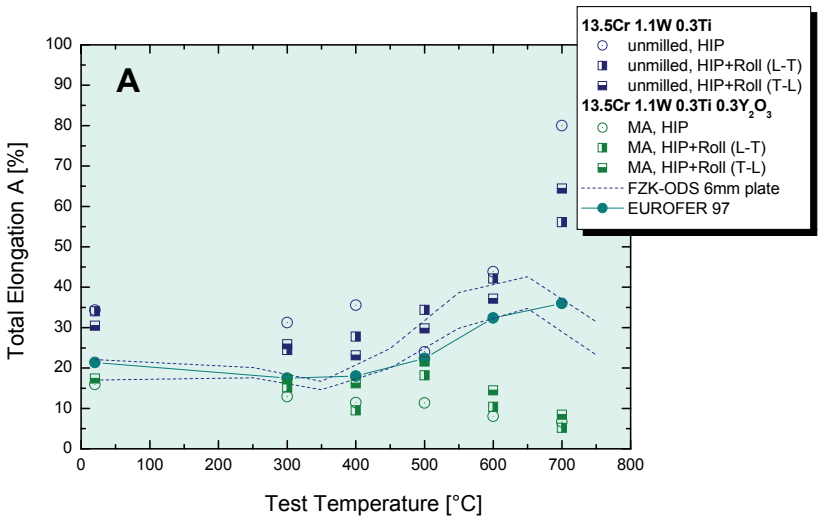

Fig. 4: Temperature dependence of total elongation for a 13.5Cr-1.1W-0.3Ti-0.3Y_2O_3 ODS alloy in the hipped and rolled state compared to 9%Cr EUROFER-ODS steel and the basic steels.

Figure 4 gives the total elongation of the same tensile specimens as before. The non-ODS base material is very soft and shows a higher total elongation than all other alloys of the whole temperature range. This can be easily understood because this steel has a simple composition and was only introduced to give the benchmark to separate the ODS effect. The ODS material shows a similar ductility up to 300 °C when compared to the EUROFER variants. Unfortunately it decreases constantly with increasing test temperature.

Figure 5 shows the impact properties of the 13.5%Cr ferritic ODS steel after hipping and after rolling in comparison to the base alloy, EUROFER 97 as well as FZK-Heat of EUROFER-ODS in the thermo-mechanical treated state and the as-hipped condition after different heat treatments. The ferritic unmilled base steel (blue squares) has a quite high upper shell energy which is comparable to that of the EUROFER ODS steel. The DBTT is around 0 °C or slightly lower. Anyway, it has poor impact behaviour compared to the optimised RAFM EUROFER steel. When Yttria is added by mechanical alloying, the impact behaviour degrades significantly. The upper shelf energy (USE) decreases to values of about 2 J and below for the only hipped material. Rolling gives a slightly higher USE than hipping and shows no dependency of the sampling direction. Nevertheless it is at least by a factor of 3 lower than that of the 9Cr ODS steel while DBTT comparable or slightly worse.

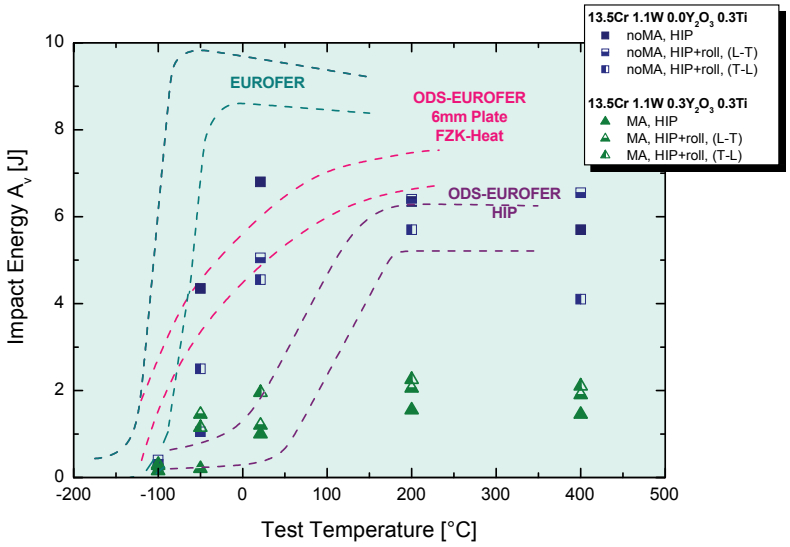

Fig. 5: Temperature dependence of total absorbed energy for a 13.5Cr-1.1W-0.3Ti-0.3Y_2O_3 ODS alloy in the hipped and rolled state compared to 9%Cr EUROFER-ODS steel and the basic steels.

Summary and conclusions

A Fe-13.5Cr-1.1W-0.3Ti-0.3Y_2O_3 ferritic ODS-steel was produced by mechanical alloying and consolidation by hot isostatic pressing. Material with the same composition was hot rolled in order to find its effect on microstructure and mechanical properties. While it shows good tensile strength, the high temperature tensile ductility and impact properties can be still improved. Anyway, hot rolling has shown a beneficial effect.

Staff:

C. Adelhelm
S. Baumgärtner
B. Dafferner
P. He
M. Hoffmann
U. Jäntsch
T. Kaiser
M. Klimenkov
R. Lindau
A. Möslang
J. Reiser
R. Ziegler
H. Zimmermann

Literature:

[1] C.C. Eiselt, M. Klimenkov, R. Lindau, A. Möslang, H.R.Z. Sandim, A.F. Padilha, D. Raabe; High-resolution transmission electron microscopy and electron backscatter diffraction in nanoscaled ferritic and ferritic-martensitic oxide dispersion strengthened steels; J. Nucl. Mater., 385 (2009) 231-235.

[2] C.C. Eiselt; Eigenschaftoptimierung der nanoskaligen ferritischen ODS-Legierung 13Cr-1W-0,3Y_2O_3-0,3TiH_2, metallkundliche Charakterisierung und Bestimmung von Struktur-Eigenschaftskorrelationen; PhD-Thesis, Scientific Report FZKA 7524 (2010).

[3] P. He, M. Klimenkov, R. Lindau, A. Möslang; Characterization of precipitates in nano structured 14% Cr ODS alloys for fusion application; J. Nucl. Mater. in press.

Acknowledgement

This work, supported by the European Communities under the contract of Association between EURATOM and Karlsruhe Institute of Technology, was carried out within the framework of the European Fusion Development Agreement. The views and opinions expressed herein do not necessarily reflect those of the European Commission.

Impact of Pulsed Operation on Lifetime of Blanket Module (WP11-DAS-PLS-P08-01)

Objectives

On the base of structural mechanical considerations of current DEMO designs the impact of pulsed operation on the thermo-mechanical fatigue and creep-fatigue lifetimes will be evaluated. Non-linear finite element (FE) analyses will be performed for the blanket design and assessed estimating the cyclic lifetime using the relevant material properties and design limits of the candidate structural alloys. Therewith the influence of the system parameters will be systematically studied deriving simplified formulae which can be implemented in system codes to optimize the system parameters for a given cyclic lifetime with minimal costs of the assembly. Close cooperation with designers and system code developers is foreseen.

Task current status

Assuming an inductive DEMO with a blanket design similar to that of the current European Helium Cooled Pebble Bed Test Blanket Module (HCPB -TBM) the influence of pulse duration on damage and lifetime of the HCPB-TBM is investigated. Therefore non-linear finite element (FE) simulations are performed considering the FE-model used in a resent non-linear failure analysis of the current European HCPB TBM design. In the simulations a loading scenario similar to that the HCPB TBM will be subjected to in ITER is assumed, where starting from a stress free state at 300°C a coolant pressure of 100 bar is applied and in a subsequent step the temperature is cycled by applying a non-homogeneous temperature field and removing it after a dwell time given by the pulse duration. Four pulse durations are investigated by selecting dwell time equal to 400 sec, 1, 3, and 8 hours, respectively. Within the reporting period the simulations of the first loading cycle with the different pulse durations could be performed. As expected, the maximum creep-fatigue damage value appearing in the component after the first cycle increases with longer dwell time and pulse duration, respectively. The increase however is not proportional and has an amplification factor less than that of the pulse duration. These trends shall be further investigated by continuing the simulations towards higher number of cycles for which the submodeling technique will be applied to overcome the problem with the extensive computing time required due to the non-linearity and huge size of the field problem.

Staff:

J. Aktaa

Literature:

[1] J. Aktaa, Szabolcs Kecskés & Fabio Cismondi: Non-linear Failure Analysis of HCPB Test Blanket Module, ISFNT-10, Portland, USA, 2011 (to be published in Fusion Engineering and Design).

Acknowledgement

This work, supported by the European Communities under the contract of Association between EURATOM and Karlsruhe Institute of Technology, was carried out within the framework of the European Fusion Development Agreement. The views and opinions expressed herein do not necessarily reflect those of the European Commission.

Corrosion Testing in PICOLO Loop (CoA)

Introduction

The HCLL concept for blankets is based on the application of the liquid breeder Pb-15.7Li which is in direct contact with the structural components, e.g. RAFM-steels. Corrosion attack of the structural material is always present and is mainly governed by operation temperature and flow velocity of the liquid breeder. At high flow velocities high dissolution rates of ca. 400 µm/year were evaluated at 550 °C leading to a high amount of dissolved corrosion products in the Pb-15.7Li. In a TBM system or also in a testing loop e.g. PICOLO these components are transported with the breeder flow to sections with cooler temperature and will form precipitates as known due to oversaturation. Effects like deposition, precipitate formation or transport were nearly completely neglected in former compatibility testing of RAFM-steels in flowing Pb-15.7Li and test evaluation. However, such formed particles may seriously affect safe and reliable operation of TBM systems. Analytical and modelling work concerning the impact of corrosion products was included into the compatibility testing program of EUROFER steel in PICOLO loop. To come to a most reliable and realistic view of all effects and also risks going on in a closed non-isothermal liquid metal system older results of corrosion testing were re-analyzed and updated by ongoing evaluation work from actual corrosion testing in PICOLO loop. The aim of the first stage of this new task is to identify corrosion phenomena correlated to precipitate formation and to form a feeling for risk in safe loop operation due to precipitate formation and transport. Surely, this task will need additional attention in future in corrosion testing as well as in modelling. The long term benefit will be the validation of predictive tools for TBMs under DEMO view and testing/qualification in ITER.

General results from compatibility testing

Compatibility testing of steels, austenitic and reduced activation ferritic-martensitic (RAFM) ones, have long-term history. A lot of data were collected concerning the corrosion behaviour of these steels at various environmental conditions. In the beginning, austenitic steels e.g. AISI 304 and AISI 316L, were tested in a small pumped Pb-17Li loop e.g. by Borgstedt [1]. In the 1990s analyzing ferritic-martensitic steels was included into the testing program [2-3]. The attack of the austenitic steels was characterized by leaching out processes mostly of nickel (Ni) with a high solubility in Pb-15.7Li, whereas the ferritic-martensitic steels showed a homogeneous dissolution attack. In the later years compatibility testing moved on to RAFM-steels and since around 2000 testing is focused on EUROFER behaviour. Due to changes in TBM operation conditions, testing temperatures were increased from moderate 480 to more aggressive 550 °C. All these tests show undoubtful that corrosion attack is increased with rising temperature and therefore the amount of corrosion products in Pb-15.7Li increases. From physics it is clear that in a non-isothermal closed system, TBM or testing loop PICOLO, oversaturation with all consequences have to appear at sections with lower temperature. Less attention was paid to the mechanism of ‘deposition’ during loop operation despite the seriousness of this effect. An early report on this is given by Torterelli [4]. It is mentioned that ‘particles’ are formed, which are able to move with the melt flow. Similar behaviour is reported in [5] for deposited ‘particles’ in a magnetic trap of PICOLO loop. However, corrosion testing at more aggressive 550 °C shifted the precipitate behaviour to high attention due to occurring severe line plugging.

Operation of PICOLO loop

Some decades ago, PICOLO loop was designed [2] for corrosion testing of steels in flowing Pb-15.7Li environment. PICOLO is a non-isothermal loop, which can operate at flow velocities of roughly some 1 cm/s to 1 m/s in the tests section. The design temperature for testing is 550 °C, however, most of the testing was done at 480 °C in the past. The cold leg of the loop containing the components magnetic trap, electro-magnetic pump, magnetic flow meter, is operated near 350 °C. The cold leg (T < 450 °C) is fabricated from austenitic steel,

whereas the hot section is made of ferritic-martensitic steel (DIN 1.4914). Cylindrical samples (diameter 8 mm) are exposed in the test section (diameter 16 mm) in a concentrically arrangement to the Pb-15.7Li flow. Fig. 1 shows the design of PICOLO loop. PICOLO operation time frame was roughly 4 years since the last general revision work with intense cleaning of tubes inside and refilling with new Pb-15.7Li, which is relevant for the results given in this paper. During this time span, PICOLO was operating for about 20,000 h at 480 °C test temperature and roughly 13,000 h at 550 °C at a flow velocity of 0.22 m/s. Due to strong corrosion of the test section component (TS) after the 550 °C cycle a new inside coated test section was installed together with heater (EH) and heat exchanger (CFHE). After that revision PICOLO run at 550 °C and 0.10 m/s with fresh Pb-15.7Li until severe plugging appeared after roughly 4000 h. Bare and Al-coated EUROFER samples were mounted during these test campaigns. PICOLO has a total loop length of about 12 m.

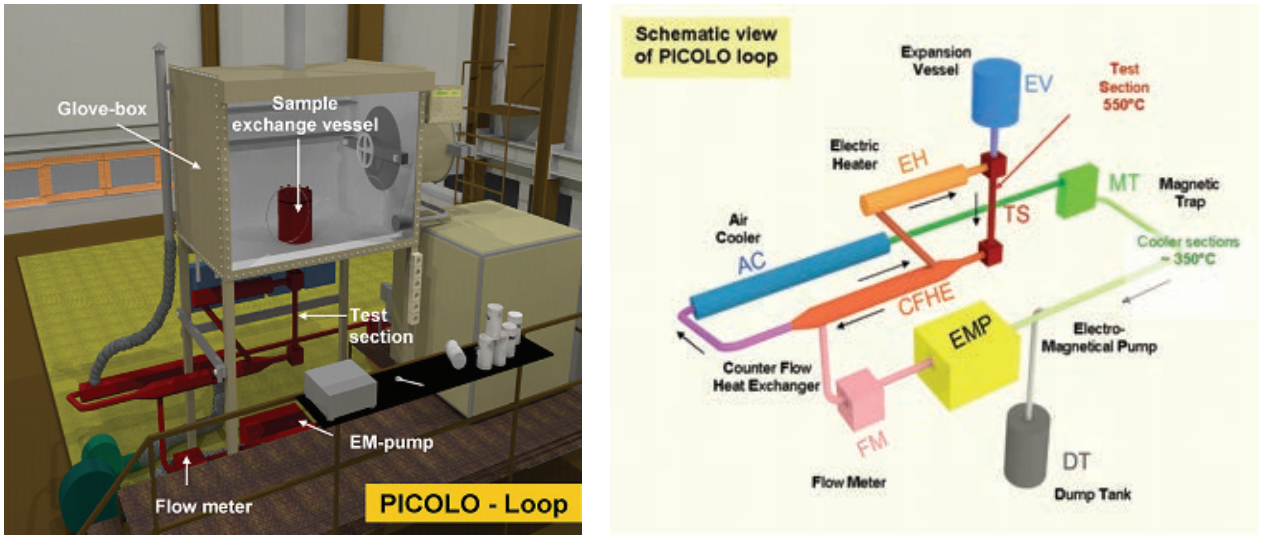

Fig. 1: Schematic view of PICOLO loop and the main components.

Corrosion testing in PICOLO loop

Different RAFM-steels (OPTIFER, MANET, F82H-mod., and EUROFER) showed rather similar corrosion attack at a flow velocity of 0.22 m/s and a testing temperature of 480 °C (753 K), with corrosion rates in the range of 80 to 100 µm/year. However with the slight increase in temperature to 550 °C (823 K) the corrosion attack increases significantly to roughly 400 µm/year. The corrosion attack dominating mechanism is for both test conditions dissolution attack. At 550 °C a square meter of EUROFER plate would lose about 4 kg per year. A reduction in flow velocity to 0.10 m/s resulted in a decrease of corrosion attack towards about 250 µm/year based on short term exposure data up to 3,000 h. The reliability of the 0.22 m/s values is much better due to long term data up to 12,000 h testing time [6]. Both test velocities which were also required for corrosion model validation of developed MATLIM-code [7] are in the turbulent flow regime, whereas, 0.10 m/s is near the boundary to mixed flow conditions (laminar-turbulent). Laminar conditions are expected for flow velocity below 0.05 m/s in PICOLO. Experimental testing and modelling using physico-chemical properties produced comparable corrosion attack values for 550 °C testing temperature and 0.22 m/s flow velocity. Fig. 2 shows both, the local temperature of PICOLO components and the corrosion ‘attack’ of each section. Thereby, negative values indicate that components will lose mass, positive ones ‘imply’ a kind of ‘coating = reduction of oversaturation’. Also in the cold leg zone, experiment and modelling are consistent and see / predict a type of ‘particle’ formation.

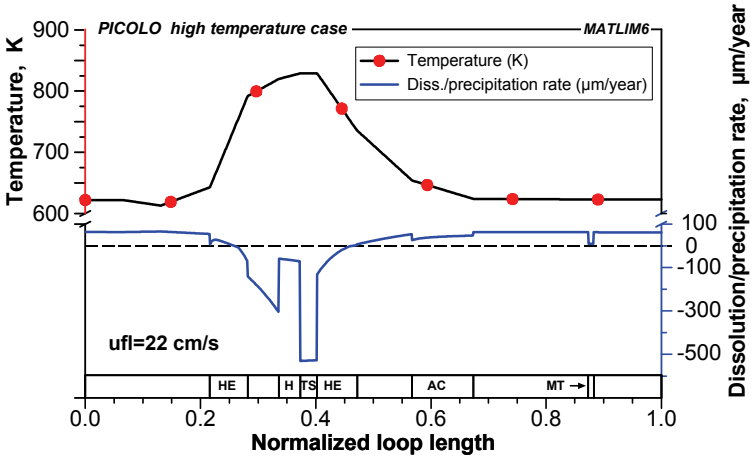

Fig. 2: Corrosion behaviour in PICOLO loop calculated by MATLIM-code over the whole loop length of PICOLO in dependence on temperature and thermo-hydraulic conditions.

Behaviour of magnetic trap and Pb-15.7Li

The magnetic trap was originally installed to collect all formed precipitates during cooling down of the Pb-15.7Li melt at the flow path length of roughly 5 m (test section to trap) from test temperature to working temperature (350 °C) of the electro-magnetic pump. The idea was that no particles will reach the pump and will re-circulate to the test section. At test temperature of 480 °C the life time of an operating magnetic trap was roughly 15,000 h. The magnetic trap is designed as a flat steel casing (ca 120 x 120 x 16 mm), where Pb-15.7Li has to pass through at low flow velocity, mounted in the field of a permanent magnet. Operation management of PICOLO showed that required pumping power, to keep flow velocity constant, was an indicator for the filling of the trap with magnetic particles. Filled traps were cut out of the loop and were replaced by fresh / empty ones. Chemical analyzes of the trap content after service showed that concentration of collected Fe/Cr particles in the Pb-15.7Li matrix are in the range of 1 to 3 at.% with a gradient from outlet to inlet. Metallurgical analyzes indicate that the particles have filigree structure similar to snow crystals and can reach length above 100 µm easily (Fig 3).

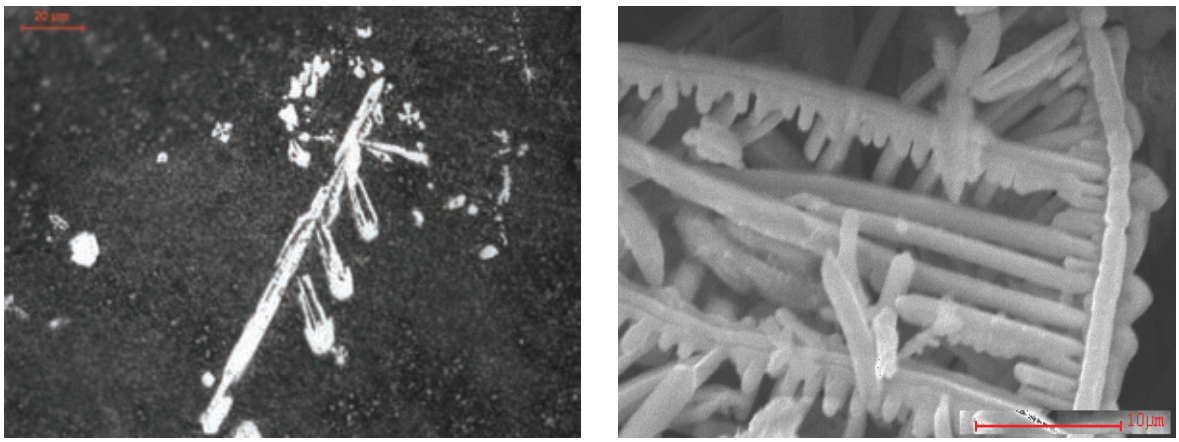

Fig. 3: Fe/Cr precipitate collected in the magnetic trap near the outlet position (optical and SEM images).

Besides, monitoring the pumping power, also the chemical composition concerning impurity elements of the flowing Pb-15.7Li was analyzed. Therefore, test samples of the melt were removed from the test section / expansion vessel in case of test-sample changes. The iron solubility as evaluated from literature and discussed in [7] may reach 10 wppm at 600 °C. The Pb-15.7Li analyzes (Fig. 4), show that the impurity content (Fe) is rather constant (< 20 wppm) over a long time span, but increases later rapidly by a factor of ca. 10. The plotted

values are the total dissolved and solid amount of Fe concentration. At least at that time (~ 9,000 h), the solubility limit is exceeded and particles have to be present. The pumping power had to be increased also significantly at that time to keep the flow of the melt constant. Both indicators are thus in agreement to decide that the trap is filled and work not properly further on. The detected Ni amount indicates that also in the cold leg corrosion takes place.

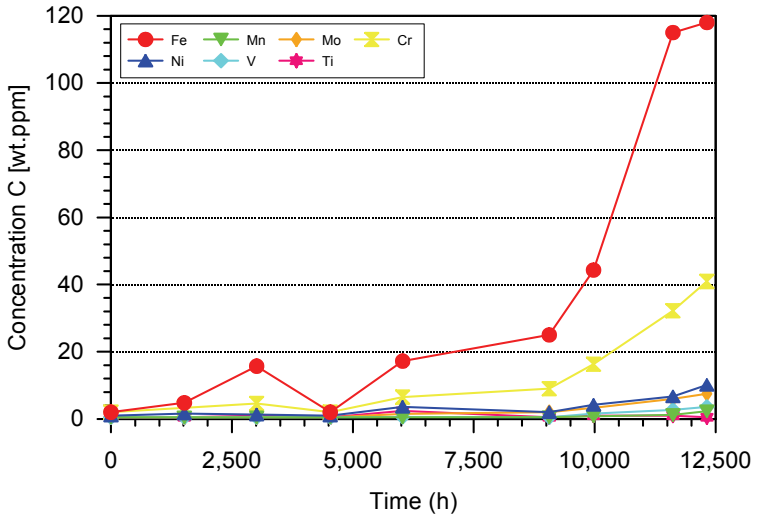

Fig. 4: Changes of impurity concentration in Pb-15.7Li extracted from TS / EV section during life time of one magnetic trap.

Precipitates in loop components

During the revision work of mounting a new test section, some loop sections were cut out to collect pieces of the tubing for metallurgical analyses. The intended issues were, detecting corrosion traces at sections with lower flow velocity e.g. EH zone (diameter ca. 42 mm) but at high temperature or to analyze 'deposition' scenarios in areas with lower temperature but without magnetic fields (CFHE) or in tubing down stream.

Fig. 5 shows the micrograph of a cut tube from the cool loop section. In the centre of the picture could be seen the adherent Pb-15.7Li layer with embedded (bright) spots of Fe/Cr particles. At the bottom a part of the steel tubing is visible. A clear separation between steel and breeder can be detected. No grown layer on top of the steel wall is visible. This underlines that no coating process takes place as expected as reverse process of dissolution in the regime of oversaturation. In contrast, similar to MT section, precipitates are found, too. Both micrographs suggest that oversaturation is reduced by precipitate formation in the melt volume. The situation after draining implies that an enrichment of particles may take place near the wall where flow velocity is a little bit smaller. Viscosity changes due to higher iron content may support this effect. The flow velocity in this zone is comparable with the conditions in the test section. The large size of the particles excludes a homogeneous flow of the 2-phase breeder mixture. The amount of Pb-15.7Li in PICOLO is about 10 liters which should circulate completely in some 4-5 minutes.

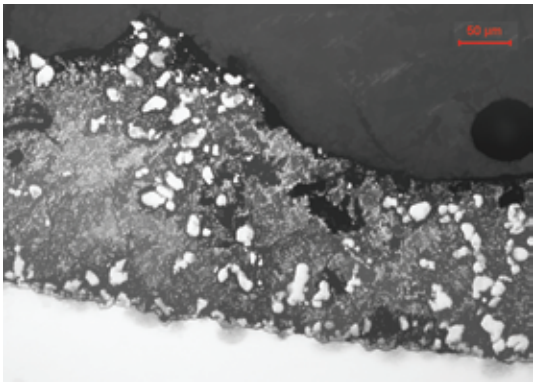

Fig. 5: Cross section of a tube (diameter 16 mm) from the cool leg. Clearly visible are particles embedded into the breeder and no coating of the tube wall.

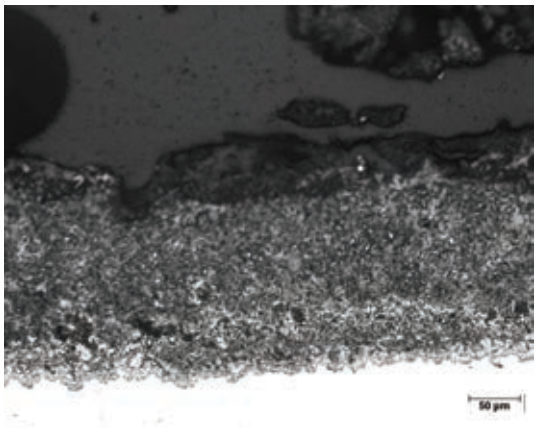

Fig. 6: Cross section of heater section (550°C, diameter ca. 42 mm).

Analyzes of the heater section were also performed. Here, temperature is comparable to conditions in test section. However, flow velocity is roughly 1/10 in heater zone (ca. 0.025 m/s) instead of 0.22 m/s in test section. The cross section shows that also at low flow velocity corrosion attack took place of the RAFM-steel visible by the roughening of the inner surface (Fig. 6). Some Pb-15.7Li is adherent at the surface and exhibits white dots. EDX showed that the white spots exhibit Fe/Cr. This may indicate that precipitates formed at the cool sections are migrating with the flow and are not completely dissolved, despite the low flow velocity in the electrical heater section.

Consequence towards ITER TBM tests

Analyzing precipitation effects in a closed loop system is complex due to the required destructive testing to get an overview of processes going on near surfaces. At the moment this corrosion related issue of precipitates gained intense attention due to plugging of pumping channel of the EM-pump. Fig. 7 shows a view into the cut channel (height inside 8 mm) where precipitates are arranged with their long axis parallel to the magnetic field lines. They formed a network of high stability which couldn't move away by switching between forward and backward flow power. Surely, the data base concerning precipitates is limited, but the 'phenomena' seen during PICOLO operation, ranging from consequent power adjustment to keep flow constant up to plugging effects, showed that additional efforts have be made in this field. In contrast to a testing loop with long tubing the observed 'problems' in operation are compressed in a breeding unit of a TBM to scales of some centimeters. Reliable operation will need the knowledge about mechanisms / phenomena and also the predictive tools for extrapolation to ITER TBM tests and DEMO.

Fig. 7: View into plugged pumping channel of PICOLO loop due to precipitate collection

Results

The performed post mortem analyses of the magnetic traps and drained components of PICOLO loop delivered valuable data concerning processes and phenomena taking place in Pb-15.7Li during circulation in a closed system. These results are a response of the system in oversaturated regime when the Pb-15.7Li leaves the hot corrosion testing section. They may be summarized as:

- The reverse process of dissolution – the deposition of corrosion products was not found.
- Precipitates are formed in the flowing breeder to reduce oversaturation.
- Precipitates were collected by the purification device magnetic trap but not completely.
- Precipitates are migrating with breeder flow.
- Pb-15.7Li layers remaining on surfaces after draining exhibit precipitates in all sections.

- Breeder analyzes in TS indicate that particles may not disappear during heating up again.
- The areas for formation and growing of precipitates incl. ‘kinetics’ is an open issue.
- Electro-magnetic pump was plugged by precipitates and highlights the risk of precipitates.

Conclusions

Performed corrosion testing of RAFM-steels produced a lot of data concerning corrosion attack of the structural components, which are in contact with flowing Pb-15.7Li at various flow and temperature conditions, however, mostly under non typical conditions present in a TBM system. At least reliability of corrosion attack at small flow velocity or surely in presence of magnetic fields is scare. Availability of predictive tools inclusively of their validation to model attack, which are essential for layout of such components towards DEMO is still a concern and needs further efforts in the future. Surely, required wall thickness can be determined to prevent leakages by corroding through under normal flow condition. But this is not enough to guarantee safe and reliable operation of such HCLL blanket systems. Corrosion testing in PICOLO loop showed that corrosion attack by dissolution is dependent on flow velocity and temperature. At designed TBM operation temperature 550 °C testing resulted in a wall thinning of roughly 0.4 mm/year at 0.22 m/s flow velocity which is reduced at smaller flow velocities but will never diminish. Thus corrosion products will always be present in the flowing Pb-15.7Li. The testing also showed that oversaturation of Fe in Pb-15.7Li leads to precipitates at cooler sections of the system and the installed magnetic trap for purification did not collect all existing ‘particles’. This led to migrating ‘particles’ in the closed loop and ‘deposition’ was observed at sections behind the ‘purification’ position. An intense ‘deposition’ was observed in other components where a magnetic field was present like flow meters or magnetic pump. Less pronounced deposits were detected in parts of the loop where Pb-15.7Li is reheated. Despite the consequent changes of the magnetic trap to keep amount of precipitates in Pb-15.7Li low, plugging of the EM pumping channel happened, indicating the risks coming from corrosion products concerning safe and reliable operation of a testing loop. A more accurate qualification of all occurring precipitate correlated mechanisms and phenomena is not possible due to the limited data base. Re-evaluation of earlier collected data like impurity levels of Pb-15.7Li in dependence on testing time / conditions in PICOLO will be used for future testing of precipitate effects. The advantage of a test loop is the local separation of dissolution and ‘deposition’ sections and ‘free’ assessable impurity parameters e.g. by adding Fe or H_2. Without special test geometries the reactions / process ongoing in a breeding unit of a TBM system with steep thermal gradients und magnetic fields inside cannot be precisely predicted.

Staff:

M. Heck
N. Holstein
J. Konys
W. Krauss
J. Lorenz
J. Novotny
A. Skrypnik
O. Wedemeyer
S.-E. Wulf
Z. Zhu

Literature:

[1] H.U. Borgstedt, G. Fress, G. Drechsler, Corrosion of stainless steel in flowing PbLi eutectic, J. Nucl. Mat., 141-143, (1986), 561-565

[2] H.U. Borgstedt, G. Drechsler, G. Frees, Z. Perit, Corrosion testing of steel X 18 CrMoVNb 12 1 (1.4914) in a Pb-17Li pumped loop, J. Nucl. Mat., 155-157, (1988), 728-731.

[3] O. K. Chopra, D. L. Smith, Compatibility of ferritic steels in forced circulation lithium and Pb-17Li systems, J. Nucl. Mat., 155-157, (1988), 715-721.

[4] P. F. Torturelli, Deposition behavior of ferrous alloys in molten lead-lithium, Fus. Eng. Design, 14, (1991), 335-345.

[5] J. Konys, W. Krauss, J. Novotny, H. Steiner, Z. Voss, O. Wedemeyer, Compatibility behavior of EUROFER steel in flowing Pb–17Li, J. Nucl. Mat., 386–388, (2009), 678–681.

[6] J. Konys, W. Krauss, H. Steiner, J. Novotny, A. Skrypnik, Flow rate dependent corrosion behavior of Eurofer steel in Pb–15.7Li, J. Nucl. Mat., 417, (2011), 1191-1194.

[7] H. Steiner, W. Krauss, J. Konys, Calculation of dissolution/deposition rates in flowing eutectic Pb–17Li with the MATLIM code, J. Nucl. Mat., 386-388, (2009), 675-677.

[8] W. Krauss, J. Konys, N. Holstein, H. Zimmermann, Al-based anti-corrosion and T-permeation barrier development for future DEMO blankets, J. Nucl. Mater., 417, (2011) 1233-1236

[9] J. Konys, W. Krauss, H. Steiner, J. Novotny, A. Skrypnik, Flow rate dependent corrosion behavior of EUROFER-steel in Pb-15.7Li, J. Nucl. Mater., 417, (2011), 1191-1194

[10] W. Krauss, J. Konys, A. Li-Puma, TBM testing in ITER: Requirements for the development of predictive tools to describe corrosion-related phenomena in HCLL blankets towards DEMO, Fus. Eng. Design, in press, Available online Dec. 14th (2011)

[11] J. Konys, W. Krauss, Corrosion and precipitation effects in a forced Pb-15.7Li loop, ICFRM-15, Charleston, SC, USA, Oct. 16-22, (2011)

[12] J. Konys, W. Krauss, N. Holstein, J. Lorenz, S. Wulf, K. Bhanumurthy, Impact of heat treatment on the behavior of Al-based anti-corrosion and T-permeation barriers in a flowing Pb-15.7Li environment, ISFNT-10, Portland, OR, USA, Sept. 11-16, (2011)

[13] K. Bhanumurthy, W. Krauss, J. Konys, Microstructural evolution of alumnide coatings on Eurofer during heat treatments, 2nd Intern. Conf. Adv. Nucl. Mater., Mumbai, India, Feb. 9-11, (2011)

[14] J. Konys, Development of advanced processes for Al-based anti-corrosion and T-permeation barriers, BARC, India, Feb. 8-11, (2011)

Goal Oriented Training Programme "Fabrication and Characterization of Materials" (WP10-GOT-FabriCharMe (FU07-CT-2010-00065))

The EFDA 2010 Work Programme covers a training activity in the field of Materials Science and Technology called FabriCharMe (Fabrication and Characterization of Materials). The general aim of the training programme is to prepare engineers and scientists for activities to support the ITER project and the long-term fusion programme within the Associations, Fusion for Energy and ITER Organization. The special aim of this training is to provide knowledge and to develop expertise of young engineers to fulfil future duties of structural materials foreseen for in-vessel components in DEMO and TBM of ITER. These materials include the low activation ferritic/martensitic steel EUROFER (foreseen to be used on the ITER TBM), nano-structured low activation Fe-Cr steels and tungsten alloys as structural, heat sink or protective elements. Thus training is needed in the procurement of these materials, managing qualification programmes and guiding the development of the materials. To achieve this, it is foreseen that the training includes practical and/or theoretical laboratory activities and educational tasks (formal courses and conferences). The main activities according the priority area "Materials Science and Technology" are specific issues of structural materials in fusion, e.g. selection of materials, alloy compositions and tailoring of properties, properties and failure mechanism under radiation (hardening, fracture, creep) and the role of gaseous transmutations, especially helium. In addition, modern tools for modelling and simulation of radiation e.g. methods to simulate evaluation of micro-structure, advanced characterization methods including electron microscopy, energy dispersive spectroscopy, diffraction methods, and micro-mechanical testing are covered as well as practice in materials technology, e.g. overview on different fabrication processes and joining techniques, qualification of base materials and welds according to nuclear standards, and non-destructive testing.

The whole network consists of 5 associations from 5 different European countries. KIT is hosting the two trainees working in this programme under WP1 and WP2, training topics are focussed on KIT's activities in post-irradiation testing, determining of irradiation damages, appropriate advanced characterization and microstructural investigation techniques, continuum mechanics modelling and design rules including radiation damage, selection and fabrication of materials, and joining techniques. CEA will provide the opportunity to work with the SYSWELD analysis software (WP2) and on the Jannus beam line (WP1). IPPLM-WUT is providing training on nanoscale microstructural characterization. CRPP will qualify a trainee on small and ultra-small specimen test techniques. CCFE-Oxford will give a training unit on focused ion beam-machined micromechanical specimens.

In 2011, there were a kick-off-meeting on February 1st and the yearly network meeting - with presentations by the trainees and by the mentors of the host associations - on November 14th and 15th, both held at KIT. The next network meeting is scheduled for November 15th and 16th, 2012.

Work package No. 1 (WP1)

Irradiation damage - advanced characterization and modelling
L. Commin, hosted at KIT since April 2011, supervised by A. Möslang
Associated Partners in this programme: CEA, IPPLM-WUT, CRPP

The trainee will be qualified in the subject of irradiation damage, appropriate advanced characterization techniques to detect and quantify them and in the implementation of such radiation damages in a continuum mechanics modelling tool to describe deformation and damage behaviour. Properties and failure mechanism under radiation and the role of helium will be studied by analyzing neutron-irradiated material which is available in the Fusion Materials Laboratory at KIT.

In 2011, the trainee has investigated the creep-fatigue interaction of EUROFER base material and welds. A literature study showed no significant influence of cyclic creep or of a creep pre-stress phase, but of a fatigue pre-stress phase: as creep I was remaining similar, creep II and lifetime are affected. Thus, different 6 mm thick samples of dissimilar EB welds have been produced: EUROFER 97/2 - EUROFER 97/2; EUROFER 3 - EUROFER 3; EUROFER 97/2 - ODS EUROFER. PWHT was 30´- 980°C + 2h - 750°C and 30´- 1050°C + 2h - 770°C. Sound welds with no porosity, no cracks and no sag of the weld pool were obtained (Fig. 1), mini LCF specimens (27 mm, 2 mm Ø) have been manufactured.

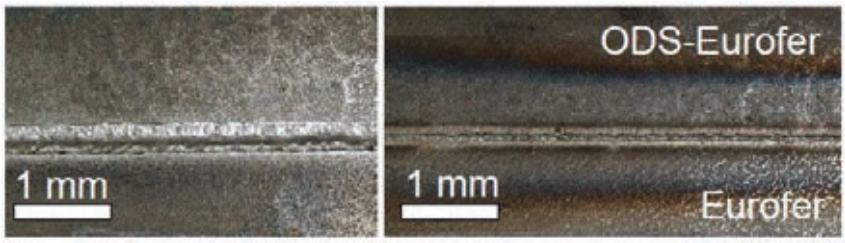

Fig. 1: EB welds of EUROFER.

For EUROFER 97/2 - ODS EUROFER, the as-welded microstructure has been characterized concerning grain and martensite laths size evolution, the M23C6 precipitations (200-400 nm in each zone / dissolved in the FZ), and Y2O3 precipitations (coarsening in the FZ). After PWHT, grain growth and EUROFER carbides precipitation in the FZ, coarsening in HAZ were observed. The Vickers hardness peak in the HAZ is correlated to smaller grains and martensite laths, the softening in the FZ is significant for a loss of the ODS strengthening. After PWHT martensite softening and carbide precipitation are found.

With the EUROFER 2 EB welds, fatigue and creep analysis was done by pure fatigue test (550 °C / ε = 0.6 %), pure creep test (550 °C / 180 MPa), $^{1}/_{3}$ fatigue life time + creep test, and $^{2}/_{3}$ Fatigue life time + creep test. EUROFER 3 EB welds and base material is tested by pure fatigue test (550 °C / ε = 0.6 %), pure creep test (550 °C / 180 MPa), and by 5 different numbers of cycles+ creep test. The results of Charpy tests on EUROFER 97/2 - ODS EUROFER EB welds are shown in Fig. 2, while Fig. 3 is representing the creep analysis of the same kind of welding.

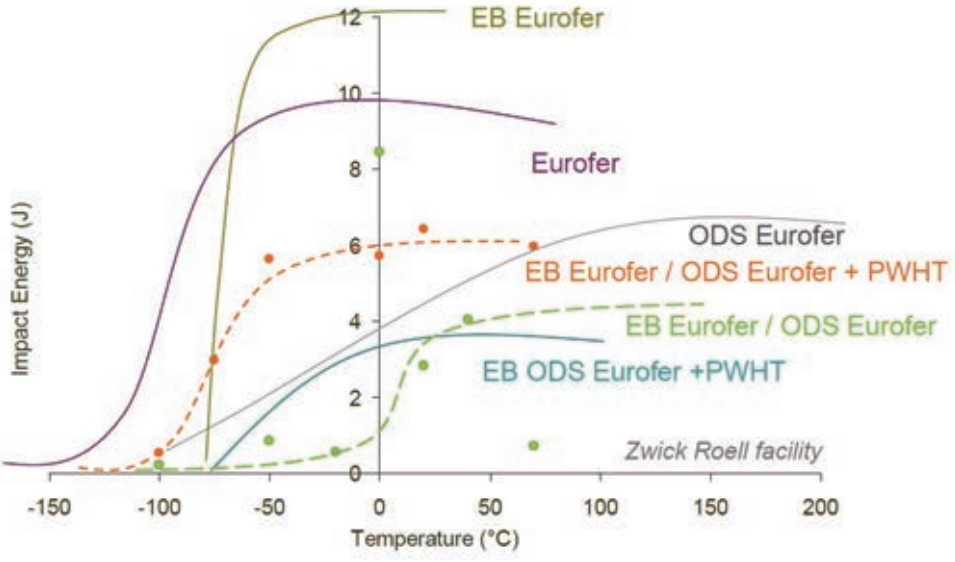

Fig. 2: Charpy tests on EUROFER 97/2 - ODS EUROFER EB welds.

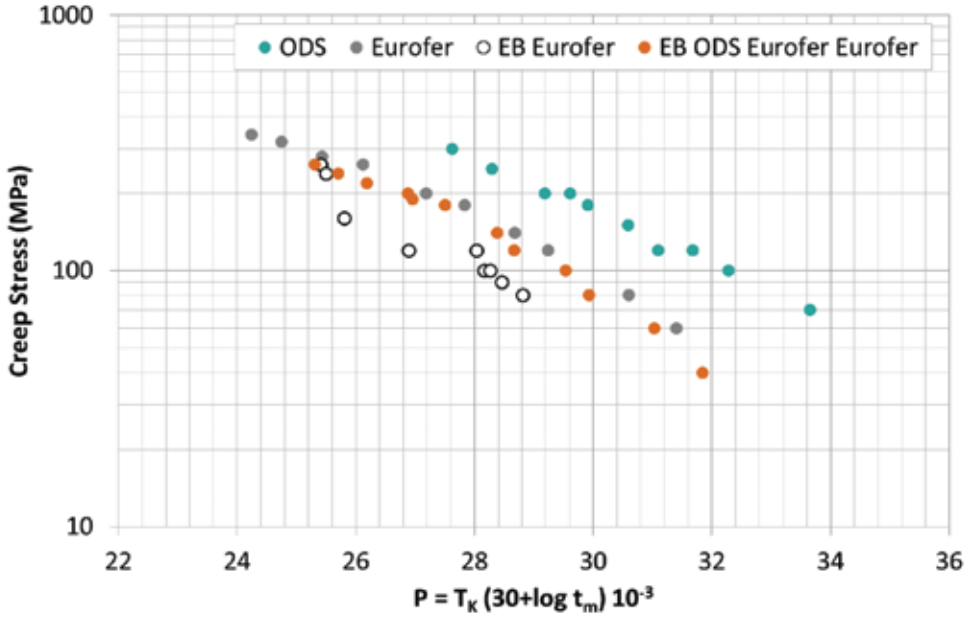

Fig. 3: Creep analysis of EUROFER 97/2 - ODS EUROFER EB welds.

Results have been presented in KIT seminars, on the ICFRM-15 and the ISFNT10 and are summarized in the 2011 trainee report. For WP1, the provisional training schedules include a stay at CRPP at the beginning of 2012 and later secondments to IPPLM-WUT and CEA, each of them 3 months.

Work package No. 2 (WP2)

Structure Materials and joining development
M. Scherwitz, hosted at KIT since October 2010, supervised by H.-C. Schneider
Associated Partners in this programme: CEA, CCFE-Oxford

The trainee will be qualified in the selection of materials, planning of irradiation experiments, post irradiation techniques, and design rules for neutron-irradiated materials in order to be able to assess materials and their joining techniques. The trainee will learn to analyze existing materials by the use of nuclear databases to further improve radiation embrittlement and high temperature creep properties.

In 2011, different activation and decay calculations using the FISPACT code have been performed in order to study the influence of impurities, neutron flux, and mass of specimens on the activation level after neutron-exposure of different alloys. The aim was to be able to estimate the activity of EUROFER test specimen for later use in micromechanical tests and especially to predict the redeposition of radioactive material in a FIB preparation device. EUROFER material has been welded by TIG, EB, and diffusion bonding in order to produce and test mini LCF specimens (27 mm, 2 mm Ø), Fig.4. Welding zones have been heat-treated and characterized by metallographic means and by hardness tests (Fig. 5), production of specimens is finished.

Development and qualification of high-temperature design rules for base materials and their welds will be done by performing isothermal and thermo-mechanical LCF of these specimens. Application and if necessary modifying the coupled deformation damage model developed for the EUROFER°97 base material helps describing the observed behaviour of welds. The aim is determining appropriate factors for considering EUROFER 97 welds and EUROFER 97 diffusion bonds in HT creep fatigue design rules.

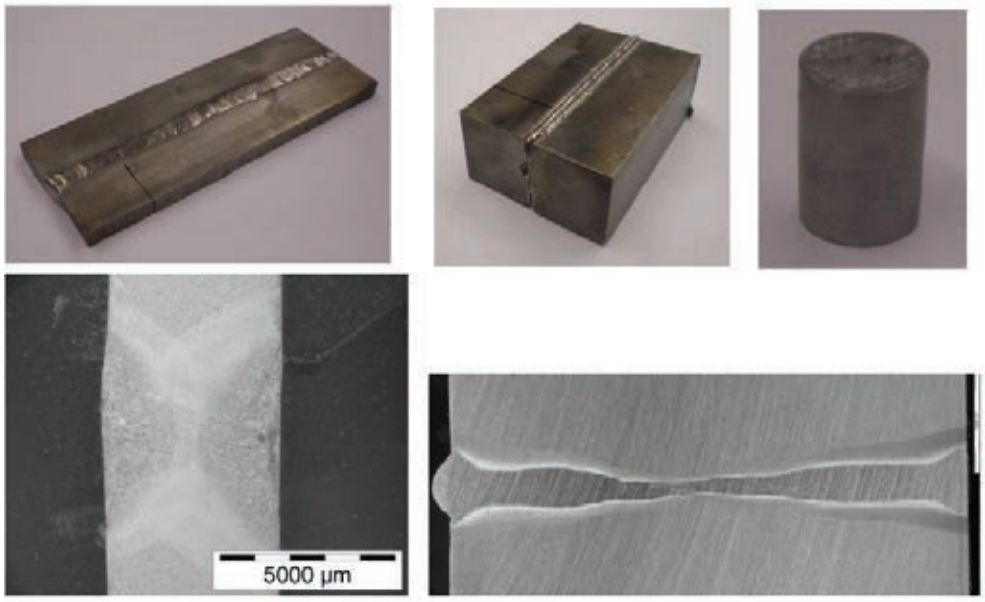

Fig. 4: Different EUROFER welds to produce 27 mm, 2 mm Ø LCF specimens. Above: TIG, EB, and diffusion bonding. Below: cross-cuts of TIG and EB weld.

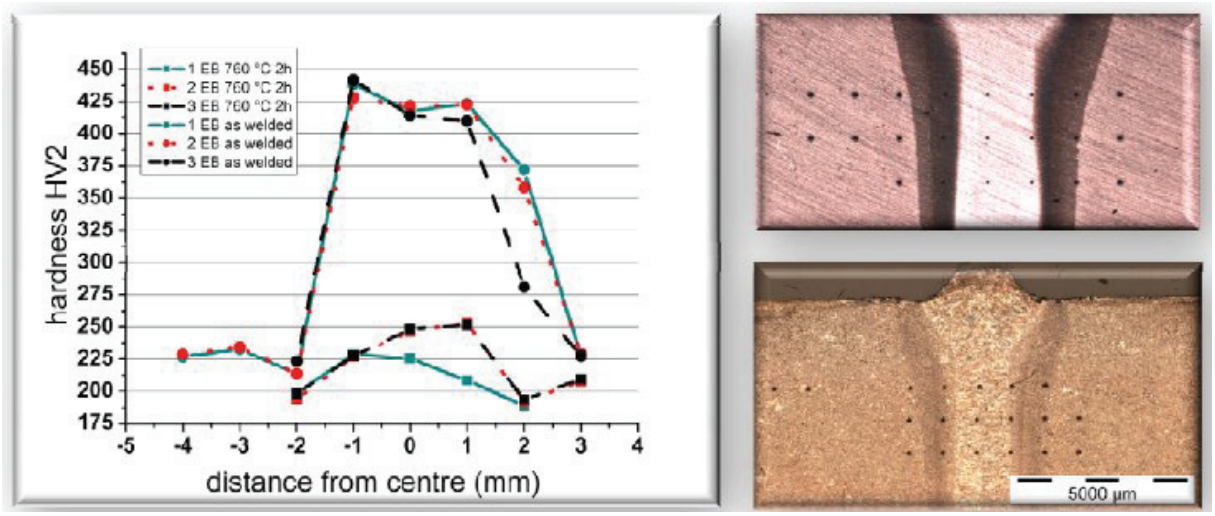

Fig. 5: Effect of 760 °C / 2h heat-treatment on hardness of EB-weld.

Further on, the trainee has attended the 2010 micromechanics workshop and the 2011 ion implantation workshop at Oxford and actually is working on micromechanical experiments during his 3 months secondment to Oxford. Micromechanical specimens have been produced and will help understanding the failure mechanisms in welds, especially helping to separate intergranular from transgranular failure by performing micromechanical bending tests on grain-sized bars.

Results have been presented in KIT seminars and on the 2011 Workshop in Oxford and are summarized in the 2011 trainee report. For WP2, the trainee was seconded to CCFE-Oxford for end of September until December 2011. His 6 months secondment to CEA is fixed to the period from April to September 2012

Future activities:

- Exchange with CRPP / CH for WP1
- Exchange with IPPLM-WUT / PL for WP1
- Exchange with CEA (Saclay) / F for WP1 and WP2
- Creep-fatigue tests and indentation; Hot Cell work (WP1)
- LCF tests and determining of parameters for damage model (WP2)

Staff:

J. Aktaa
L. Commin
A. Möslang
M. Rieth
M. Scherwitz
H.-C. Schneider
P. Vladimirov

Literature:

[1] Lindau, R., Klimenkov, M., Jäntsch, U., Möslang, A., Commin, L.: Mechanical and microstructural characterization of electron beam welded reduced activation Oxide Dispersion Strengthened - Eurofer steel, Journal of Nuclear Materials, 416 (2011) 22-29

Acknowledgement

This work, supported by the European Communities under the contract of Association between EURATOM and Karlsruhe Institute of Technology, was carried out within the framework of the European Fusion Development Agreement. The views and opinions expressed herein do not necessarily reflect those of the European Commission.

Structural Materials - Refractory Alloys

Coordination of the EFDA Fusion Materials Topical Group (WP11-MAT-WWALLOY-02-03) and Fabrication of New Tungsten Alloys and Basic Characterisation (WP11-MAT-WWALLOY-02-02)

Coordination for EFDA Fusion Materials Topical Group

During the reporting period the EFDA program 2011 on tungsten and tungsten alloys development was compiled and evaluated. The according proposals were assessed. During several working and monitoring meetings the progress was monitored and discussed. The results of the Topical Group were presented at the ICFRM15 and will be published in JNM. The final activity was the formulation of the next program for 2012 and the coordination of the calls for participation and task agreements.

Introduction

Refractory materials, in particular tungsten base materials are considered as primary candidates for structural high heat load applications in future nuclear fusion power plants. The most critical issue of tungsten materials in connection with structural divertor applications is the ductile-to-brittle transition. Therefore, fabrication and testing of Charpy specimens has been performed according to the EU standards DIN EN ISO 148-1 and 14556:2006-10. That is, small size specimens – sometimes referred to as KLST type – (27 mm x 3 mm x 4 mm, 1 mm notch depth, 0.1 mm notch root radius, 22 mm span) have been used for the tests. The specimens were fabricated by electrical discharge machining (EDM). As semi-finished products round blanks were chosen due to their simple fabrication route. They can be considered either as radially or cross rolled plates. Therefore, the specification of specimen orientation fabricated from round plates could be performed similar to that of plates (Fig. 1).

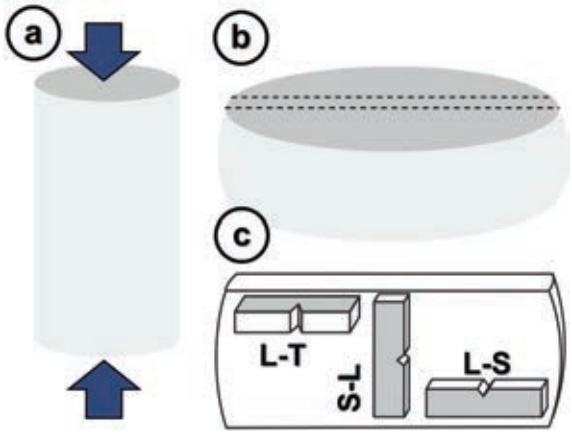

Fig. 1: (a) Round blanks are produced from sintered rods by forging them perpendicular to the axis (indicated by the arrows).
(b) The first step of specimen fabrication consisted in cutting the round blank in halves and then into a slice.
(c) For the present investigations specimens were fabricated in longitudinal-transverse (L-T), in longitudinal-short transverse (L-S), and short transverse-longitudinal (S-L) orientation.

The main requirements on tungsten materials for structural divertor applications comprise properties like high thermal conductivity, high temperature strength and stability, high recrystallization temperature, and enough ductility for an operation period of about two years under enormous neutron load. The investigations made during the recent years have shown that creep strength and recrystallization can be improved with only little effect on thermal conductivity by the use of dispersed oxides like, for example, lanthana or yttria which stabilize the grains. The intrinsic brittleness of tungsten (measured by Charpy tests), however, cannot be improved by oxide dispersion. In contrary, intercrystalline fracture is enhanced even more.

Materials, Study and Results

For the case of the ultra-high pure tungsten material it was demonstrated that due to its distinct anisotropic microstructure, commercially produced tungsten materials are difficult to use for structural applications. Like plates, round blanks show also anisotropic behaviour, that is, their microstructure can be considered as a stack of pancake-shaped grains. Therefore, the

fracture behaviour of L-S or L-T oriented specimens is much better that that of S-L orientation (Fig. 2).

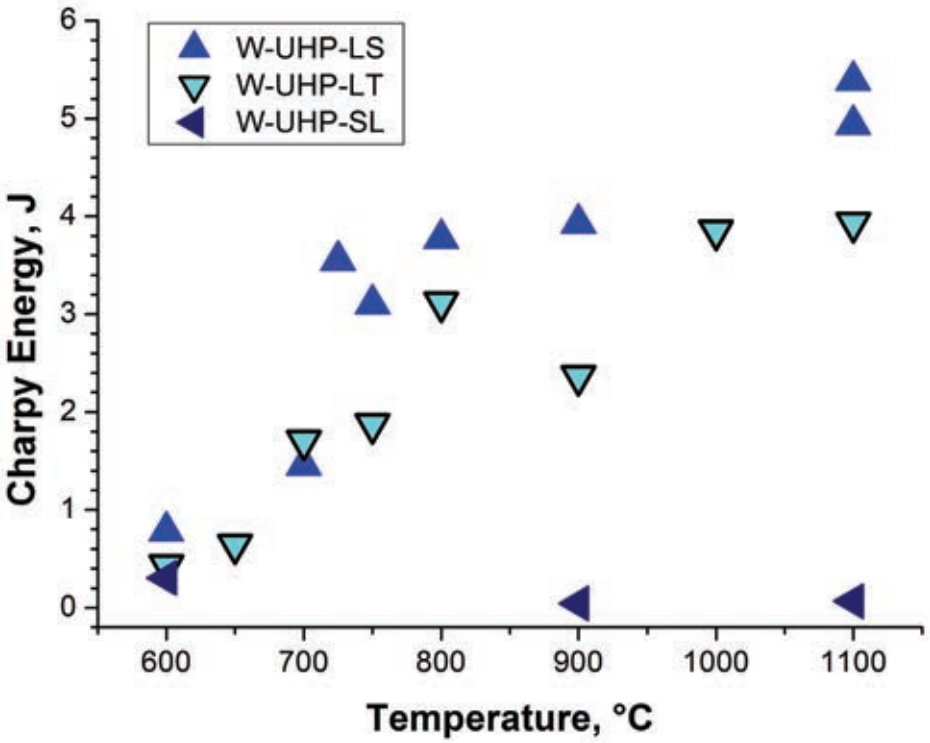

Fig. 2: Charpy test results of different oriented specimens of a round blank made of ultra-high pure tungsten. There is almost no difference between L-S and L-T oriented specimens. While DBTT is about 700-750 °C in both cases, the toughness of L-S oriented specimens is slightly higher. In L-S orientation the specimens break totally brittle without plastic deformation. Therefore, the Charpy energy of these specimens is about zero, even at testing temperatures as high as 1100 °C.

Moreover, the brittleness of tungsten materials (measured by Charpy tests) is still the main problem for their use as structural materials. And due to neutron irradiation the shift of ductile-to-brittle transition temperature (DBTT) can certainly be in the range of several hundred degrees. Therefore, the most pressing question is: How can DBTT significantly be decreased? In principle, there are three ductilisation strategies which are (1) alloying/solid solution, (2) nanostructuring, and (3) producing composite materials. The present investigations focus on the first method.

So far only rhenium is known to improve the ductility of tungsten by solid solution but its use for fusion energy applications has been ruled out for various reasons (e.g. cost and irradiation embrittlement). Iridium too is sometimes mentioned in literature to have a similar effect, though it is even more expensive. This leaves only tantalum, vanadium, molybdenum, and titanium which also form solid solution with tungsten. Round blanks of W-1%Ta, W-5%Ta, W-5%V, W-20%Mo, and W-50%Mo (weight percent) have been produced by PLANSEE. The blanks were sintered in hydrogen atmosphere and forged to a deformation degree of about 80% (Table 1). For all materials the content of several interstitial impurity elements was determined: C is less than 30 wt. ppm, S and N are less than 10 wt. ppm, and for the pure tungsten materials O is less than 30 wt. ppm.

Charpy tests in the temperature range of 400-1100 °C (in vacuum) have shown that compared to pure tungsten the DBTT of all alloys is higher, i.e. they are more brittle (Fig. 3). Only W-1%Ta shows results comparable or slightly better than pure tungsten. Therefore, it is assumed that tungsten cannot be ductilized by solid solution, except with rhenium (or maybe Iridium). As a last option, and for completeness of these studies, the effect of titanium has still to be investigated, although there is not much hope for an improvement of ductility.

Table 1: Round blanks, chemical composition, size, and fabrication details.

Material	Form	Size	Deformation Degree	Fabrication Process
W-UHP ultra-high purity	round blank	Ø180 mm, thickness 30 mm	ca. 80%	forging
WTa5 W-5wt.%Ta W-5at.%Ta	round blank	Ø180 mm, thickness 30 mm	ca. 80%	forging
WTa1 W-1wt.%Ta W-1at.%Ta	round blank	Ø180 mm, thickness 30 mm	ca. 80%	forging
WV5 W-5wt.%V W-1.4at.%V	round blank	Ø95 mm, thickness 20 mm	ca. 75%	forging
WMo50 W-50wt.%Mo W-26at%Mo	round blank	Ø95 mm, thickness 20 mm	ca. 75%	forging
WMo20 W-20wt.%Mo W-10.4at.%Mo	round blank	Ø95 mm, thickness 20 mm	ca. 75%	forging

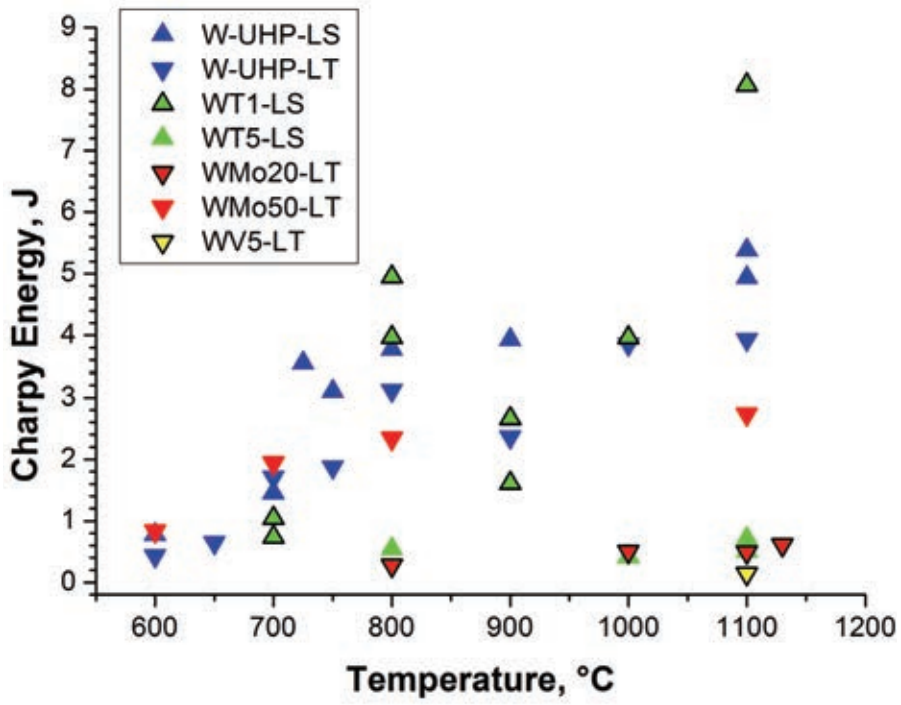

Fig. 3: Charpy test results of round blank materials with different chemical compositions (all are solid solutions).

Conclusions

The specific anisotropic microstructure of tungsten materials limits their applicability. The Charpy specimens in the present investigations have shown that real parts have to be fabricated out of plates (or blanks) with a specific orientation. The parts have to be operated with the load perpendicular to the elongated grains. In this way, tensile/bending stresses appear parallel to the plate-like grain structure which yield the highest Charpy energies and therefore, fracture toughness. But in real parts like pipes or thimbles, which play a major role in

helium-cooled divertors, the microstructure cannot be easily oriented perpendicular to the maximum bending load.

Of the three ductilisation strategies, alloying (i.e. formation of solid solution) can be almost ruled out for the case of tungsten. It has been demonstrated that Ta, V, and even Mo doesn't improve DBTT. In contrary, except for Ta in very small amounts, all solid solutions are clearly more brittle than pure tungsten. Other solid solutions with tungsten could only be formed with Ti and Nb. But first results with Ti by powder metallurgy are not promising. The use of niobium is only of academic interest (like the trial with Mo) due to its immense activation.

Staff:

S. Baumgärtner
L. Commin
B. Dafferner
S. Heger
J. Hoffmann
M. Hoffmann
U. Jäntsch
M. Klimiankou
A. Möslang
J. Reiser
M. Rieth
R. Ziegler
H. Zimmermann

Literature:

[1] Rieth, M.; Armstrong, D.; Dafferner, B.; Heger, S.; Hoffmann, A.; Hoffmann, M.D.; Jäntsch, U.; Kübel, C.; Materna-Morris, E.; Reiser, J.; Rohde, M.; Scherer, T.; Widak, V.; Zimmermann, H.; *Tungsten as a structural divertor material*; Stafa-Zürich : Trans Tech Publ., 2011, p. 11-21 (Advances in Science and Technology ; 73), ISBN 978-3-908158-56-1.

[2] Rieth, M.; Reiser, J.; Dafferner, B.; Baumgärtner, S.; *The impact of refractory material properties on the helium cooled divertor design*; 15th Internat.Conf.on Emerging Nuclear Energy Systems (ICENES 2011), San Francisco, Calif., May 15-19, 2011.

[3] Nguyen-Manh, D.; Muzyk, M.; Kurzydlowski, K.J.; Baluc, N.L.; Rieth, M.; Dudarev, S.L.; *First-principles modeling of tungsten-based alloys for fusion power plant applications*. Sandera, P. [Hrsg.] Selected, Peer-reviewed Papers from the 6th Internat.Conf.'Materials Structure and Micromechanics of Fracture (MSMF-6)', Brno, CZ, June 28-30, 2010 Stafa-Zuerich : Trans Tech Publ., 2011, p. 15-20 (Key Engineering Materials ; 465) ISBN 978-3-03785-006-0.

[4] Jäntsch, U.; Klimenkov, M.; Rieth, M.; SCherer, T.; Hoffmann, A.; *Microstructure analysis of tungsten materials produced by different fabrication routes*. 13th Internat.Workshop on Plasma-Facing Materials and Components for Fusion Applications, 1st Internat. Conf.on Fusion Energy Materials Science, Rosenheim, May 9-13, 2011.

[5] Rieth, M.; *Development of high performance materials for nuclear fusion power plants*. 2nd Brazilian – German Frontiers of Science and Technology Symposium, Potsdam, September 8-11, 2011.

[6] Rieth, M; Dudarev, S.L.; Gonzalez de Vicente, S.M.; *Review on the EFDA Programme on Tungsten Materials*. 15th International Conference on Fusion Reactor Materials (ICFRM-15), Charleston, October 16-22, 2011

Acknowledgement

This work, supported by the European Communities under the contract of Association between EURATOM and Karlsruhe Institute of Technology, was carried out within the framework of the European Fusion Development Agreement. The views and opinions expressed herein do not necessarily reflect those of the European Commission.

Two Component Powder Injection Molding (WP11-MAT-WWALLOY-01-04)

Objectives of the task

Fusion technology as possible and promising alternative energy source for the future is intensively investigated at Karlsruhe Institute of Technology. The KIT divertor design for the future DEMO fusion power plant is based on a modular concept of He-cooling finger units. More than 250,000 single parts are needed for the whole divertor system where the most promising divertor material tungsten must withstand the steady state heat loads of up to 10 MW/m².

Powder Injection Molding (PIM) as mass-oriented manufacturing method of parts with high near-net-shape precision has been adapted and developed at KIT for producing tungsten parts, which provides a cost saving alternative compared to conventional machining. While manufactured tungsten parts are normally composed of only one material composition, two component powder injection molding applied in this work allows the joining of two different materials, e.g. tungsten with a tungsten-alloy, without brazing. The motivation for this work is to manufacture the tungsten divertor parts by PIM in view of mass production aspects.

State of the art PIM R&D

First successful experiences at KIT with W-PIM were made in 2009 [1] and 2010 [2]. In the course of this work two new tungsten alloy feedstocks were developed and parts were injection molded via insert PIM. After the heat-treatment process the quality of the joining zone was investigated and characterized. This special process allows the joining of two different materials without brazing thus saving cost and time.

Materials
Two powders of pure tungsten, with an average grain size distribution in the range of 0.7 µm (W1) to 1.7 µm (W2) Fisher Sub-Sieve Size were used for preparation of binary tungsten powder particle systems. For pure tungsten parts mixtures of 50% W1 + 50% W2 are used while the doped tungsten alloys consist of 90% W1 + 10% W2.

The particle size of the powders for the preparation of the doped tungsten alloys was for the Lanthanum Oxide (La_2O_3) powder < 2.50 µm and for the Yttrium Oxide (Y_2O_3) powder < 1.50 µm.

Powder preparation
Two different tungsten compositions were produced by mechanical alloying each at 160 rpm for 2 hours in a planetary ball mill (Fritsch, Germany) using ZrO_2 balls and cans. For the first composition (W-2La_2O_3) the binary tungsten powder particle system (90% W1 + 10% W2) was doped with 2wt.% La_2O_3 powder and for the second (W-2Y_2O_3) with 2wt.% Y_2O_3.

Feedstock preparation
The most critical point of the feedstock preparation is a homogeneous distribution of agglomerate free powder in the binder matrix. After heating the powders at 80 °C for removing moisture a portion was mixed with a 50 vol.% wax/thermoplastic binder system in a kneader (Brabender, Germany) at 120 °C. After that, the feedstocks were then compounded and granulated. The feedstock compositions used for injection molding were (1) pure binary W (50% W1 + 50% W2), (2) W-2La_2O_3, and (3) W-2Y_2O_3.

Producing of parts
Injection molding was carried out on a Battenfeld Microsystem 50 injection molding machine (Battenfeld, Austria) at a feedstock temperature of 160 °C and a mold temperature of 50-60 °C. The first step is the injection molding of parts made of pure binary W. These are small discs with a thickness of 1 mm and a diameter of 11 mm. After that, the small tungsten disc

is inserted in the cavity of the machine tool, heated up to a temperature of 80-90 °C and the material composition (W-2La_2O_3 or W-2Y_2O_3) molded on it. The finished two component disc is 2 mm thick.

After injection molding and before heat-treatment the green parts have undergone solvent debinding. At first solvent debinding in n-Hexane for 48 hours at 50 °C followed by thermal debinding for ½ hour at 550 °C in dry H_2 atmosphere.

The developed heat-treatment process is a two-step procedure, first pre-sintering in a MUT sinter furnace (MUT, Germany) at 1800 °C in dry H_2 for 2 hours in order to reach a state where the material contains only closed porosity which is necessary for the HIP treatment. After that, the samples were compacted by use of a suitable HIP-cycle, performed by a HIP 3000 (Dieffenbacher, Germany). The samples were heated up to 2100 °C under 250 MPa and argon atmosphere for 3 hours. Figure 1 shows the finished parts after heat-treatment.

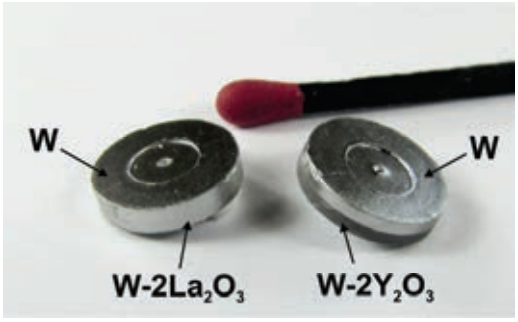

Fig. 1: 2-Component insert W-PIM: finished parts after heat-treatment.

Properties of the finished parts

Microstructure, density and hardness

Figures 2-4 show the resulting microstructure (fracture surface and metallographic section) of the finished parts after the heat-treatment process (pre-sintering and HIP). A combination of trans- and intergranular fractures typical for tungsten was observed at the SEM images of the fracture surface for pure binary (50% W1 + 50% W2) tungsten (transgranular fracture marked by arrows in Fig. 2, left). The grain size of this material is approximately between 3 and 7 µm, the theoretical density 98.6 – 99% TD and the Vickers-hardness 457 HV0.1.

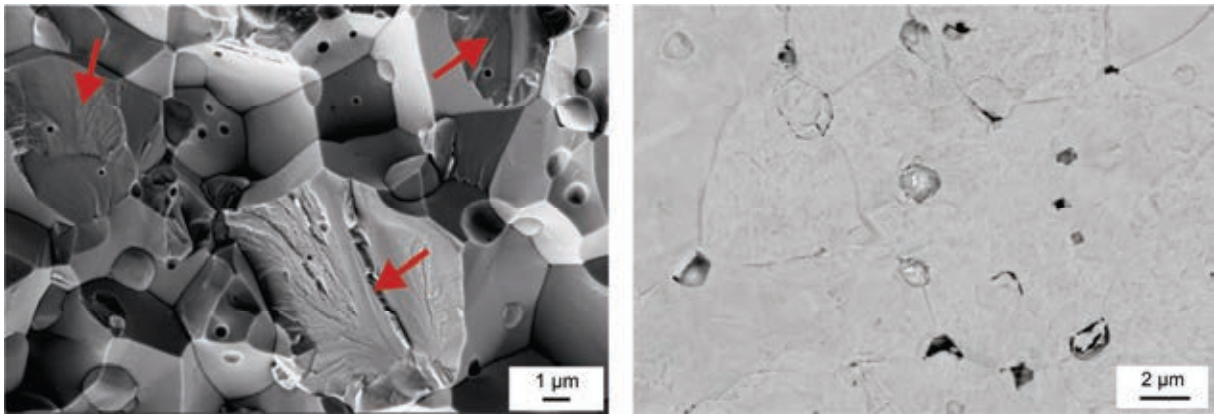

Fig. 2: SEM images of pure binary tungsten (50% W1 + 50% W2): fracture surface (left) and metallographic section (right). The areas of transgranular fracture are marked by arrows.

Figure 3 shows the result for the material composition W-2La_2O_3. The embedded spherical La_2O_3 particles in the tungsten matrix are marked by arrows. The theoretical density of this material composition is 96.5 – 97.2% TD and the Vickers-Hardness 586 HV0.1. Limited by the smaller initial grain size of the used binary tungsten powder (90% W1 + 10% W2), the grain size for this composition is also smaller, with an average value of 3 µm.

The grain size of the material composition W-2Y_2O_3 is also in a range of 3 µm. Figure 4 shows the embedded Y_2O_3 particles (see the marking) at the tungsten grain boundaries. The samples achieve a density of 96.3 – 97.1% TD and a Vickers-hardness of 617 HV0.1.

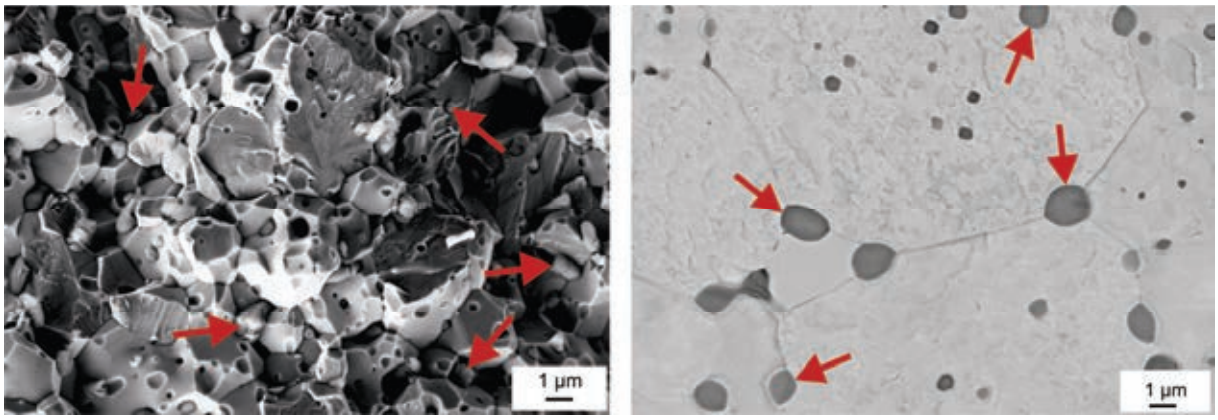

Fig. 3: SEM images of W-2La_2O_3: fracture surface (left) and metallographic section (right). A selection of the La_2O_3-particles is marked by arrows.

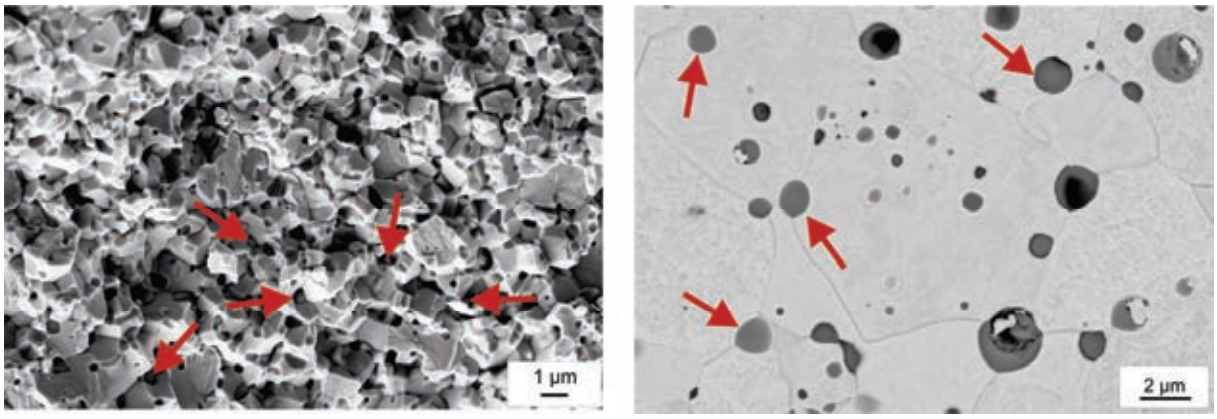

Fig. 4: SEM images of W-2Y_2O_3: fracture surface (left) and metallographic section (right). A selection of the Y_2O_3-particles is marked by arrows.

Interface characteristics

Metallographic investigations reveal that the material connection of the insert two-component powder injection molding combinations W + W-2La_2O_3 and W + W-2Y_2O_3 are successful (see Figs. 5 and 6, left and middle). In the seam of the joining zone no cracks or gaps are visible. In order to obtain detailed information on the transition from one material to the other at the interface, Auger electron spectra were recorded. Figure 5 and 6 (right) show the elemental concentration across the interface of the finished parts. The tungsten matrix is shown in red and the colour of the embedded particles (La_2O_3 respectively Y_2O_3) is black. It can be seen that a solid bond of the material interface was obtained.

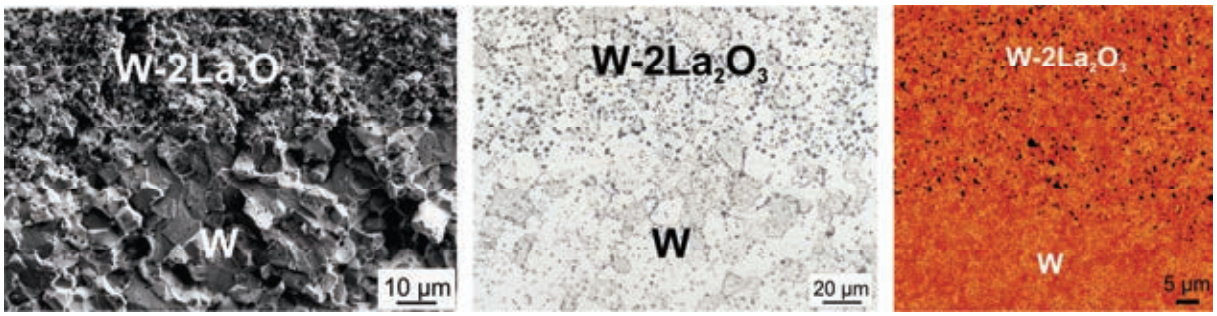

Fig. 5: Interface characteristics of W + W-2La_2O_3: SEM images of the fracture surface (left), metallographic section (middle), AES-Map (right). The W matrix is shown in red and the colour of the embedded La_2O_3 particles is black.

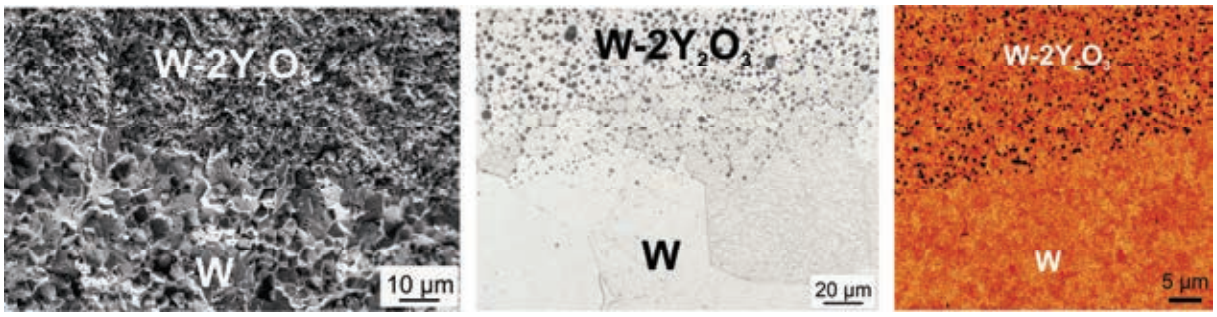

Fig. 6: Interface characteristics of W + W-2Y_2O_3: SEM images of the fracture surface (left), metallographic section (middle), AES-Map (right). The W matrix is shown in red and the color of the embedded Y_2O_3 particles is black.

Conclusions and outlook

The motivation for this work was the investigation of a joining method for two different materials by using insert two-component powder injection molding. The experience, the knowledge and the results of past pretests on conventional one-component parts such as the tungsten tile was transferred to produce basic two-component parts via insert injection molding. An investigation of the joining zone was done by analyses using scanning electron microscopy (SEM) and Auger electron spectroscopy (AES). The results of the analyses, e.g. density, hardness, microstructure of the finished samples, and the quality of the joining zone, were characterized and found to be acceptable for further investigations. This is a promising outcome for manufacturing of tungsten and tungsten alloy divertor parts by the two-component powder injection molding process. The development of new material combinations processible with a new fully automatically two-component powder injection molding tool to replicate fusion relevant components such as the tungsten tile and the tungsten alloy thimble in one step without brazing will further enhance the use of mass production PIM parts for the DEMO fusion reactor. The so produced mockups will undergo high heat flux tests at the Efremov Institute, St. Petersburg, Russia, within the frame of divertor finger mock-up test program.

Staff:

S. Antusch
I. Fuchs
P. Holzer
M. Müller
M. Offermann
G. Pintsuk (FZ Jülich)
V. Piotter
H. Walter
T. Weingärtner

Literature:

[1] S. Antusch, P. Norajitra, V. Piotter, H.-J. Ritzhaupt-Kleissl, Powder Injection Molding for mass production of He-cooled divertor parts. Journal of Nuclear Materials 417 (2011), 533-535.

[2] S. Antusch, P. Norajitra, V. Piotter, H.-J. Ritzhaupt-Kleissl, L. Spatafora, Powder Injection Molding – An innovative manufacturing method for He-cooled DEMO divertor components. Fusion Engineering and Design 86 (2011), 1575-1578.

Acknowledgement

This work, supported by the European Communities under the contract of Association between EURATOM and Karlsruhe Institute of Technology, was carried out within the framework of the European Fusion Development Agreement. The views and opinions expressed herein do not necessarily reflect those of the European Commission.

Deep Drawing of Tungsten Plates (WP11-MAT-WWALLOY-01-01)

Introduction

The reference design of a helium cooled divertor for future fusion reactors makes use of hundreds of thousands of finger units consisting of a pressurized structural part called a thimble [1-3]. Due to the high number of parts needed, the thimble has to be fabricated by mass production techniques like deep drawing. As the thimble is a pressurized part exposed to an internal pressure of 100 bars, the demands for the material are high, which means that it requires the best available tungsten material. Former work has shown that pure tungsten material has the best impact properties and has to be preferred over other commercially available tungsten materials, such as that doped with potassium (PLANSEE name WVM or WVMW) or strengthened with oxides like lanthanum oxide (PLANSEE name WL10) [4-7]. Furthermore the inherent weakness of the grain boundaries has to be taken into account, which requires the need for grains that are aligned to the contour of the part (grain boundary alignment).

This paper describes the successful deep drawing of a 1 mm tungsten plate in high vacuum at 600 °C. In doing this, a thimble can be machined with grains that follow the contour. More details can be found here [8].

Deep drawing of a tungsten thimble made from a tungsten plate

The actual design for a He-cooled divertor for DEMO makes use of a thimble like part made of tungsten that is a pressurized component and has to be made of a structural material [1]. Due to its unfavourable grain orientation, rod material cannot be used to machine a thimble by turning or milling (Fig. 1). The most promising machining route consists of deep drawing of a W plate which results in grains that follow the contour. It can be put on hold that for components made of tungsten ‘grain boundary alignment’ is a highly necessary tool in order to create the best possible arrangement for external forces acting on the weak grain boundaries. Now the still open question is: Is it possible to deep draw a thimble from a 1 mm tungsten plate?

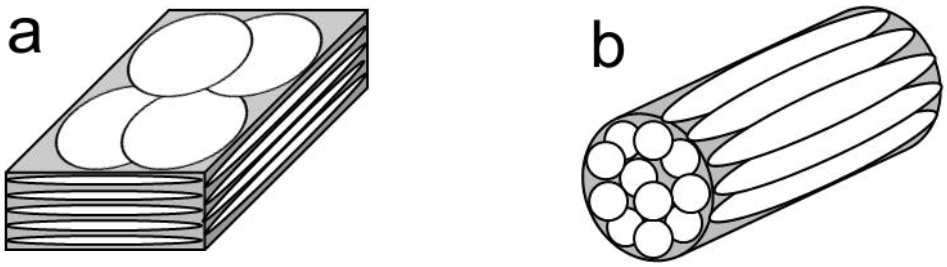

Fig. 1: Microstructure of a tungsten rod (a) and a tungsten plate (b). The grains in the rod can be seen as a bundle of ‘fibres’ and the grains in the plate can be considered as a stack of ‘pancakes’.

In a deep drawing tool, tungsten blanks with different diameter were deep drawn. The deep drawing tool is made of stainless steel (316) and consists of a hold-down device fixed with several screws, a guided male die part and a backbone (see Fig. 2). This tool is placed into the furnace of a universal test device (Zwick030). At the beginning a vacuum of about 10^{-5} mbar is created, and the temperature of the tungsten blank is adjusted to 600 °C. Then the male die part is pushed onto the tungsten blank with a velocity of 0.1 mm/min. The deep drawing was performed on blanks with a diameter of 23 mm and 26 mm. It can be seen from Figure 3 that both the blanks with a diameter of 23 mm and the blanks with a diameter of 26 mm can be deep drawn to a thimble with an inner diameter of 13 mm and an outer diameter of 15 mm. The thimbles are intact with excellent surfaces (see Fig. 4). By deep drawing a 26 mm blank, a thimble with a height of 10 mm can be manufactured. An optical micrograph of a cut, polished and etched thimble shows the grains that follow the contour (see Fig. 5).

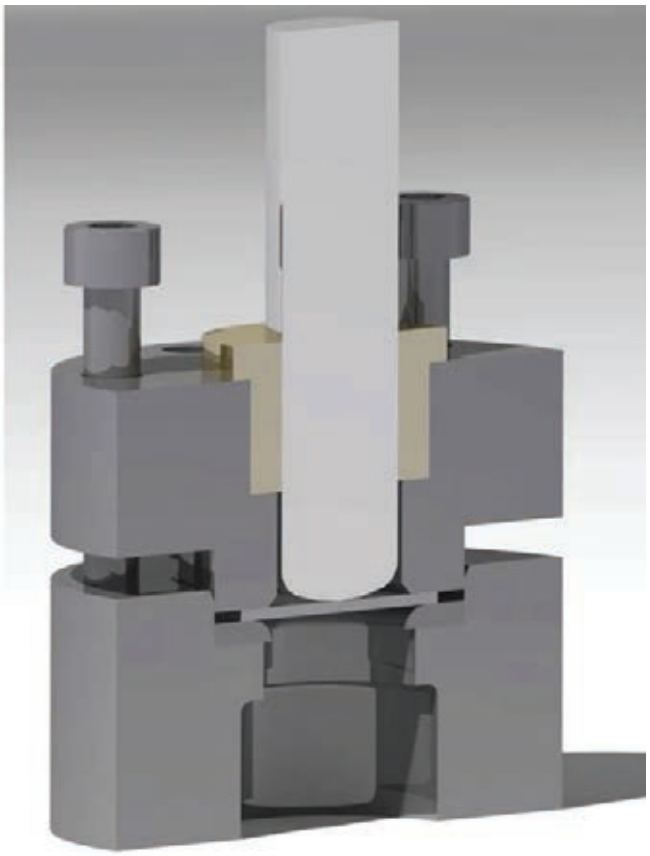

Fig. 2: The deep drawing tool is made of stainless steel (316). The tungsten plate is fixed by a hold down device pressed by screws. The whole tool is placed into the furnace of a universal test device.

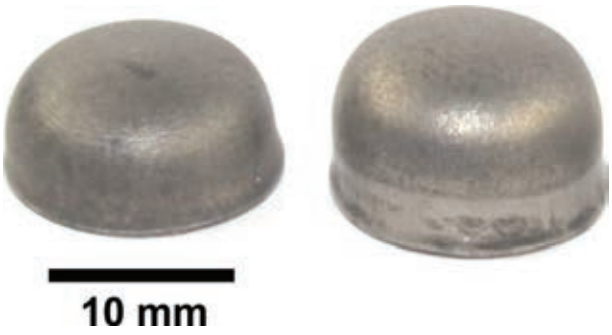

Fig. 3: Left: a blank with a diameter of 23 mm leads to a deep drawn thimble with a height of 8 mm. Right: a diameter of 26 mm leads to a height of 10 mm. Deep drawing was performed in a high vacuum at 600°C.

Fig. 4: Quality of the deep drawing process. Left: the top surface is extremely smooth. Middle: view inside the thimble. Right: the inner surface is also smooth.

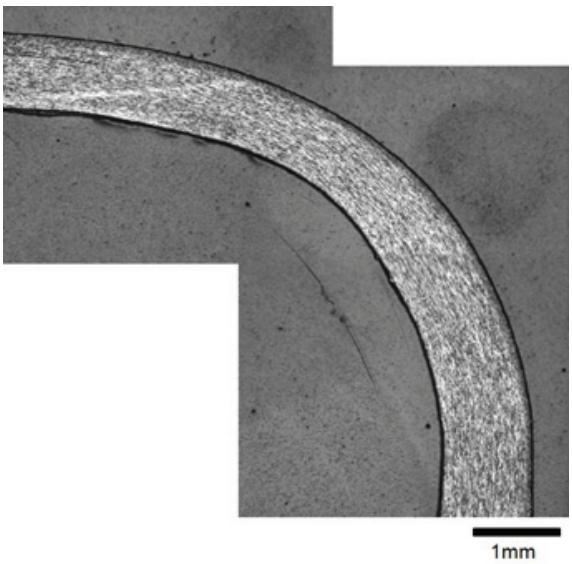

Fig. 5: Optical micrograph of a deep drawn tungsten thimble. The thimble was cut, polished and etched. The image shows the grains following the contour of the thimble.

Conclusions

The actual design of a helium cooled divertor makes use of hundreds of thousand finger units consisting of a pressurized structural part called a thimble. This thimble is made of

tungsten and exposed to an internal pressure of 100 bars. It is further known that pressurized parts always fail due to tangential stress as it is by a factor two higher than stress in axial direction. Considering the inherent weakness of the grain boundaries of tungsten, it is obvious that a thimble cannot be made of rod material since a rod has grains like 'fibres' in the axis direction. In this combination the orientation of the weak grain boundaries are congruent to the most stressed direction of the pressurized thimble.

Among all known commercially available tungsten materials, pure tungsten shows the best impact bending fracture behaviour (excluding tungsten with rhenium). This behaviour can neither be improved by doping tungsten with potassium nor by adding oxides, e.g. lanthanum oxide. So the material recommendation for the thimble is pure tungsten.

During fabrication of tungsten plate materials, the plate is exposed to hot and cold work, where cold work is defined as rolling below the recrystallisation temperature of the plate material. The outcome of this fabrication route is an anisotropic material which has different properties depending on the rolling direction. For more details on the anisotropic tungsten material properties (tensile tests and Charpy tests) see [8].

This report shows that deep drawing of a tungsten plate was successful. A tungsten plate with a thickness of 1 mm and a diameter of 26 mm can be deep drawn in a universal testing device under a high vacuum and at high temperature to a thimble with a height of 10 mm and an outer diameter of 15 mm. The deep drawing technique combines two important benefits: (i) it fits the needs of a mass production technique which is necessary taking into account the large number of several hundred thousand cooling units required, and (ii) due to the weak grain boundaries of tungsten the grains should follow the contour of the thimble which is also realized by deep drawing a plate, in other words, 'grain boundary alignment'. The on-going investigation will further focus on an improvement of the deep drawing process such as deep drawing at higher speed by increasing the temperature. A further aim is to increase the height of the thimble by using larger blanks. Additional geometries beside thimbles, e.g. u-profiles, are also under investigation.

Staff:

S. Baumgärtner
D. Bohlich
B. Dafferner
M. Hoffmann
U. Jäntsch
A. Möslang
J. Reiser
M. Rieth
R. Ziegler
H. Zimmermann

Literature:

[1] P. Norajitra, A. Gervash, R. Giniyatulin, T. Ihli, W. Krauss, R. Kruessmann, V. Kumetsov, A. Makhankov, I. Mazul, I. Ovchinnikov, Fus. Eng. and Des. 81 (2006) 341-346.

[2] P. Norajitra, L.V. Boccaccini, A. Gervash, R. Giniyatulin, N. Holstein, T. Ihli, G. Janeschitz, W. Krauss, R. Kruessmann, V. Kuznetsov, A. Makhankov, I. Mazul, A. Moeslang, I. Ovchinnikov, M. Rieth, B. Zeep, J. Nucl. Mater. 367 (2007) 1416-1421.

[3] P. Norajitra, R. Giniyatulin, T. Ihli, G. Janeschitz, W. Krauss, R. Kruessmann, V. Kuznetsov, I. Mazul, V. Widak, I. Ovchinnikov, R. Ruprecht, B. Zeep, Fus. Eng. and Des. 82 (2007) 2740-2744.

[4] M. Rieth, A. Hoffmann, Fus. Sci. Technol. 56 (2009) 1018-1022.

[5] M. Rieth, A. Hoffmann, Int. J. Refract. Met. H. Mater. 28 (2010) 679–686.

[6] M. Rieth, A. Hoffmann, Adv. Mater. Res. 59 (2009) 101-104.

[7] M. Rieth, J.L. Boutard, S.L. Dudarev, T. Ahlgren, S. Antusch, N. Baluc, M.-F. Barthe, C.S. Becquart, L. Ciupinski, J.B. Correia, C. Domain, J. Fikar, E. Fortuna, C.-C. Fu, E. Gaganidze, T.L. Galán, C. García-Rosales, B. Gludovatz, H. Greuner, K. Heinola, N. Holstein, N. Juslin, F. Koch, W. Krauss, K.J. Kurzydlowski, J. Linke, Ch. Linsmeier, N. Luzginova, H. Maier, M.S. Martínez, J.M. Missiaen, M. Muhammed, A. Muñoz, M. Muzyk, K. Nordlund, D. Nguyen-Manh, P. Norajitra, J. Opschoor, G. Pintsuk, R. Pippan, G. Ritz, L. Romaner, D. Rupp, R. Schäublin, J. Schlosser, I. Uytdenhouwen, J.G. van der Laan, L. Veleva, L. Ventelon, S. Wahlberg, F. Willaime, S. Wurster and M.A. Yar, doi:10.1016/j.jnucmat.2011.01.075.

[8] J.Reiser, M. Rieth, B. Dafferner, S. Baumgärtner, R. Ziegler, A. Hoffmann, Fusion Eng. and Des. (2011), doi:10.1016/j.fusengdes.2011.07.011

Acknowledgement

This work, supported by the European Communities under the contract of Association between EURATOM and Karlsruhe Institute of Technology, was carried out within the framework of the European Fusion Development Agreement. The views and opinions expressed herein do not necessarily reflect those of the European Commission.

Development of Composite Tungsten Foil Materials (WP11-MAT-WWALLOY-02-01)

Introduction

Strategies to ductilize tungsten and to prevent the material from delaminating are by synthesizing (i) a tungsten alloy, (ii) a nanostructured tungsten material or by (iii) synthesizing a tungsten composite. For a tungsten composite we can distinguish between a (i) particle reinforced tungsten, (ii) random short fibre reinforced tungsten, (iii) uniaxial long fiber tungsten or, and that will be introduced in this work (iv) a tungsten laminate. In this report we will present the synthesis and characterization of a tungsten laminate made by assembling several layers of thin tungsten foil. It is well known, that bcc metals can be ductilized by prior cold work [1]. Furthermore, assessment on ODS tungsten shows, that the higher the degree of deformation the higher the recrystallization temperature and the higher the fracture toughness [2]. Other authors mention that the DBTT can be reduced by cold work, and that the higher the degree of deformation the lower the DBTT [3]. The idea now consists in taking a tungsten semi-finished product that has experienced a break down rolling with a high degree of deformation, a high degree of cold work: a tungsten foil. A tungsten foil with a thickness of 0.1 mm can be bent plastically at room temperature (Fig. 1). By assembling several layers of this ductile tungsten foil followed by a subsequent joining process, the ductile material properties of the foil should be expanded to a bulk material.

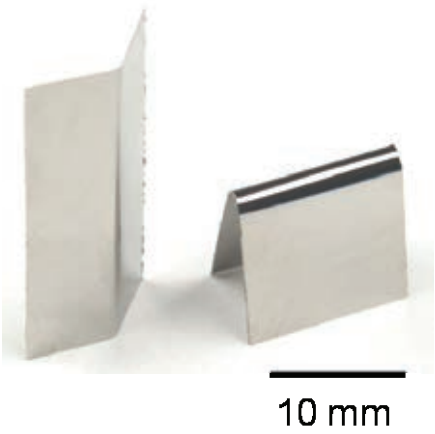

Fig. 1: Preliminary bending tests with tungsten foil with a thickness of 0.1 mm. The tests were performed at room temperature. The rolling direction (0°) is from bottom to top. It can be seen that tungsten foil is ductile at room temperature.

In this report we will examine the properties of a tungsten laminate made of several layers of ductile tungsten foil and address the following questions:

- Is it possible to expand the ductile properties of a tungsten foil to a bulk material by assembling and joining several layers of tungsten foil?
- How are the mechanical properties of a tungsten laminate if the tungsten foil was annealed (1 h / 1800 °C)?
- Can more complex structures like e.g. pipes be synthesized by such a tungsten laminate and what are their properties?

Syntheses of a tungsten laminate

The material, which has been chosen for the syntheses of a tungsten laminate, is rolled 99.97% pure tungsten foil with a thickness of 0.1 mm. This commercial material was produced by PLANSEE Metall GmbH, Reutte/Austria, in a powered metallurgical route. After sintering, the plate/foil experienced a break down rolling with a high degree of deformation resulting in grains that can be compared to a stack of ‘pancakes’ [4]. The material which has been chosen for brazing material is a commercial eutectic silver copper alloy (72 wt.% Ag and 28 wt.% Cu) with a thickness of 0.1 mm. The melting point of this material is at 780 °C. One layer of tungsten foil and one layer of copper alloy were put on each other in turn. Finally the stack of foil consists of 20 layers of tungsten foil and 19 layers of copper alloy in between. Brazing takes place in high vacuum ($1*10^{-4}$ mbar) at 800 °C. At 800 °C the furnace is shut down immediately and the sample is cooled down. In addition, a tungsten laminate was synthesized with annealed tungsten foil (1 h at 1800 °C). Afterwards the assembling and joining of a laminate took place as described above.

Charpy impact tests with laminate

The tungsten plate material used for benchmark experiments was unalloyed 99.97% pure tungsten with a thickness of 4 mm. This commercially available material was produced by PLANSEE Metall GmbH, Reutte/Austria. After sintering, the plate was rolled with a high degree of deformation resulting in elongated grains leading to a microstructure that can be considered as a stack of 'pancakes'. The optical micrograph of a longitudinal section of rolled tungsten plate can be seen elsewhere [4]. Charpy tests were performed based on the EU standards DIN EN ISO 148-1 and 14556:2006-10. According to this standard the small size specimens have the following dimensions: 3 mm x 4 mm x 27 mm, 22 mm span, 1 mm notch depth, 0.1 mm notch root radius. The samples were orientated in 0° direction (L-S type) and all samples were shaped by electrical discharged machining (EDM). Fig. 2 shows a finally shaped Charpy test sample made from tungsten laminate material. The Charpy tests were performed in vacuum (10^{-3} mbar). More details on the Charpy test device can be seen elsewhere [4-5].

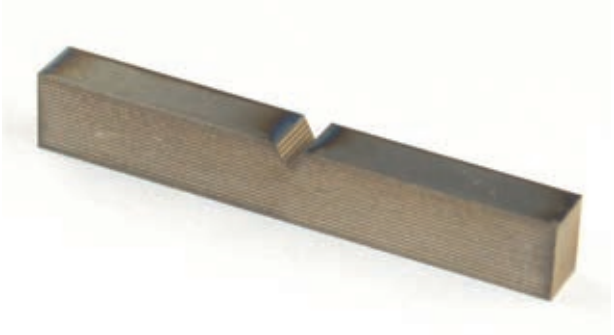

Fig. 2: Charpy test sample, synthesized by 20 layers of tungsten foil (thickness 0.1 mm), joined with 19 layers of an eutectic silver copper brazing filler (thickness 0.1 mm). The dimensions are equal to the KLST type: 3 x 4 x 27 mm^3, 1 mm notch depth.

Results of the Charpy tests

In general body centred cubic materials show classical embrittlement behaviour containing a clear transition from brittle (at lower temperatures) to ductile (at higher temperature) fracture. Tungsten however is different and has two transitions (i) one from brittle to delamination and then (ii) from delamination to ductile [6]. It can be seen clear in Fig. 3 that for the samples made from 4 mm plate material, the transition from brittle to delamination occurs at 500 °C. But unfortunately there is no transition from delamination to ductile. Even at 1000 °C, which was the highest tested temperature, the fracture is still in delamination type. A comparison of results obtained by samples made of tungsten plate material with results obtained from samples made of tungsten laminate material shows, that the idea of expanding the ductile properties from the foil to a bulk material was successful realized. The laminate material can dissipate energy at low temperatures and even at room temperature the sample made from tungsten laminate can dissipate nearly 2 J (Fig. 3). At 100 °C already 5 J can be dissipated by the laminate sample. The highest amount of energy dissipation appears at 300 °C and is about 10 J. This value is again higher than the highest energy dissipation value measured on samples made from tungsten plate material (e.g. 500 °C, 8 J). It can be concluded that the ductilisation of tungsten was successful.

Now the question arises: How are the Charpy impact properties if the tungsten foil was annealed? Fig. 3 shows a comparison of results obtained from samples made of annealed tungsten plate material (1 h / 2000 °C) and samples made of laminate that was synthesized by annealed tungsten foil (1 h / 1800 °C). The results show that annealed tungsten plate material cannot dissipate energy even at 1000 °C. At 1000 °C the fracture is still brittle. The annealed tungsten laminate material is different. Here a transition from ductile to brittle takes place at 500 °C. These results show that annealed tungsten plate material is a no go for structural plates. The behaviour of the annealed tungsten laminate material however is excellent as the transition temperature occurs in the same temperature regime as the transition temperature for tungsten plate material (as-received).

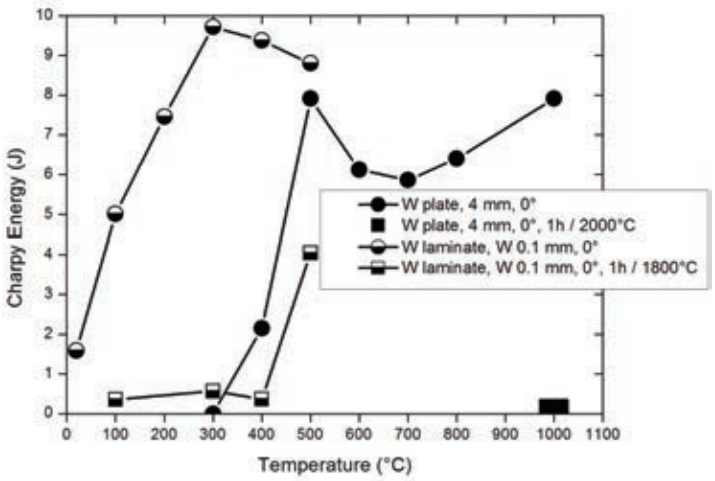

Fig. 3: Results of the Charpy impact tests. The samples cut from the 4 mm tungsten plate were oriented in L-S type and the samples made from a tungsten laminate were orientated in rolling direction (see L-S type). The comparison of the material as-received and the material in annealed condition show large improvements of the Charpy impact properties by the laminate material.

Comparing the results of the laminate material made by foil as-received and by foil annealed (1 h / 1800 °C) one can define a best case barrier (as-received foil) and a worst case barrier (annealed foil). Doing this, one can assume that the transition temperature of laminate material in any annealed state should be between these barriers.

It can be concluded, that the idea of expanding the ductile material properties of a tungsten foil to a bulk material by synthesizing a tungsten laminate was successfully realized. Even a laminate made of annealed tungsten foils is nearly as good as tungsten plate material as-received. However, a lot of high temperature applications require more complex structures than plates like e.g. tungsten pipes. So the question to address here is: Is it possible to synthesize laminate tungsten pipes and what are their properties?

Syntheses and assessment of a tungsten pipe made of tungsten foil

Till now there are no ductile tungsten pipes available that can be used as structural parts. Compared to e.g. steel or molybdenum alloys, it is not possible to extrude a tungsten pipe. So the only possibility to manufacture a tungsten pipe is by drilling a hole in a tungsten rod. It was shown in previous work that tungsten rod material with a diameter of roughly 14 mm has grains elongated in axis direction with an aspect ratio of roughly 1:3 [7] and that the microstructure can be compared to a bundle of fibres [4]. Furthermore it has to be taken into account, that the grain boundaries are the weakest chain link in a tungsten material and that cracks intent to penetrate along the weak grain boundaries resulting in anisotropic fracture behaviour.

Using a tungsten pipe made from a rod for an internal pressure component, the direction of the elongated weak grain boundaries is equal to the expected crack direction caused by tangential stresses. But how can we manufacture a tungsten pipe that can be used for structural parts? The new idea now consists in manufacturing a tungsten pipe using a ductile tungsten foil. By rolling up a tungsten foil, followed by a subsequent joining process, a tungsten pipe can be synthesized. This tungsten pipe made of tungsten foil has many advantages like e.g. that the grains of the tungsten pipe foil follow the contour of the pipe. Doing this, the requirement of ‘grain boundary alignment’, which is a highly necessary tool for structural tungsten parts, is fulfilled [8]. In this case any external force exposed to the pipe will hit the grains in the optimum way which is perpendicular to the flat grain surface, and the problem of the weak tungsten grain boundaries is avoided.

Synthesis of a tungsten pipe

Materials used to synthesize a tungsten pipe is rolled unalloyed 99.97% pure tungsten foil with a thickness of 0.1 mm as well as an interlayer of a copper alloy (eutectic silver copper, 72 wt.% Ag and 28 wt.% Cu) with a thickness of 0.1 mm. The tungsten foil and the copper alloy foil are cut with a cutting device in dimensions of 27 x 200 mm^2. The rolling direction of the tungsten foil is equal to the 200 mm side of the foil. One foil of tungsten and one foil of copper alloy is put on each other and fixed in a holder. The holder enables an easy and precise roll up of the foil. The brazing takes place in high vacuum ($1*10^{-4}$ mbar). At 800 °C the furnace is shut down immediately and the sample is cooled down. The final wall thickness of the tungsten pipe is ca. 1 mm. The final tungsten pipe made form tungsten foil can be seen in Fig. 4.

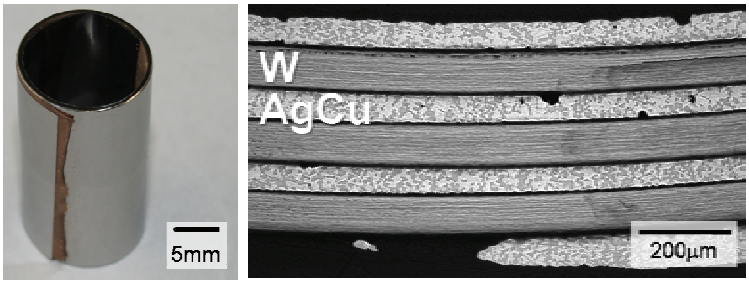

Fig. 4: Left: a tungsten pipe made of tungsten foil. Length is 27 mm, outer diameter is 15 mm, wall thickness ca. 1 mm. Right: optical micrograph of a cross section of a tungsten pipe made form tungsten foil showing several layers of tungsten foil (thickness 0.1 mm) and an eutectic silver copper brazing filler (thickness 0.1 mm).

With tungsten pipes which were synthesized as described, Charpy impact test were performed and compared to tungsten pipes made from drilling and turning a hole in a tungsten rod.

Charpy impact tests on tungsten pipes

Tungsten rod material used to manufacture tungsten pipes for benchmark experiments was rolled unalloyed 99.97% pure tungsten with a diameter of 25 mm. This commercial material was produced by PLANSEE Metall GmbH, Reutte/Austria, in a powered metallurgical route. After drilling and turning, the tungsten pipes have a length of 27 mm, an outer diameter of 15 mm and a wall thickness of 1 mm. Tungsten pipes made of tungsten foil will be compared to drilled tungsten pipes.

Charpy tests were performed on the basis of the EU standards DIN EN ISO 148-1 and 14556:2006-10. According to this standard the small size specimens have the following dimensions: 3 mm x 4 mm x 27 mm, 22 mm span, 1 mm notch depth, 0.1 mm notch root radius. However, the samples used for instrumented Charpy tests here were pipes with an outer diameter of 15 mm, a wall thickness of 1 mm and a length of 27 mm on a 22 mm span. More details on the Charpy test device can be seen elsewhere [4-5].The maximum energy of the striker is about 20 J. If the energy absorption of the test sample is higher than 20 J the striker is stuck in the sample body. All tests were performed in atmosphere. Three samples of a tungsten pipe made from rod material were tested: one at room temperature, one at 300 °C and one at 700 °C. Four samples of a tungsten pipe made from tungsten foil were tested in the temperature range from room temperature till 300 °C.

Results of the Charpy tests

Pipes made from rod material cannot absorb energy in a Charpy test. The energy dissipation at room temperature, 300 °C and 700 °C is smaller than 2 J which in again a strong proof that rod material cannot in any case be used for structural tungsten parts. Having a look at the fractured pipe tested at 300 °C shown in Fig. 5 (left) it can be seen that grain boundaries

are the preferred crack propagation direction. Even if the striker hits the pipe perpendicular to the axis direction of the pipe, the fractured pipe shows cracks in axis direction which is equal to the direction of the elongated grain boundaries. It can be concluded, that using tungsten pipes made from tungsten rods for structural applications is a no go.

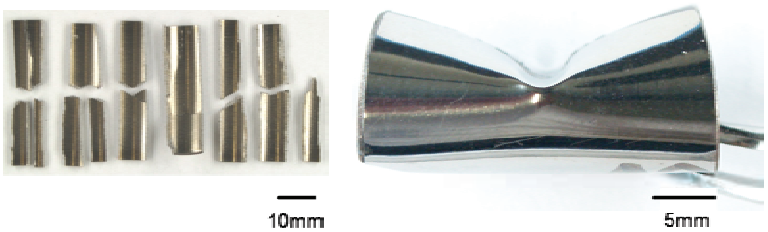

Fig. 5: Left: result of a Charpy test with a tungsten pipe made from rod material. The energy dissipation was 0 J at 300 °C. Right: result of a Charpy test with a tungsten pipe made from tungsten foil. The energy dissipation was at least 20 J. The pipe has no leak and is completely ductile.

The situation appears different for tungsten pipes made from tungsten foil. Here the energy absorption at room temperature, at 100 °C, 200 °C, and 300 °C is at least 20 J. For some samples the striker even got stuck in the sample. Moreover the samples tested at 200 °C and 300 °C are completely ductile and show no crack or leakage (Fig. 5 right). The high amount of energy absorption capability combined with the appearance of complete ductile fracture even at low temperatures makes a tungsten pipe made from a tungsten foil to the first tungsten pipe that can be used for structural applications.

Summary

In this report the potential of a tungsten laminate made from tungsten foil was assessed. It was shown by Charpy tests, that a tungsten laminate can dissipate energy at lower temperatures compared to tungsten plate material and that the idea of expanding the ductile properties of a tungsten foil to a bulk material by assembling and joining several layers of tungsten foil was successfully realized. Moreover, even Charpy test samples made from annealed (1 h / 1800 °C) tungsten foil show a brittle ductile transition at the same temperature range as tungsten plate material as-received. Finally the first tungsten component that can be used for structural applications was introduced: a tungsten pipe made by rolling-up a tungsten foil, followed by a subsequent brazing process can dissipate high amounts of energy in a Charpy test and shows complete ductile fracture already at 200 °C. One can think of using this tungsten laminate, especially the tungsten pipe, for several structural applications (e.g. divertor technology) in future fusion devices.

Staff:

S. Baumgärtner
D. Bohlich
B. Dafferner
M. Hoffmann
U. Jäntsch
A. Möslang
J. Reiser
M. Rieth
R. Ziegler
H. Zimmermann

Literature:

[1] P.B. Hirsch, S.G. Roberts, J. Samuels, *Rev. Phys. Appl.* **23**, 409 (1988).

[2] I. Stresemann, P. Heel, W. Spielmann, A. Hoffmann, 17 Plansee Seminar (2009).

[3] E. Lassner, W.-D. Schubert, *Tungsten: Properties, Chemistry, Technology of the Element, Alloys, and Chemical Compounds*, Kluwer Academic/Plenum Publishers, New York, (1999).

[4] M. Rieth, A. Hoffmann, Int. J. Refract. Met. Hard Mater. **28**, 679 (2010).

[5] M. Rieth, A. Hoffmann, Adv. Mater. Res. **59**, 101 (2009).

[6] M. Rieth et al., Adv. Sci. Tec. **73**, 11, (2010).

[7] D. Rupp, S.M. Weygand, J. Nucl. Mater. 386-388 (2009) 591-593.

[8] J.Reiser, M. Rieth, B. Dafferner, S. Baumgärtner, R. Ziegler, A. Hoffmann, Fusion Eng. and Des. (2011), doi:10.1016/j.fusengdes.2011.07.011

Acknowledgement

This work, supported by the European Communities under the contract of Association between EURATOM and Karlsruhe Institute of Technology, was carried out within the framework of the European Fusion Development Agreement. The views and opinions expressed herein do not necessarily reflect those of the European Commission.

Fracture-Mechanical (FM) and Microstructural Characterization of Tungsten Alloys (WP11-MAT-WWALLOY-02-05)

Objectives

Inherent low fracture toughness of tungsten combined with the high DBTT are major drawbacks for structural application of tungsten alloys. Furthermore, FM properties are expected to exhibit strong anisotropy due to (i) different grain shape/orientation with respect to the rolling direction and (ii) texture. The current task aims at FM characterization of different laboratory and industry scale W-alloys (W, W-Ti, W-V, W-Ta) and their ODS variants in the interesting temperature window for fusion applications (RT-1300 °C). Emphasis is put on the investigation of microstructure and load rate dependence of the fracture toughness (K_{IC}). The investigations are accompanied by fractographic and microstructural investigations.

Performed work

Fracture behaviour of commercial polycrystalline tungsten alloy fabricated through the powder metallurgic process involving sintering into rods and subsequent forging into round blanks was studied in a wide temperature range from 23 to 800 °C. Tests above 350 °C were performed in high vacuum to avoid oxidation of the specimens. Quasi-static three point bending tests were performed on pre-cracked rectangular SENB specimens with dimensions of 3x4x27 mm and with machined V-shaped notches. Sharp crack starter notches have been introduced by means of a razor blade polishing. This method allowed reduction of the notch radius down to 20 µm. During the experiments, force, displacement and temperature were recorded.

The microstructure of round blank tungsten was characterized by existence of platelet shaped grains being stacked parallel to a round blank base, see Fig. 1a and b. For the study of the influence of the fabrication route specific anisotropic microstructure on the FT and ductile-to-brittle transition the specimens have been extracted in three different, i.e. longitudinal (*L-R*), radial (*R-L*) and circumferential (*C-R*) orientations, see Fig. 1 c.

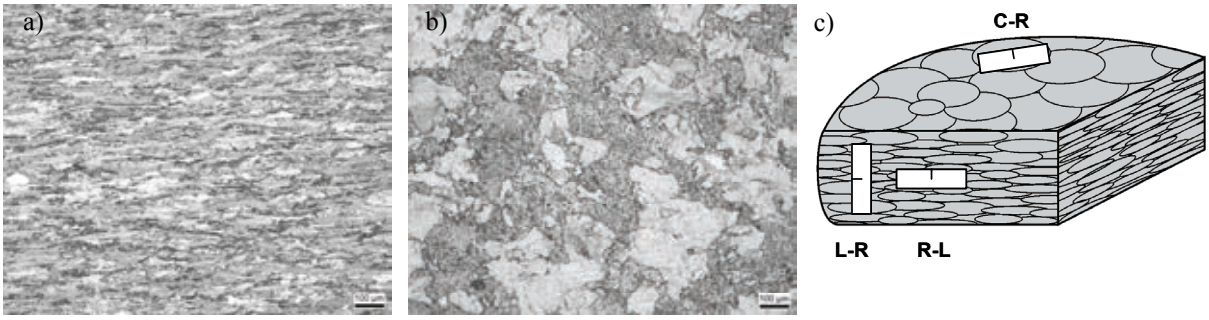

Fig. 1: Microstructure of polycrystalline round blank tungsten a) plane transverse to base; b) plane parallel to base; c) specimen orientations for the study of the influence of anisotropy on the fracture toughness.

Fig. 2 shows load vs. displacement curves of selected specimens. The fracture mechanical experiments yielded distinctive fracture behaviour for each investigated specimen orientation. At RT all specimens failed by a brittle manner. The maximum load level achieved in *L-R* orientation was however considerably lower than the maximum load levels achieved in *R-L* and *C-R* orientations. For longitudinal *(L-R)* orientation the crack propagated predominantly in intergranular manner at all test temperatures as revealed in SEM micrographs presented in Fig. 3. The lowest test temperature with an observable onset of plastic deformation was 400 °C. The specimens extracted in radial (*R-L*) and circumferential (*C-R*) orientations, in contrast, failed by a transcrystalline cleavage at RT as shown in Fig. 3. Radially oriented (*R-L*) specimens showed a crack deflection at intermediate test temperatures which was accompanied by a change of fracture behaviour from transgranular cleavage at room temperature

to predominantly intergranular fracture at test temperatures above 400 °C, see Fig. 3. The deviation from the linear load vs. displacement behaviour was observable already at 200 °C. For the specimens extracted in circumferential orientation (*C-R*) coexistence of transgranular cleavage and intergranular fracture occurring in mutually orthogonal planes has been observed from 300 °C up to the highest investigated temperatures.

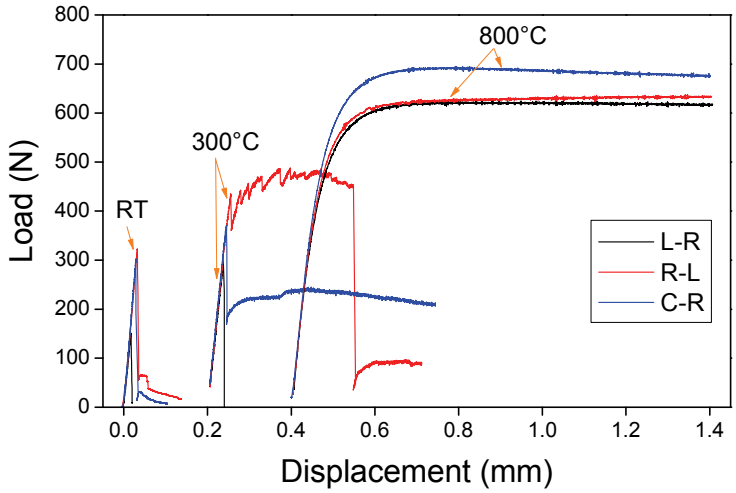

Fig. 2: Load vs. displacement of polycrystalline round blank tungsten for three different specimen orientations. Displacement controlled tests were performed at a load rate of 2 µm/s corresponding to a loading rate of 0.6-0.8 $MPam^{1/2}$/s.

The anisotropic microstructure was shown to have a strong influence on the FT and ductile-to-brittle transition. Fig. 4 shows FT vs. test temperature for the three investigated specimen orientations. On increasing temperature the stress intensity factor loses its validity with increasing ductile behaviour and the calculated values give only a lower bound of fracture toughness. The corresponding invalid values are denoted by open symbols in the diagram. For longitudinal orientation the material exhibited a low room temperature FT of about 7 $MPam^{1/2}$ and a steep increase of fracture toughness above 200 °C. For the radial and circumferential orientations, in contrast, the material exhibited relatively high room temperature fracture toughness of about 15 $MPam^{1/2}$. Such behaviour can be well understood by considering the anisotropic microstructure of polycrystalline round blank tungsten. In contrast to longitudinal orientation for radial and circumferential orientations the crack is forced to propagate in a transgranular manner which leads to an increase of apparent fracture toughness values. Fracture mechanical behaviour of round blank polycrystalline tungsten with good fracture toughness values in two of three investigated orientations is superior to fracture mechanical behaviour of commercially available polycrystalline tungsten rods investigated in detail e.g. in [D. Rupp and S. Weygand, Phil. Mag. 90 (2010), 4055]. Indeed, in the latter case only the specimens extracted in longitudinal orientation showed a high room temperature FT of about 15 $MPam^{1/2}$.

In the framework of an EFDA task we have carried out FM investigation on ODS W-2Y_2O_3 alloys manufactured at CRPP-EPFL in collaboration with PLANSEE by MA and HIPping. Quasi-static three point bending tests were performed on pre-cracked rectangular SENB specimens with dimensions of 3x4x27 mm and with machined V-shaped notches. Sharp crack starter notches have been introduced by means of a razor blade polishing. The FM investigation yielded very promising results. So, ductile behaviour and stable crack growth were observed already above test temperature of 250-300 °C. The preliminary assessment of fracture toughness yielded K_Q ~18 $MPam^{1/2}$ at temperatures of 350-600°C.

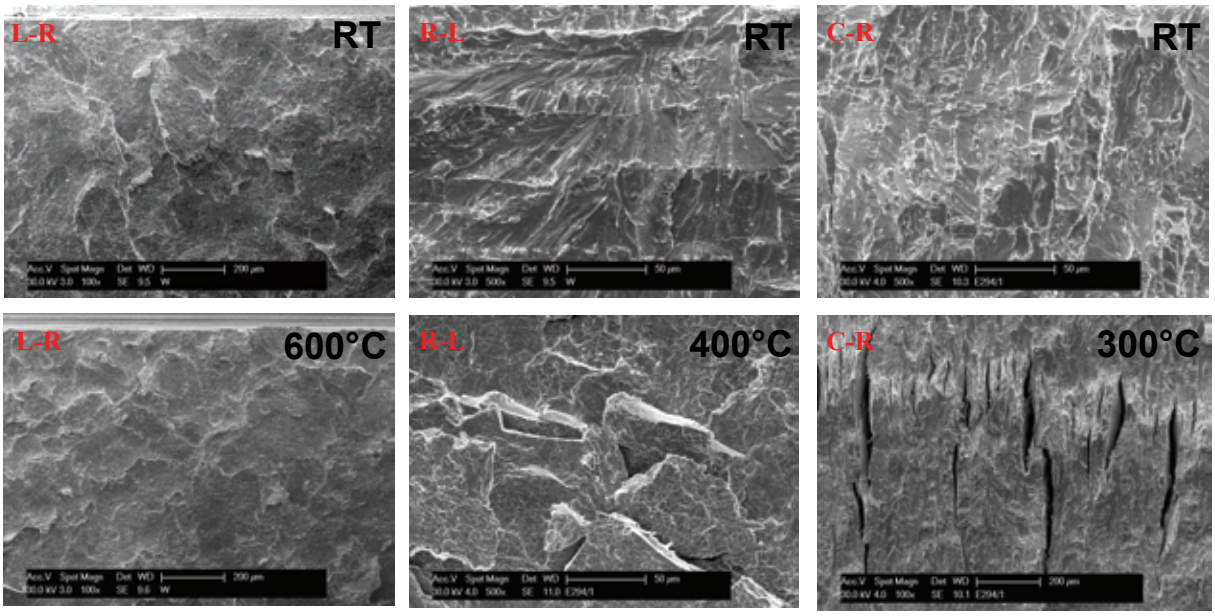

Fig. 3: SEM micrographs of fracture surfaces of polycrystalline round blank tungsten specimens tested at different temperatures.

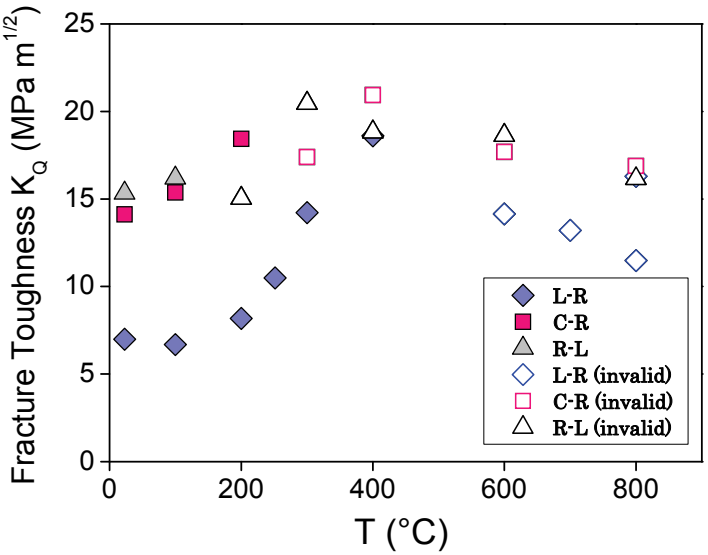

Fig. 4: Fracture Toughness of polycrystalline round blank tungsten vs. test temperature for three different specimen orientations. Values denoted by open symbols do not satisfy the ASTM 399 validity criteria. Loading rate 0.6-0.8 MPam$^{1/2}$/s.

Conclusion and Outlook

Fracture mechanical and microstructural characterization of novel tungsten alloys provided within the EFDA “Tungsten and Tungsten Alloys Development” Task Agreement has been performed. FM characterization of tungsten alloy produced by PLANSEE in a powder metallurgical route involving sintering into rods and accompanying forging into round blanks yielded very promising results. Due to the specific fabrication route the material exhibited relatively large room temperature FT values for two of three specimen orientations. This material gives more flexibility for component designing in comparison of commercially available rolled polycrystalline rod tungsten materials with only one strong orientation. The investigation of load rate dependence of the fracture behaviour is underway. The FM investigation ODS W-2Y_2O_3 alloys manufactured at CRPP-EPFL in collaboration with PLANSEE yielded very promising results.

FM characterization of different novel laboratory and industry scale W-based structural materials that are being developed under the EFDA “Tungsten and Tungsten Alloys Development” Task Agreement will be performed in the interesting temperature window for fusion applications (RT-1300 °C). The J-Integral and/or COD methods will be applied for the investigation of upper shelf fracture toughness. FM experiments will be accompanied by fractographic and microstructural investigations.

Staff:

U. Bürkle
E. Gaganidze
S. Knaak
M. Walter

Acknowledgement

This work, supported by the European Communities under the contract of Association between EURATOM and Karlsruhe Institute of Technology, was carried out within the framework of the European Fusion Development Agreement. The views and opinions expressed herein do not necessarily reflect those of the European Commission.

Development of Functionally Graded Tungsten/EUROFER 97 Joints for Divertor Applications (WP11-MAT-WWALLOY-01-03)

Objectives

The feasibility of the production of homogenous layers at different mixing ratios has been proved by PVD (magnetron sputtering) and VPS (vacuum plasma spraying). Microstructural analyses of the samples showed a sufficient small porosity and high quality for both fabrication methods.

In a next step the production and characterisation of functionally graded layers as well as their bonding to EUROFER 97 by diffusion bonding shall be aspired. In order to investigate the performance of the functional graded joints the samples will be subjected to thermal cycling at design relevant temperatures. To supplement the knowledge about the homogenous layers, micro tensile tests will be performed on standalone sprayed samples and an accurate analysis of the chemical composition will be done for the sputtered coatings by Rutherford backscattering and/or Mößbauer spectroscopy.

Task current status

Further investigations of vacuum plasma sprayed coatings with mixed W/EUROFER 97 ratios showed that they are thermally stable up to 800 °C. This has an important impact on the following diffusion bonding step, particularly on the diffusion bonding temperature. Samples were heat treated for one hour at 800 °C / 900 °C / 1000 °C and 1100 °C in vacuum and subsequently analyzed by scanning electron microscopy (SEM). Remarkable is that no cracking occurred even up to the highest temperature, neither in the EUROFER 97 nor in the tungsten regions. Rather a delamination of tungsten and EUROFER 97 regions took place at T > 1000 °C. However, the samples heat treated at 900 °C already showed creation of the intermetallic phase Fe_2W at the interface of EUROFER 97 and tungsten regions.

The production of 1 mm thick functionally graded material could be realized by VPS at FZJ-IEK-1. SEM images of the cross section view showed microstructure of high quality, uniform distribution of tungsten and EUROFER 97 and low porosity (Fig. 1). Unfortunately the adhesion with WL10 substrate is insufficient and needs further improvement.

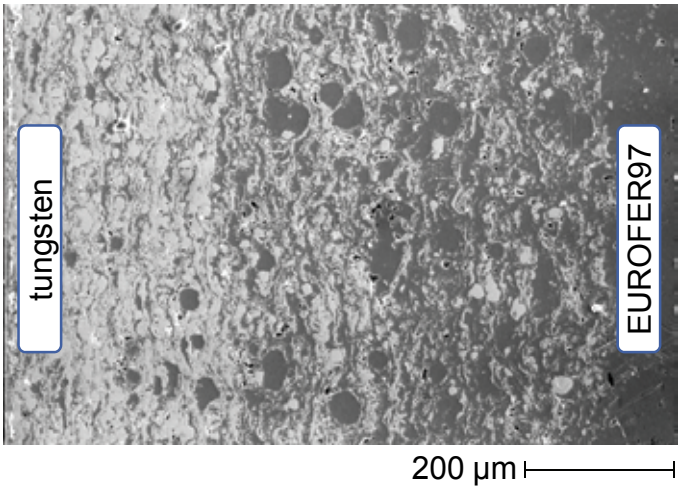

Fig. 1: SEM image of the functionally graded VPS layer.

A magnetron sputtered non-graded layer of 7 µm thickness and concentration of 40 at.% tungsten and 60 at.% EUROFER 97 deposited on WL10 has been successfully joint to EUROFER 97 by diffusion bonding at 800 °C (Fig. 2). A cross section view by SEM revealed

well bonded surfaces, but also some cracks perpendicular and parallel to the bonding surface within the sputtered coating after diffusion bonding. Although this joining technique was in principle very promising, final results can only be concluded when functionally graded coatings have been realised.

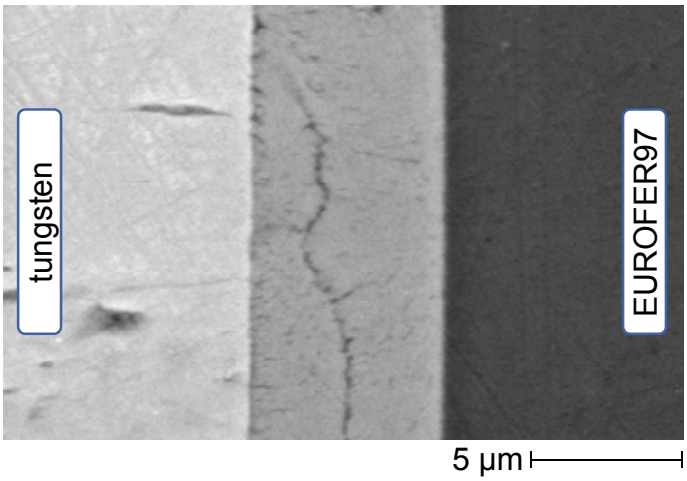

Fig. 2: SEM image of the diffusion bonded sputtered layer.

Further finite element simulations were performed to access the expected brittle failure probability in the tungsten region of an ideal functionally graded joint. The failure probability due to inherent surface and volume flaws can be significantly reduced by the reduction of joining temperature from 1000 °C to 800 °C, the increase of graded layer thickness from 2 mm to 3 mm and by inclination of the graded layer.

Staff:

T. Weber
J. Aktaa

Literature:

[1] T. Weber, J. Aktaa, Numerical Assessment of Functionally Graded Tungsten/Steel Joints for Divertor Applications, Fusion Engineering and Design, 86 (2011) 220-226.

[2] T. Weber, M. Härtelt, J. Aktaa, Considering brittleness of tungsten in failure analysis of helium-cooled divertor components with functionally graded tungsten/EUROFER97 joints, Engineering Fracture Mechanics, submitted.

Acknowledgement

This work, supported by the European Communities under the contract of Association between EURATOM and Karlsruhe Institute of Technology, was carried out within the framework of the European Fusion Development Agreement. The views and opinions expressed herein do not necessarily reflect those of the European Commission.

Development of Diffusion Bonded Tungsten / EUROFER 97 Joints (WP11-MAT-WWALLOY-01-05)

Objectives

The helium cooled divertor for DEMO reactors should withstand a very high kinetic energy and a heat flux up to 10 MW/m². Tungsten (W) as one of the refractory materials shall be used as functional material for target plates as well as for structural material. Its use as structural material however is limited to the high temperature parts which shall be connected by means of solid state diffusion bonding to the low temperature parts built from the reduced activation ferritic/martensitic steel EUROFER 97. Realizing such kind of joining is restricted by many problems related to the large differences in melting temperatures and coefficients of thermal expansion (CTE) and the forming of brittle intermetallic layers. The large difference in coefficients of thermal expansion causes high thermally induced residual stresses at the interface, which can yield failure of the joints, particularly when they are subjected to the mechanical and thermal loading.

In this task a low activation vanadium (V) (hand on level: ~20 years) sheet is introduced as an interlayer. This material with its CTE between EUROFER 97 and W is proved to be able to reduce the residual stress. Nevertheless for diffusion bonding at high temperature (> 1000 °C), the residual stress is still very high and a thick intermetallic phase is formed at EUROFER 97/V interface and additionally grain growth of V interlayer was evident. So it is necessary to find optimal diffusion bonding parameters, which can reduce all the problems mentioned above and at the same time still allow diffusion mechanisms to be sufficiently activated for the closure of the pores along the bonding interfaces. The aim is to produce joints with high strength, ductility and toughness which can survive the thermo-mechanical divertor loading.

Task current status

According to previous investigations, diffusion bonding of EUROFER 97 with tungsten using low activation V interlayer seems possible. It is also reported that a low temperature diffusion bonding method is more suitable for this material combination to reduce the formation of brittle intermetallic phases and to avoid grain growth in the materials to be bonded.

In the course of this work period the influence of bonding temperature and process duration on the microstructure and mechanical properties of the joint have been studied systematically. The bulk materials used in this work were an 18 mm diameter polycrystalline W rod with a purity of 99.96% manufactured by Plansee Metall GmbH and a 25 mm thick EUROFER 97 plate (2nd batch with a heat number of 993402). The commercial V plate used as interlayer had a thickness of 1 mm with a purity of 99.9%. For bonding experiments the tungsten-rod was cut by EDM (Electrical Discharge Machining) in cylindrical specimens with a length of 16 mm while from the EUROFER 97-plate cylindrical specimens were fabricated with a diameter of 18 mm, a length of 22 mm and a bonding surface parallel to the rolling plane. The V interlayer was cut to a disc with a diameter of 18 mm. Before diffusion bonding, the specimens were ground and polished to remove the surface impurities containing carbides and oxides. These impurities were analyzed on the surface of the V plate (about 30 nm thick) by means of AES (Auger electron spectroscopy). To exclude significant influences of the surface parameter on diffusion bonding results, the surfaces of all specimens were polished up to a surface roughness of $R_z \leq 1$ µm. After the cleaning procedures, the specimens to be bonded were piled on each other with the interlayer inserted between EUROFER 97 and W, and then diffusion bonded in the vacuum furnace (5×10^{-5} mbar). The diffusion bonding experiments were hold in true stress mode. Post bond heat treatment (PBHT) was not necessary for specimens bonded at 800 °C or less. The investigations of bonded samples were carried out by microstructural analyses before and after the chemical etching. Their mechanical behaviour was investigated by nanoindentation hardness tests locally across the

bonded interfaces, by tensile tests for the assessment of the strength and by Charpy impact tests (with KLST specimen geometry) for assessment of the toughness.

As shown in Fig. 1a), the specimens are well bonded at 800 °C and for a bonding duration of 1 h. The bonding results indicate no cracks and no remaining pores along the EUROFER 97/V and V/W bond interfaces (upper figure).

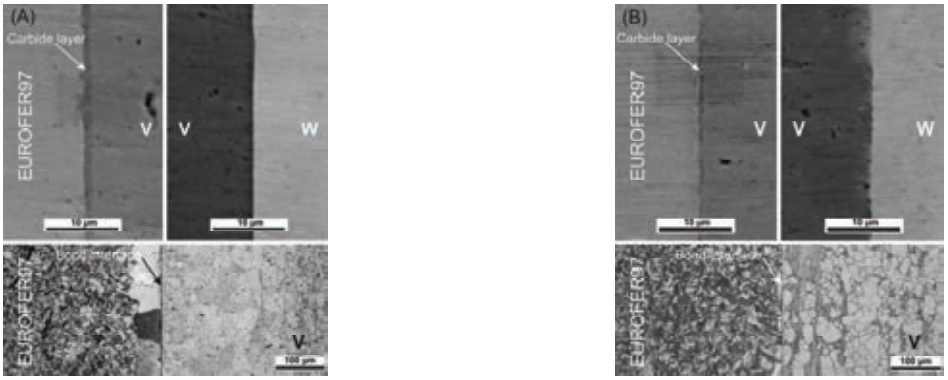

Fig. 1: Microstructure before (upper) and after (lower) the chemical etching of specimens bonded at a) 800 °C and b) 700 °C and for a bonding duration of 1 h, respectively.

Microstructure alteration is just noticeable at the EUROFER 97/V interface. Using EMPA (electron probe microanalysis), the dark layer along that bond interface has been investigated. As stated in the last report, for specimens bonded at much higher temperatures, this layer contains very high concentrations of C and is considered as a brittle carbide layer. The brittleness of this layer is confirmed by nanoindentation hardness tests showing an access of hardness value close to the interface. The microstructure alteration is also established close to the interface on the EUROFER 97 side as a result of the interdiffusion of C in this region to the V interlayer (lower figure). By reducing the bonding temperature down to 700 °C, the bond interfaces are still sound as shown in Fig. 1b). In addition to the reduction of the thermally induced residual stress, the thickness of the carbide layer was also significantly decreased due to the reduction of the diffusion rate of C from EUROFER 97. This gives a benefit to the EUROFER 97 interface that the microstructures there do not alter significantly and therefore they do not differ from that of EUROFER 97 bulk material at least visually.

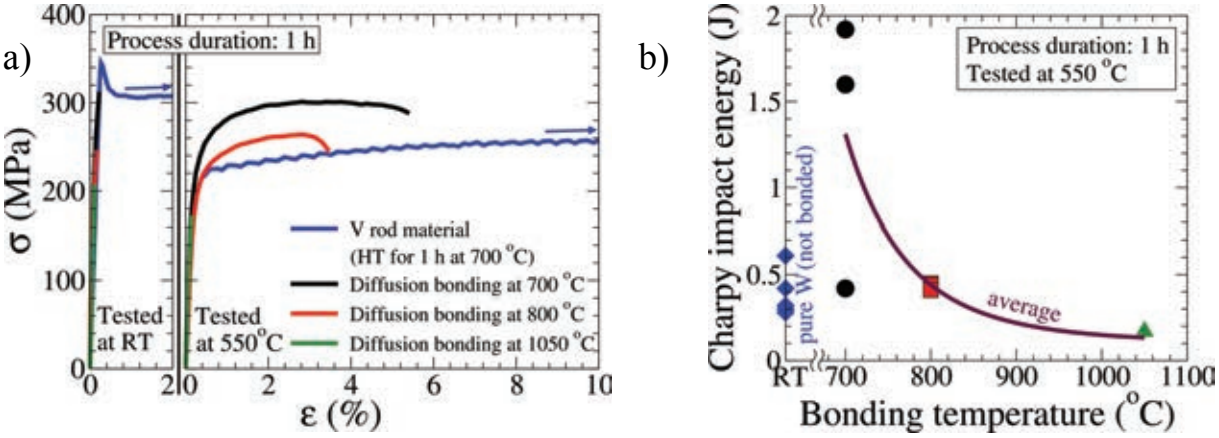

Fig. 2: Diffusion bonding in a temperature range down to 700 °C and for process duration of 1 h, a) σ – ε curves for specimens tensile tested at RT and 550 °C, b) Charpy impact energy as a function of process duration for specimens impact tested at 550 °C.

The advantages in the reduction of the thermally induced residual stress and of the microstructure alteration improve the mechanical properties of the bonded specimens. As presented in Fig. 2a), the strength increases with increasing bonding temperature. Tensile test-

ing at RT shows that the strength of specimen bonded at 700 °C reaches about 91% of the strength of the V rod material after the heat treatment (HT) at 700 °C for 1 h. By heating the specimens before tested up to 550 °C, the residual stress at the bond interfaces of the specimens bonded at low temperature are mostly released. The bond interfaces are strong enough to hold the tensile load, such that the V interlayer considered as the part with the lowest strength deforms plastically. The ductility increases with the reduction of the bonding temperature, such that a strain to rupture of about 5% is attained for specimen bonded at 700 °C. In comparison with the heat treated V rod material, the strength of the low temperature bonded specimens is higher. It can be explained by the microstructure differences between the V interlayer and the rod material and also because the aspect ratio of the V interlayer, which is very small and therefore can induce constraints in it. The improvement in strength and ductility with the reduction of bonding temperature enhances also the toughness of the material. This tendency is shown by Charpy impact tests, for which the absorbed Charpy impact energy as shown in Fig. 2b) increases with the reduction of the bonding temperature up to an average value of about 1.3 J for specimens bonded at 700 °C. The large discrepancy on the absorbed impact energy of each specimen is assumed to be caused by the inhomogeneity of the surface finish. Nevertheless, this average value is much higher than that of the specimens made of pure tungsten tested at the same temperature (~0.4 J). The bonded specimens tested mechanically are broken in different bonded interfaces depending on the bonding temperature. All specimens bonded at 800 °C and higher are broken at the EUROFER 97/V interface. This interface is strong enough for specimens bonded at 700 °C to maintain much more mechanical loading until the specimens failed at the V/W interface.

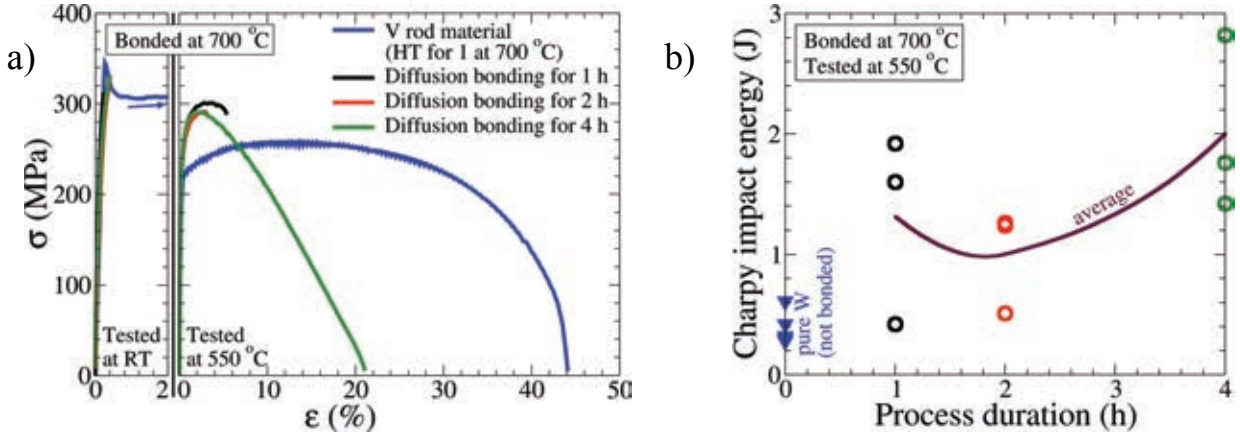

Fig. 3: Diffusion bonding at 700 °C for various process durations; a) σ – ε curves for specimens tensile tested at RT and 550 °C; b) Charpy impact energy as a function of process duration for specimens impact tested at 550 °C.

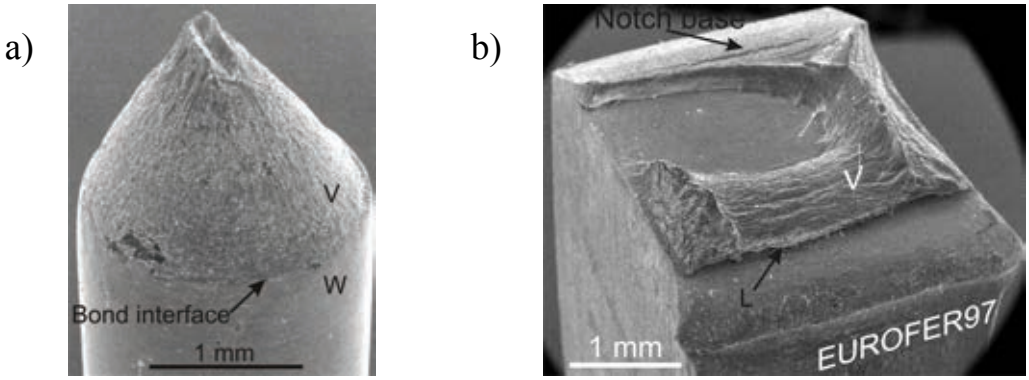

Fig. 4: Fracture micrographs of specimens bonded at 700 °C and for 4 h. The a) tensile test and b) Charpy impact test are carried out at 550 °C. After the Charpy impact test, both parts of the specimen were still together. It is broken thoroughly along L in liquid nitrogen.

The superiority of the specimens bonded at 700 °C is furthermore investigated. The diffusion bonding experiments are continued for various process duration. It is necessary to find the optimal process duration, since by its increase may cause the intermetallic phases to grow at the EUROFER 97/V interface and brings a negative influence on the mechanical properties. At the same time, the increase of the process duration increases the amount of materials transported to micro pores at the bond interfaces and makes the V/W interface stronger. By comparing the microstructure, it was evident, that the microstructure of specimens bonded for 4 h does not differ microscopically from that bonded for 1 h except a non-significant increase of the thickness of carbide layer. The tensile properties are shown in Fig. 3a). The strength of the specimens tested at RT increases slightly with the process duration. Nevertheless, for specimens bonded for 4 h, the ultimate tensile strength is very close to that of the V rod material. The grave improvement was found when the specimens were tested at 550 °C. The specimen bonded at 700 °C shows a very ductile property with a strain to rupture up of about 20%. The fracture micrograph in Fig. 4a) reveals a very strong necking mainly in the V interlayer. The high strength and increasing ductility usually yield high impact toughness. This is shown in Fig. 3, where the absorbed Charpy impact toughness of the specimens bonded with process duration of 4 h is generally higher than that with shorter process duration. The average values increase more than 50% from about 1.3 J (process duration of 1 h) to about 2.0 J. Comparing with the pure W (not bonded), this average value is with a factor 5 higher.

After the tests, all specimens with process durations of 4 h were not broken thoroughly. The fracture surface of the specimen with the highest energy is show in Fig. 4b). It is evident that the still on EUROFER 97 attached V interlayer was severely deformed. The plastic deformation is also found at the edge of the EUROFER 97 due to the compression load on the back of notch.

Considering all of the results in this period of report, it can be concluded that the joining between EUROFER 97 and W using low activation V interlayer (hand on level: ~20 years) is feasible and can be strongly recommended to be considered for the manufacturing of the divertor components in the DEMO reactor.

Staff:

J. Aktaa
W.W. Basuki

Literature:

[1] W.W. Basuki, J. Aktaa, Investigation on the diffusion bonding of tungsten and EUROFER97, Journal of Nuclear Materials 417 (2011) 524 - 527.

[2] W.W. Basuki, J. Aktaa, Investigation of tungsten/EUROFER97 diffusion bonding using Nb interlayer, Fusion Engineering and Design 86 (2011) 2585 – 2588.

[3] W.W. Basuki, J. Aktaa, Diffusion bonding between W and EUROFER97 using V interlayer, submitted to Journal of Nuclear Materials (2011).

Acknowledgement

This work, supported by the European Communities under the contract of Association between EURATOM and Karlsruhe Institute of Technology, was carried out within the framework of the European Fusion Development Agreement. The views and opinions expressed herein do not necessarily reflect those of the European Commission.

Development of W-W Joints Brazing using Ti Alloy (WP11-MAT-WWALLOY-01-06)

The use of low-activating materials in the divertor design is one of the most important requirements. This also includes proper selection of brazing materials, which have to meet the additional thermal load carrying as well as functional requirements. Titanium is favored as brazing material, since it can meet the requirements as far as possible. With its elevated melting point of 1668 ° C compared with the previously used Ni-based fillers (T_{br} ~1050 °C) [1], the titanium material provides a sufficiently large safety margin to the operating temperature of the braze joint of approximately 1200 °C.

We started our study with braze wetting experiments. First braze wetting tests were carried out using pure Ti (99.99% grade, 50 µm thick) and Ti50Ni (100 µm thick) foils as intermediate layer between two W slices of 1 mm thickness cut from rod (Ø25 mm, Plansee). A high vacuum furnace (10^{-5} mbar, heating rate ~ 10 K/min and cooling rate ~ 20 K/min) was used. Process parameters are as follows: brazing temperature T_{br} = 1750 °C for Ti and 1100 °C for Ti50Ni, respectively, hold time 30 min, no pressing weight. The wetting test results for Ti and Ti50Ni filler metals are shown in Figures 1 and 2, respectively. Test results of both cases show braze wetted area only at some places, accompanied by voids that may be caused by diffusion of titanium in tungsten. In the latter case with Ti50Ni (Fig. 2), also Ni precipitation in the brazing layer was observed. In the next step as a counter measure, some parameters will be varied, e.g. more solder, shorter hold time and the use of weight.

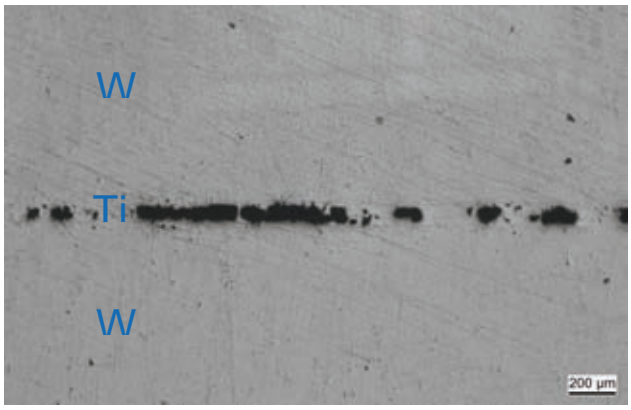

Fig. 1: Braze wetting tests on tungsten and titanium filler metal.

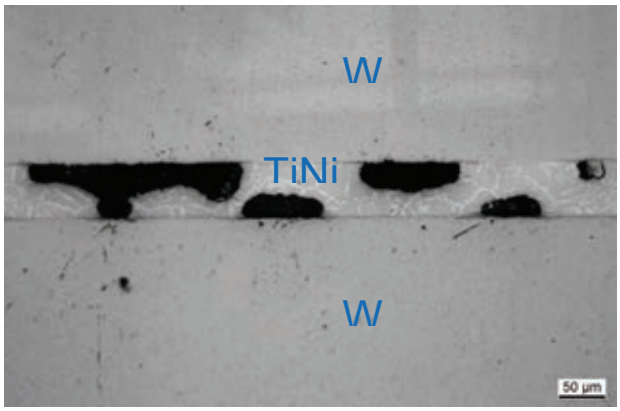

Fig. 2: Braze wetting tests on tungsten and Ti50Ni alloy filler metal.

Staff:

W. Basuki
P. Norajitra
L. Spatafora

Literature:

[1] P. Norajitra, S. Antusch, R. Giniyatulin, I. Mazul, G. Ritz, H.-J. Ritzhaupt-Kleissl, L. Spatafora, Current State-Of-The-Art Manufacturing Technology for He-Cooled Divertor Finger, J. Nucl. Mater. 417 (2011) 468–471.

Acknowledgement

This work, supported by the European Communities under the contract of Association between EURATOM and Karlsruhe Institute of Technology, was carried out within the framework of the European Fusion Development Agreement. The views and opinions expressed herein do not necessarily reflect those of the European Commission.

Development of W-EUROFER & W-W Brazed Joints. Commercial Joints Deposited by Electro-chemical Methods: (i) Aqueous Electrolytes and (ii) Organic Electrolytes (WP11-MAT-WWALLOY-01)

Introduction

For an application in a fusion power system a helium cooled divertor concept is investigated, which is projected to remove heat loads of up to 15 MW/m². This divertor design is based on a modular arrangement of cooling fingers, which is to be fabricated from a heat resistant material like tungsten alloys.

To connect the necessary components precisely, optimized to withstand high mechanical and thermal stresses without any danger of failure during the whole process time, this shall be done by brazing materials. The solders herein guarantee besides a force-fit connection also a certain ability to compensate mechanical stresses coming from the highly different thermal expansion coefficients.

Two positions in the divertor are of strategic interest:

a.) the connection between tungsten tile and tungsten/WL10 thimble in the upper part of the finger design. This connection has functional character and must withstand temperatures of approx. 1250 °C; here exists a high chemical metallurgical similarity of the both metal sides, but the high temperatures reduce drastically the choice of convenient materials for brazing.

b.) the connection between tungsten thimble and steel sleeve (ODS EUROFER) at the lower position. The operation temperatures are about 700 °C; but here the connection of two different materials underlies high pressure forces (80 bar cooling gas pressure). The connection must be gastight, furthermore stable also under cyclic conditions with repeated cold-warm changes.

Here, the differences in thermal expansion coefficients are drastic, and the metals with completely different chemical properties have to be connected by a solder with a contact affinity to both sides. The Cu is casted into the gap but no brazing to tungsten takes place. If Cu should be used as filler metal a functional scale on top of the tungsten part is required to allow a metallurgical reaction and alloy formation for good adherence. Nickel may be such a metal which has affinity to both copper and tungsten.

For the suitable brazing solders materials of both connecting sites the question arises to manufacture the layers selectively at the desired positions, even with a high degree of uniformity and reproducibility. In the light of the needed numbers of divertor units, which have to be produced in mass-production, also economic aspects are not negligible.

Electrochemical metal deposition

Electro-chemistry allows the deposition of metallic layers on a solid substrate from a liquid system; from aqueous systems generally this takes place in temperature regions of < 100 °C. So far, the electroplating does not affect the substrate material by thermal forces, does not change the metallurgical structure, which is very important especially for brittle substrate materials, and neither also the chemical nature of the substrate material. Electro-chemical deposition is also one of the few techniques, where deposition on the surface all over the substrate can take place simultaneously during one process step without complex facility.

Targets of brazing development

Investigations were carried out comprising following aspects:

- ► Development of electro-chemical technologies based on commercially known filler compositions for the Group VIII and IB elements from aqueous systems for brazing of divertor components. The main goal is the substitution of activation-sensitive metals without any loss of the coating properties, as they are established by Nickel; here Pd seems to be the most favourable candidate including its surface conditioning tools.
- ► Development for coating of tungsten with multi-layer deposition of e.g. Pd and Cu, as well as heat treatment up to 1100 °C and analyzing of inter-diffusion features.
- ► Development of electro-chemical coating technologies for deposition of electro-negative refractory metals e.g. from Group VB and VIB elements like W, Ta to Ti suitable for designing advanced brazing metals under fusion aspects. The technological challenge is to evaluate appropriate aprotic organic amine-based electrolytes, the new class of ionic liquids (IL). IL and the corresponding IL-metal salt combinations in conjunction with adjusted concentrations, temperatures and current/voltage parameters for deposition must be developed by electrochemical R&D.

Results

Palladium

Palladium (Pd) is the nearest homologue element to nickel (up to date most experienced model material) but does not have its most disadvantageous property to react nuclear-chemical with the neutron irradiation to unstable elements including helium gas evolution. As Ni also palladium allows to combine as filler material the both immiscible metals W and Cu. Therefore the electrochemical deposition is to be transferred from experienced Ni parameters to Pd. Unfortunately it is in contrast to nickel not an often used technical galvanic metal, far less for the deposition on tungsten surfaces (which is described in literature as impossible). But because of the closed relationship to Ni, the elaborated surface pretreatment methods can be applied resp. easily adopted.

Deposition of palladium on tungsten

The pretreatment of tungsten parts was carried out by applying an alkaline hexacyanoferrate solution as suitable etchant for the Pd deposition, which is based on commercial electrolytes. Deposition parameters were. T = 40 °C and pH = 7-8. The current density with homogeneous coating behaviour was found to be in the range i = 10-80 mA/cm². Therefore the scale thickness is very similar to Ni adjustable easily by current density and deposition time, in the range 5 to 100 µm depending on the requirements of joining. So it was demonstrated successfully, that the deposition of Pd on tungsten as a matter of fact could be realized despite converse statements (Fig. 1).

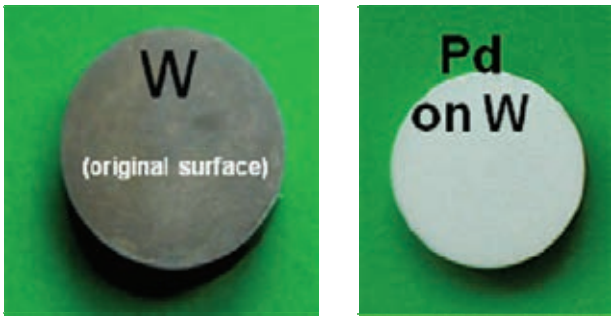

Fig. 1: Palladium on tungsten deposited from aqueous electrolyte.

Cu-Pd transition layers on tungsten

For closed joined connections, as it is needed in W-W, the filler sequence must be Pd-Cu-Pd with a stepless gradient for all possible binary metal systems. For the realization of such connections, tungsten parts covered both with Pd and Cu-layers were connected with the copper-sites and heat-treated with brazing temperatures. As Fig.2 shows, the miscibilities are sufficient high for W-Pd and Pd-Cu under the test conditions. A continuous variation of solid solutions from W via W-Pd and W-Pd-Cu to Cu-Pd as filler material, at least not exceeding a

ratio Cu/Pd = 4:1. In this concentration, the ability of Pd of a possible hydrogen (or deuterium) adsorption is drastically weakened.

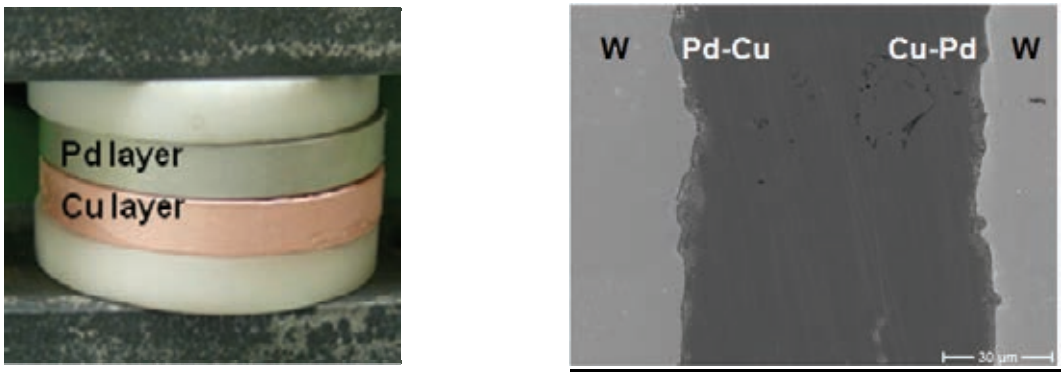

Fig. 2: Applied tungsten rods, diameter 16mm, connected by galvanic layers W-Pd-Cu-Pd-W.

Hereby it is demonstrated that Pd is a feasible material for brazing duties in W-technology. Further investigations are to be done to reach even lower Pd-contents, with the same or preferentially better joining results, which is primarily to be seen in the elaboration of optimal galvanic thicknesses. In the next step the tungsten will be joined by this electro chemically deposited multilayer system to EUROFER. The challenge is to get Pd coatings and diffusion behaviour on those steels, which are not typical substrate materials and therefore do no suit the specifications in Pd galvanotechnique because of the absence of some alloy elements in RAF steels.

Deposition from non-aqueous electrolytes: Ionic Liquids

In comparison to transition metals like Fe and Ni, refractory metals are by their electro-chemical potentials more or less more noble, and therefore, should be in theory also applicable by electro-chemical deposition. But in practice the EC reduction is bound to a reaction with water and therefore marked by a reaction sequence via hydroxides to oxides, at least forming insulating layers. As result, aqueous deposition from water is not possible for these metals (Fig. 3).

Here the absence of water during deposition is necessary. Such aprotic electrolytes can be used by the use of molten salt systems. Modern electrolytes of the ionic liquids (IL) type, are also molten salt systems, but of organic chemistry, with amine cations, as result with drastic reduced melting temperatures, which can open new paths in electrochemical deposition.

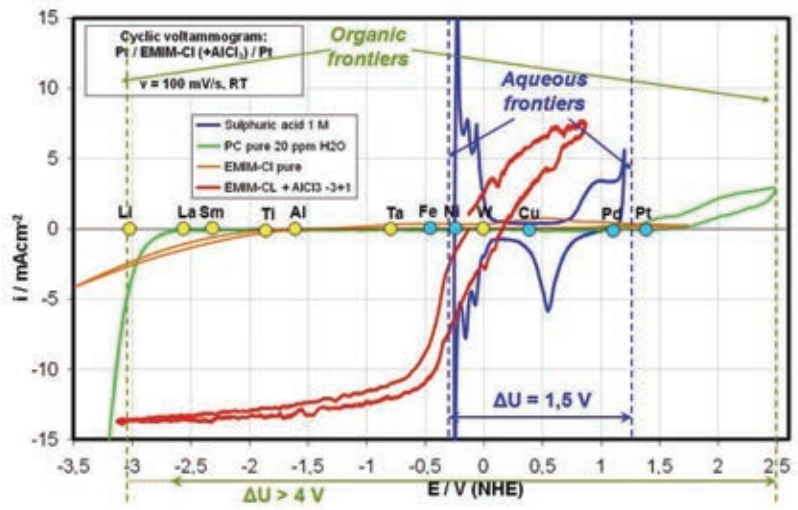

Fig. 3: Frontiers of aqueous systems and position of some electro-negative galvanic metals.

Ta deposition from IL systems

By suitable combinations of IL and corresponding metal salts, a Two Component IL Electrolyte TCILE can be designed and evaluated for deposition of refractory metal e.g. W, Ta or Ti. Because of its rather passive nature in chemical and electrochemical view, and also as problematic metal in electro-chemistry, but important in fusion technology, Ta was also investigated. From Ta, it is known that depositions can be done by fluorine systems, where the galvanic processing of fluor and fluorides as anodic by-product is not only a harsh safety problem, and the subsequent incorporation of fluor/fluoride in the matrix is a further problem. Therefore, the task was to investigate F-free electrolyte systems.

The used Ionic Liquid was the first commercial available IL, Ethyl-Methyl-Imidazolium Chloride (EMIM-Cl), which revealed already as a suitable electrolyte type for Al-deposition on EUROFER for formation of corrosion and tritium permeation barriers [2], and showing its practicable application for refractory metals. Fig. 4 shows first electro-chemical investigations of Ta-IL systems, of the type TaCl5+ EMIM-Cl in submolar concentrations. The CV shows, that there are significant hints of positions of Ta-Metal deposition in potentiostatic modi. The investigation of the EMIM-tantalum systems revealed some similarities to W systems. The mixed EMIM-Cl and TaCl5 does not form, as e.g. Al-Systems a room temperature liquid, but rise the common melting point up to 130-150 °C (pure EMIM-Cl: 80 °C). As consequence, low viscous solutions can not be handled below such working temperature. It is highly probable, that Ta will need because its higher passivation behavior (comparable to Cr, Ti and Pt) other EC Parameters at the same chemical concentrations as W.

Depositions tests from the first made EMIM-Cl did show only slight nucleus, but not fully developed coatings, also caused by the high oxidation state of 5, which means that in comparison to tungsten also high electric currents have to be processed. It is visible, that an increase of the temperature causes a drastic improvement of the electric properties, caused by the decline of the viscosity. This means that RTIL, with their temperature range under 100 °C are not suitable.

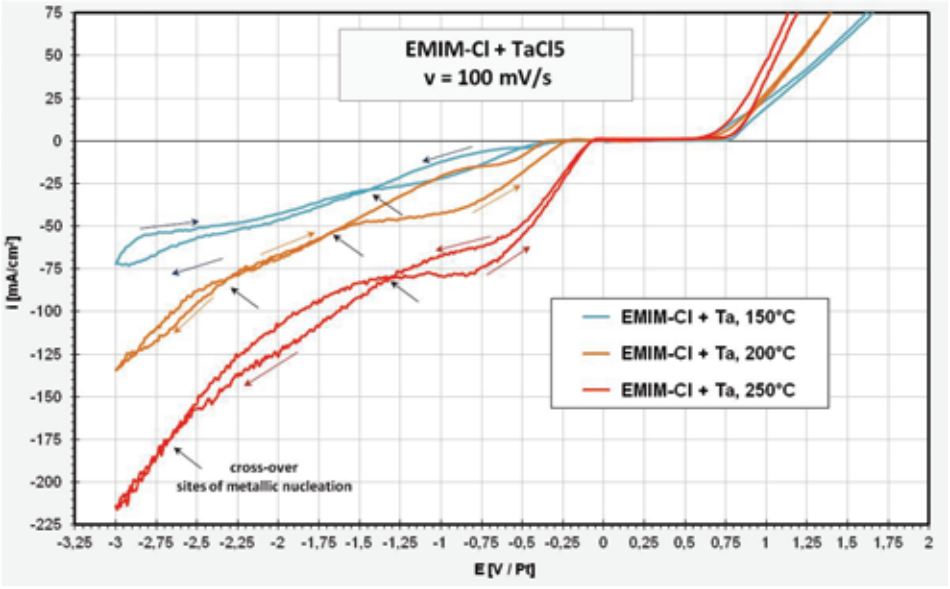

Fig. 4: LSV of a IL-tantalum solution, showing a drastic increase of current density at temperatures from RTIL temperatures up to > 200 °C.

Current investigations are carried out to get solutions without any supersaturation. Because temperatures of 300 to 350 °C count as the upper limit for IL use (to be called High Temperature Ionic Liquids, HTIL), such systems might trade preferably as MTIL systems (Medium Temperature IL).

For the future work it is planned to use carbonacid ester systems e.g. propylencarbonate or ethylencarbonate as additionally viscous minimizing agents.

Conclusions

The development of suitable and long term stable joints for He cooled divertor fingers is essential for the successful operation of this design. Challenging are both required joints, the steel / W alloy combination due to the high expansion mismatch and the strong differences in alloy characteristics and the high temperature brazing of the W alloys between tile and thimble. The general screening has shown the needs for functional interlayer's to allow brazing instead of only casting or to suppress inacceptable diffusion reactions and last not least the homogenous coating and complete wetting of surfaces to be joined.

In the first step commercially used filler metal combinations were selected for the deposition process. As electrolytes for Cu and Pd systems water based solutions were investigated. The tests established techniques for a surface cleaning and conditioning due to oxide / hydroxide scales before any coating is performed.

It was demonstrated that copper brazing instead of only casting of tungsten can be applied if functional scales were deposited on tungsten. Heat treatments and pre-brazing studies imply that such scales may be in the dimension of roughly 10 µm. A homogeneous Pd deposition on tungsten was successfully achieved as functional inter-layer by following subsequent electro-chemically coatings of Cu-layer to act as filler metal. The analyses indicate a high rate of reproducibility and excellent wetting of the joining parts a condition for defect-free brazing.

These positive results in application of electro chemical deposition of coatings point out that this technology can be applied in combination with fusion relevant alloys like tungsten and EUROFER steel. Modification of filler metals and functional scales will be the focus of next steps in the development of electro chemical brazing tools from aqueous systems.

Diffusion barriers and high temperature fillers require combinations of / or with refractory metals (e.g. W, Ta or Ti type). However, these elements cannot be deposited from aqueous electrolytes due to e.g. oxide formation. Therefore an alternative and innovative development line in electro-chemical deposition technology based on the use of novel ionic liquids was also started to achieve a Ta coating technology, using the experiences of the analogue W deposition. For first evaluation of the applicability of IL as electrolytes the aprotic component EMIM-Cl was selected. Basic potentiostatic investigations were performed in combination with metal salts e.g. $TaCl_5$ to demonstrate and verify the applicability and syntheses of electrolytes suitable for metal deposition in general. Current investigations focus on the overcoming of the passivation features of tantalum also in IL. The further development in aprotic systems will include also other IL and refractory metals with focus high temperature W&W alloy brazing.

Staff:

N. Holstein
J. Konys
W. Krauss
J. Lorenz

Literature:

[1] N. Holstein W. Krauss, J. Konys, Development of advanced processes for Al-based anti corrosion and T permeation barriers, Fus. Eng. to be published

[2] W. Krauss, N. Holstein, J. Konys, H. Zimmermann, Al-based anti-corrosion and T-permeation barrier development for future DEMO blankets, Fus. Eng. to be published

[3] N. Holstein, W. Krauss, J. Konys Development of functional scales for joining of divertor components based on electro-chemical plating technology, ICFRM-15, October 16-22, 2011, Charleston

[4] N. Holstein in “Recent progress on tungsten materials research for nuclear fusion applications in Europe”, M. Rieth (ed.) to be published in Journal of Nuclear Materials, 15-024

Acknowledgement

This work, supported by the European Communities under the contract of Association between EURATOM and Karlsruhe Institute of Technology, was carried out within the framework of the European Fusion Development Agreement. The views and opinions expressed herein do not necessarily reflect those of the European Commission.

Post Irradiation Examination (WP11-MAT-WWALLOY-04-01)

High temperature alloys (such as tungsten) are assumed to be primary materials candidates for structural application in the divertor. Different tungsten materials will be base characterised at room temperature by instrumented indentation. Registering hardness tests (Vickers, Rockwell, and Berkovich) are performed, in a further step at higher temperatures and in irradiated condition.

The applicability of the indentation method for bulk material and even for porous tungsten coatings could be demonstrated with indents made in a cross-section of a polished W-coating deposited on an EUROFER substrate (plasma-spray, material furnished by IPP Garching). In preparation for a future investigation of irradiated tungsten, indentation experiments on unirradiated tungsten samples were continued. The general feasibility of indentation tests on this materials class could be approved. The experiment series contained classical monocyclic as well as polycyclic indentation tests. Samples, provided by IPP, were PCW or SCW of different crystal orientation (100, 110, 111). The monocyclic tests confirmed the simulated results from IPP, relying on a crystal-plasticity model.

Data from polycyclic tests were used to extract viscoplastic material parameters using a neural network based analysis method. These results, shown in Fig. 1, allow simulation of a tensile test (Fig. 2). A good agreement with real tests (marked “tensile” in Fig. 2) is achieved especially for stress parameters.

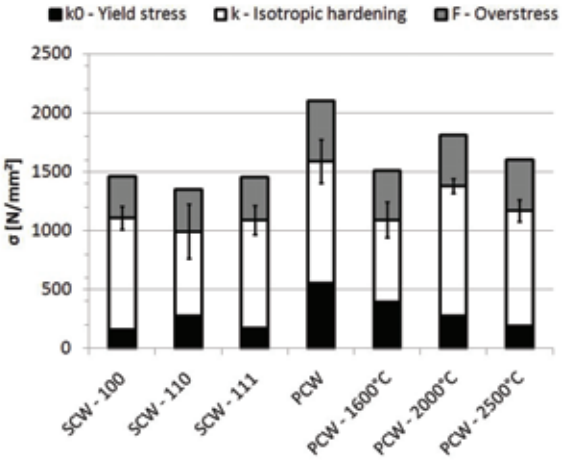

Fig. 1: Material parameters extracted from indentation data using neural network analysis.

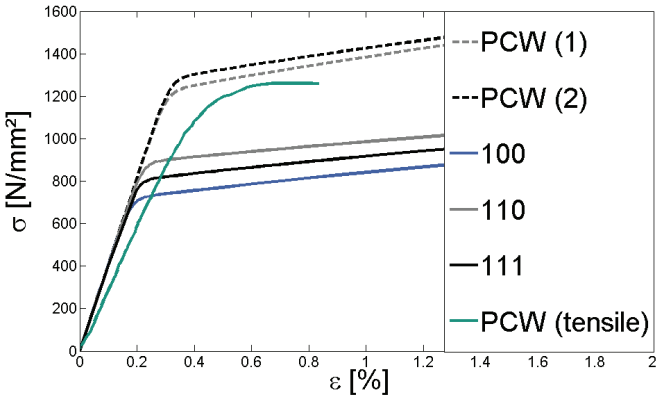

Fig. 2: Stress-strain-curves of simulated and real tensile test for tungsten.

A varying system’s overall compliance (Fig. 3) has to be taken into account when evaluating the data. Further research on determination of machine’s compliance for spherical indenters and its significance has to be done. Pile-up around the indent was determined by surface scanning in collaboration with IPP. The data is used to consider the real contact area of the indenter. Evaluation models have to be adapted to this knowledge. Further on in single-crystalline tungsten, pile-up is an evident characteristic for plastic anisotropy of tungsten.

In addition, preparing work for fracture mechanical characterization was done by investigation of sharp indents and the crack initiation in the area of highest stress concentration of the tetraedical indent. Indeed, preliminary indentations performed on tungsten with different types of indenters demonstrate the importance of the selection of the indenter geometry for the generation of high plastic deformation rates (see residual deformation for two types of indentations in tungsten in Fig. 4). The threshold of the indentation force needed for crack generation in tungsten is thus expected to be significantly reduced by using a cube-corner tip. FIB-based analyses of the indented surface as well as cross-sectional analyses of imprints on tungsten did not reveal the presence of radial, lateral or even median crack at loading up to 300 N (Fig. 5).

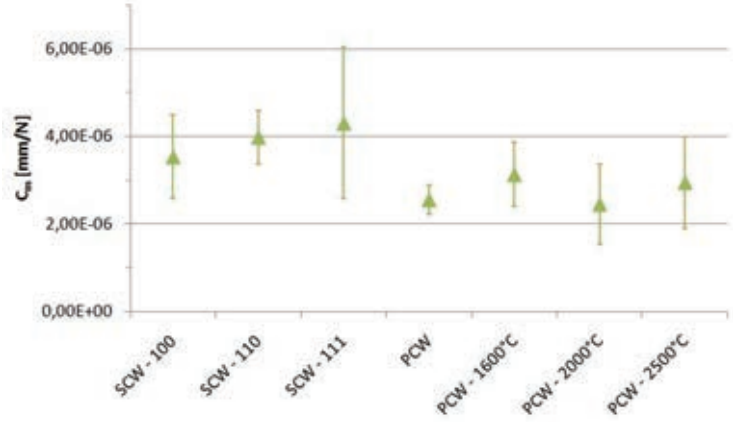

Fig. 3: Varying machine's compliance for different types of tungsten material conditions.

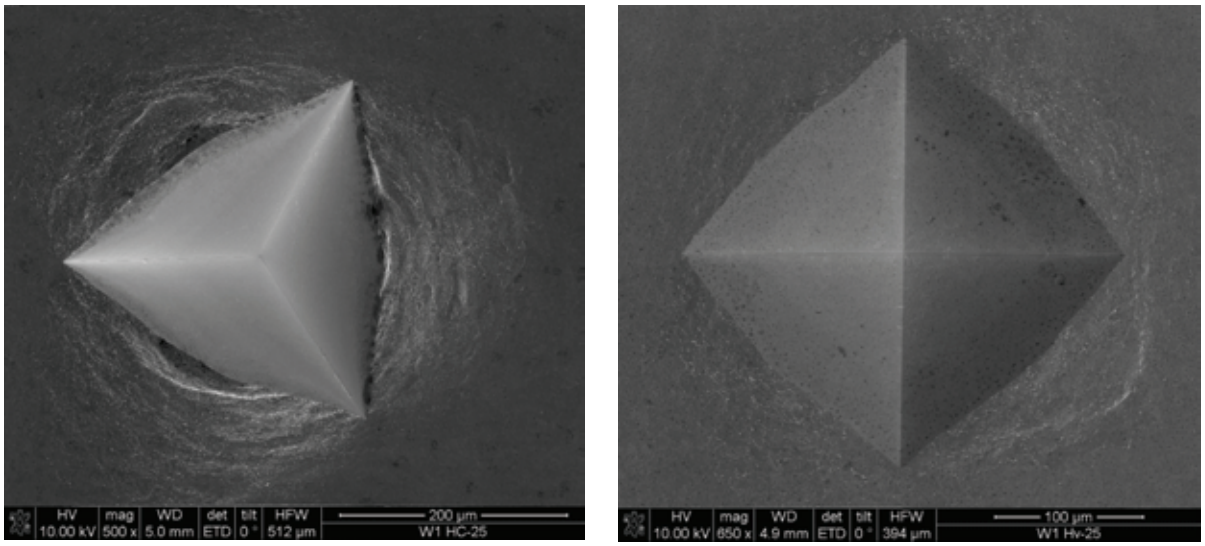

Fig. 4: Investigation of the plastic behavior depending on the indenter geometry used for an applied load of 250 N: cube corner imprint (left), Vickers imprint (right). Figures by D. Exner.

Moreover, those investigations generally point out the importance of the mechanical stability of the indenter tip at macroscale loadings on both hard and brittle materials as it is the case for tungsten. Finite-Elements-analyses will be used as predicting tool for failure of the tip under defined loading conditions (Fig. 6).

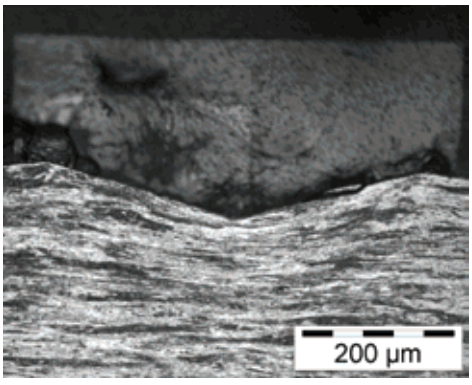

Fig. 5: Cross-section etched surface of a Vickers imprint revealing the rolling direction.

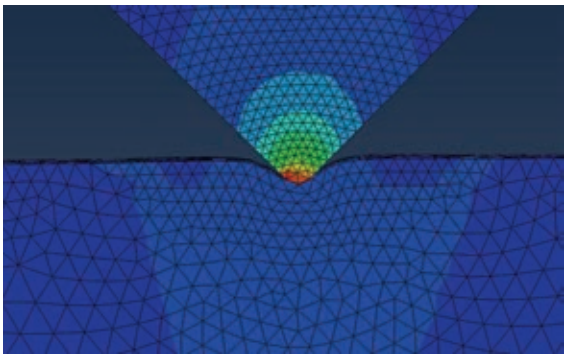

Fig. 6: High stress generation at the location of the indenter tip relatively to the specimen.

For high temperature indentation, the manufacturing of both new machines was finished in the reporting period. Both machines are designed for remote-handled use in the Hot Cell with highly active specimens; they furnish loads and maximum temperatures of 2 N and 1000 °C resp. 200 N and 600 °C. Assembly und first test runs of both machines at manufacturers are done; both machine will be delivered at end of the year, optimization of parameters is going on.

Future activities:

- Determination and significance of machine's compliance for spherical indenters
- Consideration of the pile-up-factor in evaluation of indentation data
- Investigation on anisotropic plastic deformation behaviour of single crystalline tungsten
- Investigation of crack initiation behaviour by sharp indents
- Characterisation of irradiated tungsten by instrumented indentation
- Installation of two different high temperature indentation devices
  - device 1 for temperatures up to 650 °C and forces up to 200 N
  - device 2 for temperatures up to 1000 °C and forces up to 2 N

Staff:

B. Albinski
M. Holzer
W. Ibbe
S. Lautensack
I. Sacksteder
H.-C. Schneider

Literature:

[1] Sacksteder, I., Schneider, H.C.: Development of an instrumented indentation device for further characterization of irradiated steels at high temperature. Fusion Engineering and Design, 86(2011) 2565-2568

[2] Sacksteder, I., Schneider, H.C., Materna-Morris, E.: Determining irradiation damage and recovery by instrumented indentation in RAFM steel. Journal of Nuclear Materials, 417(2011) 127-130

[3] Sacksteder, I.: Instrumented Indentation for Characterization of Irradiated Metals at Room and High Temperatures, Dissertation Fakultät für Maschinenbau, Karlsruher Institut für Technologie (KIT), 20.07.2011; http://digbib.ubka.uni-karlsruhe.de/volltexte/1000023850

Acknowledgement

This work, supported by the European Communities under the contract of Association between EURATOM and Karlsruhe Institute of Technology, was carried out within the framework of the European Fusion Development Agreement. The views and opinions expressed herein do not necessarily reflect those of the European Commission.

Mechanical Characterisation of W-Armour Materials (WP11-MAT-WWALLOY-03-01)

Background and objectives

Tungsten and tungsten alloys are presently considered for helium cooled divertor and possibly for the protection of the helium cooled first wall in DEMO designs, mainly because of their high temperature strength, good thermal conductivity, and low sputter rates. There are two types of applications for these materials which require quite different properties: one is the use as plasma-facing armour or shield component, the other is for structural purposes. An armour material needs high crack resistance under extreme thermal operation conditions while a structural material has to be ductile within the operation temperature range. Both material types have also to be stable with respect to high neutron irradiation doses and helium production rates.

The part “protection materials development” focussed on an optimisation of armour materials and high heat flux testing. Candidate materials have to be characterised by fatigue and shock tests for an assessment of their possible lifetimes. Additionally, basic mechanical characterisations have to be performed on new developed materials, to support the alloys optimisation processes.

Status

At the beginning of 2011 PSI-CRPP provided an optimized mechanically alloyed and compacted disk from W-2%Y. Specimens for both impact tests (small KLST samples) and tensile tests (sub-sized round tensile samples) were fabricated by EDM technique and tested.

The high temperature high vacuum impact tests were performed at IAM-AWP and it was found, that the **D**uctile to **B**rittle **T**ransition **T**emperature is in the region of 500 °C under dynamic loading and consequently slightly higher than the DBTT of for example WVM (potassium doped tungsten; DBTT = 435 °C) or WL 10 (tungsten with 1% lanthanum; DBTT = 465 °C)) as shown in Fig. 1. However, the **U**pper **S**helf **E**nergy is significant lower compared with the USE of such commercially available tungsten alloys.

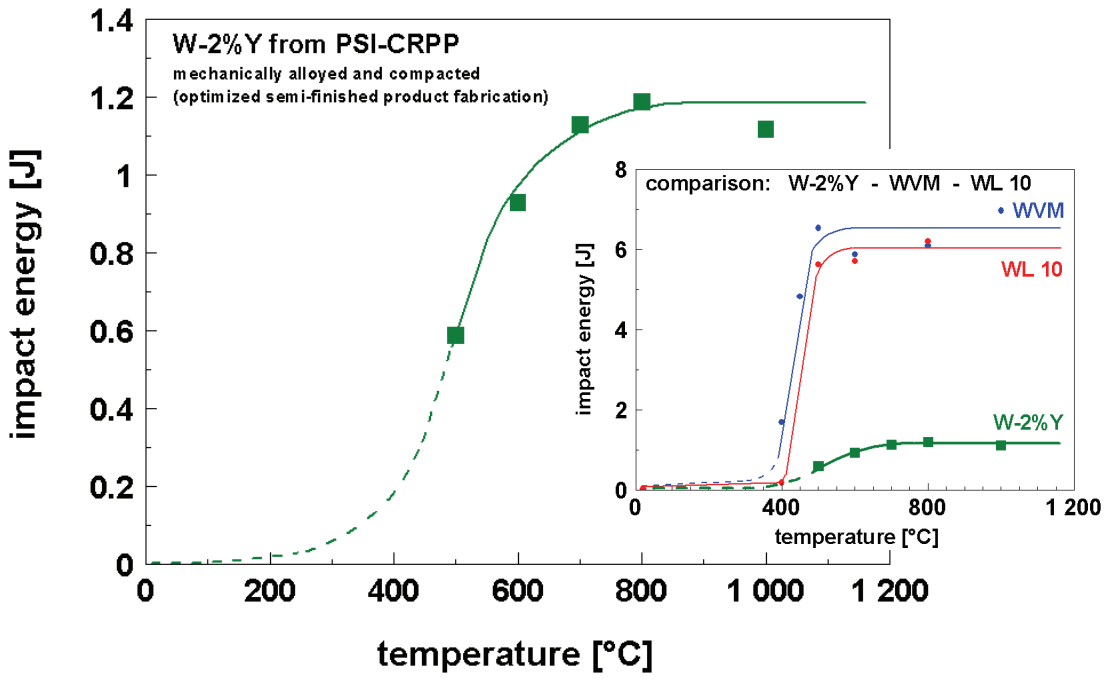

Fig. 1: Results of impact tests on W-2%Y, additionally compared with results from former tests on WVM and WL 10.

In contrast to the material behaviour under dynamic loading, the alloy shows a significant lower DBTT under quasi static loading (< 400 °C; in fracture mechanical investigations it was determined, that the DBTT is ca. 275 °C – compare Annual Report 2011, same task and activity from E. Gaganidze). Compared with both the non-compacted alloy and the first additionally forged ingot, the material shows clearly better mechanical properties in tension (Fig. 2).

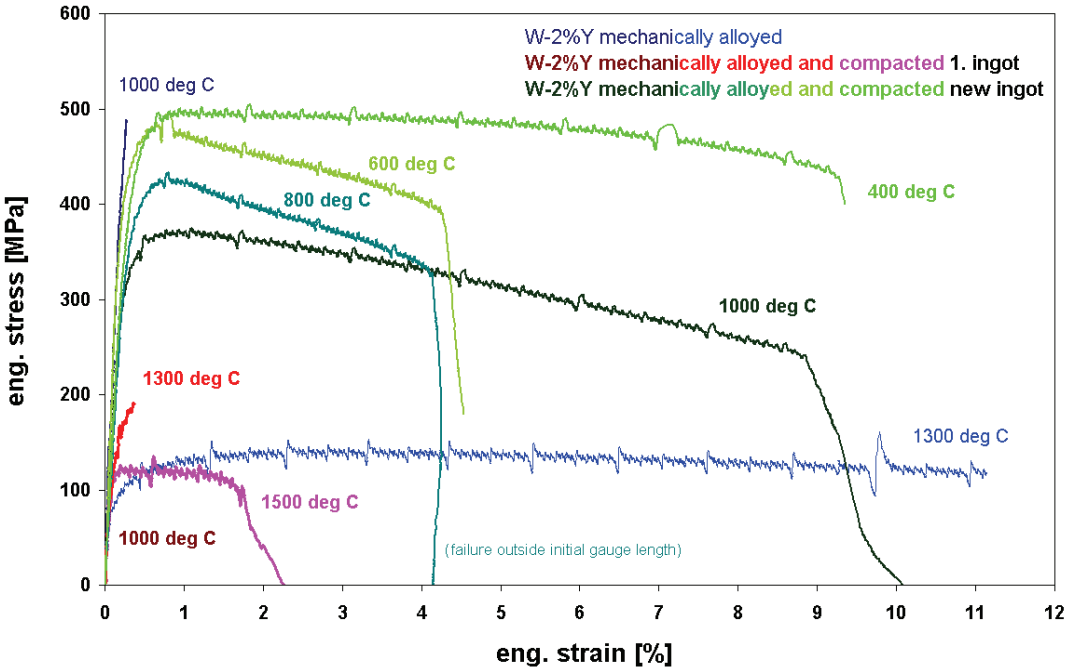

Fig. 2: Results of tensile tests on different W-2%Y alloys at relevant temperatures.

If one compares the mechanical behaviour under uniaxial loading of this novel tungsten alloy with the behaviour of pure tungsten as well as WL 10 it can be seen, that the strength at equal temperatures is comparable/slightly lower. However, the elongation at fracture is clearly lower and reveals a generally reduced plasticity in particular compared with pure W.

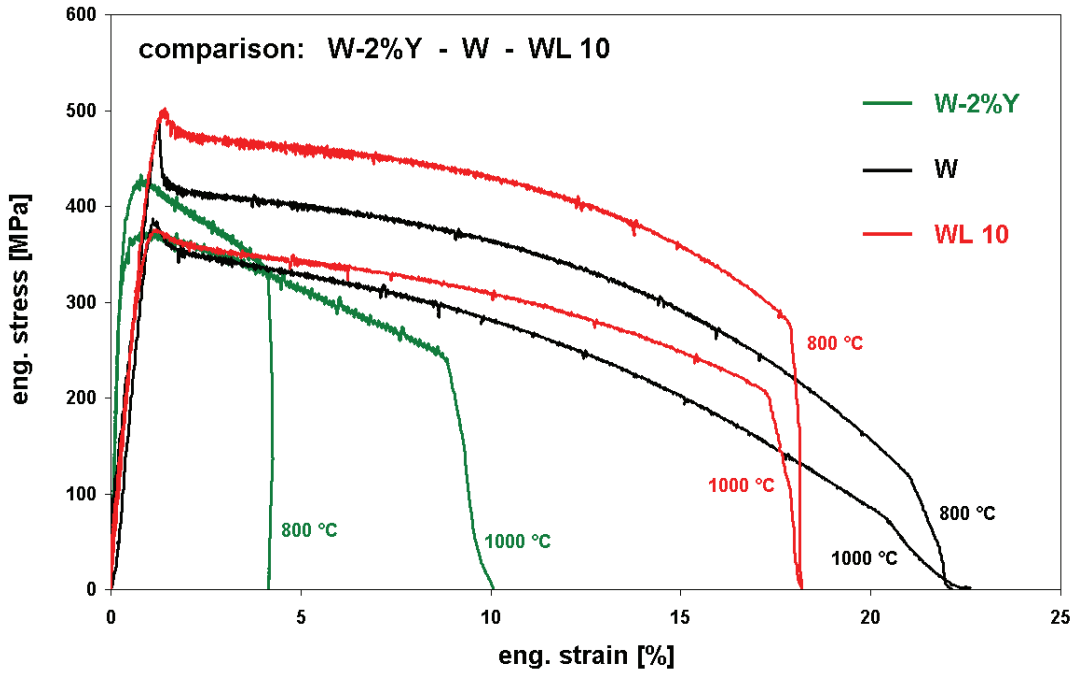

Fig. 3: Results of tensile tests on W-2%Y, W and WL 10 at selected temperatures.

In addition to the W-2%Y alloy provided by PSI – CRPP, in June/August 2011 CEIT provided two small ingots from WCr10Si10 and WCr12Ti2.5, respectively. The materials were manufactured by mechanical alloying in combination with a post HIP process (1300 °C, 1 h, 200 MPa). Due to the low amount, it was decided to fabricate small bars (3 mm x 3 mm x 30 mm) from both ingots to characterize the materials behaviour in dependence of the temperature in 3-point bending tests.

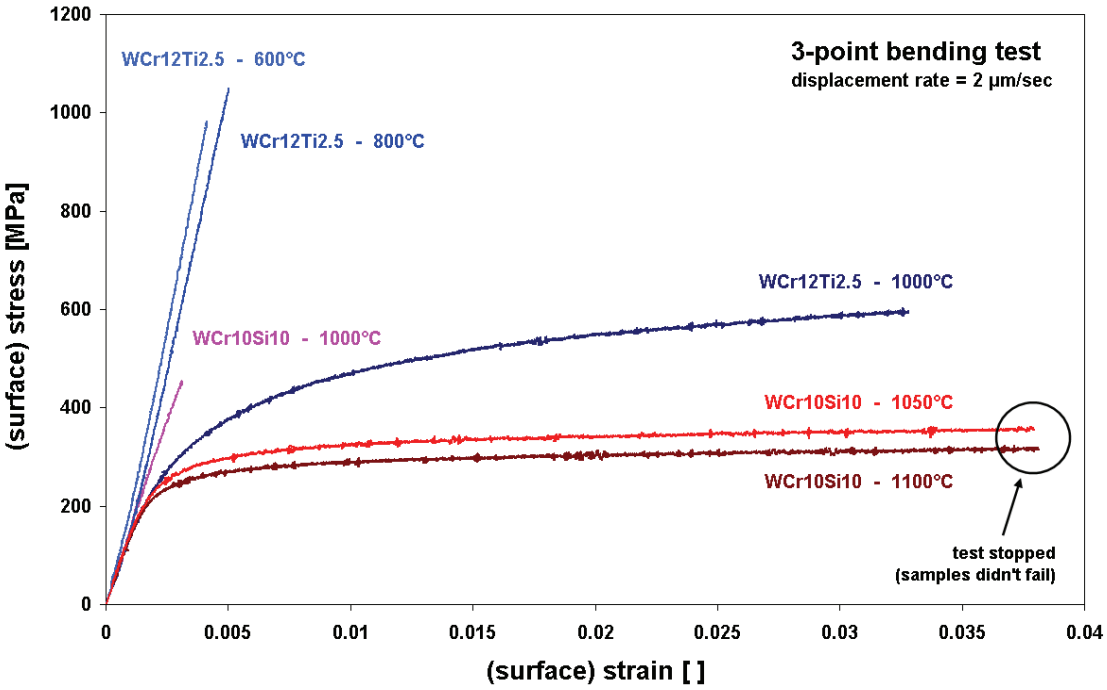

Fig. 4: Results of 3-point bending tests on both WCr10Si10 and WCr12Ti2.5.

It was found, that WCr12Ti2.5 in general shows a higher strength and a lower DBTT (probably ca. 900 °C) compared to WCr10Si10 (DBTT ca. 1025 °C). However, as illustrated in Fig. 4, the ductile to brittle transition from WCr10Si10 occurs very abrupt. It has to be clarified if this phenomenon is based on a phase transformation or a domination of the silicates $(W,Cr)_5Si_3$ on the temperature dependent deformation properties of the alloy.

Conclusion and outlook

The tests on W-2%Y, provided by PSI-CRPP were continued. It was found, that the mechanically alloyed and compressed material, manufactured with optimized semi finished product fabrication, shows clearly better mechanical properties compared to the non-compacted alloy. In impact tests, the DBTT was determined in the region of ca. 500 °C whereas in tensile tests the material still behaves ductile at 400 °C.

In addition to the tests on W-2%Y, bending tests on both WCr10Si10 and WCr12Ti2.5, manufactured and provided by CEIT, were performed. It was found, that WCr12Ti2.5 in general shows a higher strength and a lower DBTT (probably ca. 900 °C) compared to WCr10Si10 (DBTT ca. 1025 °C).

It is planned to continue the mechanical characterization of all three tungsten alloys in 2012. Beside additional bending tests on the alloys provided by CEIT, in particular WCr12Ti2.5 should also be tested in tensile experiments. Therefore, CEIT currently tries to manufacture some bigger ingots.

Staff:

M. Walter

Literature:

[1] P. López-Ruiz et al., 'Powder metallurgical processing of self-passivating tungsten alloys for fusion first wall application', 15th Conference on Fusion Reactor Materials, Charleston, 2011

[2] R. Pippan et al., 'Recent Progress in R&D on Tungsten Alloys for Divertor Structural and Plasma Facing Components', 15th Conference on Fusion Reactor Materials, Charleston, 2011

[3] M. Rieth et al., 'Recent progress on tungsten materials research for nuclear fusion applications in Europe', 15th Conference on Fusion Reactor Materials, Charleston, 2011

Acknowledgement

This work, supported by the European Communities under the contract of Association between EURATOM and Karlsruhe Institute of Technology, was carried out within the framework of the European Fusion Development Agreement. The views and opinions expressed herein do not necessarily reflect those of the European Commission.

Nuclear Data

Nuclear Data Studies/Experiments in Support of TBM Activities (F4E-GRT-056-02 (ES-AC) - Action 2, NUDATA_Exper)

Overall objective

The overall objective of the grant agreement was to provide the experimental data base required for the validation of the nuclear data libraries EFF and EAF developed in the frame of the EU Fusion Technology Programme. The focus of the KIT tasks was on experimental validation activities of ITER and TBM design calculations and on development of detectors and measuring techniques.

Task 1.1
HCLL: Determination of the relative Li content in a selection of PbLi bricks from the mock-up assembly by means of neutron flux transmission or other techniques

Recently, two experimental campaigns were performed with a neutronics mock-up of the HCLL-TBM. The first campaign was a joint tritium production rate (TPR) measurement experiment at the Frascati Neutron Generator (FNG) of ENEA Frascati [1]. Tritium measurements have been performed independently by three collaborating groups with the goal to achieve an uncertainty level as small as possible on the final combined result, since the TPR is a very crucial parameter for the self-sustaining operation of a DT fusion reactor. The second campaign was conducted at the neutron laboratory of Technical University of Dresden (TUD) with the same mock-up, which was shipped to this laboratory after the first campaign. In this campaign, fast neutron and gamma-ray spectra and the slow neutron flux by means of time-of-arrival spectra have been measured in two positions inside the mock-up [2].

The analysis of these experiments revealed that the lithium composition deviates significantly from the presumed natural composition of lithium. In the present work, we performed measurements with the aim to determine the lithium content in the LiPb, inhomogeneities in the lithium distribution and the relative ^{6}Li mass in selected bricks of the mock-up.

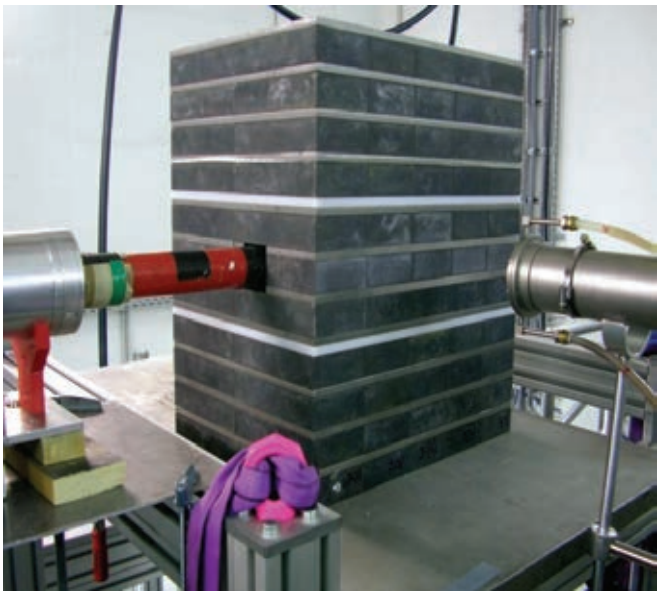

Fig. 1: The HCLL-TBM neutronics mock-up.

The HCLL-TBM mock-up was built from bricks of lithium-lead with the sizes 3.6 cm × 17 cm × 9 cm. They were arranged in 11 horizontal layers, the layers were separated by EUROFER sheets with a thickness of 9 mm. Two polyethylene sheets were inserted above and below the three central LiPb layer. Their purpose was to shape the neutron spectrum making it more similar to the spectrum expected in a breeding blanket. A photograph of the mock-up as used in the neutron and gamma-ray spectrum measurements at TUD is shown in Figure 1.

Several techniques have been applied to obtain more information on the ^{6}Li content and distribution in the LiPb:

Lithium concentration deduced from time-of-arrival spectra measurements

As part of the original neutronics experiment campaign, time-of-arrival spectra have been measured in the mock-up at TUD. Details of the experiment are described in [2]. For these measurements, the neutron generator was operated in pulsed mode with a repetition rate of 1 kHz and a DT neutron pulse length of 10 ms. The signal from a ^{3}He counter (Canberra 24NH15 type) inserted into two positions in the mock-up was accumulated in a multi-channel scaler over a time of 900 µs after the DT neutron pulse from the neutron generator. Parallel calculations using the Monte Carlo code MCNP-5 [3] show that a few tens of µs after the initial DT neutron pulse the fast neutrons have disappeared from the mock-up and the remaining neutron flux is dominated by thermal neutrons. The slope of the decay curve of this slow neutron population in the mock-up is related to the effective neutron absorption cross section of the average mock-up material, which is in turn completely dominated by the cross section of the ^{6}Li(n,a)T reaction. MCNP-5 and nuclear data from the JEFF-3.1.1 [4] and FENDL-2.1 [5] data libraries were used to calculate the time-of-arrival spectra for both experimental detector positions. The experimental and calculated decay curves are shown in Figure 2.

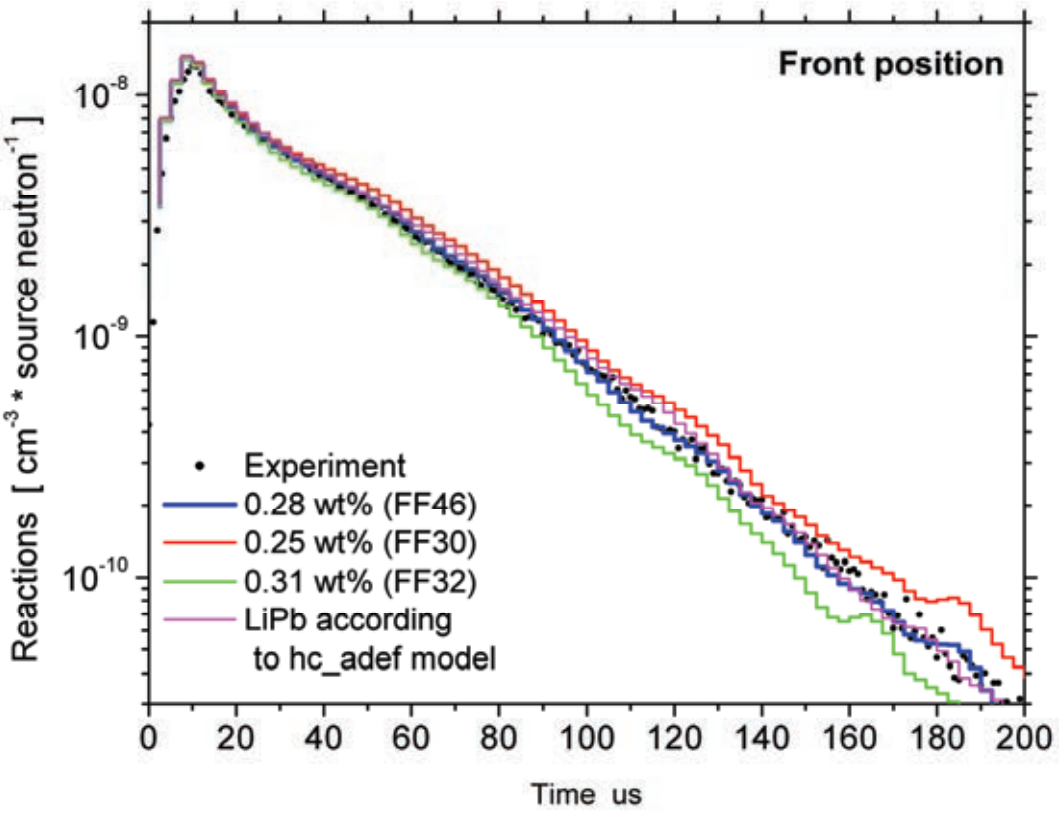

Fig. 2: Time-of-Arrival spectra in the HCLL TBM neutronics mock-up irradiated with DT neutron pulses and comparison with calculations assuming reduced ^{6}Li concentration in the LiPb. FF46, FF30, and FF32 refer to computer models with reduced Li content while the hc_adef model assumes 0.61 wt% lithium and reduced ^{6}Li abundance.

From comparison of calculated and experimental time-of-arrival spectra, a value of (0.274±0.011) wt% corresponding to the slope of the experimental decay curve was obtained.

As a result of this analysis it can be said that the ^{6}Li concentration in the LiPb of the HCLL TBM mock-up is reduced to approximately half of the nominal value either by ^{6}Li depletion or by reduced lithium content or, of course, a combination of both.

Transmission measurement

The aim of this measurement was to determine whether there are significant differences in the ^{6}Li content between bricks of the same production cast and especially between bricks from different production casts by a simple and economical procedure covering as many as possible bricks of the mock-up. The applied methodology provided relative values; an absolute determination of the ^{6}Li content would have required a very well designed thermal neutron field, which was out of scope.

An AmBe neutron source with an activity of 1.8×10^{11} Bq of ^{241}Am has been used for this experiment. It was surrounded by a layer of lead with a thickness of 5 cm and a layer of polyethylene to moderate the neutrons from the source. In order to obtain a beam of epithermal and thermal neutrons with sufficient neutron flux density, a channel was formed from tiles of LiAl.

A ^{3}He counter tube has been chosen for detecting the transmitted neutrons. It was placed in a channel made of LiAl tiles to shield it from room-returned slow neutrons.

The LiPb bricks were placed in the space between the collimator channel of the neutron source and the detector. The accumulated number of collected pulses in the ^{3}He counter was more than 10000 in each case, so that the statistical uncertainty of the counting was below 1%. The reproducibility of the measurement has been checked on some of the bricks, without changing the geometry. It was found that the ^{6}Li volume concentration between bricks even of different production batches is less than 4.4%.

Lithium content by atomic absorption spectroscopy and ICP-MS

Samples from five bricks of production cast 25 have been investigated with atomic absorption spectroscopy at VKTA Rossendorf for their lithium and lead content. The results are presented in Table 1. There is only small scattering, all relative lithium masses were the same within the average measurement uncertainty of 5.3%. The mean value of all five samples is 0.61 wt% confirming a previous analysis (0.615±0.016 wt%, 15.6 at%) by an independent institute (the Latvian Institute of Aquatic Ecology), based on atomic absorption spectroscopy measurements on a total of 60 ingots from 17 different casts.

Table 1: Lithium content in five LiPb bricks as measured with ICP-AAS at VKTA Rossendorf.

Probe	Einheit	Li [Ma%]	Pb [Ma%]	Li [At%]	Pb [At%]
1	c_i	0,61	98,7	15,5	84,5
	s	0,03	5,0	0,8	4,3
	s/c_i [%]	5,2	5,1	5,2	5,1
2	c_i	0,61	104,5	14,8	85,2
	s	0,03	5,4	0,8	4,4
	s/c_i [%]	5,1	5,2	5,1	5,2
3	c_i	0,58	102,0	14,5	85,5
	s	0,03	5,3	0,8	4,4
	s/c_i [%]	5,3	5,2	5,3	5,2
4	c_i	0,62	103,2	15,2	84,8
	s	0,03	5,3	0,8	4,3
	s/c_i [%]	5,5	5,1	5,5	5,1
5	c_i	0,62	99,2	15,6	84,4
	s	0,03	5,3	0,8	4,5
	s/c_i [%]	5,3	5,3	5,3	5,3

Small specimens from at least one brick of each production cast have been investigated also with mass spectroscopy methods at Institute of Applied Materials of KIT. The specimens were taken by drilling into the brick (Ø 5mm). The first approximately five millimetres of material were discarded to exclude surface effects from the measurements. The next approximately five millimetre were used for the specimen. From each specimen, two independent samples have been prepared for the mass spectroscopic measurement according to the published method by Misra and Froelich [6]. The results of the measurement are shown in Table 2. The average of the ^{6}Li content in the LiPb was found to be (0.0181±0.0007) wt%. Here we show an estimated error of 4% accounting for the statistical error for the average of all samples taken, 2.5 %, and an uncertainty of the enrichment of the ^{6}Li standard of 3%. The stability of the ICP-MS measurement procedure has been controlled by monitoring ^{6}Li standards before, during and after the samplemeasurements.

Table 2: ICP-MS measurements done at KIT. Two samples had been prepared from each LiPb brick specimen.

Reference	***Sample 1***		***Sample 2***	
	^{6}Li mass%	***^{7}Li mass%***	***^{6}Li mass%***	***^{7}Li mass%***
R1	0.0183	0.615	0.0182	0.601
R1 a	0.0180	0.602	0.0182	0.605
PV	0.0176	0.596	0.0172	0.584
PH	0.0177	0.597	0.0183	0.618
14.3	0.0189	0.615	0.0189	0.616
17.4	0.0179	0.589	0.0173	0.580
20.3	0.0184	0.608	0.0184	0.611
R3	0.0179	0.607	0.0182	0.615
R5	0.0180	0.608	0.0183	0.618
3.21	0.0184	0.617	0.0180	0.600
3.22	0.0186	0.618	0.0184	0.621
3.23	0.0182	0.617	0.0182	0.607
3.24	0.0184	0.614	0.0184	0.619
3.25	0.0186	0.622	0.0187	0.618
17.8	0.0170	0.564	0.0173	0.578
18.6	0.0180	0.596	0.0179	0.598
6.10	0.0175	0.591	0.0181	0.612
9.9	0.0180	0.604	0.0179	0.603
11.6	0.0183	0.609	0.0184	0.609
13.6	0.0183	0.620	0.0182	0.610
16.9	0.0186	0.615	0.0181	0.599
19.10	0.0188	0.628	0.0182	0.602
21.9	0.0183	0.605	0.0180	0.604
22.9	0.0182	0.604	0.0179	0.596
23.1	0.0171	0.574	0.0168	0.565

The scattering of the measured values of the standards was less than 1 %, therefore it was concluded that a similar margin can be assumed for a single sample. A lithium carbonate solution with 95% isotopic enrichment of ^{6}Li has been used as standard. No data about the uncertainty of the enrichment was available, but it is deemed reasonable to adopt the above mentioned value of 3%.

Staff:

Ch. Adelhelm
U. Fischer
T. Kaiser
A. Klix
D. Gehr (Technical University of Dresden, Germany)

Literature:

[1] P. Batistoni, M. Angelone, P. Carconi, U. Fischer, K. Fleischer, K. Kondo, A. Klix, I. Kodeli, D. Leichtle, L. Petrizzi, M. Pillon, W. Pohorecki, M. Sommer, A. Trkov, R. Villari, "Neutronics experiments on HCPB and HCLL TBM mock-ups in preparation of nuclear measurements in ITER", Fusion Engineering and Design, Vol. 85, (2010), p. 1675

[2] A. Klix, P. Batistoni, R. Böttger, D. Lebrun-Grandie, U. Fischer, J. Henniger, D. Leichtle, R. Villari, "Measurement and analysis of neutron flux spectra in a neutronics mock-up of the HCLL test blanket module", Fusion Engineering and Design, Vol. 85, (2010), p. 1803

[3] MCNP—A General Monte Carlo N-Particle Transport code, Version 5, Report, LA-UR 03-1987, Los Alamos, (2003)

[4] A. Santamarina, D. Bernard, Y. Rugama (Eds.), The JEFF-3.1.1 Nuclear Data Library, JEFF Report 22, Validation Results from JEF-2.2 to JEFF-3.1.1, NEA Data Bank (2009), ISBN 978-92-64-99074-6

[5] D.L. Aldama, A. Trkov, FENDL-2.1—Update of an Evaluated Nuclear Data Library for Fusion Application, INDC(NDS)-467, IAEA, (2004).

[6] S. Misra, Ph. N. Froelich, “Measurement of lithium isotope ratios by quadrupole-ICP-MS: application to seawater and natural carbonates” J. Anal. At. Spectrom., Vol. 24, (2009), p. 1524

Task 1.3
HCLL: Post-analysis of the whole experiment including sensitivity and uncertainty analysis

The EU is conducting a dedicated neutronics R&D program that includes the development of computational tools, the generation of high quality nuclear data and their validation by means of integral experiments and, later, neutronics experiments in TBMs in ITER. In the frame of this program, and integrated into the Joint European Fission Fusion File project (JEFF), neutron cross section and covariance data libraries are developed, as well as computational tools comprising sensitivity and uncertainty codes based on Monte-Carlo and deterministic approaches (MCSEN SUSD3D).

The results of the neutronics experiment at FNG on the HCPB mock-up and their analyses have already been published and the preliminary results of the experiment on the HCLL mock-up have been reported in [7]. The present, now completed task was to provide final results of the HCLL mock-up experiment, the requested sensitivity and uncertainty analyses using MCSEN are reported here.

The MCSEN code has been employed for the Monte Carlo sensitivity calculations of tritium production rates (TPR) in several lithium carbonate pellets on nuclear cross-sections of all

relevant isotopes. Available co-variance data is used to obtain nuclear response uncertainties related to nuclear data uncertainties.

The sensitivities of the TPR with respect to variations of the nuclear reaction cross sections were studied using the MCSEN and the SUSD3D code, respectively. Sensitivities were calculated at different positions, namely for the pellets containing natural lithium, located at 3.39/3.57 cm (Li-nat D1) and 28.29/28.47 cm (Li-nat D7) of penetration depth, and for the pellets enriched to 90 % in Li-6 located at 3.75/3.85 cm (Li-6 D1), and 28.65/28.75 cm (Li-6 D7) of penetration depth. Monte Carlo sensitivity calculations were performed with the MCSEN code using its track length estimator feature. The tritium production from ^{6}Li was found to be most sensitive to Pb (elastic and (n,2n)), H (elastic), ^{6}Li (n,t) and Fe(n,γ) cross-sections, as shown in Table 3. The sensitivity to the cross-sections is relatively week, and for the ^{6}Li it is even decreasing at deeper positions in the mock-up. The tritium production from ^{7}Li is most sensitive to the ^{7}Li(n,n'α)t reaction (1%/% since detector response function) itself. Additional significant negative sensitivities are due to (n,2n) cross sections in Pb. Reactions on the other involved nuclides (Fe, C) also contribute only slightly to the sensitivity. For the calculation of uncertainties in the TPR due to uncertainties of the underlying nuclear data, common sets of covariance data have been used for both methodological approaches. The covariance data were taken mainly from JEFF3.2, ENDF/B-VI.8, /B-VII, IRDF-02 and the ZZ SCALE6.0/COVA-44G libraries and COMMARA-2.0 [23] (only for SUSD3D calculations) neutron cross section covariance libraries. For the MCSEN derived uncertainties (Table 4) no correlations between different nuclides have been assumed. Very good consistency between the uncertainty predictions based on different covariance data libraries, as well as between the SUSD3D and MCSEN results, was observed. Note that the SCALE-6 covariance library is the most complete and includes, in addition to the Pb covariances, also the data for the Li, H, C and Fe cross-sections. According to these data, the associated nuclear data related uncertainties are small, generally below 3%, even for the deep positions of ~30 cm.

Acknowledgement:

The authors acknowledge the fruitful discussions with and recommendations on covariance data processing and checking by Ivo Kodeli, Institute Josef Stefan Lubljana, Slovenia. The code MCSEN has been developed by R. L. Perel, Hebrew University Jerusalem, IL.

Staff:

U. Fischer
D. Leichtle

Literature:

[7] P. Batistoni, M. Angelone, P. Carconi, U. Fischer, K. Fleischer, K. Kondo, A. Klix, I. Kodeli, D. Leichtle, L. Petrizzi, M. Pillon, W. Pohorecki, M. Sommer, A. Trkov, R. Villari, Neutronics experiments on HCPB and HCLL TBM mock-ups in preparation of nuclear measurements in ITER, Fusion Engineering and Design, In Press, Available online 18 June 2010

[8] D. Leichtle, U. Fischer, I. Kodeli, R.L. Perel et al., Sensitivity and uncertainty analyses of the HCLL mock-up experiment, Fus Eng Des 85 (2010) 1724-1727

[9] D. Leichtle, U. Fischer, R.L. Perel, Sensitivity and uncertainty analysis of nuclear responses in the EU HCLL TBM of ITER, Fus. Eng. Des. 86 (2011), 2156-2159

Table 3: Integrated relative sensitivities (in %/%) of partial TPR with respect to major cross sections for natural (7.5% 6Li) and enriched (95% 6Li) lithium pellets (MCSEN results)

Mat	MT	Position D1		Position D7	
		^{6}Li-95%	^{6}Li-7.5%	^{6}Li-95%	^{6}Li-7.5%
^{206}Pb	Tot	0.18	0.08	0.01	-0.02
	El	0.05	0.04	-0.05	-0.09
	Inel	0.04	0.02	0.02	0.01
	(n,2n)	0.07	0.01	0.02	0.05
	(n,γ)	-0.002	-0.001	-0.003	-0.004
^{207}Pb	Tot	0.27	0.09	0.11	0.11
	El	0.14	0.07	0.07	0.05
	Inel	0.03	0.01	0.01	0.02
	(n,2n)	0.07	0.01	0.02	0.03
	(n,γ)	-0.008	-0.005	-0.02	-0.02
^{208}Pb	Tot	0.44	0.11	0.05	-0.11
	El	0.25	0.09	-0.05	-0.06
	Inel	0.02	0.02	-0.007	-0.04
	(n,2n)	0.16	0.02	0.09	-0.002
	(n,γ)	<-0.001	<-0.001	-0.001	-0.001
^{6}Li	Tot	0.18	0.15	-0.34	-0.06
	El	-0.005	0.001	<-0.001	<0.001
	(n,t)	0.19	0.15	-0.34	-0.06
^{7}Li	Tot	0.06	0.53	0.03	0.007
	El	0.05	0.01	0.04	0.004
	Inel	0.008	<0.001	<0.001	-0.007
	(n,t)	0.004	0.52	-0.004	0.01
^{1}H	Tot	0.63	0.40	0.12	0.34
	El	0.64	0.41	0.15	0.37
^{nat}C	Tot	0.06	0.02	0.005	0.02
	El	0.06	0.02	0.009	0.02
	Inel	<0.001	0.001	-0.004	-0.005
	(n,γ)	<-0.001	<-0.001	<-0.001	<-0.001

Table 4: Total uncertainties (1σ, in %) of TPR due to uncertainties of nuclide reaction cross sections. Results for Pb are from ENDF/B-VI.8 and SCALE6.0 covariance data, respectively (MCSEN results). (Results for 6Li: EFF2/IRDF02, results for 7Li: ENDF/B-6.8/SCALE6, results for 1H: ENDF/B-V)

Mat	TPR from $^{95\%}$Li at D1	TPR from $^{95\%}$Li at D7	TPR from ^{nat}Li at D1	TPR from ^{nat}Li at D7
^{206}Pb	0.8/0.8	0.8/0.5	0.3/0.2	0.6/0.6
^{207}Pb	0.8/0.9	0.5/0.6	0.1/0.2	0.5/0.5
^{208}Pb	1.5/1.6	1.3/1.0	0.4/0.4	0.9/0.6
^{6}Li	0.6/<0.1	0.2/<0.1	0.3/<0.1	<0.1/<0.1
^{7}Li	<0.1/<0.1	<0.1/<0.1	0.4/4.7	<0.1/0.1
^{1}H	0.4	0.4	0.2	0.3
^{nat}C	<0.1	<0.1	<0.1	0.1
Total	**2.0/2.0**	**1.7/1.3**	**0.7/4.7**	**1.2/1.0**

Task 2.1 and 2.2
HCLL: Setting up, testing and determination of the response matrix of a spectrometer in the energy range < 2 MeV, use of the spectrometer for measurement in the mock-ups with DT neutrons

In previous experiments with the HCLL mock-up, TPR, neutron and gamma-ray spectra have been measured. A well characterized NE213 scintillator was applied to obtain neutron spectra in two locations in the mock-up under DT neutron irradiation at TUD-NG. However, the accessible neutron energy range in the proton-recoil based scintillator starts around 2 MeV. Below these energies the influence on carbon recoils on the primarily measured pulse height spectra is too high and these energies had to be excluded from previous measurements. Hydrogen filled proportional counter tubes can be used to measure neutron spectra in the range of several tens of keV up to approximately 1 MeV depending on their size and pressure of the filling gas which determines the H density and hence the mean free path of the recoil proton.

We have used a commercially available proton recoil tube for the measurement of neutron spectra in the HCLL TBM mock-up. The device was a LND 281 fabricated by LND Inc. Its active volume had a radius of 1.82 cm and a length of 17.78 cm. The tube was filled with a mixture of hydrogen (3040 torr), nitrogen (100 torr) and methane (100 torr) according to the manufacturers' data sheet. With these values it is possible to measure neutron fluxes from approx. 300 keV to 1 MeV.

The reaction $^{14}N(n,p)^{14}C$ + 625.9 keV has been used to calibrate the primary pulse height spectrum of protons. The latter will be used together with the response matrix of the proportional counter in an unfolding procedure to compute the neutron spectrum.

The response matrix is calculated with MCNPX Version 2.6 [10]. The detailed geometry including gas amplification effects are taken into account. A preliminary result of the matrix calculation is shown in Figure 3. Additional calculations are underway to improve the response matrix and to proceed with the unfolding using the MAXED code [11].

Staff:

U. Fischer
D. Förster
D. Gehre
A. Klix

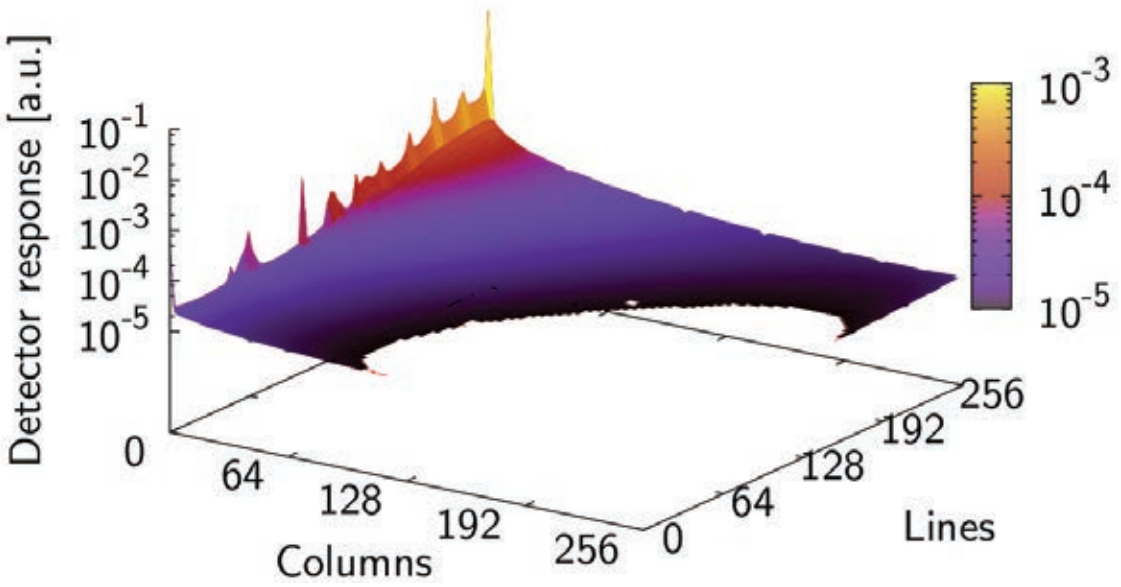

Fig. 3: Calculated response matrix.

Literature:

[10] D.B. Pelowitz, ed., “MCNPX™ User’s Manual, Version 2.6.0”,LANL Report LA-CP-07-1473, 2008

[11] M. Reginatto and P. Goldhagen. Maxed, a computer code for maximum entropy deconvolution of multisphere neutron spectrometer data. Health Physics, 77(5):579–583, November 1999.

Task 3.2
Assessment of a Li glass detector coupled to a photodiode via fiber for use in the TBM. Test in the HCLL mock-up

Neutronics experiments with the TBM in ITER will face several severe challenges. Any kind of detectors will have to withstand an extremely harsh environment, which is characterized by intense fields of ionizing radiation, temperatures on the order of several hundred grad Celsius, strong magnetic fields, etc. In addition, the access to the TBM will be very limited so that any kind of diagnostics system might have to stay in the TBM for many plasma pulses and experimental campaigns before it could be replaced in the event of a failure.

This task is devoted to preliminary investigations of the suitability of a combination of lithium glass scintillators, optical fibers and photodiodes as candidates for TBM diagnostics. At this point we do not address the radiation hardness of the system; we test only the principal functionality.

The detector used in these tests is a ^{6}Li-enriched lithium glass GS2 from Nuclear Enterprises. The cylindrical scintillator has a diameter of 1 cm and a height of 1 cm. In a first step it was coupled to a custom design avalanche photo diode (APD) from Hamamatsu. The APD had a sensitive area of 5 mm by 5 mm and a peak sensitivity at 450 nm. It was operated at a bias voltage of 384.7 V. Under these conditions it produced a pulse signal approximately proportional to the energy deposition by the charged particles in the scintillator.

Figure 4 shows a comparison of a typical pulse height spectrum taken with the scintillator coupled directly to the APD and, for comparison, to a photo multiplier tube (PMT). Apparently the energy resolution of the combination scintillator–APD is slightly lower than that of the combination scintillator–PMT. The source of neutrons for the irradiation was a Cf-252 spon-

taneous fission source with an activity of 2.27E+08 Bq delivering approximately 2.64E+07 neutrons per second. The source neutrons were moderated with polyethylene blocks.

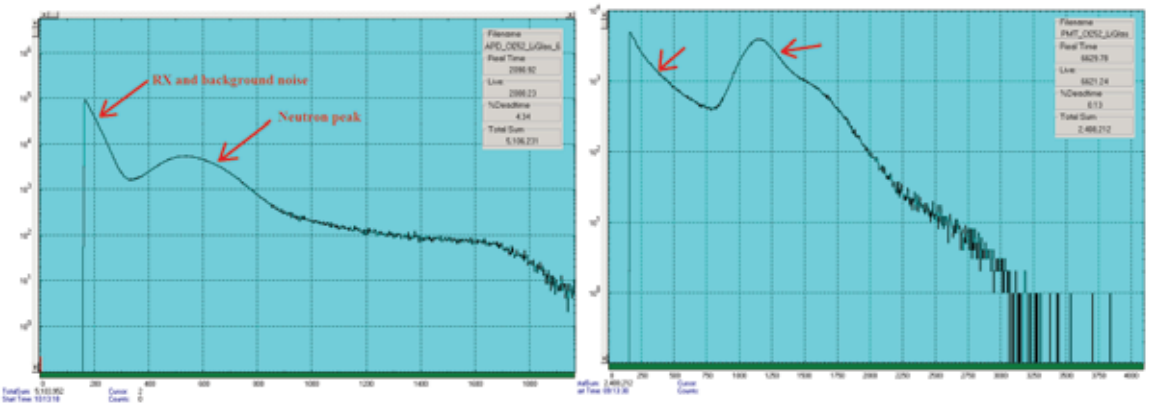

Fig. 4: Pulse height spectra taken with the combination Li-glass–APD (left) and Li-glass–PMT (right)

Tests with the combination Li-glass scintillator, APD and an available optical fiber have been performed but no clear output signal was found. Additional experiments with a special UV/Vis fiber are underway.

Staff:

U. Fischer
A. Klix
Th. Lafargue

Task 3.5
Selection of suitable foil combinations with respect to cross section, half-lives of daughters, temperature and expected measurement regime to be used in an automatic system for insertion/removal

An important aim of neutronics TBM experiments in ITER will be to assess the prediction accuracy of nuclear responses in an environment more closely resembling that of a future fusion reactor than could be achieved so far with existing facilities. Quantities to be measured are for example tritium production rates and nuclear heating. These quantities have to be related to the time-dependent spectral neutron flux through the TBM. The local spectral flux density in the TBM will depend on the particular plasma conditions and hence not only the total flux density and spacial flux distribution but also the spectrum may change during a plasma pulse [12]. There are currently only a few measurement techniques available which are compatible with the harsh environment conditions in the TBM during operation such as high temperatures, strong EM fields and intense ionizing radiation. We are therefore studying a “traditional” but promising technique for neutron flux measurements based on activation foils and a pneumatic transport system into the TBM and back. Such a transport system would allow also for measurement cycles shorter than a plasma pulse and hence to obtain a temporal neutron flux profile if suitable activation foils are used.

Selection of the activation foil set

A fast pneumatic measurement system could produce nearly real-time data if the exposure to the neutron field can be kept short (on the order of a few tens of seconds) and the measurement of the induced gamma-ray activity is done immediately after extraction. However, under these conditions the use of "classic" dosimetry reactions would not be very suitable since the gamma lines due to induced activity of interest may be much smaller than gamma lines from "parasitic" induced activity (mostly meta-stable states with short half-lives).

It appears interesting to look at short-living induced activities and utilize the nuclear reactions from which they originate as dosimetry reactions. We have therefore investigated several candidate materials for their suitability to short cycle measurements. Initial criteria were a gamma line intensity of at least 10% and a half-life time between 30 and 300 seconds. This generated a collection of possibly useful dosimetry reactions. In a further step, detailed calculations have been performed to assess whether the induced gamma activity can be measured indeed with acceptable signal-to-noise ratio and as few corrections as possible such as coincidence summing due to the presence of several intense gamma lines from the same isotope.

The induced gamma activity in 0.1 g of each investigated material has been calculated with the European Activation System EASY-2007 [13]. The choice of the mass is somewhat arbitrary; however, since the activity would scale linearly with mass, this value appears to be a suitable choice. At this moment there are no fixed choices for measurement positions in the TBM. Therefore a position in the equatorial plane of ITER, central breeder unit of the HCPB TBM and 3 cm behind the first wall, adjacent to the vertical part of the breeder layer in the breeder unit has been selected to proceed with the assessment. The neutron spectrum was calculated with MCNP-5 [14] and nuclear data from FENDL-2.1 [15]. A total neutron flux density of $1.42*10^{14}$ $n*cm^{-2}$ as a result of the MCNP calculation was used as input for the EASY calculation. An irradiation time of 30 seconds followed by a cooling (sample transport) time of 10 seconds has been adopted. The induced activities calculated by FISPACT have been used together with gamma line data from ENSDF to construct a gamma source term for a gamma transport calculation simulating a HPGe detector with MCNP-5 and nuclear data from the mcplib04 and el3 libraries. The size of the HPGe detector was chosen to be 5.52 cm diameter and 5.83 cm height following the dimensions of a commercial detector routinely used in the neutron laboratory of TUD. Pulse height tallies have been used to simulate the gamma-ray detector.

Results

Several candidate foil materials have been investigated with the calculation method described above. In many cases metastable states emitting gamma lines in cascades were found. In such a case the measurement can be in principle performed. However, depending on the geometrical setting of the gamma ray measurement, severe corrections for coincidence summing might be necessary or the simultaneous measurement of a set of foils might become difficult, since each gamma-ray line in the energy range up to 2..3 MeV produces a Compton background, which could reduce extremely the signal-to-noise ratio for lines of interest from other foils. Therefore, only materials with a few lines from the induced activity were given preference. A preferred selection of foils is shown in Table 5, together with their relevant proposed dosimetry reactions. All materials in this Table have melting points above the temperatures which are expected in the ITER TBMs.

For each of these four materials the expected pulse height spectra in a typical HPGe detector were calculated for a measurement regime described in section 2.2. An example of such a calculated spectrum is shown for illustration in Fig. 5.

Of same importance as the measurability of the emitted gamma lines is the coverage of the neutron energy range for energies from 0 to approximately 14.5 MeV as expected in the TBM. The reactions $^{140}Ce(n,\alpha)^{137m}Ba$ and $^{93}Nb(n,\alpha)^{89m}Y$ do have a slow neutron energy part, but the cross section is very low there. Therefore only the reactions $^{27}Al(n,\gamma)^{28}Al$ and $^{93}Nb(n,\gamma)^{94m}Nb$ should be considered for the measurement of the slow neutron energy range. The remaining proposed dosimetry reactions from Table 5 cover the fast neutron energy range. Approximate threshold energies are given in Table 5. The energy where the cross section is approximately 10% of the maximum value has been adopted as criterion for the threshold energy. From the threshold energy column in Table 5 it is clear that there is no threshold reaction covering the energy range between a few hundred keV and about 4 MeV

well in this foils set. Information on this energy range would be only included in the reaction rates of the n,γ reactions on aluminium and niobium.

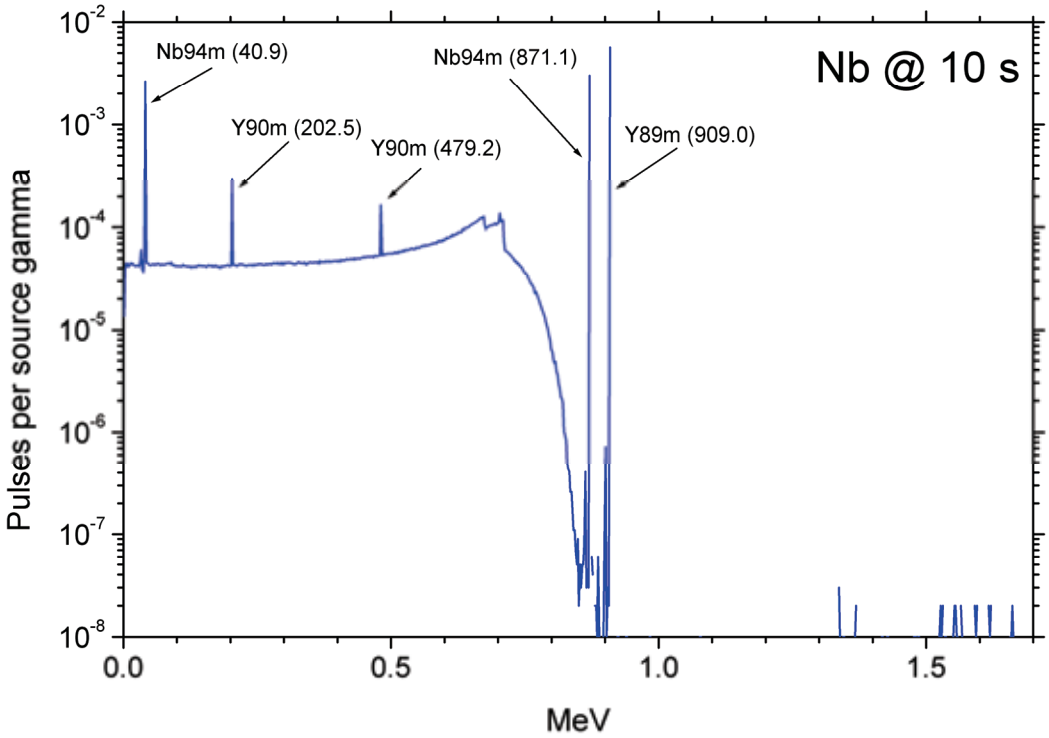

Fig. 5: Calculated pulse height spectra in a HPGe gamma-ray detector from Nb following.

Table 5: Proposed dosimetry reactions for TBM neutronics experiments (based on JEFF-3.1.1).

Dosimetry Reaction	**Half-life (sec)**	**Approx. threshold energy (MeV)**	**Gamma-ray energy / Intensity of gamma line**		
$^{140}Ce(n,2n)^{139m}Ce$	56.1	10	754.2 / 0.92		
$^{140}Ce(n,\alpha)^{137m}Ba$	153.12	12	661.7 / 0.90		
$^{27}Al\ (n,g)\ ^{28}Al$	134.46	--	1778.7 / 1.00		
$^{27}Al(n,p)^{27}Mg$	567.48	4.5	843.7 / 0.72	1014.4 / 0.28	
$^{52}Cr(n,p)^{52}V$	224.7	5.5	1434.1 / 1.00		
$^{53}Cr(n,p)^{53}V$	97.2	6	1006.3 / 0.90	1289.5 / 0.10	
$^{54}Cr(n,p)^{54}V$	49.8	11	834.8 / 0.97	989.1 / 0.80	2259.3 / 0.46
$^{54}Cr(n,p)^{51}Ti$	348.0	8.2	320.1 / 0.94		
$^{93}Nb(n,g)^{94m}Nb$	375.6	--	41.0 / 7.3e-4	871.1 / 4.95e-3	
$^{93}Nb(n,a)^{90m}Y$	11484	6.9	202.5 / 0.97	479.5 / 0.91	
$^{93}Nb(n,na)^{89m}Y$	15.663	12.5	909.0 / 0.99		
$^{93}Nb(n,2n)^{92m}Nb$	876960	9.5	934.5 / 0.99		

Staff:

U. Fischer
A. Klix

Literature:

[12] A. Murari, M. Angelone, G. Bonheure, E. Cecil, T. Craciunescu, D. Darrow, et.al., New Developments in the Diagnostics for the Fusion products on JET in Preparation for ITER, Report EFDA-JET-CP(10)03/09.

[13] R.A. Forrest, The European Activation System: EASY-2007 overview, Report Culham Science Centre, UKAEA FUS 533, 2007.

[14] MCNP - A General Monte Carlo N-Particle Transport code, Version 5, Report LA-UR-03-1987, LANL (2003).

[15] D. Lopez Aldama, A. Trkov, FENDL-2.1 -- Update of an evaluated nuclear data library for fusion application, INDC(NDS)-467, IAEA (2004).

Acknowledgement

This work was supported by Fusion for Energy under the grant contract No. F4E-GRT-056-02 (ES-AC).- Action 2 with collaboration by ENEA, Italy; AGH-UST, Poland; JSI, Slovenia and ASCR, Czech Republic. The views and opinions expressed herein reflect only the author's views. Fusion for Energy is not liable for any use that may be made of the information contained therein.

Neutronics Analysis of ITER Diagnostic Components (ITER/IO/10/4300000298)

Objective

The general objective of this work was to provide neutronics computational service for the ITER Diagnostics Team in order to improve the shielding performance of the Diagnostic Generic Equatorial Port Plug (EPP) in ITER. Systematic neutronics analyses need to be conducted to assess the EPP radiation shielding performance and identify important parameters for optimizing the design, with the objective to find technical solutions for reducing the neutron streaming through the port in such a way that the ITER design limit for the shut-down dose rate for personnel access can be met.

Introduction

The ITER components must withstand the irradiation of 14 MeV neutrons generated in the D-T fusion nuclear reactions in the plasma chamber and impinging on the First Wall (FW) as shown in Fig. 1. The ITER design encompasses many engineering details, some of them, such as gaps and channels, provide streaming paths for neutron and secondary photon radiation and degrade the shielding performance of the blanket or port plugs. These geometry details must be properly modeled, while for other ITER parts (blanket bulk shield, vacuum vessel shield) the homogenization of shield materials is possible. The challenges arising in the neutronics modeling of ITER are associated with the deep-penetrating radiation with attenuation factors by ~8 orders of magnitude for total neutron fluxes. Such problems were addressed in Ref. [1] devoted to the analysis of the ITER Upper Port which is shown in Fig. 2. The Monte Carlo code MCNP5 [2] was selected as the reference radiation transport 3D computer code. The R2Smesh interface code [3] and the 3D CAD geometry conversion tool McCad [4], both of them developed at KIT and integrated in a fusion neutronics toolkit [5] are routinely applied for the ITER design activities [5, 6]. Responding to actual ITER demands, the R2S approach [7] was extended to the updated R2Smesh system by inclusion the possibility of coupling the MCNP5 transport and FISPACT-2007 [8] activation calculations through the common use of mesh-tally distributions. In the R2Smesh scheme, the results of neutron fluxes, generated decay photon sources and the final results of shutdown dose rates are calculated on a 3D mesh representation, which can have a high spatial resolution. Distributions of neutrons, secondary photons, and decay photons and other nuclear responses can thus be represented in the geometry required preserving original heterogeneities, such as small gaps around the diagnostic Equatorial Port Plug (EPP) shown in Fig. 1.

The EPP gap allows manufacturing tolerance of 2 cm; the gaps of 0.5-cm thick separate the EPP drawers inside which the diagnostic equipment is packed. In the calculations, the content of the EPP drawers was not followed geometrically explicit, and instead, it was modeled homogeneously as mixture of 80 vol.% of steel and 20% of water. It was assessed separately, that the radiation streaming through the EPP diagnostic channels inside the drawers contributes ~50 μSv/hr into the shutdown dose rate at the Port Extension (PE) interspace pinpointed in Fig. 1. Therefore, the ITER design limit of 100 μSv/h for personnel access has been changed to 50 μSv/h in application to the diagnostic EPP modeling with the homogenized material composition of its shielding. The challenges of physics, engineering and technology of the EPP diagnostic systems are well presented in [9]. Early neutronics studies [10] of several systems of plasma diagnostic in the Upper and Equatorial Ports have served for diagnostics development in ITER. The results of nuclear heating and neutron flux distributions for the Radial Neutron Camera inside EPP are provided in [11], where it is shown that shutdown dose rate levels at the PE interspace are much higher than the design target of 100 μSv/h. Some recent results of the EPP shielding and activation parametric analyses [12] have revealed substantial progress in mitigating the radiation streaming through the EPP gaps by means of arrangement of gap labyrinth, stoppers, and rails.

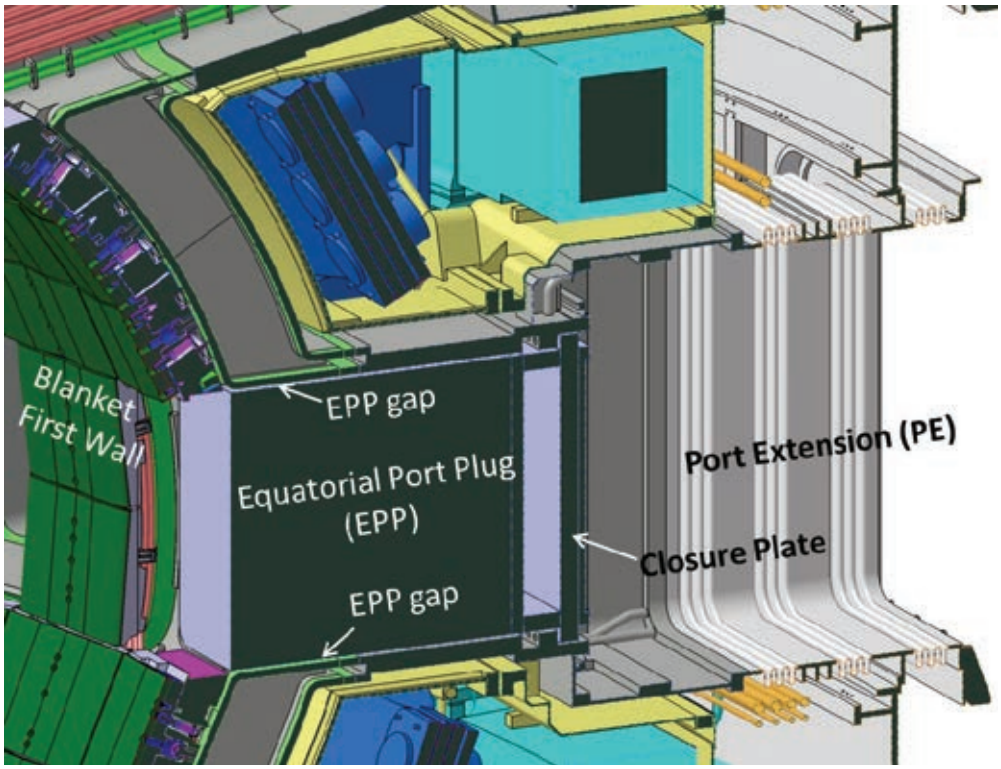

Fig. 1: Computer Aided Design (CAD) view of the Blanket First Wall (FW), Equatorial Port Plug (EPP) and its back-side interspace behind Closure Plate inside Port Extension (PE).

MCNP model approximations

A local EPP MCNP model has been created by extracting the Equatorial Port area with adjacent blanket modules and vacuum vessel from the global ITER model called A-lite 4.1, as shown in Fig. 2. The extracted parts (blanket insertions, port structures such as walls, closure plate, and extension box) were modified in accordance with the CAD drawings of ITER. A proper surface neutron source has been generated by recording the source neutrons passing the EPP first wall in a MCNP run with full neutron source definition in plasma volume. On the four lateral sides of the extracted local EPP model, reflective or vacuum boundary conditions were assumed, as shown in Fig. 2. A straight gap of 2 cm width between EPP and port frame was considered as initial variant of the EPP neutronics parametric analysis. Two zones behind the closure plate were selected for the detecting of fluxes and doses.

The R2Smesh scheme applied for the local modeling includes MCNP5 radiation transport and FISPACT-2007 activation calculations coupled through the use of mesh-tallies covering the whole space of the local model shown on the right of Fig. 2. The maps of shutdown dose rates have been produced around EPP, taking into account the decay photon sources generated in materials of whole local model.

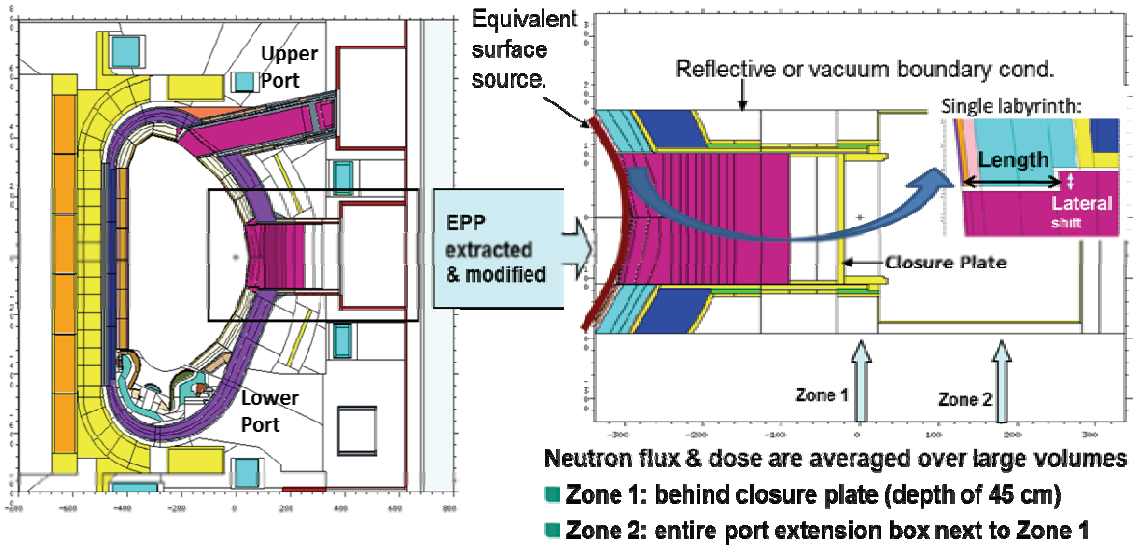

Fig. 2: MCNP plots of local modeling approach for the ITER Equatorial Port Plug (EPP).

Results

As result of a series of EPP parametric neutronic calculations [12], a labyrinth was arranged behind the blanket as shown in Fig. 2 for reducing the neutron streaming inside the EPP gap, which dominates in fluxes and doses in the detecting zones. To find its optimal dimensions the 1st gap segment length and the lateral shift of the labyrinth have been systematically varied. The resulting flux and dose values are presented in Figs. 3 and 4 for the 1st segment length, where zero value of the length corresponds to the straight gap and 70-cm length is located in the middle of vacuum vessel. Due to EPP engineering design reasons, the optimal single labyrinth is set at 40 cm for the 1st segment length and 8 cm for the lateral shift. The results shown in Figs. 3, 4 obtained with reflective and vacuum boundary conditions in the local model give upper and lower limits of the real results, which can be obtained in the full 3D ITER model. Such results are presented in Table 1 for the ITER global B-lite model, the successor model of A-lite, with three variants of the EPP and ITER Lower Port description.

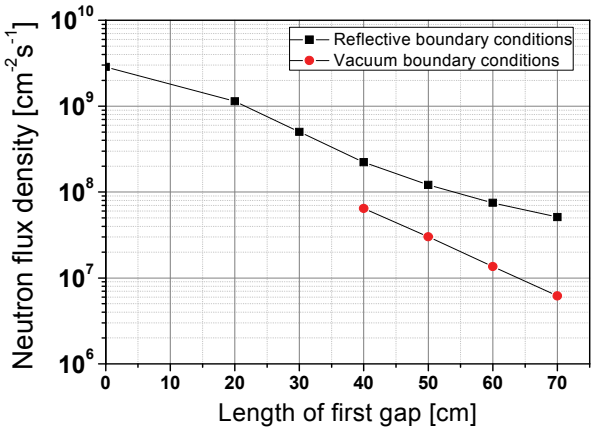

Fig. 3: Total neutron flux (n/cm^2/s) profiles in **Zone 2** as function of 1st segment length of the labyrinth (see Fig. 2) of the EPP local model.

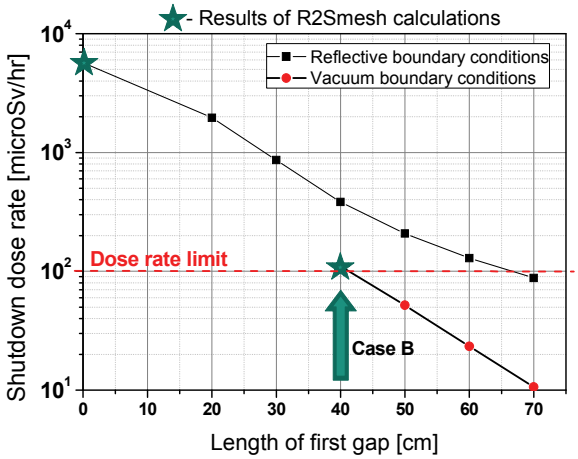

Fig. 4: Shutdown dose rate (μSv/hr) profiles for **Zone 2** as function of 1st segment length of the gap labyrinth shown in Fig. 2.

The dose rates have been calculated [12] at 10^6 s after ITER operation along the SA2 scenario with R2Smesh for two local models: with straight gap and optimal labyrinth, as pinpointed by stars in Fig.4, while for the intermediate labyrinth variants the flux-to-dose scaling factor of 1.6e-6 μSv/hr*cm^2*s has been applied for the dose estimations. The highest shut-

down dose rate of 6090 μSv/hr is obtained in Zone 1 of the local EPP model **L1** with straight EPP gaps. These gaps open line-of-sight from the plasma to the EPP connective flange at the back closure plate, as shown in Fig. 5 of the dose rate map with two symmetrical peaks at flange. By introducing the optimal labyrinth in the model **L2** (schematically shown in Fig. 7), the dose is reduced to 512 μSv/hr, which is still 10 times above the target 50 μSv/hr. Also, lateral boundary conditions affect the fluxes and doses in the detecting zones, e.g. in the model **L2** with vacuum boundaries the dose map is presented in Fig. 6 with 345 μSv/hr and 111 μSv/hr in Zones 1 and 2, respectively. For the same locations of the model **L2** with reflective boundaries, the doses are 512 μSv/hr and 384 μSv/hr (see Table 1) due to preserving the radiation inside the local model boundaries, bouncing from its lateral sides. As multivariant parametric analysis [12] proved, only a configuration with double labyrinth in the model **L3** as shown in Fig. 8 makes it possible to satisfy the dose limit of personnel access. From the activation analysis of the EPP materials follows that the dose at 10^6 s after shutdown is dominated by decay photon emission from the SS316L(N)-IG steel isotopes of ^{60}Co (~50% of dose), ^{58}Co (~20% of dose), ^{54}Mn and ^{182}Ta (~10% each).

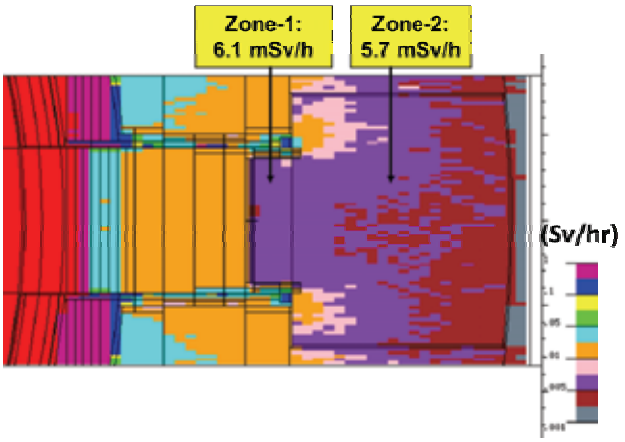

Fig. 5: Shutdown dose rate (μSv/h) map for the local EPP model L1 with straight gap and reflective boundary conditions.

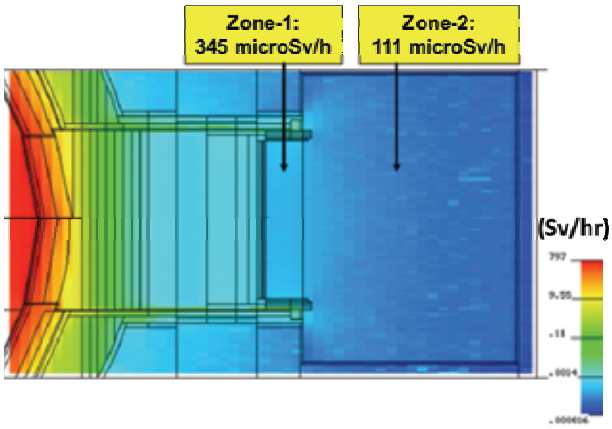

Fig. 6: Shutdown dose rate (μSv/h) map for the local EPP model L2 with optimal single labyrinth and vacuum boundary conditions.

Table 1: Comparison of local vs. global MCNP5 modeling.

Model description	EPP gap	Shutdown dose rate (μSv/h)	
		Zone 1	Zone 2
Local EPP – L1 (reflective boundaries)	Straight gap	6090	5700
Local EPP – L2 (reflective boundaries)	Optimal single labyrinth	512	384
Local EPP – L3 (reflective boundaries)	Double labyrinth	29	45
Global B-lite-V1: pre-designed EPP, no inter-drawer gaps	Some labyrinth	~ 578	~ 390
Global B-lite-V2: integrated EPP design, with 0.5-cm gaps between EPP drawers, and un-shielded Lower Port	Optimal single labyrinth	~ 1290	~ 979
Global B-lite-V3: integrated EPP design with closed gaps between EPP drawers and shielded Lower Port	Optimal single labyrinth	~ 403	~ 229

The comparison of doses obtained with local and global modeling approaches is presented in Table 1. The doses inside the EPP zones of the global B-lite models were obtained with

the flux-to-dose factor calculated before for EPP. The B-lite-V1 model demonstrates similar to the local EPP model doses (578 μSv/hr in Zone 1). B-lite-V1 is characterized by preliminary description of EPP with some labyrinth, no lateral gaps between blanket and EPP, and absence of 0.5cm drawer gaps. The insertion in B-lite-V2 of the EPP design with optimal labyrinth results in ~1290 μSv/hr, due to open EPP drawer gaps and adverse streaming from the Lower Port. In the B-lite-V3 global model, by means of closing the 0.5cm gaps between the EPP drawers and shielding the Lower Port, it was possible to reach ~403 μSv/hr in Zone 1. The dose difference between the B-lite variants V2 and V3 demonstrates the cross-influence effect causing by Lower Port to the EPP interspace.

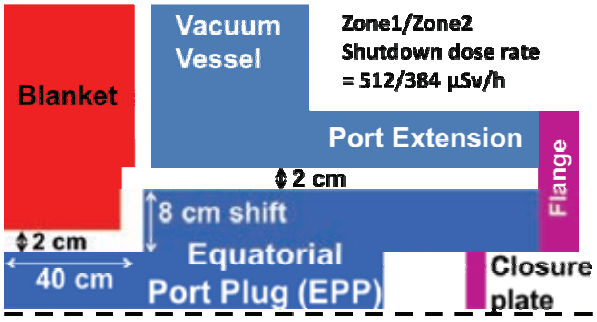

Fig. 7: Schematic view of local EPP model with optimal single labyrinth – model **L2.**

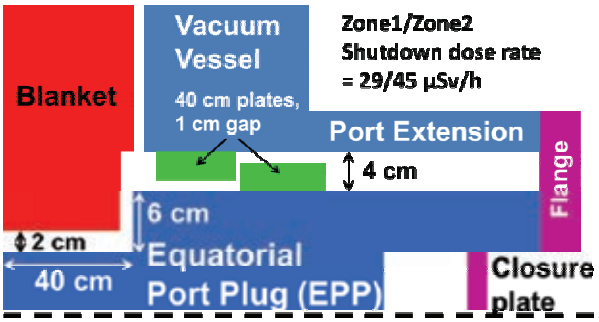

Fig. 8: Schematic view of local EPP model with double labyrinth – model **L3.**

The MCNP neutron fluxes were achieved with ~10% statistical precision for the track-length estimations, using the parallel computations on the JUROPA/HPC-FF cluster in the most effective way following to the recommendations [13] of optimal parallel computing.

Staff:

A. Serikov
U. Fischer
D. Leichtle

Literature:

[1] A. Serikov, et al., “Neutronic modeling challenges for the ITER ECRH launcher shielding design,” Nuclear Technology, 168, November (2), (2009), pp. 411-416.

[2] X-5 Monte Carlo Team, “MCNP—A general Monte Carlo N-particle Transport Code, Version 5, Vol. I: Overview and Theory,” LA-UR-03-1987, Los Alamos National Laboratory (Apr. 24, 2003).

[3] D. Leichtle, M. Majerle, U. Fischer, A. Serikov, “Verification and validation of the R2Smesh approach for the calculation of high resolution shutdown dose rate distributions,” Proceedings of the ISFNT-10, Portland, Oregon, USA, Sep. 11–16, 2011.

[4] D. Grosse, H. Tsige-Tamirat, “Current Status of the CAD Interface Program McCad for MC Particle Transport Calculations,” Proc. M&C 2009, Saratoga Springs, May 3-7, 2009.

[5] A. Serikov, U. Fischer, et al., “Toolkit for High Performance Monte Carlo Radiation Transport and Activation Calculations for Shielding Applications in ITER,” Proc. M&C 2011, Rio de Janeiro, RJ, Brazil, May 8-12, 2011, LAS/ANS (2011); http://mathematicsandcomputation.freezoka.net/MC11/_pdf/mc27_256_paper.pdf

[6] U. Fischer, et al., “Neutronics R&D efforts in support of the European breeder blanket development programme,” Nuclear Fusion 49 (2009) 065009.

[7] Y. Chen, U. Fischer, “Rigorous MCNP based shutdown dose rate calculations: computational scheme, verification calculations and applications to ITER,” Fusion Engineering and Design 63–64 (2002) 107–114.

[8] R. A. Forrest et al., “FISPACT 2007 user manual,” UKAEA FUS 534 report, March 2007.

[9] M. Walsh, et al., “ITER diagnostic challenges,” Proceedings of 2011 IEEE/NPSS 24th Symposium on Fusion Engineering (SOFE 2011), 26-30 June 2011, Chicago, USA.

[10] G. Shatalov, A. Borisov, S. Sheludjakov, A. Serikov, “Neutronics for ITER diagnostic systems and ports,” Fusion Engineering and Design 42 (1998) 221–228.

[11] F. Moro et al., “Neutronic Analysis of the ITER Equatorial Port Plug 1,” Proceedings of the ISFNT-10, Portland, Oregon, USA, Sep. 11–16, 2011.

[12] A. Serikov, U. Fischer, D. Leichtle, C. S. Pitcher, “Monte Carlo radiation shielding and activation analyses for the Diagnostic Equatorial Port Plug in ITER,” Proceedings of the ISFNT-10, Portland, Oregon, USA, Sep. 11–16, 2011.

[13] A. Serikov, U. Fischer, et al., “MCNP5 parallel computations on JUROPA/HPC-FF supercomputer for ITER applications,” Proceedings of the German Annual Meeting on Nuclear Technology (Jahrestagung Kerntechnik JK-2010), Berlin, May 4-6, 2010.

Acknowledgment

This work has been funded by the ITER Organization under the ITER service contract Nr. IO/10/4300000298 (ITER RFQ-10-14) using an adaptation of the Alite and Blite MCNP models which were developed as a collaborative effort between the FDS team of ASIPP China, University of Wisconsin-Madison, ENEA Frascati, CCFE UK, JAEA Naka, and the ITER Organization. The views and opinions expressed herein reflect only the author’s views. The ITER Organization is not liable for any use that may be made of the information contained therein.

Monte Carlo Calculations of Covariances for Nuclear Reactions in Fusion Technology Applications (EFDA HPC-FF-FSNMCCO)

Objective

The objective of the HCP-FF project FSNMCCO was to utilize the HPC-FF parallel super computer for Monte Carlo calculations of covariances for nuclear reaction cross-sections, as required for uncertainty assessments in fusion neutronic applications.

Computational approach for covariances

Covariance matrices for cross-sections predicted by nuclear models are obtained using the Monte Carlo method described in Ref.[1]. The generation of covariances implies: i) the definition of the "best" set of parameters for the "best" nuclear models used for the cross-section calculation, defined basing on the available measurements ii) the definition of uncertainties of model parameters, iii) the Monte Carlo sampling of N number of input data sets for the code implementing selected "best" models, iv) the execution of calculations for obtained input data files, and v) the calculation of covariance matrices for particular reactions

$$V_{ij} = N^{-1} \sum_{k=1}^{N} (\sigma_{ik} - \sigma_{i0})(\sigma_{jk} - \sigma_{j0}) \qquad (1)$$

where σ_{ik} is the cross-section corresponding to the "*i*"-th primary neutron energy in the "*k*"-th Monte Carlo history, σ_{i0} is the cross-section obtained using the set of "optimal" model parameters as described below.

The corresponding correlation matrix is equal to

$$C_{ij} = V_{ij} (V_{ii} \times V_{jj})^{-1/2} . \qquad (2)$$

The search of optimal nuclear model parameters to be used as the "basic" set for the calculation of cross-section correlations

The first part of the work concerns the computation of the "optimal" nuclear model parameters corresponding to calculated σ_{i0} cross-sections.

An uncertainty of calculated reaction cross-sections results mainly from the uncertainty of nuclear model parameters used for calculations. Nuclear level density parameters play here a crucial role [2]. In order to find the set of "optimal" parameters and to decrease the uncertainty of calculated cross-sections for reactions with missing measurements it is possible to use nuclear model parameters, corrected using available experimental data for other reactions producing the same residual nuclei, which appear in investigated reactions. Mathematically the search of the "optimal" values of parameters for reactions with $X_0, X_1, \ldots X_N$ residuals implies the finding of the minimum of one of the following functions with "a" parameters considered as variables

$$H(a_0', a_1', a_2', \ldots, a_N') = \sum_{j=1}^{N_{\exp}} \left((\sigma_j^{calc}(a_0', a_1', a_2', \ldots, a_N') - \sigma_j^{\exp}) / \Delta\sigma_j^{\exp} \right)^2 , \qquad (3)$$

or

$$S(a_0', a_1', a_2', \ldots, a_N') = 10^{\left\{ \left(\sum_{j=1}^{N_{\exp}} \left[\frac{\lg(\sigma_j^{\exp}) - \lg(\sigma_j^{calc})}{(\Delta\sigma_j^{\exp} / \sigma_j^{\exp})} \right]^2 \right) \left(\sum_{j=1}^{N} \left[\sigma_j^{\exp} / \Delta\sigma_j^{\exp} \right]^2 \right)^{-1} \right\}^{1/2}} , \qquad (4)$$

where a_0', a_1', …, a_N' are nuclear level density parameters for X_0, X_1, … X_N nuclei from intervals $[a_i - \Delta a_i, a_i + \Delta a_i]$ with i=0,1,.., N relating to the model of nuclear level density adopted for calculations; σ_j^{calc} is the calculated cross-section for the "j"-th reaction; σ_j^{exp} and $\Delta\sigma_j^{exp}$ are measured value of cross-section and its error.

The values of $a_i \pm \Delta a_i$ for i=0,1,...,N define the domain of H and S. The errors Δa_i relate to the method used for the a_i determination: systematics and experimental data, namely the unavoidable use of systematics for calculations a_i makes the finding of "optimal" parameters for cross-section calculations essential. In practice, the calculation of H or S for each set of a_0', a_1', …, a_N' and available experimental points σ_j^{exp} , j=0,1,…M assumes a bulk of computations, which makes the use of various mathematical methods to find the minimum of Eq.(3) or Eq.(4) ineffective. In the present work the method, close to Hastings-Metropolis algorithm [3,4], is used to find the optimal "a" parameters. The search assumes "m" parallel computer calculations and is performed as follows. A proposed sample, or a "move", is calculated by

$$a_i^{(k)}(t+1) = a_i(t)+(2\gamma_i^{(k)} - 1)\,\delta\Delta\, a_i \qquad (5)$$

where "t+1" concerns the new state [4]; "k" value relates to one set of independent calculation, k= 1,…m; γ is a random number from the interval [0,1]; δ defines the maximal possible change of "a".The "n" proposal is accepted if

$$H(a(n)(t+1))=\min\{H(a(1)(t+1)), H(a(2)(t+1)),\ldots H(a((m)(t+1))\} < H(a(t)), \qquad (6)$$

If Eq.(6) is not satisfied, a new "m" number of calculations is performed or the search of the minimum Eq.(6) is finished.

The search of "optimal" nuclear level density parameters was applied for the evaluation of neutron induced reaction cross-sections for chromium isotopes with A = 50, 52, 53, 54. The (n,x) and (p,x) reaction cross-sections from EXFOR at the incident nucleon energy, E_n below 30 MeV for targets with atomic number from 21 to 24 and atomic mass from 45 to 54, and residual nuclei with Z from 22 to 24, and A from 44 to 54 were used for the correction of model parameters. The total number of experimental points, N_{exp} is equal to 289.

Fig. 1 shows the changes of $H^{1/2}$ values at different steps of the finding of the minimum of Eq.(6) applying various models for the calculation of the nuclear level density. Each step corresponds to several thousands parallel calculations using TALYS code [5].

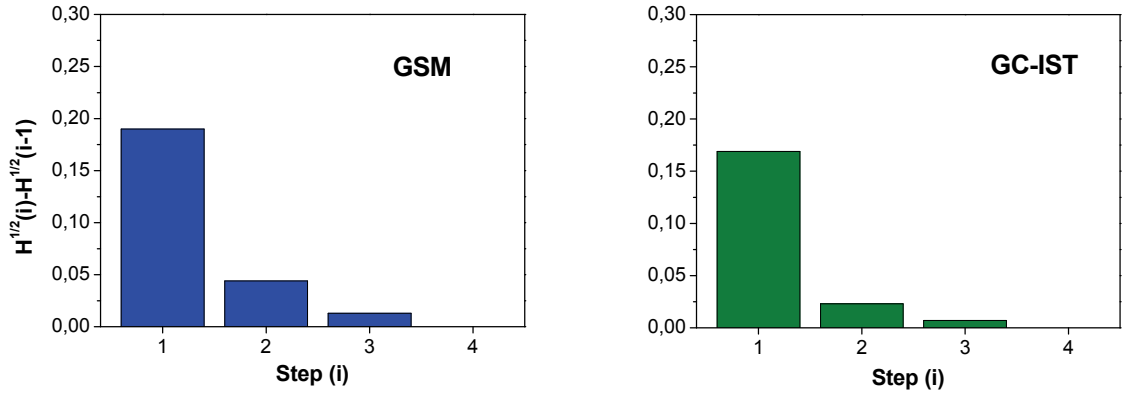

Fig. 1: The step-by-step approximation to the minimum of Eq.(3). The calculation of nuclear level density was performed using the generalized superfluid model (GSM) (left figure) and Gilbert-Cameron model combined with Ignatyuk-Smirenkin-Tishin model (GC-IST) (right figure).

Table 1 shows the $H^{1/2}$ and S-values after the search of the minimum of Eq.(3) for nuclei and reactions discussed above and the ratios to $H_0^{1/2}$ and S_0 values obtained using the initial values of model parameters. Fig.2 shows the examples of cross-sections calculated using nuclear level density parameters before and after correction.

Table 1: The $H^{1/2}$ and S values corresponding to the "optimal" parameters of various models for the calculation of nuclear level density and the ratios $H^{1/2}/H_0^{1/2}$ and $S^{1/2}/S_0^{1/2}$ calculated using corrected and uncorrected parameters. See the captions to Fig. 2.

Final values	GSM	GC-IST
$H^{1/2}$	7.2	8.4
S	1.20	1.22
$(H/H_0)^{1/2}$	0.75	0.80
S/S_0	0.96	0.97

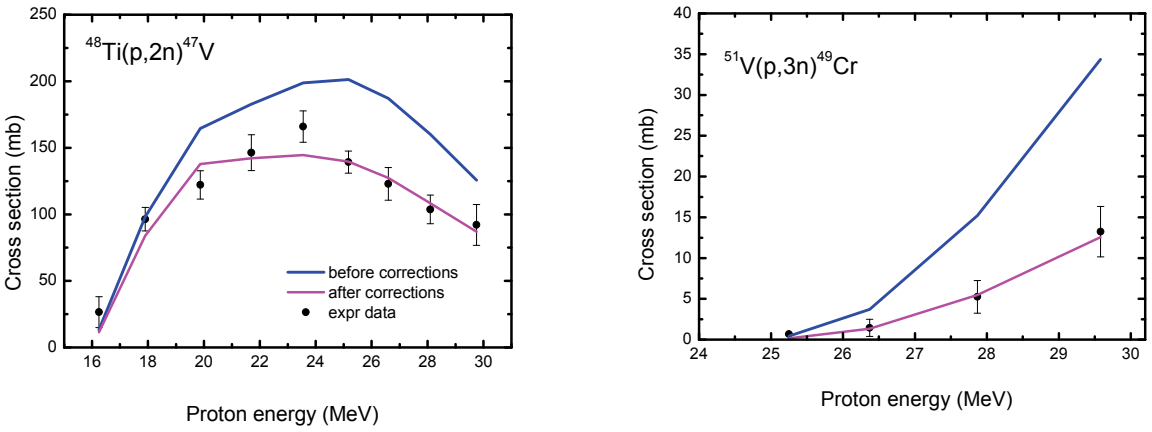

Fig. 2: Examples of cross-sections calculated using GSM model with nuclear level density parameters before and after the search of minimum of Eq.(3).

Calculation of covariances using the Monte Carlo method

The calculations of covariance matrices for nuclear cross-sections were performed using a set of computer programs, BEKED, elaborated in KIT [2].

Using BEKED the computation of covariances can be performed with the help of TALYS [5], ALICE/ASH [6], and ECIS [7] codes. Fig. 3 shows the example of correlation matrices for the (n,p) reaction cross-sections for ^{52}Cr obtained using nuclear model calculations by TALYS and ALICE/ASH codes.

Fig. 4 shows the examples of obtained matrices for (n,x) reactions.

The calculated values were converted in ENDF/B format and introduced in files, prepared by KIT, suitable for general applications.

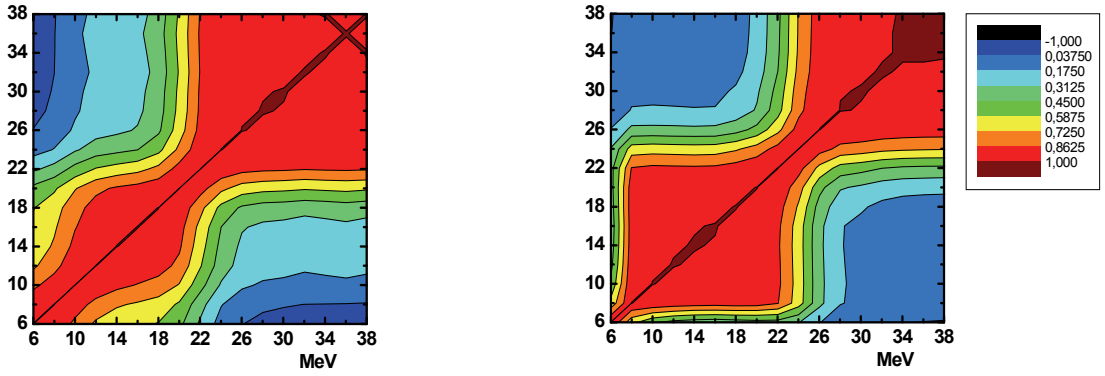

Fig. 3: Correlation matrix for the ^{52}Cr(n,p) reaction cross-section obtained nuclear models implemented in the TALYS code (left figure) and ALICE/ASH code (right figure).

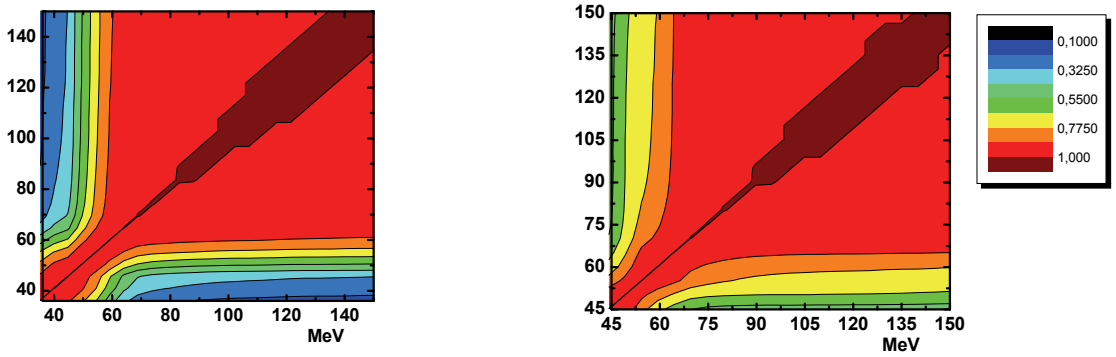

Fig. 4: Calculated correlation matrices for ^{52}Cr(n,4n)^{49}Cr (left) and ^{52}Cr(n,x4np) ^{48}V (right) reactions.

Staff:

A. Konobeev
U. Fischer
P. Pereslavtsev

Literature:

[1] D. L. Smith, Covariance Matrices for Nuclear Cross Sections Derived from Nuclear Model Calculations, ANL/NDM-159, Argonne National Laboratory (2004).

[2] A.Yu. Konobeyev, U. Fischer, P.E. Pereslavtsev, Computational Approach for Evaluation of Nuclear Data Including Covariance Information, Int. Conf. Nucl. Data for Sci. and Technology, Jeju Island, Korea (2010)

[3] W.K. Hastings, Biometrika 57 (1970) 97.

[4] R. Capote, D.L. Smith, Nuclear Data Sheets, 109 (2008) 2768

[5] A.J. Koning_, S. Hilaire, M. Duijvestijn, TALYS-1.0, Int. Conf. Nucl. Data for Sci. and Technology, Nice, France (2007) 058 DOI: 10.1051/ndata:07767

[6] C.H.M. Broeders, A.Yu. Konobeyev, A.Yu. Korovin, V.P. Lunev, M. Blann, ALICE/ ASH - Pre-Compound and Evaporation Model Code System for Calculation of Excitation Functions, Energy and Angular Distributions of Emitted Particles in Nuclear Reactions at Intermediate Energies, FZKA 7183, Forschungszentrum Karlsruhe (2006)

[7] J. Raynal, “ECIS96,” *Proc. Specialists' Meeting on the Nucleon Nucleus Optical Model up to 200 MeV,* Bruyères-le-Chatel, France, Nov. 13-15, 1996

Acknowledgement

This work, supported by the European Communities under the contract of Association between EURATOM and Karlsruhe Institute of Technology, was carried out within the framework of the European Fusion Development Agreement. The views and opinions expressed herein do not necessarily reflect those of the European Commission.

Monte Carlo Radiation Transport Calculations for Nuclear Fusion Facilities (EFDA HCP-FF-FSNMCFU)

Objective

The objective of the HCP-FF project FSNMCFU was to exploit and utilize the capabilities of the HPC-FF super computer for massive parallel Monte Carlo radiation transport simulations in applications to ITER.

In the framework of the FSNMCFU project, a couple of fusion neutronics R&D activities [1-5] were conducted utilizing the HPC-FF supercomputer resources [6] for massive parallel Monte Carlo particle transport simulations. It was demonstrated that the parallel use of hundreds of the HPC-FF CPUs substantially accelerates the Monte Carlo calculations with the MCNP5 code [7]. The challenging tasks of deep-penetration radiation transport for fusion neutronics in ITER were addressed successfully, e.g. nuclear heating and helium production rate have been calculated with high spatial resolution using the MCNP5 mesh tally capability. The experience of performing the neutronics analyses for the ITER Upper Electron Cyclotron Heating (ECH) launcher [1, 2] has shown that some tasks could be solved only on supercomputers. The Monte Carlo statistical errors associated with the mesh-tally results were reduced by applying variance reduction techniques and by taking the advantages of massive parallel computations on the HPC-FF system.

The performance of the MCNP5 parallel runs on the HPC-FF supercomputer at JSC, together with the OpusIB and HC3 systems at KIT has been evaluated and compared in terms of speed-up and efficiency. A considerable increase of the number of CPUs exploiting the resources of the HPC-FF at JSC enables to accomplish shielding tasks for the ITER design development much faster than before at KIT, e.g. a job for one month running on 27 CPUs on the OpusIB cluster with a speed-up of 24, can be accomplished on HPC-FF in one day with a speed-up of ~700 on ~1600 CPUs. This is an evident benefit of running MCNP5 radiation transport simulations on HPC with massive parallel multiprocessing. Performance assessments of the MCNP5 code were carried out to find an efficient way to run the code in a parallel regime. The parallel version of the code has been compiled with the Intel Fortran and C/C++ compilers, and the MPI libraries.

The practice of the MCNP5 MPI parallel computations [8, 9] shows that it is important to keep the master-slave communication as little as possible. This is achieved by setting the number of intermediate data exchange, called “rendezvous”. The optimal number of CPUs used in MCNP5 parallel calculations is dependent on the complexity of the model, physical process involved in particle tracks and the particle histories lengths. An important issue for scaling is keeping or increasing the calculation load on each processor: the higher ratio of computation per communication, the closer speed-up scaling to linear law. From the experience of the MCNP5 parallel runs for the ITER fusion neutronic applications, the optimal number of CPUs depends on the size of the MCNP5 task and the number of available processors on the cluster. In our practice, the averaged number of CPUs we have set on HPC-FF is around 800, while the usual number of CPUs on HC3 (another cluster at KIT) and OpusIB is around 96. These are rough numbers of CPUs, which can be used without a long task queuing. The maximum speed-up was found on HPC-FF at around 700 with 1600 CPUs. This means that the wall-clock time to run the same job on one CPU was 700 times longer than running on 1600 CPUs in parallel on the HPC-FF cluster.

Staff:

U. Fischer
D. Leichtle
A. Serikov

Literature:

[1] A. Serikov, U. Fischer, et al., “Overview of recent nuclear analyses for the Upper ECH launcher in ITER,” Fusion Engineering and Design, vol. 85, issues 10-12, (2010), pp. 1885-1895; http://dx.doi.org/10.1016/j.fusengdes.2010.06.016.

[2] A. Serikov, U. Fischer, et al., “Evolution of shielding computations for the ITER upper ECH launcher,” Nuclear Technology, vol. 175, no. 1, pp. 238-250, July 2011.

[3] A. Serikov, U. Fischer, et al., “High performance computations of Monte Carlo radiation transport for ITER fusion neutronics,” Proceedings of the Workshop “Computational Methods in Science and Engineering” (SimLabs@KIT 2010), November 29 - 30, 2010, Karlsruhe, Germany, KIT Scientific Publ., 2011, ISBN 978-3-86644-693-9, http://digbib.ubka.uni-karlsruhe.de/volltexte/1000023323; http://books.google.de/books?id=KgGCchbdi6MC&lpg=PA3&dq=SimLab%40KIT%20workshop%2C%20Karlsruhe%2C%20Nov.%2029-30%2C%20KIT%20Scientific%20Publishing%202010&hl=de&pg=PA135#v=onepage&q&f=false.

[4] A. Serikov, U. Fischer, et al., “Toolkit for High Performance Monte Carlo Radiation Transport and Activation Calculations for Shielding Applications in ITER,” Proc. M&C 2011, Rio de Janeiro, RJ, Brazil, May 8-12, 2011, Latin American Section / American Nuclear Society (2011); http://mathematicsandcomputation.freezoka.net/MC11/_pdf/mc27_256_paper.pdf

[5] A. Serikov, U. Fischer, D. Grosse, “High Performance Parallel Monte Carlo Transport Computations for ITER Fusion Neutronics Applications,” Proc. of SNA + MC 2010, Tokyo, Japan, October 17-20 (2010), accepted in Progress in Nuclear Science and Technology journal.

[6] HPC-FF system: http://www2.fz-juelich.de/jsc/juropa/, and http://www2.fz-juelich.de/jsc/juropa/configuration/

[7] X-5 Monte Carlo Team, “MCNP—A General Monte Carlo N-Particle Transport Code, Version 5, Volume I, MCNP Overview and Theory,” LA-UR-03-1987, Los Alamos National Laboratory (Apr. 24, 2003; revised Oct. 3, 2005).

[8] A. Serikov, U. Fischer, et al., “Performance assessments of the MCNP5 parallel computations for the ITER ECRH launcher,” Proc. German Ann. Meet. on Nuclear Technology (Jahrestagung Kerntechnik JK-2008), May 27-29, 2008, Hamburg, Germany, (2008).

[9] A. Serikov, U. Fischer, et al., “MCNP5 parallel computations on JUROPA/HPC-FF supercomputer for ITER applications,” Proc. German Annual Meeting on Nuclear Technology (Jahrestagung Kerntechnik JK-2010), May 4-6, 2010, Berlin, Germany, (2010).

Acknowledgement

This work, supported by the European Communities under the contract of Association between EURATOM and Karlsruhe Institute of Technology, was carried out within the framework of the European Fusion Development Agreement. The views and opinions expressed herein do not necessarily reflect those of the European Commission.

Definition of Radiation Map in DEMO (WP11-DAS-RH-07-01)

Objective

The objective of the WP11-DAS-RH-07 task was first, to define the radiation map in DEMO (if possible in 2011) during a plasma pulse and at different points in time after termination of a plasma shot, and, second, identify further work to be carried out in 2012-2013 to refine the radiation map.

This task was jointly conducted by KIT and UNED. At the DEMO RH kick-off meeting, EFDA Garching, October 5, 2011, the approaches were presented available at KIT and UNED for assessing radiation maps during operation and shut-down times. For operation periods, neutron and gamma radiation fields (as well as resulting doses) are obtained by means of coupled neutron and gamma transport calculations using e. g. the MCNP Monte Carlo code with a suitable DEMO reactor model. For the radiation maps during shut-down times, the gamma radiation fields are required (as well as the resulting doses) which are due to the radioactive decay of activated materials by emission of decay photons. This requires a coupled computational approach linking neutron transport calculations (using e. g. the MCNP code), activation calculations (using the FISPACT or ACAB code), and, finally, decay photon transport calculations (using again MCNP). Such approaches are available with the so-called rigorous 2-step system (R2S) of KIT (MCNP coupled with FISPACT), and a similar system by UNED based on the coupling of MCNP and the ACAB activation code.

Activities performed

At the Kick-off Meeting it was agreed to use the DEMO 2008 MCNP model, developed by KIT in the framework of the EFDA DEMO study activities 2006-2008, for providing already in 2011 first (rough) assessments of radiation maps relevant to the remote handling. The underlying DEMO CAD neutronics model was provided by KIT to EFDA for further dissemination, and, in addition, the MCNP input deck was provided to UNED. This model was then used by UNED for calculating neutron flux and He production profiles in specific areas of the upper and the divertor port, as well as activity and decay heat distributions of the blanket and the divertor. The MCNP model had to be modified in the divertor port area by cutting-off the lower outboard blanket module so as to enable the removal of the divertor cassette.

The calculations were performed for an average neutron wall loading of 1.2 MW/m^2 and an irradiation time of 5 full power years (fpy) for the blanket, and 2.5 fpy for the divertor. The He production calculated for the upper port blanket cooling pipe connection was shown to be not critical since the pipe is well shielded from the plasma neutron source by the upper blanket/shield modules. The He production after the assumed lifetime is one to two orders below the limit of 1 appm He in steel. The divertor port, on the other hand, is not well shielded from the plasma neutron radiation. The He production therefore exceeds the 1.0 appm limit by up to one order of magnitude for the assumed lifetime. The specific activity and afterheat density were calculated for a blanket module at the central inboard side of the DEMO and the divertor considering decay times up to 10 years after irradiation. The maximum specific activity is obtained for the first wall at levels of 10^{12} Bq/cm^3 decreasing by one to two orders of magnitude after 10 years. In the blanket structure the activation is lower by about a factor three. The activation level of the divertor is about 5 10^{12} Bq/cm^3 at maximum, thus about a factor two less than at the first wall of the central inboard blanket module.

For comparison, average values of the specific activity and the decay heat were also derived for the steel structure irradiated in a DEMO type HCPB reactor. Such data were available at KIT from some previous analyses on the so-called DEMONET reactor with an average neutron wall loading of 2.2 MW/m^2 and an irradiation time of 2.2 fpy. This results in a first wall fluence of 5.0 MWa/m^2 (corresponding to 50 dpa in steel) which is very close to the assumed target values for the present DEMO. The obtained values are at a level of 10^{12} Bq/cm^3 and

0.1 W/cm^3 for the specific activity and the afterheat density, respectively, and thus are in good agreement with the data obtained by UNED for the DEMO 2008 model.

A rough assessment was performed for the absorbed radiation dose rate expected for silicon after shut-down as result of the activation of the Eurofer structure. To this end, a semi-infinite slab of Eurofer was assumed to be irradiated over 5 full power years in a radiation field corresponding to the first wall location in a blanket module at the central inboard side of DEMO. The resulting decay photon radiation, calculated for decay times up to 10 years after shut-down at the surface of the semi-infinite slab, was then assumed to be entirely absorbed in a silicon layer. For the decay times 1d to 1 year after shut-down, which cover the relevant period to be considered for remote handling to take place, the resulting absorbed dose rate level for silicon is around 3 Gy/h. The dominant contributor to the absorbed dose rate is Mn-54 which is produced during irradiation from the Eurofer constituents Fe (90%) and Mn (10%).

Further work to be carried out in 2012-2013

The activation and radiation doses to specific components depend significantly on the material build of the considered components and the imposed irradiation conditions (neutron radiation field, irradiation time, surrounding, etc.). It is thus required to develop a suitable DEMO reactor model with a more realistic representation of the relevant components. Radiation doses to the components during and after operation, activation and decay heat distributions, gas production data etc. can then be assessed on a more reliable basis as required for remote handling/maintenance investigations.

Staff:

U. Fischer
J. Sanz (UNED)
J.P Catalán (UNED)
R. Juárez (UNED)

Acknowledgement

This work, supported by the European Communities under the contract of Association between EURATOM and Karlsruhe Institute of Technology, was carried out within the framework of the European Fusion Development Agreement. The views and opinions expressed herein do not necessarily reflect those of the European Commission.

Shutdown Dose Rate Prediction: Study of Feasibility of an Integral Experiment in Positions Relevant for ORE Evaluation (JW8-FT-5.28)

Objective

The overall objective of Task JW8-FT-5.28 was to validate the available computational methodologies for shutdown dose rate calculations, the Direct One Step (D1S) and the Rigorous 2 Step (R2S), through the comparison with dose rates measured in an integral experiment on JET for positions relevant for the evaluation of the Occupational Radiation Exposure (ORE).

Dose rate measurements

Dose rate measurements were performed by the ENEA experimental team and the JET health physics group for several positions along the mid port horizontal axis of JET Octant 1 as shown in Fig. 1. The measurements were performed during the 2009/2010 shutdown period of JET using different radiation dose meters including two Geiger Müller type detectors (Automess Teletector 6112D and Mini Rad series 1000R) and a ionization chamber (Eberline R02-W type) mounted on a mascot system. Measurements were performed at 81, 84, 109, 137, 145 and 263 days after shutdown.

Dose rate calculations

Calculations of the shutdown dose rates have been performed using the Advanced D1S method of ENEA [1] and the R2Smesh method of KIT [2]. For these calculations, the original MCNP 45° geometry model of Octant 1 has been modified to match the real masses and volumes of the JET main components, and including the proper material chemical compositions with impurities.

The deuterium-tritium (DT) and deuterium-deuterium (DD) neutron sources were described by a parametric representation of a typical JET plasma emissivity used as reference for JET MCNP calculations. JEFF 3.1.1 nuclear cross section data [3] and EAF 2007 [4] activation cross-sections have been used for the transport and activation calculations, respectively.

Both the Advanced-D1S and the R2Smesh approaches employed the same geometry, data, irradiation conditions and tallies to record the photon flux spectra. The assumed DD and DT irradiation histories are based on measured neutron yield data covering the full JET operation from 1983 until shut-down in 2009. It is noted that the radiation dose after the 2009 shutdown is due to the activation of the last thirteen years of irradiation while the contribution from the first decade of the JET operation is negligible.

For the R2Smesh calculations, the entire JET octant was overlaid with a fine spatial (rectangular) grid of 3 cm mesh size for the neutron fluxes and a coarse grid with 15 cm mesh size for the neutron spectra. In total $3.9 \cdot 10^6$ cells were used in the fine mesh model. $1 \cdot 10^9$ source neutrons histories were tracked in the calculations of the neutron flux spectra. The achieved statistical accuracy is < 1% for the total neutron flux densities and less than 10% for the neutron flux spectra.

R2Smesh calculations were performed for 81, 109, 137 and 263 days after shutdown for comparison with the Teletector and Mini Rad dose rate measurements. For each irradiation history (D-T and D-D) and cooling time around 30.000 inventory calculations using the FISPACT code [5] were performed. The R2S approach requires running a decay gamma transport calculation for each cooling time considered. This calculation provides the photon flux spectra on the specified mesh grid. These spectra are then converted to dose rates using the ICRP-74 [6] photon fluence-to-dose conversion coefficients. $1 \cdot 10^9$ source photons were tracked in each decay gamma transport calculation. The resulting statistical error for

the decay photon flux is less than 0.5% in the plasma region and less than 5% at the distances of 1m away from the port window.

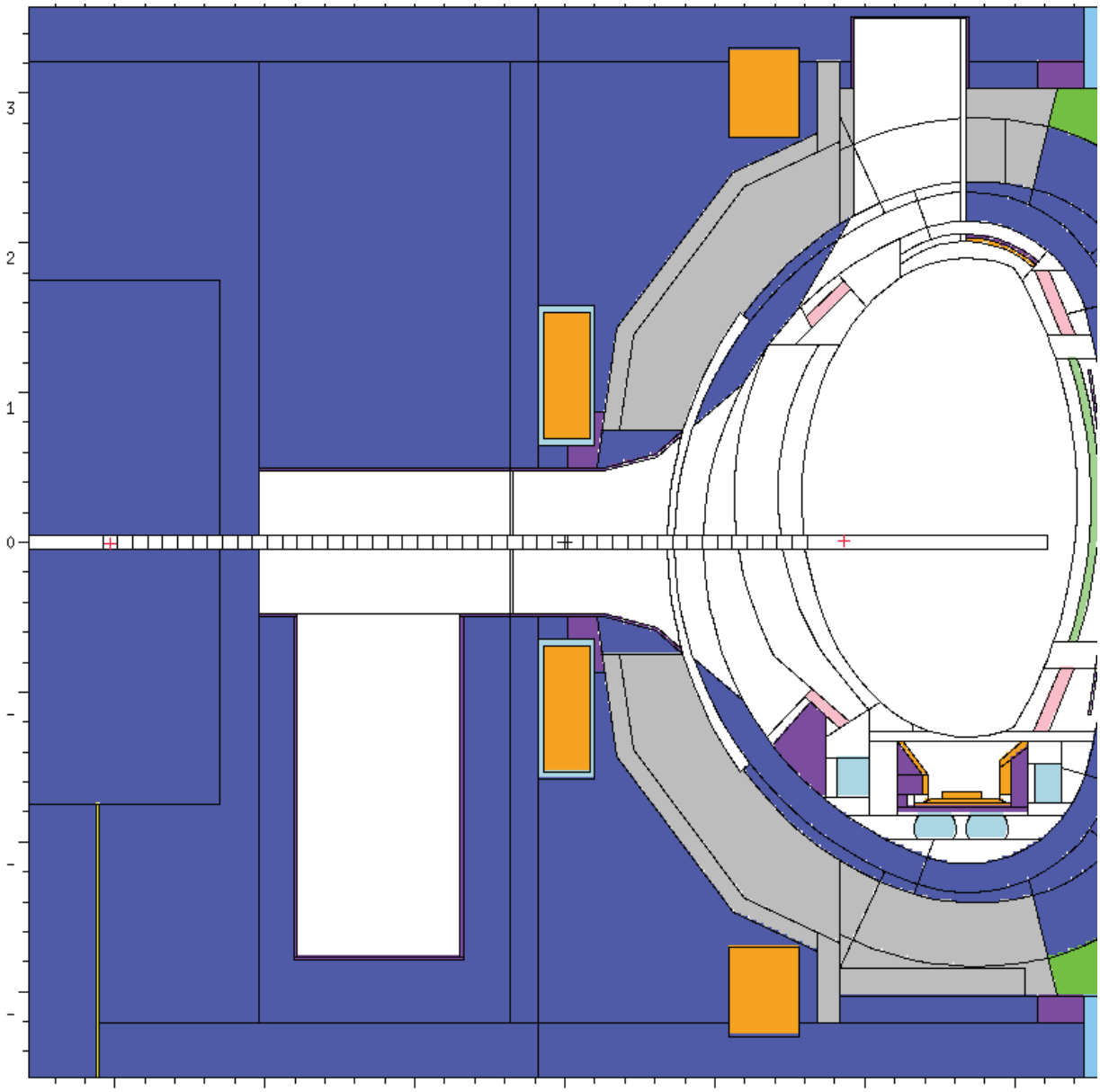

Fig. 1: Dose rate measurements positions along the mid port horizontal axis of JET Octant 1.

Results and analysis

The R2Smesh results for the shutdown dose rates are shown in Fig. 2 in comparison with the measurements at the considered decay times 81, 109, 137 and 263 days after shutdown. They refer to the designated positions in the mid-plane port where the dose measurements were performed with the Teletector and the Mini rad detectors.

There is an overall good agreement between the calculated and the measured dose rates with C/E (calculation/experiment) ratios in the range between 0.7 and 1.3 with two exceptions in case of the Mini Rad measurements at 263 days after shutdown. It is noted, however, that there is a trend for underestimating the measurements at short cooling times (81 days) and for overestimating at longer cooling times (263 days). ^{60}Co was shown to be the dominant radionuclide contributing to the shutdown dose at all considered cooling times. The contribution of ^{58}Co was found to be not significant.

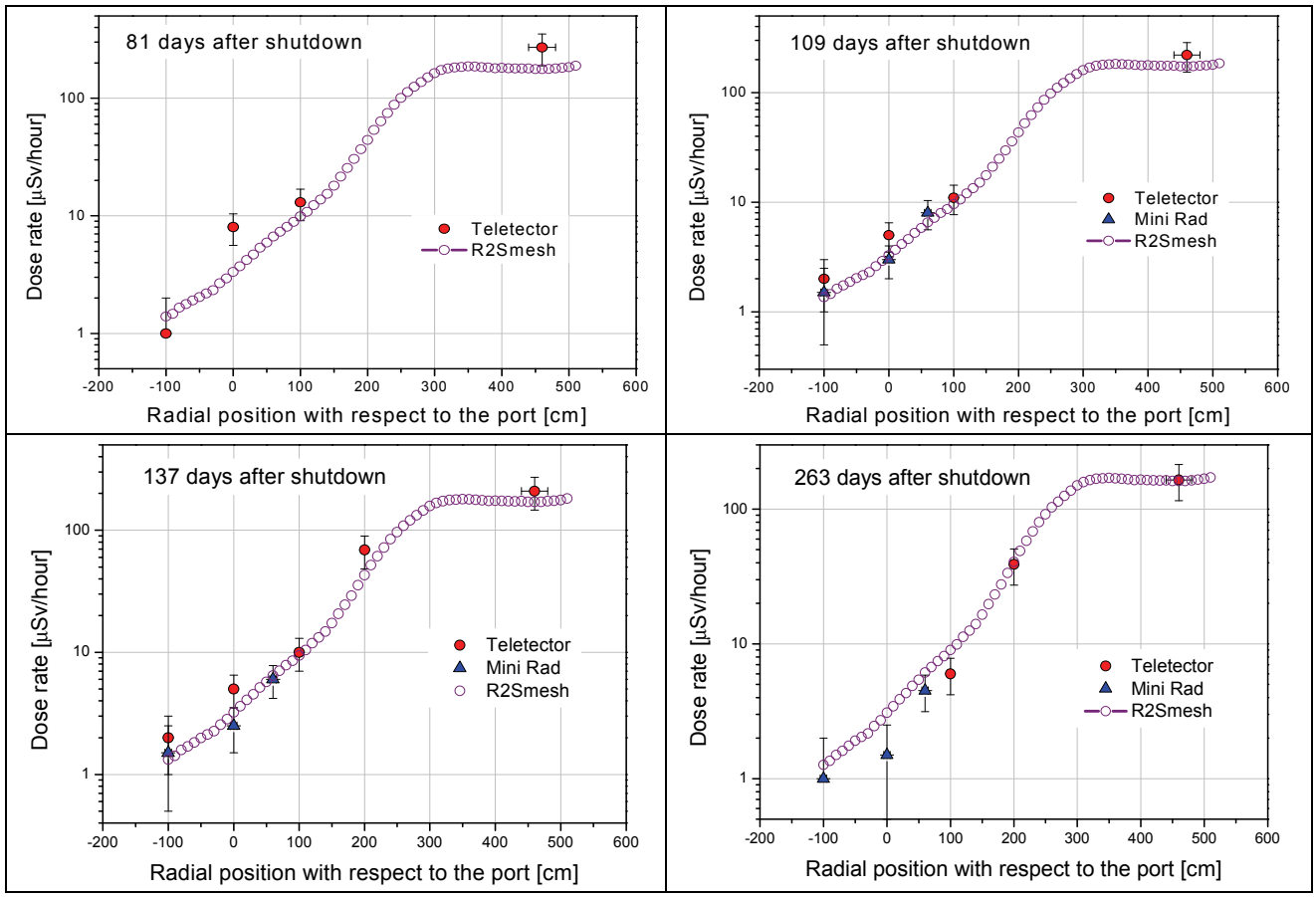

Fig. 2: R2Smesh results for the shutdown dose rates along the mid-plane port compared with experimental results available at the designated positions.

Staff:

U. Fischer
P. Pereslavtsev
R. Villari (ENEA Frascati)
F. Moro (ENEA Frascati)
L. Petrizzi (ENEA Frascati)

Literature:

[1] H. Iida, D. Valenza, R. Plenteda, R. T. Santoro AND J. Dietz, Radiation Shielding for ITER to allow for Hands-on Maintenance inside the Cryostat, J. of Nuc. Sci. and Tech., Supplement 1. (March 2000) 235-242.

[2] Y. Chen, U. Fischer, Rigorous MCNP based shutdown dose rate calculations: computational scheme, verification calculations and applications to ITER, Fusion Eng. Des. 63-64 (2002) 107-114.

[3] A. Koning et al., Status of the JEFF nuclear data library, , Internat. Conf. on Nuclear Data for Science and Technology (ND2010), Jeju Island, Korea, April 26-30, 2010; Journal of the Korean Physical Society, 59(2011),1057-1062, DOI:10.3938/jkps.59.1057.

[4] R. A. Forrest, J. Kopecky, J.-Ch. Sublet, 'The European Activation File: EAF-2007 cross section library', Report UKAEA FUS535, March 2007.

[5] R. Forrest, FISPACT-2007 User Manual EASY 2007 Documentation Series UKAEA FUS 534

[6] M. Majerle, D. Leichtle, U. Fischer, A. Serikov, Verification and validation of the R2Smesh approach for the calculation of high resolution shutdown dose rate distributions, 10th Int. Symp. on Fusion Nuclear Technology (ISFNT-10), Portland, USA, Sept. 12-16, 2011

[7] ICRP publication 74, Conversion Coefficients for Use in Radiological Protection, Annals of ICRP 26/3 (1997)

Acknowledgement

This work, supported by the European Communities under the contract of Association between EURATOM and Karlsruhe Institute of Technology, was carried out within the framework of the European Fusion Development Agreement. The views and opinions expressed herein do not necessarily reflect those of the European Commission.

Benchmarking of CAD to MCNP Interface (JW8-FT-5.29)

Objective

The object of Task JW8-FT-5.29 was to evaluate the CAD to MCNP interface programme McCad, developed previously at KIT, by independent users at ENEA through a test application for an existing fusion device of high complexity. Its portability and user-friendliness should be evaluated, as well as the impact of the geometrical approximation introduced on the neutronic analyses. Furthermore, useful feedback for the optimization of the tool should be provided to the McCad developers.

The McCad conversion tool

McCad has been developed at KIT to enable the automatic conversion of CAD models into the semi-algebraic geometry representation as utilized in Monte Carlo particle transport simulations. McCad is entirely based on open source software; it is running under the Linux operating system and utilizes the Open Cascade CAD kernel with the Qt4 libraries for the graphical user interface (GUI). The GUI allows the visualization of the geometry models and the exchange of CAD and Monte Carlo geometry data. Such data can be imported in the STEP, IGES, and BREP data format (CAD) and as well as MCNP input deck. Available MCNP surface types are planes, spheres, cylinders, cones, tori and a few macro bodies. The converted geometry models can be output in the syntax of the Monte Carlo codes MCNP and TRIPOLI. McCad is in routine use at KIT for the conversion of CAD geometry models for neutronics analyses with the MCNP code.

McCad implementation and tests at ENEA

The McCad beta test version 0.1, released in August 2010, was provided to ENEA for conducting Task JW8-FT-5-29. At ENEA, McCad was installed on a Debian based Ubuntu 7.10 Linux system with the support and assistance of KIT.

First application tests were performed at ENEA with simple geometries to evaluate the MCNP converted file syntax with the focus on the generation of void geometry cells. Feedback was provided to KIT initiating a review of the McCad algorithm for the void generation. An improved void generation procedure has been subsequently developed and implemented in an advanced version of McCad.

Advanced application tests were performed for a CAD model of the FAST (Fusion Advanced Studies Torus) Vacuum Vessel and Equatorial Port prepared with the CATIA V5 software where the toroidal non-analytical surfaces were replaced with a sequence of cylindrical sectors. The conversion of the model with void spaces around the solids and the void spaces filled by some materials showed a well-known but crucial issue: The void spaces are usually not defined in the CAD models but need to be defined for neutronics analyses. The void cells generated to this end by McCad are in general very complex. This can be avoided if the void spaces can be defined as solids in the CAD model.

Test application to the JET Ultra Violet Optical Spectrometer

The JET Ultra Violet Optical Spectrometer has been chosen for a real application test of the McCad conversion process.

The geometrical structure of the spectrometer was first analysed and then simplified by replacing solids that were described by non-analytic surfaces and by removing all elements which are not relevant for neutronic calculations. Next the STEP data file describing the spectrometer was divided into four independent files that were converted separately. Each

STEP file was imported to McCad using its GUI and then successively converted and output in the MCNP geometrical description.

To validate the converted geometry model, a stochastic volume calculation has been performed with MCNP using the converted spectrometer elements. The obtained values were compared with the volumes obtained directly with CATIA V5 for the CAD geometry. In general, good agreement was obtained confirming that the conversion process reproduces properly the CAD geometry.

The numerous tests performed in the frame of this Task highlighted the reliability of the McCad software tool in converting CAD geometry data into MCNP representation for Monte Carlo calculations. McCad is a CAD to Monte Carlo interface programme with a high potential. It is under continuous development to optimise its performance, enhance and extend its capabilities. The void generation algorithm, in particular, is a crucial issue which requires further optimisation. The only severe limitation of the McCad conversion process is currently the constraint to use only analytical surfaces when defining the CAD geometry. In fusion technology, non-analytic surfaces are frequently present in the CAD models thus necessitating modifications and simplifications of the geometry models on the CAD software platform.

Staff:

U. Fischer
D. Grosse
F. Moro (ENEA Frascati)

Acknowledgement

This work, supported by the European Communities under the contract of Association between EURATOM and Karlsruhe Institute of Technology, was carried out within the framework of the European Fusion Development Agreement. The views and opinions expressed herein do not necessarily reflect those of the European Commission.

Assessment of the Suitability of Neutron and Gamma Detectors in the Future Experiment at JET for the Validation of Shutdown Dose Rate Prediction (JW9-FT-5.31)

Overall objective

The general aim of the task was the assessment of the suitability of NE213 scintillator and GEM detectors for neutron fluxes/spectra measurements as well as CdTe and BrilLanCe 380 detectors for gamma ray spectra measurements outside the JET vessel through preliminary irradiation tests.

Characterization of the new semi-conductor detector CZT

Local shut-down dose rate assessments for areas near a fusion reactor vessel are necessary input for the design of maintenance schemes and accident scenarios and hence also of importance for the licensing procedure. These assessments are based on calculations with particle transport and inventory codes using evaluated nuclear data libraries. Experimental checking of their performance is therefore required.

A CdTe detector for gamma-ray spectrum measurements of dominating induced gamma-ray activity at least near the JET reactor vessel has been tested before. Such detectors are very small and light and therefore well-suited for measurements near the JET vessel especially in places with very limited space. However, also for these reasons the gamma-ray efficiency is comparably low.

Aim of the work of D8 of this task is the test of a CZT detector with a special electrode design and a larger volume than the detectors investigated in D2 and D5 of this task.

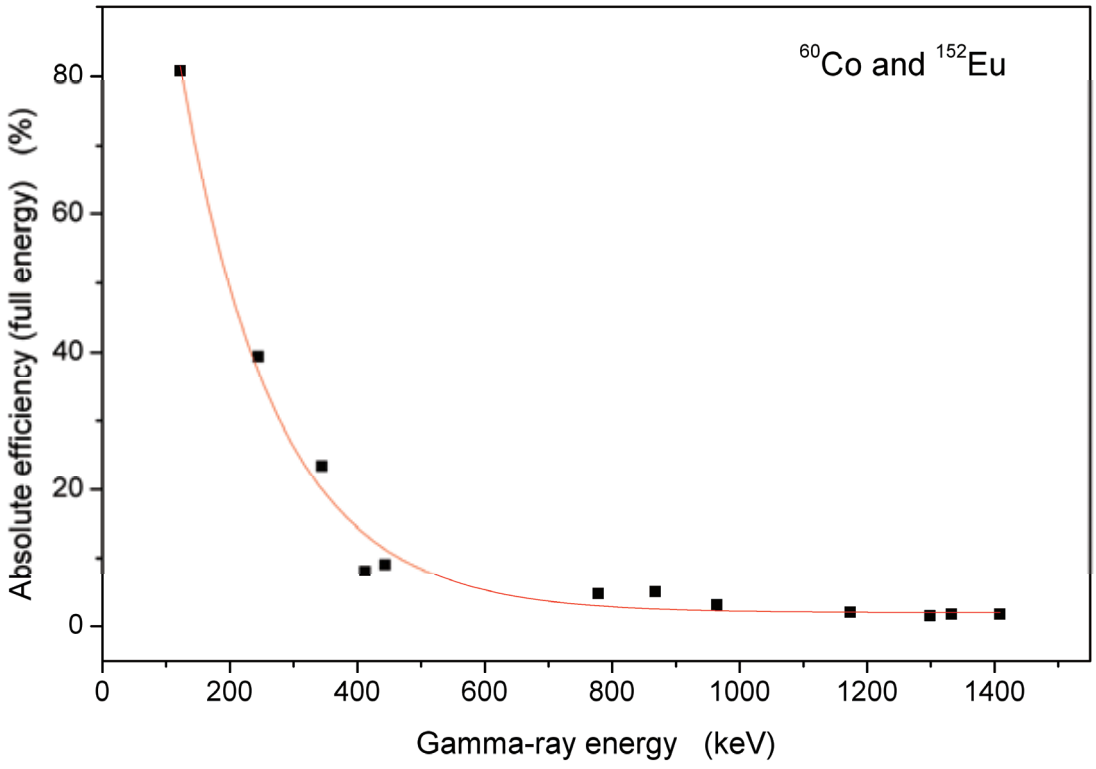

Fig. 1: Efficiency curve of TUD's CZT detectors obtained with 60Co and 152Eu calibration sources.

CZT detectors are based on Cadmium-Zinc-Telluride wide-band gap material and can be operated at room temperature. However, charge-collection efficiency and resolution is not as excellent as that of HPGe detectors which need liquid nitrogen cooling. These parameters can be improved by introducing a special electrode design on the detector. We have investigated a CZT of cubic shape with a side length of 1 cm and hence a volume of 1 ccm with gamma-ray calibration sources. The detector is equipped with a so-called co-planar grid, two comb-shaped anodes on one side and a cathode at the back side. Both anodes are kept at a slightly different potential. Evaluating the difference signal of these two anodes, the contribution to the signal from less mobile holes can be removed and only the contribution from electrons is preserved. Tests at TUD show that energy resolutions better than 4% at a gamma-ray energy of 661 keV (Cs-137) can be achieved.

The efficiency calibration curve obtained with ^{60}Co and ^{152}Eu standard calibration sources is shown in Figure 1. It should be noted that the figure shows absolute values of the efficiency for the selected geometry only. However, it can be inferred that the ratio of the efficiencies at 121 keV and at 1332 keV is a factor of about 50. Applying this detector for measurements at JET would require a preceding DT operation to achieve reasonable count rates. The detector would provide information on dominant radio nuclides on the base of gamma-ray lines and half-lives. However, the energy resolution is considerably lower than that of a HPGe detector. The advantage of the CZT detector is its small size and the operability at room temperature. This provides the possibility to place it near structures of interest for a measurement and thereby analyse the dominant nuclides in this specific structure with less influence from radiation from the surroundings.

Staff:

A. Klix
D. Gehre (Technical University of Dresden, D-1062 Dresden, Germany)
R. Villari (ENEA Fusion and Nuclear Technologies Department, I-00044 Frascati, Italy)

Acknowledgement

This work, supported by the European Communities under the contract of Association between EURATOM and Karlsruhe Institute of Technology, was carried out within the framework of the European Fusion Development Agreement. The views and opinions expressed herein do not necessarily reflect those of the European Commission.

International Fusion Materials Irradiation Facility (IFMIF)

Broader-Approach Activity: IFMIF Testcell and High Flux Test Module (BMBF Reference No. 03FUS0008)

Introduction

Scope of work

In the Engineering Validation and Engineering Design Activities (EVEDA) for the International Fusion Material Irradiation Facility IFMIF, which is an element of the Broader Approach activities launched jointly by several European countries and Japan, the german contribution includes engineering tasks for the IFMIF Testcell and the IFMIF High Flux Test Module. This report covers tasks performed at the Institute for Neutron Physics and Reactor technology at the KIT attributed to the following procurement arrangements (PAs):

- PA TF-1 EU : Engineering design and Validation of the IFMIF High Flux Test Module
- PA TF-2: Irradiation in fission reactor (Responsible SCK-CEN, contribution by KIT)
- PA TF-4: Other irradiation modules (Responsible CIEMAT, contribution by KIT)
- PA ED-04: Test Cell, Access Cell, Test Module Handling Cell and Technology Rooms

According to the planning for EVEDA, these tasks will be performed in the timeframe up to 12/2013.

System overview

The IFMIF facility is dedicated to fusion-relevant irradiation of structural and functional material specimens, with the objective to create an experimentally validated material properties database suitable for design and licensing of future fusion power plants. The facility is composed of several subsystems, namely the 40MeV 250mA deuteron accelerator facility (AF), the lithium target facility (LF) and the test facilities (TF). The target- and testcell (TTC) is part of the test facilities, containing the lithium target neutron source and the test modules. It has the primary function to shield the environment against the intense radiation generated by the target, and to safely contain all hazardous materials. Inside the TTC, the target and test modules are arranged, as shown in Fig. 1.

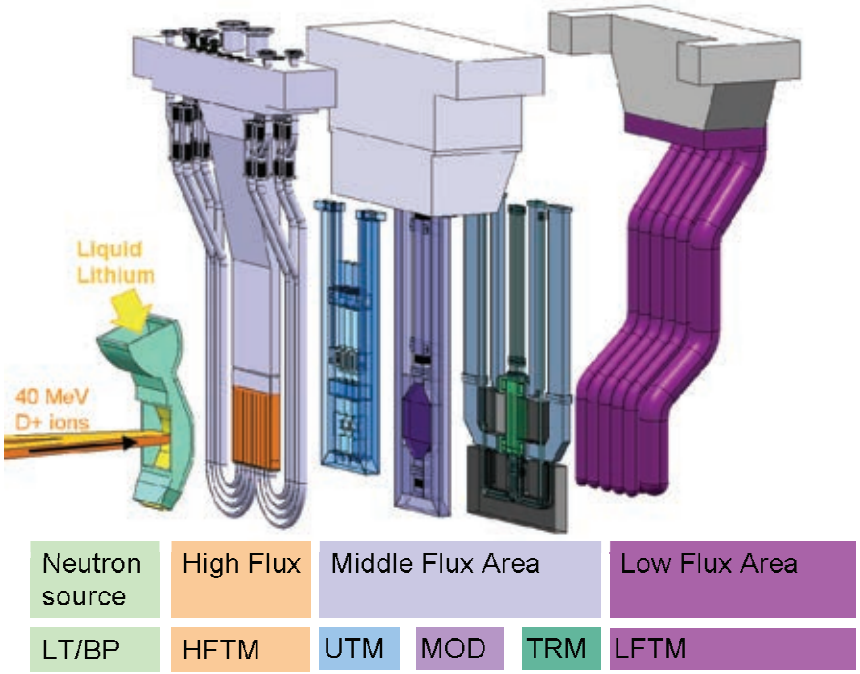

Fig. 1: Overview on the irradiation experiments inside the IFMIF Target- and Testcell (TTC).

The High Flux Test Module (HFTM) is the irradiation device for miniaturized SSTT samples of structural materials. The HFTM is positioned immediately behind the neutron source inside the TTC. The HFTM contains up to 24 irradiation rigs/capsules with approximately 80 SSTT samples each. It is possible to adjust individual temperatures for the specimens in each rig, in the range of 250 – 550°C (A high temperature option 650°C is additionally investigated).

The Tritium Release Test Module (TRM) is filled with specimen of tritium breeding materials, such as Li_2SiO_4, Beryllium, and others. The tritium release can be measured in situ during the irradiation, and the change in specimen structure (porosity etc.) can be examined after the irradiation.

Engineering Design and Validation for the HFTM

HFTM-Assembly engineering design

The design of the HFTM-Assembly has been improved regarding the assembly/disassembly process, which has to be performed partially under hot cell conditions by remote handling tools. It was sought to remove cost-driving and time consuming processes from the assembly, in order to improve the overall process in the IFMIF irradiation operation. A major step was the simplification of the finalizing weld-seams to close the HFTM-Assembly after insertion of the capsules. By re-design of the attachment between the thin-walled container and the stiff Attachment-Adapter (upper part), it is now possible to reduce the welding process to a simpler operation with access from only one side, which drastically simplifies the specifications for the equipment to handle the HFTM inside the hotcell. The improvements were implemented in the CAD Model of the HFTM double-compartment mockup, which will be the next manufactured mockup for test in the helium loop.

HFTM Irradiation Capsule and Rig

The irradiation capsule, which contains a set of material specimen for irradiation inside the HFTM, was already developed and analysed to a considerable degree of maturity. Three capsules have been produced, quality-checked and filled with material specimens (Fig. 2). During the production, issues of the construction have been identified, and according improvements have been implemented in the design.

In the same viewpoint as for the HFTM-Assembly, the irradiation rig was improved for easier assembly in the hot cells. This was reached by inserting the upper reflector into the rig hull, so that gas tight, circumferential weld seams are no longer necessary, only spot welding needs to be performed in the hot cell (Fig. 3).

The upper reflector is now made from two “sandwiched” parts, so that the feeding through of cables can be performed, even if their electrical connectors or feedthroughs are already installed (before delivery to the hot cell). This is especially necessary to be compatible with the new interface to the testcell, where brazed-on feedthroughs are used instead of removable connectors.

Fig. 2: Three fabricated capsules filled with specimens for irradiation in the BR2 MTR reactor.

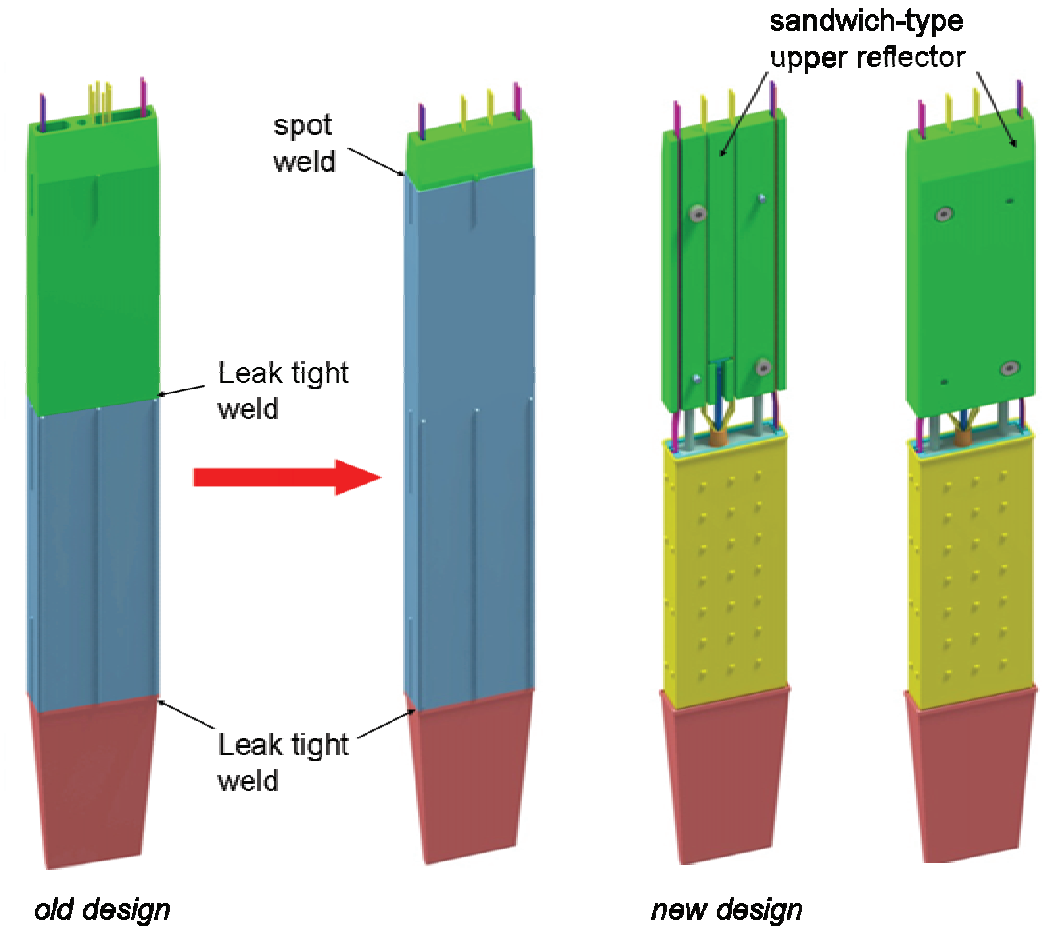

Fig. 3: Design improvement of irradiation rig.

HFTM Mockup experiments

The HFTM single rig experiment aims to investigate the behaviour of a 1:1 rig inside a compartment mockup. The experiment was installed at the ITHEX facility and was tested hydraulically. The performed tests verify, that the pressure drop is within the acceptable and predicted range, and that the perfusion of parallel minichannels by the coolant gas is of uniform quality.

Engineering Design of the Target- and Testcell

The design of the TTC has been significantly modified from the previous MTC concept. A driving motivation was the necessity to avoid polymer-based electrical connectors within the irradiation cavity. The following changes characterize the new design (Fig. 4):

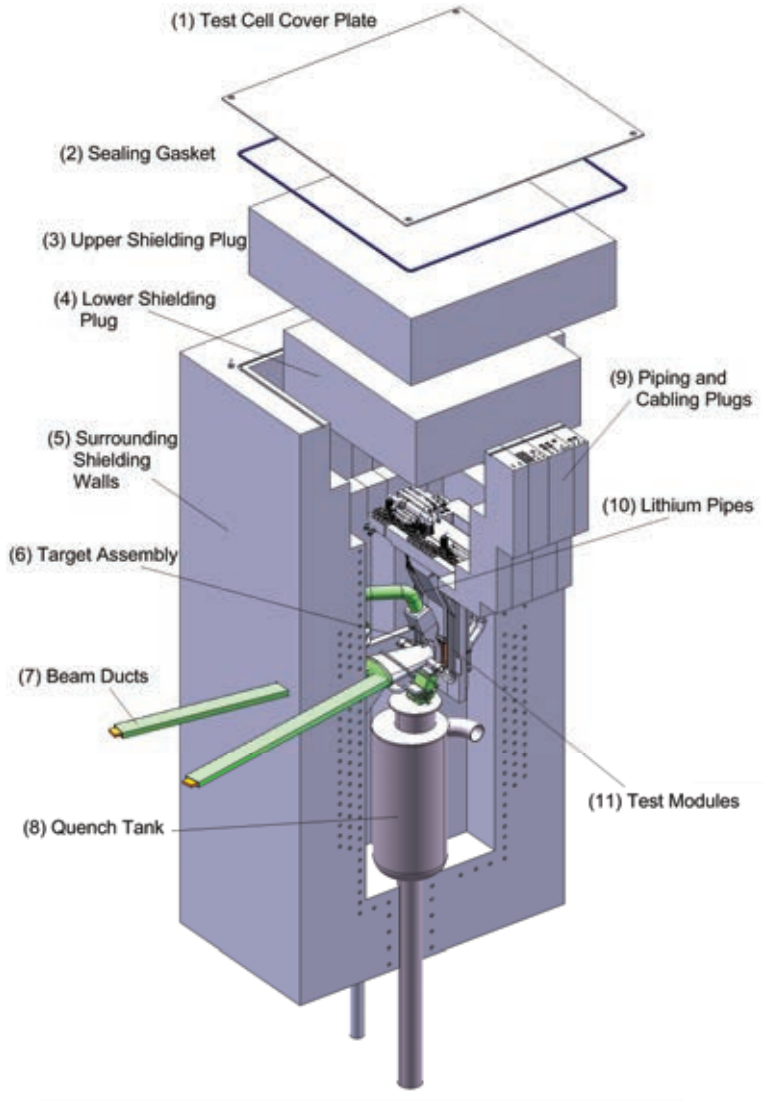

Fig. 4: The IFMIF testcell with “piping and cabling plugs”.

- The cross-section has been changed to a rectangular shape to adapt better to the test modules
- Instead of a vessel (bearing both mechanical and vacuum-pressure loads), the supporting walls are now made directly from the concrete of the radiation shield, with a steel liner inside to provide an inert and gas tight surface.

- The gas-sealing function has been moved above the top shielding plug, enabling the use of polymer-based sealing materials instead of difficult to handle metal gaskets.
- The electrical interfaces to the test modules is no longer performed by electrical connectors. Instead, the cables from the modules are fed-through gas tight plugs on the top of the modules.

The Preliminary Design Review for the new testcell design has been performed in 09/2011.

Engineering Design of the Tritium Release Test Module

The design of the Tritium Realease Test Module (TRM) was started in the report period. The requirements and a candidate test scenario were assessed based on the R&D needs for future ceramic breeding material candidates and breeding blanket design parameters. A geometrical design for the irradiation capsules and the module with the according instrumentation was drafted. Some design features (temperature control concept) were adopted from the HFTM in order to benefit from the validation activities performed for the HFTM. Thermal and mechanical analyses, as well as calculations on the tritium budget were performed. It could be shown, that the goals for the temperature range and limits for temperature spread can be reached. Issues remain for the high temperature variants (900°C and higher), where no adequate materials have been selected.

The Preliminary Design Review for the TRM has been performed in 07/2011.

Staff:

F. Arbeiter
Y. Chen
B. Dolensky
J. Freund
T. Heupel
Ch. Klein
M. Mittwollen
A.-L. Muche
G. Schlindwein
N. Scheel
P. Schubert
K. Tian
K. Zinn

Cooperation with industrial partners:
Babcock Noell (BNG), Germany, contractor:
The task of BNG is to review the testcell design under the aspect of construction technologies. Improvements coherent with state-of-the-art nuclear construction technologies are to be proposed by the company. Innovative aspects are the realization of highly heat loaded radioprotective walls against energetic neutrons and gammas.

Literature:

[1] Arbeiter, F.; Abou-Sena, A.; Chen, Y.; Dolensky, B.; Heupel, T.; Klein, C.; Scheel, N.; Schlindwein, G. Development and validation status of the IFMIF high flux test module. Fusion Engineering and Design, 86(2011) S.607-610 DOI:10.1016/j.fusengdes.2011.01.031

[2] Chen, Y.; Arbeiter, F. Flow and heat transfer characteristics of helium cooled IFMIF high flux test module. 10th Internat.Symp.on Fusion Nuclear Technology (ISFNT 2011), Portland, Oreg., September 11-16, 2011

[3] Klix, A.; Arbeiter, F.; Fischer, U.; Heinzel, V.; Serikov, A. Assessment of the operational dose rate in polymer insulators in the test cell of the IFMIF neutron source. 38th IEEE Internat.Conf.on Plasma Science (ICOPS) and 24th Symp.on Fusion Engineering (SOFE), Chicago, Ill., June 26-30, 2011

[4] Serikov, A.; Arbeiter, F.; Fischer, U.; Heinzel, V.; Klix, A.; Simakov, S.P. Shutdown dose rate analyses for the IFMIF HFTM. Fusion Engineering and Design, 86(2011) S.2639-2642 DOI:10.1016/j.fusengdes.2010.11.030

Acknowledgement

This work was financially supported by the Ministry of Research and Education (BMBF) under the grant No. 03FUS0008. The views and opinions expressed herein do not reflect necessarily those of the BMBF or the European Commission.

Broader-Approach Activity: Commissioning and First Tests of the Low Pressure He Loop HELOKA-LP (BMBF Reference No. 03FUS0005 and 03FUS0008)

Introduction

The work performed for IFMIF EVEDA (see respective section in this annual report) encompasses extensive experimental validation activities for the IFMIF High Flux Test Module (HFTM), developed at KIT. It is envisaged to build a prototype of the HFTM, and test it in 1:1 operation conditions (without irradiation) in a helium loop. This helium loop is named HELOKA-LP and has been built at KIT-INR as a preparative activity for the Broader Approach. This final status report describes the planning, construction, taking into service and tested performance of the facility, which has been prepared in the frame of the BMBF project 03FUS0005 and finalized in the ongoing IFMIF EVEDA phase within the frame of the BMBF project 03FUS0008.

Planning, construction and operation

HELOKA-LP has been specified to encompass 1:1 the hydraulic test conditions for the planned IFMIF HFTM, as given in Table 1:

Table 1: Requirements and specifications for HELOKA-LP

	Requirements by HFTM	**HELOKA-LP specifications**
HFTM helium mass flow	0.11 kg/s	0.012 – 0.12 kg/s
HFTM inlet pressure	0.3 MPa	0.3-0.6 MPa
HFTM outlet pressure	0.22 MPa	≥ 0.15 MPa
HFTM inlet temperature	50°C	RT – 250°C
HFTM outlet temperature	80-100°C	RT – 350°C

Other requirements on the facility are:

- The availability of a suitable process control system, to enable a long-term steady state operation and guided transitions for start-up and shut-down.
- The availability of a data acquisition system, to acquire, process, display and store the signals coming from the loop and from the HFTM test device (Thermocouples, pressures, strain, etc.).
- The availability of controllable electrical power supply units, to operate the electrical heaters which are integrated into the central 4x3 irradiation rigs. (thus, 36 units are required).

An overview of the process layout is given in Fig. 1. Fig. 2 gives some photographic impressions of the facility.

The helium gas flow is generated by an air cooled screw driven compressor with a nominal electric power of 355 kW and with a maximum delivered overpressure of about 0.8 MPa. At the typical inlet pressure of 0.15MPa absolute, the compressor generates a helium mass flow of around 190 g/s. The gas flow is divided to a bypass and a test section strand. This way the mass flow through the test section can be adjusted. The temperature at the test section entrance is controlled by dividing the gas stream between a electrical heater (300kW) and a parallel cooler, and mixing both streams again before the test section. A set of valves behind

the test section is used to control the test section pressure. The process control system can automatically adjust and control the valve openings according to the set points for mass flow, pressure and temperature given by the operator.

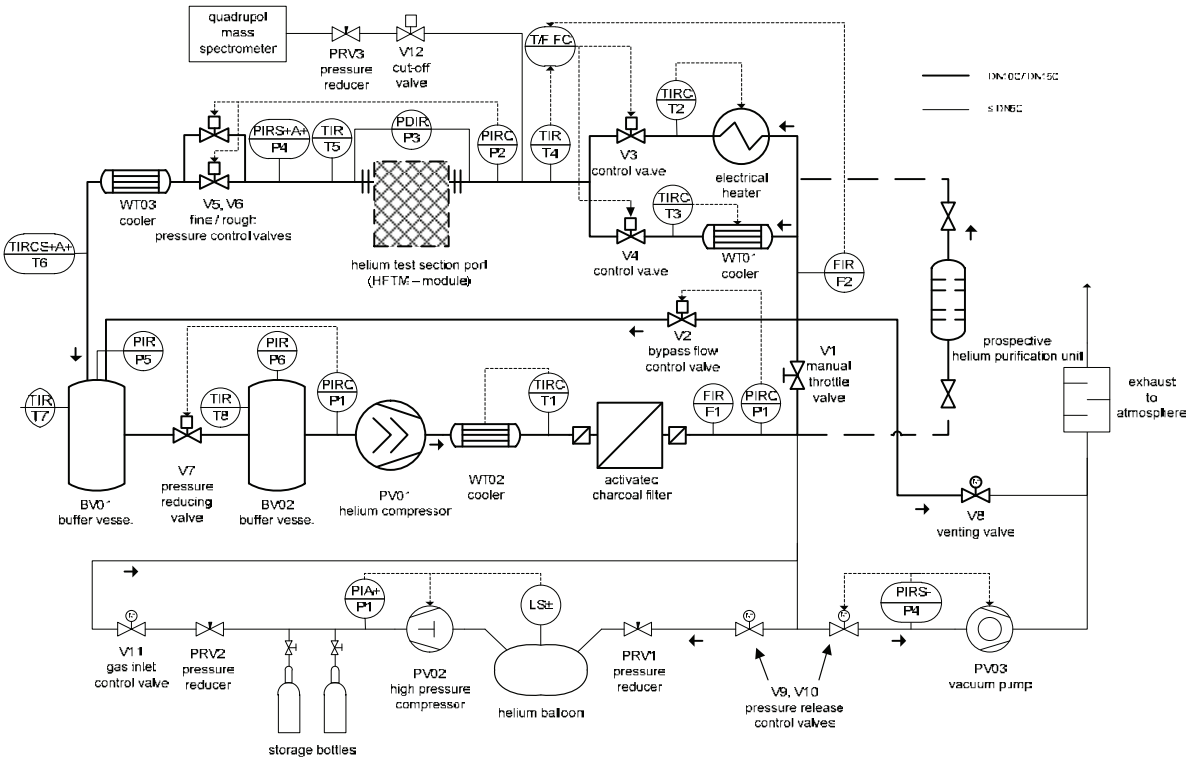

Fig. 5: Simplified piping and instrumentation diagram (P&ID) of the HELOKA-LP facility.

The detailed process dimensioning, planning and construction was performed by the industrial company Kraftanlagen Heidelberg GmbH. The planning, testing and taking into service was performed in close cooperation with KIT. The construction has been finalized in 12/2009. Further testing and optimization was performed by KIT between 2010 and 2011. The facility has also been upgraded with 36 controllable DC power sources to supply the HFTM heater circuits. It was proven, that the facility fully meets the specifications from Table 1, and that a very good stability of the process parameters can be maintained.

The operational experiences include optimization of the control parameters, to reach a stable pressure at the test module even in large mass flow transients. Also, the cooling gas chemistry (impurities) has been monitored and analyzed. Based on the design of HELOKA-LP, the Test Module Helium Cooling System for IFMIF, which requires an approximately fivefold higher total mass flow, has been specified.

Fig. 6: Views of the HELOKA-LP facility. Top: the compressor station showing the helium compressor with two buffer vessels. Bottom: The test facility where the HFTM will be integrated, showing the piping, the switch cabinets for data acquisition and 36 power supplies and the test stand for gas analysis.

Conclusions and outlook

The HELOKA-LP facility has been constructed, taken into operation and has been verified to meet the full scope of requirements for its mission as a testbed for the IFMIF High Flux Test Module in the IFMIF EVEDA phase. It is available without delay for the planned experimental series. It is expected, that HELOKA-LP will contribute to the success of IFMIF not only be the test of the HFTM, but also by providing experience and benchmark data on the operation of low pressure helium cooling. A numerical model (RELAP-3D) to model the transient behaviour of the full loop including the test module is under preparation. First tests against experimental data from HELOKA-LP have been performed.

HELOKA-LP is a worldwide unique facility, which can contribute to a broad range of research applications, also beyond IFMIF. Among possible applications are tests of gas cooled accelerator targets and irradiation experiments (as foreseen for the European Spallation Source, ESS), or low pressure high temperature solar heated systems. It is especially well suited to facilitate basic fluid dynamics research on efficient heat transfer, due to the favorable conditions of low pressure gas systems to incorporate complex instrumentation of the test sections.

Staff:

F. Arbeiter
J. Freund
X. Jin
Ch. Klein
G. Schlindwein
K. Zinn

Cooperation with industrial partners:
Kraftanlagen Heidelberg GmbH (KAH), Germany, contractor:
Kraftanlagen Heidelberg has planned, dimensioned and built the HELOKA-LP facility. Low pressure helium loops are a new task for the industry. New competences in the transient control of gas loops was built up in the company by cooperation with KIT.

Literature:

[1] G. Schlindwein, F. Arbeiter, J. Freund, Start-up phase of the HELOKA-LP low pressure helium test facility for IFMIF irradiation modules, Proceedings of the 10th International Symposium on Fusion Nuclear Technology, Portland, Oregon, USA, Sep. 2011 (under review)

[2] Arbeiter, F.; Abou-Sena, A.; Chen, Y.; Dolensky, B.; Heupel, T.; Klein, C.; Scheel, N.; Schlindwein, G. Development and validation status of the IFMIF high flux test module. Fusion Engineering and Design, 86(2011) S.607-610 DOI:10.1016/j.fusengdes.2011.01.031

[3] F. Arbeiter, Y. Chen, B. Dolensky, J. Freund, T. Heupel, Christine Klein, Nicola Scheel, Georg Schlindwein (2011): Overview of results of the first phase of validation activities for the IFMIF High Flux Test Module, Proceedings of the 10th International Symposium on Fusion Nuclear Technology, Portland, Oregon, USA, Sep. 2011 (under review)

Acknowledgement

This work was financially supported by the Ministry of Research and Education (BMBF) under the grants No. 03FUS0005 and 03FUS0008. The views and opinions expressed herein do not reflect necessarily those of the BMBF or the European Commission.

Broader-Approach Activity: Neutronics Analysis for the IFMIF Test Facility and High Energy Beam Transport Section (BMBF Reference No. 03FUS0008)

Objective

The objective of this work was to support the engineering design of the IFMIF Test Facility (TF) with the Test Cell (TC) and the high energy beam transport (HEBT) section within the IFMIF-EVEDA/BA framework. The TC is the central part of IFMIF where two deuteron beams react with the liquid lithium target and the Test Modules (TMs) are placed for irradiation. The HEBT section is required to transport two deuteron beams accelerated to 40 MeV with the beam current of 125 mA from the exit of the accelerator to the lithium target. Neutronic analyses are performed to provide various nuclear responses which are required for the engineering design of the facility (material damage, gas productions, heating, etc.) and for safety related assessments (activation of various components, air and gas, biological doses to work personnel and the public).

Computational approach

In the IFMIF lithium target, neutrons are generated through d-Li(d,xn) reactions. The McDeLicious Monte Carlo code [1] was developed as an enhancement to MCNP in order to simulate the neutron and photon generation in the transport calculation with the comprehensive evaluated d + ^{6,7}Li cross-section data. A standard set based on the LA150 evaluated library has been used in previous IFMIF nuclear analyses. Currently a new FENDL-3 library is prepared by the IAEA with an energy range of incident particles up to 150 MeV. FENDL-3 is planned as new standard nuclear data library for IFMIF nuclear analyses and several starter libraries of FENDL-3 are already available. Here we have utilized the FENDL-3 starter library, release 2, except for several lighter nuclides which were evaluated only for neutron energies up to 20 MeV.

Nuclear analysis for IFMIF Test Cell

All previous nuclear analyses were conducted with a standard TC model that has been manually devised according to the CDR design. However, the TC presently designed has a very different geometry with significant impact on neutronic aspects. Therefore, a new TC model based on the MTC-2009 concept [2] developed on the CAD platform with CATIA V5 was converted into the geometry representation by utilizing the McCad conversion software developed at KIT [3]. This new Monte Carlo geometry model includes the deuterium beam ducts, the lithium target assembly with the back plate, lithium loop components within the TC, three TMs, the vessel and vessel cover, and concrete shielding walls around the vessel (Fig. 1). This model is quite complex and the total number of cells is around 18,000.

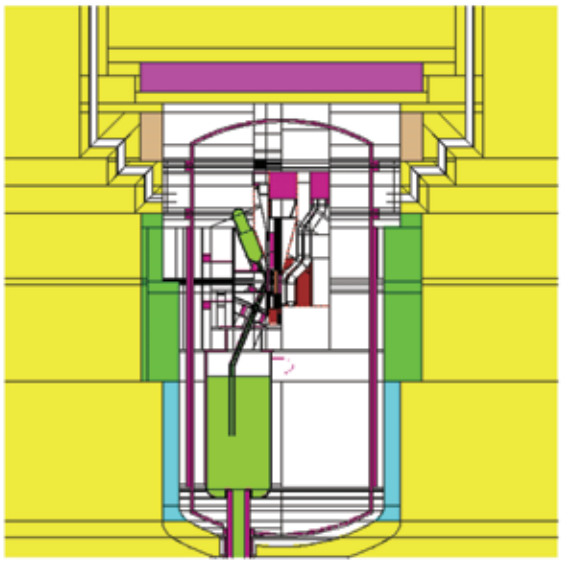

Fig. 1: Vertical cut of the new IFMIF TC neutronic model based on the MTC concept.

The nuclear heating rate, displacement damage and gas production rates in the TC vessel wall were calculated with the new geometry model. Fig. 2 shows the nuclear heating distribution calculated for the vessel wall as an example. Pronounced peaks were obtained around the beam ducts entrance region due to back-streaming neutrons. The helium production was shown to be too high if re-welding is considered. A wall thickness of more than 350 cm is needed to satisfy the dose rate limit during operation of less than 10 μSv/h in rooms adjacent to TC. The dose rate on the top access cell floor is estimated to be around 20 μSv/h and well less than 100 μSv/h. Thus substantial improvement has been achieved in the shielding capability for the access cell in the present TC design.

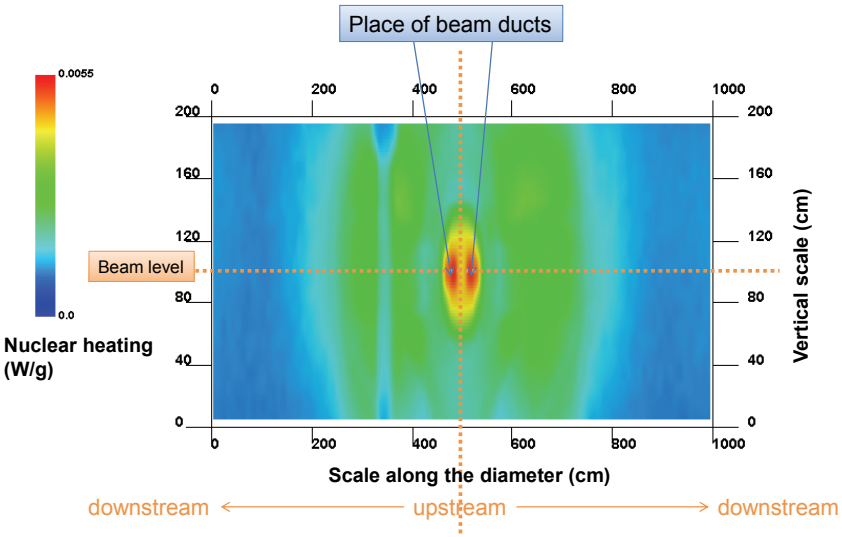

Fig. 2: Nuclear heating distribution calculated for the cylindrical plane of the vessel liner.

Nuclear analysis for IFMIF HEBT section

In the HEBT section, neutrons back streaming from the lithium target can cause significant damage to accelerator components and result in their activation. In order to estimate the resulting radiation doses, detailed neutron and photon flux distributions inside the Target Interface Room (TIR) and the Radiation Isolation Room (RIR) during operation are evaluated. A new calculation model for the IFMIF accelerator building up to 41.2 m upstream from the Li target was prepared according to the latest HEBT system design. Fig. 3 shows the geometrical configuration of the present calculation model. A calculation with the full TC model was used to generate a surface source located on the inner concrete wall of TIR downstream as indicated in the figure. Neutron and photon particles have been recorded along the McDeLicious runs on the surface source and then sampled in subsequent MCNP5 runs. Fig. 4 shows the neutron flux distribution during IFMIF full power operation calculated for TIR and RIR as an example. The present analysis shows that the largest contribution to the TIR dose will come from neutrons streaming from the Li target through the beam ducts. It seems to be impossible to use any semiconductor devices inside TIR, while there will be no problem on other mechanical devices. The dose after shutdown due to decay gamma was preliminary estimated for the beam duct in TIR with the FISPACT-2007 inventory code. In order to reduce the shutdown dose rate, the use of a low-Mn content aluminium alloy is proposed.

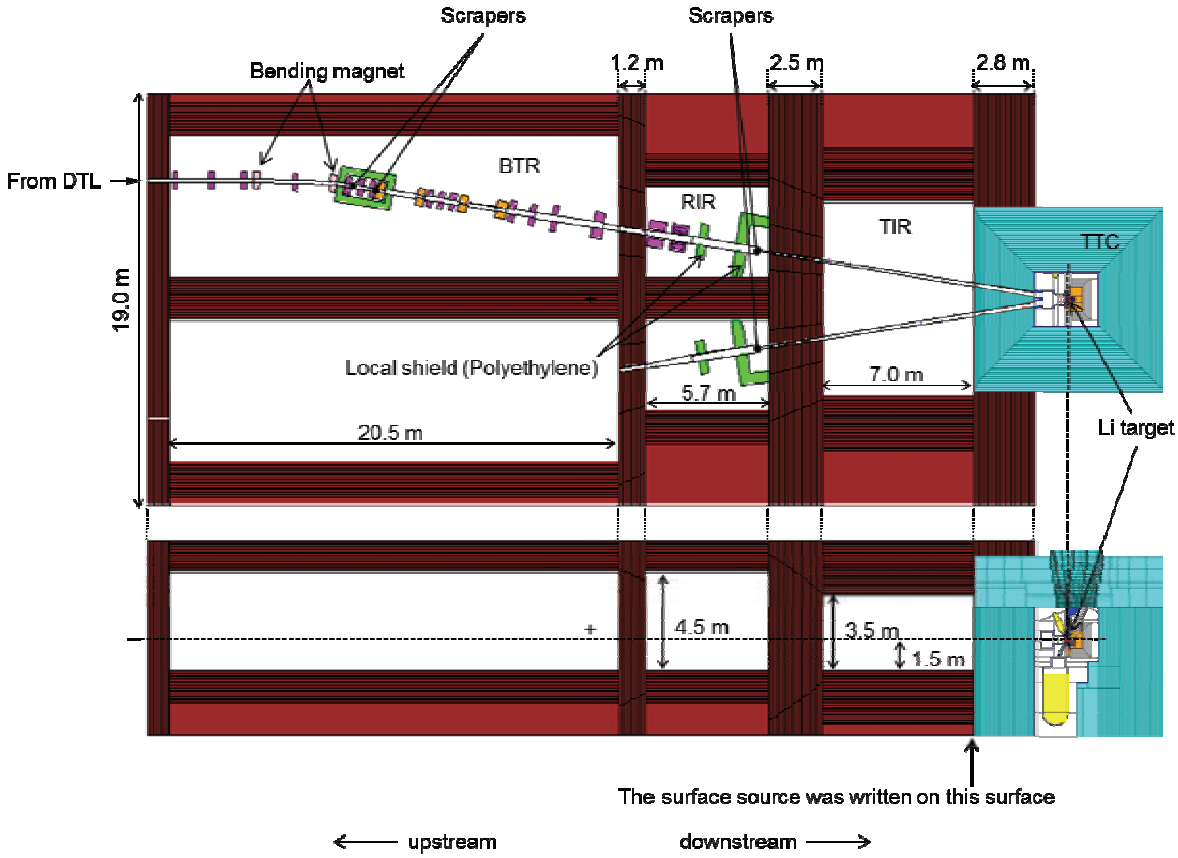

Fig. 3: Geometrical configuration of the present analysis for the IFMIF HEBT section.

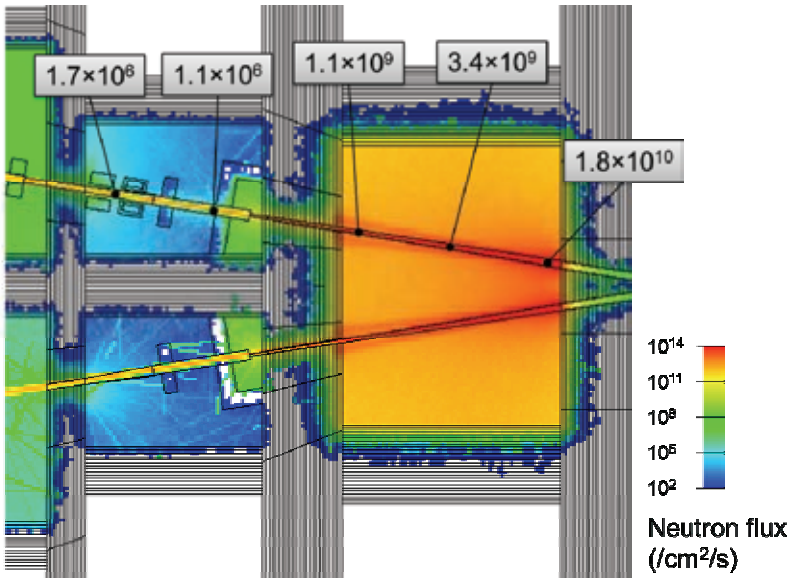

Fig. 4: Neutron flux distribution during IFMIF full power operation calculated for TIR and RIR.

Staff:

K. Kondo
A. Serikov
A. Klix
U. Fischer

Literature:

[1] S.P. Simakov et al., Advanced Monte Carlo procedure for the IFMIF d-Li neutron source term based on evaluated cross section data, Journal of Nuclear Materials 307–311 (2002), pp. 1710-1714.

[2] K. Tian et al., IFMIF target and test cell—Conceptual designs, boundary condition definitions and current status of preliminary engineering design, Fusion Engineering and Design 85 (2010), pp. 2282-2287.

[3] D. Große and H. Tsige-Tamirat, Current Status of the CAD Interface Program McCad for MC Particle Transport Calculations, Proceedings of International Conference on Mathematics, Computational Methods & Reactor Physics (M&C 2009), on CD-ROM, American Nuclear Society, 2009.

Acknowledgement

This work was financially supported by the Ministry of Research and Education (BMBF) under the grant No. 03FUS0008. The views and opinions expressed herein do not reflect necessarily those of the BMBF or the European Commission.

Fuel Cycle –
Vacuum Pumping

Completion of Final Design for the Prototype Torus Cryopump (F4E-2009-GRT-018-01)

Background and objectives

The reference design of the ITER exhaust gas pumping includes 8 cryopumps to pump the torus via 5 ducts (configuration under change). The design of these cryopumps has to consider the different requirements for vacuum pumping, remote handling and safety, and provides strong interfaces to the surrounding environment of the installation port plugs of the ITER machine.

The aim of this task is to provide the build-to-print design of the pre-production cryopump (PPC) including a solid mechanical, thermal, seismic, safety event and engineering limit analysis to demonstrate compliance with EN13445, the chosen design code for this ITER component [1]. In this sense, the PPC represents a real prototype that is presently also intended to be used as a spare. After manufacturing, the cryopump will be tested in the TIMO-2 facility.

Design development and verification

The concept design of the torus cryopump as developed in 2007 [2] was used as starting point of this design task. The detailed design development had to undergo various stages to reflect changing ITER requirements. The final design is depicted in Fig. 1. The PPC is circular shaped with a maximum outer diameter of 1776 mm and a total length of about 2054 mm. The cryopanel system at 4.5 K with a total pumping surface of 11.2 m² consists of 28 cryopanels in a circular arrangement. The outer thermal shield system at 80 K forms an enclosure around the cryopanel system against the heat radiation from inside and outside the cryopump. The pumping speed can be varied by throttling the main valve, which opens towards the torus with a maximum stroke of 470 mm. The valve inlet diameter is 800 mm. The prototype torus cryopump can be separated into four main subassemblies: the pump housing including the pump plug, the thermal shield system, the cryopanel system and the pump inlet valve. For all subassemblies analyses of the different operational and accidental scenarios were done by finite element analysis (FEM). In Figs. 2 and 3 the schemes for the different cases are summarised which include the dead weight of the components (DW), the internal and external pressures and additional acceleration caused by seismic events with different probability and spectrum (SL1 and SL2).

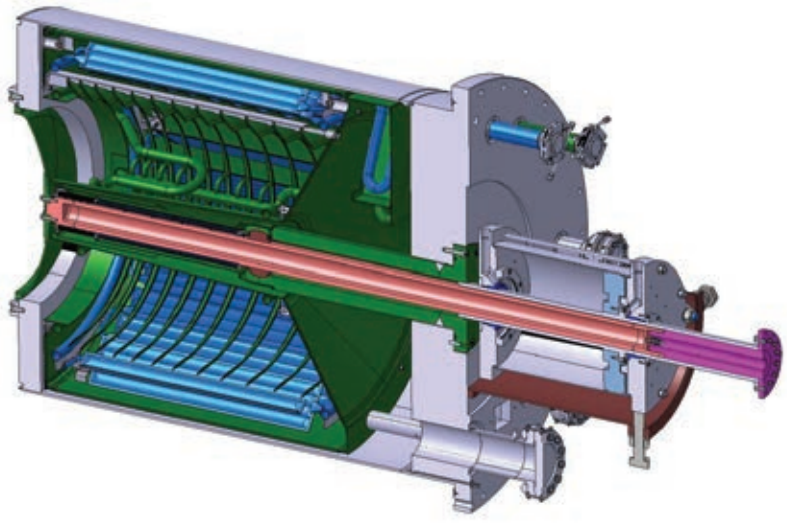

Fig. 1: Final design of the torus pump as single unit, showing the main subassemblies: the housing (grey), the thermal shield system (green), the cryopanel system (blue) and the inlet valve system (pink/orange).

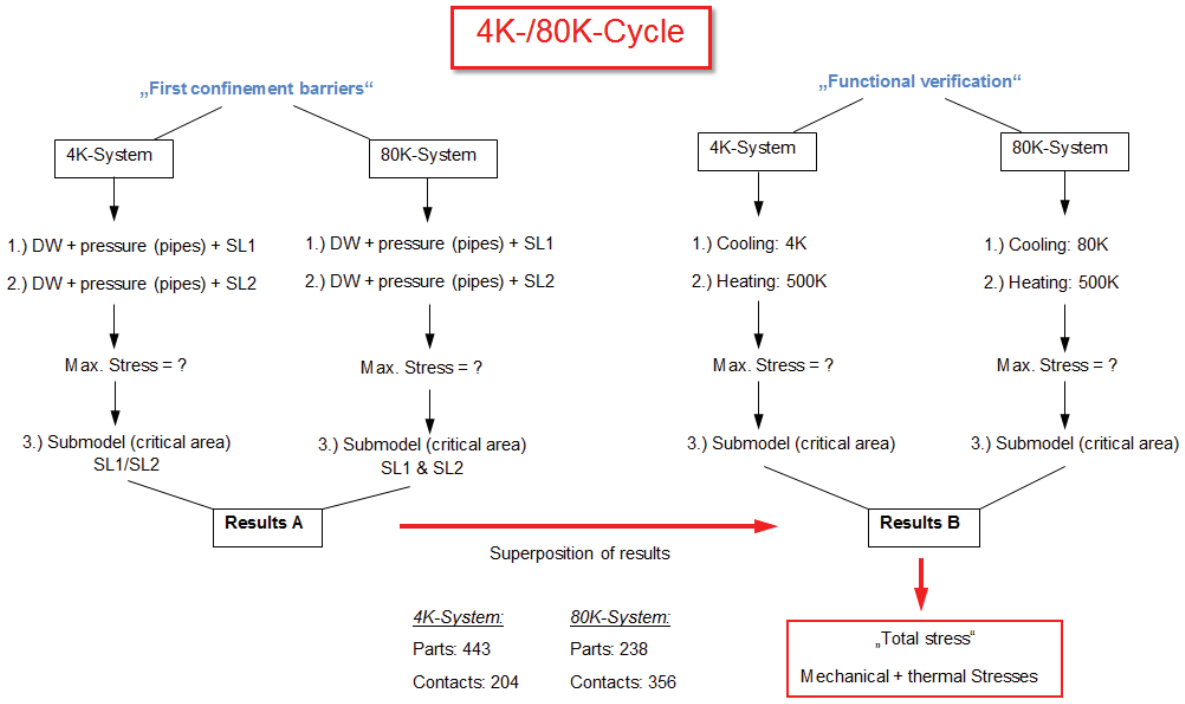

Fig. 2: Investigated load cases for the FEM analyses of the cryopanel and thermal shield system.

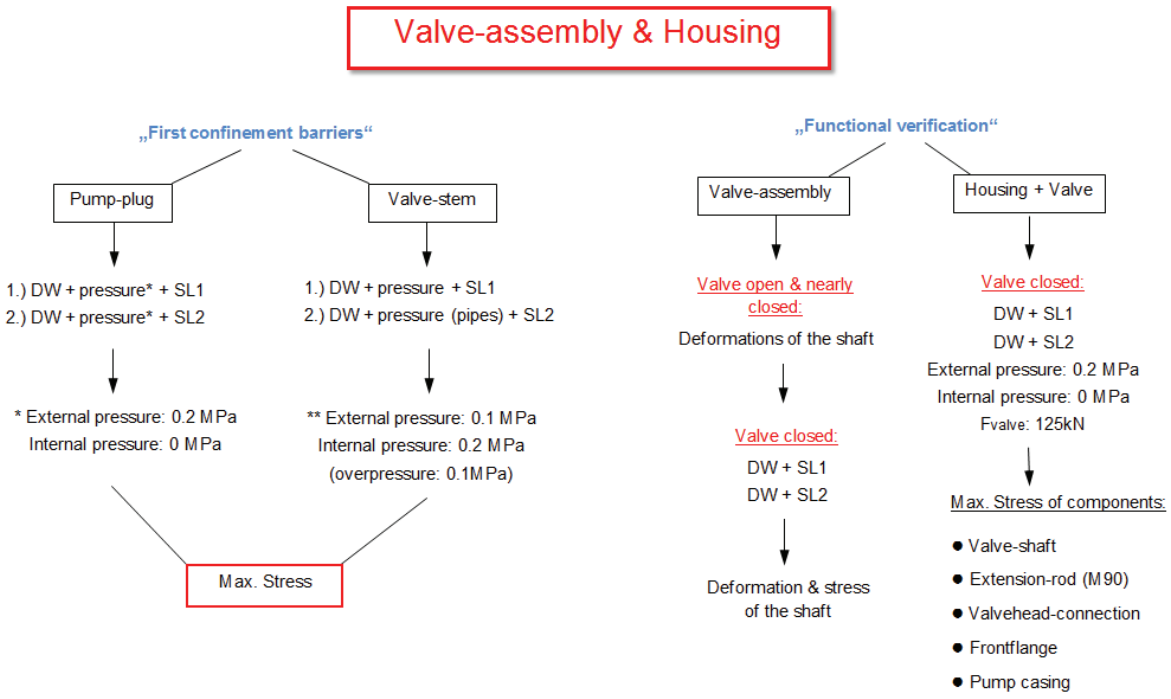

Fig. 3: Investigated load cases for the FEM analyses of the valve assembly and PPC housing.

The results of the FEM work are the displacements and mechanical/thermal/seismic stresses for the subassemblies under the different operational and accidental scenarios. The resulting maximum stresses were always compared with the values requested by the standards. In cases where the stresses were too high the design was optimised and the displacements and stresses were recalculated. As an example, Fig. 4 shows the displacement along the symmetry axis for a seismic event of class SL2 after design optimisation of the pipe supports. The resulting stresses in the supply manifold of the thermal shield system are shown in Fig. 5. Both, displacements and maximum stresses, could be reduced significantly.

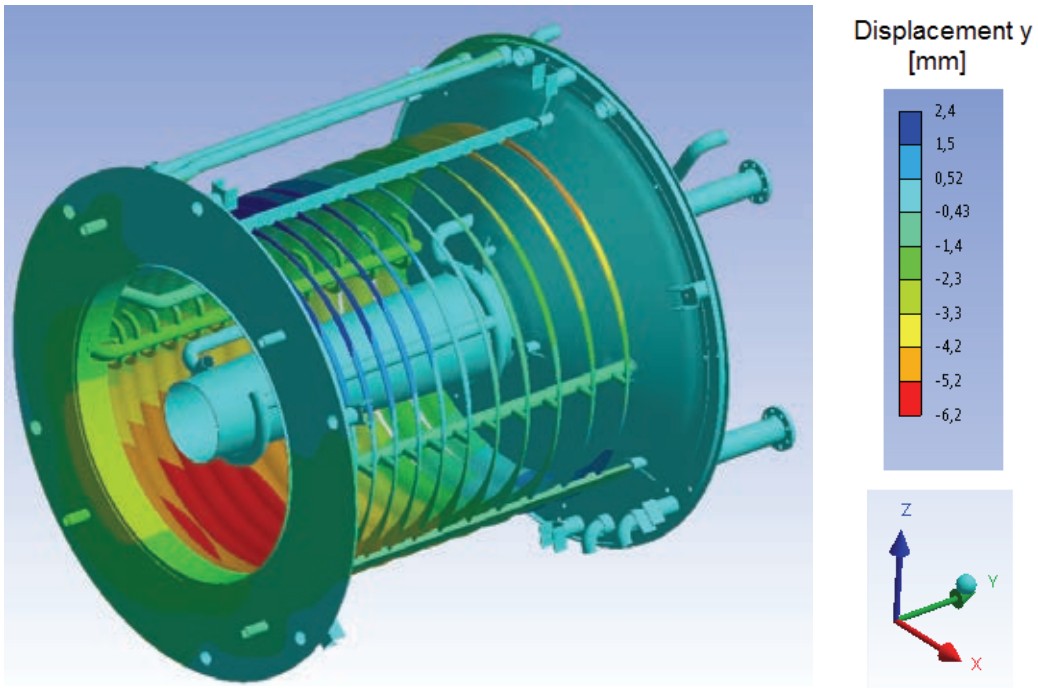

Fig. 4: Displacement of the thermal shield system in direction of the symmetry axis (SL2).

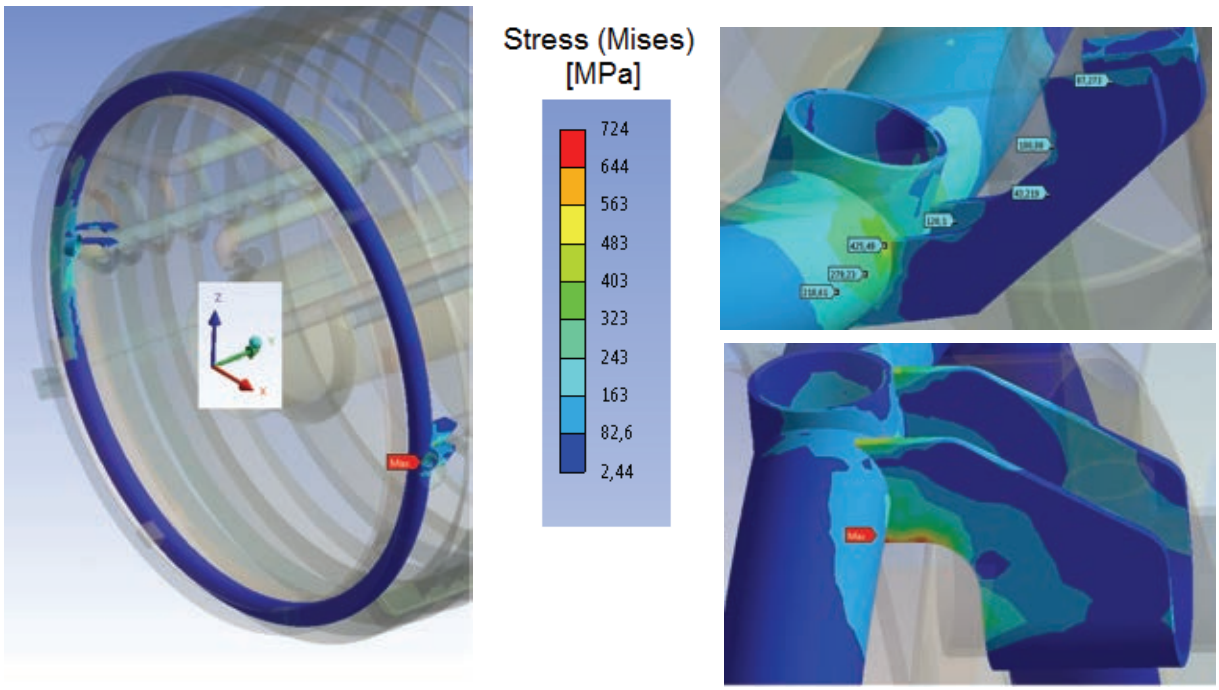

Fig. 5: FEM calculations of the stresses in the thermal shied system (supply manifold for SL2).

Calculation of the maximal acceptable heat flux to the PPC

Different calculations were performed in order to assess the maximal acceptable heat flux to the PPC in case of an accidental situation in a loss-of-vacuum event (LOVA) [3]. The maximum acceptable heat load value is directly linked to the maximum acceptable cryogenic mass flow in the cryopump's circuits which is limited by the pressure design of the circuits. Both cryopanel circuit (normal operation at about 0.5 MPaA and 4.5 K) and thermal shield circuit (normal operation at about 1.8 MPaA and 80 K) were investigated.

In order to protect a helium circuit in a LOVA situation (leading to excessive heat load due to air, water, or helium ingress), the safety components (relief valve, burst disk, etc…) must be correctly sized and the maximal pressure reached in the circuit must be assessed. Indeed, when the helium is released from the circuit during an accidental situation, a pressure gradient occurs in the circuit and a peak pressure is reached at a certain point within the system.

Defining the heat load value for a specific accident (air, water, and helium ingress) is the critical point of the problem. Unfortunately, it is very difficult to calculate this value as it is depending on the heat transfer coefficient inside the circuit and on complex phenomena occurring outside the circuit (such as ice layers formation). Moreover, no reliable experimental data exist on heat fluxes in case of ingress for circuits operated with supercritical helium. This is why a reverse approach was taken in the present study. This means, the maximum acceptable mass flow that can be handled according to the design pressure of the circuit was calculated. Once the maximal mass flow is calculated, the corresponding heat load is calculated and compared to the maximum acceptable value of heat load defined by ITER.

The maximum mass flow that can be released from the cryopanel circuit was assessed with about 10.6 kg/s, which corresponds to a heat load of 800 kW and a heat flux of 6.2 W/cm². The maximum mass flow that can be released from the thermal shield circuit was assessed with about 3.7 kg/s, which corresponds to a heat load of 2200 kW and a heat flux of 7.8 W/cm².

The following Fig. 6 illustrates the results for the cryopanel circuit. One block of cryopanels is made of 4 parallel cryopanels, and one block of connection pipes is made of 4 parallel connection pipes. The mass flow profile to the two protecting relief valves (RV1 and RV2) and the pressures in the circuit are represented along the circuit.

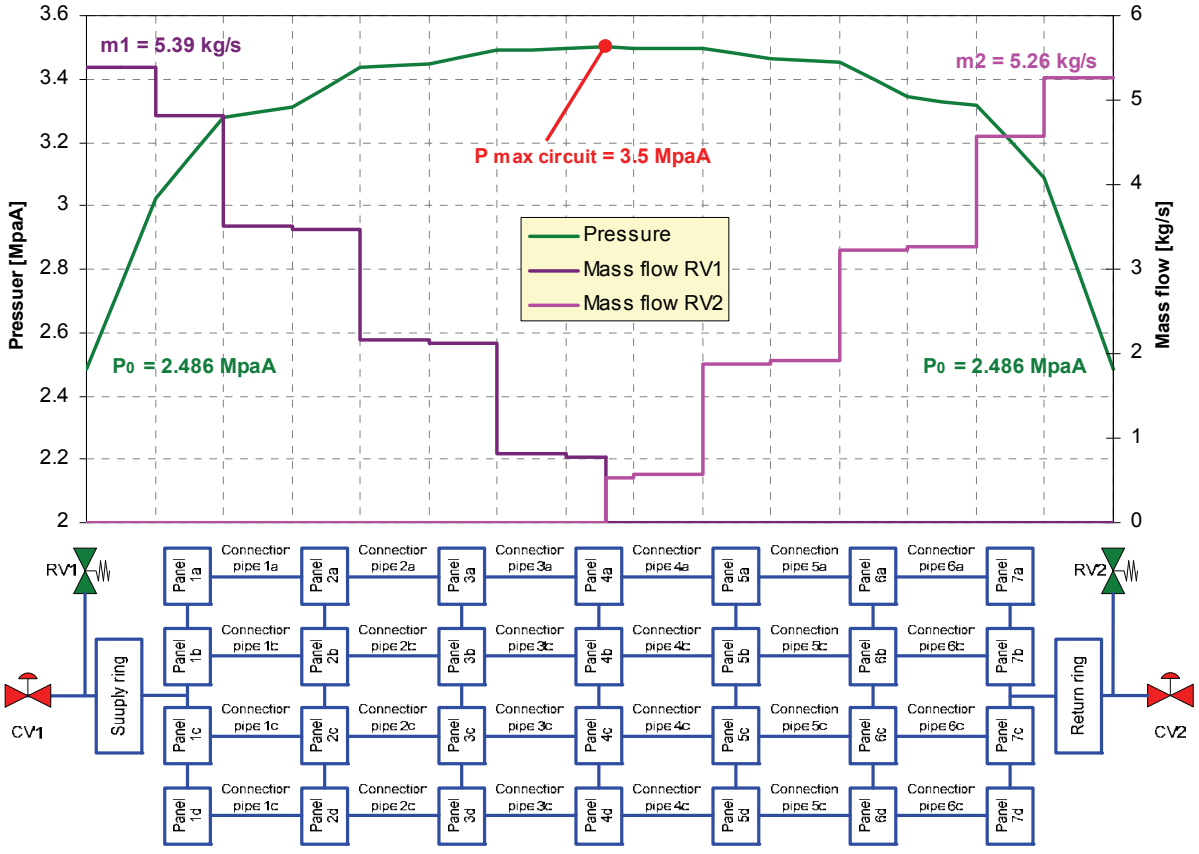

Fig. 6: Mass flows and pressure build-up in the PPC cryopanel circuit.

In order to perform this work, a specific code has been developed by KIT. The code offers the possibility to size a safety component for a given mass flow or for a given heat load on a helium circuit, according to the norms related to pressure devices (API520, EN13648-3).

Current status and outlook

The complete build-to-print design of the PPC together with the documentation catalogue of performed studies, analyses and assessments is finalised. The 3D CATIA products have been transferred according to the ITER format requirements. A number of 230 2D drawings have been produced including a detailed list of 1400 weld descriptions. The design was approved from F4E and ITER and will be given to the manufacturer who will be identified until mid 2012 in a call-for-tender procedure. If invited, KIT is ready to provide expertise to F4E in cryopump manufacturing. Finally, when built, the pump will be tested in the TIMO-2 facility to validate the design [4].

Industry involvement

This work has been supported by the company WEKA AG, Switzerland, who were acting as Third Party to KIT. WEKA was contributing their expertise in cryogenic valve design and industrial manufacturability, especially in the areas of sealing, bearing choice and position control.

Staff:

Chr. Day
A. Demsoreanu
H. Haas
V. Hauer
M. Lux
M. Scannapiego
R. Simon
H. Strobel

Literature:

[1] Chr. Day et al., Design progress for the ITER torus and neutral beam cryopumps, Fusion Engineering and Design 86 (2011) 2188-2191.

[2] V. Hauer et al., Design of the ITER torus prototype cryopump, Fusion Engineering and Design 82 (2007) 2113–2119.

[3] Chr. Day, Th. Giegerich, St. Hanke, V. Hauer, R. Lässer, St. Papastergiou, Design development of the cryopumping systems of ITER in view of future DT fusion devices, ISFNT-10, Portland, OR, USA, Sept. 2011.

[4] H. Haas, Chr. Day, F. Herzog, TIMO-2 – a cryogenic test bed for the ITER cryosorption pumps, Cryogen. Engng. Conf., Spokane, W, USA, June 2011.

Acknowledgement

This work was supported by Fusion for Energy under the grant contract No. F4E-2009-GRT-018-01 with collaboration by WEKA AG, Switzerland. The views and opinions expressed herein reflect only the author's views. Fusion for Energy is not liable for any use that may be made of the information contained therein.

Simulation of Vacuum Flows in Fusion Reactors (EFDA HPC-FF-SIMVAC, WP11-HCD-01-05-05-01)

Background

The prediction and modelling of vacuum flows is of key importance for the design and operation of fusion machines. In particular, there are high vacuum pumping systems for evacuation and maintenance of the needed pressure levels in the torus, in the cryostat and in the neutral beam injectors. Each of the aforementioned vacuum systems consists of networks with various channels and complicated cross sections and is characterised by large temperature gradients and distributed gas loads. The flow in such systems covers the whole range of the Knudsen number, varying from the free molecular regime all the way up to the hydrodynamic limit.

KIT has developed the ProVac3D software, which is a stochastic approach to describe gas flows based on the time-of-flight accumulation method [1]. It has become the reference tool for the vacuum design of the ITER cryopump systems, see [2-4], and has been applied successfully to flow simulations of the ITER divertor system. This success encouraged us to investigate the feasibility of ProVac3D to describe transient flow problems. Non-equilibrium flows are of central importance in fusion machines where not only ramp-up and -down, but also keeping steady-state conditions requires the con-current performance of many actuators (fuelling, heating, seeding, etc.), each with specific dynamic characteristics.

Parallelization and transient flow applications

Due to the underlying idea of monitoring a single particle travel path and velocity, ProVac3D is intrinsically able to describe transient phenomena and is intrinsically able to be parallelized without problem. Because of the complexity of the geometries of interest and the demand for a large number of modelled particles - especially in transient cases - to reduce the statistical error, parallel calculations are highly desirable. Hence, the computational demands (speed and time) are expected to be reasonably low for ProVac3D whereas other codes valid in the transitional range (such as DSMC or kinetic equation solvers) are very complicated to be parallelized. In view of this promising situation, the main target for 2011 was to demonstrate that ProVac3D is a reasonable approach to describe transient phenomena in fusion problems.

As first step, an effective parallelization was successfully accomplished in 2011. Figure 1 shows the results on the High Performance Computer for Fusion (HPC-FF) at Jülich Supercomputing Centre (JSC) and on the HC3 supercomputing system at KIT. One can see that the speed-up efficiency is still quite good by using hundreds cores.

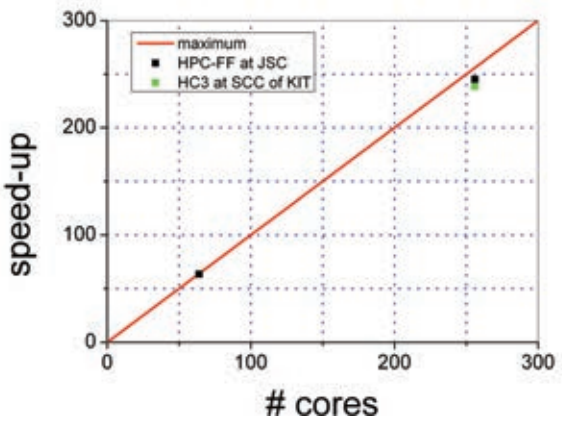

Fig. 1: The speed-up efficiency of ProVac3D after parallelization.

This allowed us to re-simulate many previous design cases with higher statistical precision. With the parallelisation, we had the capability to start activities in modelling of transient flows, which are, by their nature asking for much more computational power than steady-state flows. Up to now, there is very little literature about transient phenomena in a vacuum system [5].

Under this task, we have modified successfully the ProVac3D code to include new subroutines, in which the time-dependent trajectory tracings are handled and the existing good con-

vergence characteristics are preserved. The model chosen in a test simulation was a cylindrical tube of the length of 10 m and the diameter of 300 mm. The test molecules of nitrogen at 300 K were injected into the tube inlet according to the Maxwellian velocity distribution. 100 equally distributed virtual discs along the tube axis were implemented to record the time-dependent incident hits. The time resolution was 1 ms for the first 5 s. This means that there were 5000 time windows in total. As many as 10^{10} molecules were simulated with 640 cores on the supercomputer of HPC-FF. The computation time was less than 5 hours. This work was performed under the SIMVAC project of HPC-FF. Figure 2 shows the simulation result. The incident hits are a measure for the local pressure. Compared to [5], which is considered as the present state-of-the art in this field, the resolution could be improved significantly.

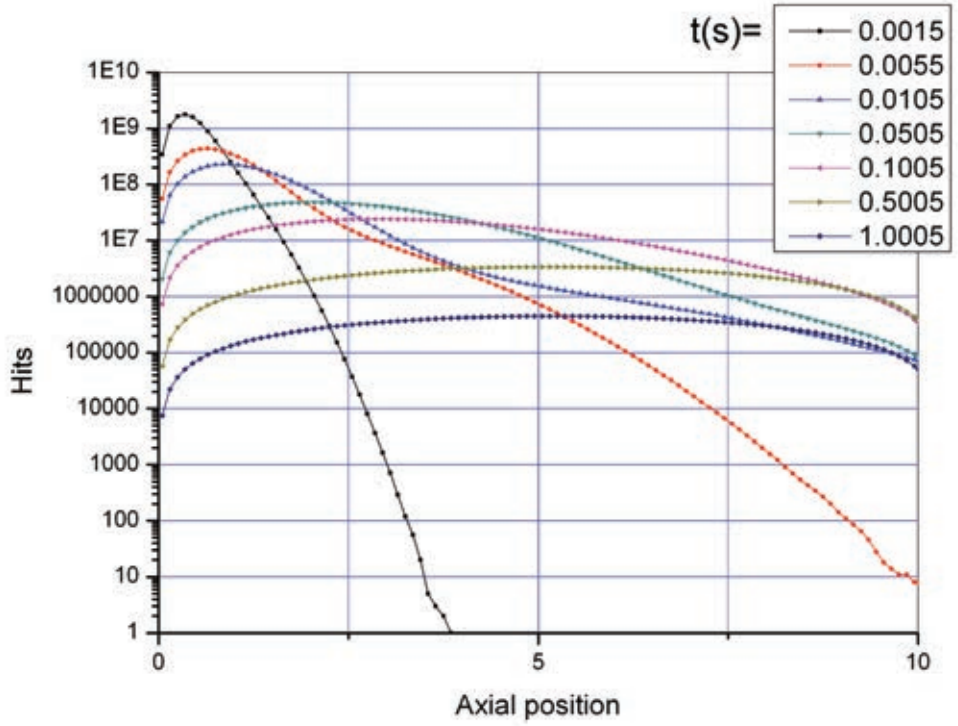

Fig. 2: Time-dependent incident hits of nitrogen molecules at 300 K along the 10 m length of the modelled tube.

Conclusions and outlook

It has been demonstrated that the ProVac3D code is a reasonable approach to describe the transient gas flows in a vacuum system. This was enabled by a full parallelization of the code and by the development of subroutines to record the time-dependent trajectories of the test molecules. By these two essential steps the objectives of the task are fulfilled. However, we still need to cross-check the simulation results with experimental data. As the published database is almost non-existing, this activity will be supported by our experimental test rig TRANSFLOW.

Staff:

X. Luo

Literature:

[1] X. Luo, Chr. Day, Investigation of a new Monte Carlo method for transitional gas flow, Proc. 27th Int. Symp. on RGD, AIP Conference Proceedings 1333, Melville, W, USA, 2011, pp. 272-276.

[2] X. Luo, Chr. Day, H. Haas, St. Varoutis, Experimental results and numerical modelling of a high-performance large-scale cryopump I, Journal Vac. Sci. Technol. A 29 (2011) 041601/1-7.

[3] X. Luo, V. Hauer, Chr. Day, Monte-Carlo calculation of the radiation heat load of the ITER pre-production cryopump, ISFNT, Portland, OR, USA, Sept. 2011, accepted for publication in Fusion Engineering and Design.

[4] X. Luo, Chr. Day, 3D Monte Carlo modeling of the neutral beam injection systems of ITER, Fusion Engineering and Design 85 (2010) 1446-1450.

[5] M. Cox, Towards modelling a vacuum accident in a x-ray beamline, Oral presentation at 64th IUVSTA Workshop, Leinsweiler, Germany, May 2011.

Acknowledgement

This work, supported by the European Communities under the contract of Association between EURATOM and Karlsruhe Institute of Technology, was carried out within the framework of the European Fusion Development Agreement. The views and opinions expressed herein do not necessarily reflect those of the European Commission.

Components and Infrastructures of PRIMA: Cryopumps for MITICA and the ITER Heating Neutral Beam (F4E-2009-GRT-032-PMS-H.CD and F4E-GRT-303 (PMS-H.CD))

Background and objectives

The 2011 activities in the area of the cryopumps for Neutral Beams (NB) were focussed on the continuation of the design development to a build-to-print (BtP) level that can be directly employed for a call for tender and the manufacturing. The NB cryopump package has two elements: firstly, the cryopumps for the ITER HNB, which have to be addressed initially; secondly and starting from the ITER HNB design, the cryopumps to be used in the MITICA testbed, which will be testing a full 1:1 scale ITER NB [1, 2]. To make full benefit of the diagnostic capabilities of the testbed, some adaptations have to be made to the cryopumps. But they have to be made such that the pump stays fully representative for the ITER HNB environment.

The 2011 work was first organised under Grant F4E-2009-GRT-032, which started in spring 2009 and was running until March 2011. The continuation of the work was performed under GRT-303 which is the direct successor of GRT-032 with the same lead parties involved and running since May 2011. Thereby, GRT-303 covers the elaboration of the BtP design of the cryopump for the ITER HNB as well as for the MITICA cryopump. The MITICA facility is currently being set up on site of Consorzio RFX in Padova, Italy.

Design development

For the ITER HNB cryopump many open design details have been solved, in all cases accompanied by FEM analyses and the development of all needed documentation and plans [3-4].

Solving open design issues

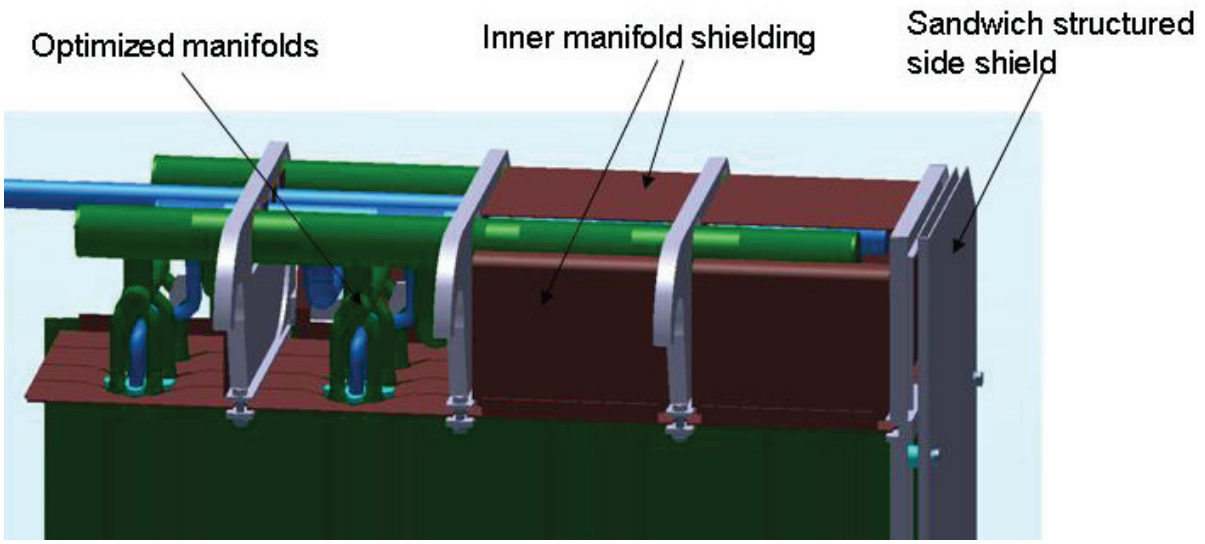

Fig. 1: Upper part of one module of the pump showing some details of the final design. The outer manifold cover is hidden to show the internal parts.

Solutions have been developed and integrated for the side shields at both ends of the pump, for the outer manifold shielding, being the outer cover at the top and bottom region, for the inner manifold cover, reducing the heat load onto the cryogenic manifolds in the pump, for the spacers between the cryopanels and the front shielding, and for the mechanical support of all the panels and shields, which has to insulate cooled components from the warm frame

while allowing the thermal movements of all components. Fig. 1 illustrates some of these design details.

Conceptual design for MITICA cryopump adaptations

The required beam diagnostics in MITICA ask for additional openings in the cryopump at two different positions along the beamline. An investigation on potential design options and consequences has been performed to assess already at an early point in the design development if an adequate adaptation of the HNB design is possible without a significant impact to the pump performance. The developed solution is basing on a marginal shift of the entire pump to not affect the cryosections in the pump. Consequently, the needed openings have only to be realized in the shielding backwalls. These openings have to be equipped with small additional shieldings to guarantee that no direct thermal radiation coming from the beamline vessel through these openings will reach the cryopanels. Fig. 2 shows the conceptual design of this additional shielding system. Since this additional shielding system will slightly reduce the capture probability of its neighboring pumping sections, a detailed pump model, including these adaptations, was integrated in a ProVac3D model of the entire HNB system. This led to a reliable prediction of the resulting reduction of the global pump performance, caused by the two local adaptations, which was found being negligible and not causing any significant difference between the HNB pump and the adapted MITICA pump.

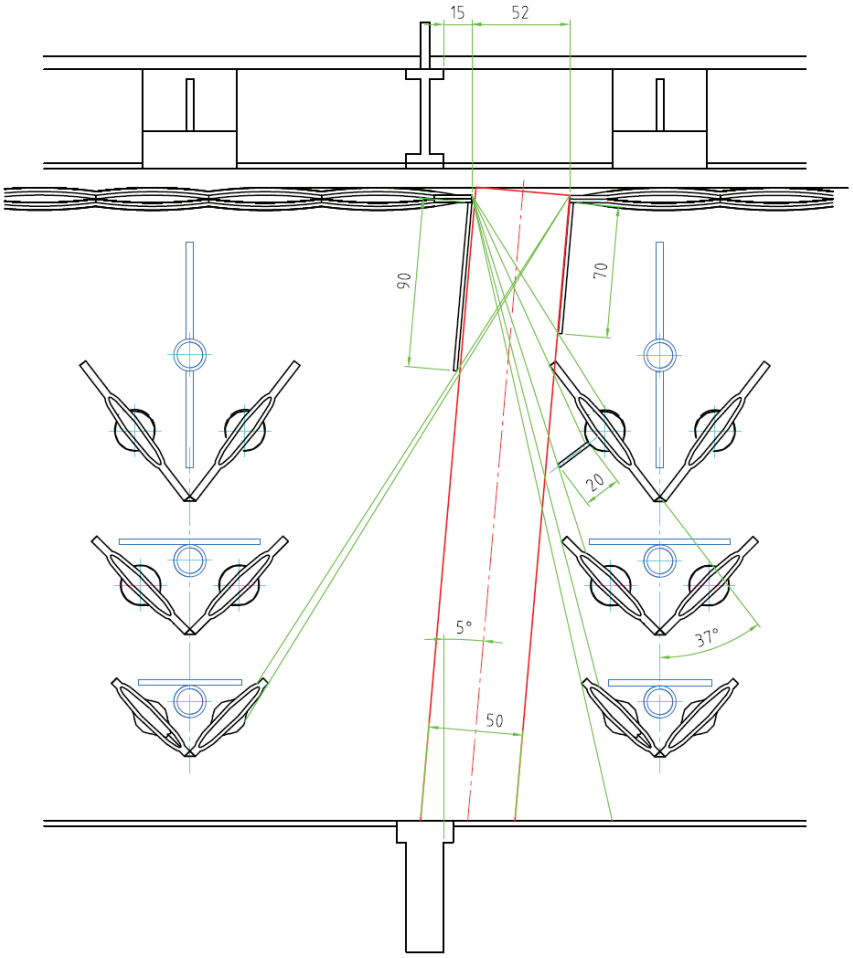

Fig. 2: Drawing of the conceptual design for the openings in the shielding backwall to achieve the diagnostic openings required for MITICA and for the additional shielding needed to avoid any direct thermal radiation on the cryopanels.

FEM analyses of all scenarios

Due to the size of the pump and the demanding temperature range of the pump components during the different operation scenarios, extensive FEM analyses are needed to check all the individual components, sub arrangements and the whole pump. The thermal loads have to be determined considering that the pump parts are at different temperatures (4 K, 80 K, 300 K or 470 K). Fig. 3 shows a typical result of FEM analyses concerning the estimated deformation of the radiation back wall when it is cooled down from 300 K to 80 K.

These analyses have to accompany the design process continuously, this means that almost every design step has to be checked and the result is often leading to an iterative redesign and optimisation of the related component [5].

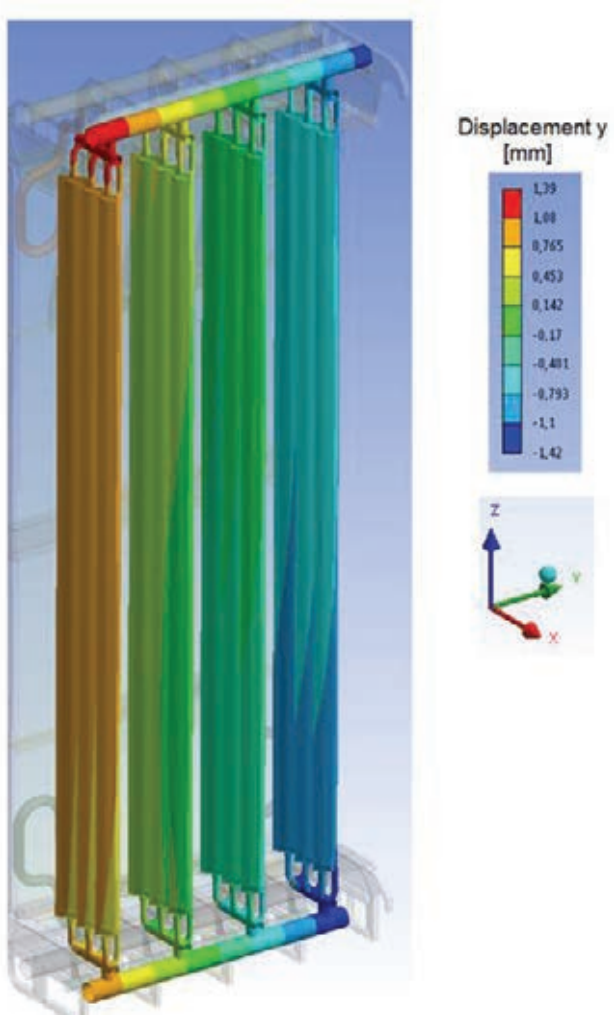

Fig. 3: Example for FEM analyses: movement of the front shielding panels when cooled down from 300 K to 80 K during pump operation.

Assembly and manufacturability studies

To deliver a BtP design ready for manufacturing, it must be accompanied by design supporting investigations. Therefore, in parallel to the design process, the question of how to assemble all these components and subassemblies has to be answered. Consequently, a major step was the development of a detailed assembly procedure and investigations on several manufacturing details to guarantee that the manufacturing of the entire pump is possible at all. One detail of many others that needed deep investigations and discussions was the

manufacturing of the cryopanels. Assuming the enormous heat loads to be handled by the 4 K circuit, an investigation of the expected panel temperature showed a potentially critical value. To improve the design and to reduce the panel temperature, a Cu plating of an adapted stainless steel structure was implemented to increase the thermal conductivity. This problem was addressed within the NIPEE EFDA Goal Oriented Training Programme on Negative Ion Physics and Engineering Expertise, and is described in a separate chapter in this annual report.

NBI cryopump safety analysis

Calculations have been performed in order to assess the minimum number and size of the safety components (relief valve, burst disk) and the maximal acceptable heat flux to the NB cryopumps in case of an accidental situation due to loss of vacuum (air or water ingress). A loss of vacuum is leading to an excessive heat load, and the pressure inside the helium circuit is increasing. Then, when the helium is released above a certain pressure, flow and pressure gradients occur in the cryopump circuits, given by the thermohydraulic characteristics of the circuits [6, 7]. As the direct calculation of this safety case is too complex and can therefore not be done in a reliable way, a reverse approach has been taken, namely to start from the design pressure of the circuit and to derive the maximum mass flow which can be released by the devices in such a way that the peak pressure is still below the design pressure. The maximum mass flow can then be converted to a heat load and this can be compared with the ITER values.

By this method, it could be demonstrated that the chosen pipe diameters in the NB cryopump design satisfy the requirements. Furthermore, the heat loads (1.7 W/cm² of the thermal shield circuit and 4 W/cm² for the effective cryopanel circuit) were found to be acceptable.

Conclusions and future work

The design evolution of the ITER HNB cryopump has seen much progress and is very close to the final stage [8]. When this will be achieved, the final BtP design will be adapted to the needs of the MITICA test bed on site of Consorzio RFX, Italy. The pump for this test bed will be the first NB pump to be manufactured and the test bed operation also serves the purpose to confirm and validate the design for ITER.

The remaining scope of GRT-303 includes the following activities to be performed in 2012:

- Final 3D design of all 16 modules.
- Preparation of 2D drawings.
- Finalization of ongoing FEM analyses of the whole pump for all scenarios including seismic events.
- Mechanical analyses of the load case caused by ice formation from a water leak.
- Improvement of the manufacturing and assembly plans.
- Adaptation of the finalized HNB design for MITICA.

Staff:

Chr. Day
A. Demsoreanu
St. Hanke
X. Luo
S. Ochoa
M. Scannapiego
R. Simon
H. Strobel

Literature:

[1] P. Sonato et al., The ITER neutral beam facility in Padua, Italy, Proc. 23rd IAEA Fusion Energy Conf., Daejeon, Korea, Oct. 2010

[2] A. Masiello et al., The European contributions to the developments of the ITER NB injector, Fusion, Fusion Engineering and Design 86 (2011) 860-863.

[3] St. Hanke, Chr. Day, X. Luo, P. Sonato, Status of the cryosorption pumping system for the neutral beam test facility MITICA, Ann. Congr. of the Italian Vacuum Society, Padova, Italy, May 2011.

[4] St. Hanke, M. Scannapiego, X. Luo, Chr. Day, F. Fellin, P. Zaccaria, The large cryopump system for the heating neutral beam injection of ITER, 58th Int. Symp. of the American Vacuum Society, Nashville, TN, USA, Nov. 2011.

[5] Chr. Day, Th. Giegerich, St. Hanke, V. Hauer, R. Lässer, St. Papastergiou, Design development of the cryopumping systems of ITER in view of future DT fusion devices, ISFNT 2011, Portland, OR, USA, Sept. 2011.

[6] M. Scannapiego, Chr. Day, St. Hanke, V. Hauer, Thermohydraulic investigation of the ITER neutral beam injector cryopump, in: M. Chorowski (Ed.): Proc. Int. Cryogenic Engng. Conf., Wroclaw, Poland, 2011, pp. 827-832.

[7] M. Scannapiego et al., Thermohydraulic investigation on the operation of the ITER torus and neutral beam cryopumps, 26th SOFT, Porto, Portugal, Sept. 2010.

[8] Chr. Day et al., Design progress for the ITER torus and neutral beam cryopumps, Fusion Engineering and Design 86 (2011) 2188-2191.

Acknowledgement

This work was supported by Fusion for Energy under the grant contracts No. F4E-2009-GRT-032-PMS-H.CD and F4E-GRT-303 (PMS-H.CD) with collaboration by RFX, Italy; CNRS, France; IPP, Germany and CCFE, United Kingdom. The views and opinions expressed herein reflect only the author's views. Fusion for Energy is not liable for any use that may be made of the information contained therein.

Development of the Cryogenic Plant of PRIMA (F4E-GRT-306 (PMS-H.CD))

Background and objectives

KIT is charged with the development of the cryopumps for the ITER Heating Neutral Beam Injector (HNB) and for the PRIMA/MITICA test bed which is currently being built at Consorzio RFX, Padova, Italy. MITICA is an ITER facility in which the performance of a full 1:1 scale HNB will be tested. Contrary to the cryopumps, which will be very much identical in ITER and MITICA, the cryoplants to supply the pumps can obviously be different. For ITER, the cryopumps are only a small client among many others, whereas in MITICA, the only purpose of the cryoplant is to supply the cryopump. The design of the cryoplant has therefore to match closely the cryopump requirements. Hence, KIT was contracted to support RFX with the cryoplant specification.

Assessment of the required flows for the HNB cryopump operation

According to the heat load to the HNB cryopump and the required inlet and outlet temperatures, the required mass flows during steady-state pulse and stand-by modes have been calculated. During these steady-state phases the cryopanels of the cryopump are supplied with supercritical helium at about 4.5 K and the thermal shield system with gaseous helium at 80 K. The most demanding operation regarding the cryogenic power and the complexity of the operation is the regeneration of the cryopanels at 100 K, which has to be performed in only 3 hours in some cases. The 100 K regeneration is divided in three phases: the warm-up, the exhaust phase at 100 K, and the cool-down to 4.5 K. During the cool-down phase, the HNB cryopanels are supplied with supercritical helium at about 4.5 K. Then a large quantity of this “cold” helium is warmed up and has to be re-liquefied, which is consuming a lot of cryogenic power. The required mass flows during the transient warm-up and cool-down phases have been estimated using a simplified approach, in order to assess the required cryogenic power of the cryoplant. The final numbers to be included in the cryoplant Technical Specification are currently under negotiation.

Depending on the different pump operation modes the found values can be used as a starting point for the detailed overall design of the cryoplant. The final design including all the vessels und transfer lines will be included in the scope of the supplier.

Conceptual design for the cryogenic plant of PRIMA

The necessary cryogenic infrastructure was developed on the basis of the experience collected during the different test campaigns with the ITER model pump at TIMO [1]. The conceptual design is illustrated in Fig. 1.

Following a verification of the technical feasibility of this cryoplant concept by RFX and a check of the spatial situation on site, a draft technical specification was prepared and discussed with F4E. Finally, after some loops of iteration a final draft was agreed.

Outlook

This grant has been closed with the end of 2011. F4E and RFX are discussing the best way for how to go ahead with the call for tender procedure. Most probably, there will be an initial phase with technical discussions with the industry prior to the official start of the tender procedure in 2012. It is planned that KIT will be further involved in this development.

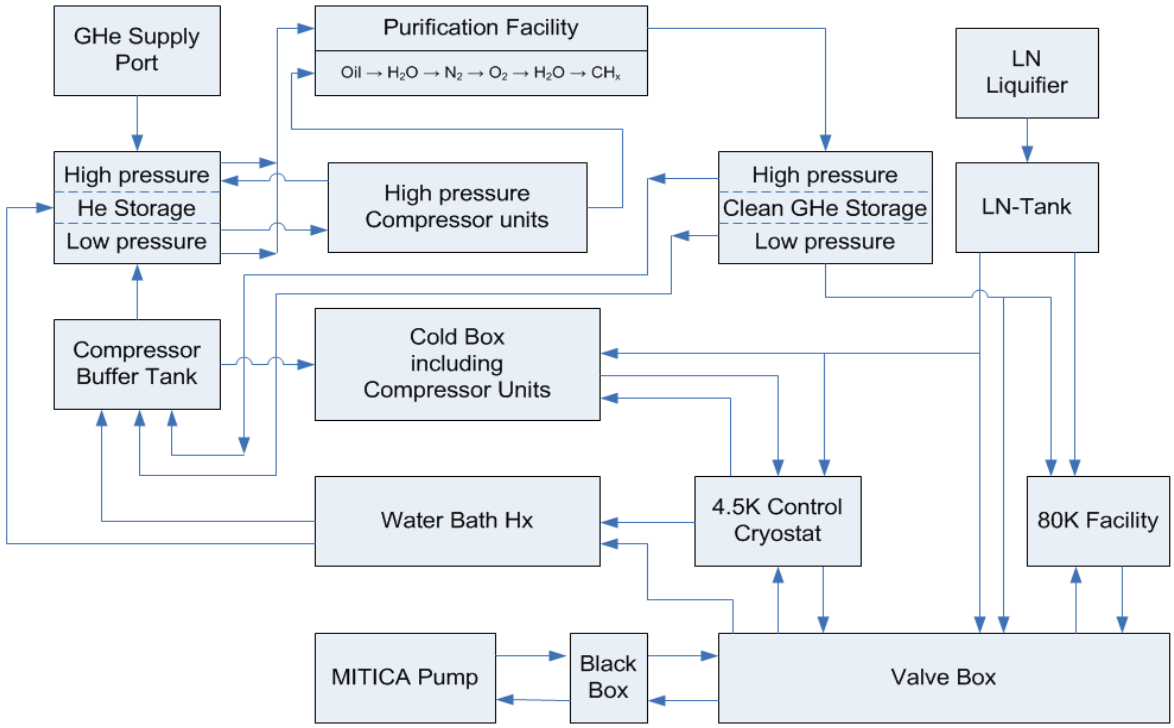

Fig. 1: KIT concept for the cryogenic infrastructure of PRIMA. It gives an overview of the components which are necessary for the successful operation of the MITICA pump under ITER relevant conditions.

Staff:

A. Demsoreanu
H. Haas
St. Hanke
R. Müller
M. Scannapiego

Literature:

[1] H. Haas, Chr. Day, F. Herzog, TIMO-2 – a cryogenic test bed for the ITER cryosorption pumps, Cryogen. Engng. Conf., Spokane, W, USA, June 2011.

Acknowledgement

This work was supported by Fusion for Energy under the grant contract No. F4E-GRT-306 (PMS-H.CD) with collaboration by RFX, Italy. The views and opinions expressed herein reflect only the author's views. Fusion for Energy is not liable for any use that may be made of the information contained therein.

Integration of Particle Control in ITER Plasma Scenario Simulations: Modelling of ITER Gas Fuelling Systems (WP11-HCD-01-05-03-01)

Background and objectives

The gas injection system (GIS) of ITER is a system used for the normal fuelling of the machine in the ignition phase, for wall conditioning, for radiative seeding and for rapid and precise injection of impurities for the fusion power shutdown [1]. The GIS consists of two main branches namely the system in the upper port region of the torus and a system in the lower port region of the divertor. These systems are capable of controlling the injection rate of gases, such as D_2, H_2, N_2, Ne, He or Ar, which are needed to be routed from the tritium plant through various piping networks, which consist of channels with different lengths and cross section. As a result, information on the gas flow dynamics is of vital importance for the design and optimization of the above system and subsequently for the performance and efficiency of the fusion reactor especially during the discharge phase. The objective of this EFDA task was to analyse the dynamics of the gases flowing through the GIS pipework.

ITER GIS system description

As first step a good understanding of the piping system had to be developed in order to do an appropriate modelling. In brief, the individual sub-systems of the GIS are required to provide the following functions:

- Provide hydrogen isotopes, He and impurity gas input to the vacuum vessel for plasma initiation, maintenance and control and for wall conditioning;
- Supply H_2 and D_2 gases to the heating and diagnostics Neutral Beam injectors;
- Provide a safety important emergency shutdown system (Fusion Power Shutdown System FPSS);
- Provide the pellet forming and propellant gases for the pellet injection system.

The gas supply and distribution system supplies gases from the tritium plant and distributes them to the various gas supply boxes and incorporates a common pumping and flushing line. The supply line is routed from the tritium plant to the upper vault where it intersects a distribution ring manifold which encircles the bio-shield. Circumferentially of this ring manifold (Fig. 1-left) are the local distribution manifolds which route the gas supplies to each valve box. Each of these valve boxes is charged with a gas pressure of 0.1 MPa. The routing of these local manifolds is through the vertical pipe shafts to the valve boxes located at the various levels. The fuel delivery line design conditions are the same for most of the individual sub systems, where a 10 mm diameter cylindrical pipe with length limited to 20 m is installed.

In order to provide the flexibility for physics operations (e.g. between minimum neutral density in the main chamber and a strong plasma flow in the scrape-off layer gas injection is provided at two poloidal elevations. These are the top port GIS, for fuelling at the top of the plasma chamber, and the divertor GIS, for fuelling at the divertor chamber. To minimise erosion of the first wall and the generation of high local peak heat fluxes at the top port injection point, the gas has to be injected uniformly. To achieve this, the gas is injected at five discrete toroidal locations behind the blanket and the gaps between adjacent blanket modules used to promote poloidal spreading of the injected gas (Fig 1-right). The system allows the injection of any combination of hydrogenic (H_2, D_2, T_2 depending on the type of discharge) and impurity gas species simultaneously.

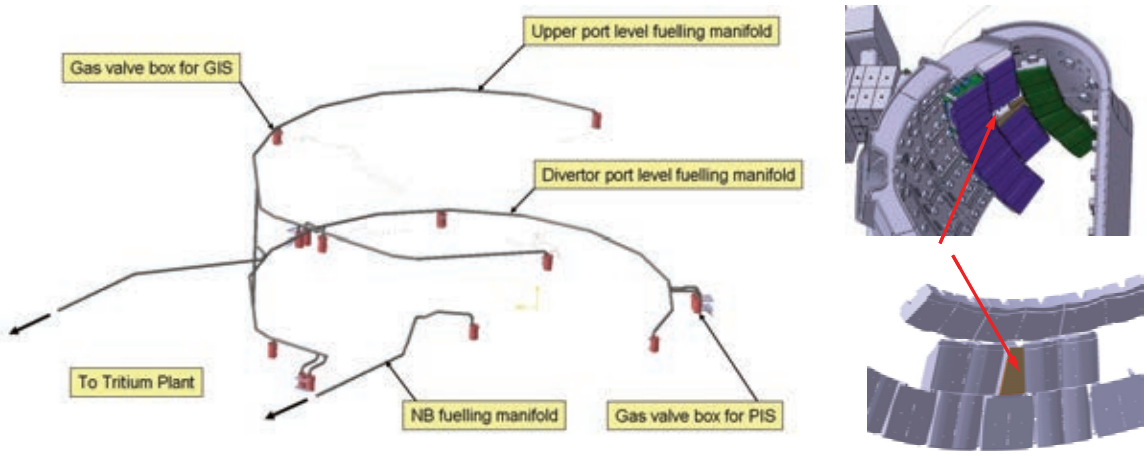

Fig. 1: Gas fuel manifold layout (left) and typical injection points (right).

The top port GIS consists of four valve boxes uniformly distributed around the biological shield. The valve boxes are cylindrical in shape, shrouded in a magnetic shield and mounted on a support platform. The typical distance between the torus and the valve boxes is around 17 m. The exposed connections, between the supply lines and the valve box, are made using demountable metal sealed connections. The gas injection delivery line is assembled in a similar manner.

The divertor GIS system consists of six valve boxes evenly distributed around the machine at the divertor pit level. The configuration of these valve boxes is identical to the top port GIS valve boxes with the exception that the magnet shielding is thicker to accommodate the higher magnetic field in this location. The gas delivery line is routed from the valve box in a secondary confinement line to the divertor port where it is routed through the fixed portion of the port secondary to the vacuum vessel flange where it passes through the fixed portion of this flange, below the cryopump, under the divertor to end at the divertor chamber.

Performance requirements

For a typical DT fuelling scenario a maximum combined DT fuelling rate of 400 (Pa m³)/s will be provided for at least 50 s for start-up and density ramp-up and between 50 (Pa m³)/s and 200 (Pa m³)/s used for the remainder of the pulse depending on the plasma operating conditions. During flat top, the fuelling will be modulated up to 400 (Pa m³)/s in 10 second bursts for density/fusion power control. The maximum fuelling rate provided for pure tritium, under all operating scenarios, will be 110 (Pa m³)/s.

Three impurity gases, normally He, N_2, Ne or Ar, are provided for irradiative cooling of the divertor and/or plasma experiments. The impurity gas delivery system provides a maximum fuelling rate of 100 (Pa m³)/s, with an average value of 10 (Pa m³)/s required during plasma operation, impurity gases such as N_2, Ne and Ar.

Within this present task, it has to be demonstrated that the GIS is able to provide a response time to 63% at 20 (Pa m³)/s for H_2, D_2, T_2 and He species in < 1 second [1].

Numerical modeling

In the above framework, numerical calculations, which include the transient behaviour of gas flow through long tubes for various gases, flow conditions and geometrical parameters, were performed, using the commercial package ANSYS-CFX (see Fig. 2). The fully transient, turbulent flow described by the well-known Navier-Stokes equations, subject to non-slip boundary conditions, were solved in an iterative manner. The numerical results of pressure and mass flow rate evolution and the lag time, have been compared with the corresponding ex-

perimental results obtained by the experimental facility in SWIP-China [2], who is the ITER Domestic Agency responsible for the GIS package. In general, it is seen that the numerical calculations seem to predict with acceptable accuracy (Fig. 3) the corresponding experimental data.

Fig. 2: Piping scheme of the gas injection system.

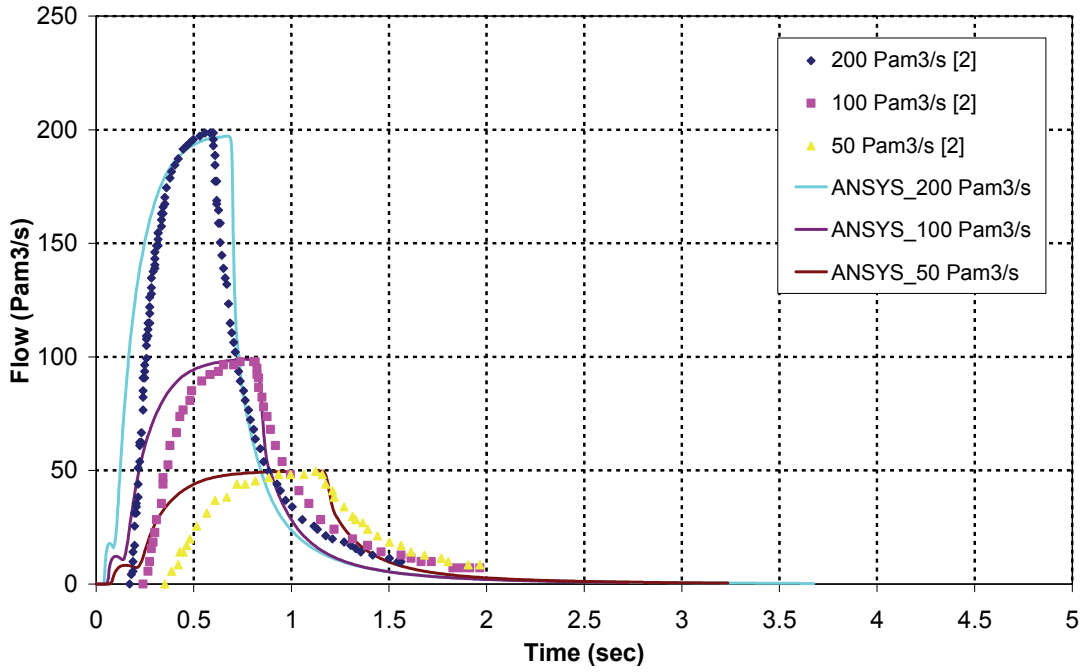

Fig. 3: Comparison between ANSYS-CFX results and experimental results [2] for various injected throughputs of Ar. The upstream pressure is p=0.1 MPa, the tube length is L=20 m and the tube radius is R= 5 mm.

Another study that was performed supported the design of the upstream tank (see Fig. 2). By a parametric analysis, it could be shown how the time needed to inject the specified gas amount into the torus chamber is related to the upstream pressure and volume of the supply tank, see Figure 4. It was found that for high initial pressures of the upstream tank the time needed for its complete evacuation is significantly lower. As a result, since for the ITER FPSS the time is a vital performance parameter, high pressure puffing (30 bar) will be implemented at ITER.

Conclusions

It was successfully demonstrated that numerical models of the Gas Injection System of ITER can be developed that are suitable for benchmarking with corresponding experimental results and provide results to justify design decisions. The design of ITER GIS is still an open issue and a lot of research is under way. As a result, numerical models like the ones described in the present report can play a significant role during the optimisation phase.

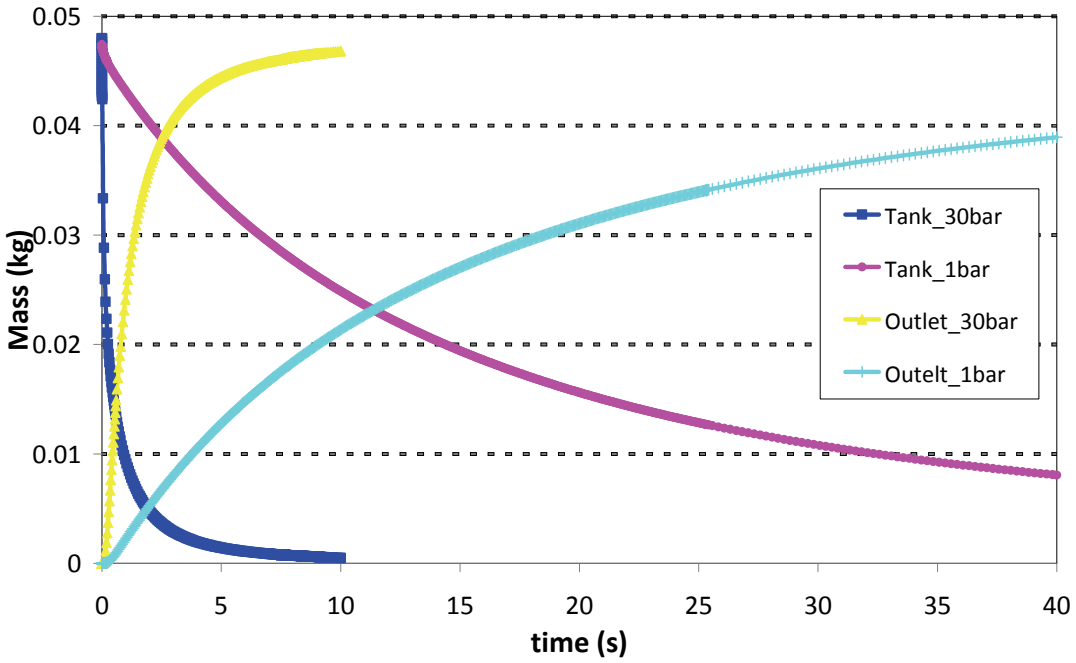

Fig. 4: Time evolution of total mass of Ar inside the upstream tank and the amount of gas injected in the vacuum vessel (outlet) for the cases with initial tank pressure 30 bar and 1 bar. The tube length and radius are L=25 m and R=5 mm respectively.

Staff:

Chr. Day
X. Luo
S. Ochoa
S. Varoutis

Literature:

[1] S. Maruyama et al., ITER fuelling system design and challenges, Proc. 23rd IAEA Fusion Energy Conference, Daejaeon, Korea, Oct. 2010.

[2] Z. Jian-er, W. Ming-xu, R. Hong, Z. Gui-qing, L. Bo, L. Wei, Gas Fuelling System and Glow Discharge System Design, ITA 18-02 Task, Final Report, Chengdu, China, 2008.

Acknowledgement

This work, supported by the European Community under the contract of Association between EURATOM and Karlsruhe Institute of Technology, was carried out within the framework of the European Fusion Development Agreement. The views and opinions expressed herein do not necessarily reflect those of the European Commission.

Design Assessment and Development Needs of Fuelling and Pumping Systems for DEMO (WP11-DAS-HCD-FP-01 and -02)

Background

The fuelling and pumping systems of a fusion device are the pacemaker of all torus and plasma operation under nominal and off-normal conditions. The technology for ITER is very much customized and a direct scale-up towards the power plant level is problematic. In 2011, a review assignment task was launched under the EFDA Power Plant Physics & Technology Work Programme on the technological maturity and development needs of fuelling and pumping systems for DEMO. For this reason, two DEMO options were studied, an early and conservative DEMO 1, which is incorporating as much as possible existing and scaled-up technology from ITER, and a DEMO 2, which is based on challenging plasma physics and full steady-state operation. On top of the technology assessment, recommendations for further R&D needs have also been developed.

KIT was in charge to co-ordinate this review. The fuelling part was elaborated by CCFE with some expert input from KIT, whereas the pumping part was mainly provided by KIT with some expert input from the Hellenic Association.

Fuelling systems

Fuelling systems comprise in general gas injection for plasma density control, for supply to neutral beams and diagnostic neutral beams, for injecting impurity gases into the divertor to provide radiative cooling, and for wall conditioning. Pellet injection is used for plasma density control, for ELM control, for enhanced edge radiative cooling and finally for better coupling of the RF injectors with the plasma. Specialized systems comprise injecting impurity gases to mitigate disruptions and for emergency power shutdown. All these functionalities were carefully analysed as they impact on the fuelling throughput and therefore on the pumping system.

Fuelling in ITER relies on pellets at relatively low velocities, injected from the high field side, and on the ∇B-drift to increase core fuelling efficiency. The design of ITER does not allow high speed pellet injection, which is under debate for a power plant. As result to the performed study, it was re-confirmed that the fuelling of DEMO will require a step change compared to existing tokamaks, neither the technology nor the physics can be regarded as mature. Most models predict a very low efficiency of gas puffing inside the separatrix. Hence, gas injection fuelling is not considered to be a candidate for DEMO.

As potential fuelling technologies we have considered pellets, supersonic gas injection, compact toroid (CT) injection and unmagnetized plasma injection.

Pellets will have high fuelling efficiency, but cannot create centrally a peaked density profile in a full-scale reactor. Unfortunately, there are no experimental data on purely pellet-fuelled high density plasmas in a metal-wall (low outgassing) tokamak. This is an important issue which must be addressed to provide a better base for any decision on the next step development.

Compact toroid fuelling has been demonstrated on small tokamaks. The behaviour of a CT when approaching and entering a large tokamak is not well understood. An existing CT generator could be equipped with a flight tube and simulated tokamak stray field.

Pumping systems

A suitable pumping system for a fusion power plant also has to include an embedded control function for gas throughputs (fuel gas and He ash recycle flows) to assist the plasma control

system and has to be compatible to the disruption mitigation techniques used at the power device (today still unknown). An additional functionality which will be asked from the torus exhaust pumping system (or an additional, dedicated pumping system) is to provide improved density control to achieve above Greenwald conditions for the specific magnetic configuration the power plant device will have (divertor concept, plasma shape etc.) [1].

Concerning pumping systems, cryosorption pumping at 5 K is the reference primary pumping concept for ITER. Expertise in the design of customized cryopumps is available, and any DEMO 1 requirements for more pumping speed is more or less a question of giving more cross-section to pump out.

The situation is more critical for the backing pumps, because tritium-compatible mechanical pumping is still an issue. Dedicated R&D had been started in Europe to develop a tritium-compatible screw or roots pump, but the programme was stopped because the ITER fore-pumping procurement package was given to US. Hence, ITER is now using a customized cryogenic forevacuum compressor (JET-style) - which is clearly not an option for a fusion power plant – and combines this with a dry piston pump, which needs further development to reduce the high maintenance requirements.

The lessons ITER will teach are useful for the areas of cryogenic pumping at 5 K and tritium plant systems. However, these two areas are just the ones expected to change for a power plant.

For primary pumping purposes of a DEMO 2, a viable alternative to the 5 K cryopump for burn operation with reduced operating costs and equivalent availability would be desirable. In view of the unacceptably high processing times and the build-up of large tritium inventories in case of a simple scale-up of the ITER fuel cycle towards DEMO, a rigid simplification is needed. To achieve this, the concept of direct internal recycling (DIR concept) [2] of the unburnt fuel fractions upstream of the torus vacuum pumps was elaborated, see Figure 1, thus resulting in significantly reduced throughputs for the tritium plant and vacuum pumping systems. The ultimate goal is to go from a batch-wise, cryogenic, non-separating vacuum pumping systems, as is the case for ITER, towards a continuous, non-cryogenic and separating (He from hydrogens) pumping system [3].

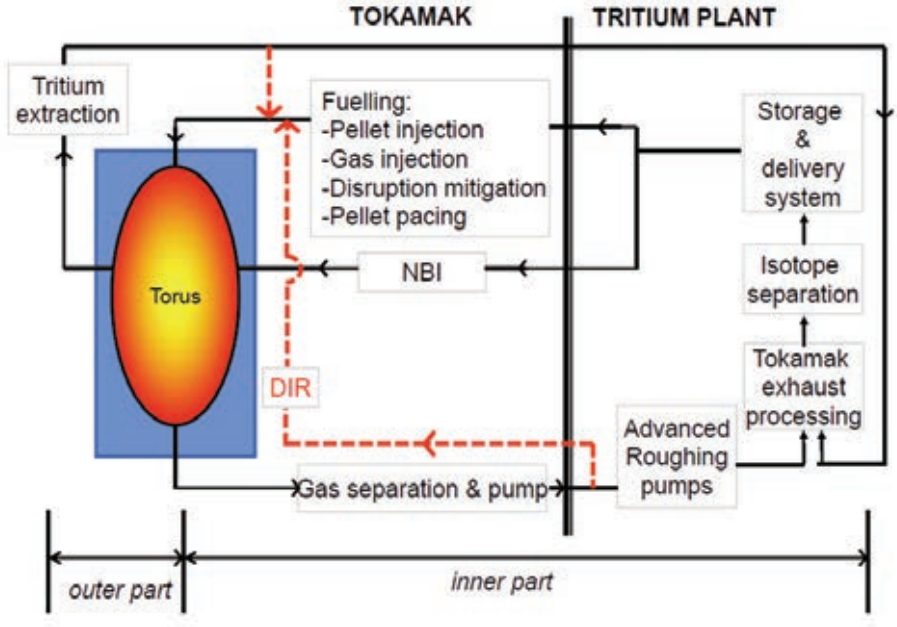

Fig. 1: Concept of Direct Internal Recycling (DIR) to simplify the fuel cycle of a fusion power plant.

As a first step in this direction, a theoretical approach was taken to assess all different pump types which are available on the market. A quantitative ranking scheme was elaborated, that gives the quality of a certain pumping solution. This was based on a pairwise comparison procedure based on 18 categories which classify aspects such as tritium compatibility, design simplicity, suitability for extrapolation, maintainability etc. In a second step, costs have been estimated to develop these pumps and/or to make these pumps tritium compatible. As a result of this process, two figures have been obtained (see Figure 2), one for the high vacuum (HV) pumps and one for roughing pumps, which plot the cost versus the calculated quality rating. The best solution can be found in these figures in the lower right corner, where R&D costs are low and the quality is high.

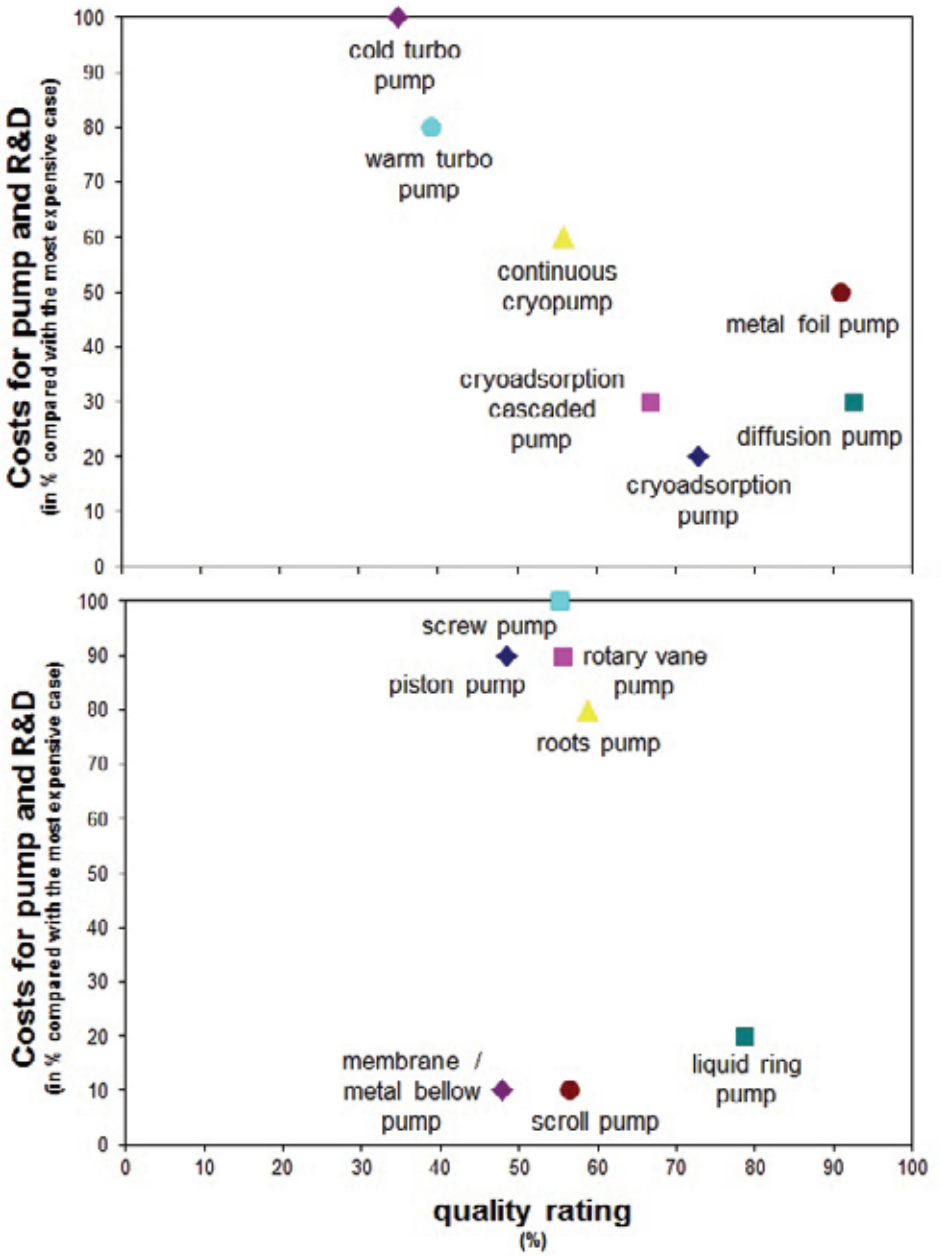

Fig. 2: Result of the technical-economic examination of different high vacuum pumps (top) and roughing pumps (bottom).

In a final step, SWOT tables were elaborated for the most promising pump types. From this result, a pumping train has been identified as a very promising solution that consists of a vapour diffusion pump as HV pump and a liquid ring pump as roughing pump, both with a working liquid that was replaced from water or oil to a liquid metal (for tritium reasons). For the

separation of the exhaust gas close to the divertor, a metal foil based pump is considered to be a promising candidate.

This novel pumping system configuration is considered to offer significant advantages over the ITER solution or any scale-up version thereof and is most promising to work successfully, but asks for experimental demonstration [4]. KIT is therefore currently conceptuating the test facility THESEUS (see the report on the work done under the VACU-TEC GOT) and first proof-of-principle tests are planned to be performed under the EFDA Power Plant Physics and Technology Programme 2012.

Conclusions

The assessment of the fuelling and pumping systems has clearly shown that a simple extrapolation of the ITER systems to a DEMO device would be not a good choice. Possible solutions with new technology have been identified and a R&D programme for their development was proposed.

Staff:

Chr. Day
Th. Giegerich
St. Varoutis
M. Kovari (CCFE, UK)
D. Valougeorgis (University of Thessaly, Volos, Greece)

Literature:

[1] Chr. Day, R. Wolf, An integrated view on high density plasma operation and fuel cycle, Int. Workshop on MFE roadmapping in the ITER era, Princeton, NJ, USA, Sept. 2011.

[2] Chr. Day, I. Cristescu, B. Pégourié, B. Weyssow, Considerations towards the fuel cycle of a steady-state fusion device, IAEA Fusion Energy Conference, Daejon, Korea, Oct. 2010.

[3] Th. Giegerich, Chr. Day, V. Hauer, Development of a tritium compatible vapor diffusion pump for a commercial fusion power plant, ISFNT-10, Portland, OR, USA, Sept. 2011.

[4] Chr. Day, Th. Giegerich, St. Hanke, V. Hauer, R. Lässer, St. Papastergiou, Design development of the cryopumping systems of ITER in view of future DT fusion devices, ISFNT-10, Portland, OR, USA, Sept. 2011.

Acknowledgement

This work, supported by the European Communities under the contract of Association between EURATOM and Karlsruhe Institute of Technology, was carried out within the framework of the European Fusion Development Agreement. The views and opinions expressed herein do not necessarily reflect those of the European Commission.

Revision of the JT-60SA Research Plan – Chapter 9: Fusion Engineering (WP11-JTA-RWP)

Background

The research objectives and strategy of the JT-60SA experiment are described in the "JT-60SA Research Plan", and the most recent version v2.1 was issued end February 2011. This version of the JT-60SA Research Plan outlines the scientific objectives and operation strategy of the JT-60SA tokamak in the views of the JAEA Home Team and the collaborators from several Japanese Universities. It contains a detailed description of the foreseen research phases, with a tentative planning covering 20 years of operation, describes the various operational regimes of the machine, and treats different subjects in separate chapters.

In a Broader Approach management meeting was agreed that the next version of the Research Plan should be issued as a common document between EU and Japan. In order to organize this, each chapter was given to a responsible EU officer for review and amendment. In this task, KIT was charged to work on the chapter on fusion engineering.

The role of JT-60SA in fusion research

The target of JT-60SA is to contribute to early realization of fusion energy by two missions.

Support of ITER exploitation

Support of the exploitation of ITER is the first main mission of JT-60SA. This is based on a favorable phasing between the operation planning of the two machines. A part of the results expected makes use of unique JT-60SA capabilities and can be classified as a confirmation or consolidation of the ITER physics and operation basis (demonstration of an ITER Q=10 equivalent discharge, study of the operational boundaries, confirmation of the transport and L-H transition scaling laws, study of pedestal structure and ELMs, etc.). Other studies will be certainly useful, although they could also be carried out on other tokamaks. Most interesting is the versatile heating and current drive systems (positive NB, negative NB, off- and on-axis) allowing for burning plasma studies and the long pulse length, allowing the possibility of preparing a full ITER reference H-mode scenario.

Issues for DEMO

The second main mission of JT-60SA is the investigation of key physics and engineering issues for DEMO. The main plasma physics and operational issues on which JT-60SA could contribute to the DEMO design are identified in the JT-60SA Research Plan as: (i) understanding self-regulating plasma systems (since the burning plasma will be a physical system with a very high fraction of self-generated heating and current), (ii) demonstrate steady-state sustainment of the required integrated plasma performance, and (iii) extend operational boundaries (high beta, bootstrap and Greenwald fractions).

Fusion technology aspects

JT-60SA addresses a variety of fusion technology aspects. A series of component tests (structural inserts and diagnostics), e.g. ferromagnetic insert tests to study the ripple effects for breeding blankets, are foreseen right from the start of the machine. However, due to the fact that JT-60SA starts as carbon machine, the plasma facing components will be upgraded - to tungsten (divertor) and beryllium (first wall) - only at a later stage. The increasing neutron budget from D-D operation is planned to be exploited for instrument characterization.

In the amended version of the research plan, a new section on testing and validating peripheral technology, especially in the area of pumping and fuelling, see Table 1, has been added. JT-60SA will be the first plasma device with the capability to have a variable divertor pump-

ing speed, as ITER will also have (although with a different technology). This may give an additional way to control plasma detachment and studies on this influence are now being integrated in the detail planning of JT-60SA operation. Installation of the ITER rough pumps and/or a DEMO relevant rough pump train is also an option. The study of pellet injection under ITER relevant conditions (where most of the pellet is ablated in the edge and the material transport has to rely on the gradB drift only) is another important category which has been brought in by the EU working group.

Table 1: Additional research items defined in the Research Plan review and their relevance for ITER and/or DEMO.

Research items	**ITER and DEMO**	**ITER**	**DEMO**
A. Primary pumping Effect of spatial and speed variation on plasma *Utilizes existing hardware*	x		
B. Rough pumping *Includes test hardware (different for ITER and DEMO)*		x	x
C1. Pellet fuelling Assess performance for ITER and DEMO relevant conditions (consumption of the pellets in the edge) *Utilizes existing hardware*	x		
C2. Pellet fuelling *Includes ITER test hardware*		x	
D. Disruption mitigation by MGI Characterise *Own hardware to be developed*		x	

Conclusions

The revision of the chapter 9 of the JT-60SA Research Plan has been finalized and a new version of the whole document (v3) has been issued at the end of 2011. The discussions held between EU and Japan (Fig. 1) have been very open, fruitful and characterized by a collaborative attitude. A list of collaboration proposals to continue common work on specific issues has been elaborated and integrated in the draft of the EFDA Work Programme 2012.

Staff:

L. Boccaccini
Chr. Day
H. Haas
V. Hauer

Acknowledgement

This work, supported by the European Communities under the contract of Association between EURATOM and Karlsruhe Institute of Technology, was carried out within the framework of the European Fusion Development Agreement. The views and opinions expressed herein do not necessarily reflect those of the European Commission.

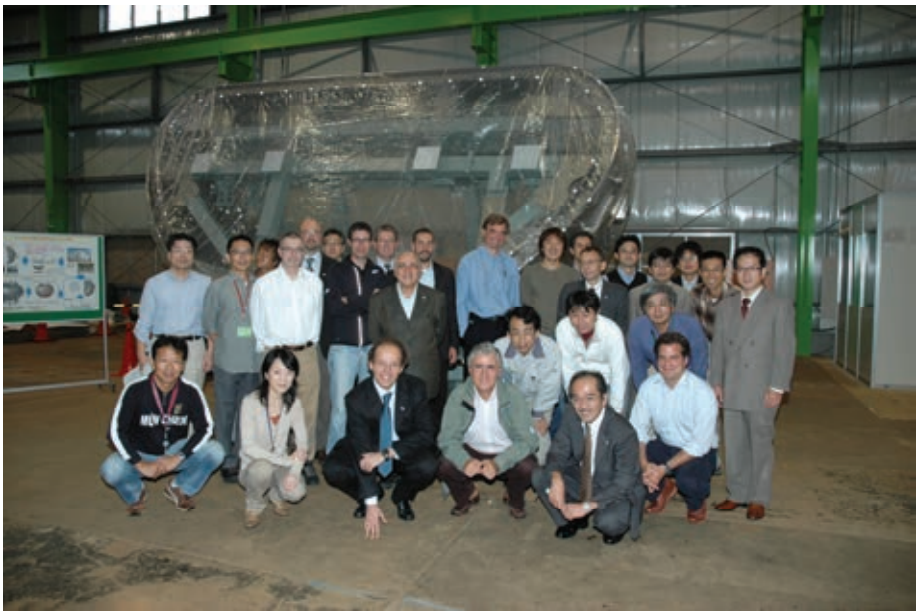

Fig. 1: The EU working group with their Japanese counterparts in front of the first segment of the JT-60SA vacuum vessel at Naka site on the occasion of the first Research Coordination Meeting, October 2011.

Goal Oriented Training Programme on Negative Ion Physics and Engineering Expertise (WP08-GOT-NIPEE (FU07-CT-2008-00043))

Background and objectives

The NIPEE programme is supporting the development of the PRIMA/MITICA neutral beam test facility which is currently being built at Consorzio RFX, Padova, Italy. This facility features a full 1:1 scale testing environment of the complete ITER Heating Neutral Beam (HNB). To provide training and experience in the design, specification and construction of high power Neutral Beam Injection systems and their integration with the test facility, six engineers receive expert training in the relevant aspects. The goal oriented training programme is coordinated by Consorzio RFX. KIT is hosting a trainee.

Within the NIPEE Programme the KIT trainee shall specifically contribute to the final design of the large cryopumping system of MITICA, but also gain general expertise in basic fusion and vacuum technology and understanding of Neutral Beam Systems. To build up experience in this wide field, the trainee was involved in different on-going cryopump projects.

Design support activities

Capture assessment of a pump configuration for MAST-Upgrade

UK's fusion energy experiment MAST (Fig. 1) is equipped with a special Super-X divertor for which a new open structure cryopump is under consideration. In preparation of a potential collaboration in the area of the divertor cryopumping systems, KIT was investigating the most promising geometry and position of the pumps in such a novel divertor environment (Fig. 2).

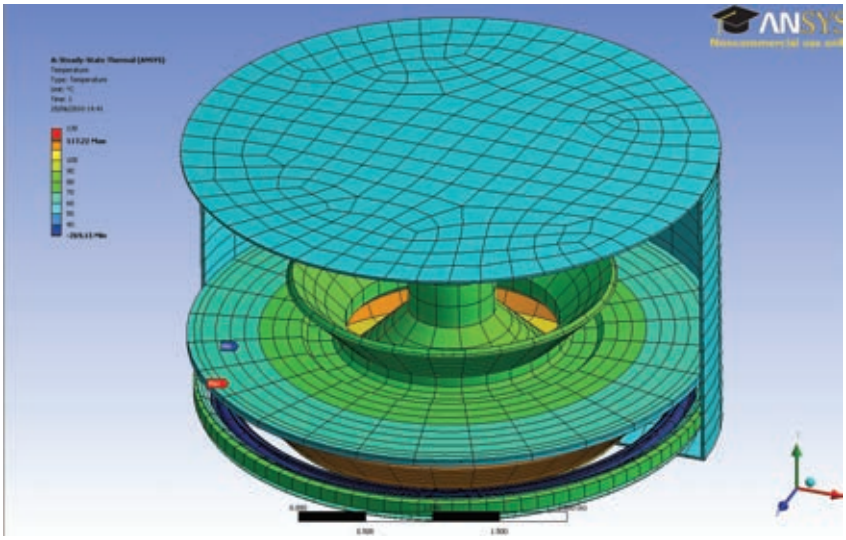

Fig.1: Open structure divertor cryopump.

For this investigation the capture coefficient of the different geometries was calculated using the 3D Monte Carlo Simulation MOVAK, see Fig. 3. The capture coefficient is defined as the ratio of pumped particles over incoming particles balanced at the reference inlet cross-section. These data, together with calculated heat loads, were used to select the optimal cross-section geometry of the pump. Additionally, the influence of the position of the pump in the divertor region on the pump performance was investigated.

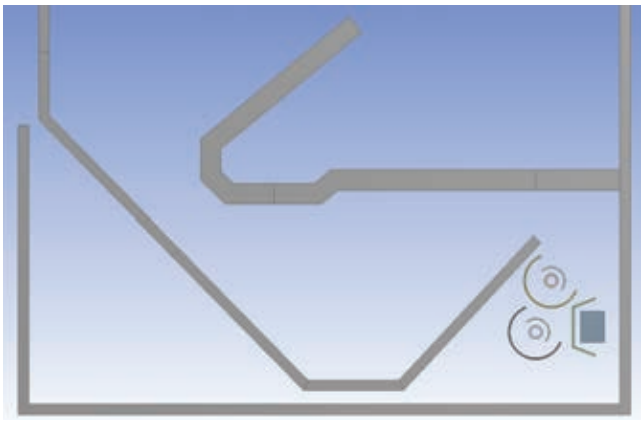

Fig. 2: 2D-Illustration of the divertor with a candidate cryopump configuration.

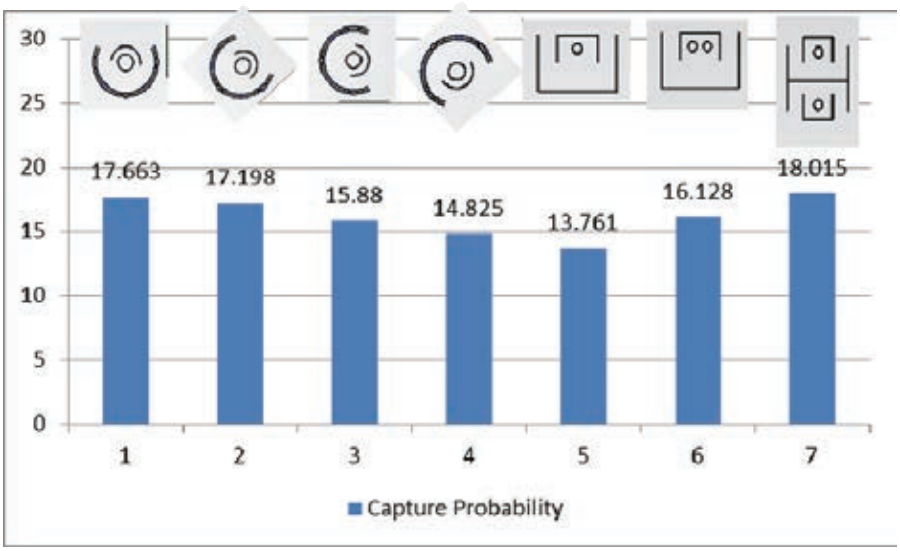

Fig. 3: Capture coefficient (in%) for different cross-sections of the cryopump.

Temperature of the HNB beamline vessel

On request by IO, the temperature of the outer wall of the HNB beamline vessel (BLV) was investigated. The motivation was the concern of potential ice formation due to frozen humidity on the outer BLV cooled down by the cryopump in operation or standby. Also, the heating of the BLV during the high temperature regeneration of the pump was an issue under investigation. For every scenario the corresponding internal conditions (temperature and pressure) - (1) nominal condition (pumping or stand by), (2) normal regeneration at 100 K with internal convection, (3) high temperature regeneration with internal convection - were combined with the worst case outer air temperature conditions. Fig. 4 shows a typical result regarding the temperature distribution on the outer BLV wall and the time dependent behaviour of this cool down until thermal equilibrium steady-state conditions are reached.

The achieved results showed clearly that no ice formation will occur. However, formation of liquid water is very likely and should be suppressed by air conditioning measures.

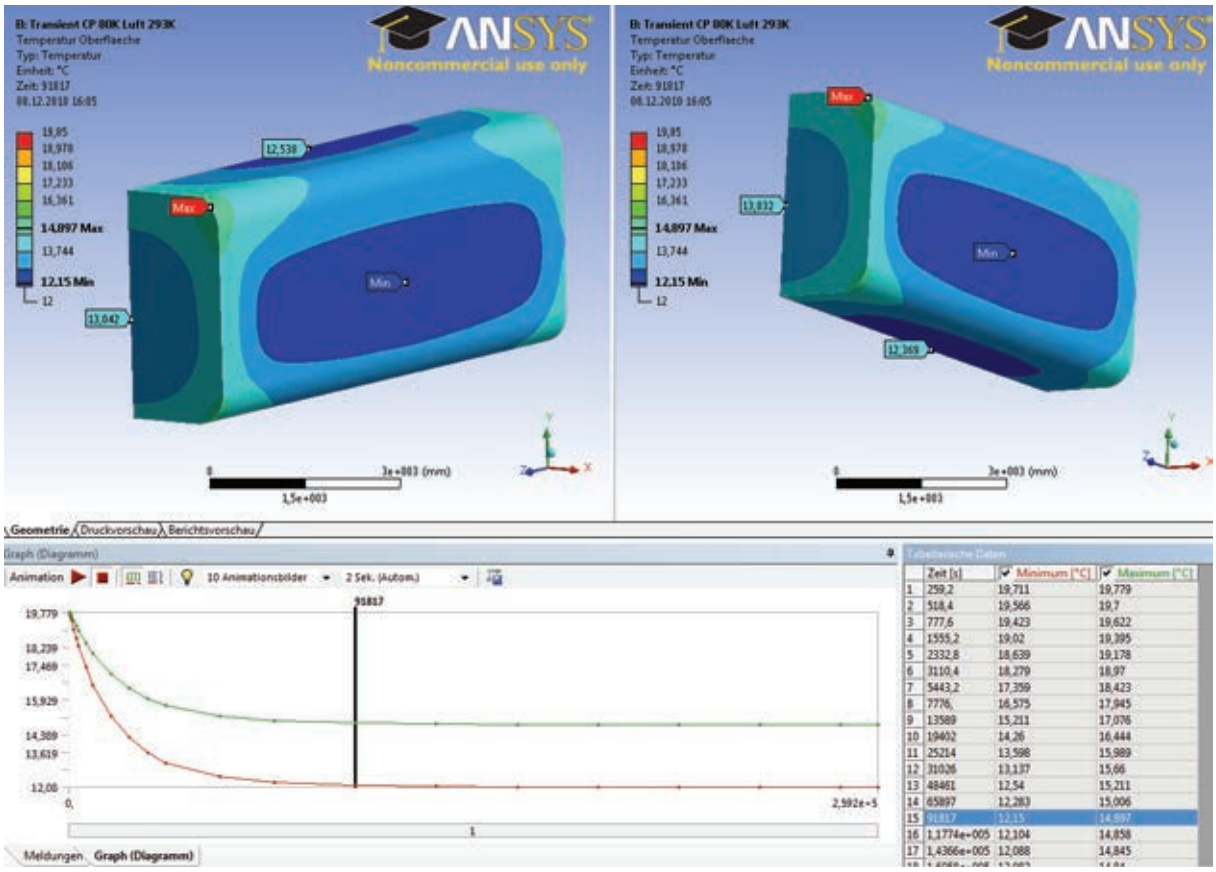

Fig. 4: Example of a result of the BLV temperature cooled down by the cold cryopump inside. On top the temperature distribution on the BLV, on bottom the development of the cool down in time to reach asymptotically the local maximum (green) and minimum (red) temperature values.

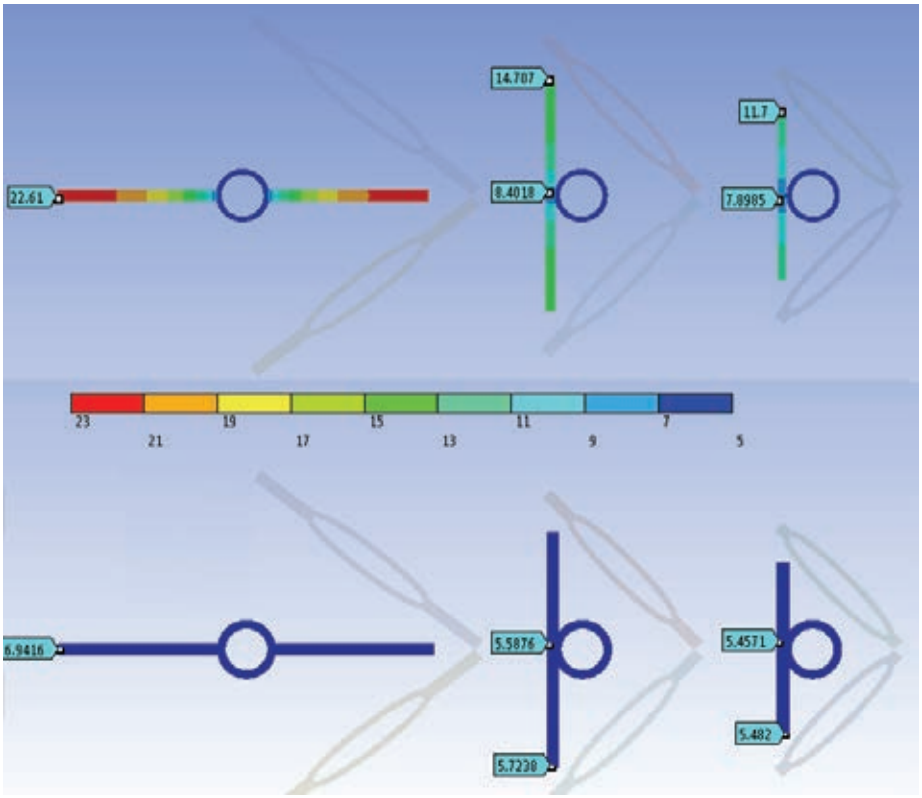

Fig. 5: Comparison of the calculated temperature distribution (in K) for the old cryopanel design (top) consisting of SS only and the improved design (bottom) consisting of thinner SS fins plated with 1 mm Cu all around.

Investigations on cryofin temperature in the HNB pump

The enormous heat loads to be handled by the HNB pump, especially the additional load onto the first 1.5 m caused by the energetic electrons emitted from the ion source, necessitated a thorough investigation on the resulting temperature of the cryopanels. Since the cryopanels consist of a SS pipe and an attached SS fin, the area coated with charcoal is cooled via passive thermal conduction only. The investigations lead to the result that the low thermal conductivity of the pure SS arrangement causes a critically high temperature of above 20 K. Consequently, the design was improved. The new concept still consists of an arrangement of SS pipe and fin but the fin is now reduced in thickness and after the connection between pipe and fin the arrangement is plated by Cu to increase the effective thermal conductivity drastically. Fig. 5 shows both, the pure SS version compared with the improved design which guarantees a proper cooling of the entire fin.

Calculation of the thermal radiation heat load on the cryogenic manifolds in the HNB pump

To optimize the pump design and to predict reliably the heat loads to be handled, the manifold areas in the pump (top and bottom region) have been investigated. To further reduce the heat load from warm components like the mounting structure onto the 4 K manifolds, an additional manifold shielding had to be developed. For this purpose, a submodel of the manifold region was integrated to ANSYS and an iterative calculation and design optimization was performed. Fig. 6 shows the resulting sandwich structure of the inner cooled Cu plates and a warm outer SS shell which was found to be the optimal solution.

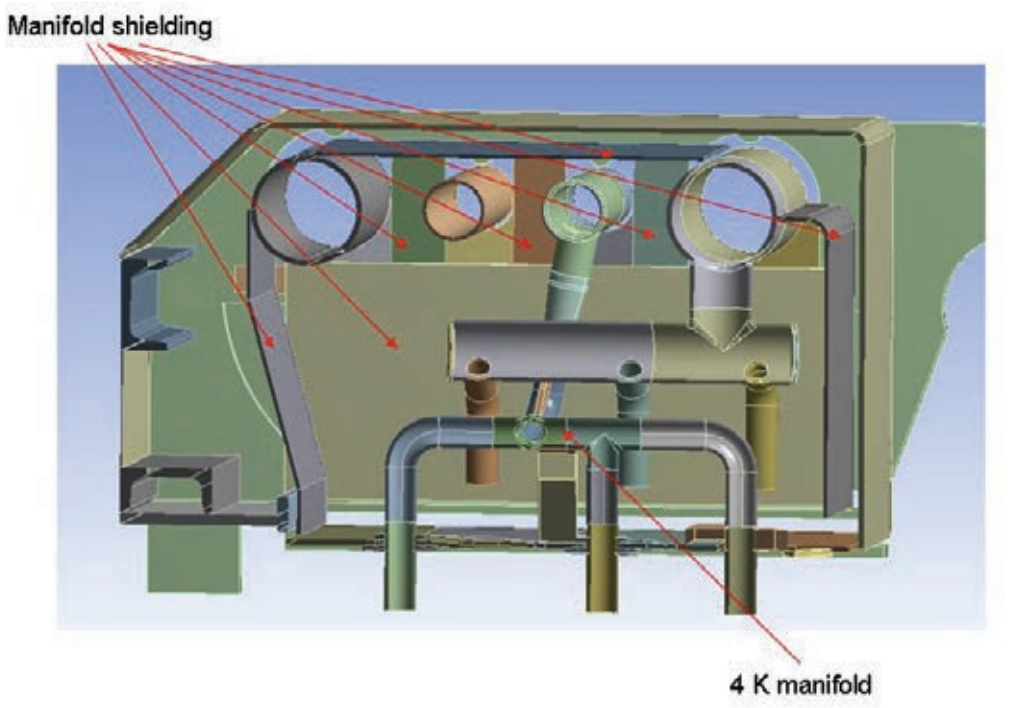

Fig. 6: Design of the manifold region with all shieldings after the optimization process.

Conclusions and future work

The EFDA Goal oriented training programme scheme demonstrated to be an excellent framework for young researchers to get a thorough education in fusion and be able to deliver own selfstanding work packages. The ongoing design work of the NBI cryopump has seen a real benefit by this support so that this scheme will be continued in the next year.

Staff:

Chr. Day
St. Hanke (mentor)
S. Ochoa (trainee)
H. Strobel
S. Varoutis

Acknowledgement

This work, supported by the European Communities under the contract of Association between EURATOM and Karlsruhe Institute of Technology, was carried out within the framework of the European Fusion Development Agreement. The views and opinions expressed herein do not necessarily reflect those of the European Commission.

Goal Oriented Training Programme on Vacuum Technologies and Pumping (WP10-GOT-VACU-TEC (FU07-CT-2010-00065))

Background and objectives

The aim of the VACU-TEC training programme is to prepare five scientists for activities to support the ITER project and the long-term fusion programme in Europe in the area of vacuum technologies and pumping.

The European procurement for ITER in the area of vacuum technologies and pumping systems covers activities for the supply of cryopumps for torus, cryostat, heating and diagnostics neutral beam systems as well as the supply of cold valve boxes, instrumentation and the R&D needed to finalize the design of these components. All these requested areas are fully covered in the VACU-TEC Goal oriented training programme (GOT) and each area is reflected by an individual work package (WP 1 to 5):

- *Cryogenic Engineering:* Cold turbo pump development (WP1 by CEA Grenoble)
- *Instrumentation:* Identification of total and high resolution partial pressure measurements for ITER leak detection (WP2 by KIT)
- *Leak Localization:* Development of remote devices for ITER in-vessel leak localization (WP3 by CEA Cadarache)
- *Mechanical Vacuum Engineering:* Mechanical design of large scale cryopumps for ITER and mechanical pumps (WP4 by KIT)
- *Physics:* Vacuum gas dynamics and flow modelling (WP5 by the Hellenic Association, Volos)

The training programme for all trainees follows the same generic scheme with four main elements:

1. *General education* by participation in introductory as well as specialized courses, lectures and seminars all along the first year of the project
2. *Practical education* by being involved in the group activities related to the corresponding training topic
3. *Secondments* to other partners of the training programme at various stages of the project as project introduction, improvement or conclusive training
4. *Participation in conferences, workshops* and *meetings*

KIT is co-ordinating this network which started in Nov 2010. However, the recruitment phase could only be concluded in July 2011.

VACU-TEC Work Package 2 (Instrumentation)

The main objective for Work Package 2 is to develop and characterize vacuum pressure instrumentation and to improve the ITER leak detection system as well as to study outgassing behaviour of materials which will be employed in the ITER vacuum systems. Additionally test vacuum chambers should be set up in the vacuum laboratory for benchmarking, calibration and outgassing measurements.

<u>Test rig for outgassing rate measurements</u>

A test facility for measuring outgassing rates is being set up, since outgassing plays an important role, especially if ultra-high vacuum conditions shall be reached. Hydrogen desorption from stainless steel is a common problem. For building large vacuum systems such as ITER, the outgassing rates of the materials should be strongly considered. Often, outgassing

rates of different materials have to be reduced by a pre-treatment like electro-polishing, baking or vacuum-firing. But the theory of outgassing is quite complicated and not yet fully understood. Also experimental results reported in the literature are often not consistent. This is why new experimental efforts are under way at KIT to provide a better understanding.

The two main methods to measure outgassing rates are the pressure-rise method and the throughput method. The new outgassing measurement apparatus, currently being built at KIT, uses the difference method (a modified throughput method). With this method, the pressure difference between two identical vacuum chambers, with one containing the sample and the other acting as a reference, is measured to achieve the outgassing rate of the sample. Like this, the outgassing of the vacuum chamber can be subtracted and also very low sample outgassing rates can be measured.

Another advantage of this concept is the lock system, with which simultaneous transfer of sample and reference is possible. Thus, there is no influence on the measurement if the outer conditions change with time. In addition there is an extra-heating for the sample that should be installed to improve the relation between sample and chamber outgassing. The size of the apparatus allows to measure samples with a surface of 250 cm^2. The measurements can be taken at room temperature and at 100 °C, in agreement with the requirements of the ITER Vacuum Handbook.

The flowchart of the facility is shown in Figure 1. The central part of the test facility consists of two identical vacuum chambers (Figure 1, 4+5) which are connected by a cross piece. The system is pumped down by two turbo molecular pumps (2) with membrane fore pumps (1), since dry pumps are needed to achieve sufficiently low pressures and to exclude contaminations. The orifices (3) have a known conductance of 10 l/s for H_2. Two bakeable Bayard-Alpert gauges (6) are used to measure the total pressure in the sample and the reference chamber. The whole apparatus, with the exception of the lock system, can be baked at 300°C. For the samples, extra heating is provided. Additionally to the total pressure measurement, the partial pressure is measured by a quadrupole mass spectrometer (9) to receive the composition of the gas and quantify the different gas species. Another total pressure gauge is used to check if the pressure is low enough to start the mass spectrometer, which can be in-situ calibrated via a calibrated leak (10).

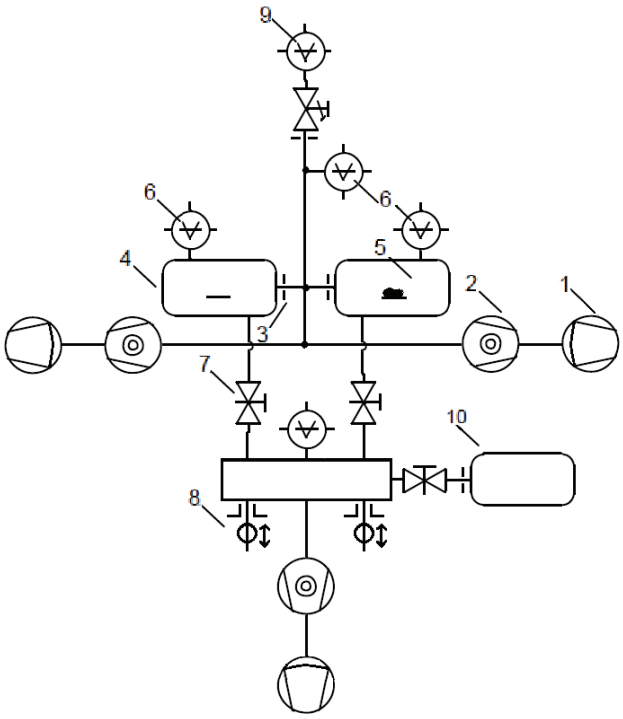

Fig. 1: Concept of the Outgassing Measurement Apparatus.

One lock chamber can be used for both vacuum chambers. Like this, simultaneous transfer of sample and reference is possible. Here, the pumping system consists of a turbo molecular pump and a membrane pump, too. Two magnetical rotational and linear feedthroughs are used for sample transportation. To separate lock and vacuum chambers two all-metal gate valves are provided. A vacuum gauge is used to measure the pressure in the lock chamber, since a pressure of about 10^{-5} Pa should be reached before transferring to the vacuum chambers.

According to this concept, CAD drawings (Figure 2) of the test facility have been made. At present, the design phase is concluded and various components have already been delivered, so that the main part of the measurement apparatus can be set up in the beginning of next year.

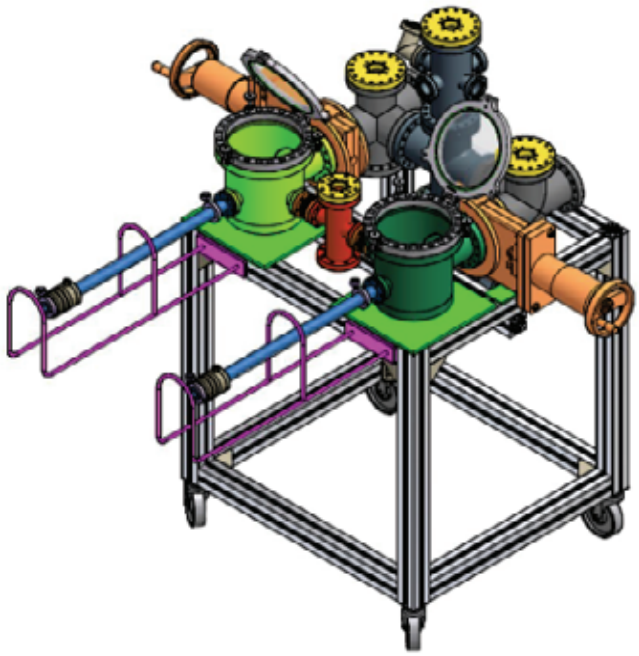

Fig. 2: CAD-drawing of the vacuum components of the Outgassing Measurement Apparatus. The footprint of the apparatus is 1.5 mx1.5 m.

VACU-TEC Work Package 4 (pumps)

The research activities in 2011 under the VACU-TEC work package 4 focused mainly on the investigation of tritium compatible vacuum pumps for fusion applications and the improvement of the ITER vacuum pumping system (including the simplification of the fuel cycle) starting with an assessment of the existing ITER solution. This work was done not only for ITER but also in view of a commercial fusion power plant (DEMO), see also the report on the complementary activity under the EFDA power plant physics and technology activity WP11-DAS-HCD-FP.

During this work, four main topics turned out to become the central elements of this work package:

- Development of a continuously working, non-cryogenic and tritium compatible high vacuum pump fulfilling high RAMI (Reliability, Availability, Maintainability and Inspectability) requirements.
- Development of a continuously working, non-cryogenic and tritium compatible fore-vacuum pump (roughing pump) fulfilling high RAMI requirements.
- Development of a gas separation concept that allows a gas fore-separation in order to reduce the size of the tritium plant significantly.
- Set up a test facility that allows testing the proposed solution/components. (THESEUS; Test facility for helium separating units)

Development of an improved tritium compatible pumping system for DEMO providing a capability for direct internal recycling

The vacuum pumping system for ITER is based on a cryogenic solution: Cryogenic high vacuum pumps are used to pump the exhaust gas out of the torus. These pumps are gas binding pumps that need to be frequently regenerated. For this regeneration, a roughing pump is needed. This pump is also a cryogenic pump: The gas which is released of the torus pumps during regeneration is cooled down again into a smaller volume where all gases except of helium are condensed. The pressures that are achieved during regeneration of this small volume cryo viscous compressor are high enough to use a dry piston pump to compress the gas to atmospheric pressure.

This cryo-based pumping system is considered to be a good solution for an experimental device such as ITER, but for DEMO, requirements are completely different: Cost and RAMI-issues become more and more important [1]. For this reason, a generic assessment of various pump types was performed (see WP11-DAS-HCD-FP) which identified a novel, promising pumping train concept that consists of a vapour diffusion pump as high vacuum pump and a liquid ring pump as roughing pump, both with a working liquid that was replaced from water or oil to a liquid metal (for tritium reasons) [2].

Figure 3 shows the full fuel cycle (without detailed fuelling systems and the tritium plant) that has been proposed in 2011 by KIT for use in a fusion power plant /DEMO. Central part of this fuel cycle is the gas separation by special metal foil modules, the Separator Pumping Modules. By these heated metal foils, the gas is pumped and separated in a helium enriched part and the pure unburnt deuterium/tritium fuel. Deuterium and tritium is recycled directly into the reactor and thus, it is called Direct Internal Recycling (DIR) concept.

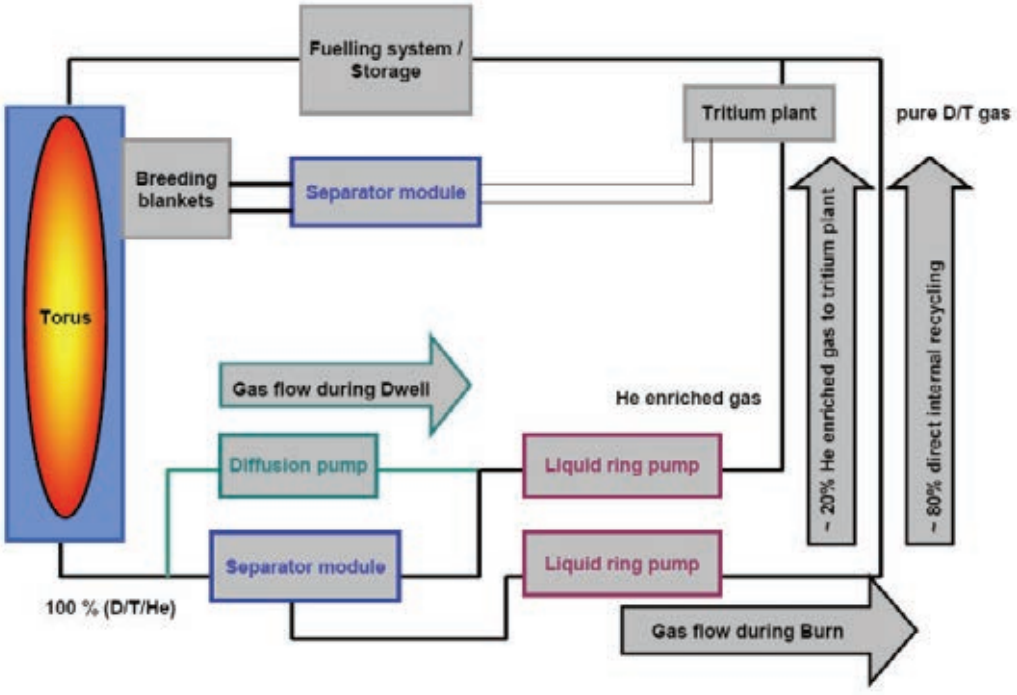

Fig. 3: Summary of a new fuel cycle concept proposed by KIT for a fusion power plant including the Direct Internal Recycling concept to keep the total tritium inventory small and the tritium processing times short.

All these pumps have never been tested before. Therefore a proof-of-principle-test is absolutely necessary. In addition, a fundamental understanding of the underlying physics in these three pump types has to be gained. Based on this, software tools (lumped parameter or rigorous) have to be developed which allow for predictive modelling and thus, would support a dedicated design approach for DEMO. To perform parametric experiments and to learn how

to operate such a complex vacuum system is a major task of the THESEUS facility, which is planned to be fully constructed in 2012. The main tasks of this facility are the

1. Testing of tritium compatible, continuous working vacuum pumps.
2. Testing of the Separator Pumping Modules.
3. Demonstration of the functionality of the Direct Internal Recycling (DIR) concept.

This test facility is needed in a technical scale as the reasonable minimum size of the available components is already big. The simulation of the fuel cycle pumping situation is a complex task with high demands on safety (hydrogen and deuterium handling), control and data acquisition. This work was started in spring 2011 and was co-funded by the KIT start-up budget provided by the German Helmholtz Society.

Figure 4 gives an overview of the THESUS facility. Gas is dosed via the dosing system in a test vessel that represents the torus of a fusion machine. Then it is pumped out by the test pumps or the separator pumping module. The infrastructure (cooling system, electronic switchboards, control room) is also installed on the upper level. When the gas is pumped out of the test vessel, it is recycled to the dosing dome in a closed loop. For investigation of the separating performance, it is planned to employ a three channel gas analyzing system.

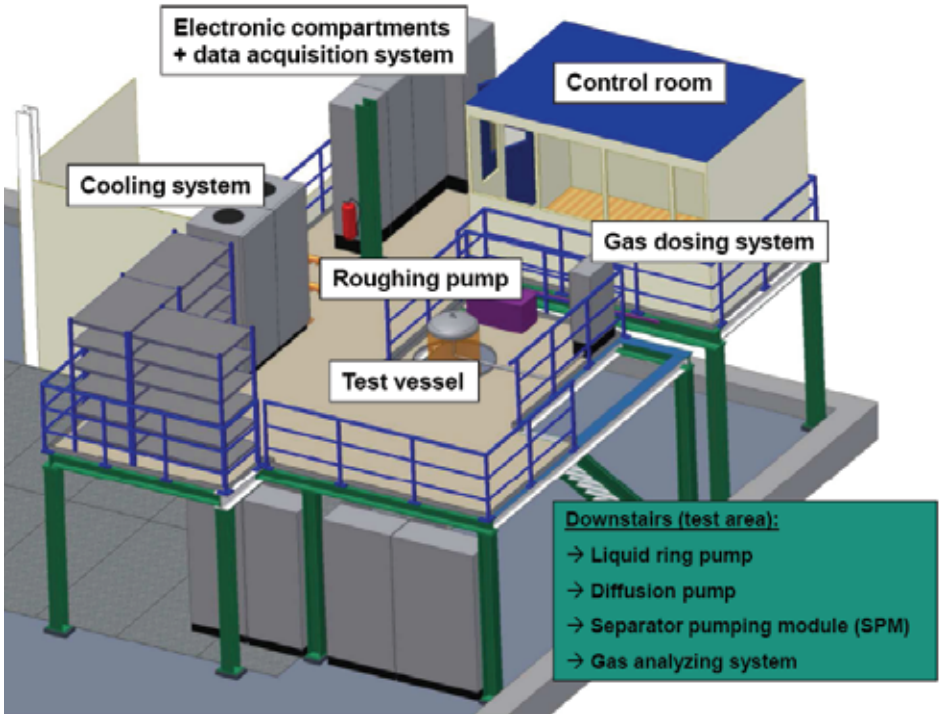

Fig. 4: The THESEUS facility.

The whole facility can be controlled remotely by a PLC (SIEMATIC S7) and a human machine interface (SIEMENS WinCC). This is necessary because during hydrogen and deuterium operation of THESEUS, no people are allowed close to the facility for safety reasons. All pressures, temperatures and flows are measured with high accuracy by a 23 bit data acquisition system (Delphin TopMassage ©). A Hydrogen Interlock System is installed to guarantee the safety during the experiments. First results of the component tests are expected for late 2012.

Conclusions

The EFDA GOT VACU-TEC training programme was established in 2011, see Figure 5. It demonstrated to be an excellent framework for young researchers to get a thorough education in fusion and be able to deliver own and selfstanding work for fusion research.

Fig. 5: Kick-off meeting of VACU-TEC, held in October 2011 at KIT. The front row features the five trainees.

Staff:

K. Battes (trainee for WP2)
Chr. Day (for co-ordination)
A. Edinger
Th. Giegerich (trainee for WP4)
V. Hauer (mentor)
Th. Johann
R. Müller
P. Pfeil
H. Stump
J. Weinhold

Literature:

[1] Th. Giegerich, Chr. Day, View on challenges in operating fusion power plant vacuum systems, OLAV-III Workshop, Oak Ridge, TN, USA, July 2011.

[2] Th. Giegerich, Chr. Day, V. Hauer, Development of a tritium compatible vapor diffusion pump for a commercial fusion power plant, ISFNT-10, Portland, OR, USA, Sept. 2011.

Acknowledgement

This work, supported by the European Communities under the contract of Association between EURATOM and Karlsruhe Institute of Technology, was carried out within the framework of the European Fusion Development Agreement. The views and opinions expressed herein do not necessarily reflect those of the European Commission.

Fuel Cycle –
Tritium Processing

Testing of Isotope Separation System (ISS) with the WDS (TW6-TTFD-TR 63)

In view of mitigation the concern over tritium release into the environment during pulsed operation of the Torus, the Water Detritiation System (WDS) and Isotope Separation System (ISS), based on cryogenic distillation (CD), will operate in such a way that WDS will be a final barrier of tritium for the processed protium waste gas stream discharged from ISS. To investigate the capability of the WDS to achieve this goal, the influence of the additional basically hydrogen stream from ISS and its feeding location into the WDS, the separation performances of Liquid Phase Catalytic Exchange process has to be investigated and accurately mathematically modelled.

In order to develop the experimental data base needed for design of ITER WDS and ISS, the following modes of operation have been considered during the design of the combination WDS-ISS:

- Operation of the LPCE column with composition fluctuation in the stream returned from the CD column
- Operating of the CD column with composition and flow rate fluctuations in the feeding stream
- Operation in different dynamic modes in order to validate and bench mark the TRIMO code.

To support the research activities an experimental facility, called TRENTA, has been constructed and is in operation at TLK. The design of the facility was developed in view of the experimental program mainly dedicated to investigate the combination WDS-ISS processes during isotopic and thermal transitory regimes. Therefore, a detailed investigation of the control system and separation performances of the CECE process when working as a final barrier of the top product of the CD column to be discharged into the environment is under investigation.

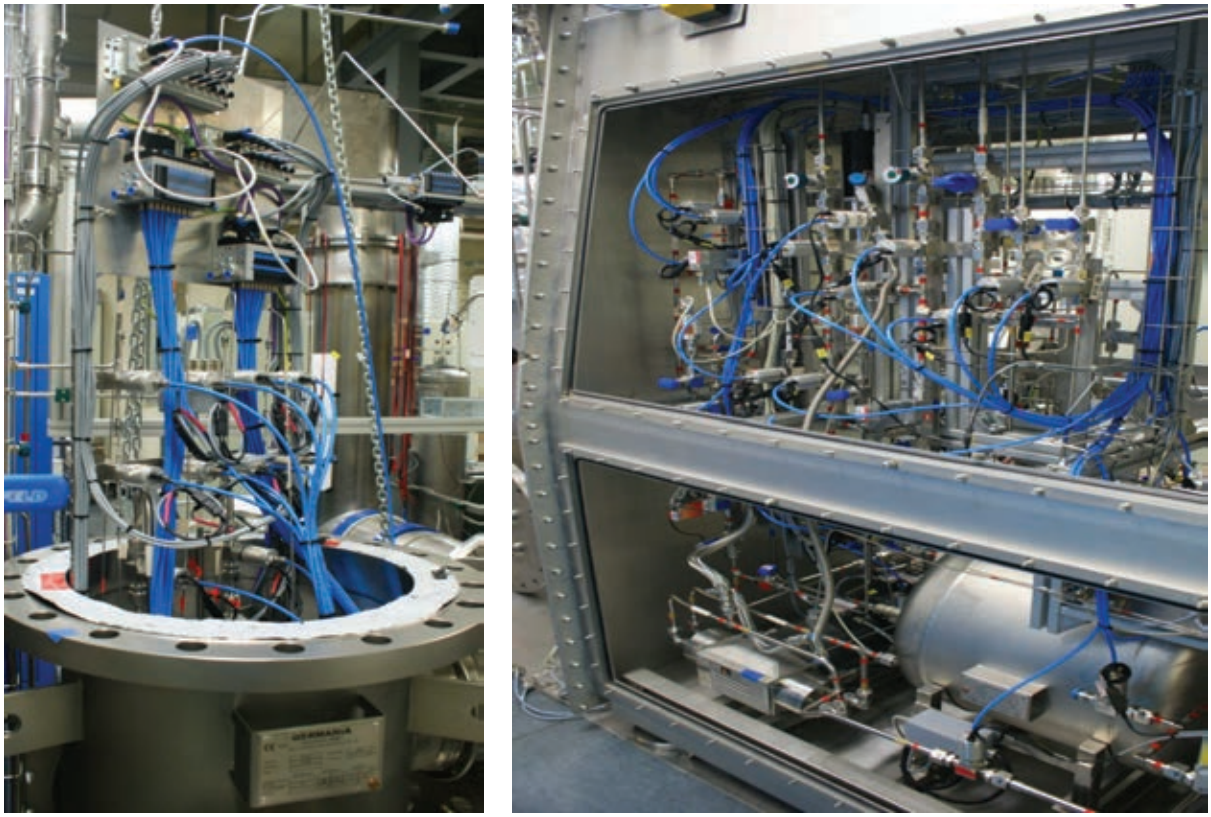

Fig. 1: The valve box and the glove box of TRENTA facility in view of CD-CECE operation.

In support of the above program the following activities have been carried out in 2011:

- Installation of the heat exchangers within the cryogenic distillation cold box.
- Completion and commissioning of the valve box in between the cryogenic distillation cold box and glove box. The role of the valve box is to isolate the glove box from the cryogenic distillation cold box in case of abnormal conditions to prevent any pressurization of the glove box.
- Completion and commissioning of the glove box where all the components for gas processing in between the cryogenic distillation cold box and the CECE process at ambient temperature are accommodated.
- A dedicated software based on TRIMO++ software have been developed aiming to simulate the operation of the combination cryogenic distillation process with the CECE process. The software has been developed according to the real configuration of TRENTA plant, i.e. including all major components relevant for operation of the facility.
- Several runs of the dedicated software have been performed considering various operation modes at different parameters. In view of calibration of the software developed at TLK the predicted performances, such as decontamination factor and isotopic profiles along the LPCE column, will be benchmarked against the experimental results.

Staff:

D. Adami
I. Cristescu
N. Lohr
C. Petrutiu
C. Plusczyk
R. Michling
S. Welte

Acknowledgement

This work, supported by the European Communities under the contract of Association between EURATOM and Karlsruhe Institute of Technology, was carried out within the framework of the European Fusion Development Agreement. The views and opinions expressed herein do not necessarily reflect those of the European Commission.

Finalization of the System Capacity, Enhancements Studies and Detailed Design of WDS Components including HAZOP Studies (F4E-2010-GRT-045 (PNS-VTP))

The assignment of WDS is to recover tritium from tritiated water and to discharge decontaminated hydrogen, which is oxidized to water before released to the atmosphere. The recovered tritium is available in the gas phase (tritiated hydrogen) and partially transferred to ISS for final enrichment and separation. The CECE process is applied for WDS, which consists mainly of two processing steps. First tritiated water is converted to gaseous hydrogen by electrolyser units, and secondly along an isotopic exchange column (LPCE) one part of the generated hydrogen stream is decontaminated for discharge and whereas the other part is fed to the ISS for final enrichment and separation of the required hydrogen isotopologues.

To control the process in an efficient manner, all tritiated water will be intermediately stored in the holding tanks of WDS, from where the water is constantly fed to the exchange columns or to the electrolyser units, depending on the tritium content and the operation modes of WDS. The main sources of tritiated water are the scrubber columns (SC) and the molecular sieve drier (MS) from the Detritiation System (DS).

The water input to WDS is cleaned over a purification stage prior to be sent to the different holding tanks regarding the tritium content. Tritiated water emerged from accidents/incidents is collected in emergency tanks, which are capable to receive larger amounts of tritiated water.

The basic functions of the WDS can be summarized as follows:

- Temporary storage of tritiated water in holding tanks coming from the scrubber columns and molecular sieve drier of DS during normal operation and maintenance duties
- Temporary storage in emergency tanks of tritiated water coming mainly from DS.
- Processing of tritiated water for tritium recovery
- Enrichment of tritium from processed water into the gaseous phase to be fed to ISS for further enrichment and separation
- Decontamination of ISS off-gas by processing through the catalytic exchange column in WDS prior to discharge to atmosphere
- Discharge of decontaminated hydrogen stream generated from the tritiated water by electrolysis.

In view of the Preliminary Design Review (PDR) prior to the signature of the Procurement Arrangement (PA) the following activities have been carried out:

- Development of the P&ID for the entire ITER WDS
- 3-D layout of the B2 level, where the largest components of ITER WDS shall be placed such as emergency holding tanks of 100 m3, tritiated water holding tanks of 20 m3 , electrolysers, etc.
- Detailed design for the emergency holding tanks of 100 m3 and tritiated water holding tanks of 20 m3 has been completed.
- The procedure for the seismic analysis of the major WDS components has been developed and used to check the behaviour of holding tanks of 100 m3 and tritiated water holding tanks of 20 m3 during an earth quake (s. Fig.1).

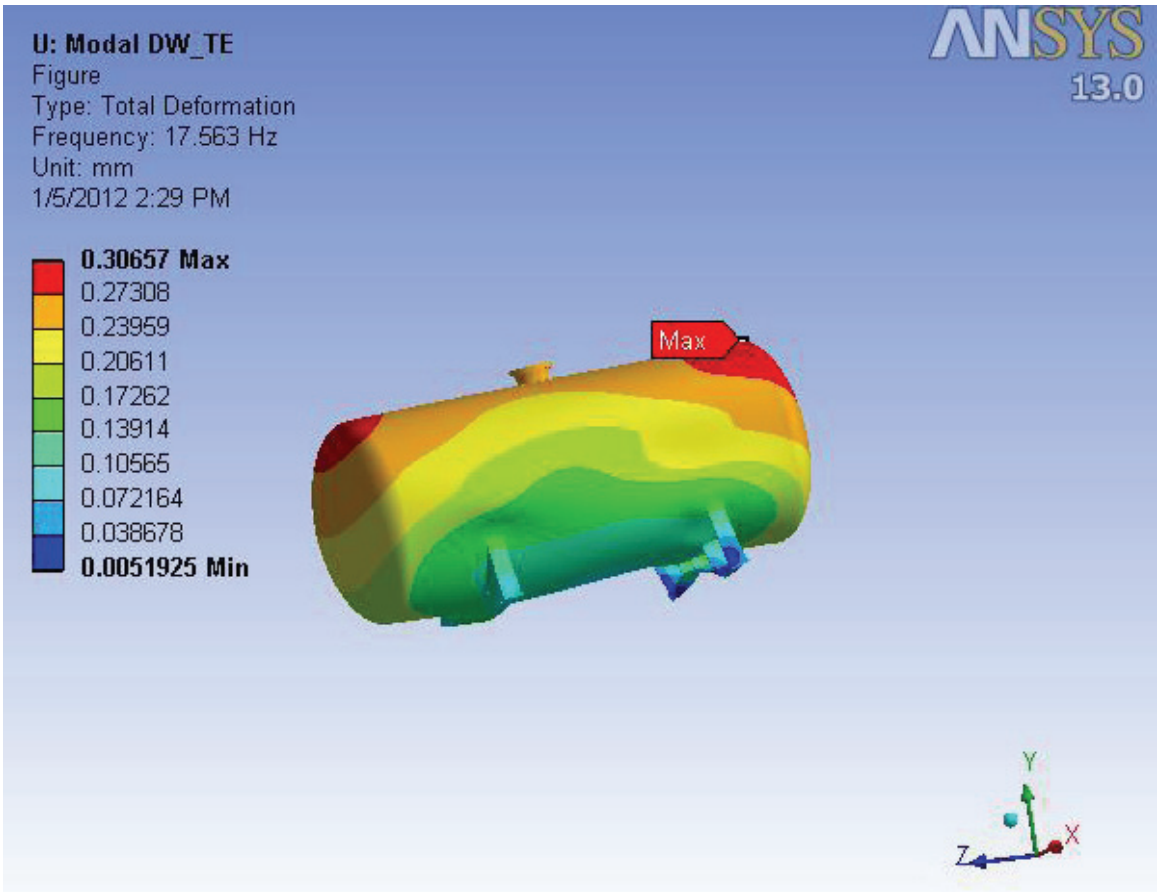

Fig. 1: Example for seimic analysis of the 100 m^3 holding tank.

- Detailed investigation of separation performances of 8 m LPCE column from TRENTA facility have been carried out aiming to quantify the influence of deuterium content in the tritiated water to be processed on the decontamination factor that can be achieved along the column. Various concentrations of deuterium have been used, ranging from natural level up to 45% atomic deuterium concentration; the decontamination factor and deuterium and tritium profile along the LPCE column have been measured.
- The experimental results have been used as input data for the TRIMO++ software and the mass transfer coefficients for various chemical reactions, relevant for ITER WDS design, have been calculated.

Staff:

I. Cristescu
N. Lohr
R. Michling
C. Petrutiu
C. Plusczyk
S. Welte
G. Ana – ICIT Romania
A. Niculescu – ICIT Romania

Acknowledgement

This work was supported by Fusion for Energy under the grant contract No. F4E-2010-GRT-045 (PNS-VTP).with collaboration by ENEA Frascati, Italy; ICIT, Rm. Vâlcea, Romania and CEA Saclay, France. The views and opinions expressed herein reflect only the author's views. Fusion for Energy is not liable for any use that may be made of the information contained therein.

Water Detritiation after Purification using TRENTA-3 (JW11-FT-2.38)

Introduction

The normal operation of any type of Fusion machine, such as JET, inevitably produces not only large amounts of solid waste material but also tritiated liquids (oils and water). Amongst them tritiated water (HTO), is the major liquid waste, which needs to be processed with a view not only to reduce the tritium content in order to comply with the disposal regulations relating to the upper limit of tritium concentration, but also with the aim to recover tritium.

During the last years of operation through many experimental campaigns JET generated tritiated water with an average rate of approximately 10 tonnes per year. This amount of tritiated water has been collected and temporarily stored on site and currently, there are about 250 drums waiting for detritiation, each one of them containing approximately 180 litres of tritiated water with the average tritium concentration of 1.5 GBq/l (0.04 Ci/l).

Until recently, the tritiated water has been shipped to Ontario Power Generation Inc. (OPGI), Canada for detritiation and final disposal. However, lately the costs for the processing of the JET tritiated water did increase considerably as well as, the criteria for the water quality. Indeed, after chemical analysis it appeared that the JET tritiated water is contaminated by a large variety of anions and cations, which are “poisoning” the detritiation facility at OPGI. Therefore, the specifications of the water quality have been increased and therefore, there are serious concerns that this “route to Canada” might not be available in the future. If this route becomes unavailable JET needs to find a viable alternative, which means that JET has been looking after a substitute solution, either on-site or in collaboration with another Association, which will be able to provide the adequate facility for the processing of its tritiated water.

In this regard, the choice of using the TRENTA detritiation facility located at the Tritium Laboratory Karlsruhe (TLK) was an obvious solution and therefore, a Fusion Technology task has been initiated in the frame of the JET 2011 Work-programme, The aim of this task is to demonstrate that it is possible to reduce to a minimum volume large amounts of JET tritiated water with the aim to possibly appoint TLK as the substitute route for the detritiation (in fact enrichment) of the JET tritiated water. However, in order to perform this task, prior to the detritiation of the JET water it was also necessary to use water, which has been purified i.e. depleted from the major part of metal and ion contaminants.

In a previous task undertaken under the Fusion Technology Task Force, it has been successfully demonstrated that such purification can be achieved very efficiently, in order to meet the purity criteria set up by OPGI (JW9-FT-2.33) [1]. Therefore, after having reduced the concentration of all major impurities such as, chlorine, fluorine and other heavy metals such as gadolinium, the detritiation of the purified water was a second and necessary step in the way of establishing a new route for the detritiation of the JET water.

In this task it is proposed to demonstrate an efficient detritiation of one drum of tritiated water (after purification), using the existing TRENTA-3 experimental facility, which is already in operation at the TLK. In fact, in this task we propose an enrichment of the JET tritiated water or in order words we propose to reduce the tritiated volume of one single drum to a minimum (few litres) but keeping the total tritium concentration. For this task it is proposed to detritiate the drum sent previously to SCK•CEN i.e. drum 476.

Experimental

Working in the field of detritiation of many types of liquids and gaseous mixtures, the TLK acquired huge and worldwide-acknowledged expertise. In this respect, for the detritiation of tritiated water in liquid phase, TLK developed a semi-technical scale plant facility, the so-

called TRENTA facility [2]. In order to perform the needed experiments, the TRENTA team investigated and optimised the various experimental parameters involved in the detritiation process. These parameters are affecting the separation performances of the TRENTA system and therefore, various tests have been carried out extended over a period of several years. During this investigation, we did explore many experiment conditions using several catalysts/packing mixtures. The aim was to establish and finely tune up the most critical experimental parameters, in order to provide the highest possible decontamination factor [3].

The TRENTA-3 test rig, used for this task is combining two well-established methods, which appear to be the most suitable processes for water detritiation and tritium recovery. These processes, are involving the electrolysis of the tritiated water, followed by a **L**iquid **P**hase **C**atalytic **E**xchange (LPCE). During the first step tritiated water is electrolysed generating oxygen and a tritiated hydrogen stream, which in a second step is enriched after being sent into a catalytic column (the LPCE column). This column is filled with an appropriate mixture made of an active catalytic material and an appropriate packing material.

The whole process is known as being the CECE process, which stands for **C**ombination of **E**lectrolysis and **C**atalytic **E**xchange of hydrogen isotopes. In a third step, it is also possible to recover the tritium contained into the enriched mixture of hydrogen isotopes, by sending the latter into a cryogenic distillation column operating at very low temperatures (20 K-25 K).

The TRENTA-3 facility, developed with the support of a previous work programme of the TF-FT (JW0-FT-2.01) [4, 5], is currently under regular operation at the TLK. It is an experimental facility, which allows us to systematically investigate the influence of deuterium (or tritium) content on the decontamination factor in relation with the location of the feeding points. The facility also allows the evaluation of the separation performances for transitory regimes and is fully validated by well-established simulation models, developed at the TLK.

More in details, the TRENTA-3 facility consists of two following systems:

- Two upgraded electrolyser units from Proton Energy Systems (HOGEN 40)
- An 8 m length LPCE column having an internal diameter of 55 mm and operating at the average temperature of 70°C and at the pressure of 1.2-1.8 bar absolute.

The electrolysis unit consist of two electrolysers using a Solid Polymer Membrane (SPM) electrolyte made from *Nafion*. The *Nafion* has received a considerable amount of attention as it is a very good proton conductor and therefore, has been extensively used as main material for proton exchange membrane (PEM) fuel cells, because of its excellent thermal and mechanical stability. The chemical basis of Nafion's superior conductive properties should be regarded on its sulfonic groups ($^{-}SO_3$) as in these groups, hydrogen can very easily "hop" from one acid site to another.

In comparison with the electrolyser using the alkaline electrolyte potassium hydroxide (KOH), electrolysers using a SPM electrolyte have the big advantages to not release K^+ anions, which can be transported with the hydrogen stream and finally deposited into the packing and catalyst material of the LPCE column. No less important is that SPM has a lower inventory of tritiated water and therefore, it does not generate additional tritiated liquid waste.

On the other hand, filling the LPCE column with an appropriate catalyst and packing material is of paramount importance, as it enhances the catalytic exchange taking place within the column and need to remain free of any ion contamination other than the hydrogen isotopes (thus importance of the purification process of the JET tritiated water prior to its detritiation).

The LPCE column consists of four sections of 2 m each, with liquid distributors between them. In addition to the catalyst/packing mixture the column is also equipped at the bottom with an integrated electric boiler and an external cooler at the top, while a jacket in which

warm water is circulating assures a constant temperature along the whole length of the column (Fig. 1).

The LPCE column was designed to allow processing water with different tritium and/or deuterium concentration. Therefore, beside the tritiated water, directly feeding into the electrolysers, several feeding points along the column could also be used. This allows feeding the LPCE column with tritiated water at a various locations, the feeding point depending on the tritium concentration of the tritiated water to be processed.

During our experiment for this task, only demineralised water has been supplied, at the top of the LPCE column, while the enriched tritiated water is collected in the boiler located at the bottom of the LPCE column from where it is sent to the electrolysis unit. The hydrogen–deuterium–tritium mixture produced by the electrolysis of tritiated water is fed at the bottom of the LPCE column. In the boiler of the LPCE column, the hydrogen and tritium gas mixture is saturated with water vapours flowing down the column, and then flows upstream in counter-current mode across the LPCE column. During the whole process the demineralised liquid water feeding the top of the column, is flowing down up to the boiler, while simultaneously the tritiated gaseous mixture is flowing upstream across the LPCE column. The isotopic exchange process as well as the chemical reactions taking place across the LPCE column are illustrated in Fig.1.

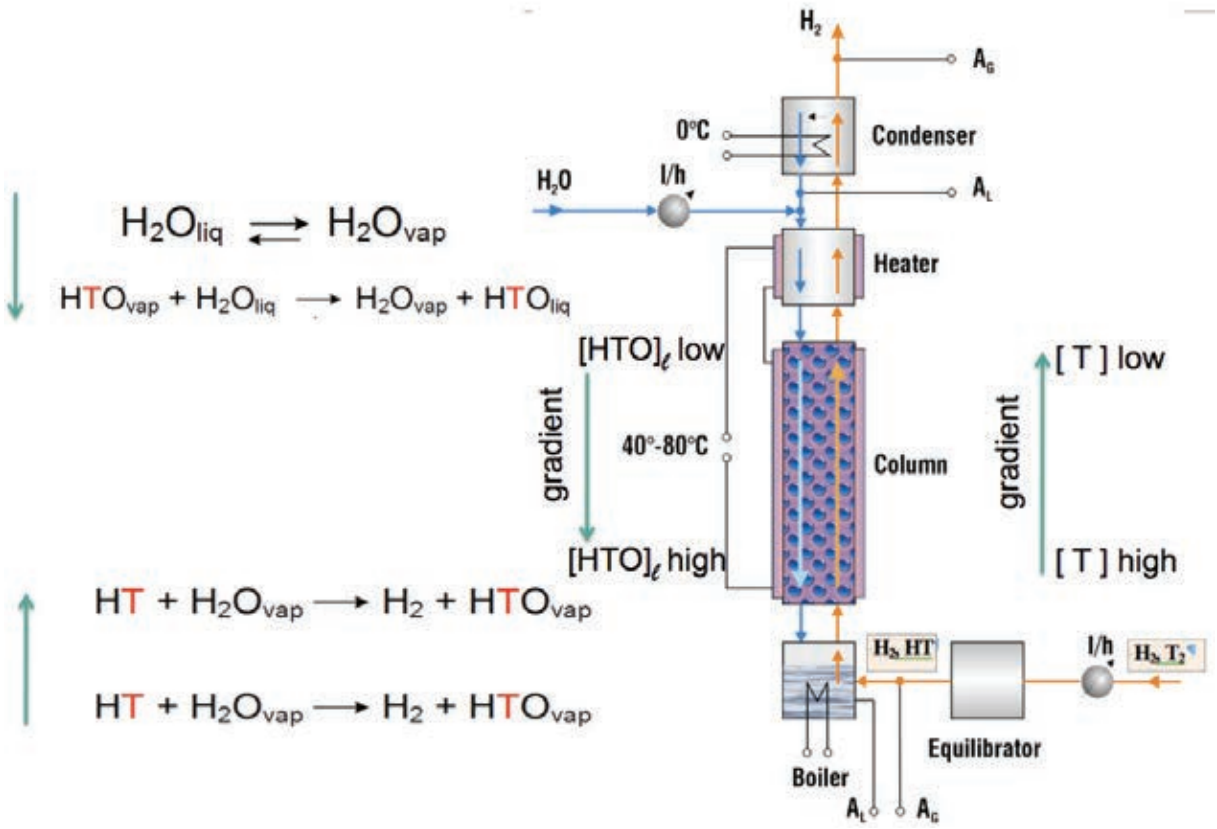

Fig. 1: The LPCE column and the chemical reactions taking place at the TRENTA-3 experimental test rig.

As it is clearly illustrated, as the liquid water trickles down the LPCE column, it becomes more and more enriched in tritium whereas simultaneously the tritiated hydrogen gas flowing upstream across the LPCE column becomes more and more depleted in tritium (compared to the initial electrolyte solution from which it evolved). During the process and in steady state operation of the column, a gradient in tritium concentration is established across the column leading finally to the release of the tritium depleted hydrogen stream at the top of the column and then to the stack.

A condenser is also included at the top of the LPCE column just to trap the traces of tritium that might have escaped the isotopic exchange. Regular sampling of the tritiated water was controlling the efficiency of the isotopic exchange, taking place across at column.

The nominal feed rate of tritiated water of the CECE process at TLK is 2 kg/h compared with 60 kg/h foreseen for ITER-WDS (Water Detritiation System), however during routine operation we were processing about 1.7 kg/h (94.4 mol/h).

Description of the facility

The flow diagram of the entire water detritiation facility (TRENTA-3) as it is in operation at the TLK is given in Fig. 2. It comprises two electrolysers able to provide up to 2 Nm3/h and an 8m height LPCE column. The column has been filled with catalyst and inert packing (as layers or as mixture) according to the manufacturer specifications. The isotopic exchange column has an outer jacket, through which thermostated water flows to maintain a constant temperature along the column. In addition, the power of the heater for the feed water and the heater of the boiler are controlled. The boiler ensures heating and saturation of the hydrogen with water vapour.

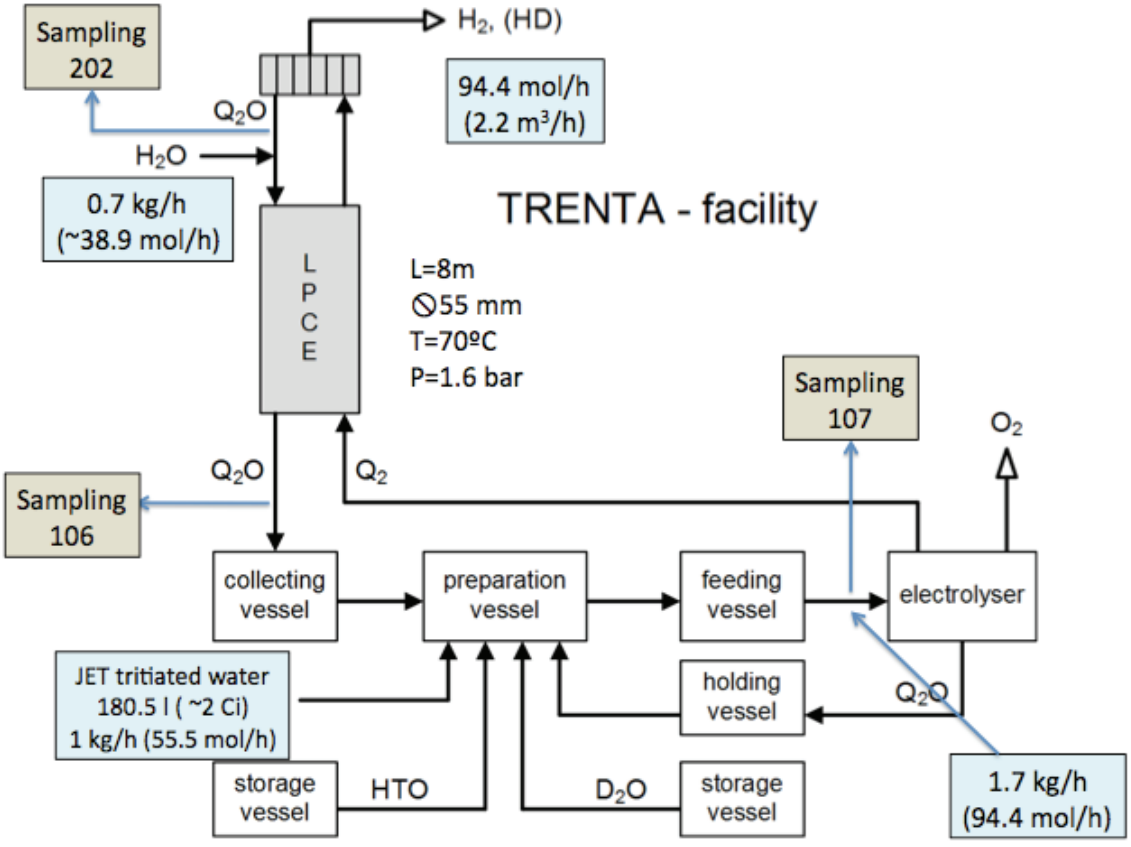

Fig. 2: Schematic illustration of the entire TRENTA-3 facility.

The electrolyser is fed with one single stream of liquid water. It is a mixture of the tritiated water collected at the bottom of the LPCE column (0.7 kg/h), to which we add the JET tritiated water (1 kg/h). Therefore the electrolyser receives about 1.7 kg/h (94.4 mol/h) tritiated water. After the electrolysis 94.4 mol/h tritiated hydrogen is sent to the bottom of the LPCE column or approximately 2.28 m^3/h. The isotopic exchange process takes place between the pre-heated distillated water feeding the top of the column (0.7 kg/h) and the tritiated hydrogen coming from the electrolysed at the bottom of the column. The ratio between the tritiated hydrogen gas entering at the bottom of the LPCE column to the molar wa-

ter amount feeding the top of the column is known as the molar gas to liquid flow rate ratio, and in this case it was equal to 2.4.

Several sampling locations have been foreseen along the whole process and their position is indicated on Fig. 2. This allows us to control the whole process and follow the evolution of the tritium concentration in respect to the time. The main sampling points were performed for the liquid phase at the bottom of the column and in the gas phase at the top of the column, which give us an indication when the steady state is reached. Moreover, at the column outlet it is also possible to proceed with on-line measurements of the gas phase composition as there is a connection leading to a Quadrupole mass spectrometer. After the steady state conditions have been established, comparative measurements have been performed on regular basis, using the Omegatron mass spectrometer.

The evolution of the tritium concentration, at the various sampling point, in respect to the time, is illustrated in the Figure 3.

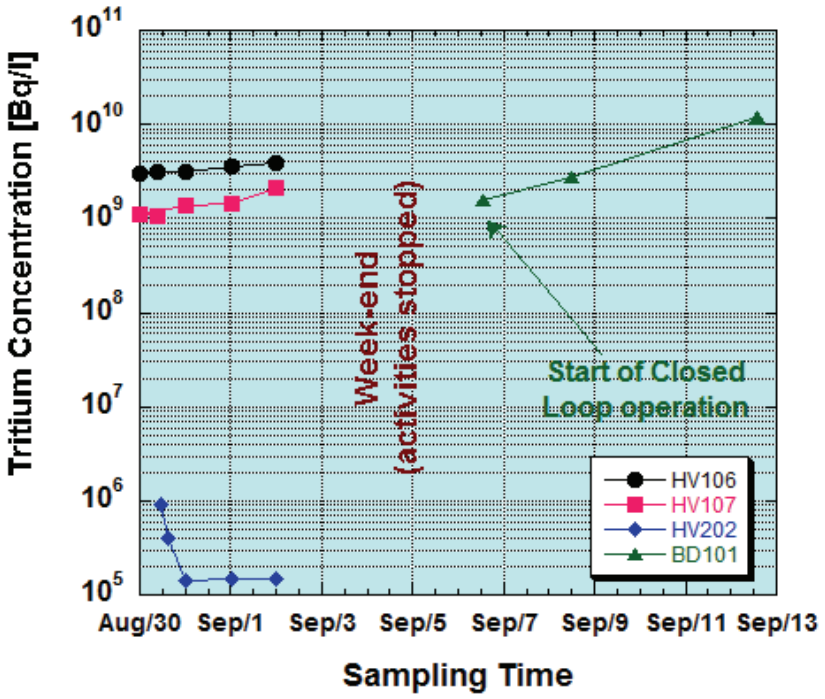

Fig. 3: Evolution of the tritium concentration against time at the various sampling points (the location of the various points it is indicated in Fig. 2).

We may notice that we needed approximately one week to introduce the whole amount of JET tritiated water into the system and during this time the tritium concentration at the top and the bottom of the column and at the feeding position was constant or slightly increasing. However, once the total amount of the JET tritiated has been introduced into the system we started operating in close loop and therefore, the tritium concentration was constantly increasing. This is showing by the sampling measurement performed for the holding vessel BD101 feeding the electrolyser.

It is also worth mentioning that the tritium concentration at the condensed water at the top of the column is about 4 orders of magnitude lower than the tritium concentration of the water leaving the bottom of the LPCE column.

After processing, the 180.5 l of JET tritiated water have been reduced to 6.25 l with an average tritium concentration of 11.85 GBq/kg, i.e. a total tritium activity of 74.01 GBq (2.00 Ci).

Conclusions

The goal of this task was to demonstrate, on a representative scale, that the tritiated water produced during normal operation at JET could be efficiently detritiated using the TRENTA-3 facility at TLK.

For this task one drum of tritiated water containing about 180.5 l of tritiated water, with an average tritium concentration of 0.41 GBq/kg i.e. a total activity of 74.01 GBq (2.00 Ci) was

sent to TLK for volume reduction and therefore tritium enrichment. The tritiated water has been previously purified at SCK•CEN in order to meet the admission criteria requested by OPGI, i.e. before its detritiation many anions and cations impurities which were contaminating the tritiated water have been removed by passing the water through a series of ion filters.

After processing the JET water into the TRENTA-3 facility at the TLK, the final reduced volume was only 6.25 kg with an average tritium concentration of 11.85 GBq/kg, i.e. a total tritium activity of 74.01 GBq (2.00 Ci), which gives us a volume reduction factor of about 29.

The process showed that it is possible to efficiently reduce large amounts of tritiated water to a minimum volume. We are only limited by the tritium concentration of 10 Ci/kg which is the highest concentration for which the two electrolysers have been licensed. Having this limit in mind and taking into account that presently there are about 250 drums of tritiated water stored at JET (45 m^3) with an average concentration of 1.5 GBq/l (0.04 Ci), it is possible to reduce this volume to approximately 182 l i.e. to one single drum with an average tritium concentration of 10 Ci/l. This means that for the JET water, we can reach a volume reduction factor of about 250.

Staff:

N. Bekris
N. Lohr
R. Michling
Chr. Plusczyk
S. Welte

Literature:

[1] K. Dylst, J. Seghers. Experimental demonstration of a chemical process for the purification before detritiation of tritiated water from JET. EFDA-JET Report JW9-FT-2.33, or SCK-CEN Report 4941, Feb-2010.

[2] I. Cristescu, Ioana R. Cristescu, L. Dörr, M. Glugla, G. Hellriegel, R. Michling, D. Murdoch, P. Schäfer, S. Welte, W. Wurster. Commissioning of water detritiation and cryogenic distillation systems at TLK in view of ITER design. Fusion Engineering and Design, Volume 82, (2007), 2126-2132.

[3] R. Michling, I. Cristescu, L. Dörr, S. Welte, W. Wurster. Modification, enhancement and operation of a water detritiation facility at the Tritium Laboratory Karlsruhe. Fusion Engineering and Design, 84, (2009),338-343.

[4] I. Cristescu, Ioana-R. Cristescu, U. Tamm, C.J. Caldwell-Nichols, M. Glugla, D. Murdoch, S. Welte . Simultaneous tritium and deuterium transfer in a water detritiation CECE facility at TLK. Fusion Engineering and Design, 69, (2003), 109-113.

[5] I. Cristescu, U. Tamm, Ioana-R. Cristescu, M. Glugla, C.J. Caldwell-Nichols. Investigation of simultaneous tritium and deuterium transfer in a catalytic isotope exchange column for water detritiation. Fusion Engineering and Design, Volumes 61-62, November 2002, Pages 537-542.

Acknowledgement

This work, supported by the European Communities under the contract of Association between EURATOM and Karlsruhe Institute of Technology, was carried out within the framework of the European Fusion Development Agreement. The views and opinions expressed herein do not necessarily reflect those of the European Commission.

Goal Oriented Training Programme “Tritium Technologies for the Fusion Fuel Cycle” (WP08-GOT-TRI-TOFFY (FU07-CT-2008-00047))

Background

The overall objective of the project is to support EU activities in the Deuterium-Tritium Fuel Cycle area for ITER by the training of six Early-Stage Researchers. The training programme is developed along existing projects in the framework of the European procurement package for the ITER Fuel Cycle with the main focus on water detritiation (WDS) and isotope separation (ISS) systems, detritiation processes, gas analytics and tritium measurements (see overview table: list of Work Packages). The participating Associations are: KIT, CEA, ENEA, HAS/MTA ATOMKI, MEdC/ICIT, and CCFE.

No.	Title	Partners involved
1	Combined operation of WDS and ISS	KIT (ICIT, CCFE)
2	Detritiation of waste	CEA (KIT, CCFE)
3	Technologies for tritium recovery and trapping	ENEA (KIT, CCFE)
4	Calorimeter with large sample volume	MTA ATOMKI (KIT, CCFE)
5	Experimental Pilot Plant for Tritium and Deuterium Separation	ICIT (KIT, CCFE)
6	Participation in JET operation	CCFE (KIT)

The project was started in late 2008. The last 2 recruitments were done in the first part of 2010 and all trainees started their traineeship.

Status of project

All trainees are now fully involved in R&D work and part of them (those who started earlier) have already submitted papers. Two of the trainees have joined the ISFNT 2011 conference in Portland contributing by presentations.

An educational highlight in 2011 was the 4 weeks stay of all trainees at JET. The trainees got a dedicated training covering all aspects of a fusion machine. The course was well prepared and given with a lot of enthusiasm by our JET partners.

Outlook

In the next reporting period almost all trainees will have finished their programme. Therefore, the responsible people in the different countries now will have to see to it that these well educated trainees get a possibility to stay “in fusion”.

Programme Coordinator:

B. Bornschein

Acknowledgement

This work, supported by the European Communities under the contract of Association between EURATOM and Karlsruhe Institute of Technology, was carried out within the framework of the European Fusion Development Agreement. The views and opinions expressed herein do not necessarily reflect those of the European Commission.

Safety

Development of In-vessel Dust Measurement Techniques (F4E-2010-GRT-050 (ES-SF)

Subtask 3: Hot dust measurement using water vapour injection

The aim of the work is a feasibility study for a diagnostic method proposed recently to measure the hot beryllium dust inventory accumulated inside the ITER vacuum vessel during its normal operation. The method is to inject intentionally a small amount of water vapour into the evacuated vacuummvessel and to monitor the hydrogen release due to the Be-steam reaction $Be+H_2O=BeO+H_2$. The measurement results could allow extrapolation to loss of coolant (LOCA) events and evaluation of the hydrogen production to be expected in this case. Because of the high toxicity of beryllium dust, it was decided to use a substitute material instead of beryllium.

The following experimental scheme has been elaborated to perform the study. Based upon the analysis of the physical and chemical properties of Be and on the mechanism of its surface oxidation, aluminum has been chosen as a Be substitute to study the feasibility of the method. As it is known from the literature, the beryllium oxide layer forming on the pure Be surface during its oxidation provides an efficient protection of the Be surface from its further oxidation. The protective capability remains up to 600° C. The same is valid for Al. So the most interesting and informative data can be obtained at the initial stage of the dust oxidation, when the surfaces are still clean and have no oxide layer.

A test matrix has been produced and the methods of the dust specification have been elaborated. The methods include:

- Carrier gas heat extraction CGHE: to measure the oxygen content of dusts;
- BET method: to measure the specific dust surface;
- Scanning electron microscopy: to measure the dust size distribution;
- Optic ICP Emission Spectroscopy: to measure the bulk purity of the dust.

The experiments will be performed in a modified DUSTEX facility. The modification has been designed: it is a measuring chamber of about 2 l volume, that will be evacuated down to several hundredths of Pa with a dust sample inside. The chamber is connected to a steam injector providing a defined amount of steam let inside the chamber, and to a mass-spectrometer to measure the hydrogen release due to steam/Be-substitute reaction. The chamber is heated to 200-450°C to investigate the reaction sensitivity to temperature.

Dust samples will be prepared in a special box filled with argon. A coarse Al dust will be milled inside the box using a ball-mill machine. Then it will be placed inside the chamber keeping the atmosphere/environment oxygen-free. After that, the chamber will be detached from the box, closed, evacuated, and heated to the desired temperature. A defined amount of steam will be let inside the chamber to react with the sample. The test scheme is shown in Fig. 1.

The facility modification has been designed; some parts have been manufactured, the others have been procured:

1. Measuring chamber. The chamber integrates a support to place the samples, and temperature sensors to measure the inner temperature and its homogeneity (manufactured).
2. Heater to bring the chamber to the desired temperature and keep it during the tests (procured, Horst GmbH).

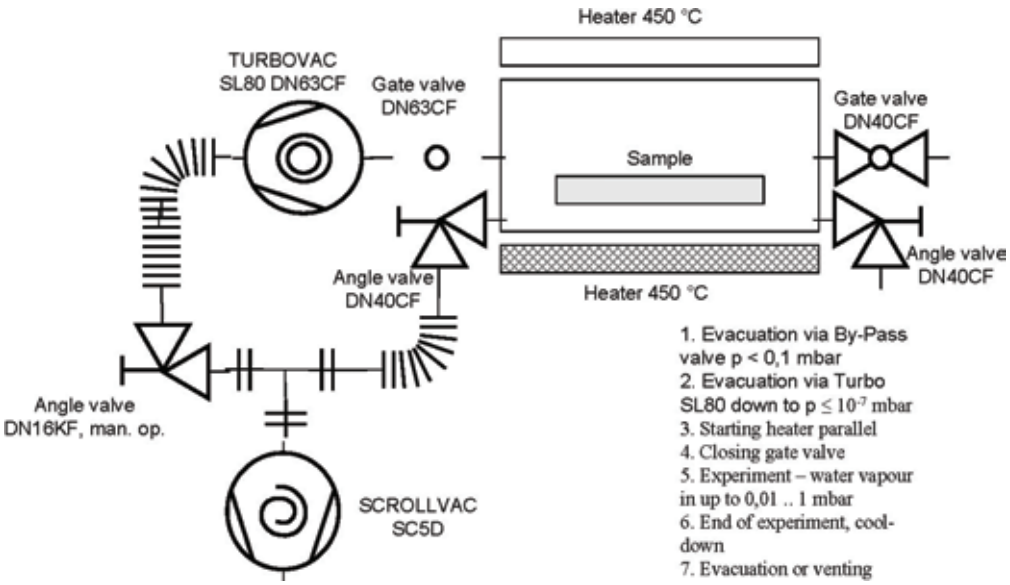

Fig. 1: Test scheme.

3. Steam injector connected to the chamber via a heated line (procured, WAGNER Mess- und Regeltechnik).
4. Vacuum pump/system to evacuate the chamber to several hundredths of Pa (procured, OERLIKON).
5. Mass-spectrometer connected to the measuring chamber to monitor/measure the dynamics of hydrogen release after steam injection (adopted to low vacuum conditions).
6. Glove box to prepare dust samples and store them for the tests (lent and equipped with procured parts).
7. Test preparation and run control system (developed at KIT).

Fig. 2: Modified facility to measure hydrogen release due to Be-substitute/steam reaction at high temperatures and low pressures.

The facility has been assembled and tested (see Fig. 2). Commissioning and calibration tests will be finished beginning of 2012. The measurements will be completed April 2012.

Staff:

A. Denkevits
T. Jordan
B. Ochsler
F. Prestel

Acknowledgement

This work was supported by Fusion for Energy under the grant contract No. F4E-2010-GRT-050 (ES-SF). The views and opinions expressed herein reflect only the author's views. Fusion for Energy is not liable for any use that may be made of the information contained therein.

Appendix I: KIT Departments Contributing to the Fusion Programme

KIT Department	KIT Institut/Abteilung	Director	Ext.
Institute for Applied Materials - Applied Materials Physics	Institut für Angewandte Materialien – Angewandte Werkstoffphysik (IAM-AWP)	Prof. Dr. H.J. Seifert Dr. A. Möslang (Acting Head)	23895 24029
Institute for Applied Materials - Materials and Biomechanics	Institut für Angewandte Materialien - Werkstoff- und Biomechanik (IAM-WBM)	Prof. Dr. O. Kraft	24815
Institute for Applied Materials - Material Processing Technology	Institut für Angewandte Materialien - Werkstoffprozesstechnik (IAM-WPT)	Dr. R. Knitter (Acting Head)	22518
Institute for Pulsed Power and Microwave Technology	Institut für Hochleistungsimpuls- und Mikrowellentechnik (IHM)	Prof. Dr. J. Jelonnek	22440
Institute for Nuclear and Energy Technology	Institut für Kern- und Energietechnik (IKET)	Prof. Dr. T. Schulenberg	23450
Institute for Neutron Physics and Reactor Technology	Institut für Neutronenphysik und Reaktortechnik (INR)	Dr. R. Stieglitz	22550
Institute for Technical Physics	Institut für Technische Physik (ITeP)	Prof. Dr. M. Noe	23500
- Tritium Laboratory Karlsruhe	- Tritiumlabor Karlsruhe (TLK)	Dr. B. Bornschein	23239
Institute for Data Processing and Electronics	Institut für Prozessdatenverarbeitung und Elektronik (IPE)	Prof. Dr. M. Weber	25612

Appendix II: Fusion Programme Management Staff

Head of the Research Unit	Dr. K. Hesch	ext. 25460 e-mail: klaus.hesch@kit.edu
Secretariat:	Mrs. A. Knoll	ext. 25461 e-mail: anja.knoll@kit.edu
	Mrs. M.-E. Tuzia	ext. 22435 e-mail: maria-elena.tuzia@kit.edu
Program Budget, Administration, Reports, EU-Affairs	BW. M. Henn	ext. 25547 e-mail: michael.henn@kit.edu
	Mrs. I. Pleli	ext. 28292 e-mail: ingrid.pleli@kit.edu
Blanket and Divertor Development, HELOKA, IFMIF, Public Relations	Dr. D. Radloff	ext. 28750 e-mail: dirk.radloff@kit.edu
Fuel Cycle, Structural Materials, Superconducting Magnets, CAD-Office	DI. S. Gross	ext. 25468 e-mail: sigurd.gross@kit.edu
Plasma Heating Technology, Safety Studies, Neutronics, Physics	Dr. K. Hesch	ext. 25460 e-mail: klaus.hesch@kit.edu
Quality Management, Resource Loaded Planning, Document Management	Dr. J. Gafert	ext. 22923 e-mail: juergen.gafert@kit.edu
	Dr. I. Ignatiadis	ext. 85465 e-mail: Ioannis.ignatiadis@kit.edu
	Dr. M. Ionescu-Bujor	ext. 28325 e-mail: mihaela.ionescu-bujor@kit.edu
	Mrs. DI. B. Keim	ext. 24194 e-mail: birgit.keim@kit.edu
	Mrs. DI. Ch. Schweier	ext. 28325 e-mail: christine.schweier@kit.edu

Address: **Karlsruhe Institute of Technology**
Nuclear Fusion Programme Management

Post Office Box 3640, D - 76021 Karlsruhe / Germany

Telephone No: **0721-608-Extensions .....**

Telefax No: **0721-608-25467**

world wide web: **http://www.fusion.kit.edu/**

Appendix III: Publications

Plasma Wall Interaction

[1] Arnoux, G.; Bazylev, B.; Lehnen, M.; Loarte, A.; Riccardo, V.; Bozhenkov, S.; Devaux, S.; Eich, T.; Fundamenski, W.; Hender, T.; Huber, A.; Jachmich, S.; Kruezi, U.; Sergienko, G.; Thomsen, H.; JET EFDA Contributors
Heat load measurement on the JET first wall during disruptions.
Journal of Nuclear Materials, 415(2011) S.S817-S820, DOI:10.1016/j.jnucmat.2010.11.042

[2] Bazylev, B.; Arnoux, G.; Fundamenski, W.; Igitkhanov, Yu.; Lehnen, M.; JET EFDA Contributors.
Modeling of runaway electron beams for JET and ITER.
Journal of Nuclear Materials, 415(2011) S.S841-S844, DOI:10.1016/j.jnucmat.2010.11.086

[3] Bazylev, B.; Igitkhanov, Yu.; Landman, I.; Pestchanyi, S.; Loarte, A.
Erosion simulation of first wall beryllium armour after ITER transient heat loads and runaway electrons action.
Journal of Nuclear Materials, 417(2011) S.655-658, DOI:10.1016/j.jnucmat.2011.01.074

[4] Bazylev, B.; Landman, I.; Pitts, R.A.
Simulations of transient heat flux damage on leading edges in the ITER all-tungsten divertor.
15th Internat.Conf.on Fusion Reactor Materials, Charleston, S.C., October 16-22, 2011

[5] Coenen, J.W.; Bazylev, B.; Brezinsek, S.; Philipps, V.; Hirai, T.; Kreter, A.; Linke, J.; Sergienko, G.; Pospieszczyk, A.; Tanabe, T.; Ueda, Y.; Samm, U.;
TEXTOR-Team
Tungsten melt layer motion and splashing on castellated tungsten surfaces at the Tokamak TEXTOR.
Journal of Nuclear Materials, 415(2011) Suppl.1, S.S78-S82, DOI:10.1016/j.jnucmat.2010.09.046

[6] Garkusha, I.E.; Landman, I.; Linke, J.; Makhlay, V.A.; Medvedev, A.V.; Malykhin, S.V.; Peschanyi, S.; Pintsuk, G.; Pugachev, A.T.; Tereshin, V.I.
Performance of deformed tungsten under ELM-like plasma exposures in QSPA Kh-50.
Journal of Nuclear Materials, 415(2011) S.S65-S69
DOI:10.1016/j.jnucmat.2010.11.047

[7] Igitkhanov, Y.
Modelling of multi-component plasma for TOKES. KIT Scientific Reports, KIT-SR 7564 (März 2011)

[8] Igitkhanov, Y.; Bazylev, B.
Electric field and hot spots formation on divertor plates. Journal of Modern Physics, 2(2011) S.131-135, DOI:10.4236/jmp.2011.23020

[9] Igitkhanov, Y.; Bazylev, B.
The PFC erosion in DEMO due to runaway electrons. Fusion Science and Technology, 60(2011) S.349-353

[10] Igitkhanov, Yu.
On generation of runaway electrons during massive gas injection.
13th Internat.Workshop on Plasma Edge Theory in Fusion Devices (PET 13), South Lake Tahoe, Calif., September 19-21, 2011, European Fusion Theory Conf., Frascati, I, September 26-29, 2011

[11] Igitkhanov, Yu.; Bazylev, B.; Landman, I.
Calculation of runaway electrons stopping power in ITER. Journal of Nuclear Materials, 415(2011) S.S845-S848, DOI:10.1016/j.jnucmat.2010.11.071

[12] Igitkhanov, Yu.; Bazylev, B.; Pestchanyi, S.; Boccaccini, L.
Plasma facing materials lifetime in DEMO reactor. 10th Internat.Symp.on Fusion Nuclear Technology (ISFNT 2011), Portland, Oreg., September 11-16, 2011, Abstract on CD-ROM

[13] Klimov, N.; Podkovyrov, V.; Zhitlukhin, A.; Kovalenko, D.; Linke, J.; Pintsuk, G.; Landman, I.; Pestchanyi, S.; Bazylev, B.; Janeschitz, G.; Loarte, A.; Merola, M.; Hirai, T.; Federici, G.; Riccardi, B.; Mazul, I.; Giniyatulin, R.; Khimchenko, L.; Koidan, V.
Experimental study of PFCs erosion and eroded material deposition under ITER-like transient loads at the plasma gun facility QSPA-T. Journal of Nuclear Materials, 415(2011) S.S59-S64
DOI:10.1016/j.jnucmat.2011.01.013

[14] Landman, I.S.; Pestchanyi, S.E.; Igitkhanov, Y.; Pitts, R.
Two-dimensional modelling of disruption mitigation by massive gas injection.
Fusion Engineering and Design, 86(2011) S.1616-1619
DOI:10.1016/j.fusengdes.2010.12.017

[15] Litnovsky, A.; Philipps, V.; Wienhold, P.; Kreter, A.; Kirschner, A.; Matveev, D.; Brezinsek, S.; Sergienko, G.; Pospieszczyk, A.; Schweer, B.; Schulz, C.; Schmitz, O.; Coenen, J.W.; Samm, U.; Krieger, K.; Hirai, T.; Emmoth, B.; Rubel, M.; Bazylev, B.; Breuer, U.; Stärk, A.; Richter, S.; Komm, M.; TEXTOR Team
Overview of material migration and mixing, fuel retention and cleaning of ITER-like castellated structures in TEXTOR. Journal of Nuclear Materials, 415(2011) S.S289-S292
DOI:10.1016/j.jnucmat.2010.12.018

[16] Neudorfer, J.; Munz, C.D.; Stindl, T.; Schneider, R.; Roller, S.; Auweter-Kurtz, M.
Three-dimensional particle-in-cell simulation of a pulsed plasma truster: modelling and challenges.
32nd Internat.Electric Propulsion Conf., Wiesbaden, September 11-15, 2011

[17] Neudorfer, J.; Stindl, T.; Schneider, R.; Roller, S.; Munz, C.D.; Auweter-Kurtz, M.
Three-dimensional particle-in-cell simulation of a pulsed plasma truster: modelling and challenges.
32nd Internat.Electric Propulsion Conf., Wiesbaden, September 11-15, 2011
Proc.publ.online ; Fairview Park, Ohio : Electric Rocket Propulsion Society, 2011 Paper 116

[18] Pestchanyi, S.; Garkusha, I.; Landman, I.
Simulation of residual thermostress in tungsten after repetitive ELM-like heat loads.
Fusion Engineering and Design, 86(2011) S.1681-1684
DOI:10.1016/j.fusengdes.2011.01.034

[19] Pestchanyi, S.; Landman, I.
Verification of TOKES simulations against the MGI experiments in JET.
10th Internat.Symp.on Fusion Nuclear Technology (ISFNT 2011), Portland, Oreg., September 11-16, 2011

Physics: Heating and Current Drive – ECRH

[1] Aiello, G.; Meier, A.; Scherer, T.; Schreck, S.; spaeh, P.; Strauss, D.; Vaccaro, A.
Outgassing measurements for the ITER EC H&CD upper launcher.
23rd Joint Russian-German Meeting on ECRH and Gyrotrons, Karlsruhe/Stuttgart/Garching, May 23-28, 2011, Folien auf CD-ROM

[2] Aiello, G.; Meier, A.; Scherer, T.; Schreck, S.; Spaeh, P.; Strauss, D.; Vaccaro, A.
Outgassing measurements for the ITER EC H&CD upper launcher.
26th Symp.on Fusion Technology (SOFT 2010), Porto, P, September 27 - October 1, 2010

[3] Aiello, G.; Meier, A.; Scherer, T.; Schreck, S.; Spaeh, P.; Strauss, D.; Vaccaro, A.
Outgassing measurements for the ITER EC H&CD upper launcher.
Fusion Engineering and Design, 86(2011) S.2474-2477, OI:10.1016/j.fusengdes.2011.01.128

[4] Albajar, F.; Bonicelli, T.; Alberti, S.; Avramides, K.A.; Cirant, S.; Gantenbein, G.; Goodman, T.P.; Illy, S.; Ioannidis, Z.; Hogge, J.P.; Jin, J.; Kern, S.; Latsas, G.; Pagonakis, I.G.; Piosczyk, B.; Rzesnicki, T.; Thumm, M.; Tigelis, I.; Tran, M.Q.; Vomvoridis, J.; Benin, P.; Lievin, C.; Darbos, C.; Gassmann, T.; Henderson, M.
The European 2 MW gyrotron for ITER.
Prater, R. [Hrsg.]
Electron Cyclotron Emission and Electron Cyclotron Resonance Heating (EC-16) : Proc.of the 16th Joint Workshop, Sanya, China, April 12-15, 2010; Singapore [u.a.] : World Scientific, 2011 S.331-338, Incl.CD-ROM, ISBN 978-981-4340-26-7

[5] Beringer, M.H.
Design studies towards a 4 MW 170 GHz coaxial-cavity gyrotron.
Dissertation, Karlsruher Institut für Technologie 2010, Karlsruhe : KIT Scientific Publ., 2011 (Karlsruher Forschungsberichte aus dem Institut für Hochleistungsimpuls- und Mikrowellentechnik; Bd.1), ISBN 978-3-86644-663-2

[6] Beringer, M.H.; Illy, S.; Jin, J.; Kern, S.; Thumm, M.; Lievin, C.
Physical component designs and thermo-mechanical studies towards a 4 MW 170 GHz coaxial-cavity gyrotron.
ITG Vacuum Electronics Workshop, Bad Honnef, November 15-16, 2010, Folien auf CD-ROM

[7] Borie, E.
Computation of RF-behavior in gyrotrons.
10th School of Fusion Physics and Technology, Volos, GR, May 9-13, 2011

[8] Borie, E.; Gantenbein, G.; Illy, S.; Kern, S.; Leonhardt, W.; Smartsev, A.; Schlaich, A.; Schmid, M.; Thumm, M.
Development of 140 GHz, 1 MW, CW gyrotrons for fusion applications. Status and recent results.
10th School of Fusion Physics and Technology, Volos, GR, May 9-13, 2011

[9] Braune, H.; Erckmann, V.; Laqua, H.P.; Michel, G.; Noke, F.; Purps, F.; Schulz, T.; Wagner, D. ; W7-X ECRH Teams at IPP, IPF and KIT
Gyrotron high power long pulse operation. Challenges and solutions.
23rd Joint Russian-German Meeting on ECRH and Gyrotrons, Karlsruhe/Stuttgart/Garching, May 23-28, 2011, Folien auf CD-ROM

[10] Damyanova, M.; Kern, S.; Illy, S.; Thumm, M.; Sabchevski, S.; Zhelyazkov, I.; Vasileva, E.; Balabanova, E.
Simulation tools for computer aided design and numerical investigations of powerful gyrotrons.
17th Internat.Summer School on Vacuum, Electron and Ion Technologies, Sunny Beach, BG, September 19-23, 2011

[11] Erckmann, V. ; PMW- and W7-X Teams at KIT and IPP W7-X and ECRH. Status and prospects.
23rd Joint Russian-German Meeting on ECRH and Gyrotrons, Karlsruhe/Stuttgart/Garching, May 23-28, 2011, Folien auf CD-ROM

[12] Erckmann, V.; Kasparek, W.; Petelin, M.I.; Bruschi, A.; Bin, W.; Braune, H.; van den Braber, R.; Doelman, N.; Gantenbein, G.; Laqua, H.P.; Lechte, C.; Lubiako, L.; Marushchenko, N.B.; Michel, G.; Plaum, B.; Thumm, M. ; W7-X ECRH-Teams at IPP Greifswald, IPF Stuttgart, and KIT
ECRH with advanced CW systems.
8th Internat.Workshop 'Strong Microwaves and Terahertz Waves : Sources and Applications', Nizhny Novgorod, Russia, July 9-16, 2011

[13] Erckmann, V.; Kasparek, W.; Petelin, M.I.; Bruschi, A.; Bin, W.; Braune, H.; van den Braber, R.; Doelman, N.; Gantenbein, G.; Laqua, H.P.; Lechte, C.; Lubiako, L.; Marushchenko, N.B.; Michel, G.; Plaum, B.; Thumm, M. ; W7-X ECRH-Teams at IPP Greifswald, IPF Stuttgart, and KIT
ECRH with advanced CW systems.
8th Internat.Workshop 'Strong Microwaves and Terahertz Waves : Sources and Applications', Nizhny Novgorod, Russia, July 9-16, 2011, Proc. S.15-16
Nizhny Novgorod : Russian Academy of Sciences, 2011

[14] Erckmann, V.; Kasparek, W.; Plaum, B.; Lechte, C.; Petelin, M.I.; Bruschi, A.; D'Arcangelo, O.; Bin, W.; Braune, H.; van den Braber, R.; Doelman, N.; Gantenbein, G.; Laqua, H.P.; Lubiako, L.; Marushchenko, N.B.; Michel, G.; Thumm, M. ; W7-X ECRH-Teams at IPP Greifswald, IPF Stuttgart, and KIT
Large scale CW ECRH systems: meeting a challenge.
Joint Meeting of the 19th Topical Conf.on Radio Frequency Power in Plasmas and the US Japan RF Physics Workshop, Newport, R.I., June 1-3, 2011

[15] Erckmann, V.; Kasparek, W.; Plaum, B.; Lechte, C.; Petelin, M.I.; Bruschi, A.; D'Arcangelo, O.; Bin, W.; Braune, H.; van den Braber, R.; Doelman, N.; Gantenbein, G.; Laqua, H.P.; Lubiako, L.; Marushchenko, N.B.; Michel, G.; Thumm, M. ; W7-X ECRH-Teams at IPP Greifswald, IPF Stuttgart, and KIT
Large scale CW ECRH systems: meeting a challenge.
Radio Frequency Power in Plasmas : Proc.of the 19th Topical Conf., op, Newport, R.I., June 1-3, 2011, Melville, N.Y. : American Inst.of Physics, 2011 S.165-172 (AIP Conference Proceedings ; 1406) ISBN 978-0-735-0978-1

[16] Flamm, J.; Jin, J.; Thumm, M.
Comparison of different models of wave propagation in launchers of quasi-optical mode converters.
23rd Joint Russian-German Meeting on ECRH and Gyrotrons, Karlsruhe/Stuttgart/Garching, May 23-28, 2011, Folien auf CD-ROM

[17] Flamm, J.; Jin, J.; Thumm, M.
An FFT based spectral method for analysis of launchers in advanced gyrotron output couplers.
ITG Vacuum Electronics Workshop, Bad Honnef, November 15-16, 2010, Folien auf CD-ROM

[18] Flamm, J.; Jin, J.; Thumm, M.
Cylindrical wave decomposition in launchers of gyrotron quasi-optical mode converters.
2011 IEEE Internat.Vacuum Electronics Conf. (IVEC 2011), Bangalore, IND, February 21-24, 2011

[19] Flamm, J.; Jin, J.; Thumm, M.
Cylindrical wave decomposition in launchers of gyrotron quasi-optical mode converters.
2011 IEEE Internat.Vacuum Electronics Conf. (IVEC 2011) : Proc.of a meeting held in Bangalore, IND, February 21-24, 2011, Piscataway, N.J. : IEEE, 2011 S.111-112
ISBN 978-1-4244-8662-5

[20] Flamm, J.H.; Jin, J.; Thumm, M.K.
Wave propagation in advanced gyrotron output couplers.
Journal of Infrared, Millimeter, and Terahertz Waves, 32(2011) S.887-896
DOI:10.1007/s10762-011-9800-y

[21] Gantenbein, G.; Braune, H.; Dammertz, G.; Erckmann, V.; Illy, S.; Kern, S.; Kasparek, W.; Lechte, C.; Leonhardt, W.; Lievin, C.; Michel, G.; Noke, F.; Purps, F.; Samartsev, A.; Schlaich, A.; Schmid, M.; Thumm, M.
New results of the 140 GHz / 1 MW series gyrotrons for W-7X.
23rd Joint Russian-German Meeting on ECRH and Gyrotrons, Karlsruhe/Stuttgart/Garching, May 23-28, 2011, Folien auf CD-ROM

[22] Gantenbein, G.; Braune, H.; Dammertz, G.; Erckmann, V.; Illy, S.; Kern, I.S.; Kasparek, W.; Lechte, C.; Leonhardt, W.; Lievin, C.; Michel, G.; Noke, F.; Purps, F.; Samartsev, A.; Schlaich, A.; Schmid, M.; Thumm, M.
Status of 1 MW, 140 GHz series gyrotrons for W7-X.
36th Internat.Conf.on Infrared, Millimeter and Terahertz Waves (IRMMW-THz 2011), Houston, Tex., October 2-7, 2011

[23] Gantenbein, G.; Dammertz, G.; Kern, S.; Latsas, G.; Piosczyk, B.; Rzesnicki, T.; Samartsev, A.; Schlaich, A.; Thumm, M.; Tigelis, I.
Progress in stable operation of high power gyrotrons.
Prater, R. [Hrsg.]
Electron Cyclotron Emission and Electron Cyclotron Resonance Heating (EC-16) :
Proc.of the 16th Joint Workshop, Sanya, China, April 12-15, 2010
Singapore [u.a.] : World Scientific, 2011 S.347-352, Incl.CD-ROM, ISBN 978-981-4340-26-7

[24] Gantenbein, G.; Erckmann, V.; Illy, S.; Kern, S.; Kasparek, W.; Lechte, C.; Leonhardt, W.; Lievin, C.; Samartsev, A.; Schlaich, A.; Schmid, M.; Thumm, M.
140 GHz, 1 MW CW gyrotron development for fusion applications. Progress and recent results.
Journal of Infrared, Millimeter, and Terahertz Waves, 32(2011) S.320-328
DOI:10.1007/s10762-010-9749-2

[25] Gospodchikov, E.D.; Shalashov, A.G.; Smolyakova, O.B.; Bagryansky, P.A.; Malygin, V.I.; Gorbatushkov, V.N.; Amirov, V.Kh.; Thumm, M.
Design of auxiliary ECR heating system for the gas dynamic trap.
23rd Joint Russian-German Meeting on ECRH and Gyrotrons, Karlsruhe/Stuttgart/Garching, May 23-28, 2011, Folien auf CD-ROM

[26] Gospodchikov, E.D.; Shalashov, A.G.; Smolyakova, O.B.; Bagryansky, P.A.; Malygin, V.I.; Gorbatushkov, V.N.; Amirov, V.Kh.; Thumm, M.
Design of auxiliary ECR heating system for the gas dynamic trap.
8th Internat.Workshop 'Strong Microwaves and Terahertz Waves : Sources and Applications', Nizhny Novgorod, Russia, July 9-16, 2011

[27] Gospodchikov, E.D.; Shalashov, A.G.; Smolyakova, O.B.; Bagryansky, P.A.; Malygin, V.I.; Gorbatushkov, V.N.; Amirov, V.Kh.; Thumm, M.
Design of auxiliary ECR heating system for the gas dynamic trap.
8th Internat.Workshop 'Strong Microwaves and Terahertz Waves : Sources and Applications', Nizhny Novgorod, Russia, July 9-16, 2011, Proc. S.175-176
Nizhny Novgorod : Russian Academy of Sciences, 2011

[28] Henderson, M.; Albajar, F.; Alberti, S.; Baruah, U.; Bigelow, T.; Becket, B.; Bertizzolo, R.; Bonicelli, T.; Bruschi, A.; Caughman, J.; Chavan, R.; Cirant, S. ; Darbos, C.; deBaar, M.; Denisov, G.; Farina, D.; Gandini, F.; Gassmann, T.; Goodman, T.P.; Heidinger, R.; Hogge, J.P.; Kajiwara, K.; Kasparak, W.; Kasugai, A.; Kern, S.; Kobayashi, N.; Landis, J.D.; Moro, A.; Nazare, C.; Oda, J.; Omori, T.; Pagonakis, I.; Parmar, D.; Platania, P.; Plaum, B.; Poli, E.; Porte, L.; Piosczyk, B.; Purohit, D.; Ramponi, G.; Rao, S.L.; Rasmussen, D.; Ronden, D.; Saibene, G.; Sakamoto, K.; Sanchez, F.; Scherer, T.; Singh, N.P.; Shapiro, M.; Sozzi, C.; Spaeh, P.; Strauss, D.; Sauter, O.; Takahashi, K.; Temkin, R.; Thomas, P.; Thumm, M.; Zohm, H.
Present status of the 24 MW 170 GHz ITER EC H & D system.
8th Internat.Workshop 'Strong Microwaves and Terahertz Waves : Sources and Applications', Nizhny Novgorod, Russia, July 9-16, 2011

[29] Henderson, M.; Albajar, F.; Alberti, S.; Baruah, U.; Bigelow, T.; Becket, B.; Bertizzolo, R.; Bonicelli, T.; Bruschi, A.; Caughman, J.; Chavan, R.; Cirant, S. ; Darbos, C.; deBaar, M.; Denisov, G.; Farina, D.; Gandini, F.; Gassmann, T.; Goodman, T.P.; Heidinger, R.; Hogge, J.P.; Kajiwara, K.; Kasparak, W.; Kasugai, A.; Kern, S.; Kobayashi, N.; Landis, J.D.; Li, F.; Litvak, A.; Moro, A.; Myasnikov, V.; Nazare, C.; Oda, J.; Omori, T.; Pagonakis, I.; Parmar, D.; Peters, B.; Platania, P.; Plaum, B.; Poli, E.; Porte, L.; Piosczyk, B.; Purohit, D.; Ramponi, G.; Rao, S.L.; Rasmussen, D.; Ronden, D.; Saibene, G.; Sakamoto, K.; Sanchez, F.; Scherer, T.; Schreck, S.; Singh, N.P.; Shapiro, M.; Sozzi, C.; Spaeh, P.; Strauss, D.; Sauter, O.; Tai, E.; Takahashi, K.; Temkin, R.; Thomas, P.; Thumm, M.; Zohm, H.
Present status of the 24 MW 170 GHz ITER EC H & D system.
8th Internat.Workshop 'Strong Microwaves and Terahertz Waves: Sources and Applications', Nizhny Novgorod, Russia, July 9-16, 2011, Proc. S.21-22
Nizhny Novgorod : Russian Academy of Sciences, 2011

[30] Henderson, M.; Becket, B.; Cox, C.; Darbos, C.; Gandini, F.; Gassman, T.; Jean, O.; Nazare, C.; Omori, T.; Purohit, D.; Tanga, A.; Udintsev, V.; Albajar, F.; Bonicelli, T.; Heidinger, R.; Saibene, G.; Alberti, S.; Bertizzolo, R.; Chavan, R.; Collazos, A.; Goodman, T.P.; Hogge, J.P.; Landis, J.D.; Paganakis, I.; Porte, L.; Sanchez, F.; Sauter, O.; Tran, M.Q.; Zucca, C.; Baruah, U.; Kushwah, M.; Singh, N.P.; Rao, S.L.; Bigelow, T.; Caughman, J.; Rasmussen, D.; Bruschi, A.; Cirant, S.; Farina, D.; Moro, A.; Platania, P.; Ramponi, G.; Sozzi, C.; De Baar, M.; Ronden, D.; Denisov, G.; Kajiwara, K.; Kasugai, A.; Kobayashi, N.; Oda, Y.; Sakamoto, K.; Takahashi, K.; Kasparek, W.; Kumric, H.; Plaum, B.; Aiello, G.; Gantenbein, G.; Illy, S.; Jin, J.; Kern, S.; Meier, A.; Piosczyk, B.; Rzesnicki, T.; Scherer, T.; Schreck, S.; Serikov, A.; Spaeh, P.; Strauss, D.; Thumm, M.; Vaccaro, A.; Poli, E.; Zohm, H.; Shapiro, M.; Temkin, R.
The ITER EC H&CD system.
Prater, R. [Hrsg.]
Electron Cyclotron Emission and Electron Cyclotron Resonance Heating (EC-16) :
Proc.of the 16th Joint Workshop, Sanya, China, April 12-15, 2010
Singapore [u.a.] : World Scientific, 2011 S.353-363, Incl.CD-ROM, ISBN 978-981-4340-26-7

[31] Illy, S.; Gantenbein, G.; Schmid, M.; Weggen, J.
Design, construction and first tests of a stainless steel load for high power mm-wave radiation.
23rd Joint Russian-German Meeting on ECRH and Gyrotrons, Karlsruhe/Stuttgart/Garching,
May 23-28, 2011, Folien auf CD-ROM

[32] Illy, S.; Gantenbein, G.; Schmid, M.; Weggen, J.
Design, construction and first tests of a stainless steel load for high power mm-wave radiation.
38th IEEE Internat.Conf.on Plasma Science (ICOPS) and 24th Symp.on Fusion Engineering (SOFE), Chicago, Ill., June 26-30, 2011, Abstracts publ.online

[33] Jin, J.; Flamm, J.; Kern, S.; Rzesnicki, T.; Thumm, M.
Theoretical and experimental investigation of a quasi-optical mode converter for a coaxial-cavity gyrotron.
ITG Vacuum Electronics Workshop, Bad Honnef, November 15-16, 2010, Folien auf CD-ROM

[34] Jin, J.; Gantenbein, G.; Kern, S.; Rzesnicki, T.; Thumm, M.
A matching optics unit (MOU) for coaxial-cavity ITER gyrotron.
23rd Joint Russian-German Meeting on ECRH and Gyrotrons, Karlsruhe/Stuttgart/Garching,
May 23-28, 2011, Folien auf CD-ROM

[35] Jin, J.; Gantenbein, G.; Kern, S.; Rzesnicki, T.; Thumm, M.
Design matching optics unit (MOU) for coaxial ITER gyrotron.
2011 IEEE Internat.Vacuum Electronics Conf. (IVEC 2011), Bangalore, IND,
February 21-24, 2011

[36] Jin, J.; Gantenbein, G.; Kern, S.; Rzesnicki, T.; Thumm, M.
Design matching optics unit (MOU) for coaxial ITER gyrotron.
2011 IEEE Internat.Vacuum Electronics Conf. (IVEC 2011) : Proc.of a meeting held in Bangalore, IND, February 21-24, 2011, Piscataway, N.J. : IEEE, 2011 S.271-272, ISBN 978-1-4244-8662-5

[37] Jin, J.; Rzesnicki, T.; Kern, S.; Thumm, M.
High-efficiency quasi-optical mode converter for the coaxial cavity gyrotron.
Fusion Science and Technology, 59(2011) S.742-748

[38] Kalaria, P.C.; Kartikeyan, M.V.; Thumm, M.
Design considerations of a 170 GHz, 0.5 MW, CW gyrotron.
Internat.Conf.on Microwaves, Antenna, Propagation and Remote Sensing (ICMARS),
Jodhpur, IND, December 7-10, 2011

[39] Kalaria, P.C.; Kartikeyan, M.V.; Thumm, M.
Design studies of quasi-optical launcher of a 170 GHz, CW gyrotron for ECRH application.
Internat.Conf.on Microwaves, Antenna, Propagation and Remote Sensing (ICMARS),
Jodhpur, IND, December 7-10, 2011

[40] Kasparek, W.; Erckmann, V.; Hollmann, F.; Michel, G.; Noke, F.; Purps, F.; Plaum, B.; Brand, P.; Lechte, C.; Filipovic, E.; Saliba, M.; Doelmann, N.; van den Braber, R.; Bongers, W.; Krijger, B.; Petelin, M.; Shchegolkov, D.; Koposova, E.; Lubyako, L.; Bruschi, A.; Bin, W.; D'Arcangelo, O.; Stober, J.; Wagner, D. ; Groups at IPF Stuttgart, IAP N.Novgorod, IPP Garching and Greifswald, IFP Milano, KIT Karlsruhe, TNO Delft and FOM Rijnhuizen
Status of development of compact diplexers for ECRH applications.
23rd Joint Russian-German Meeting on ECRH and Gyrotrons, Karlsruhe/Stuttgart/Garching, May 23-28, 2011, Folien auf CD-ROM

[41] Kern, S.; Avramides, K.A.; Roy Choudhury, A.; Dumbrajs, O.; Gantenbein, G.; Illy, S.; Samartsev, A.; Schlaich, A.; Thumm, M.
Simulation and experimental investigation on dynamic after cavity interaction (ACI).
36th Internat.Conf.on Infrared, Millimeter and Terahertz Waves (IRMMW-THz 2011), Houston, Tex., October 2-7, 2011

[42] Kern, S.; Roy Choudhury, A.; D'Andrea, D.; Schlaich, A.; Avramides, K.; Alberti, S.
Recent advances in gyrotron interaction simulations.
23rd Joint Russian-German Meeting on ECRH and Gyrotrons, Karlsruhe/Stuttgart/Garching, May 23-28, 2011, Folien auf CD-ROM

[43] Li, F.; ALberti, S.; Hogge, J.P.; Pagonakis, I.G.
Calculation of stray magnetic field effects on the operation of the ITER electron cyclotron system.
38th IEEE Internat.Conf.on Plasma Science (ICOPS) and 24th Symp.on Fusion Engineering (SOFE), Chicago, Ill., June 26-30, 2011

[44] Li, F.; Alberti, S.; Hogge, J.P.; Pagonakis, I.G.
Calculation of stray magnetic field effects on the operation of the ITER electron cyclotron system.
38th IEEE Internat.Conf.on Plasma Science (ICOPS) and 24th Symp.on Fusion Engineering (SOFE), Chicago, Ill., June 26-30, 2011, Piscataway, N.J. : IEEE, 2011 Paper SP2-27
ISBN 978-1-4577-0669-1
Proc.also publ.online, e-ISBN 978-1-4577-0667-7, DOI:10.1109/SOFE.2011.6052289

[45] Litvak, A.; Sakamoto, K.; Thumm, M.
Innovation on high power long pulse gyrotrons.
38th EPS Conf.on Plasma Physics, Strasbourg, F, June 27 - July 1, 2011

[46] Litvak, A.; Sakamoto, K.; Thumm, M.
Innovation on high-power long-pulse gyrotrons.
Plasma Physics and Controlled Fusion, 53(2011) S.124002/1-14
DOI:10.1088/0741-3335/53/12/124002

[47] Malygin, A.V.; Pagonakis, I.Gr.; Illy, S.; Avramides, K.A.; Piosczyk, B.; Kern, S.; Thumm, M.
Three-dimensional numerical studies of non-uniform emission in magnetron injection guns.
8th Internat.Workshop 'Strong Microwaves and Terahertz Waves : Sources and Applications', Nizhny Novgorod, Russia, July 9-16, 2011

[48] Malygin, A.V.; Pagonakis, I.Gr.; Illy, S.; Avramides, K.A.; Piosczyk, B.; Kern, S.; Thumm, M.
Three-dimensional numerical studies of non-uniform emission in magnetron injection guns.
8th Internat.Workshop 'Strong Microwaves and Terahertz Waves : Sources and Applications', Nizhny Novgorod, Russia, July 9-16, 2011, Proc. S.99-100
Nizhny Novgorod : Russian Academy of Sciences, 2011

[49] Neudorfer, J.; Munz, C.D.; Schneider, R.
High order PIC simulation of high power millimeter wave sources.
38th IEEE Internat.Conf.on Plasma Science (ICOPS) and 24th Symp.on Fusion Engineering (SOFE), Chicago, Ill., June 26-30, 2011, Abstract publ.online

[50] Neudorfer, J.; Stindl, T.; Stock, A.; Schneider, R.; Petkow, D.; Roller, S.; Munz, C.D.; Auweter-Kurtz, M.
Three-dimensional simulation of rarefied plasma flows using a high order particle in cell method.
Nagel, W. [Hrsg.]
High Performance Computing in Science and Engineering '10 : Transactions of the High Performance Computing Center, Stuttgart (HLRS) 2010
Berlin [u.a.] : Springer, 2011 S.593-604; ISBN 978-3-642-15747-9
DOI:10.1007/978-3-642-15748-6_43

[51] Neudorfer, J.; Stock, A.; D'Andrea, D.; Illy, S.; Kern, S.; Munz, C.D.; Schneider, R.
High order parallel PIC simulations of microwaves devices.
23rd Joint Russian-German Meeting on ECRH and Gyrotrons, Karlsruhe/Stuttgart/Garching, May 23-28, 2011, Folien auf CD-ROM

[52] Neudorfer, J.; Stock, A.; D'Andrea, D.; Illy, S.; Kern, S.; Schneider, R.; Roller, S.; Munz, C.D.
High-order PIC simulations of microwave sources.
36th Internat.Conf.on Infrared, Millimeter and Terahertz Waves (IRMMW-THz 2011), Houston, Tex., October 2-7, 2011

[53] Omori, T.; Henderson, M.A.; Albajar, F.; Alberti, S.; Baruah, U.; Bigelow, T.; Beckett, B.; Bertizzolo, R.; Bonicelli, T.; Bruschi, A.; Caughman, J.; Chavan, R.; Cirant, S.; Collazos, A.; Cox, D.; Darbos, C.; de Baar, M.R.; Denisov, G.; Farina, D.; Gandini, F.; Gassmann, T.; Goodman, T.P.; Heidinger, R.; Hogge, J.P. ; Illy, S.; Jean, O.; Jin, J.; Kajiwara, K.; Kasparek, W.; Kasugai, A.; Kern, S. ; Kobayashi, N.; Kumric, H.; Landis, J.D.; Moro, A.; Nazare, C.; Oda, Y.; Pagonakis, I.; Piosczyk, B.; Platania, P.; Plaum, B.; Poli, E.; Porte, L.; Purohit, D.; Ramponi, G.; Rao, S.L.; Rasmussen, D.A.; Ronden, D.M.S.; Rzesnicki, T.; Saibene, G.; Sakamoto, K.; Sanchez, F.; Scherer, T.; Shapiro, M.; Sozzi, C. ; Spaeh, P.; Strauss, D.; Sauter, O.; Takahashi, K.; Temkin, R.; Thumm, M.; Tran, M.Q.; Udintsev, V.; Zohm, H.
Overview of the ITER EC H&CD system and its capabilities.
Fusion Engineering and Design, 86(2011) S.951-954, DOI:10.1016/j.fusengdes.2011.02.040

[54] Pagonakis, I.Gr.; Illy, S.; Piosczyk, B.; Kern, S.; Hogge, J.P.; Alberti, S.
A new criterion for gyrotron gun design.
23rd Joint Russian-German Meeting on ECRH and Gyrotrons, Karlsruhe/Stuttgart/Garching, May 23-28, 2011, Folien auf CD-ROM

[55] Pagonakis, I.Gr.; Illy, S.; Piosczyk, B.; Li, F.; Alberti, S.; Darbos, C.; Henderson, M.
The effect of the ITER stray magnetic field on the operation of the EU 2 MW coaxial cavity gyrotron.
23rd Joint Russian-German Meeting on ECRH and Gyrotrons, Karlsruhe/Stuttgart/Garching, May 23-28, 2011, Folien auf CD-ROM

[56] Pagonakis, I.Gr.; Li, F.; Alberti, S.; Illy, S.; Piosczyk, B.; Hogge, J.P.; Kern, S.; Ferran, A.; Henderson, M.; Darbos, C.
The effect of the ITER stray magnetic field on the operation of the EU 2 MW coaxial cavity gyrotron.
8th Internat.Workshop 'Strong Microwaves and Terahertz Waves : Sources and Applications', Nizhny Novgorod, Russia, July 9-16, 2011

[57] Roy Choudhury, A.; Kern, S.; D'Andrea, D.; Schlaich, A.; Thumm, M.
Influence of tapered magnetic field on gyrotron interaction calculation.
23rd Joint Russian-German Meeting on ECRH and Gyrotrons, Karlsruhe/Stuttgart/Garching, May 23-28, 2011, Folien auf CD-ROM

[58] Rzesnicki, T.; Piosczyk, B.; Gantenbein, G.; Illy, S.; Jin, J.; Kern, S.; Losert, M.; Pagonakis, I.; Samartsev, A.; Schlaich, A.; Thumm, M.
2 MW, 170 GHz coaxial-cavity gyrotron for ITER. Experimental results obtained with a short-pulse pre-prototype tube.
US-EU-JPN RF Heating Technology Workshop, Austin, Tex., October 10-12, 2011

[59] Rzesnicki, T.; Piosczyk, B.; Gantenbein, G.; Illy, S.; Jin, J.; Kern, S.; Pagonakis, I.; Samartsev, A.; Schlaich, A.; Thumm, M.
Recent experimental investigations on the 2 MW, 170 GHz coaxial cavity pre-prototype gyrotron for ITER.
23rd Joint Russian-German Meeting on ECRH and Gyrotrons, Karlsruhe/Stuttgart/Garching, May 23-28, 2011, Folien auf CD-ROM

[60] Rzesnicki, T.; Piosczyk, B.; Illy, S.; Jin, J.; Kern, S.; Pagonakis, I.; Samartsev, A.; Schlaich, A.; Thumm, M.
2 MW, 170 GHz coaxial-cavity gyrotron for ITER. Results obtained with a short pulse pre-prototype at KIT.
8th Internat.Workshop 'Strong Microwaves and Terahertz Waves : Sources and Applications', Nizhny Novgorod, Russia, July 9-16, 2011

[61] Rzesnicki, T.; Piosczyk, B.; Illy, S.; Jin, J.; Kern, S.; Pagonakis, I.; Samartsev, A.; Schlaich, A.; Thumm, M.
2 MW, 170 GHz coaxial-cavity gyrotron for ITER. Results obtained with a short pulse pre-prototype at KIT.
8th Internat.Workshop 'Strong Microwaves and Terahertz Waves : Sources and Applications', Nizhny Novgorod, Russia, July 9-16, 2011, Proc. S.121-122
Nizhny Novgorod : Russian Academy of Sciences, 2011

[62] Rzesnicki, T.; Piosczyk, B.; Roy Choudhury, A.; Illy, S.; Jin, J.; Kern, S.; Samartsev, A.; Schlaich, A.; Thumm, M.
Recent improvements on the 2 MW, 170 GHz coaxial-cavity pre-prototype gyrotron.
ITG Vacuum Electronics Workshop, Bad Honnef, November 15-16, 2010
Folien auf CD-ROM

[63] Samartsev, A.; Gantenbein, G.; Dammertz, G.; Illy, S.; Kern, S.; Schlaich, A.; Thumm, M.
Current status of multi-frequency gyrotron development.
23rd Joint Russian-German Meeting on ECRH and Gyrotrons, Karlsruhe/Stuttgart/Garching, May 23-28, 2011, Folien auf CD-ROM

[64] Samartsev, A.; Gantenbein, G.; Dammertz, G.; Illy, S.; Kern, S.; Leonhardt, W.; Schlaich, A.; Schmid, M.; Thumm, M.
Development of frequency step tunable 1 MW gyrotron at 131 to 146.5 GHz.
2011 IEEE Internat.Vacuum Electronics Conf. (IVEC 2011), Bangalore, IND, February 21-24, 2011

[65] Samartsev, A.; Gantenbein, G.; Dammertz, G.; Illy, S.; Kern, S.; Leonhardt, W.; Schlaich, A.; Schmid, M.; Thumm, M.
Development of frequency step tunable 1 MW gyrotron at 131 to 146.5 GHz.
2011 IEEE Internat.Vacuum Electronics Conf. (IVEC 2011) : Proc.of a meeting held in Bangalore, IND, February 21-24, 2011, Piscataway, N.J. : IEEE, 2011 S.269-270
ISBN 978-1-4244-8662-5

[66] Samartsev, A.; Gantenbein, G.; Illy, S.; Kern, S.; Latsas, G.; Thumm, M.; Tigelis, I.
Numerical simulation of parasitic gyro-BWO interaction in a gyrotron beam tunnel.
36th Internat.Conf.on Infrared, Millimeter and Terahertz Waves (IRMMW-THz 2011), Houston, Tex., October 2-7, 2011

[67] Scherer, T.; Strauss, D.; Meier, A.
CVD diamond for sub-mm and THz applications.
Frühjahrstagung DPG, Fachverband Dielektrische Festkörper, Dresden, 13.-18.März 2011
Verhandlungen der Deutschen Physikalischen Gesellschaft, R.6, B.46(2011) DF 18.3

[68] Scherer, T.; Strauss, D.; Meier, A.; Mathis, Y.L.; Judin, V.; Müller-Sebert, W.; Smirnov, W.; Nebel, C.
Investigation of microwave and THz radiation losses in CVD diamond and chemically modified diamond.
Materials Research Society Fall Meeting 2010, Boston, Mass., November 29 - December 3, 2010
Diamond Electronics and Bioelectronics : Fundamentals to Applications IV ;
Proc.of Symp.A of MRS Fall Meeting 2010, Boston, Mass., November 29 - December 3, 2010, Warrendale, Pa. : MRS, 2011 mrsf10-1282-a15-01
(Materials Research Society Symposium Proceedings ; 1282), DOI:10.1557/opl.2011.452

[69] Scherer, T.A.; Meier, A.; Landmann, A.
Dielectric properties of natural grown Tourmaline at 100 GHz.
36th Internat.Conf.on Infrared, Millimeter and Terahertz Waves (IRMMW-THz 2011), Houston, Tex., October 2-7, 2011

[70] Scherer, T.A.; Meier, A.; Strauss, D.; Schreck, S.; Takahashi, K.; Kajiwara, K.; Oda, Y.; Sakamoto, K.; Saibene, G.
Experimental analysis of the inserted waveguide CVD diamond window prototype for the ITER ECRH upper launcher.
36th Internat.Conf.on Infrared, Millimeter and Terahertz Waves (IRMMW-THz 2011), Houston, Tex., October 2-7, 2011

[71] Scherer, T.A.; Meier, A.; Strauss, D.; Schreck, S.; Takahashi, K.; Kajiwara, K.; Oda, Y.; Sakamoto, K.
Low and high power microwave testing of the new prototype II ITER torus CVD diamond window with inserted waveguides.
23rd Joint Russian-German Meeting on ECRH and Gyrotrons, Karlsruhe/Stuttgart/Garching, May 23-28, 2011, Folien auf CD-ROM

[72] Scherer, T.A.; Strauss, D.; Schreck, S.; Meier, A.; Müller-Sebert, W.; Nebel, C.
Investigations of microwave absorption of surface modified CVD diamond disks for fusion applications.
22nd European Conference on Diamond, Diamond-Like Materials, Carbon Nanotubes and Nitrides (DIAMOND 2011), Garmisch-Partenkirchen, September 4-8, 2011

[73] Scherer, T.A.; Strauss, D.; Vaccaro, A.; Aiello, G.; Schreck, S.; Meier, A.; Späh, P.
Recent upgrades of the ITER ECRH CVD torus diamond window design and investigation of dielectric diamond properties.
Prater, R. [Hrsg.]
Electron Cyclotron Emission and Electron Cyclotron Resonance Heating (EC-16) :
Proc.of the 16th Joint Workshop, Sanya, China, April 12-15, 2010
Singapore [u.a.] : World Scientific, 2011 S.396-400, Incl.CD-ROM, ISBN 978-981-4340-26-7

[74] Scherer, T.A.; Strauss, D.; Vaccaro, A.; Aiello, G.; Schreck, S.; Meier, A.; Späh, P.; Takahashi, K.; Kajiwara, K.; Oda, Y.; Sakamoto, K.
Recent upgrades of the ITER ECRH launcher double wall structure and the new CVD torus diamond window design II.
US-EU-JPN RF Heating Technology Workshop, Austin, Tex., October 10-12, 2011

[75] Schlaich, A.; Choudhury, A.R.; Gantenbein, G.; Illy, S.; Kern, S.; Lievin, C.; Samartsev, A.; Thumm, M.
Examination of parasitic after-cavity oscillations in the W7-X series gyrotron SN4R.
US-EU-JPN RF Heating Technology Workshop, Austin, Tex., October 10-12, 2011

[76] Schlaich, A.; Flamm, J.; Gantenbein, G.; Kern, S.; Samartsev, A.; Thumm, M.
Characterization of undesired RF oscillations in megawatt gyrotrons.
ITG Vacuum Electronics Workshop, Bad Honnef, November 15-16, 2010, Folien auf CD-ROM

[77] Schlaich, A.; Illy, S.; Kern, S.; Samartsev, A.; Thumm, M.
Recent examinations of the W7-X-SN4R gyrotron RF output spectrum.
23rd Joint Russian-German Meeting on ECRH and Gyrotrons, Karlsruhe/Stuttgart/Garching, May 23-28, 2011, Folien auf CD-ROM

[78] Schmid, M.; Erckmann, V.; Gantenbein, G.; Illy, S.; Kern, S.; Lievin, Ch.; Samartsev, A.; Schlaich, A.; Rzesnicki, T.; Thumm, M.
Technical developments at the KIT gyrotron test facility.
Fusion Engineering and Design, 86(2011) S.518-521, DOI:10.1016/j.fusengdes.2011.01.072

[79] Schreck, S.; Scherer, T.A.; Strauss, D.; Meier, A.; Sakomoto, K.; Takahashi, K.; Kajiwara, K.; Oda, Y.; Saibene, G.
CVD diamond torus windows for ITER ECRH prototype design and experimental investigations.
8th Internat.Workshop 'Strong Microwaves and Terahertz Waves : Sources and Applications', Nizhny Novgorod, Russia, July 9-16, 2011

[80] Schreck, S.; Scherer, T.A.; Strauss, D.; Meier, A.; Sakomoto, K.; Takahashi, K.; Kajiwara, K.; Oda, Y.; Saibene, G.
CVD diamond torus windows for ITER ECRH prototype design and experimental investigations.
8th Internat.Workshop 'Strong Microwaves and Terahertz Waves : Sources and Applications', Nizhny Novgorod, Russia, July 9-16, 2011, Proc. S.335-336
Nizhny Novgorod : Russian Academy of Sciences, 2011

[81] Sozzi, C.; Giruzzi, G.; Lennholm, M.; Parkin, A.; Aiello, G.; Bellinger, M.; Bird, J.; Bouquey, F.; Braune, H.; Bruschi, A.; Butcher, P.; Clay, R.; de la Luna, E.; Denisov, G.; Edlington, T.; fanthome, J.; Farina, d.; Farthing, J.; Figini, L.; Garavaglia, S.; Garcia, J.; Gardener, M.; Gerbaud, T.; Granucci, G.; Hay, H.; Henderson, M.; Hotchin, S.; Ilyin, V.N.; Jennison, M.; Kasparek, W.; Khilar, P.; Kirneva, N.; Kislov, D.; Knipe, S.; Kuyanov, A.; Litaudon, X.; Litvak, A.G.; Moro, A.; Nowak, S.; Parail, V.; Plau, B.; Saibene, G.; Späh, P.; Strauss, D.; Trukhina, E.; Vaccaro, A.; Vagdama, A.; Vdovin, V. ; JET EFDA Contributors
Conceptual design of an ECRH system for JET.
8th Internat.Workshop 'Strong Microwaves and Terahertz Waves : Sources and Applications', Nizhny Novgorod, Russia, July 9-16, 2011

[82] Sozzi, C.; Giruzzi, G.; Lennholm, M.; Parkin, A.; Aiello, G.; Bellinger, M.; Bird, J.; Bouquey, F.; Braune, H.; Bruschi, A.; Butcher, P.; Clay, R.; de la Luna, E.; Denisov, G.; Edlington, T.; fanthome, J.; Farina, d.; Farthing, J.; Figini, L.; Garavaglia, S.; Garcia, J.; Gardener, M.; Gerbaud, T.; Granucci, G.; Hay, H.; Henderson, M.; Hotchin, S.; Ilyin, V.N.; Jennison, M.; Kasparek, W.; Khilar, P.; Kirneva, N.; Kislov, D.; Knipe, S.; Kuyanov, A.; Litaudon, X.; Litvak, A.G.; Moro, A.; Nowak, S.; Parail, V.; Plau, B.; Saibene, G.; Späh, P.; Strauss, D.; Trukhina, E.; Vaccaro, A.; Vagdama, A.; Vdovin, V. ; JET EFDA Contributors
Conceptual design of an ECRH system for JET.
8th Internat.Workshop 'Strong Microwaves and Terahertz Waves : Sources and Applications', Nizhny Novgorod, Russia, July 9-16, 2011, Proc. S.163-164
Nizhny Novgorod : Russian Academy of Sciences, 2011

[83] Spaeh, P.; Aiello, G.; de Baar, M.; Chavan, R.; Elzendoorn, B.; Goodman, T.; Henderson, M.; Kleefeldt, K.; Landis, J.D.; Meier, A.; Ronden, D.; Saibene, G.; Scherer, T.; Schreck, S.; Serikov, A.; Strauss, D.; Vaccaro, A.
The ITER EC H&CD upper launcher: structural design.
26th Symp.on Fusion Technology (SOFT 2010), Porto, P, September 27 - October 1, 2010

[84] Spaeh, P.; Aiello, G.; de Baar, M.; Chavan, R.; Elzendoorn, B.; Goodman, T.; Henderson, M.; Kleefeldt, K.; Landis, J.D.; Meier, A.; Ronden, D.; Saibene, G.; Scherer, T.; Schreck, S.; Serikov, A.; Strauss, D.; Vaccaro, A.
The ITER EC H&CD upper launcher: structural design.
Fusion Engineering and Design, 86(2011) S.724-727, DOI:10.1016/j.fusengdes.2011.03.115

[85] Späh, P.; Aiello, G.; Kleefeldt, K.; Meier, A.; Scherer, T.; Schreck, S.; Strauss, d.; Vaccaro, A.; Serikov, A.; Goldmann, A.; Kroiss, A.; Obermeier, C.
Manufacturing studies of double wall components for the ITER EC H&CD upper launcher.
10th Internat.Symp.on Fusion Nuclear Technology (ISFNT 2011), Portland, Oreg., September 11-16, 2011

[86] Späh, P.; Vaccaro, A.; Aiello, G.; Giruzzi, G.; Lennholm, M.; Sozzi, C.; Strauss, D.
Structural design and analysis of an ECRH launcher for JET.
38th IEEE Internat.Conf.on Plasma Science (ICOPS) and 24th Symp.on Fusion Engineering (SOFE), Chicago, Ill., June 26-30, 2011

[87] Späh, P.; Vaccaro, A.; Aiello, G.; Giruzzi, G.; Lennholm, M.; Sozzi, C.; Strauss, D.
Structural design and analysis of an ECRH launcher for JET.
38th IEEE Internat.Conf.on Plasma Science (ICOPS) and 24th Symp.on Fusion Engineering (SOFE), Chicago, Ill., June 26-30, 2011, Proc.publ.online, Piscataway, N.J. : IEEE, 2011 Paper SP3-17, DOI:10.1109/SOFE.2011.6052319

[88] Stindl, T.; Neudorfer, J.; Stock, A.; Auweter-Kurtz, M.; Munz, C.D.; Roller, S.; Schneider, R.
Comparison of coupling techniques in a high-order discontinuous Galerkin-based particle-in-cell solver.
Journal of Physics D, 44(2011) S.194004/1-9, DOI:10.1088/0022-3727/44/19/194004

[89] Stober, J. ; ASDEX Upgrade Team; GYCOM, IAP, KIT, IPF, IPP Greifswald
The ECRH system of ASDEX upgrade. Status and plans.
23rd Joint Russian-German Meeting on ECRH and Gyrotrons, Karlsruhe/Stuttgart/Garching, May 23-28, 2011, Folien auf CD-ROM

[90] Stober, J.; Leuterer, F.; Monaco, F.; Müller, S.; Münich, M.; Schubert, M.; Schütz, H.; Wagner, D.; Zohm, H.; Thumm, M.; Scherer, T.; Meier, A.; Gantenbein, G.; Flamm, J.; Kasparek, W.; Lecht, C.; Litvak, A.G.; Denisov, G.G.; Chirkov, A.; Popov, L.G.; Nichiporenko, V.O.; Myasnikov, V.E.; Tai, E.M.; Solyanova, E.A. ; Malygin, S.A.; Belov, Y.
Status and plans for an extension of the ECRH systems on ASDEX upgrade.
23rd Joint Russian-German Meeting on ECRH and Gyrotrons, Karlsruhe/Stuttgart/Garching, May 23-28, 2011, Folien auf CD-ROM

[91] Stober, J.; Wagner, D.; Giannone, L.; Leuterer, F.; Maraschek, M.; Mlynek, A.; Monaco, F.; Münich, M.; Poli, E.; Reich, M.; Schmid-Lorch, D.; Schütz, H.; Schweinzer, J.; Treutterer, W.; Zohm, H.; Meier, A.; Scherer, T.; Flamm, J.; Thumm, M.; Höhnle, H.; Kasparek, W.; Stroth, U.; Chirkov, A.V.; Denisov, G.G.; Litvak, A.; Malygin, S.A.; Myasnikov, V.E.; Nichiporenko, V.O.; Popov, L.G.; Soluyanova, E.A.; Tai, E.M.
ECRH on ASDEX upgrade. System extension, new modes of operation, plasma physics results.
Prater, R. [Hrsg.]
Electron Cyclotron Emission and Electron Cyclotron Resonance Heating (EC-16) : Proc.of the 16th Joint Workshop, Sanya, China, April 12-15, 2010
Singapore [u.a.] : World Scientific, 2011 S.28-41, Incl.CD-ROM, ISBN 978-981-4340-26-7

[92] Stock, A.; Neudorfer, J.; D'Andrea, D.; Munz, C.D.; Schneider, R.; Roller, S.
High-order PIC simulation of high power millimeter wave sources components.
38th EPS Conf.on Plasma Physics, Strasbourg, F, June 27 - July 1, 2011

[93] Strauss, D.; Aiello, G.; Chavan, R.; Cirant, S.; deBaar, M.; Farina, D.; Gantenbein, G.; Goodman, T.; Henderson, M.A.; Kasparek, W.; Kleefeldt, K.; Landis, J.D.; Meier, A.; Moro, A.; Plaum, B.; Poli, E.; Ramponi, G.; Ronden, D.; Saibene, G.; Sanchez, F.; Sautter, O.; Scherer, T.; Schreck, S.; Serikov, A.; Sozzi, C.; Spaeh, P.; Vaccaro, A.; Zohm, H.
Preliminary design of the ITER ECH upper launcher.
38th IEEE Internat.Conf.on Plasma Science (ICOPS) and 24th Symp.on Fusion Engineering (SOFE), Chicago, Ill., June 26-30, 2011, Abstract online
DOI:10.1109/SOFE.2011.6052319

[94] Strauss, D.; Flamm, J.; Gantenbein, G.; Meier, A.; Scherer, T.A.; Thumm, M.; Vaccaro, A.; Stober, J.; Wagner, D.; Denisov, G.G.
ECH beyond ITER: broadband diamond windows.
23rd Joint Russian-German Meeting on ECRH and Gyrotrons, Karlsruhe/Stuttgart/Garching, May 23-28, 2011, Folien auf CD-ROM

[95] Strauss, D.; Scherer, T.; Aiello, G.; Meier, A.; Schreck, S.; Späh, P.; Vaccaro, A.
Deflections and vibrations of the ITER ECRH upper launcher.
Prater, R. [Hrsg.]
Electron Cyclotron Emission and Electron Cyclotron Resonance Heating (EC-16) : Proc.of the 16th Joint Workshop, Sanya, China, April 12-15, 2010
Singapore [u.a.] : World Scientific, 2011 S.370-375, Incl.CD-ROM, ISBN 978-981-4340-26-7

[96] Thumm, M.
Lecture series on high-power quasi-optical mm-wave transmission and mode converters for ECRH. 5: High-power millimetre wave quasi-optical components and mode converters.
Vortr.: Budker Institute of Nuclear Physics, Novosibirsk, Russia, 20.April 2011

[97] Thumm, M.
Lecture series on high-power quasi-optical mm-wave transmission and mode converters for ECRH. 6: 10 MW, 140 GHz, CW gyrotron and optical transmission system for the stellarator Wendelstein 7-x (W7-X).
Vortr.: Budker Institute of Nuclear Physics, Novosibirsk, Russia, 21.April 2011

[98] Thumm, M.
Progress on gyrotrons for ITER and future thermonuclear fusion reactors.
IEEE Transactions on Plasma Science, 39(2011) S.971-979
DOI:10.1109/TPS.2010.2095042

[99] Thumm, M.
Progress on gyrotrons for ITER, W7-X and future magnetic confinement fusion reactors.
Vortr.: Novosibirsk State Technical University, 6.Dezember 2011

[100] Thumm, M.
Lecture series on overmoded waveguide transmission. 1: Attenuation and mode conversion in overmoded waveguide.
Vortr.: Budker Institute of Nuclear Physics, Novosibirsk, Russia, 10.März 2011

[101] Thumm, M.
Lecture series on overmoded waveguide transmission. 2: Diagnostics and adiabatic mode converters in overmoded waveguide.
Vortr.: Budker Institute of Nuclear Physics, Novosibirsk, Russia, 10.März 2011

[102] Thumm, M.
Lecture series on overmoded waveguide transmission. 3: Mode converters and components in overmoded waveguides I.
Vortr.: Budker Institute of Nuclear Physics, Novosibirsk, Russia, 11.März 2011

[103] Thumm, M.
Lecture series on overmoded waveguide transmission. 4: Mode converters and components in overmoded waveguides II.
Vortr.: Budker Institute of Nuclear Physics, Novosibirsk, Russia, 11.März 2011

[104] Thumm, M.
State-of-the-art of high power gyro-devices and free electron masers. Update 2010.
KIT Scientific Reports, KIT-SR 7575 (April 2011)

[105] Thumm, M.; Braune, H.; Dammertz, G.; Gantenbein, G.; Erckmann, V.; Illy, S.; Kern, S.; asparek, W.; Lechte, C.; Leonhardt, W.; Lievin, C.; Michel, G.; Noke, F.; Purps, F.; Samartsev, A.; Schlaich, A.; Schmid, M.; Schulz, T.
Recent progress on the 1 MW, 140 GHz, CW series gyrotrons for W7-X.
8th Internat.Workshop 'Strong Microwaves and Terahertz Waves : Sources and Applications', Nizhny Novgorod, Russia, July 9-16, 2011

[106] Thumm, M.; Braune, H.; Dammertz, G.; Gantenbein, G.; Erckmann, V.; Illy, S.; Kern, S.; Kasparek, W.; Lechte, C.; Leonhardt, W.; Lievin, C.; Michel, G.; Noke, F.; Purps, F.; Samartsev, A.; Schlaich, A.; Schmid, M.; Schulz, T.
Recent progress on the 1 MW, 140 GHz, CW series gyrotrons for W7-X.
8th Internat.Workshop 'Strong Microwaves and Terahertz Waves : Sources and Applications', Nizhny Novgorod, Russia, July 9-16, 2011, Proc. S.45-46

[107] Thumm, M.; Gantenbein, G.; Illy, S.; Kern, S.; Leonhardt, W.; Samartsev, A.; Schlaich, A.; Schmidt, M.; Erckmann, V.; Kasparek, W.; Lechte, C.; Lievin, C.
140 GHz, 1 MW, CW gyrotron development for the ECRH system of the stellarator Wendelstein 7-X.
2011 IEEE Internat.Vacuum Electronics Conf. (IVEC 2011), Bangalore, IND, February 21-24, 2011

[108] Thumm, M.; Gantenbein, G.; Illy, S.; Kern, S.; Leonhardt, W.; Samartsev, A.; Schlaich, A.; Schmidt, M.; Erckmann, V.; Kasparek, W.; Lechte, C.; Lievin, C.
140 GHz, 1 MW, CW gyrotron development for the ECRH system of the stellarator Wendelstein 7-X.
2011 IEEE Internat.Vacuum Electronics Conf. (IVEC 2011) : Proc.of a meeting held in Bangalore, IND, February 21-24, 2011, Piscataway, N.J. : IEEE, 2011 S.105-106
ISBN 978-1-4244-8662-5

[109] Thumm, M.K.A.
Recent developments on high-power gyrotrons. Introduction to this special issue.
Journal of Infrared, Millimeter and Terahertz Waves, 32(2011) S.241-252
DOI:10.1007/s10762-010-9754-5

[110] Vaccaro, A.; Aiello, G.; Kleefeldt, K.; Scherer, T.; Schreck, S.; Spaeh, P.; Strauss, D.
The ITER EC H&CD upper launcher: transient mechanical analysis.
26th Symp.on Fusion Technology (SOFT 2010), Porto, P, September 27 - October 1, 2010

[111] Vaccaro, A.; Aiello, G.; Kleefeldt, K.; Scherer, T.; Schreck, S.; Spaeh, P.; Strauss, D.
The ITER EC H&CD upper launcher: transient mechanical analysis.
Fusion Engineering and Design, 86(2011) S.851-854, DOI:10.1016/j.fusengdes.2011.01.073

[112] Vaccaro, A.; Aiello, G.; Meier, A.; Scherer, T.; Schreck, S.; Spaeh, P.; Strauss, D.; Gantenbein, G. Silicon oil DC200(R)5CST as an alternative coolant for CVD diamond windows.
Prater, R. [Hrsg.]
Electron Cyclotron Emission and Electron Cyclotron Resonance Heating (EC-16) : Proc.of the 16th Joint Workshop, Sanya, China, April 12-15, 2010 Singapore [u.a.] : World Scientific, 2011 S.401-409, Incl.CD-ROM, ISBN 978-981-4340-26-7

[113] Vaccaro, A.; Aiello, G.; Meier, A.; Scherer, T.; Schreck, S.; Späh, P.; Strauss, D.; Stober, J.; Wagner, D.; Denisov, G.G.; de Wit, H.G.M.
Grooved CVD diamond windows: grooves' profiles and structural simulations.
US-EU-JPN RF Heating Technology Workshop, Austin, Tex., October 10-12, 2011

[114] Vaccaro, A.; Aiello, G.; Meier, A.; Scherer, T.; Schreck, S.; Späh, P.; Strauss, D.; Stober, J.; Wagner, D.; de Wit, H.G.M.
Grooved CVD diamond windows: grooves' profiles and structural simulations.
36th Internat.Conf.on Infrared, Millimeter and Terahertz Waves (IRMMW-THz 2011), Houston, Tex., October 2-7, 2011

[115] Vaccaro, A.; Aiello, G.; Scherer, T.; Schreck, S.; Meier, A.; Späh, P.; Strauss, D.; Stober, J.; Wagner, D.
Grooved CVD diamond windows: Grooves' profiles and structural simulations.
23rd Joint Russian-German Meeting on ECRH and Gyrotrons, Karlsruhe/Stuttgart/Garching, May 23-28, 2011, Folien auf CD-ROM

[116] van't Klooster, C.G.M.; Petelin, M.; Aloisio, M.; Thumm, M.
Large MM-wave groundbased antenna for telecommunication and radar and associated system considerations.
33rd ESA Antenna Workshop on Challenges for Space Antenna Systems, Noordwijk, NL, October 18-21, 2011

[117] Wagner, D.; Kasparek, W.; Leuterer, F.; Monaco, f.; Münich, M.; Schütz, H.; Stange, T.; Stober, J.; Thumm, M.
Band stop filter for ECE at WEGA.
23rd Joint Russian-German Meeting on ECRH and Gyrotrons, Karlsruhe/Stuttgart/Garching, May 23-28, 2011, Folien auf CD-ROM

[118] Wagner, D.; Kasparek, W.; Leuterer, F.; Monaco, F.; Münich, M.; Schütz, H.; Stange, T.; Stober, J.; Thumm, M.
Bragg reflection band stop filter for ECE on WEGA.
36th Internat.Conf.on Infrared, Millimeter and Terahertz Waves (IRMMW-THz 2011), Houston, Tex., October 2-7, 2011

[119] Wagner, D.; Kasparek, W.; Leuterer, F.; Monaco, F.; Münich, M.; Schütz, H.; Stange, T.; Stober, J.; Thumm, M.
Bragg reflection band stop filter for ECE on WEGA.
Journal of Infrared Millimeter and Terahertz Waves, 32(2011) S.1424-1433
DOI:10.1007/s10762-011-9833-2

[120] Wagner, D.; Stober, J.; Leuterer, F.; Monaco, F.; Müller, S.; Münich, M.; Schubert, M.; Schütz, H.; Zohm, H.; Erckmann, V.; Thumm, M.; Scherer, T.; Strauss, D.; Meier, A.; Gantenbein, G.; Flamm, J.; Kasparek, W.; Höhnle, H.; LEchte, C.; Litvak, A.G.; Denisov, G.G.; Chirkov, A.; Petelin, M.I.; Popov, L.G. ; Nichiporenko, V.O.; Myasnikov, V.E.; Tai, E.M.; Solyanova, E.A.; Malygin, V.E.; ASDEX Upgrade Team
Multi-frequency ECRH system at ASDEX upgrade status and activities.
US-EU-JPN RF Heating Technology Workshop, Austin, Tex., October 10-12, 2011

[121] Wagner, D.; Stober, J.; Leuterer, F.; Monaco, F.; Münich, M.; Schmid-Lorch, D.; Schütz, H.; Zohm, H.; Thumm, M.; Scherer, T.; Meier, A.; Gantenbein, G.; Flamm, J.; Kasparek, W.; Höhnle, H.; Lechte, C.; Litvak, A.G.; Denisov, G.C.; Chirkov, A.; Popov, L.G.; Nichiporenko, V.O.; Myasnikov, V.E.; Tai, E.M.; Solyanova, E.A.; Malygin, S.A.
Recent upgrades and extensions of the ASDEX upgrade ECRH system.
Journal of Infrared, Millimeter and Terahertz Waves, 32(2011) S.274-282
DOI:10.1007/s10762-010-9703-3

[122] Wagner, D.; Stober, J.; Leuterer, F.; Monaco, F.; Münich, M.; Schubert, M.; Schütz, H.; Zohm, H.; Thumm, M.; Scherer, T.; Meier, A.; Gantenbein, G.; Flamm, J.; Kasparek, W.; Höhnle, H.; Lechte, C.; Litvak, A.G.; Denisov, G.G.; Chirkov, A.; Popov, L.G.; Nichiporenko, V.O.; Myasnikov, V.E.; Tai, E.M.; Solyanova, E.A.; Malygin, S.A.
Operation of the multifrequency ECRH system at ASDEX upgrade.
36th Internat.Conf.on Infrared, Millimeter and Terahertz Waves (IRMMW-THz 2011), Houston, Tex., October 2-7, 2011

[123] Zeile, C.; Neuberger, H.; Dolensky, B.
ITER port plug engineering trainee program: design, manufacturing and integration of structural components (analysis of the attachment).
Fusion Engineering and Design, 86(2011) S.2029-2032, DOI:10.1016/j.fusengdes.2011.04.052

Magnets and Affiliated Components

[1] Bagrets, N.; Schlachter, S.I.; Goldacker, W.; Kudymow, A.; Barth, C.; Weiss, K.P.
Thermal properties of materials for coated conductor Rutherford cables (CCRC).
6th Workshop of Mechanical-Electromagnetic Properties of Superconductors, Okinawa, J, December 5-7, 2011

[2] Bagrets, N.; Weiss, E.; Wesenfelder, S.; Weiss, K.P.
Cryogenic test facility CryoMaK.
22nd Internat.Conf.on Magnet Technology (MT-22), Marseille, F, September 12-16, 2011

[3] Barth, C.; Vojenciak, M.; Weiss, K.P.; Schlachter, S.
Electro- mechanical analysis of Roebel cables with different geometries.
Cryogenic Engineering Conf.and Internat.Cryogenic Materials Conf. (CEC-ICMC), Spokane, Wash., June 13-17, 2011

[4] Barth, C.; Weiss, K.P.; Goldacker, W.
Influence of shear stress on current carrying capabilities of high temperature superconductor tapes.
Applied Superconductivity Conf., Washington, D.C., August 1-6, 2010

[5] Barth, C.; Weiss, K.P.; Goldacker, W.
Influence of shear stress on current carrying capabilities of high temperature superconductor tapes.
IEEE Transactions on Applied Superconductivity, 21(2011) S.3098-3101, DOI:10.1109/TASC.2010.2086420

[6] Cismondi, F.; Kiss, B.; Legradi, G.; Hernandez, F.
About the fundamental role of fluid dynamic analyses in the design of the solid EU test blanket module.
10th Internat.Symp.on Fusion Nuclear Technology (ISFNT 2011), Portland, Oreg., September 11-16, 2011

[7] Drotzinger, S.; Fietz, W.H.; Heiduk, M.; Heller, R.; Lange, C.; Lietzow, R.; Möhring, T.
Investigation of HTS current leads under pulsed operation for JT-60SA.
22nd Internat.Conf.on Magnet Technology (MT-22), Marseille, F, September 12-16, 2011

[8] Fietz, W.H.; Drotziger, S.; Fink, S.; Heiduk, M.; Heller, R.; Kopmann, A.; Lange, C.; Lietzow, R.; Möhring, T.; Rohr, P.; Rummel, T.; Süßer, M.
Test arrangement for the W7-X HTS-current lead prototype testing.
IEEE Transactions on Applied Superconductivity, 21(2011) S.1058-1061
DOI:10.1109/TASC.2010.2095401

[9] Fietz, W.H.; Fink, S.; Lange, C.; Noe, M.; Winkler, A.
Internal transient over-voltages in large fusion coils.
22nd Internat.Conf.on Magnet Technology (MT-22), Marseille, F, September 12-16, 2011

[10] Fietz, W.H.; Heller, R.; Schlachter, S.I.; Goldacker, W.
Application of high temperature superconductors for fusion.
Fusion Engineering and Design, 86(2011) S.1365-1368, DOI:10.1016/j.fusengdes.2010.11.018

[11] Fink, S.; Winkler, A.; Fietz, W.H.; Noe, M.
Transient electrical voltages within ITER poloidal field coils.
22nd Internat.Conf.on Magnet Technology (MT-22), Marseille, F, September 12-16, 2011

[12] Heiduk, M.; Bagrets, N.; Weiss, K.P.
Data acquisition of a tensile test stand for cryogenic environment.
22nd Internat.Conf.on Magnet Technology (MT-22), Marseille, F, September 12-16, 2011

[13] Heller, R.
Wendelstein 7-X current leads successfully tested.
Fusion News - Newsletter, December 2010

[14] Heller, R.; Drotzinger, S.; Fietz, W.H.; Fink, S.; Heiduk, M.; Kienzler, A.; Lange, C.; Lietzow, R.; Möhring, T.; Rohr, P.; Rummel, T.; Mönnich, T.; Buscher, K.P.
Test results of the high temperature superconductor prototype current leads for Wendelstein 7-X.
IEEE Transactions on Applied Superconductivity, 21(2011) S.1062-1065
DOI:10.1109/TASC.2010.2096371

[15] Heller, R.; Fietz, W.H.; Kienzler, A.; Lietzow, R.
High temperature superconductor current leads for fusion machines.
Fusion Engineering and Design, 86(2011) S.1422-1426, DOI:10.1016/j.fusengdes.2010.12.077

[16] Lange, C.; Baldzuhn, J.; Fink, S.; Heller, R.; Hollik, M.; Fietz, W.H.
Paschen problems in large coil systems.
22nd Internat.Conf.on Magnet Technology (MT-22), Marseille, F, September 12-16, 2011

[17] Lietzow, R.; Fietz, W.H.; Heiduk, M.; Heller, R.; Lange, C.
A current lead test facility for the cryogenic test of the W7-X and JT-60SA HTS-current leads.
Cryogenic Engineering Conf.and Internat.Cryogenic Materials Conf. (CEC-ICMC), Spokane, Wash., June 13-17, 2011

[18] Nyilas, A.; Weiss, K.P.; Sgobba, S.; Scheubel, M.; Libeyre, P.
Fatigue crack growth rate and fracture toughness of ITER central solenoid jacket materials at 7 K.
Cryogenic Engineering Conf.and Internat.Cryogenic Materials Conf. (CEC-ICMC), Spokane, Wash., June 13-17, 2011

[19] Osamura, K.; Nyilas, A.; Weiss, K.P.; Shin, H.S.; Katagiri, K.; Ochiai, S.; Hojo, M.; Sugano, M.; Ohsawa, K.
International round Robin test for mechanical properties of BSCCO-2223 superconductive tapes at room temperature.
Cryogenics, 51(2011) S.21-26, DOI:10.1016/j.cryogenics.2010.10.005

[20] Rizzo, E.; Heller, R.; Savoldi Richard, L.; Zanino, R.
Heat exchanger CFD analysis for the W7-X high temperature superconductor current lead prototype.
Fusion Engineering and Design, 86(2011) S.1571-1574, DOI:10.1016/j.fusengdes.2011.04.077

[21] Rizzo, E.; Heller, R.; Savoldi Richard, L.; Zanino, R.
Analysis and performance assessment for a 68 kA HTS current lead heat exchanger.
22nd Internat.Conf.on Magnet Technology (MT-22), Marseille, F, September 12-16, 2011

[22] Savoldi Richard, L.; Heller, R.; Zanino, R.
Thermal-hydraulic simulation of 80 kA safety discharge in the ITER toroidal field model coil (TFMC) using the 4C code.
15th Internat.Conf.on Emerging Nuclear Energy Systems (ICENES 2011), San Francisco, Calif., May 15-19, 2011

[23] Weiss, K.P.; Goldacker, W.; Nannini, M.
Finite element analysis of torsion experiments on HTSC tapes.
IEEE Transactions on Applied Superconductivity, 21(2011) S.3102-3106
DOI:10.1109/TASC.2010.2090121

[24] Weiss, K.P.; Jung, A.; Westenfelder, S.; Vostner, A.; Jewell, M.
Impact of cold work on ductility of ITER TF jacket material.
22nd Internat.Conf.on Magnet Technology (MT-22), Marseille, F, September 12-16, 2011

[25] Weiss, K.P.; Westenfelder, S.; Fietz, W.H.
Determination of mechanical and thermal properties of electrical insulation material at 4.2 K.
Cryogenic Engineering Conf.and Internat.Cryogenic Materials Conf. (CEC-ICMC),
Spokane, Wash., June 13-17, 2011

Blanket Breeding

[1] Abou-Sena, A.; Löbbecke, B.; von der Weth, A.; Knitter, R.
Effect of post welding heat treatment of the HCPB TBM on Eurofer and lithium orthosilicate pebbles.
Fusion Engineering and Design, 86(2011) S.2254-2257, OI:10.1016/j.fusengdes.2011.03.038

[2] Boccaccini, L.V.
Status of the EFDA goal oriented training programme EUROBREED.
EFDA GOTP Satelite Meeting during 26th Symp.on Fusion Technology (SOFT 2010),
Porto, P, September 27 - October 1, 2010

[3] Boccaccini, L.V.; Aiello, A.; Bede, O.; Cismondi, F.; Kosek, L.; Ilkei, T.;
Salavy, J.F.; Sardain, P.; Sedano, L. ; European TBM Consortium of Associates
Present status of the conceptual design of the EU test blanket systems.
Fusion Engineering and Design, 86(2011) S.478-483, DOI:10.1016/j.fusengdes.2011.02.036

[4] Boccaccini, L.V.; Cismondi, F.; Norajitra, P.
Overview on fusion technology development for DEMO in KIT. In vessel component design and integration.
Japan-US Workshop on Fusion Power Plants and Related Advanced Technologies,
Toki, J, February 22-24, 2011

[5] Bühler, L.
Asymptotic methods for modeling of liquid-metal flows in strong magnetic fields. (eingeladen)
10th School and Workshop on Fusion Physics and Technology, Volos, GR, May 9-13, 2011

[6] Bühler, L.
Impact of magnetohydrodynamics on the development of liquid metal blankets for fusion reactors. (eingeladen)
Guest Colloquium Research Training Group Lorentz Force Velocimetry and Lorentz Force Eddy Current Testing, TU Ilmenau, 17.Mai 2011

[7] Bühler, L.; Mistrangelo, C.
Analysis of liquid-metal MHD flows in the European test blanket module. (eingeladen)
10th School of Fusion Physics and Technology, Workshop on MHD Flows and Plasma Stability, Volos, GR, May 9-13, 2011

[8] Bühler, L.; Mistrangelo, C.
Determination of flow distribution in a HCLL blanket mock-up through electric potential measurements.
Fusion Engineering and Design, 86(2011) S.2301-2303, DOI:10.1016/j.fusengdes.2011.01.132

[9] Bühler, L.; Mistrangelo, C.
Effects of radial variation of the magnetic field on the pressure distribution in the European liquid-metal blanket concept. Fusion Science and Technology, 60(2011) S.257-263

[10] Bühler, L.; Mistrangelo, C.
Liquid metal flow in the European concept for a fusion test blanket under the influence of spatially varying magnetic fields.
8th PAMIR Internat.Conf.on Fundamental and Applied MHD, Borgo, F, September 5-9, 2011

[11] Bühler, L.; Mistrangelo, C.
Liquid metal flow in the European concept for a fusion test blanket under the influence of spatially varying magnetic fields.
8th PAMIR Internat.Conf.on Fundamental and Applied MHD, Borgo, F, September 5-9, 2011
Proc.on CD-ROM

[12] Bühler, L.; Mistrangelo, C.; Horanyi, S.
Experimental detection of MHD flow reversals in sub channels of a liquid metal test blanket for ITER.
3th Internat.Symp.on Bifurcations and Instabilities in Fluid Dynamics, Barcelona, E, July 18-21, 2011

[13] Bühler, L.; Mistrangelo, C.; Köhly, C.
Design of a flexible liquid metal loop for investigation of MHD flows related to fusion blanket applications.
38th IEEE Internat.Conf.on Plasma Science (ICOPS) and 24th Symp.on Fusion Engineering (SOFE), Chicago, Ill., June 26-30, 2011

[14] Bühler, L.; Mistrangelo, C.; Köhly, C.
Design of a flexible liquid metal loop for investigation of MHD flows related to fusion blanket applications.
38th IEEE Internat.Conf.on Plasma Science (ICOPS) and 24th Symp.on Fusion Engineering (SOFE), Chicago, Ill., June 26-30, 2011, Proc.publ.online
Piscataway, N.J. : IEEE, 2011 Paper SP2-51, DOI:10.1109/SOFE.2011.6052306

[15] Chakin, V.; Klimenkov, M.; Rolli, R.; Kurinskiy, P.; Moeslang, A.; Dorn, C.
Microstructural and tritium release examination of titanium beryllides.
Journal of Nuclear Materials, 417(2011) S.769-774, DOI:10.1016/j.jnucmat.2010.12.142

[16] Chakin, V.; Möslang, A.; Kurinskiy, P.; Rolli, R.; Schneider, H.C.; Alves, E.; Alves, L.C.
Tritium permeation, retention and release properties of beryllium pebbles.
Fusion Engineering and Design, 86(2011) S.2338-2342, DOI:10.1016/j.fusengdes.2011.01.091

[17] Chakin, V.; Rolli, R.; Moeslang, A.; Kurinskiy, P.; Vladimirov, P.; Ferrero, C.; Pieritz, R.; Van Renterghem, W.
Study of helium bubble evolution in highly neutron-irradiated beryllium by using X-ray micro tomography and metallography methods.
Physica Scripta, T145(2011) S.014012/1-6, DOI:10.1088/0031-8949/2011/T145/014012

[18] Ciampichetti, A.; Aiello, A.; Nitti, S.; Ricapito, I.; Liger, K.; Demange, D.; Sedano, L.; Moreno, C.; Succi, M.
Design of tritium extraction system for the European HCPB test blanket module.
10th Internat.Symp.on Fusion Nuclear Technology (ISFNT 2011), Portland, Oreg., September 11-16, 2011

[19] Cismondi, F.
Basics of breeding blanket technology. (eingeladen)
Course 'Engineering of Nuclear Fusion Reactors', Politecnico di Torino, I, January 18, 2011

[20] Cismondi, F.; Aiello, G.; Kecskes, S.; Rampal, G.
Thermo mechanical performance of the EU TBMs under a typical ITER transient.
19th Topical Meeting on the Technology of Fusion Energy (TOFE), Las Vegas, Nev., November 7-11, 2010

[21] Cismondi, F.; Aiello, G.; Kecskes, S.; Rampal, G.
Thermomechanical performance of the EU TBMs under a typical ITER transient.
Fusion Science and Technology, 60(2011) S.123-127

[22] Cismondi, F.; Kecskes, S.; Aiello, G.
HCPB TBM thermo mechanical design: assessment with respect codes and standards and DEMO relevancy.
26th Symp.on Fusion Technology (SOFT 2010), Porto, P, September 27 - October 1, 2010

[23] Cismondi, F.; Kecskes, S.; Aiello, G.
HCPB TBM thermo mechanical design: assessment with respect codes and standards and DEMO relevancy.
Fusion Engineering and Design, 86(2011) S.2228-2232, DOI:10.1016/j.fusengdes.2011.02.067

[24] Cismondi, F.; Kiss, B.; Legradi, G.
Fluid dynamic design of the manifold system in the HCPB TBM.
29th National Heat Transfer Conf., Torino, I, June 20-22, 2011

[25] Cismondi, F.; Magnani, E.; Boccaccini, L.V.
Segmentation of internal components and impact on maintenance for DEMO.
Japan-US Workshop on Fusion Power Plants and Related Advanced Technologies,
Toki, J, February 22-24, 2011
10th Internat.Symp.on Fusion Nuclear Technology (ISFNT 2011), Portland, Oreg.,
September 11-16, 2011

[26] Jin, X.Z.; Ghidersa, B.E.
Investigation of accident cases for high pressure, high temperature experimental helium loop using RELAP5-3D code.
Fusion Engineering and Design, 86(2011) S.2739-2742, DOI:10.1016/j.fusengdes.2011.01.074

[27] Knitter, R.; Chaudhuri, P.; Feng, Y.J.; Hoshino, T.; Yu, I.K.
Recent developments of solid breeder fabrication.
15th Internat.Conf.on Fusion Reactor Materials, Charleston, S.C., October 16-22, 2011

[28] Knitter, R.; Kolb, M.H.H.; Kaufmann, U.; Goraieb, A.A.
Fabrication of modified lithium orthosilicate pebbles by addition of titania.
15th Internat.Conf.on Fusion Reactor Materials, Charleston, S.C., October 16-22, 2011

[29] Kolb, M.; Bruns, M.; Knitter, R.; van Til, S.
Characterization of the surface of lithium orthosilicate and the effect on tritium release.
15th Internat.Conf.on Fusion Reactor Materials, Charleston, S.C., October 16-22, 2011

[30] Kolb, M.; Knitter, R.
Advancements in the melt-based fabrication of tritium breeder pebbles.
Meeting on Tritium and Blanket Technologies, Portland, Or., September 14, 2011

[31] Kolb, M.; Knitter, R.
Enhanced melt-spraying process for tritium breeder pebbles.
16th Internat.Workshop on Ceramic Breeder Blanket Interactions (CBBI-16), Portland, Or.,
September 8-10, 2011

[32] Kolb, M.; Knitter, R.; Kaufmann, U.; Mundt, D.
Enhanced fabrication process for lithium orthosilicate pebbles as breeding material.
Fusion Engineering and Design, 86(2011) S.2148-2151, DOI:10.1016/j.fusengdes.2011.01.10

[33] Kolb, M.; Odemer, C.; Knitter, R.
Synthesis of tritium breeder ceramics from metallic lithium.
10th Internat.Symp.on Fusion Nuclear Technology (ISFNT 2011), Portland, Oreg.,
September 11-16, 2011

[34] Mistrangelo, C.
Topological analysis of separation phenomena in liquid metal flow in sudden expansions. Part 2. Magnetohydrodynamic flow.
Journal of Fluid Dynamics, 674(2011) S.132-162, DOI:10.1017/S0022112011000607

[35] Mistrangelo, C.
Topological analysis of separation phenomena in liquid metal flow in sudden expansions. Part 1. Hydrodynamic flow.
Journal of Fluid Mechanics, 674(2011) S.120-131, DOI:10.1017/S0022112010006439

[36] Mistrangelo, C.; Bühler, L.
Development of a numerical tool to simulate magnetohydrodynamic interactions of liquid metals with strong applied magnetic fields.
Fusion Science and Technology, 60(2011) S.798-803

[37] Mistrangelo, C.; Bühler, L.
Instabilities in electrically driven MHD flows.
8th PAMIR Internat.Conf.on Fundamental and Applied MHD, Borgo, F, September 5-9, 2011

[38] Mistrangelo, C.; Bühler, L.
Instabilities in electrically driven MHD flows.
8th PAMIR Internat.Conf.on Fundamental and Applied MHD, Borgo, F, September 5-9, 2011
Proc.on CD-ROM, Vol.1 S.175-179 (Paper A 3_4)

[39] Mistrangelo, C.; Bühler, L.
Magnetohydrodynamic pressure drops in geometric elements forming a HCLL blanket mock-up.
Fusion Engineering and Design, 86(2011) S.2304-2307, DOI:10.1016/j.fusengdes.2011.03.011

[40] Mistrangelo, C.; Bühler, L.
Numerical analysis of buoyant-convective liquid metal flow in channels exposed to strong magnetic fields.
38th IEEE Internat.Conf.on Plasma Science (ICOPS) and 24th Symp.on Fusion Engineering (SOFE), Chicago, Ill., June 26-30, 2011

[41] Mistrangelo, C.; Bühler, L.
Numerical analysis of buoyant-convective liquid metal flow in channels exposed to strong magnetic fields.
38th IEEE Internat.Conf.on Plasma Science (ICOPS) and 24th Symp.on Fusion Engineering (SOFE), Chicago, Ill., June 26-30, 2011, Proc.publ.online, Piscataway, N.J. : IEEE, 2011
Paper SO1D-3, DOI:10.1109/SOFE.2011.6052204

[42] Munakata, K.; Mochizuki, K.; Wajima, T.; Wada, K.; Hara, K.; Shinozaki, T.; Takeishi, T.; Knitter, R.; Bekris, N.; Fujii, T.; Yamana, H.; Okuno, K.
Tritium release from ceramic breeder materials deposited with noble metals.
Journal of Nuclear Materials, 417(2011) S.731-734, DOI:10.1016/j.jnucmat.2011.01.079

[43] Odemer, C.; Maciejewski, U.; Kolb, M.H.H.; Knitter, R.
Gefügeuntersuchungen an schmelzprozessierten Lithiumorthosilikatkugeln. Materialographie : Metalle - Keramik - Polymere ; 45.Metallographie-Tagung mit Ausstellung, Karlsruhe, 14.-16.September 2011

[44] Panayotov, D.; Sardain, P.; Boccaccini, L.V.; Salavy, J.F.; Cismondi, F.; Jourd'Heuil, L.
System engineering approach in the EU test blanket systems design integration.
Fusion Engineering and Design, 86(2011) S.2241-2245, DOI:10.1016/j.fusengdes.2011.01.006

[45] Pieritz, R.A.; Reimann, J.; Ferrero, C.
3D tomography analysis of the inner structure of pebbles and pebble beds.
Advanced Engineering Materials, 13(2011) S.145-155, DOI:10.1002/adem.201000256

[46] von der Weth, A.; Felde, A.; Hellmeier, H.; Rey, J.; Rudolf, S.
Theoretical investigation of a first wall fabrication process.
Journal of Nuclear Materials, 417(2011) S.25-28, DOI:10.1016/j.jnucmat.2011.05.022

[47] Ying, A.; Reimann, J.; Boccaccini, L.; Enoeda, M.; Kamlah, M.; Knitter, R.; Gan, Y.; Van der Laan, J.; Magielsen, L.; Tincani, A.; Abou-Sena, A.; Annabattula, R.K.; Narula, M.; Tanigawa, H.
Status of ceramic breeder pebble bed thermo-mechanics R&D and impact on breeder material mechanical strength. (eingeladen)
10th Internat.Symp.on Fusion Nuclear Technology (ISFNT 2011), Portland, Oreg., September 11-16, 2011

[48] Zhao, S.
Multiscale modeling of thermomechanical properties of ceramic pebbles.
KIT Scientific Reports, KIT-SR 7573 (September 2011)
Dissertation, Karlsruher Institut für Technologie 2010

[49] Zmitko, M.; Poitevin, Y.; Boccaccini, L.; Salavy, J.F.; Knitter, R.; Möslang, A. ; Magielsen, A.J.; Hegemann, J.B.J.; Lässer, R.
Development and qualification of functional materials for the EU test blanket modules: strategy and R&D activities.
Journal of Nuclear Materials, 417(2011) S.678-683, DOI:10.1016/j.jnucmat.2011.02.009

Divertor

[1] Antusch, S.; Norajitra, P.; Piotter, V.; Ritzhaupt-Kleissl, H.J.
Powder injection molding for mass production of He-cooled divertor parts.
Journal of Nuclear Materials, 417(2011) S.533-535, DOI:10.1016/j.jnucmat.2010.12.122

[2] Hesch, K.; Aktaa, J.; Antusch, S.; Boccaccini, L.V.; Day, C.; Demange, D.; Fietz, W.; Gantenbein, G.; Möslang, A.; Norajitra, P.; Rieth, M.
Technology developments at KIT towards a magnetic confinement fusion power plant.
15th Internat.Conf.on Emerging Nuclear Energy Systems (ICENES 2011), San Francisco, Calif., May 15-19, 2011

[3] Koncar, B.; Kosmrlj, S.; Norajitra, P.
Cyclic surface heating of the cooling finger mock-up.
10th Internat.Symp.on Fusion Nuclear Technology (ISFNT 2011), Portland, Oreg., September 11-16, 2011

[4] Norajitra, P.; Antusch, S.; Basuki, W.; Spatafora, L.
Fabrication of parts and joining process development. Development of Ti-alloy brazing for tungsten divertor component joints.
Fusion Materials Topical Group W and W-alloy Development Monitoring Meeting, Frascati, I, June 6-7, 2011

[5] Norajitra, P.; Antusch, S.; Basuki, W.; Spatafora, L.; Toth, V.
Newly developed innovative manufacturing technologies for He-cooled DEMO divertor.
38th IEEE Internat.Conf.on Plasma Science (ICOPS) and 24th Symp.on Fusion Engineering (SOFE), Chicago, Ill., June 26-30, 2011

[6] Norajitra, P.; Antusch, s.; Basuki, W.; Spatafora, L.; Toth, V.
Newly developed innovative manufacturing technologies for He-cooled DEMO divertor.
38th IEEE Internat.Conf.on Plasma Science (ICOPS) and 24th Symp.on Fusion Engineering (SOFE), Chicago, Ill., June 26-30, 2011, Proc.publ.online, Piscataway, N.J. : IEEE, 2011 Paper SP1-36, DOI:10.1109/SOFE.2011.6052260

[7] Norajitra, P.; Antusch, S.; Boccaccini, L.V.; Kuzmic, M.; Maione, I.; Spatafora, L.
He-cooled DEMO divertor: design verification testing against impact loads.
10th Internat.Symp.on Fusion Nuclear Technology (ISFNT 2011), Portland, Oreg., September 11-16, 2011

[8] Norajitra, P.; Spatafora, L.
Technological study on manufacturing of multi-finger module of He-cooled DEMO divertor.
15th Internat.Conf.on Fusion Reactor Materials, Charleston, S.C., October 16-22, 2011

Structural Materials

[1] Aktaa, J.; Petersen, C.
Modeling the constitutive behavior of RAFM steels under irradiation conditions.
Journal of Nuclear Materials, 417(2011) S.1123-1126, DOI:10.1016/j.jnucmat.2010.12.295

[2] Albinski, B.; Schneider, H.C.; Sacksteder, I.; Yao, Q.; Kraft, O.
A new high-temperature indentation device for characterization of materials for fusion applications.
20.testXpo : Fachmesse für Prüftechnik, Ulm, 10.-13.Oktober 2011
15th Internat.Conf.on Fusion Reactor Materials, Charleston, S.C., October 16-22, 2011

[3] Albinski, B.; Schneider, H.C.; Sacksteder, I.; Yao, W.; Kraft, O.
Characterization of materials for fusion applications by indentation experiments at high temperatures.
15th Internat.Conf.on Fusion Reactor Materials, Charleston, S.C., October 16-22, 2011

[4] Albinski, B.; Yao, W.; You, J.H.; Schneider, H.C.
Characterisation of poly- and singlecrystalline tungsten by instrumented indentation.
13th Internat.Workshop on Plasma-Facing Materials and Components for Fusion Applications, 1st Internat. Conf.on Fusion Energy Materials Science, Rosenheim, May 9-13, 2011

[5] Aleev, A.A.; Iskandarov, N.A.; Klimenkov, M.; Lindau, R.; Möslang, A.; Nikitin, A.A.; Rogozhkin, S.V.; Vladimirov, P.; Zaluzhnyi, A.G.
Investigation of oxide particles in unirradiated ODS Eurofer by tomographic atom probe.
Journal of Nuclear Materials, 409(2011) S.65-71, DOI:10.1016/j.jnucmat.2010.09.008

[6] Annabattula, R.K.; Gan, Y.; Kamlah, M.
Thermomechanics of pebble beds in fusion reactors.
World Materials Summit 2011, Washington, D.C, October 9-12, 2011

[7] Annabattula, R.K.; Zhao, S.; Kamlah, M.; Gan, Y.
Crushing analysis of the ceramic pebbles using DEM.
16th Internat.Workshop on Ceramic Breeder Blanket Interactions (CBBI-16), Portland, Or., September 8-10, 2011

[8] Annabattula, R.K.; Zhao, S.; Kamlah, M.; Gan, Y.
Mechanics of polydisperse spherical pebble assembly.
16th Internat.Workshop on Ceramic Breeder Blanket Interactions (CBBI-16), Portland, Or., September 8-10, 2011

[9] Antusch, S.; Müller, M.; Norajitra, P.; Pintsuk, G.; Piotter, V.; Ritzhaupt-Kleissl, H.J.; Weingärtner, T.
Two component tungsten powder injection molding for mass production of the He-cooled DEMO divertor parts.
15th Internat.Conf.on Fusion Reactor Materials, Charleston, S.C., October 16-22, 2011

[10] Arbeiter, F.; Abou-Sena, A.; Chen, Y.; Dolensky, B.; Heupel, T.; Klein, C.; Scheel, N.; Schlindwein, G.
Development and validation status of the IFMIF high flux test module.
Fusion Engineering and Design, 86(2011) S.607-610, DOI:10.1016/j.fusengdes.2011.01.031

[11] August, A.; Nestler, B.; Kneer, A.; Wendler, F.; Rölle, M.; Selzer, M.
Offenporige metallische Schäume. Werkstoffe in der Fertigung, (2011) Nr.6, S.45-46

[12] Basuki, W.W.
Investigation of diffusion bonding between tungsten and EUROFER97 using V interlayer.
MAT-W&Walloys Monitoring Meeting, Garching, February 9-10, 2011

[13] Basuki, W.W.; Aktaa, J.
Investigation of tungsten/EUROFER97 diffusion bonding using Nb interlayer.
Fusion Engineering and Design, 86(2011) S.2585-2588, DOI:10.1016/j.fusengdes.2011.03.017

[14] Basuki, W.W.; Aktaa, J.
Investigation on the diffusion bonding of tungsten and EUROFER97.
Journal of Nuclear Materials, 417(2011) S.524-527, DOI:10.1016/j.jnucmat.2010.12.121

[15] Basuki, W.W.; Aktaa, J.
Low temperature diffusion bonding between EUROFER97 and W using V interlayer.
Fusion Materials Topical Group W and W-alloy Development Monitoring Meeting, Frascati, I,
June 6-7, 2011

[16] Bhanumurthy, K.; Krauss, W.; Konys, J.
Micro-structural evolution of alumnide coatings on Eurofer during heat treatments.
2nd Internat.Conf.on Advances in Nuclear Materials (ANM-2011), Mumbai, IND,
February 9-11, 2011

[17] Chakin, V.; Moeslang, A.; Vladimirov, P.; Kurinski, P.; Rolli, R.; Schneider, H.C.; van Til, S.; Hegeman, J.B.J.; Zmitko, M.
Tritium release and retention properties of highly neutron irradiated beryllium pebbles from HIDOBE-01 experiment.
15th Internat.Conf.on Fusion Reactor Materials, Charleston, S.C., October 16-22, 2011

[18] Chakin, V.; Möslang, A.; Kurinskiy, P.; Rolli, R.; Schneider, H.C.; Alves, E.; Alves, L.c.
Tritiumpermeation, retention and release properties of beryllium pebbles.
26th Symp.on Fusion Technology (SOFT 2010), Porto, P,
September 27 - October 1, 2010

[19] Chakin, V.; Rolli, R.; Schneider, H.C.; Moeslang, A.; Kurinsky, P.; Van Renterghem, W.
Pores and cracks in highly neutron irradiated beryllium.
Journal of Nuclear Materials, 416(2011) S.3-8, DOI:10.1016/j.jnucmat.2010.11.098

[20] Coppola, R.; Klimenkov, M.; Lindau, R.; Möslang, A.; Valli, M.; Wiedenmann, A.
Comparison microstructural investigation of neutron irradiated Eurofer-97 and
ODS Eurofer-97 steel.
15th Internat.Conf.on Fusion Reactor Materials, Charleston, S.C., October 16-22, 2011

[21] Coppola, R.; Klimenkov, M.; Lindau, R.; Möslang, A.; Valli, M.; Wiedenmann, A.
Recent applications of small-angle neutron scattering in the characterization of irradiated steels for nuclear technologies.
Journal of Nuclear Materials, 409(2011) S.100-105, DOI:10.1016/j.jnucmat.2010.09.012

[22] Dethloff, C.; Gaganidze, E.; Svetukhin, V.; Aktaa, J.
Modeling of helium bubble growth in ^{10}B-doped RAFM steels under neutron irradiation.
15th Internat.Conf.on Fusion Reactor Materials, Charleston, S.C., October 16-22, 2011

[23] Dethloff, C.; Gaganidze, E.; Svetukhin, V.V.
Modeling of helium bubble growth. Recent achievements.
6th Meeting of the Helmholtz-Russia Joint Research Group 13, Karlsruhe, May 4, 2011

[24] El-Guebaly, L.; Kurtz, R.; Rieth, M.; Kurishita, H.; Robinson, A.; ARIES Team.
W-based alloys for advanced divertor designs: options and environmental impact of state-of-the-art alloys.
Fusion Science and Technology, 60(2011) S.185-189

[25] Gaganidze, E.
Issues related to radiation on blanket and divertor materials.
Materials Assessment Report Monitoring Meeting, Garching, December 1, 2011

[26] Gaganidze, E.; Dethloff, C.; Weiß, O.J.; Svetukhin, V.; Tikhonchev, M.; Aktaa, J.
Modeling and TEM investigation of helium bubble growth in RAFM steels under neutron irradiation.
25th Symp.on Effects of Radiation on Nuclear Materials, Anaheim, Calif., June 15-17, 2011
Book of Abstracts S.45

[27] Gaganidze, E.; Petersen, C.
Post irradiation examination of RAFM steels after fast reactor irradiation up to 71 dpa and < 340^{0}C (ARBOR 2).
KIT Scientific Reports, KIT-SR 7596 (Oktober 2011)

[28] Gaganidze, E.; Petersen, C.; Aktaa, J.; Povstyanko, A.; Prohkorov, V.; Diegele, E.; Lässer, R.
Low cycle fatigue properties of reduced activation ferritic/martensitic steels after high-dose neutron irradiation.
Nuclear Fusion, 51(2011) S.083012/1-6, DOI:10.1088/0029-5515/51/8/083012

[29] Gaganidze, E.; Petersen, C.; Materna-Morris, E.; Dethloff, C.; Weiß, O.J.; Aktaa, J.; Povstyanko, A.; Fedoseev, A.; Makarov, O.; Prokhorov, V.
Mechanical properties and TEM examination of RAFM steels irradiated up to 70 dpa in BOR-60.
Journal of Nuclear Materials, 417(2011) S.93-98

[30] Gaganidze, E.; Rupp, D.; Bürkle, U.
Fracture mechanical and microstructural characterization of W-alloys.
MAT-W&Walloys Monitoring Meeting, Garching, February 9-10, 2011

[31] He, P.; Klimenkov, M.; Lindau, R.; Möslang, A.
Microstructure-property correlation of 13.5%Cr nanostructured ODS steels for fusion application.
1st Internat.Workshop on Dispersion Strengthened Steels for Advanced Nuclear Applications (DIANA I), Aussois, April 4-8, 2011

[32] He, P.; Klimenkov, M.; Lindau, R.; Möslang, A.
Microstrutural response on high temperature low cycle fatigue of ODS Eurofer and 13.5% Cr ODS steels.
15th Internat.Conf.on Fusion Reactor Materials, Charleston, S.C., October 16-22, 2011

[33] Holstein, N.; Krauss, W.; Konys, J.
Development of novel tungsten processing technologies for electro-chemical machining (ECM) of plasma facing components.
Fusion Engineering and Design, 86(2011) S.1611-1615, DOI:10.1016/j.fusengdes.2010.11.003

[34] Jäntsch, U.; Klimenkov, M.; Rieth, M.; SCherer, T.; Hoffmann, A.
Microstructure analysis of tungsten materials produced by different fabrication routes.
13th Internat.Workshop on Plasma-Facing Materials and Components for Fusion Applications, 1st Internat. Conf.on Fusion Energy Materials Science, Rosenheim, May 9-13, 2011
Book of Abstracts S.178

[35] Klimenkov, M.
Quantitative measurement of argon inside of nano-sized bubbles in ODS steels.
Journal of Nuclear Materials, 411(2011) S.160-162, DOI:10.1016/j.jnucmat.2011.01.104

[36] Klimenkov, M.
TEM study of hydrogen-containing precipitates in Al-containing ODS steel.
Journal of Nuclear Materials, 417(2011) S.197-200, DOI:10.1016/j.jnucmat.2010.12.070

[37] Klimenkov, M.; Materna-Morris, E.; Lindau, R.
Analytical TEM investigation of boron alloyed EUROFER 97.
13th Internat.Workshop on Plasma-Facing Materials and Components for Fusion Applications, 1st Internat. Conf.on Fusion Energy Materials Science, Rosenheim, May 9-13, 2011
Book of Abstracts S.175

[38] Klimenkov, M.; Materna-Morris, E.; Lindau, R.; Möslang, A.
Analytical TEM characterization of precipitates in EUROFER 97.
European Materials Research Society Bilateral Energy Conf., Nice, F, May 9-13, 2011

[39] Klimenkov, M.; Materna-Morris, E.; Möslang, A.
Characterization of radiation induced defects in EUROFER 97 after neutron irradiation.
Journal of Nuclear Materials, 417(2011) S.124-126, DOI:10.1016/j.jnucmat.2010.12.261

[40] Klimenkov, M.; Materna-Morris, E.; Möslang, A.; Schneider, H.C.
Microstructural characterisation of boron alloyed EUROFER 97 after neutron irradiation.
15th Internat.Conf.on Fusion Reactor Materials, Charleston, S.C., October 16-22, 2011

[41] Klimenkov, M.; Materna-Morris, E.; Vladimiriov, P.; Möslang, A.; Schneider, H.C.
TEM study of irradiation induced copper precipitation in the presence of helium.
15th Internat.Conf.on Fusion Reactor Materials, Charleston, S.C., October 16-22, 2011

[42] Klimenkov, M.; Vladimirov, P.; Möslang, A.; Materna-Morris, E.; Schneider, H.C.
TEM study of irradiation induced copper precipitation in boron alloyed EUROFER97 steel.
International Journal of Materials Research, 102(2011) S.1089-1093
DOI:10.3139/146.110570

[43] Konys, J.
Development of advanced processes for Al-based anti-corrosion and T-permeation barriers.
Vortr.: Bhabha Atomic Research Center, Mumbai, IND, 8.Februar 2011

[44] Konys, J.; Krauss, W.
Corrosion and precipitation effects in a forced-convection Pb-15.7Li loop.
15th Internat.Conf.on Fusion Reactor Materials, Charleston, S.C., October 16-22, 2011

[45] Konys, J.; Krauss, W.; Holstein, N.; Lorenz, J.; Wulf, S.; Bhanumurthy, K.
Impact of heat treatment on the behavior of Al-based anti-corrosion and T-permeation barriers in a flowing Pb-15.7Li environment (1).
10th Internat.Symp.on Fusion Nuclear Technology (ISFNT 2011), Portland, Oreg., September 11-16, 2011

[46] Konys, J.; Krauss, W.; Holstein, N.; Lorenz, J.; Wulf, S.; Bhanumurthy, K.
Impact of heat treatment on the behavior of Al-based anti-corrosion and T-permeation barriers in a flowing Pb-15.7Li environment (2).
10th Internat.Symp.on Fusion Nuclear Technology (ISFNT 2011), Portland, Oreg., September 11-16, 2011

[47] Konys, J.; Krauss, W.; Schroer, C.
Non-metal chemistry of heavy liquid metal corrosion of iron-based structural materials.
Internat.Conf.on Vistas in Chemistry, Kalpakkam, IND, October 11-13, 2011

[48] Konys, J.; Krauss, W.; Schroer, C.
Non-metal chemistry of heavy liquid metal corrosion of iron-based structural materials.
Ganesan, V. [Hrsg.]
Internat.Conf.on Vistas in Chemistry, Kalpakkam, IND, October 11-13, 2011, Proc. S.10-11
Indira Gandhi Centre for Atomic Research

[49] Konys, J.; Krauss, W.; Steiner, H.; Novotny, J.; Skrypnik, A.
Flow rate dependent corrosion behavior of Eurofer steel in Pb-15.7Li.
Journal of Nuclear Materials, 417(2011) S.1191-1194, DOI:10.1016/j.jnucmat.2010.12.277

[50] Krauss, W.; Holstein, N.; Konys, J.; Lorenz, J.
Electro-chemical processes for W manufacturing and joining.
15th Internat.Conf.on Fusion Reactor Materials, Charleston, S.C., October 16-22, 2011

[51] Krauss, W.; Konys, J.; Holstein, N.; Zimmermann, H.
Al-based anti-corrosion and T-permeation barrier development for future DEMO blankets.
Journal of Nuclear Materials, 417(2011) S.1233-1236, DOI:10.1016/j.jnucmat.2010.12.278

[52] Krauss, W.; Konys, J.; Li-Puma, A.
TBM testing in ITER: requirements for the development of predictive tools to describe corrosion-related phenomena in HCLL blankets towards DEMO (1).
10th Internat.Symp.on Fusion Nuclear Technology (ISFNT 2011), Portland, Oreg., September 11-16, 2011

[53] Krauss, W.; Konys, J.; Li-Puma, A.
TBM testing in ITER: requirements for the development of predictive tools to describe corrosion-related phenomena in HCLL blankets towards DEMO (2).
10th Internat.Symp.on Fusion Nuclear Technology (ISFNT 2011), Portland, Oreg., September 11-16, 2011

[54] Krauss, W.; Lorenz, J.; Holstein, N.; Konys, J.
Alternative electro-chemically based processing routes for joining of plasma facing components.
Fusion Engineering and Design, 86(2011) S.1607-1610, DOI:10.1016/j.fusengdes.2011.03.106

[55] Krauss, W.; Lorenz, J.; Holstein, N.; Konys, J.
Development of functional scales for joining of divertor components based on electro-chemical plating technology.
15th Internat.Conf.on Fusion Reactor Materials, Charleston, S.C., October 16-22, 2011

[56] Kurinskiy, P.; Chakin, V.; Moeslang, A.; Rolli, R.; Alves, E.; Alves, L.C.; Franco, N.; Dorn, Ch.; Goraieb, A.A.
Comparative study of fusion relevant properties of $Be_{12}V$ and $Be_{12}Ti$.
Fusion Engineering and Design, 86(2011) S.2454-2457, DOI:10.1016/j.fusengdes.2010.12.065

[57] Kurinskiy, P.; Moeslang, A.; Chakin, V.; Rolli, R.; Alves, E.; Alves, L.C.; Franco, N.; Dorn, Ch.; Goraieb, A.A.
Comparative study of fusion relevant properties of $Be_{12}V$ and $Be_{12}Ti$.
26th Symp.on Fusion Technology (SOFT 2010), Porto, P, September 27 - October 1, 2010

[58] Lindau, R.; Klimenkov, M.; Jäntsch, U.; Möslang, A.; Bergmann, L.; Staron, P.; Fischer, T.; dos Santos, J.F.
Microstructural and mechanical characterization of friction stir welded reduced activation Eurofer and Eurofer-ODS steels.
15th Internat.Conf.on Fusion Reactor Materials, Charleston, S.C., October 16-22, 2011

[59] Materna-Morris, E.; Möslang, A.; Rolli, R.; Schneider, H.C.
Effect of 16.3 dpa neutron irradiation on fatigue lifetime of the RAFM steel EUROFER97.
Fusion Engineering and Design, 86(2011) S.2607-2610, DOI:10.1016/j.fusengdes.2011.03.060

[60] Materna-Morris, E.; Möslang, A.; Schneider, H.C.
Low cycle fatigue behavior of EUROFER97-steel after 16.3 dpa neutron irradiation at 250, 350 and 450^0C.
15th Internat.Conf.on Fusion Reactor Materials, Charleston, S.C., October 16-22, 2011

[61] Möslang, A.
Hocheistungswerkstoffe für den Fusionsreaktor. (eingeladen)
Physikalisches Kolloquium, Friedrich-Schiller-Universität, Jena, 10Januar 2011

[62] Nguyen-Manh, D.; Muzyk, M.; Kurzydlowski, K.J.; Baluc, N.L.; Rieth, M.; Dudarev, S.L.
First-principles modeling of tungsten-based alloys for fusion power plant applications.
Sandera, P. [Hrsg.]
Selected, Peer-reviewed Papers from the 6th Internat.Conf.'Materials Structure and Micromechanics of Fracture (MSMF-6)', Brno, CZ, June 28-30, 2010
Stafa-Zuerich : Trans Tech Publ., 2011 S.15-20 (Key Engineering Materials ; 465)
ISBN 978-3-03785-006-0

[63] Reiser, J.; Rieth, M.
Optimization and limitations of known DEMO divertor concepts.
10th Internat.Symp.on Fusion Nuclear Technology (ISFNT 2011), Portland, Oreg., September 11-16, 2011

[64] Reiser, J.; Rieth, M.; Dafferner, B.
Tungsten for structural divertor parts.
Fusion PhD Seminar, Bad Herrenalb, 27.-28.Juni 2011

[65] Reiser, J.; Rieth, M.; Dafferner, B.; Hoffmann, A.
Influence of thickness and notch on impact bending properties of pure tungsten plate material.
15th Internat.Conf.on Fusion Reactor Materials, Charleston, S.C., October 16-22, 2011

[66] Reiser, J.; Rieth, M.; Dafferner, B.; Möslang, A.; Schlulmeyer, W.; Hoffmann, A.
Ductile tungsten (W) pipes for structural applications.
Conf.on Intellectual Property, Dispute Prevention and Technology Transfer, Barcelona, E, November 28-29, 2011

[67] Renzetti, R.A.; Sandim, H.R.Z.; Sandim, M.J.R.; Santos, A.D.; Möslang, A.; Raabe, D.
Annealing effects on microstructure and coercive field of ferritic-martensitic ODS Eurofer steel.
Materials Science and Engineering A, 528(2011) S.1442-1447, DOI:10.1016/j.msea.2010.10.051

[68] Rieth, M.
Development of high performance materials for nuclear fusion power plants.
2nd Brazilian-German Frontiers of Science and Technology Symp.2011, Potsdam, September 8-11, 2011

[69] Rieth, M.
International tungsten development efforts and the gas cooled divertor design.
15th Internat.Conf.on Fusion Reactor Materials, Charleston, S.C., October 16-22, 2011

[70] Rieth, M.
Tungsten - Properties, possible and impossible applications.
Institutsseminar, Karlsruher Institut für Technologie, 8.Dezember 2011

[71] Rieth, M.; Armstrong, D.; Dafferner, B.; Heger, S.; Hoffmann, A.; Hoffmann, M.D. ; Jäntsch, U.; Kübel, C.; Materna-Morris, E.; Reiser, J.; Rohde, M.; Scherer, T. ; Widak, V.; Zimmermann, H.
Tungsten as a structural divertor material.
Vincenzini, P. [Hrsg.]
Selected Papers from the 5th Forum on New Materials, Part of CIMTEC 2010 – 12th Internat.Conf.on Modern Materials and Technologies, Montecatini Terme, I, June 6-18, 2010
Stafa-Zürich : Trans Tech Publ., 2011 S.11-21 (Advances in Science and Technology ; 73)
ISBN 978-3-908158-56-1

[72] Rieth, M.; Boutard, J.L.; Dudarev, S.L.; Ahlgren, T.; Antusch, S.; Baluc, N.; Barthe, M.F.; Becquart, C.S.; Ciupinski, L.; Correia, J.B.; Domain, C.; Fikar, J.; Fortuna, E.; Fu, C.C.; Gaganidze, E.; Galan, T.L.; Garcia-Rosales, C.; Gludovatz, B.; Greuner, H.; Heinola, K.; Holstein, N.; Juslin, N.; Koch, F.; Krauss, W.; Kurzydlowski, K.J.; Linke, J.; Linsmeier, Ch.; Luzginova, N.; Maier, H.; Martinez, M.S.; Missiaen, J.M.; Muhammed, M.; Munoz, A.; Muzyk, M.; Nordlund, K.; Nguyen-Manh, D.; Norajitra, P.; Opschoor, J.; Pintsuk, G.; Pippan, R.; Ritz, G.; Romaner, L.; Rupp, D.; Schäublin, R.; Schlosser, J.; Uytdenhouwen, I.; van der Laan, J.G.; Veleva, L.; Ventelon, L.; Wahlberg, S.; Willaime, F.; Würster, S.; Yar, M.A.
Review of the EFDA programme on tungsten materials technology and science.
Journal of Nuclear Materials, 417(2011) S.463-467, DOI:10.1016/j.jnucmat.2011.01.075

[73] Rieth, M.; Dudarev, S.L.; Gonzalez de Vicente, S.M.
Review on the EFDA programme on tungsten materials.
15th Internat.Conf.on Fusion Reactor Materials, Charleston, S.C., October 16-22, 2011

[74] Rieth, M.; Reiser, J.; Dafferner, B.; Baumgärtner, S.
The impact of refractory material properties on the helium cooled divertor design.
15th Internat.Conf.on Emerging Nuclear Energy Systems (ICENES 2011), San Francisco, Calif., May 15-19, 2011

[75] Rogozhkin, S.V.; Aleev, A.A.; Zaluzhnyi, A.G.; Nikitin, A.a.; Iskandarov, N.A.; Vladimirov, P.; Lindau, R.; Möslang, A.
Atom probe characterization of nano-scaled features in irradiated ODS Eurofer steel.
Journal of Nuclear Materials, 409(2011) S.94-99, DOI:10.1016/j.jnucmat.2010.09.021

[76] Rölle, M.; August, A.; Selzer, M.; Nestler, B.
Generierung offenporiger metallischer Schaumstrukturen zur Simulation der Wärmeübertragungseigenschaften.
Forschung aktuell, Karlsruhe : Hochschule Karlsruhe Technik und Wirtschaft, 2011 S.21-23

[77] Römmelt, M.; August, A.; Nestler, B.; Kneer, A.
Analysis of thermal evolution in textile fabrics using advanced microstructure simulation techniques.
5th Internat.Conf.on Textile Composites and Inflatable Structures (Structural Membranes 2011), Barcelona, E, October 5-7, 2011

[78] Römmelt, M.; August, A.; Nestler, B.; Kneer, A.
Analysis of thermal evolution in textile fabrics using advanced microstructure simulation techniques.
Onate, E. [Hrsg.]
5th Internat.Conf.on Textile Composites and Inflatable Structures (Structural Membranes 2011), Barcelona, E, October 5-7, 2011, Proc.publ.online

[79] Rupp, D.
Bruch und Spröd-duktil-Übergang in polykristallinem Wolfram.
Vortr.: Fraunhofer-Institut für zerstörungsfreie Prüfverfahren, Saarbrücken, 17.Januar 2011

[80] Rupp, D.; Gaganidze, E.
Preparation and fracture mechanical testing of tungsten microbeams.
MAT-W&Walloys Monitoring Meeting, Garching, February 9-10, 2011

[81] Sacksteder, I.; Cherville, J.H.; Weingärtner, T.; Trouillet, V.
Effect of the heat-induced corrosion on the mechanical behavior of EUROFER97 derived by instrumented indentations.
7th Internat.Workshop on Direct and Inverse Problems in Piezoelectricity, Oer- Erkenschwick, October 4-7, 2011

[82] Sacksteder, I.; Cherville, J.H.; Weingärtner, T.; Trouillet, V.
Effect of the heat-induced corrosion on the mechanical behavior of EUROFER97 derived by instrumented indentations.
15th Internat.Conf.on Fusion Reactor Materials, Charleston, S.C., October 16-22, 2011

[83] Sacksteder, I.; Schneider, H.C.
Development of an instrumented indentation device for further characterization of irradiated steels at high temperature.
Fusion Engineering and Design, 86(2011) S.2565-2568, DOI:10.1016/j.fusengdes.2011.01.082

[84] Sacksteder, I.; Schneider, H.C.; Materna-Morris, E.
Determining irradiation damage and recovery by instrumented indentation in RAFM steel.
Journal of Nuclear Materials, 417(2011) S.127-130, DOI:10.1016/j.jnucmat.2011.02.012

[85] Scherwitz, M.; Schneider, H.C.; Materna-Morris, E.; Aktaa, J.
Approach of a new testing method on the basis of Eurofer-Eurofer welding joints.
Workshop on Ion Implantation as a Neutron Irradiation Analogue, Oxford, GB,
September 26-28, 2011

[86] Suty, M.
Einflüsse gängiger Gussfehler auf die Werkstoffkennwerte des Gusseisens EN-GHS-400.
Jahrestagung Kerntechnik, Berlin, 17.-19.Mai 2011

[87] Svetukhin, V.; L'vov, P.; Gaganidze, E.; Tikhonchev, M.; Dethloff, C.
Kinetics and thermodynamics of Cr nanocluster formation in Fe-Cr system.
Journal of Nuclear Materials, 415(2011) S.205-209, DOI:10.1016/j.jnucmat.2011.06.005

[88] Svetukhin, V.; L'vov, P.; Gaganidze, E.; Tikhonchev, M.; Krestina, N.
Modeling of chromium nanocluster growth under neutron irradiation.
15th Internat.Conf.on Fusion Reactor Materials, Charleston, S.C., October 16-22, 2011

[89] Tikhonchev, M.; Svetukhin, V.; Gaganidze, E.
MD simulation of atomic displacement cascades near chromium-rich clusters in FeCr alloy.
15th Internat.Conf.on Fusion Reactor Materials, Charleston, S.C., October 16-22, 2011

[90] Tikhonchev, M.Yu.; Svetukhin, V.V.; Kadochkin, A.S.; Gaganidze, E.
Molecular dynamics simulation of atomic displacement cascades in Fe-9 at % Cr and Fe-9 at % Cr-0.1 at % C alloys.
Russian Metallurgy, (2011) Nr.5, S.314-422, Metally, (2011) No.3, S.22-30 (in russian)

[91] Weber, T.; Aktaa, J.
Functionally graded tungsten / EUROFER 97 joints for divertor applications.
MAT-W&Walloys Monitoring Meeting, Garching, February 9-10, 2011
Fusion Materials Topical Group W and W-alloy Development Monitoring Meeting,
Frascati, I, June 6-7, 2011

[92] Weber, T.; Aktaa, J.
Numerical assessment of functionally graded tungsten/steel joints for divertor applications.
Fusion Engineering and Design, 86(2011) S.220-226, DOI:10.1016/j.fusengdes.2010.12.084

[93] Weber, T.; Zhou, Z.; Qu, D.; Aktaa, J.
Resistance sintering under ultra high pressure of tungsten/EUROFER97 composites.
Journal of Nuclear Materials, 414(2011) S.19-22, DOI:10.1016/j.jnucmat.2011.04.024

[94] Weiß, O.J.; Gaganidze, E.
Quantitative TEM investigation of neutron irradiated EUROFER97 from WTZ and ARBOR 1.
6th Meeting of the Helmholtz-Russia Joint Research Group 13, Karlsruhe, May 4, 2011
Monitoring Meeting 'Radiation Effects Modelling and Experimental Validation',
Garching, November 21-23, 2011

[95] Weiß, O.J.; Gaganidze, E.
Quantitative TEM investigation of helium bubbles in neutron irradiated boron doped steels from ARBOR 1.
Radiation Effects Modelling and Experimental Validation Monitoring Meeting, Frascati, I, June 9-10, 2011

[96] Weiß, O.J.; Gaganidze, E.; Aktaa, J.
Quantitative microstructural characterisation of high-dose irradiated EUROFER97.
15th Internat.Conf.on Fusion Reactor Materials, Charleston, S.C., October 16-22, 2011

[97] Weiß, O.J.; Gaganidze, E.; Aktaa, J.
Quantitative TEM investigations on EUROFER 97 up to 32 dpa.
Vincenzini, P. [Hrsg.]
Selected Papers from the 5th Forum on New Materials, Part of CIMTEC 2010 – 12th Internat.Conf.on Modern Materials and Technologies, Montecatini Terme, I, June 6-18, 2010
Stafa-Zürich : Trans Tech Publ., 2011 S.118-123 (Advances in Science and Technology ; 73)

Nuclear Data

[1] Anikeev, A.V.; Dagan, R.; Fischer, U.; Tsidulko, Yu.A.
A fusion neutron source for the incineration of radioactive waste based on the gas dynamic trap.
23rd IAEA Fusion Energy Conference, Daejeon, Korea, October 11-16, 2010

[2] Anikeev, A.V.; Dagan, R.; Fischer, U.; Tsidulko, Yu.A.
A fusion neutron source for the incineration of radioactive waste based on the gas dynamic trap.
23rd IAEA Fusion Energy Conference, Daejeon, Korea, October 11-16, 2010, Proc.publ.in the Web, Wien : IAEA, 2011 FTP/P1-10

[3] Anikeev, A.V.; Dagan, R.; Fischer, U.; Tsidulko, Yu.A.
A fusion neutron source for the incineration of radioactive waste based on the gas dynamic trap.
23rd IAEA Fusion Energy Conference, Daejeon, Korea, October 11-16, 2010

[4] Anikeev, A.V.; Dagan, R.; Fischer, U.; Tsidulko, Yu.A.
A fusion neutron source for the incineration of radioactive waste based on the gas dynamic trap.
23rd IAEA Fusion Energy Conference, Daejeon, Korea, October 11-16, 2010, Proc.publ.in the Web, Wien : IAEA, 2011 FTP/P1-10

[5] Fischer, U.; Batistoni, P.; Dupont, E.; Forrest, R.A.; Hendrikson, H.; Izquierdo, J.; sublet, J.C.
The European effort on the evaluation and validation of nuclear data for fusion technology applications.
Journal of the Korean Physical Society, 59(2011) S.1369-1373, DOI:10.3938/jkps.59.1369

[6] Fischer, U.; Batistoni, P.; Große, D.; Klix, A.; Konobeyev, A.; Leichtle, D.; Perel, R.L.; Pereslavtsev, P.
Progress in R&D efforts on neutronics and nuclear data for fusion technology applications.
23rd IAEA Fusion Energy Conference, Daejeon, Korea, October 11-16, 2010
Proc.publ.in the Web, Wien : IAEA, 2011 FTP/P6-25

[7] Fischer, U.; Große, D.; Moro, F.; Pereslavtsev, P.; Petrizzi, L.; Villari, R.; Weber, V.
Integral approach for neutronics analyses of the European test blanket modules in ITER.
Fusion Engineering and Design, 86(2011) S.2176-2179, DOI:10.1016/j.fusengdes.2011.01.067

[8] Fischer, U.; Klix, A.; Li, J.; Pereslavtsev, P.; Simakov, S.P.; Forrest, R.A.; Wasastjerna, F.
State-of-the-art of computational tools and data for IFMIF neutronics and activation analyses.
Journal of Nuclear Materials, (2011), DOI:10.1016/j.jnucmat.2010.12.266

[9] Fischer, U.; Leichtle, D.; Serikov, A.
Neutronics analysis for the IVVS/GDC plug in ITER.
16th Internat.Workshop on Ceramic Breeder Blanket Interactions (CBBI-16),
Portland, Or., September 8-10, 2011

[10] Fischer, U.; Pereslavtsev, P.; Grosse, D.; Weber, V.; Li Puma, A.; Gabriel, F.
Nuclear design analyses of the helium cooled lithium lead blanket for a fusion power demonstration reactor.
Fusion Engineering and Design, 85(2010) S.1133-1138, DOI:10.1016/j.fusengdes.2010.02.023

[11] Klix, A.; Angelone, M.; Eid, M.; Fischer, U.; Lebrun-Grandie, D.
Neutronikexperimente für die Entwicklung europäischer Fusionsreaktor-Brutblankets.
Frühjahrstagung DPG, Arbeitskreis Energie, Dresden, 13.-18.März 2011
Verhandlungen der Deutschen Physikalischen Gesellschaft, R.6, B.46(2011) AKE 4.3

[12] Klix, A.; Arbeiter, F.; Fischer, U.; Heinzel, V.; Kondo, K.; Serikov, A.
Assessment of the operational dose rate in polymer insulators in the test cell of the IFMIF neutron source.
38th IEEE Internat.Conf.on Plasma Science (ICOPS) and 24th Symp.on Fusion Engineering (SOFE), Chicago, Ill., June 26-30, 2011
Piscataway, N.J. : IEEE, 2011 Paper SP2-19, ISBN 978-1-4577-0669-1
Proc.also publ.online, e-ISBN 978-1-4577-0667-7, DOI:10.1109/SOFE.2011.6052282

[13] Klix, A.; Arbeiter, F.; Fischer, U.; Heinzel, V.; Serikov, A.
Assessment of the operational dose rate in polymer insulators in the test cell of the IFMIF neutron source.
38th IEEE Internat.Conf.on Plasma Science (ICOPS) and 24th Symp.on Fusion Engineering (SOFE), Chicago, Ill., June 26-30, 2011

[14] Klix, A.; Arbeiter, F.; Fischer, U.; Heinzel, V.; Serikov, A.; Simakov, S.P.
Calculations of the operational dose rate in polymer insulators in the test cell of IFMIF.
Jahrestagung Kerntechnik, Berlin, 17.-19.Mai 2011
Berlin : INFORUM GmbH, 2011, CD-ROM

[15] Klix, A.; Batistoni, P.; Böttger, R.; Lebrun-Grandie, D.; Fischer, U.; Henniger, J.; Leichtle, D.; Villari, R.
Measurement and analysis of neutron flux spectra in a neutronics mock-up of the HCLL test blanket module.
Fusion Engineering and Design, 85(2010) S.1803-1806, DOI:10.1016/j.fusengdes.2010.05.038

[16] Klix, A.; Domula, A.; Fischer, U.; Gehre, D.; Pereslavtsev, P.; Rovni, I.
Test facility for a neutron flux spectrometer system based on the foil activation technique for neutronics experiments with the ITER TBM.
Fusion Engineering and Design, 86(2011) S.2322-2325, DOI:10.1016/j.fusengdes.2011.02.090

[17] Klix, A.; Domula, A.; Forrest, R.; Zuber, K.
Measurement and analysis of activation induced in titanium with fusion peak neutrons.
Journal of Nuclear Materials, 417(2011) S.688-691, DOI:10.1016/j.jnucmat.2011.03.039

[18] Klix, A.; Fischer, U.; Lebrun-Grande, D.; Batistoni, P.; Villari, S.; Boettger, R.; Fleischer, K.; Henniger, J.; Gehre, D.; Sommer, M.
Integral neutronics experiment with a mock-up of the European HCLL-TBM for ITER.
Journal of the Korean Physical Society, 59(2011) S.1957-1960, DOI:10.3938/jkps.59.1957

[19] Konobeev, A.Yu.; Fischer, U.; Pereslavtsev, P.E.; Capote, R.
Improved data evaluation methodology for energy ranges with missing experimental data.
Internat.Workshop on Accelerator Radiation Induced Activation (ARIA 2011),
Jerusalem, IL, May 15-19, 2011

[20] Kuznetsov, M.; Grune, J.; Kobelt, S.; Sempert, K.; Jordan, T.
Experiments for the hydrogen combustion aspects of ITER LOVA scenarios.
Fusion Engineering and Design, 86(2011) S.2747-2752, DOI:10.1016/j.fusengdes.2011.01.050

[21] Kuznetsov, M.; Redlinger, R.; Breitung, W.; Grune, J.; Friedrich, A.; Ichikawa, N.
Laminar burning velocities of hydrogen-oxygen-steam mixtures at elevated temperatures and pressures.
Proceedings of the Combustion Institute, 33(2011) S.895-903, DOI:10.1016/j.proci.2010.06.050

[22] Le Guern, F.; Gulden, W.; Ciattaglia, S.; Counsell, G.; Bengaouer, A.; Brinster, J.; Dabbene, F.; Denkevitz, A.; Jordan, T.; Kuznetsov, M.; Porfiri, M.T.; Redlinger, R.; Roblin, Ph.; Roth, J.; Segre, J.; Sugiyama, K.; Tkatschenko, I.; Xu, Z.
F4E R&D programme and results on in-vessel dust and tritium.
Fusion Engineering and Design, 86(2011) S.2753-2757, DOI:10.1016/j.fusengdes.2010.12.029

[23] Leichtle, D.; Fischer, U.; Perel, R.L.; Serikov, A.
Sensitivity and uncertainty analysis of nuclear responses in the EU HCLL TBM of ITER.
Fusion Engineering and Design, 86(2011) S.2156-215, DOI:10.1016/j.fusengdes.2011.01.004

[24] Leichtle, D.; Serikov, A.; Fischer, U.
Absorbed decay-photon dose analysis of the IVVS/GDC plug in ITER.
Jahrestagung Kerntechnik, Berlin, 17.-19.Mai 2011
Berlin : INFORUM GmbH, 2011, CD-ROM

[25] Majerle, M.; Simakov, S.P.; Fischer, U.
Modelling D-Be and D-C neutron sources for SPIRAL-2.
10th Internat.Topical Meeting on Nuclear Applications of Accelerators (AccApp 2011), Knoxville, Tenn., April 3-7, 2011

[26] Pereslavtsev, P.; Fischer, U.; Grosse, D.; Leichtle, D.; Majerle, M.
Shutdown dose rate analysis for the European TBM system in ITER.
10th Internat.Symp.on Fusion Nuclear Technology (ISFNT 2011), Portland, Oreg., September 11-16, 2011

[27] Pereslavtsev, P.; Konobeyev, A.; Fischer, U.; Leal, L.
Evaluation of ^{50}Cr, ^{52}Cr, ^{53}Cr, ^{54}Cr neutron cross section data for energies up to 200 MeV.
Journal of the Korean Physical Society, 59(2011) S.931-934, DOI:10.3938/jkps.59.931

[28] Pereslavtsev, P.; Konobeyev, A.; Fischer, U.; Leal, L.
Evaluation of ^{50}Cr, ^{52}Cr, ^{53}Cr, ^{54}Cr neutron cross section data for energies up to 200 MeV.
Internat.Conf.on Nuclear Data for Science and Technology (ND2010), Jeju Island, Korea, April 26-30, 2010

[29] Serikov, A.; Arbeiter, F.; Fischer, U.; Heinzel, V.; Klix, A.; Simakov, S.P.
Shutdown dose rate analyses for the IFMIF HFTM.
Fusion Engineering and Design, 86(2011) S.2639-2642, DOI:10.1016/j.fusengdes.2010.11.030

[30] Serikov, A.; Fischer, U.; Grosse, D.
High performance parallel Monte Carlo transport computations for ITER fusion neutronics application.
Joint Internat.Conf.of the 7th Supercomputing in Nuclear Application and the 3rd Monte Carlo (SNA + MC2010), Tokyo, J, October 17-21, 2010

[31] Serikov, A.; Fischer, U.; Grosse, D.
High performance parallel Monte Carlo transport computations for ITER fusion neutronics application.
Progress in Nuclear Science and Technology, 2(2011) S.294-300

[32] Serikov, A.; Fischer, U.; Grosse, D.; Leichtle, D.; Majerle, M.
Toolkit for high performance Monte Carlo radiation transport and activation calculations for shielding applications in ITER.
Internat.Conf.on Mathematics and Computational Methods Applied to Nuclear Science and Engineering (MC 2011), Rio de Janeiro, BR, May 8-12, 2011, Proc.on CD-ROM
American Nuclear Society, Latin American Section, 2011, ISBN 978-85-63688-00-2

[33] Serikov, A.; Fischer, U.; Grosse, D.; Leichtle, D.; Strauss, D.
High performance computations of Monte Carlo radiation transport for ITER fusion neutronics.
Workshop SimLabs @ KIT, Karlsruhe, November 29-30, 2010

[34] Serikov, A.; Fischer, U.; Grosse, D.; Leichtle, D.; Strauss, D.
High performance computations of Monte Carlo radiation transport for ITER fusion neutronics.
Kondov, I. [Hrsg.]
Workshop Computational Methods in Science and Engineering (SimLabs @ KIT), Karlsruhe, November 29-30, 2010, Proc.S.135-148
Karlsruhe : KIT Scientific Publ., 2011, ISBN 978-3-86644-693-9

[35] Serikov, A.; Fischer, U.; Grosse, D.; Loughlin, M.J.; Majerle, M.; Schreck, S.; Spaeh, P.; Strauss, D.
Neutronic analyses for the upper ports in the neutral beam cell of ITER.
Fusion Science and Technology, 69(2011) S.708-714

[36] Serikov, A.; Fischer, U.; Grosse, D.; Spaeh, P.; Strauss, D.
Evolution of shielding computations for the ITER upper ECH launcher.
Nuclear Technology, 175(2011) S.238-250

[37] Serikov, A.; Fischer, U.; Leichtle, D.
Neutronic analyses for the IVVS/GDC system in ITER.
Transactions of the American Nuclear Society, 104(2011) S.637-638

[38] Simakov, S.P.; Fischer, U.; Bem, P.; Burjan, V.; Götz, M.; Honusek, M.; Kroha, V.; Novak, J.; Simeckova, E.; Forrest, R.A.
Analysis of the dosimetry cross sections measurements up to 35 MeV with a ^{7}Li(p,xn) quasi-monoenergetic neutron source.
Journal of the Korean Physical Society, 59(2011) S.1856-1859, DOI:10.3938/jkps.59.1856

[39] Simakov, S.P.; Li, J.; Fischer, U.
Radiation deep penetration calculations for the IFMIF test cell wall.
Fusion Engineering and Design, 85(2010) S.1924-1927, DOI:10.1016/j.fusengdes.2010.06.025

International Fusion Materials Irradiation Facility (IFMIF)

[1] Borodin, V.A.; Vladimirov, P.V.
Three-dimensional atomistic modeling of microcrack propagation in iron.
Journal of Nuclear Materials, 416(2011) S.49-54, DOI:10.1016/j.jnucmat.2010.12.224

[2] Borodin, V.A.; Vladimirov, P.V.; Moeslang, A.
The effects of temperature on crack propagation in Bcc iron.
15th Internat.Conf.on Fusion Reactor Materials, Charleston, S.C., October 16-22, 2011

[3] Chen, Y.; Arbeiter, F.
Flow and heat transfer characteristics of helium cooled IFMIF high flux test module.
10th Internat.Symp.on Fusion Nuclear Technology (ISFNT 2011), Portland, Oreg., September 11-16, 2011

[4] Gopejenko, A.; Zhukovskii, Y.F.; Vladimirov, P.V.; Kotomin, E.A.; Möslang, A.
Modeling of yttrium, oxygen atoms and vacancies in □-iron lattice.
Journal of Nuclear Materials, 416(2011) S.40-44, DOI:10.1016/j.jnucmat.2010.11.088

[5] Vladimirov, P.V.; Moeslang, A.
Ab initio static and molecular dynamics studies of helium behavior in beryllium.
15th Internat.Conf.on Fusion Reactor Materials, Charleston, S.C., October 16-22, 2011

Fuel Cycle – Vacuum Pumping

[1] Day, C.
Kryovakuumtechnik und Kryopumpen.
VDI-Wissensforum Kryotechnik, Karlsruhe, 23.-25.März 2011

[2] Day, C.
Seminar on the ITER vacuum systems.
Engineering on Nuclear Fusion Reactors, Politecnico Torino, I, January 25, 2011

[3] Day, C.; Cristescu, I.; Pegourie, B.; Weyssow, B.
Considerations towards the fuel cycle of a steady-state DT fusion device.
23rd IAEA Fusion Energy Conference, Daejeon, Korea, October 11-16, 2010
Proc.publ.in the Web, Wien : IAEA, 2011 FTP/P1-04

[4] Day, Chr.; Giegerich, Th.; Hanke, St.; Hauer, V.; Lässer, R.; Papastergiou, S.
Design development of cryopumping systems for ITER in view of future DT fusion devices. (eingeladen)
10th Internat.Symp.on Fusion Nuclear Technology (ISFNT 2011), Portland, Oreg., September 11-16, 2011

[5] Day, Chr.; Haas, H.; Hanke, St.; Hauer, V.; Luo, X.; Scannapiego, M.; Simon, R.; Strobel, H.; Fellin, F.; Lässer, R.; Masiello, A.; Papastergiou, St.; Dremel, M.; Mayaux, Chr.; Pearce, R.
Design progress for the ITER torus and neutral beam cryopumps.
Fusion Engineering and Design, 86(2011) S.2188-2191, DOI:10.1016/j.fusengdes.2010.11.023

[6] Day, Chr.; Haas, H.; Hanke, St.; Hauer, V.; Luo, X.; Varoutis, St.
Modeling and simulation of the ITER cryopumping systems.
American Vacuum Society 58th Internat.Symp.and Exhibition, Nashville, Tenn., October 30 - November 4, 2011

[7] Day, Chr.; Wolf, R.
An integrated view on high density plasma operation and fuel cycle. eingeladen
Internat.Workshop 'MFE Roadmapping in the Iter Era, Princeton, N.J., September 7-10, 2011

[8] Giegerich, T.; Day, C.; Hauer, V.
Development of a tritium compatible vapor diffusion pump for a commercial fusion power plant.
10th Internat.Symp.on Fusion Nuclear Technology (ISFNT 2011), Portland, Oreg., September 11-16, 2011

[9] Giegerich, T.; Day, Chr.
View on challenges in operating fusion power plant vacuum systems.
3rd Workshop on the Operation of Large Vacuum Systems (OLAV III), Oak Ridge, Tenn., July 11-14, 2011

[10] Giegerich, T.; Varoutis, S.; Hauer, V.; Day, C.
Measurements in the transflow facility.
64th IUVSTA Workshop on Practical Applications and Methods of Gas Dynamics for Vacuum Science and Technology, Leinsweiler, May 16-19, 2011

[11] Giegerich, Th.; Day, Chr.
Development of vacuum flow modeling tools.
3rd Workshop on the Operation of Large Vacuum Systems (OLAV III), Oak Ridge, Tenn., July 11-14, 2011

[12] Haas, H.; Day, Chr.; Herzog, F.
TIMO-2 - a cryogenic test bed for the ITER cryosorption pumps.
Cryogenic Engineering Conf.and Internat.Cryogenic Materials Conf. (CEC-ICMC), Spokane, Wash., June 13-17, 2011

[13] Hanke, St.; Day, Chr.; Luo, X.; Sonato, P.
Status of the cryosorption pumping system for the neutral beam test facility MITICA.
Italian Vacuum Association 20.Congresso, Padova, I, 17-19 Maggio 2011

[14] Hanke, St.; Scannapiego, M.; Luo, X.; Day, Chr.; Fellin, F.; Zaccaria, P.
The large cryopump system for the heating neutral beam injection of ITER.
American Vacuum Society 58th Internat.Symp.and Exhibition, Nashville, Tenn., October 30 - November 4, 2011

[15] Hauer, V.; Day, C.
Network modelling of complex vacuum systems.
64th IUVSTA Workshop on Practical Applications and Methods of Gas Dynamics for Vacuum Science and Technology, Leinsweiler, May 16-19, 2011

[16] Luo, X.; Day, C.; Haas, H.; Varoutis, S.
Experimental results and numerical modeling of a high-performance large-scale cryopump. I. Test particle Monte Carlo simulation.
Journal of Vacuum Science and Technology A, 29(2011) S.041601/1-7
DOI:10.1116/1.3585665

[17] Luo, X.; Day, Chr.
Investigation of a new Monte Carlo method for transitional gas flow.
27th Internat.Symp.on Rarefied Gas Dynamics (RGD 2010), Pacific Grove, Calif., July 10-15, 2010
Proc.Part 1 S.272-276, Melville, N.Y. : American Institute of Physics, 2011
(AIP Conference Proceedings ; 1333), ISBN 978-0-7354-0889-0

[18] Luo, X.; Haas, H.; Day, C.
Systematic vaccum study of the ITER model cryopump by test particle Monte Carlo simulation.
Frühjahrstagung DPG, Fachverband Vakuumphysik und Vakuumtechnik, Dresden, 13.- 18.März 2011
Verhandlungen der Deutschen Physikalischen Gesellschaft, R.6, B.46(2011) VA 2.1

[19] Luo, X.; Varoutis, S.; Hass, H.; Hanke, S.; Day, C.
ProVac3D - a test particle Monte Carlo program for complex vacuum systems.
64th IUVSTA Workshop on Practical Applications and Methods of Gas Dynamics for Vacuum Science and Technology, Leinsweiler, May 16-19, 2011

[20] Maruyama, S.; Yang, Y.; Pitts, R.A.; Sugihara, M.; Putvinski, S.; Carpentier-Chouchana, S.; Li, B.; Li, W.; Baylor, L.R.; Meitner, S.J.; Day, C.; LaBombard, B.; Reinke, M.
ITER fuelling system design and challenges. Gas and pellet injection and disruption mitigation
23rd IAEA Fusion Energy Conference, Daejeon, Korea, October 11-16, 2010
Proc.publ.in the WEB, Wien : IAEA, 2011 ITR/P1-28

[21] Masiello, A.; Agarici, G.; Bonicelli, T.; Simon, M.; Alonso, J.; Bigi, M.; Boilson, D.; Chitarin, G.; Day, C.; Franzen, P.; Hanke, S.; Heinemann, B.; Hemsworth, R.; Luchetta, A.; Marcuzzi, D.; Milnes, J.; Minea, T.; Pasqualotto, R.; Pomaro, N.; Serianni, G.; Rigato, W.; Sonato, P.; Toigo, V.; Villecroze, F.; Waldon, C.; Zaccaria, P.
The European contribution to the developments of the ITER NB injector.
Fusion Engineering and Design, 86(2011) S.860-863, DOI:10.1016/j.fusengdes.2011.03.035

[22] Pantazis, S.; Varoutis, S.; Hauer, V.; Day, C.; Valougeorgis, D.
Gas-surface scattering effect on vacuum gas flows through rectangular channels.
Vacuum, 85(2011) S.1161-1164, DOI:10.1016/j.vacuum.2010.12.019

[23] Pearce, R.J.H.; Antipenkov, A.; Bersier, J.L.; Boussier, B.; Bryan, S.; Hughes, I.; Sekachev, I.; Worth, L.; Baylor, L.; Gardner, W.; Meitner, S.; Wickus, P.; Lässer, R.; Papastergiou, S.; Day, Chr.
Gas species, their evolution and segregation through the ITER vacuum systems.
10th Internat.Symp.on Fusion Nuclear Technology (ISFNT 2011), Portland, Oreg., September 11-16, 2011

[24] Scannapiego, M.; Day, C.; Hanke, S.; Hauer, V.
Thermohydraulic investigation on the ITER neutral beam injector cryopump.
Chorowski, M. [Hrsg.]
Proc.of the 23rd Internat.Cryogenic Engineering Conf.(ICEC 23) and Internat.Cryogenic Materials Conf.(ICMC 2010), Wroclaw, PL, July 19-23, 2010
Wroclaw : Oficyna Wydawnicza Politechniki Wroclawskieij, 2011 S.827-832
ISBN 978-83-7493-589-0

[25] Sonato, P.; Bonicelli, T.; Chakraborty, A.K.; Hemsworth, R.; Watanabe, K.; Day, C.; Franzen, P.; Waldon, C.
The ITER neutron beam facility in Padua - Italy: a joint international effort for the development of the ITER heating neutral beam injector prototype.
23rd IAEA Fusion Energy Conference, Daejeon, Korea, October 11-16, 2010
Proc.publ.in the Web, Wien : IAEA, 2011

[26] Varoutis, S.
Numerican and experimental investigation of rarefied gas flows over the whole range of the Knudsen number.
Graduiertenkolleg PoreNet, Universität Bremen, 2011

[27] Varoutis, S.; Day, C.
Numerical modeling of an ITER type cryopump.
10th Internat.Symp.on Fusion Nuclear Technology (ISFNT 2011), Portland, Oreg., September 11-16, 2011

[28] Varoutis, S.; Sharipov, F.; Day, C.; Luo, X.; Haas, H.
Follow-up vacuum study of the ITER model cryopump by the direct simulation Monte Carlo method.
Frühjahrstagung DPG, Fachverband Vakuumphysik und Vakuumtechnik, Dresden, 13.- 18.März 2011
Verhandlungen der Deutschen Physikalischen Gesellschaft, R.6, B.46(2011) VA 2.2

[29] Varoutis, S.; Sharipov, F.; Valougeorgis, D.; Sazhin, O.
Benchmark problem. Direct simulation Monte Carlo of gas flow through an orifice and short tube.
64th IUVSTA Workshop on Practical Applications and Methods of Gas Dynamics for Vacuum Science and Technology, Leinsweiler, May 16-19, 2011

Fuel Cycle – Tritium Processing

[1] Bekris, N.; Sirch, M.
On the mechanism of the disproportionation of ZrCo hydride.
15th Internat.Conf.on Fusion Reactor Materials, Charleston, S.C., October 16-22, 2011

[2] Borisevich, O.; Demange, D.; Parracho, T.; Pera-Titus, M.; Nicolas, C.H.
Permeance and selectivity of helium and hydrogen in nanocomposite MFI-alumina hollow fibre for tritium processes.
5th Internat.FEZA Conf., Valencia, E, July 3-7, 2011

[3] Demange, D.
Tritium coupled phenomena in solid breeder blanket concepts: state of the art and rationale for future work plan.
16th Internat.Workshop on Ceramic Breeder Blanket Interactions (CBBI-16), Portland, Or., September 8-10, 2011

[4] Demange, D.; Alecu, C.; Bekris, N.; Borisevich, O.; Bornschein, B.; Fischer, S.; Köllö, Z.; Le, T.L.; Michling, R.; Schlösser, M.; Sturm, M.; Wagner, R.; Welte, S.
Process and analytical issues for tritium management in breeder blanket of ITER and DEMO.
10th Internat.Symp.on Fusion Nuclear Technology (ISFNT 2011), Portland, Oreg., September 11-16, 2011

[5] Demange, D.; Bekris, N.; Besserer, U.; Le, L.T.; Kramer, F.; Parracho, A.; Wagner, R.
Overview of processes using zeolite at the Tritium Laboratory Karlsruhe.
5th Internat.FEZA Conf., Valencia, E, July 3-7, 2011

[6] Parracho, A.I.R.T.; Demange, D.; Knipe, S.; Le, L.T.; Simon, K.H.; Welte, S.
Process of highly tritiated water desorbed from molecular sieve bed using PERMCAT.
10th Internat.Symp.on Fusion Nuclear Technology (ISFNT 2011), Portland, Oreg., September 11-16, 2011

[7] Plusczyk, C.; Cristescu, I.; Michling, R.; Cilbir, E.; Welte, S.
Computational 2 phase fluid dynamic simulation to design a cryogenic reboiler for liquid hydrogen isotopologues distillation.
10th Internat.Symp.on Fusion Nuclear Technology (ISFNT 2011), Portland, Oreg., September 11-16, 2011

[8] Welte, S.; Demange, D.; Wagner, R.; Gramlich, N.
Development of a technical scale PERMCAT reactor for processing of highly tritiated water.
10th Internat.Symp.on Fusion Nuclear Technology (ISFNT 2011), Portland, Oreg., September 11-16, 2011

Appendix IV: Glossary

AAS	Atomic Absorption Spectroscopy
AC	Alternating Current
ACAB	UNED Code for Activation Calculations
ACI	After Cavity Interaction
AEUL	Association EURATOM – University of Latvia, Riga
AF	Accelerator Facility
ALICE/ASH	The code for the calculation of nuclear reaction cross-sections and secondary particle distributions using geometry dependent hybrid model
APD	Avalance Photo Diode
AREVA	French Nuclear Company
ASG magnet	Superconducting magnet at CRPP for the ITER gyrotron manufactured by ASG Superconductors
ASTM	American Society for Testing and Materials
BA	Broader Approach
BDT	Brittle-to-Ductile Transition
BEKED	The code package for the evaluation of nuclear data
BF	Bright-Field
BLV	Beamline Vessel
BMBF	Bundesministerium für Bildung und Forschung
BTR	Beam Transport Room
BSM	Blanket Shield Module
BtP	Built-to-print
BU	Breeder Unit
CAD	Computer Aided Design
CATIA V5	CAD Software, Version 5
CBED	Convergent Beam Electron Diffraction
CCFE	Culham Centre for Fusion Energy, UK
CCRC	Coated Conductor Rutherford Cable
CD	Cryogenic Distillation
CdTe	Cadmium Telluride
CEA	Commissariat à l'Énergie Atomique, Saclay (France)
CEBSR	Continuous Edge Bending Strain Rig
CECE	Combined Electrolysis Catalytic Exchange
CFC	Carbon Fibre Composite
CFD	Computational Fluid Dynamic
CHF	Critical Heat Flux

CIEMAT	Centro de Investigaciones Energeticas Medioambientales y Tecnologicas
CNR	Consiglio Nazionale delle Ricerche, Milano, Italy
COD	Crack Opening Displacement
CPS	Capillary Porous System
CPU	Central Processing Unit
C-R	Circumferential Orientation
Cr	Chromium
CRPP-EPFL	Centre de Recherces en Physique des Plasmas, - Ècole polytechnique fédérale de Lausanne, Switzerland
CS	Central Solenoïd
CT	Compact Toroid
CTE	Coefficient of Thermal Expansion
Cu	Copper
CuLTKa	Current Lead Test Facility Karlsruhe
CVD	Chemical Vapor Deposition
CW	Continuous Wave
CZT	Cadmium-Zinc-Telluride
D1S	Direct One-step Method for Shut-down Dose rate Calculations
DAS	Design Assessment Studies
DBH	Dispersed Barrier Hardening
DBTT	Ductile-to-Brittle Transition Temperature
DCLL	Dual Coolant Lithium Lead
DD	Deuterium Deuterium Fusion Process
DDA	DEMO Design Activities
DEMO	DEMOnstration Fusion Reactor
DEMONET	DEMO Version of the Next European Torus (NET)
DIR	Direct Internal Recycling
DSC	Differential Scanning Calorimetry
DSMC	Direct Simulation Monte Carlo
DT	Deuterium Tritium
DTC	Drift Tube Linac
EAF	European Activation File
EASY	European Activation System
EB	Electron Beam Welding
ECCD	Electron Cyclotron Current Drive
ECH & CD	Electron Cyclotron Heating and Current Drive
ECIS	The code for the calculation of total and elastic cross-sections and particle transmission coefficients using the coupled channel model

ECRF	Electron Cyclotron Range of Frequences
ECRH	Electron Cyclotron Resonance Heating
ECRH & CD	Electron Cyclotron Resonance Heating and Current Drive
EDM	Electrical Discharge Machining
EDX	Energy Dispersive X-ray Spectrocopy
EELS	Electron Energy Loss Spectroscopy
EF	Equilibrium Field
EFDA	European Fusion Development Agreement
EFF	European Fusion File
EFREMOV	Scientific Research Institute, Saint Petersburg, Russia
EGYC	European Gyrotron Consortium
ELM	Edge Localized Model
EM	Electromagnetic
EMIM-$AlCl_4$	Ethyl-Ethyl-Imidazolium Tetrachloroaluminium Chloride
EMIM-Cl	Ethyl-Ethyl-Imidazolium Chloride
ENDF	Evaluated Nuclear Data File
ENEA	Italian National Agency for New Technologies, Energy and Sustainable Economy Development
ENSDF	Evaluated Nuclear Structure Data File
EPP	Diagnostic Generic Equatorial Port Plug in ITER
EU	European
EUROFER	European RAF/M Steel
EVEDA	Engineering Validation and Engineering Design Activities
EXFOR	Exchange Format for Nuclear Reaction Data and the file containing the compilation of measurements
F4E	Fusion for Energy
FE	Finite Element
FEM	Finite Element Method
FENDL	Fusion Evaluated Nuclear Data Library
FGMC	Fundamental Gaussian Mode Content
FIB	Focused Ion Beam Microscope
FISPACT	Nuclear Inventory Code for Activation Calculations
FM	Fracture-Mechanical
FML	Fusion Materials Laboratory (KIT, Germany)
FNG	Frascati Neutron Generator
FPP	Fusion Power Plant
FPSS	Fusion Power Shutdown System
FPY	Full Power Year

FT	Fracture Toughness
FW	First Wall
FZ	Fusion Zone
FZJ	Forschungszentrum Jülich
GEM	Gas Electron Multiplier
GIS	Gas Injection Fuelling System
GOT	Goal Oriented Training Programme
GS2	Lithium Glass Scintallator
GUI	Graphical User Interface
H_2	Hydrogen
H&CD	Heating and Current Drive
HAADF	High Angle Annular Dark Field (detector)
HAS	Hungarian Academy of Sciences
HAZ	Heat Affected Zone
HC3	High Performance Computer cluster at KIT
HCF	Hot Cell Facility
HCLL	Helium Cooled Lithium Lead
HCPB	Helium Cooled Pebble Bed
He	Helium
HEBLO	HElium BLOwer (Helium facility at FZK)
HELLAS	A synonym for the collaborating Greek Institutions National Technical University of Athens, Greece and the National and Kapodistrian University of Athens, Greece
HELOKA	Helium Loop Karlsruhe
HETRA	Heat TRAnsfer Experiment
HFR	High Flux Reactor (Petten)
HFTM	High Flux Text Module
HHF	High Heat Flux
HIP	Hot Isostatic Pressing
HNB	Heating Neutral Beam Injector
HPC-FF	High Performance Computer for Fusion, Jülich
HPGe	High-Purity Germanium (detector)
HR	Hot Rolling
HRJRG-13	Helmholtz Russia Joint Research Group-13
HTIL	High Temperature Ionic Liquids
HTO	Tritiated Water Vapour
HTS	High Temperature Superconductor
HV	High Vacuum

IAEA	International Atomic Energy Agency
IAP	Institute of Applied Physics, Nizhny Novgorod, Russia
I_c	Critical Current
ICIT	National Institute of Research and Development for Cryogenics and Isotope Technology, Rm. Valcea, Romania
ICP-MS	Inductively Coupled Plasma Mass Spectroscopy
ICRP	International Commission on Radiation Protection
IFMIF	International Fusion Materials Irradiation Facility
IGES	Data Format for the Exchange of CAD Geometry Data
IL	Ionic Liquids
IPE	Institute for Data Processing and Electronics
IPF	Institut für Plasmaforschung, Universität Stuttgart, Germany
IPP	Max Planck Institut für Plasmaphysik, Garching,/Greifswald, Germany
IPPLM-WUT	Institute of Plasma Physics and Laser Microfusion – Warsaw University of Technology, PL
ISS	Isotope Separation System
ISSP	Institute of Solid State Physics, Riga, Latvia
ITEP	Institute for Technical Physics
ITER	International Thermonuclear Experimental Reactor
IVCC	In-vessel Components Coolants Assessment
JAERI	Japan Atomic Energy Agency
JEFF	Joint Evaluated Fission Fusion File
JET	Joint European Torus
JSC	Jülich Supercomputing Centre
JSC “SSC RIAR”	Joint Stock Company “State Scientific Centre Research Institute of Atomic Reactors”
JT-60	Japan Torus with D-shape Cross Section
JUROPA/HPC-FF	High Performance Computing for Fusion cluster at Juelich Supercomputing Centre at Forschungszentrum Juelich, Germany
KALOS	Karlsruhe Lithium Orthosilicate
KBHF	Karlsruhe Beryllium Handling Facility
K_{IC}	Critical Stress Intensity Factor for Model I Loading
KIT	Karlsruhe Institute of Technology
K_Q	Stress Intensity Factor as defined ASTM 399
LCF	Low Cycle Fatigue
LF	Lithium Target Facility
LHT	Launcher Handling Test Facility at KIT
LLL	Liquid Lithium Limiter
LOM	Light Optical Microscope / Microscopy
LOVA	Loss of Vacuum Accident

LPMS	Large Port Maintenance System
LPCE	Liquid Phase Catalytic Exchange
L-R	Longitudinal Orientation
MA	Mechanical Alloying
MAXED	Unfolding Code
McCAD	Software Tool for the Conversion of CAD Geometry Data into Monte Carlo Representation
MCNP	Monte Carlo Neutron Photon (code for particle transport simulations)
CPX	Monte Carlo Code for Multi Particle Transport Simulations
MCSEN	Monte Carlo Sensitivity Code based on MCNP
MGI	Massive Gas Injection for Disruption Mitigation
MHD	Magneto Hydrodynamic
MITICA	Neutral Beam test bed in Padova, Italy
MOU	Matching Optics Unit
MPI	Message Passing Interface
MTC	Modular Test Cell
MTIL	Medium Temperature Ionic Liquids
NB	Neutral Beam
NC	Normal Conducting
NDT	Non-destructive Testing
NE213	Liquid scintillator with capability to discriminate between gamma-ray and neutron interaction
NG	Neutral Gas
Ni	Nickel
NRG	Nuclear Research and Consultancy Group, National Nuclear Research Institute of the Netherlands, located in Petten
ODS	Oxygen Dispersion Strengthened
ODSFS	Oxygen Dispersion Strengthened ferritic steels
OI magnet	Superconducting magnet at KIT, manufactured by Oxford Instruments
OM	Optical Microscopy
ORE	Occupational Radiation Exposure
OSi	Lithium Orthosilicate
P/R	Ratio of Power over the Major Radius
PAS	Positron Annihilation Spectroscopy
PCW	Poly-Crystalline Tungsten
Pd	Palladium
PEX	Power Exhaust
PF	Poloïdal Field
PFC	Plasma Facing Component

PIE	Post Irradiation Examination
PIM	Power Injection Molding
PLT	Princeton Large Tokamak
PMT	Photo Multiplier Tube
PPC	ITER Pre-production Torus Cryopump
PPCS	Power Plant Conceptual Study
PPE	Port Plug Engineering
PPPT	Power Plant Physics Technology
PRIMA	Neutral Beam Test d Facility in Padova, Italy
ProVac3D	KIT Code for Vacuum Flow Calculations
PS	Power Distribution System
PWHT	Post Weld Heat Treatment
QD	Quench Detection
QDU	Quench Detection Unit
R2S	Rigorous Two-step Methode for Shut-down Dose Rate Calculations
RAFM	Reduced Activation Ferritic Martensitic (Steel)
RAMI	Reliability, Availability, Maintainability, Inspectability
RD	Rolling direction
RE	Runaway Electrons
RF	Radio Frequency, within this report above 100 GHz
RF	Russian Federation
RH	Remote Handling
RIR	Radiation Isolation Room
R-L	Radial Orientation
rpm	rotations per minute
RT	Room Temperature
RTIL	Room Temperature Ionic Liquids
SA2	Safety scenario of irradiation in ITER for activation calculations
SANS	Small Angel Neutron Scattering
Sc	Superconducting
SCD	Single Crystal Diffraction
SCK-CEN	Studiecentrum voor Kernenergie, Mol, Belgium
SCW	Single-Crystalline Tungsten
SEM	Scanning Electron Microscopy
SENB	Single Edged Notched Bar
SL1, SL2	Seismic Load Case

SOL	Scrape-off Layer
SS	Stainless Steel
STEM	Scanning Transmission Electron Microscope
STEP	Data Format for the Exchange of CAD Geometry Data
T-3M	Russian Tokamak with Materials Testing Stand
TAP	Technical Advisory Panel for F4
TALYS	The code for the calculation of nuclear reaction cress-sections and secondary particle distributions using pre-equilibrium exciton model
TBM	Test Blanket Module
T_{br}	Brazing Temperature
TCILE	Two Component Ionic Liquids Electrolyte
TD	Theoretical Density
TED	Thales Electron Devices at Velizy, France
TEM	Transmission Electron Microscope / Microscopy
TF	Test Facility
TF	Toroidal Field
THESEUS	Test Facility for DEMO Vacuum Pumps
Ti	Titanium
TIG	Tungsten Inert Gas Welding
TIMO	Test Facility for ITER Model Pump
TIR	Target Interface Room
TiT target	Titanium-Tritium, solid target used in accelerator-based neutron generators.
TLD	Thermo Luminescence Detector
TLK	Tritium Laboratory Karlsruhe
TOL-F	Name of a measurement device for the local dose rate
TOSKA	Torusspulen Testanordnung Karlsruhe
TPR	Tritium Production Rate
TQ	Thermal Quench
TRANSFLOW	Test Facility for Vacuum Flows
TRIPOLI	Monte Carlo Code for Particle Transport Calculations
TRM	Tritium Release Test Module
TTC	Target- and Test Cell
TUD	Technical University of Dresden
TUD-NG	Technical University of Dresden Neutron Generator
TZM	Molybdenum, stabilized by small amounts of titanium and zirconium
UNED	Universidad Nacional de Educación a Distancia, Madrid, Spain
UNIQD	Universal Quench Detector

VDE	Vertical Displacement Event
VMS	Vertical Maintenance System
VNWA	Vectorial Network Analyzer
VV	Vacuum Vessel
W	Tungsten
W7-X	The Wendelstein 7-X Stellarator Project in Greifswald, Germany
WCD	Water-cooled Divertor
WDS	Water Detritiation System
WL10	Tungsten with 10 % of La2O3
Zr	Zirconium

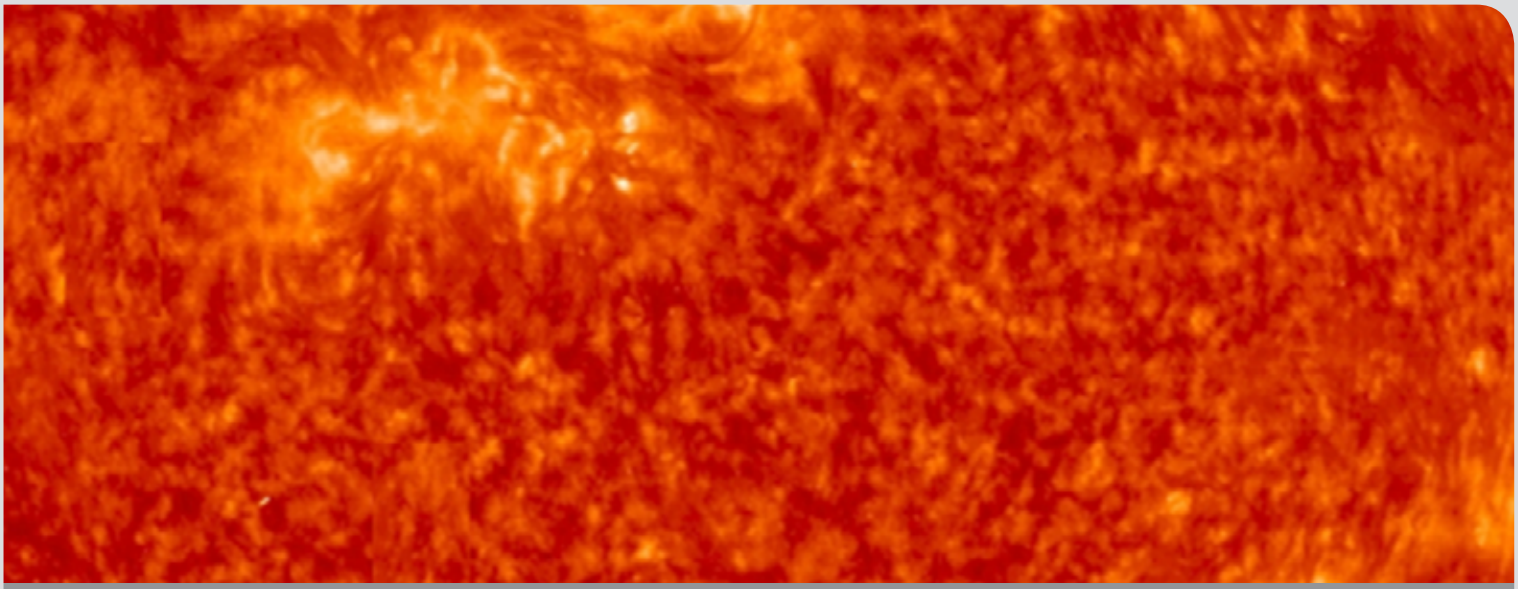

ISSN 1869-9669